

**INVESTIGATION OF ENGINE DESIGN PARAMETERS ON
THE EFFICIENCY AND PERFORMANCE OF THE HIGH
SPECIFIC POWER DOWNSIZED SI ENGINE**

A thesis submitted for the degree of Doctor of Philosophy

By

Barnaby Coates

School of Engineering and Design

Brunel University

United Kingdom

November 2012

Abstract

This study investigates the impact of employing the Miller cycle on a high specific power downsized gasoline engine by means of Early Intake Valve Closing (EIVC) and Late Intake Valve Closing (LIVC). This investigation assesses the potential for the Miller cycle to improve fuel economy at part load points, as well as high load points with significantly elevated boost pressures (Deep Miller) of up to 4 bar abs. The impact of geometric Compression Ratio (CR) and Exhaust Back Pressure (EBP) has also been investigated. The knock mitigating qualities of Deep Miller have been assessed, and its ability to increase maximum engine load explored. Low Speed Pre-ignition (LSPI) and autoignition tendencies with reduced coolant flow rates and with aged and new fuels have also been studied.

This study comprises both experimental and analytical studies. A Ricardo Hydra single cylinder thermodynamic engine was developed and used for the experimental component of the study. This engine features a high specific power output (120kW/l) cylinder head from the Mahle 1.2l 3 cylinder aggressively downsized engine. The analytical component was carried out using a 1-dimensional GT-Power model based on the Ricardo Hydra experimental engine. A Design of Experiments (DoE) based test plan was adopted for this analytical study.

The experimental study found that EIVC was the optimal strategy for improving fuel economy at both part-load and high-load conditions. LIVC yielded a fuel economy penalty at part-load operations and a fuel economy improvement at high-loads. The unexpected part-load LIVC result was attributed to the engine breathing dynamics of the experimental engine. The analytical study found moderate LIVC to be the optimal strategy at lower speeds, unless compensation for the increased degree of scavenging experienced with EIVC was compensated for, in which case EIVC was optimum. At higher speeds EIVC was found to be optimum regardless of whether or not compensation for scavenging was employed. It was generally found that less sensitivity to EBP was exhibited the more extreme the EIVC and LIVC. It was also found that a higher geometric CR could be tolerated with extreme EIVC and LIVC, and a fuel economy benefit could be obtained through the elevation of Geometric CR.

Acknowledgements

I would firstly like to express my thanks and utmost respect to my supervisor Professor Hua Zhao for offering me this PhD opportunity in his world renowned Centre for Advanced Powertrain and Fuels Research, and for his guidance and support over the last 4 years.

I would also like to express my thanks to Neil Fraser and Paul Freeland of Mahle Powertrain for giving me this opportunity, and for their patience. Without their support and assistance, and their donation of numerous engine components and instrumentation, this project could not have happened.

I also owe a great deal of thanks to other staff at Brunel University and Mahle Powertrain who have given me guidance, advice and support on many occasions including Alan Todd, Andrew Jaimeson, Carol Jackson, Dave Hancock, Dave OudeNijeweme, Greg Taylor, Ian Reynolds, James Taylor, Phil Toon, Rob Beevers, Cheryl Cramer, Chris Alan, Clive Barrett, John Langdon, Michael Low, Ray Kirby and Reza Herfatmanesh. I would like to extend special thanks to Jens Neumeister, Justin Mape, Tony Cains, Al Cairns and Yan Zhang for going out of their way to help me out and assist me on a number occasions.

I also wish to express my gratitude to the engine lab technicians Andy Selway and Ken Anstiss, with thanks in particular to Andy who has helped me out so greatly over the last 4 years.

Finally I would like to thank my family and friends without whom I simply could not have coped for the first 2 and a half years whilst the test cell was being constructed, and during the various occasions the engine was not working and no results could be obtained. I owe you all so much.

Abbreviations, Symbols and Chemical Symbols

General Abbreviations

ABDC	After Bottom Dead Centre
AC	Alternating Current
AFR	Air Fuel Ratio
ATDC	After Top Dead Centre
BBDC	Before Bottom Dead Centre
BDC	Bottom Dead Centre
BEV	Battery Electric Vehicle
BLD	Borderline Detonation
BMEP	Brake Mean Effective Pressure
BSFC	Brake Specific Fuel Consumption
BTDC	Before Top Dead Centre
BTDCF	Before Top Dead Centre Firing
CA	Crank Angle
CAAA	Clean Air Act Amendments
CAD	Crank Angle Degrees
CAFE	Corporate Average Fuel Economy
CAI	Controlled Autoignition
CARB	Californian Air Resources Board
CAT	Charge Air Temperature
CFD	Computational Fluid Dynamics
CGI	Compacted Graphite Iron
CI	Compression Ignition
COST	Changing One Separate factor at a Time
COV	Coefficient Of Variation
CR	Compression Ratio
DC	Direct Current

DI	Direct Injection
DOC	Diesel Oxidation Catalyst
DoE	Design of Experiment
DPF	Diesel Particulate Filter
eBoost	Electric Boosting
ECU	Electronic Control Unit
EE	Extended Expansion
EGR	Exhaust Gas Recirculation
EGT	Exhaust Gas Temperature
EIVC	Early Intake Valve Closing
EMOP	Exhaust Maximum Opening Point
EMS	Engine Management System
EOC	End Of Compression
EOR	End Of Ramp
EPA	Environmental Protection Agency
E-REV	Extended-Range Electric Vehicle
EU	European Union
EVC	Exhaust Valve Closing
FCEV	Fuel Cell Electric Vehicle
FID	Flame Ionization Detector
GDI	Gasoline Direct Injection
GE	General Electric
GIMEP	Gross indicated Mean Effective Pressure
GVW	Gross Vehicle Weight
HC	Hydrocarbons
HCCI	Homogeneous Charge Compression Ignition
HEV	Hybrid Electric Vehicle
ICE	Internal Combustion Engine
IMEP	Indicated Mean Effective Pressure
IMOP	Intake Maximum Opening Point
IMPR	Intake Manifold Pressure Referencing

ISFC	Indicated Specific Fuel Consumption
IVC	Intake Valve Closing
IVO	Intake Valve Opening
KI	Knock Intensity
LBDI	Lean Boost Direct Injection
LEV	Low Emission Vehicle
LF	Low-pass Filter
LHR	Low Heat Rejection
LIVC	Late Intake Valve Closing
LIVO	Late Intake Valve Open
LNT	Lean NOx Trap
LSPI	Low Speed Pre-ignition
LUSIE	Leeds University Spark Ignition Engine
MAF	Mass Air Flow
MAP	Manifold Absolute Pressure
MBT	Minimum spark advance for Best Torque
MFB	Mass Fraction burn
NA	Naturally Aspirated
NEDC	New European Driving Cycle
NI	National Instruments
NIMEP	Net Indicated Mean Effective Pressure
NLT	New Long Term
NMHC	Non-methane Hydrocarbons
NMOG	Non-methane Organic Gasses
NOx	Nitrogen Oxides
NST	New Short Term
NVH	Noise, Vibration and Harshness
PC	Passenger Car
PFI	Port Fuel Injection
PID	Proportional Integral Derivative
PIPR	Polytropic Index Pressure Referencing

PM	Particulate Matter
PMEP	Pumping Mean Effective Pressure
PN	Particulate Number
PNLT	Post New Long Term
PRT	Platinum Resistance Thermometer
RBF	Radial Base Function
RM	Reference Mass
RON	Research Octane Number
rpm	revolutions per minute
SCR	Selective Catalytic Reduction
SI	Spark Ignition
SOI	Start Of Injection
SULEV	Super Ultra Low Emission Vehicle
TC	Time Constant
TDC	Top Dead Centre
TKE	Turbulent Kinetic Energy
UEGO	Universal Exhaust Gas Oxygen
UGMF	Unburned Gas Mass Fraction
ULEV	Ultra Low Emission Vehicle
ULG	Unleaded Gasoline
US	United States
VVA	Variable Valve Actuation
VVT	Variable Valve Timing
WOT	Wide Open Throttle
ZEV	Zero Emissions Vehicle

Symbols

a	Wiebe model constant
A	Knock index multiplier, Activation energy multiplier, Flow area

A_s	Heat transfer surface area
b	Bore
C_f	Skin friction coefficient
C_p	Specific heat capacity at constant pressure, Pressure loss coefficient
CL	Connecting rod length
D	Equivalent diameter
e	Total internal energy per unit mass
h	Heat transfer coefficient
H	Total enthalpy
$ISem$	Indicated specific emission
K_m	Percentage cylinder unburned at knock initiation
m	Wiebe model constant, mass
\dot{m}	Boundary mass flux into the volume
M	Molecular weight
n	Polytropic exponent/specific heat ratio
ON	Octane number
p	In-cylinder pressure, pressure
p_f	Pressure feedback
p_n	Predicted pressure
Δp	Change in pressure
Δp_c	Change in pressure due to combustion
Δp_v	Change in pressure due to volume change
P	Precursor reaction rate multiplier
Q	Heat input
r_v	Geometric compression ratio
R	Specific gas constant
s	Stroke

t	Time
$thkn$	Start of compression angle
T	Livengood-Wu integral, Temperature
T_a	Activation temperature
T_{fluid}	Fluid temperature
T_u	Instantaneous unburned gas temperature
T_{wall}	Wall temperature
ΔT	Temperature difference
u	Velocity at the boundary
V	Volume
VC	Volumetric concentration
V_I	Cylinder volume at knock initiation
V_{TDC}	Volume at TDC
x	MFB, Crank-pin offset
x_b	Mass fraction burned
ρ	Density
θ	Crank angle
θ_0	Crank angle at combustion start
θ_b	Combustion duration
η	Thermodynamic efficiency
η_{Otto}	Otto cycle efficiency
φ	Equivalence ratio
τ	Douaud and Eyzat component

Chemical symbols

CHO	Carbohydrate
CO	Carbon Monoxide

CO ₂	Carbon dioxide
H	Hydrogen atom
H ₂ SO ₄	Sulphuric acid
HCHO	Formaldehyde
N	Nitrogen atom
N ₂	Nitrogen
NO	Nitric oxide
NO ₂	Nitrogen dioxide
O	Oxygen atom
O ₂	Oxygen
O ₃	Ozone
OH	Hydroxyl radical
SO ₂	Sulphur dioxide
SO ₃	Sulphur trioxide

Contents

	Page
Abstract	
Acknowledgements	
Abbreviations, Symbols and Chemical Symbols	
Chapter 1: Introduction	1
1.1 Introduction	1
1.2 Objectives	5
1.3 Outline of Thesis	5
Chapter 2: Literature Review	8
2.1 Introduction	8
2.2 Gasoline Engine Emissions	10
2.2.1 Current Worldwide Emission Legislation	10
2.2.1.1 Carbon Monoxide (CO)	16
2.2.1.2 Unburned Hydrocarbons (HC)	17
2.2.1.3 Nitrogen Oxides (NO _x)	18
2.2.1.4 Particulate Matter (PM)	19
2.3 Current Automotive Engines, Technologies and Trends	19
2.3.1 Hybrid and Electric Powertrains	20
2.3.2 Fossil Fuel Powertrains	21
2.3.3 Gasoline Engine Developments	22
2.3.4 Downsizing and Turbocharging	25
2.4 Atkinson/Miller Cycle	28
2.4.1 Introduction	28

2.4.2 History	29
2.4.3 Pumping Losses	33
2.4.4 Combustion Stability	36
2.4.5 Engine Breathing	39
2.4.6 Emissions	40
2.4.7 Knock Mitigation and Deep Miller	43
2.5 Summary	44
Chapter 3: Experimental Test Facility	46
3.1 Introduction	46
3.2 Experimental Setup	46
3.2.1 Engine Description	47
3.2.1.1 Single Cylinder Engine Description	49
3.2.1.2 Cylinder Block Design	51
3.2.2 Oil System	53
3.2.3 Coolant System	55
3.2.4 Fuel System	59
3.2.5 Intake System	62
3.2.5.1 Pipes	62
3.2.5.2 System Details	63
3.2.6 Exhaust System	67
3.2.6.1 Design	67
3.2.6.2 System Details	67
3.2.6.3 Conversion of Emissions to Specific Emissions	69
3.2.7 Dynamometer and EMS	70
3.3 Data Acquisition and Instrumentation	75

3.3.1 Data Acquisition Software	77
3.3.2 Calibration of Sensors	82
3.3.3 Accuracy of Data and Known Measurement Errors	84
3.4 Daily Test Point	86
Chapter 4: Development of a Single Cylinder Engine GT-Power Model	87
4.1 Introduction	87
4.2 Development of the Single Cylinder Engine Model	88
4.2.1 Single Cylinder Engine Model Details	89
4.2.1.1 Flow Modelling	89
4.2.1.2 Combustion Modelling	91
4.2.1.3 Modelling Limitations	92
4.2.1.4 Other Modelling Parameters	93
4.3 Single Cylinder Engine Model 1: DoE Based Test Plan	93
4.3.1 Single Cylinder Engine Knock Model	96
4.3.1.1 Functionality of the Knock Model	96
4.3.1.2 Irresolvable Issues with the Knock Model	101
4.4 Single Cylinder Engine Model 2: Correlation of Thermodynamic Data	103
4.5 Mahle Powertrain 3 Cylinder Engine Model	104
Chapter 5: Application of the Deep Miller Cycle to Improve Fuel Economy and Increase Maximum Load	106
5.1 Introduction	106
5.2 Development of a DoE Based Test Plan	107
5.2.1 Introduction	107
5.2.2 Screening	107

5.2.3 DoE Type	110
5.2.4 Limitations of the DoE	111
5.2.5 Test Point Description	114
5.2.5.1 1000rpm, 14 bar BMEP	116
5.2.5.2 2000rpm, 24 bar BMEP	117
5.2.5.3 5000rpm, 24 bar BMEP	117
5.3 ISFC optimisation	118
5.3.1 Introduction	118
5.3.2 ISFC Trends	119
5.3.2.1 1000rpm, 14 bar BMEP	119
5.3.2.1.1 EBP Effects	119
5.3.2.1.2 Geometric CR Effects	123
5.3.2.2 2000rpm, 24 bar BMEP	128
5.3.2.2.1 EBP Effects	128
5.3.2.2.2 Geometric CR Effects	134
5.3.2.3 5000rpm, 24 bar BMEP	137
5.3.2.3.1 EBP Effects	137
5.3.2.3.2 Geometric CR Effects	143
5.3.3 Cam Timing Trends	146
5.3.4 Scavenging Effects	150
5.3.4.1 Scavenging	151
5.3.4.2 Charge Scavenging	159
5.3.5 Engine Breathing	161
5.3.6 General Compression Ratio Effects	169
5.4 Maximum Load Comparison	174
5.5 Summary	177

Chapter 6: Single Cylinder Engine Performance Evaluation	179
6.1 Introduction	179
6.2 Comparison of the Single Cylinder Engine to the 3 Cylinder Engine	179
6.2.1 Introduction	180
6.2.2 Description of Test Points	180
6.2.3 Results	182
6.2.3.1 ISFC	182
6.2.3.2 Engine Breathing	184
6.2.3.3 Knocking Tendency	192
6.2.3.4 Correct EBP Determination	195
6.3 Impact of Coolant Flow Rate on Autoignition Tendency	198
6.3.1 Introduction	198
6.3.2 The Effect of Coolant Temperature Gradient	199
6.3.2.1 Results	202
6.3.3 Effect of Coolant Flow Rate at Higher Load Operations	210
6.3.3.1 Results	211
6.4 Impact of Cam Timing on Autoignition Tendency	213
6.4.1 Introduction	213
6.4.2 Test Plan	213
6.4.3 Results	214
6.4.4 GT-Power Analysis	223
6.4.4.1 Introduction	223
6.4.4.2 Results	224
6.5 Effects of Fuel Age	228
6.5.1 Introduction	228

6.5.2 Test Plan	229
6.5.3 Results	229
Chapter 7: Experimental Studies of Miller Cycle on Engine Performance and Fuel Consumption	232
7.1 Introduction	232
7.2 Achieving EIVC and LIVC	233
7.3 Description of Test Points	234
7.4 Low Load Operations with EIVC and LIVC (Region 1)	237
7.4.1 Introduction	237
7.4.2 Results	238
7.4.2.1 Discrepancy at 1000rpm	244
7.4.2.2 Emissions	248
7.4.2.3 Analysis of the Individual Components of EIVC and LIVC	253
7.4.2.4 Optimum Cam Timing Observations	260
7.4.2.5 Combustion Phasing Observations	261
7.4.3 Summary	264
7.5 High Load Operations with EIVC and LIVC (Deep Miller)	265
7.5.1 Introduction	265
7.5.2 Results	266
7.5.2.1 EBP Effects	273
7.5.2.2 Analysis of the Individual Components of EIVC and LIVC	274
7.5.2.3 Turbocharging/Supercharging Feasibility for Deep Miller	280
7.5.3 Summary	282
Chapter 8: Summary and Conclusions	284

8.1 Introduction	284
8.2 Analytical Study of Deep Miller	285
8.3 Experimental Engine Study of Miller Cycle	287
8.4 Recommendations for Future Work	289
References	290
Appendix	300

List of Figures

Figure 3.1 The Mahle 1.2l 3 Cylinder Advanced Downsizing Engine	47
Figure 3.2 The Mahle Downsized Demonstrator Vehicle	48
Figure 3.3 The Brunel Single Cylinder Downsized Engine	49
Figure 3.4 Cylinder Block Plumbing	51
Figure 3.5 Ansys Plot of Factor of Safety	52
Figure 3.6 Oil System Schematic Diagram	54
Figure 3.7 Coolant Jacket Height Relative to Coolant Tank Height	56
Figure 3.8 Coolant System Schematic Diagram	58
Figure 3.9 Fuel System Schematic Diagram	61
Figure 3.10 Intake System Schematic Diagram	66
Figure 3.11 Exhaust System Schematic Diagram	69
Figure 3.12 Dynamometer Torque Curve and Engine Torque Curve Comparison	71
Figure 3.13 Dynamometer Schematic Diagram	72
Figure 3.14 ECU Loom Connection List	73
Figure 3.15 Transient Combustion Analyzer Data Acquisition Software Interface	77
Figure 3.16 Graph Window Layout	78
Figure 3.17 Band-pass Filtering Calculation	79
Figure 3.18 Accuracy of Fuel Rail Pressure Control at 3000rpm and 4 bar BMEP	85
Figure 4.1 Staggered Grid Arrangement	90
Figure 4.2 Single Cylinder Engine Model 1	94
Figure 4.3 TDC Determination with a <i>Hold Object</i>	99

Figure 4.4 Livengood-Wu Integral Accuracy at 1 CAD Resolution	100
Figure 4.5 Mahle Powertrain 3 Cylinder Engine Model	105
Figure 5.1 Latin Hypercube (left) and D-Optimum (right) Quadratic Point Distribution Comparison	110
Figure 5.2 Latin Hypercube (left) and D-Optimum (right) Quadratic Curve Fitting Comparison with Lips Circled	111
Figure 5.3 Comparison of GT-Power Calculated Intake Cam Profiles for 152, 196, 240, 276 and 312 CAD Durations Cams	113
Figure 5.4 Impact of EBP on ISFC at a Geometric CR of 9	120
Figure 5.5 Comparison of Effective CR and ISFC for Each EBP at a Geometric CR of 9	123
Figure 5.6 Comparison of Different Geometric CRs with an EBP of 1.5 bar	125
Figure 5.7 Comparison of Different Geometric CRs with an EBP of 2 bar	125
Figure 5.8 Comparison of Different Geometric CRs with an EBP of 2.5 bar	126
Figure 5.9 Impact of EBP on ISFC at a Geometric CR of 9	128
Figure 5.10 Optimum ISFC Cam IMOPs for an EBP of 2 bar at a Geometric CR of 9	129
Figure 5.11 Optimum ISFC cam IMOPs for an EBP of 3 bar at a Geometric CR of 9	129
Figure 5.12 Optimum ISFC cam IMOPs for an EBP of 4 bar at a Geometric CR of 9	130
Figure 5.13 Optimum IVO Cam Timing Points for EBPs of 2 and 3 bar Compared to the IVO Limit for a Geometric CR of 9	131
Figure 5.14 Log P-V IVC Sweep for 196 CAD Duration Intake Cam at a Geometric CR of 9 and an EBP of 2 bar	132
Figure 5.15 Log Temperature Vs. Volume Ratio IVC Sweep for 196 CAD Duration Intake Cam at a Geometric CR of 9 and an EBP of 2 bar	133
Figure 5.16 Comparison of Different Geometric CRs with an EBP of 2 bar	135

Figure 5.17 Comparison of Different Geometric CRs with an EBP of 3 bar	135
Figure 5.18 Comparison of Different Geometric CRs with an EBP of 4 bar	136
Figure 5.19 Comparison of 2, 3 and 4 bar EBPs at a Geometric CR of 9	138
Figure 5.20 Effective CR and Lambda Plots at a Geometric CR of 9, EBP of 2 bar and a Cam Duration of 276 CAD	141
Figure 5.21 Comparison of Different Geometric CRs with an EBP of 2 bar	143
Figure 5.22 Comparison of Different Geometric CRs with an EBP of 3 bar	144
Figure 5.23 Comparison of Different Geometric CRs with an EBP of 4 bar	144
Figure 5.24 The Theoretical Gain in Thermodynamic Efficiency Through the Adoption of Optimum Cam Positioning	147
Figure 5.25 Number of Points where a Theoretically Non-optimal Cam Timing was found to be Optimal in the Test Work	148
Figure 5.26 Maximum Benefit over Baseline Case (IVC at BDC) with each Cam at each Geometric CR	149
Figure 5.27 Demonstration of Optimum Cam Timings for EIVC and LIVC	151
Figure 5.28 3 Cylinder Engine Speed and Load Map Showing where Exhaust Lambda Enrichment and Leaning is Used	152
Figure 5.29 Scavenging Compensation (%) for each of the Different Cams at each EBP and CR for 1000rpm and 14 bar BMEP	153
Figure 5.30 Scavenging Compensation (%) for each of the Different Cams at each EBP and CR for 2000rpm and 24 bar BMEP	154
Figure 5.31 Scavenging Compensation (%) for each of the Different Cams at each EBP and CR for 5000rpm and 24 bar BMEP	155
Figure 5.32 Comparison of In-cylinder Lambdas for the 152 CAD Duration Cam at 2 bar EBP and a Geometric CR of 9 for all Speeds	156

Figure 5.33 1000rpm, 14 bar BMEP, EBP of 1.5 bar, Geometric CR of 9. With and without Scavenge Compensation	157
Figure 5.34 2000rpm, 24 bar BMEP, EBP of 2 bar, Geometric CR of 9. With and without Scavenge Compensation	157
Figure 5.35 5000rpm, 24 bar BMEP, EBP of 2 bar, Geometric CR of 9. With and without Scavenge Compensation	158
Figure 5.36 Estimated Charge Scavenging at 1000rpm and 14 bar BMEP for 1.5, 2 and 2.5 bar EBP	160
Figure 5.37 Charge Scavenging at 2000rpm and 24 bar BMEP with an EBP of 2 bar and a Geometric CR of 9, 10.75 and 12.5	161
Figure 5.38 EBP Resolved on a CAD Basis for an EBP of 2 bar, a Cam Duration of 152 CAD for Speeds of 1000, 2000 and 5000rpm	162
Figure 5.39 Log P-V Overlay at an EBP of 2 bar, a Cam Duration of 152 CAD, and for Speeds of 1000, 2000 and 5000rpm	163
Figure 5.40 Intake Mass Flow Rate Overlay for 240 CAD Cam Duration at an EBP of 2.5 bar, and a Speed and Load of 1000rpm and 14 bar BMEP	164
Figure 5.41 2000rpm, 24 bar BMEP, 196 CAD Duration Cam, EBP 4 bar, Geometric CR of 9. Intake Valve Mass Flow Rate Profiles from an IMOP Sweep	165
Figure 5.42 2000rpm, 24 bar BMEP, 196 CAD Duration Cam, EBP 4 bar, Geometric CR of 9. MAP Requirements for an IMOP Sweep	166
Figure 5.43 Influence of Exhaust Gas Temperature (EGT) on Exhaust Pressure/Rarefaction Wave at 5000rpm, 24 bar, 2 bar EBP and a Geometric CR of 9	167
Figure 5.44 Comparison of Single Cylinder and 3 Cylinder EBP Profiles Resolved on CAD Basis at 5000rpm and 24 bar BMEP	169
Figure 5.45 Log P-V Diagram at 2000rpm, 24 bar BMEP, 312 CAD Duration Cam, EBP of 2 bar. Comparison of Different Geometric CRs	170

Figure 5.46 1000rpm, 14 bar BMEP 50% MFB Points for EBPs of 1.5, 2 and 2.5 bar at Geometric CRs of 9, 10.75 and 12.5	171
Figure 5.47 2000rpm, 24 bar BMEP 50% MFB Points for EBPs of 2, 3 and 4 bar at Geometric CRs of 9, 10.75 and 12.5	172
Figure 5.48 5000rpm, 24 bar BMEP 50% MFB Points for EBPs of 2, 3 and 4 bar at Geometric CRs of 9, 10.75 and 12.5	172
Figure 5.49 Peak Load (NIMEP) at 1000, 2000 and 5000rpm for each Cam Profile for an EBP of 2 bar	175
Figure 5.50 Peak Load (NIMEP) at 1000, 2000 and 5000rpm for each Cam Profile for an EBP of 3 bar at 2000 and 5000 rpm, and an EBP of 2.5 bar at 1000rpm	175
Figure 6.1 Baseline Data Test Points	181
Figure 6.2 ISFC Comparison of 3 Cylinder and Single Cylinder Engines	183
Figure 6.3 Single Cylinder and 3 Cylinder Spark Timing Comparison	185
Figure 6.4 Single Cylinder and 3 Cylinder 50% MFB Point Comparison	186
Figure 6.5 Single Cylinder and 3 Cylinder 10-90% MFB Duration Comparison	186
Figure 6.6 Single Cylinder and 3 Cylinder MAP Requirement Comparison	187
Figure 6.7 Single Cylinder and 3 Cylinder EBP Comparison	187
Figure 6.8 Comparison of Intake Manifold Pressures and Intake Valve Mass Flow Rate at 5000rpm and 24 bar BMEP	189
Figure 6.9 5000rpm 24bar BMEP logP-V Comparison	190
Figure 6.10 2000rpm, 15 bar BMEP Single Cylinder and 3 Cylinder Simulation In-cylinder Pressure Comparison	193
Figure 6.11 2000rpm, 15 bar BMEP Single Cylinder and 3 Cylinder Simulation EBP Comparison	193
Figure 6.12 3000rpm, 15 bar BMEP Single Cylinder and 3 Cylinder Simulation In-cylinder Pressure Comparison	194
Figure 6.13 3000rpm, 15 bar BMEP Single Cylinder and 3 Cylinder Simulation EBP Comparison	195

Figure 6.14 2000rpm EBP Comparison at Various Loads with the EBP Valve Applied	197
Figure 6.15 2000rpm, Various Loads Single Cylinder EBP Overlay Vs. Valve Overlap Period	198
Figure 6.16 Severe Autoignition Frequency	202
Figure 6.17 Peak Autoignition Cylinder Pressure Vs. Total Engine Coolant Flow Rate	203
Figure 6.18 Peak Autoignition Cylinder Pressure Vs. Block Coolant Flow Rate	203
Figure 6.19 Head Coolant Delta T (deg C)	205
Figure 6.20 Block Coolant Delta T (deg C)	205
Figure 6.21 Head Coolant Flow Rate (l/min)	207
Figure 6.22 Block Coolant Flow Rate (l/min)	208
Figure 6.23 Cylinder Head Coolant Jacket Geometry	208
Figure 6.24 Average Band-pass Filtered KI (bar)	209
Figure 6.25 BLD 50% MFB (CAD ATDCF)	210
Figure 6.26 Autoignition Frequency in Percentage of Autoignition Cycles at Different Coolant Flow Points	212
Figure 6.27 Peak Autoignition Cylinder Pressure	215
Figure 6.28 Frequency of Autoignition Events at Specific Cam Timings	215
Figure 6.29 Ridge 1 and Ridge 2 Definitions	216
Figure 6.30 Comparison of 2 Superknock Events, 1 Occurring Under Ridge 1, the Other Under Ridge 2	217
Figure 6.31 Comparison of Pressure Histories for 2 Superknock Events, 1 Occurring Under Ridge 1, the Other Under Ridge 2	218
Figure 6.32 Polytropic Exponents	219
Figure 6.33 50% MFB Angle (CAD ATDCF)	220
Figure 6.34 EMOP Sweep at Constant Load and IMOP Demonstrating the Impact of EMOP Timing on GIMEP	220

Figure 6.35 Autoignitions Under Ridge 1 (Units of IMOP and EMOP are CAD ATDC and CAD BTDC Respectively)	221
Figure 6.36 Autoignitions Under Ridge 2 (Units of IMOP and EMOP are CAD ATDC and CAD BTDC Respectively)	222
Figure 6.37 Exhaust Port Temperatures ($^{\circ}\text{C}$)	223
Figure 6.38 Experimental (left) and Simulated (right) ISFC Comparison	225
Figure 6.39 Equivalent AFR at Cycle Start	226
Figure 6.40 Residual Gas Concentration at Cycle Start	226
Figure 6.41 EOC Pressure (bar)	227
Figure 6.42 EOC Temperature ($^{\circ}\text{C}$)	227
Figure 6.43 Autoignitions with Aged ULG95	230
Figure 6.44 Autoignitions with Fresh ULG95	230
Figure 7.1 Cam Profile Comparison (as Shown in Their Maximum Valve Overlap Positions)	233
Figure 7.2 Cam Phasing Ranges	234
Figure 7.3 Regions of Miller Cycle Studied	235
Figure 7.4 ISFC Comparison of Short, Standard and Long Cams at Low Loads	238
Figure 7.5 1000rpm, 8 bar BMEP Short, Standard and Long Cam Overlay	240
Figure 7.6 PMEP Comparison of Short, Standard and Long Cams at Low Loads	241
Figure 7.7 4000rpm, 4 bar BMEP Short, Standard and Long Cam Overlay	242
Figure 7.8 Intake Temperature Comparison of Short, Standard and Long Cams at Low Loads	244
Figure 7.9 Comparison of the Intake Valve Mass Flow Rates for the 3 Different Duration Cams at 1000rpm and 4 bar BMEP	245
Figure 7.10 MFB Profiles for the 3 Different Cams at 1000rpm and 4 bar BMEP	246
Figure 7.11 Comparison of COV for 1000rpm and 4 bar BMEP for Short (left), Standard (middle) and Long (right) Cams	247

Figure 7.12 HC Emissions Comparison of Short, Standard and Long Cams at Low Loads	249
Figure 7.13 NO _x Emissions Comparison of Short, Standard and Long Cams at Low Loads	250
Figure 7.14 HC and NO _x Emissions as Obtained from Test Work Carried out by Mahle Powertrain	251
Figure 7.15 MAP Comparison of Short, Standard and Long Cams at Low Loads	252
Figure 7.16 Theoretical Temperatures at Various Points in the 4-Stroke Atkinson and Otto Cycles	254
Figure 7.17 Comparison of 2-Stroke (left) and 4-Stroke (right) Theoretical Atkinson Cycles	255
Figure 7.18 Theoretical Benefit with EIVC at 3000rpm and 4 bar BMEP	256
Figure 7.19 Actual Benefit with EIVC at 3000rpm and 4 bar BMEP	256
Figure 7.20 Theoretical Benefit with LIVC at 3000rpm and 4 bar BMEP	258
Figure 7.21 Actual Benefit with LIVC at 3000rpm and 4 bar BMEP	259
Figure 7.22 Map of 10-90% MFB Rates for an IMOP-EMOP Sweep with the Short Cam at 3000rpm and 4 bar BMEP	261
Figure 7.23 MBT Comparison of Short, Standard and Long Cams at Low Loads	262
Figure 7.24 Spark Timing Comparison of Short, Standard and Long Cams at Low Loads	263
Figure 7.25 Optimum IMOP Timing Comparison of Short, Standard and Long Cams at Low Loads	264
Figure 7.26 2000rpm, 24 bar BMEP ISFC Comparison for Short, Standard and Long Cams at 2 EBPs	266
Figure 7.27 HC Emissions for Different IVC Timings and 2 Different EBPs with the Short Cam at 2000rpm and 24 bar BMEP with an EMOP of 100 CAD BTDC (Maximum Valve Overlap Position)	267
Figure 7.28 COV for Short, Standard and Long Cams at 2000rpm, High Load with and without EBP	269
Figure 7.29 10-90% MFB Duration for Short, Standard and Long Cams at 2000rpm, High Load with and without EBP	270

Figure 7.30 50% MFB Angle for Short, Standard and Long Cams at 2000rpm, High Load with and without EBP	271
Figure 7.31 Spark Timing for Short, Standard and Long Cams at 2000rpm, High Load with and without EBP	272
Figure 7.32 2000rpm, 15 bar BMEP ISFC Comparison for Short, Standard and Long Cams at 2 EBPs	272
Figure 7.33 EBP Profile Comparison between Short, Standard and Long Cams with 2 bar Average EBP at 2000rpm and 24 bar BMEP	274
Figure 7.34 Theoretical Benefit with EIVC at 2000rpm and 24 bar BMEP with no EBP	275
Figure 7.35 Theoretical Benefit with EIVC at 2000rpm and 24 bar BMEP with an EBP of 2 bar	276
Figure 7.36 Actual Benefit with EIVC at 2000rpm and 24 bar BMEP with no EBP	277
Figure 7.37 Actual Benefit with EIVC at 2000rpm and 24 bar BMEP and 2 bar EBP	277
Figure 7.38 Theoretical Benefit with LIVC at 2000rpm and 24 bar BMEP with an EBP of 2 bar	278
Figure 7.39 Actual Benefit with LIVC at 2000rpm and 24 bar BMEP with no EBP	279
Figure 7.40 Actual Benefit with LIVC at 2000rpm and 24 bar BMEP with an EBP of 2 bar	279
Figure 7.41 MAP Requirement Vs. BMEP for Short, Standard and Long Cams at an Engine Speed of 2000rpm	281

List of Tables

Table 2.1 Euro Standards Implementation Map	12
Table 2.2 Vehicle Categories Applicable to Euro Standards	12
Table 2.3 Current Worldwide Emissions Standards	15
Table 3.1 Daily Test Point Test Variables and Control Criteria	86
Table 4.1 Description of the Various Crank Angle Sensors in the Knock Model	98
Table 4.2 MAP Correction Factors	102
Table 4.3 EBP Correction Factors	102
Table 4.4 Geometric CR Correction Factors	102
Table 4.5 IMOP Correction Factors	102
Table 4.6 MAP and IMOP 3 Cylinder Map of BLD 50% MFB Points at a Speed and Load of 5000rpm and 24 bar BMEP Respectively	103
Table 5.1 DoE Ranges, Levels and Resolution (1000rpm)	109
Table 5.2 Intake Valve IMOP Ranges for Different Duration Cams	109
Table 5.3 SOI Timings for Each of the Speed and Load Points	116
Table 5.4 1000rpm, 14 bar BMEP, Geometric CR of 9, EBP of 1.5 bar. With and without Scavenge Compensation Effects on ISFC for an IMOP Sweep with the 152 CAD Duration Cam	158

Table 6.1 Baseline Data Test Points	181
Table 6.2 Test Variables and Control Criteria	182
Table 6.3 Table of Average EBP during the Exhaust Valve Open Phase	196
Table 6.4 Test Plan Showing Desired ΔT s and the Corresponding Flow Rate Required to Achieve that ΔT	201
Table 6.5 Test Variables and Control Criteria	201
Table 6.6 Test Plan Showing Desired ΔT s and the Corresponding Flow Rate Required to Achieve that ΔT	211
Table 6.7 Test Variables and Control Criteria	214
Table 6.8 Test Variables and Control Criteria	229
Table 7.1 Test Points for De-throttling Studies (BMEPs are the 3 Cylinder Equivalent Values)	236
Table 7.2 Test Points for Region 2 (BMEPs are the 3 Cylinder Equivalent Values)	236
Table 7.3 Test Variables and Control Criteria	237
Table 7.4 MOPs and Corresponding Valve Opening/Closing Points for Each of the Cams	237

Chapter 1

Introduction

1.1 Introduction

The advent of the Internal Combustion Engine (ICE) represents a huge milestone in human progress, and has dramatically changed the world we live in today. ICEs were made possible by an engineer called Nikolaus Otto who gave his name to the famous Otto cycle process that allows energy and mechanical power to be extracted from the combustion of air and fuel, more often than not by means of the reciprocating motion of a piston in a cylinder.

ICEs represented a great leap forward in terms of power creation, providing a smaller, neater, and much more diverse solution to the steam engine. ICEs are now used extensively in a wide variety of applications. The ICE is now the most common form of prime mover in the world today, and is regarded as a key enabler of globalisation (Smil [1]).

Since a very early stage efforts were made to refine and optimise the ICE. Oil reserves initially represented the greatest incentive to optimise the ICE and the greatest hindrance to their widespread adoption. As better techniques were developed to extract oil so the ICE gained popularity.

The main focus of early research and development was on improvement of fuel economy and increasing power. The main motivation for this was for aircraft

applications which were responsible for technologies such as supercharging, turbocharging and Direct Injection (DI) (Zhao [2]). These technologies are being reincarnated today to improve fuel economy and increase power output.

After World War II emissions also became the focus of ICE research and development. In the UK this was prompted by a new act of parliament called the "Clean Air Act 1956" [3] which was introduced to combat increasing levels of air pollution and photochemical smog.

In more recent history as the popularity of ICEs and the automotive sector have increased drastically due to emerging global markets such as China and India, the demand for fossil fuels has also increased massively, to the extent that relatively minor conflicts in the world can see the price of fuel fluctuate considerably. This coupled with growing concerns over the impact of carbon dioxide (CO₂) on the environment and the introduction of a new fining system for cars that produce more than a certain quantity of CO₂ has prompted a new flurry of research into cleaner and more fuel efficient ICEs.

Manufacturers facing the proposition of having to "pay" to be in-efficient and polluting are now resorting to technologies that hitherto have been too expensive or too advanced to justify, such as Gasoline Direct Injection (GDI), turbocharging for gasoline engines, 2-stage turbocharging, Electrical Boosting (eBoost) systems, fully Variable Valve Trains (VVT), Selective Catalytic Reduction (SCR) systems, and many more technologies besides.

These new technologies allow far greater freedom, and real time variation of engine parameters that would historically have been fixed, such as valve timing, valve duration, Intake Manifold Absolute Pressure (MAP), fuel injection pressure, fuel injection duration, fuel injection timing etc. all of which can be used to improve fuel economy and reduce emissions. This in turn results in different engine concepts.

One such engine concept that has great synergies with the above technologies is engine downsizing. A great deal of work has been invested in the concept of engine downsizing over the last decade and has shown great potential to reduce engine out emissions and CO₂ whilst also providing a significant improvement in fuel economy.

The concept of turbocharging an engine is nothing new, and it has been carried out successfully on many occasions throughout history, but it is important to understand that downsizing is not simply turbocharging an engine. Turbocharging is usually employed on premium “sporty” vehicles in an effort to boost performance rather than to reduce emissions or improve fuel economy. For downsizing the turbocharger is not there for “bolt on” performance, it is integral to the engine and is required to compensate for the reduction in swept cylinder capacity. Turbocharged engines in “sporty” vehicles still have the engine capacity to accelerate adequately at low engine speeds, so the turbocharger performance at low engine speeds is usually not of great importance to driver satisfaction. For a downsized engine though, the turbocharger must be employed to accelerate adequately, and is therefore required to function well at low speed and with very little lag time. What is more it must also function well at every other engine speed and load point without compromising reliability and/or Noise Vibration and Harshness (NVH).

Turbocharged engines are traditionally poor at low engine speeds in comparison to their performance at higher engine speeds for 2 main reasons. Firstly the turbocharger is receiving insufficient energy to compress the intake air and secondly the low engine speed means the compression process takes a long time, and the charge motion in the cylinder is usually quite slow resulting in a comparatively long combustion duration. This makes knocking combustion much more likely. This problem is further exacerbated in downsized engines because the MAP will need to be higher for an equivalent load site in comparison to a larger naturally aspirated engine. This has the effect of increasing the End Of Compression (EOC) pressure and correspondingly temperature thus making knocking combustion even more probable.

A great deal of research effort is being invested in mitigating this problem, including investigating 2 techniques known as Early Intake Valve Closing (EIVC) and Late Intake Valve Closing (LIVC). EIVC refers to the technique of closing the intake valve early of Bottom Dead Centre (BDC) and depressurising the charge in the cylinder slightly, lowering its temperature which results in lower EOC pressures and temperatures. LIVC involves closing the intake valve after BDC thus filling the cylinder completely but expelling some air from the cylinder to the intake. EIVC and LIVC both

operate by reducing the effective Compression Ratio (CR), thus allowing greater scope to increase the geometric CR and improving fuel economy at lower speeds and loads.

Both EIVC and LIVC strategies lower the volumetric efficiency of an engine considerably and will therefore require an elevated MAP relative to running with more “typical” intake cam durations and valve closing points. This can be advantageous at low engine loads due to the reduction of pumping losses, however, at high engine loads and with boost (“Deep Miller”) the success of EIVC and LIVC is heavily dependent on the boosting strategy employed.

In this thesis the viability of EIVC and LIVC and its synergies have been assessed with the following future technologies/techniques:

- Downsizing
- Downspeeding
- Turbocharging
- Supercharging/eboosting
- Increased geometric CR
- Internal Exhaust Gas Recirculation (EGR)

By means of varying the following:

- Intake cam duration
- Intake Maximum Opening Point (IMOP) timing
- Exhaust Maximum Opening Point (EMOP) timing
- MAP
- Exhaust Back Pressure (EBP)
- Geometric CR

Low load and speed EIVC and LIVC have been studied before, however, high/maximum load EIVC and LIVC is still the subject of investigation. It was not until GDI was considered a mainstream technology that EIVC and LIVC operation became feasible.

1.2 Objectives

The objective of this study is to ascertain the benefits of EIVC and LIVC on a downsized engine with the intention of using the de-throttling effect at low engine load to optimise fuel economy, and the over-expansion effect at high load to mitigate knock at high engine loads.

EIVC and LIVC shall be employed by means of cam phasing as well as the employment of different duration intake cam profiles to achieve different effective CRs. Another objective of this test work is to determine the maximum load that can be achieved through the use of EIVC and LIVC to test its synergies with engine downspeeding. The impact of other variables on the successful operation of EIVC and LIVC shall also be assessed, including speed, load, EBP and geometric CR.

A single cylinder GT-Power model was developed during the course of this project in an effort to better understand the differences in engine breathing when EIVC and LIVC are employed. This model will also be used to determine the differences in performance between the single cylinder engine and the 3 cylinder engine.

1.3 Outline of Thesis

Immediately following this brief introduction is a literature review which summarises all of the relevant literature in the field of downsizing and effective CR

reduction through both EIVC and LIVC techniques. The current and future emissions legislation shall also be discussed, as well as the details of the current and future laws regarding CO₂ emissions and other emissions too. An overview of the new technologies that can now justifiably be used on current ICEs will also be discussed.

The third chapter will cover the experimental facility that has been built at Brunel University for this project, as well as detailing all of the instrumentation and sensors that have been installed to the engine. An overview of the data acquisition software used will also be given in this chapter, as well as all of the equations used to calculate various engine operating parameters. This chapter will also detail all of the techniques used to setup and install the engine instrumentation accurately.

Chapter 4 will comprise the development of a one-dimensional single cylinder analytical engine model, as developed in GT-Power [4]. It includes an explanation as to why it was developed, details of the gas dynamic and combustion models used, and also explains how knocking combustion has been predicted and how this was implemented into a closed loop control system of combustion phasing. The techniques used to calibrate this knock model will also be described. It also contains a brief description of the 3 cylinder engine GT-Power model developed by Mahle Powertrain.

Chapter 5 comprises an analytical study of the Miller cycle based on the single cylinder GT-Power model described in chapter 4. It will describe how a Design of Experiments (DoE) based test plan was implemented to simultaneously analyse the impact of several different variables. The results of 2 studies into the use of Deep Miller to optimize fuel economy and the use of Deep Miller to maximize engine load are also presented.

Chapter 6 consists of a performance evaluation of the single cylinder experimental engine. This comprises test plan descriptions and results for studies on the impact of fuel age on knocking characteristics and autoignition tendency, and the impact of coolant flow rate on engine knocking and autoignition tendency. Comparisons between the single cylinder experimental engine and the Mahle 3 cylinder 1.2l downsized engine on which the single cylinder experimental engine is based will also be made in this chapter.

Chapter 7 consists of an experimental investigation into the Miller cycle and its impact on engine performance and fuel consumption. This chapter contains 2 studies, the first on the de-throttling potential of the Miller cycle and the second on the low speed high load knock mitigating properties of Deep Miller. The results of both of these studies will be presented, and their potential to improve fuel economy assessed.

Summary and conclusions from this study are given in chapter 8. Recommendations for future work will also be given in this chapter. Please note that all values of EBP given in this thesis are in absolute pressure.

Chapter 2

Literature Review

2.1. Introduction

Ever increasing fuel prices and climate change have shifted the focus of powertrain development to the reduction of fuel consumption and emissions rather than focusing on outright performance. The transport sector has been found to be a high contributor to global emissions (approximately 21% according to Fuglestvedt, et al [5]) of CO₂ (with road vehicles representing 70% of all transport sector CO₂ emissions in the EU in 2008 [6]), and is also responsible for 55% of the world's oil consumption [7]. Reduction of emissions is also very important given concerns over climate change and an increase in respiratory diseases in humans.

The key transport sector emissions that have been targeted as having the biggest impact on the environment are carbon monoxide (CO), nitrogen oxides (NO_x), unburned hydrocarbons (HC) and particulates (PM). Recent attention has also turned to emissions of CO₂ although there is – at this moment in time - no legislation stipulating maximum permissible quantities of CO₂ for a single vehicle, but, future EU legislation (EC 443/2009 [8]) dictates fleet average emissions of CO₂ for all new cars from 2015 onwards should be no more than 130g/km, and any cars in contravention of this will result in the manufacturer of that car being fined. This limit could be further reduced to 95g/km from 2020 onwards, and an even heavier fining structure imposed for new vehicles in excess of this [9].

Numerous technologies that will reduce emissions and fuel consumption have been investigated and researched with mixed results. Many of the technologies involve optimisation of existing fossil fuel burning powertrains, whereas other systems utilize different sources of energy such as electrical, hydrogen or fuel cell. The current fuel infrastructure favours the optimisation of existing fossil fuel combustion technologies. Hydrogen or fuel cell systems would require a significant fuel infrastructure reconstruction. Extensive research is also being carried out into hybrid powertrain designs. The success of a powertrain design also depends heavily on the additional cost.

Some of these alternative powertrain designs have been developed to the point where mass production is feasible and, crucially, existing fuel infrastructure has not needed to be modified. Hybrid powertrains have been the most successful to date with several vehicles from several big brand names utilising this technology and showing great commercial success. Other powertrain technologies that have proven to be successful are downsizing and boosting, which is another area that has been researched heavily in recent years. Downsizing is also seen as a way of improving fuel consumption and is used in conjunction with boosting. Downsizing reduces frictional losses and also permits higher geometric CRs (greater stroke lengths) to be used.

Downsizing of an engine is the most promising near term means of improving fuel consumption. Downsizing refers to the process of replacing a large Naturally Aspirated (NA) engine with a smaller turbocharged engine of the same, or similar, power output. Downsizing of an engine offers the greatest performance benefit at part load operating points. Part load operating points are shifted to higher, more efficient Brake Mean Effective Pressures (BMEP) in the engine speed load map thus reducing the frictional and pumping losses for the engine. The emissions of downsized engines generally speaking are also reduced, this depends greatly on the fuel injection and exhaust after treatment strategies employed on the vehicle though.

2.2 Gasoline Engine Emissions

2.2.1 Current Worldwide Emission Legislation

There are numerous emission standards enforced around the world (an overview of all of them is given in [10]), the majority of which concern the following pollutants:

- Carbon monoxide (CO)
- Nitrogen oxides (NO_x)
- Unburned hydrocarbons (HCs)
- Particulate matter (PM)
- Particulate number (PN)

At this moment in time there is no legislation on the horizon that dictates maximum permissible quantities of CO₂. This is because CO₂ is not regarded as a pollutant, however, measures are in place to reduce the emissions of CO₂.

There are currently 4 major types of pollutant legislation enforced around the world; European standards (Euro, EC), American standards (EPA, CARB, CAAA), Japanese and Brazilian standards. The applicability of these standards depends on the type of vehicle in question.

European standards:

The current standards applicable to European vehicles are the Euro standards [11]. There are different categories of Euro standards denoted by number (Euro 1/2/3 etc.) with the higher number corresponding to the more rigorous standards. The date of adoption of these mandatory standards is as shown in Table 2.1. The dates of adoption depend on the vehicle type, Gross Vehicle Weight (GVW) and Reference Mass (RM). Vehicle type descriptions are shown in Table 2.2.

American standards:

The US federal standards [12] are currently enforced in America (with the exception of Brazil who have their own standards). There are at present 2 sets of standards denoted tier I and tier II, tier II is what is currently being enforced for light duty road vehicles. The tier II standards can be split up into sub categories denoted bin 1 to bin 8. Different emissions criteria apply to each bin, the lower the bin number the more stringent the criteria, hence, the cleaner the vehicle. Newly registered cars can fall into any 1 of the 8 bins as long as the vehicle manufacturer still meets a fleet average of bin 5.

A tier III [13] has also been introduced recently stipulating that fleet average fuel economy for cars must be 42mpg, and 26mpg for light duty trucks with a GVW not exceeding 8,500lbs. The fleet average fuel economy for all light duty vehicles (GVW not exceeding 10,500lbs) for a manufacturer must be 35.5mpg. This is due to be implemented in 2016. Failure to achieve this fuel economy will result in vehicle manufacturers incurring fines.

California has additional, more stringent, emissions criteria that must be satisfied. This criterion was stipulated by the California Air Resources Board (CARB) [14]. As of 2008 the CARB standards had also been adopted in 12 other American states (Lyons, et al [15]).

Table 2.1 Euro Standards Implementation Map [10]

Spark Ignition Vehicles		2009	2010	2011	2012	2013	2014	2015	2016	2017	2018	2019
M, N1 CI I	Type Approval		Euro 5a 01Sep09		Euro 5b OR Euro 5b+ 01Sep11		Euro 6 01Sep14				Euro 6-2 01Sep17	
	First Registration	Euro 4		Euro 5a		Euro 5b	Euro 5b+		Euro 6 01Sep15			Euro 6-2 01Sep18
N1 CI II, III, N2	Type Approval		Euro 5a 01Sep		Euro 5b OR Euro 5b+ 01Sep11				Euro 6 01Sep15			Euro 6-2 01Sep18
	First Registration	Euro 4			Euro 5a	Euro 5b	Euro 5b+			Euro 6 01Sep16		*
Compression Ignition Vehicles												
M, N1 CI I	Type Approval		Euro 5a 01Sep09		Euro 5b OR Euro 5b+ 01Sep11		Euro 6 01Sep14				Euro 6-2 01Sep17	
	First Registration	Euro 4		Euro 5a		Euro 5b	Euro 5b+		Euro 6 01Sep15			Euro 6-2 01Sep18
Exempted M1 off-road	Type Approval		Euro 5a as N1 CI III		Euro 5b OR Euro 5b+ 01Sep11		No exemption					
	First Registration	Euro 4			Euro 5a N1	Euro 5b as M	Euro 5b+		No exemption			
Exempted non off-road	Type Approval		Euro 5a as N1 CI III		Euro 5b OR Euro 5b+ 01Sep11		No exemption					
	First Registration	Euro 4 as N1 CI III			Euro 5a	Euro 5b	Euro 5b+		No exemption			
N1 CI II, III, N2	Type Approval		Euro 5a 01Sep		Euro 5b OR Euro 5b+ 01Sep11				Euro 6 01Sep15			Euro 6-2 01Sep18
	First Registration	Euro 4			Euro 5a	Euro 5b	Euro 5b+			Euro 6 01Sep16		*

*Euro 6-2 01Sep19

Table 2.2 Vehicle Categories Applicable to Euro Standards [10]

Category	Description	Sub-category	Number of Persons	Mass Limit	Category	Description	Sub-category	Number of Persons	Mass Limit	
M	Carriage of Passengers Min. 4 wheels Passenger Car	M1	Up to 9 Persons	GVW ≤ 3,500 kg*	N	Carriage of Goods Min. 4 wheels	N1 CI 1	N.A.	Max GVW ≤ 3,500 kg	RM ≤ 1,305 kg
		M2	Over 9 Persons	GVW ≤ 5.000 kg			N1 CI 2			1,305 kg < RM ≤ 1,760 kg
		M3		5.000 kg < GVW			N1 CI 3			1,760 kg < RM ≤ 3,500 kg
				N2			3,500 kg < GVW ≤ 12.000 kg			
				N3			12.000 kg < GVW			

* Until EU4: Two subgroups: M1 with GVW ≤ 2,500 kg and M1 with 2500 kg < GVW ≤ 3,500 kg

Japanese standards:

The current Japanese standards [16] are the Post New Long Term (PNLT) and have been enforced since October 2009. These standards supersede the New Long Term (NLT) standards which in turn superseded the New Short Term (NST) standards.

Brazilian standards:

The Brazilian standards [17] are a mix of the European and American standards in that the FTP-75 cycle is adopted whilst the emissions themselves are based on EURO standards. The reason why Brazil has adopted different standards is because the fuel in Brazil contains high quantities of ethanol and the standards must be altered accordingly.

These 4 standards represent what is currently adopted throughout most of the world. Many countries adopt different levels of this criteria adopted some years ago by the region of the emission standards origin (China for instance have adopted Euro 4 standards whereas the EU currently conforms to Euro 5b standards). These emissions standards are comparable with each other and impose similar restrictions on the same emissions. An overview of the main criteria of these standards (applicable to light duty vehicles) is shown in Table 2.3.

The largest difference between them exist between the European (and Japanese) and American standards. The American standards show a greater focus on Non-Methane Organic Gasses (NMOG) and formaldehyde (HCHO) than HC and Non-Methane Hydrocarbons (NMHC).

The CO emissions are also much less rigorous in the American standards than in the Japanese and European standards. Although downsizing of engines in American light duty vehicles is beginning to occur, the extent of downsizing being applied is not

as considerable as that being applied to European and Japanese engines. The reason for this is fuel is considerably cheaper in America (58.3 pence per litre in America [18] compared to 132 pence per litre in the UK [19]), larger engines are therefore more affordable and commonplace in comparison to European and Japanese engines, and the less rigorous American CO emissions requirements reflect this fact.

There are various reasons why the emissions shown in Table 2.3 require close regulation. Sher [20] has documented extensively the reasons why these emissions are monitored. What follows is a brief explanation of what the emission is and what its impact is on the environment and general health and wellbeing, as well as an explanation of the processes that bring about that particular emission. Heywood [21] provides a very detailed review of emissions, and Cole, et al [22] provides a review of the differences in emission characteristics between GDI and Port Fuel Injection (PFI) applications.

Table 2.3 Current Worldwide Emissions Standards

Standard	Standard level	Standard type	Date of Introduction	Unit	CO	HC	NMHC	NOx	HC + NOx	PM	PN	HCHO	NMOG	CAFE (mpg)	CO2 (g/km)	
European	5b	SI	09/2011	g/km	1	0.1	0.068	0.06	0.23	0.0045	6e11					
		CI	09/2011	g/km	0.5		0.18	0.0045								
	6-1	SI	09/2014	g/km	1	0.1	0.068	0.06	0.17	0.0045	6e11					
		CI	09/2014	g/km	0.5		0.08	0.0045		6e11						
	6-2	SI	09/2017	g/km	1	0.1	0.068	0.06	0.17	0.0045	6e11					
		CI	09/2017	g/km	0.5		0.08	0.0045		6e11						
	EC 443/2009			2015												130
American	Tier II	Bin 6	2004	g/km	2.1131			0.0497		0.0062		0.0093	0.0466			
		Bin 5	2004	g/km	2.1131			0.0311		0.0062		0.0093	0.0466			
		Bin 4	2004	g/km	1.3052			0.0249		0.0062		0.0068	0.0435			
	CARB	LEV	2004	g/km	2.1131			0.0311		0.0062		0.0093	0.0466			
		ULEV	2004	g/km	1.0566			0.0311		0.0062		0.0050	0.0249			
		SULEV	2004	g/km	0.6215			0.0124		0.0062		0.0025	0.0062			
	EPA		2016										35.5			156
Japanese	PNLT	PC (SI)	09/2009	g/km	1.15	0.05		0.05		0.005						
		PC (CI)	09/2009	g/km	0.63	0.024		0.08		0.005						
Brazilian	PROCONVE L6	Otto	01/2014	g/km	1.3	0.3*	0.05	0.08				0.02				
		Diesel	01/2013	g/km	1.3		0.05	0.08		0.025						

* Applies to natural gas vehicles only

2.2.1.1 Carbon Monoxide (CO)

CO is toxic to humans. It combines with haemoglobin in the blood stream to form CO₂, thus considerably reducing the oxygen carrying capacity of blood and depriving tissues of O₂. CO can result in dizziness/light headedness, and large quantities of it can lead to loss of consciousness and eventually death (Sher [20]).

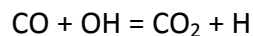
CO production is influenced heavily by the Air Fuel Ratio (AFR). Harrington, et al [23] found that when running with an equivalence ratio > 0.95 CO production can be seen to increase dramatically. Conversely, mixture inhomogeneity may give rise to high rates of CO production due to locally rich areas. The oxidation rate of CO is influenced by burned gas temperatures and temperature gradients during the expansion and exhaust strokes. Shimotani, et al [24] found that GDI offers no significant benefit over PFI with regard to CO production at normal running conditions.

Due to the fact diesel combustion is always lean, CO production is minimal and does not impose as significant an operating constraint as it does on gasoline engines.

Bowman [25] derived the chemical kinetic process responsible for the production of CO which is as shown below:



where R is a hydrocarbon radical. The CO is slowly oxidised to CO₂ in the exhaust by the following reaction:



Johnson, et al [26] found that the concentration of CO present at the end of the exhaust stroke, although lower than in the cylinder, is still significantly greater than at equilibrium conditions.

2.2.1.2 Unburned Hydrocarbons (HC)

HC emissions typically result in respiratory issues caused by bronchoconstriction, this results in coughing, dry throat and wheezing. They can also result in eye irritation. HC emissions can react with oxides of nitrogen to form ozone (O_3) which is detrimental to human health (Sher [20]).

HC is a very general term that applies to many different types of organic hydrocarbon compounds that are emitted from vehicles. The term HC applies to paraffins, olefins, acetylene and aromatics, and other types of hydrocarbon, all of which can be found in exhaust gasses. Various HC emissions can contribute to photochemical smog production and are considered quite harmful. Hydrocarbons are therefore classed by their reactivity with highly reactive HC emissions receiving the strictest regulation in the case of the American standards (formaldehyde receiving its own emissions classification due to its propensity to cause respiratory and eye irritation).

The main reason for HC emission production is usually incomplete combustion or through the use of fuel enrichment. There are numerous other reasons for HC emissions as well. Impingement on cylinder surfaces has been shown to contribute to HC emissions. Zhao, et al [27] found that this is highly dependent on the injection strategy employed (wall guided, spray guided etc.) and injector orientation relative to the cylinder axis and the surfaces of the cylinder (particularly the piston crown). Daniel [28] determined that flame quenching also contributes to HC emissions on cylinder surfaces (due to the incomplete oxidation of fuel). A study by Wentworth [29] found that HC emissions are also produced from crevices where the flame front cannot propagate to oxidise the fuel. Lubricating oil is also a known source of HC emissions as it can be partially oxidised along with the charge.

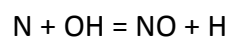
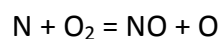
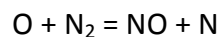
HC emissions will increase significantly when fuel enrichment is employed, due to the fact unburned fuel is unavoidable. However, due to the major drive cycles

requiring the engine to run at just low load points, enrichment has a negligible impact on overall HC emissions.

2.2.1.3 Nitrogen Oxides (NO_x)

NO_x refers to 2 specific emissions; nitric oxide (NO) and nitrogen dioxide (NO₂). NO has been found to react with haemoglobin having potentially lethal consequences. NO₂ is an irritant and reacts with the lungs and, if inhaled in a certain concentration, can cause severe damage to them (Sher [20]).

Stone [30] reports that for gasoline engines NO is produced in a far greater quantity than NO₂ in the cylinder itself through a basic chemical equilibrium analysis. Miller, et al [31] confirmed that NO is principally formed through oxidation of atmospheric nitrogen, but can sometimes form through oxidation of the nitrogen in the fuel as well, this is in addition to that which is formed by atmospheric nitrogen. The NO_x is formulated by means of the well established Zeldovich mechanism (Zeldovich [32] with an addition by Lavoie, et al [33]) which is as follows:



Burned gas temperature is a very large contributory factor in NO_x formation. Higher burned gas temperatures usually result in greater NO_x concentration. EGR is employed to suppress NO_x and is a particularly powerful NO_x suppressant, as it greatly decreases the charge temperature. Komiyama, et al [34] determined that employing 15 - 25% EGR results in a significant reduction of NO_x concentration. Spark timing was found to have a very dramatic affect on the burned gas temperature in the cylinder and has a great influence on NO_x production.

2.2.1.4 Particulate Matter (PM)

PM consists of organic particles (including soot) and sulphates. The danger PM imposes on human health greatly depends on the type of PM and the size. PM has been linked to respiratory diseases and, in the case of very fine particles ($\leq 10\text{nm}$) contamination of the lungs which the body itself cannot clear due to the particle being too small (Sher [20]).

Organic particles (soot) occur in greater quantities in diesel engines than they do in gasoline engines, depending on how the engine has been configured. Therefore, in some circumstances, diesel engines require Diesel Particulate Filters (DPFs) to reduce them.

Sulphide emissions are caused by sulphur present in the fuel. Kummer [35] found that three way catalytic converters can increase the sulphide emissions by oxidising sulphur dioxide (SO_2) to sulphur trioxide (SO_3). When emitted from the exhaust and into the atmosphere this can create aerosol sulphuric acid (H_2SO_4). Sulphuric acid is a major constituent part to acid rain.

The majority of PM emissions are simply by-products of a normal combustion process and therefore impossible to eradicate completely. Black smoke can however be produced in a gasoline engine when the charge is too rich.

2.3 Current Automotive Engines, Technologies and Trends

Although emissions standards around the world are striving toward the Zero Emissions Vehicle (ZEV), scientists and engineers are still somewhat short of achieving this on a global or even a fleet-wide scale. For now and the medium to long term future this is not achievable, but new technologies and techniques have allowed emissions to be dramatically reduced. What follows is a summary of these technologies and techniques.

2.3.1 Hybrid and Electric Powertrains

At present there are 3 main categories of hybrid and electric vehicles; Hybrid Electric Vehicle (HEV), Fuel Cell Electric Vehicle (FCEV) and Battery Electric Vehicle (BEV). FCEVs and BEVs are similar in that if the energy they use comes from a renewable source, and if one ignores the CO₂ cost of manufacturing the vehicle, some vehicle manufacturers can claim to have produced a true ZEV.

The Nissan Leaf, Peugeot iOn and Mitsubishi i-MiEV are examples of BEVs that have been put into production, and if powered from a solar or nuclear energy source they can be considered ZEVs. Owing to the fully electric powertrain BEVs can be incredibly efficient (up to 80% according to Helms, et al [36]) BEVs do suffer some considerable drawbacks however, such as a very limited range (a constraint imposed by the current generation of lithium ion battery technology) and a very long charging time using a typical domestic power supply.

The Honda FCX Clarity and Hyundai ix35 FCEV are examples of FCEVs. Like BEVs they have the potential to be classed as true ZEVs. Thomas [37] documents that owing to the much higher power density of compressed hydrogen FCEVs typically have a much greater range than BEVs, they also have a refill time comparable to fossil fuel powertrains. They are however less efficient than BEVs (48% efficient) and face additional logistical constraints such as how to safely transport highly pressurised hydrogen.

Both BEVs and FCEVs are lacking the energy infrastructure required to be successful in the short term and are both prohibitively expensive to justify over a fossil fuel powertrain at this moment in time. HEVs, though not ZEVs face no such constraint and can considerably improve emissions over fossil fuel only powertrains. The Toyota Prius is one such example of a HEV that has seen great commercial success, which has prompted an influx of other HEVs from large manufacturers such as Honda, Mercedes, Lexus, Ford, BMW and Volkswagen to name just a few. Plotkin, et al [38] determined that the efficiency benefit offered by hybrids was approximately 25% in 2005, but this

is declining due to advancements in fossil fuel powertrain technologies (such as engine downsizing) closing the gap.

Other hybrid technologies are also being researched such as range extending ICEs designed to be employed on BEVs to generate electricity, resulting in a new classification of vehicle known as the Extended-Range Electric Vehicle (E-REV). One such example of this is the Mahle range extender engine (Basset, et al [39]). Another novel concept is the air hybrid system as developed at Brunel University which regenerates approximately 15% of a vehicles kinetic energy that would have been lost under braking (Lee, et al [40]).

2.3.2 Fossil Fuel Powertrains

While BEVs and FCEVs offer great potential in terms of reduced emissions there is still a great deal of work that needs to be done to make them a true global transport solution. Until such a time as these technologies are ready, fossil fuel ICEs will still be the dominant powertrain for automotive applications.

Ever tighter emissions standards and ever higher fuel prices are forcing fossil fuel powertrains to become more versatile however, for instance, they are now applied in HEVs and E-REVs, and will continue to be applied in far different applications for the rest of their lifespan. This means that both gasoline and diesel ICEs will play a pivotal role in automotive applications for many years to come, and both will need to continue to evolve to satisfy the emissions legislation.

The key to this (particularly for diesel applications) is exhaust aftertreatment. Gasoline ICEs require a 3-way catalytic converter in their exhausts to reduce emissions of CO, NO_x and HCs, whereas diesel ICEs require a Diesel Oxidation Catalyst (DOC) because they run lean. Unlike 3-way catalytic converters, DOCs do not actively reduce NO_x emissions, so EGR is typically used instead to replace un-needed air with exhaust gasses to eliminate any unnecessary NO_x forming reactions.

Diesel ICEs can also suffer from increased soot emissions in comparison to gasoline, so in some circumstances a DPF is required as well as a DOC. Euro 6 emissions standards will require additional equipment still to reduce NOx emissions such as SCR or Lean NOx Traps (LNT). This will invariably make diesel ICEs more expensive than gasoline ICEs.

This will likely have a detrimental effect on the popularity of diesels in the future and could see a rise in the popularity of gasoline ICEs. Gasoline ICEs also have the added advantage of many new cost effective technologies that can be used to greatly improve performance and emissions. These technologies are described in section 2.3.3

2.3.3 Gasoline Engine Developments

In previous years, improvements in fuel economy for gasoline fuelled engines have been achieved in the following ways:

- Downsizing and downspeeding (reducing gear ratios)
- Developing GDI fuel injection technology
- Increased engine specific power output (turbocharging/supercharging/eboosting)
- Optimising In-cylinder flow (allowing increased homogeneity or stratified charge)
- Using lighter materials (aluminium or Compacted Graphite Iron (CGI))
- Introducing VVT systems
- Using EGR at part and full load with boost
- Using alternative thermodynamic operating cycles (Miller/Atkinson, HCCI/CAI)
- Increasing geometric CR

This list is not exhaustive and it has not been possible to develop each of the techniques listed in isolation. Many of the technologies above have synergies with each other.

Extensive use of aluminium is now made in engine manufacture. Alloys (particularly those of magnesium) are also used more for component design because of their high strength properties. Austenitic steel has also received application in exhaust manifolds where high temperature endurance, low weight and good thermal expansion properties to prevent catalyst blow by are required. CGI could also find application in block design for downsized gasoline engines in the near future, due to increased cylinder pressures and loads.

Stratified charge has already been employed on production engines and is now in its second generation (stratified charge with spray guided direct injection) and has been documented by Schwarz, et al [41] to result in improvements of Brake Specific Fuel Consumption (BSFC) of up to 20% on the New European Driving Cycle (NEDC). Stratified charge shows great promise for reducing BSFC but can only be employed at low - medium loads (as documented by Missy, et al [42]), and requires a DeNOx catalyst or LNT to pass emissions regulations. Ricardo's Lean Boost Direct Injection (LBDI) (Lake, et al [43]) is an alternative concept that also allows the engine to run homogeneous lean at higher loads and with boost. This is better suited to downsized applications and can also result in a BSFC benefit of up to 20% when applied to a downsized turbocharged engine and compared to a larger NA engine of equivalent power and torque.

Homogeneous Charge Compression Ignition (HCCI) or Controlled Autoignition (CAI) is a medium term technology that enables an engine to run homogeneous lean. Unlike stratified charge and LBDI, combustion is not initiated by a spark but by compression ignition. The mechanism of combustion is also different. Spark initiated combustion relies on a flame front propagating through the end gas which is susceptible to quenching, flame stretch and turbulence. HCCI results in the entire end gas region undergoing simultaneous reactive envelopment. In spite of the fact HCCI is a lean burn technology Zhao, et al [44] documented a significant reduction of NOx

emissions to the extent that a LNT is not required, which gives it a large advantage over stratified charge and LBDI operating regimes. CO emissions are also massively improved in comparison to stratified charge and LBDI, while HC emissions are similar. Osborne, et al [45] found that HCCI yielded an 8% improvement in ISFC. However, HCCI is restricted to low load operation only at this moment in time.

EGR is a well established means of improving fuel economy and dramatically reducing exhaust emissions. At low load EGR can be used to partially fill the cylinder with exhaust gas, thus reducing the size of the pumping loop. EGR can also be used at high load Wide Open Throttle (WOT) conditions too. Cooled exhaust gasses have the effect of reducing peak combustion temperatures which allows the combustion to be advanced considerably. Cairns, et al [46] documents reductions of CO and HC emissions of up to 70% and 80% respectively. In regions where enrichment is required WOT EGR can yield an improvement in BSFC of up to 17%. Significant NO_x reductions have been seen when comparing WOT EGR to excess air too, but not so much compared to stoichiometric operation.

The Atkinson/Miller cycle process is a near term means of improving fuel economy and has already seen application on some production engines. Both Atkinson and Miller cycles work on the same principle of changing the compression ratio relative to the expansion ratio so the expansion ratio is greater than the compression ratio. This technique is known as over-expansion. This technique has only become feasible relatively recently due to the mechanical complexity of making the expansion ratio longer than the compression ratio. This has been circumvented by the use of fully variable valve trains and cam phasing devices by closing the intake valve slightly earlier or later than BDC reducing the effective compression ratio relative to the expansion ratio.

Although the full benefits of the Atkinson/Miller cycle process can only be realised with a fully variable valve train, a benefit to BSFC can be obtained simply by changing the intake cam profile, with no further work required (depending on the application and the type of engine). Intake cam phasing (as is employed on many automotive engines) can increase this BSFC benefit further still, while circumventing

the issues associated with reduced volumetric efficiency for higher load cases. Of all of the technologies above it is also the cheapest to incorporate, with no need for any additional exhaust after treatment systems beyond that required for a standard Otto cycle engine. The Atkinson/Miller cycle process also offers synergies with all of the technologies mentioned above (with the arguable exception of EGR).

The Atkinson/Miller cycle process has only really been automotive production engine feasible since the introduction of VVT and GDI. Perhaps the most promising aspect of the Atkinson/Miller cycle is its knock mitigating properties at high load.

Of all of the technologies discussed in this section it is downsizing that is of greatest interest at this moment in time for the reasons described in section 2.3.4.

2.3.4 Downsizing and Turbocharging

Downsizing is already seeing widespread interest with many downsized engines already in production (Volkswagen 1.4 R4 TSI, Bentley 4.0L V8, BMW 2.0L TVDI). At the time of writing the most aggressively downsized production engine is the Ford Ecoboost with a peak BMEP of over 25 bar (Friedfeldt, et al [47]). Many prototype aggressively downsized engines have been designed such as the Mahle 1.2l downsized engine (Hancock, et al [48]), the MCE-5 VCR engine [49] and the Jaguar Land Rover Ultraboost engine (Turner, et al [50]), all of which surpass the extent of downsizing demonstrated by the Ford Ecoboost by a significant margin.

The Mahle 1.2l downsized engine was designed to replace a 2.4l V6 NA PFI engine and has achieved the same power output as the V6 and yielded an increase in efficiency of 30%. It can also run at 30 bar BMEP, and in a study by Lumsden, et al [51] it was run in excess of this. Turner, et al [50] expects similar benefits (35%) with the Jaguar Land Rover Ultraboost engine, which is downsized to a greater extent still (replacing a 5.0l V8 with a 2.0l I4 engine) and is required to run at a peak load of 35 bar BMEP, and 25 bar BMEP at 1000rpm.

Downsized engines reduce the number of cylinders on an engine and the overall engine displacement, this results in a considerable reduction of frictional losses. An additional benefit is obtained through the concept of load point shifting too (a smaller engine must produce a higher BMEP than a larger engine for the same power output) which dramatically reduces the part load pumping losses.

In order to compensate for a lack of displacement the engine must be boosted (usually turbocharged) to increase the specific power output. Unlike most conventional turbocharged engines the turbocharger must provide sufficient boost from a very low engine speed because a reduction of swept cylinder capacity will impact all speeds, not just high. The selection of boosting system is therefore of great importance, as it not only has to provide sufficient boost from low speeds but it also has to offer very little transient delay.

Turbocharger technology has also come a long way in recent years. The introduction of novel boosting strategies such as a 2-stage system (known as “twincharging”) and wastegate boost pressure regulation are examples of 2 technologies that have made downsizing possible. Twincharging involves complementing either a small turbocharger or supercharger with a large turbocharger or supercharger either in series or in parallel. If a small supercharger is used it is usually electrical or connected to the crankshaft by means of an electromagnetic clutch so it can be disengaged at higher speeds to prevent high parasitic losses occurring. This system is capable of providing high quantities of boost across the entire engine operating envelope with minimal lag time. This concept first entered production in 1985 on the Lancia Delta S4 Stradale [52]. Copeland, et al [53] detail a similar twincharging system that was determined to be optimal on the Jaguar Land Rover Ultraboost engine, for this engine a turbocharger has been employed for the low pressure stage and a supercharger employed for the high pressure stage.

Wastegate boost pressure regulation refers to the process of using a wastegate to divert flow away from a turbocharger turbine when it is not required, thus reducing the EBP. Conversely it can also be used to limit the maximum pressure ratio and speed of a turbocharger by purging exhaust gas that would ordinarily go through the turbine.

This permits the use of a smaller diameter turbine (good for transient response) without sacrificing the overall pressure ratio. One such wastegate boost pressure regulation system is the Mahle E-Actuator (Fraser, et al [54]) which offers improved transient response and reduced pumping losses at part load conditions.

Both of the above systems have made turbocharging a much more viable option, even for low engine speeds, and have improved it to the point where conventional supercharging offers little to no advantage any more. It may even be considered inferior to modern turbocharging due to the fact that superchargers typically demonstrate lower adiabatic efficiency than turbochargers and therefore require bigger intercoolers.

Fraser, et al [55] of Mahle powertrain investigated the impact of several different boosting systems on the Mahle 1.2l downsized engine and found that a twincharger system provided highest low speed load, while the turbocharger with electric supercharger system gave the best transient response.

Overcoming the boosting issues at low speed is not the only problem with downsizing however. Running at high load and low speed greatly increases the propensity for an engine to experience autoignition in both knocking combustion and Low Speed Pre-ignition (LSPI) form. Amann, et al [56] provides a definition of LSPI and the speeds at which it applies. LSPI is basically pre-ignition that only occurs at engine speeds of 3000rpm or less, and completely absent above 3000rpm. According to the description in Heywood [21] this is more likely at lower speeds due to reduced charge motion and also due to the elevated pressure and temperature histories during the compression process. This phenomenon has the effect of greatly reducing the maximum load at which the engine can run.

Anderson, et al [57] found that the Atkinson/Miller cycle process exhibits end gas temperature reducing properties which may reduce the propensity for LSPI and knocking combustion. The Atkinson/Miller cycle will also theoretically improve efficiency at higher load points too. This is due to the fact lower end gas temperatures will result in more spark advance relative to a baseline Otto case, which will accordingly result in lower exhaust gas temperatures. This will reduce the amount of

enrichment required for component protection which will improve fuel economy and HC emissions markedly at high speed and high load.

In spite of a great deal of interest very little research has been carried out on this concept known as Deep Miller. For this study “Deep Miller” is defined by using the Miller cycle at engine loads of at least 15 bar BMEP. One of the aims of this study is to ascertain exactly what benefit can be obtained by running with the Miller cycle at high load and low engine speed.

2.4 Atkinson/Miller Cycle

2.4.1 Introduction

With the rate at which the global transport sector is growing the automotive industry and ICEs have been forced to evolve in a very short space of time. Engine downsizing is the key to this rapid evolutionary process, as the infrastructure and technology required already exists to make it a reality. GDI is also a key to this evolution as it affords a great deal of freedom over how an engine can be run. Downsizing, though relatively easy to implement, has its own set of unique problems. High specific power outputs are what downsizing relies upon in order to be successful, but knocking combustion is a side effect of running at high specific power, so in order to elevate specific power, techniques for increasing the knock limit or Borderline Detonation (BLD) limit must be researched.

The Miller cycle process is one near term solution to increasing the BLD limit of an engine. It also has synergies with many other techniques to increase the BLD limit of an engine. It does face challenges though such as whether or not in-cylinder charge motion is affected by closing the intake valve either before or after BDC and what impact this has on combustion stability and Coefficient Of Variation (COV) of the Indicated Mean Effective Pressure (IMEP). There are also many questions left to be answered on the concept of Deep Miller and whether or not it benefits the engine, and

whether or not an increase in the geometric CR can be utilised by running with a reduced effective CR.

2.4.2 History

The Miller cycle was patented by an American engineer called Ralph Miller in 1947 (Miller [58]). It is very similar to the Atkinson cycle with the biggest difference between them being the Miller cycle requires a supercharger to compensate for the power lost by closing the intake valve away from BDC. There are however points where the definition of the 2 become blurred.

There is a great deal of literature on the benefits offered by the Atkinson cycle, and the benefits offered by a reduced pumping loop size. The Atkinson cycle engine in spite of its relatively complicated geometry received a great deal of attention from a very early stage. The British gas company built over 1000 2-stroke Atkinson cycle engines between 1886 and 1893.

Various attempts were made to implement an Atkinson cycle in an automotive engine with varying degrees of success. The most recent attempt was carried out by Honda with the extended expansion linkage engine (EXlink) [59]. There are 2 different types of Atkinson cycle engine, the original style Atkinson engine that achieves different compression to expansion ratios by employing linkages to give different geometric compression to expansion ratios, and the modern type which uses intake valve closure timing to provide a different effective compression ratio and the expansion ratio is still dictated by engine geometry. It is the second, modern, type of Atkinson cycle that blurs the boundary with Miller cycle. Miller cycle actually stipulates that the effective compression ratio is controlled by the Intake Valve Closing (IVC) timing, but it also stipulates that a supercharger must be present.

In the majority of the literature (particularly in recent years [57][60-74]) the Atkinson process referred to is the modern process, it is sometimes referred to as Miller cycle and in other papers it is referred to as the Atkinson cycle. It can also be

referred to as EIVC, LIVC and Extended Expansion (EE). In some cases it can be referred to as Deep Miller, this definitely applies to the Miller cycle only and the deep part refers to the fact that very high levels of boost pressure are employed rather than boosting simply to make up for the loss of volumetric efficiency incurred by closing the intake valve away from BDC. For the sake of clarity any system that achieves effective CR reduction by means of phasing the valves relative to BDC, whether NA or under forced induction, shall henceforth be referred to as the Miller cycle.

The Miller cycle was first utilised in large engines for marine or power generation applications. Very little regard for emissions was given then, the Miller cycle was employed purely as a means of increasing power output for greater fuel economy. In later years it gained the interest of manufacturers of smaller, more mobile applications such as earth movers and other large off-road vehicles. Miller cycle was also considered for use with Low Heat Rejection (LHR) engines. Ishizuki, et al [75] of Komatsu started researching diesel engines that employed the Miller cycle (or “extended expansion”) in the mid 1980s.

With the technologies available in those days Miller cycle was not feasible due to problems with excessive smoke emissions at part load conditions associated with reduced EOC temperatures. This was mainly due to the fact there was no convenient way to change the intake valve timing for varying degrees of Miller cycle in real time with engine load. Also EGR was found to give a similar performance benefit without the need for novel cam phasing technologies.

The US military also showed some interest in Miller cycle LHRs for tank applications slightly later in 1995 (Kamo, et al [76]). LHRs are of great importance to military vehicles owing to the fact they operate in such hostile environments and are constantly subject to attack. The majority of ballistic missile weaponry is heat seeking, lowering the thermal footprint of a vehicle is therefore of great importance and massively desirable.

The greatest commercial success of the Miller cycle has been in cogeneration applications (engines generating both power and thermal energy). The Miller cycle has been employed in natural gas cogeneration systems since 2000 in the Mitsubishi

GS16R. This particular series of engines represented a milestone in cogeneration technology in that it was the first engine to exceed a thermal efficiency of 40% for that class of generator at that time according to Kado, et al [77].

In 2010 a Miller cycle engine was released for commercial sale designed for use in locomotive applications. It was developed by General Electric (GE) and is called the powerhaul, this engine achieves 22 bar BMEP at 1500rpm with a BSFC of just 192 g/kWhr, a 9% reduction over any equivalent engine at that moment in time [78]. Due to the fact transient response is not such an issue, this engine was turbocharged which greatly improves the BSFC.

Engines of this type benefit from having a very small range of speeds and loads to operate at, and can therefore adopt fixed valve timings for Miller, this reduces the complexity of the engine massively and means the valve timings can be finely tuned for just a few speeds and loads.

Its adoption on smaller vehicles such as passenger cars and gasoline applications was slower due to the fact a supercharger was required. The cost of supercharging an engine proved too great in comparison to the amount of fuel saved for typical passenger cars. There is the added challenge of making the vehicle run at a variety of different speed and load points, and a requirement for good transient response.

Miller cycle for passenger vehicle type applications was still the subject of some research work at a relatively early stage however. There is not a great deal on Miller cycle work specifically due to the fact it is basically an extension of the Atkinson cycle. Research commenced in the mid 80's with a study from Sakai, et al [79] on the prospect of using the Miller cycle on gasoline engines.

For all applications the Miller cycle engine was found to improve the thermal efficiency greatly (in the region of 7–35% over baseline Otto cases depending on the degree of Miller, and whether or not a turbocharger or supercharger was employed). The reduction in EOC pressure and temperature was also found to greatly reduce NOx emissions.

The Miller cycle has been employed on some passenger car engines for production, such as the Mazda KJ-ZEM engine (Goto, et al [80]). The KJ-ZEM engine is a 2.3l V6 with a geometric CR of 10. This engine was used in the prestige Mazda model of the time, the Mazda Millenia. The variant with the KJ-ZEM Miller cycle engine was \$3000 more than the equivalent Otto cycle engine model, but developed 24% more power for the same fuel economy [81]. The KJ-ZEM engine was not a great commercial success due mainly to the fact that maintaining the engine was very expensive, and the new Lysholm supercharger on the engine was very expensive to replace too.

The Lysholm compressor was developed purely for this application and its development has been documented by Takabe, et al [82]. It is a supercharger because no turbochargers of that day could provide the transient response required for automotive applications. It exhibits a very high adiabatic efficiency at very high pressure ratios but ultimately still impacts heavily on the overall efficiency benefit in comparison to a turbocharger.

The majority of work in the 80's and 90's was carried out by the Japanese researchers such as Hiroshi Sakai and his team at the University of Tokyo in conjunction with mainly Japanese industry [79][83-84]. One of the reasons for this great Japanese interest is due to concerns over the quantity of NO_x emitted in large cities such as Tokyo. In 1992 a new law was introduced called the "The Law Concerning Special Measures for Total Emission Reduction of Nitrogen Oxides from Automobiles in Specified Areas" [85] aimed at radically reducing NO_x emissions. Power plants were also under greater pressure to become cleaner and more efficient, which is the reason why the Japanese also invested very heavily in the Miller cycle for LHR and power generation systems too.

In the case of passenger vehicles the price of fuel has risen to the extent that the technology required for implementation of the Miller cycle is now justifiable for the gain in efficiency obtained. The widespread introduction of VVT systems is also a key enabler to the successful implementation of the Miller cycle on passenger vehicles. With the growing number of downsized and turbocharged engines, boosting is

becoming cheaper and is now cheap enough to become viable for typical vehicle models, not just prestige models.

The trend for engines to become smaller and turbocharged also means knocking combustion poses a far greater constraint on engine performance than it has ever done before. The EOC pressure and temperature reducing qualities of the Miller cycle helps to inhibit knock which enables peak loads to be elevated.

2.4.3 Pumping Losses

One of the biggest reasons for adopting the Miller cycle is the reduction of pumping losses. The benefit obtained through this is particularly marked at very low load conditions where the pumping losses are similar in magnitude to the power output of the engine. Depending on the speed and load condition, and the type of boosting system employed, the pumping losses can actually become inverted and produce a Pumping Mean Effective Pressure (PMEP) of less than zero.

In earlier work the maximum reduction in PMEP was very significant and of the order of 80% in some cases, although this did not always give acceptable performance [86-89]. The main reason for this is earlier work was mainly focussed on running the engine completely unthrottled with symmetrical valve timing rather than simply reducing the throttling. The potential benefit of running completely unthrottled was very inviting and Theobald, et al [56] estimated it could return a theoretical fuel economy benefit of up to 24% in the then current driving schedule. It should be noted that this theoretical fuel economy improvement is not accurate for future engines. The widespread use of downsized engines has resulted in load point shifting, and as a result of this the required MAP in a downsized engine for a specific load is much higher than that for an engine from when the Theobald, et al [90] study was conducted. The maximum fuel economy benefit for today's or even tomorrow's downsized engines can be estimated but is not actually known to the author's best knowledge. One of the aims of this study is to investigate this.

In subsequent years the actual PMEP benefit obtained varied significantly depending on the type of valve actuation system employed and whether or not EIVC or LIVC was being used. In the work of Tuttle [91-92] EIVC was found to be the optimum strategy for reducing pumping losses, and the maximum PMEP benefit obtained was approximately 40%. Other works on EIVC with symmetrical valve timing also confirm that 40 - 60% is the maximum PMEP contribution reduction that can be obtained for typical gasoline engine CRs [93-94]. Symmetrical LIVC typically demonstrates a greater tolerance to effective CR reduction, this enables greater extents of LIVC to be attained and pumping loop reductions of the order of 80% [86-87]. Although pumping loop reductions of this size could be attained this yielded no benefit to BSFC, and in some cases actually returned worse BSFC than the baseline engine/setup.

In 2007 Honda developed a prototype genuine Atkinson cycle engine (Koga, et al [95]). This engine has fixed valve geometry. The reduction in PMEP peaked at approximately 37% which is another indicator that this is the maximum extent the PMEP can be reduced by with fixed geometry in order to still make an engine usable and perform acceptably.

Another major problem with extreme EIVC and LIVC cases yielding PMEP reductions of the order of 80% is that the cam profiles required to achieve this would achieve only very low maximum loads, therefore PMEP benefits of this magnitude were reserved only for costly Variable Valve Actuation (VVA) and VVT systems. It must also be taken into consideration that extreme LIVC is much easier to achieve logistically than extreme EIVC with conventional valves due to the fact that EIVC requires very short valve open durations and correspondingly only very low valve lifts can be obtained. This means choked flow through the valves is more likely to occur thus restricting the maximum PMEP benefit that can be obtained with EIVC.

Many techniques and systems have been employed for increasing the effectiveness of EIVC and LIVC strategies and for increasing the degree of Miller effect. These techniques include increasing the geometric CR to compensate for low effective CRs, employing tumble flaps to induce more turbulence, reducing valve lift and lean

combustion. The most commonly employed technique in the literature is asymmetric valve timing.

Asymmetric valve timing and valve deactivation have been studied extensively over the years [49][60-66][89]. Valve asymmetry and deactivation are both beneficial to EIVC and LIVC in most cases, however, the benefit is not always obtained through PMEP reduction. In most cases valve deactivation and asymmetric valve timing have been combined with low valve lift. This usually has the effect of reducing the Indicated Specific Fuel Consumption (ISFC) due to increased charge motion, however, for some engine/load/valve lift combinations, this can actually have the effect of increasing the PMEP contribution but still resulting in an improvement in BSFC due to better combustion [64][67], although the benefit is usually marginal. Cleary, et al [67] discovered that if the valve lift is too low and the engine load too high it can be possible for “sonic throttling” to occur. This describes the case when the flow is choked by the intake valve. This massively increases the pumping work contribution to the point where running unthrottled is no longer beneficial.

Work on other strategies to improve the effectiveness of EIVC and LIVC with tumble flaps is also underway with the Mahle cam in cam system (Taylor, et al [64]). These technologies are not necessarily intended to reduce PMEP directly but mostly through increasing charge motion. Tumble flaps have the effect of increasing tumble and in-cylinder charge motion at the expense of pumping losses. Kapus, et al [60] documented that the intake port needed to be blocked by up to 70% in-order to induce adequate amounts of tumble. Late Intake Valve Opening (LIVO) is another example of another strategy that achieves a benefit in economy through charge motion rather than pumping loss minimisation [67-69].

LIVO is also the subject of research at this moment in time. This involves phasing a short low lift intake cam toward BDC rather than Top Dead Centre (TDC). This however offers no benefit to PMEP in comparison to the throttled case.

2.4.4 Combustion Stability

One of the drawbacks of the Miller cycle, particularly of EIVC, is the reduced charge motion in the cylinder leads to a relatively slow flame front speed and a higher COV of IMEP. This problem is particularly pronounced at very low load conditions where the quality of combustion is very degraded and HC emissions increase rapidly.

Almost all of the literature available on EIVC and LIVC report this issue. Combustion degradation is particularly pronounced at low load and with very extreme degrees of EIVC and LIVC. All of the available literature is unanimous in the fact it is caused by low EOC pressure and temperature making the charge harder to ignite and burn in its entirety.

EIVC has the added drawback of exhibiting very low levels of tumble/bulk flow due to the fact the valve is closed very early on in the cycle giving the charge a very long time in which to dissipate its motion. This greatly reduces the speed of the combustion process [63][70] and greatly restricts the extent of EIVC that can be employed for gasoline engines with typical geometric CRs. Sellnau, et al [72] reported that the tumble motion can be reduced by up to 70% over baseline cases.

Zhao, et al [96] documents that tumble motion is very beneficial to combustion as it encourages mixing and is converted to turbulent motion near TDC. The conversion to turbulence at TDC is crucial as this is what increases the rate of entrainment and combustion, and increases the combustion stability. Swirl is another form of bulk motion but this is less useful to homogeneous charge GDI engines due to the fact it is not as effective at creating turbulence as tumble, and the combustion stability is not improved markedly as a result of this.

Many attempts have been made to increase the degree of bulk flow with EIVC. The most successful method of achieving this is through the use of valve asymmetry. Battistoni, et al [63] discovered that valve asymmetry can greatly increase the swirl component of motion but not so much tumble, which can actually decrease with valve asymmetry and reduce the amount of turbulence at TDC. Sellnau, et al [68] found that

tumble is dependent on valve lift and the tumble index shows a strong, almost linear, correlation with valve lift. But this is highly dependent on the engine (particularly piston) geometry (as was found by Akihisa, et al [71]), and whether or not a tumble flap or any form of masking has been incorporated [64][68].

Lee, et al [73] discovered that swirl motion can improve combustion stability and improve the Mass Fraction Burn (MFB) duration to an extent, but if the swirl component is too elevated it can have a detrimental effect. However, swirl is not best suited to this application (it is better suited to stratified applications as described by Zhao, et al [96]). Battistoni, et al [63] discovered that the swirl component is greatly reduced for symmetrical EIVC.

With tumble motion being very dependent on valve lift, EIVC has an inherent disadvantage over LIVC due to the fact that the intake open duration is very short, and this greatly reduces the peak valve lift. Urata, et al [88] stated that even fully variable valve train systems at low speed and low load struggle to open the intake cam by a large extent.

Low valve lift does have some advantages over high lift though. Although the tumble motion is reduced the initial Turbulent Kinetic Energy (TKE) can be seen to be very high with low valve lift due to the fact the flow velocity through the intake valve is very elevated [63][66]. The elevated TKE is very short lived however and typically reduces very rapidly once the intake valve has closed. Asymmetric valve timing and valve deactivation increase the TKE even more still (by up to 250% compared to symmetric timing according to Matsumoto, et al [66]), this is a likely result of increased swirl motion.

Valve asymmetry has the effect of increasing tumble by a small amount too but this tumble component is increased by a greater extent still when masking/tumble flaps are employed. This therefore provides a cross tumble (or "Swumble") type motion within the cylinder.

The effectiveness of this elevated charge motion is highly questionable. It can be seen to improve the MFB duration slightly and improve combustion stability but

ultimately with EIVC the majority of the charge motion is lost at TDC firing regardless of what charge motion stimulus has been employed on the engine. The increase of charge motion comes at the expense of increased PMEP losses in most cases. In some cases the increase of charge motion and the corresponding increase of PMEP losses required return no significant improvement over the throttled cases [67][94].

In the majority of LIVC cases (with both symmetric and asymmetric timing) the bulk flow is improved at TDC owing to the fact the valve closes later in the cycle. The flow behaviour and components of flow depend on the engine being tested. Söderberg, et al [94] reported that the components of tumble and swirl with LIVC were similar to the baseline valve timings, this means that LIVC typically exhibits greater turbulence at TDC which gives it a much improved MFB duration. However, the TKE obtained with symmetrical LIVC is typically much lower which means the mixing is inferior to the EIVC case.

Valve asymmetry and deactivation have been employed to remedy this issue, as well as exploring the effect of low lift cams. Matsumoto, et al [66] found valve deactivation to be a very effective method of increasing the TKE whilst maintaining good bulk motion. A similar strategy has been employed in another study by Söderberg, et al [94] and it was found that this was an effective method for increasing the TKE, but, like the EIVC case, this was at the expense of increased PMEP losses. The same study also confirmed that the maximum lift symmetrical LIVC case was the optimum for net efficiency for this reason, in spite of the fact that 10-90% MFB duration was one of the highest of all the LIVC strategies tested at this condition.

LIVO is another strategy for boosting charge motion. Cleary, et al [67] has concluded that it is an unsuitable replacement for throttled operation due to the fact the PMEP is so high. It does however result in similar levels of TKE as seen for EIVC only much later in the cycle. It also gives a very high effective CR close to the geometric CR which results in elevated EOC temperatures. This coupled with the increased TKE gives very fast burn durations which is useful for cold start applications.

2.4.5. Engine Breathing

Both EIVC and LIVC have the potential to change engine breathing dynamics considerably. Both strategies require the MAP to be elevated above what it would be for conventional Otto operation. This will drastically change the quantity of residuals in the cylinder, and the temperature.

EIVC is relatively insensitive to engine breathing due to the fact no charge is purged back into the intake manifold at any point during the cycle. With LIVC however a great deal of charge will be purged into the intake manifold which can have a dramatic effect on engine performance.

One of the biggest problems with EIVC operation is charge heating during depressurisation, this has been reported by Hitomi, et al [74]. LIVC has been found to achieve reduced EOC temperatures compared to EIVC due to the fact the charge is depressurised with EIVC, this causes the charge temperature to drop dramatically. The charge is then heated up by the cylinder walls thus elevating the overall charge temperature.

Blakey, et al [86] carried out an investigation on LIVC and found that the resulting PMEP reduction did not correspond to a BSFC benefit compared to the throttled case, it was in fact worse. A very high degree of LIVC was employed in order to run at part load completely unthrottled and the higher the degree of LIVC the worse this discrepancy became. This problem was traced back to the 8 branch intake manifold installed on the engine at the time. The fuel rejected through LIVC running was returning to the manifold plenum and was being distributed to other cylinders.

Taylor, et al [64] observed an increase in the intake port temperature during testing with LIVC. The temperature reached up to 60⁰C due to residuals being purged to the intake manifold. This required the combustion phasing to be retarded significantly due to the excessive temperature of the incoming air, thus impacting heavily on the perceived benefit of running with LIVC. A similar observation was made by Anderson, et al [57].

Residuals are effective at reducing NO_x and CO emissions but other than this they are generally detrimental to EIVC and LIVC combustion stability, particularly at very low loads.

The general consensus from the literature is that LIVC is harder to execute successfully than EIVC as it relies heavily on the engine tuning, particularly the intake system.

2.4.6 Emissions

Both EIVC and LIVC are inherently effective at reducing NO_x emissions due to the lower cycle temperatures. The literature states this benefit is typically in the region of 30 – 60% reduction in comparison to the baseline Otto cases [57][61][64][67-68][89-90][97]. In certain circumstances, particularly with LIVC, the reduction in NO_x can be attributed to increased residual gas concentration. It is very difficult to gauge from the literature which technique is optimum for reducing NO_x emissions, the closest is the work of Moore, et al [65] who compared NO_x emissions for EIVC and LIVC in the same study but failed to compare them at the same speed and load point. Gould, et al [98] found that for the same extent of EIVC and LIVC in a 2 valve engine, EIVC returned higher NO_x emissions (approximately 10% higher) than LIVC, but that both were considerably reduced below the Otto cycle baseline case. It was also found that EGR could reduce NO_x emissions further still but at the expense of thermal efficiency, CO emissions and HC emissions.

Internal residuals as well as external EGR have the effect of reducing NO_x and CO emissions, however, Cleary, et al [67] attempted to implement EGR in a Miller cycle engine and it resulted in a reduction in efficiency compared to just Miller on its own. This was attributed to a reduction in combustion stability.

Asymmetric valve timing and valve deactivation generally show no strong trends with regard to NO_x emissions [61-62][65]. Stansfield, et al [61-62] have run 2 separate studies on the impact of Miller cycle on NO_x emissions. In one study [61] the

NOx emissions were greater with valve deactivation in comparison to symmetrical valve actuation, although this has been attributed in part to poor engine running and misfiring. The engine also demonstrated a sensitivity to which intake cam was deactivated, with one giving slightly different NOx emissions to the other.

In a later study by Stansfield, et al [62] valve deactivation and symmetrical valve timing were analysed once again, only in this study several different valve lifts were tested as well. The impact of valve deactivation on NOx emissions was found to be dependent on speed and load in this study, with the low speed and low load point generally favouring valve deactivation and low valve lift. The advantage of valve deactivation was lost with increasing speed however. For higher load points valve deactivation with low lift valves was not feasible without boost, and only 1 valve deactivation point could be tested and this yielded no benefit over symmetrical valve timing.

In most cases EIVC and LIVC result in a slight increase in HC emissions due to lower EOC temperatures reducing the rate of HC oxidation [67][86], however Urata, et al [88] found little to no difference in HC emissions and may even be marginally improved. This reveals that the HC emissions are very dependent on the engine breathing dynamics.

HC emissions can generally be seen to decrease with increasing speed with both EIVC and LIVC in a similar manner to Otto cycle engines [62][86], and they can also be seen to decline with load (Boggs, et al [89]). Whether or not the Miller cycle HC profile intersects with the Otto HC emission profile depends on the engine. In the case of Blakey, et al [86] LIVC produces fewer HC emissions than the Otto baseline at low speed but produces more HC emissions at high speed than the baseline. Boggs, et al [89] on the other hand show elevated HC emissions at low loads (up to 94% higher than baseline at idle) but HC emissions near enough the same as the baseline at higher loads.

Cleary, et al [67] investigated numerous valve profiles for EIVC and showed that as the degree of EIVC increased (the cam duration reduced) the HC emissions

increased almost linearly to give a HC emission increase of 20% relative to the baseline to the most extreme EIVC profile.

The impact of valve deactivation can be seen to have very little effect on HC emissions. Moore, et al [65] saw a slight reduction (6%) in HC emissions at low speed and high load LIVC with valve deactivation compared to symmetric LIVC, but no gain was obtained with EIVC with valve deactivation compared to symmetric EIVC. Stansfield, et al [62] recorded a similar result with valve deactivation and low lift, in that study it made very little difference to overall HC emissions.

CO emissions with Miller cycle are generally reduced compared to baseline Otto cases with the notable exception of Sellnau, et al [68] which reports an increase of 123% compared to the baseline case. This however was a result of the engine being tuned to reduce NOx emissions for an EPA cycle rather than a reflection of the Miller cycle process as a whole. In the literature the CO emissions are typically reduced by 30 – 60% over baseline with asymmetric valve timing/valve deactivation [61-62][89].

CO is dependent upon how homogenous the charge is at the time of ignition. Of the limited data available on CO emissions and the Miller cycle, symmetrical EIVC was found to massively increase CO emissions compared to baseline for some speeds and loads. Stansfield, et al [61-62] found that both EIVC and LIVC benefit CO emissions compared to the baseline points with asymmetric valve timing though. CO emissions are largely insensitive to valve lift with EIVC which is somewhat unexpected, this would imply that the TKE generated through asymmetric valve timing/valve deactivation is sufficient for mixing the charge.

In a study by Sellnau, et al [68] LIVO was found to improve the cold start performance of an engine. In a later study by Turner, et al [69] a CFD study revealed that LIVO greatly improved the charge motion in the cylinder. When employed for just the first 20 cycles this system can achieve a reduction in HC emissions of 35% over the baseline case and prevent the use of accidental enrichment.

2.4.7 Knock Mitigation and Deep Miller

There is a wealth of literature on genuine Miller cycle engines for heavy diesel applications but there is unfortunately very little on Miller cycle gasoline engines. The majority of the papers are on Atkinson cycle only, or employing EIVC and LIVC without forced induction.

An early study of the knock mitigating effects of the Miller cycle was carried out by Ke, et al [93]. This was an analytical study of using EIVC to mitigate knock and dramatically increase maximum load. This is the first study (to the authors best knowledge) to focus on increasing engine load to what would be considered Deep Miller levels of IMEP and predicted a maximum load with EIVC of almost 22 bar IMEP.

This study predicted that the EOC temperature reducing effects of EIVC could yield a thermal efficiency benefit of approximately 7%, furthermore, it also predicted a torque increase of 7.8%. This torque benefit was maximum at approximately 3000rpm and the thermal efficiency benefit was predicted to be maximum for approximately 4250rpm and above where the need for enrichment was circumvented.

Another noteworthy study of knock mitigation was carried out by Sakata, et al [99]. This study focussed on the effects of increased geometric CR on both knock and thermal efficiency. This study demonstrates the impact of high geometric CR and LIVC on spark timing. It was discovered that the combustion had to be retarded significantly for the high geometric CR cases and the maximum knock limited load was reduced significantly as a consequence of this. However, even with very retarded combustion phasing the highest geometric CR case tested was still the optimum for ISFC. The peak load was however obtained at a much lower geometric CR.

The most recent study to encroach on what would be considered Deep Miller is that of Taylor, et al [64] who tested at a peak load of 15 bar BMEP with the Mahle cam in cam system. The increased load on the intercooler, runner temps, 50% MFB point and various other attributes were monitored to see what impact high load LIVC had on them.

The intake manifold temperature was observed to increase significantly due to the back flow of residual gasses and charge that had been purged from the cylinder as part of the LIVC process. This elevated the charge temperature markedly. In spite of this the 50% MFB point could still be advanced by 4 Crank Angle Degrees (CAD). With the intake manifold temperature elevating effects of LIVC cancelled out, the 50% MFB point could be advanced by up to 12 CAD. This yielded a thermal efficiency benefit of up to 3.2%.

Turner, et al [50] carried out an analytical investigation into the use of EIVC at high loads of up to 35 bar BMEP on the Jaguar Land Rover Ultraboost engine. EIVC and low peak valve lift was found to offer the greatest improvement at low engine speeds (approximately 6%). The BSFC improvement was lost very rapidly with increasing speed however, with there being negligible difference in BSFC between the shorter 214 CAD duration cam and the standard 250 CAD duration cam above a speed of approximately 2500rpm.

This area is of great research interest at this moment in time due to the need for ever higher engine loads to be achieved at lower engine speeds. Current projects such as the Jaguar Land Rover Ultraboost project and the likes of Ricardo have expressed a great deal of interest in Deep Miller.

2.5 Summary

This chapter contains all of the past work and results from all of the major publications in the history of the Miller/Atkinson cycle. It has also explained the future direction of Miller cycle research such as exploring Deep Miller operation. It also reflects how the Miller cycle has great potential to be employed on future gasoline ICEs as both a short term and long term technology for reducing emissions and improving fuel economy. The current and future emission limits that all ICEs must adhere to has also been explained and outlined.

This chapter explains all of the relevant literature for the Miller/Atkinson cycle work carried out in this thesis. It also helps to explain what has been discovered in this thesis and whether or not a similar discovery has been obtained before and whether or not the result obtained contradicts any of the results obtained in previous test work. It has also demonstrated where the gaps in knowledge with regard to the Miller cycle exist and how best to research this subject further.

Chapter 3

Experimental Test Facility

3.1 Introduction

This chapter describes the experimental test facility used to obtain all the experimental data contained in this thesis. It also describes the data acquisition system used and how the raw in-cylinder pressure data was analysed to retrieve key experimental data.

The test facility used for this test work was designed from new by the author. This includes installation of a new dynamometer, AC drive, dynamometer control unit, boost rig, exhaust system, extractor fan, gas sensor, fuel supply, data acquisition system as well as 3-phase and single phase power.

The engine used is a Mahle downsized 3 cylinder head mated to a single cylinder Ricardo Hydra bottom end. A cylinder block therefore had to be designed, an additional plate also had to be designed to accommodate the cam drive system.

3.2 Experimental Setup

3.2.1 Engine Description

The crankcase used for all test work was from a Ricardo Hydra single cylinder engine. It is a single cylinder crankcase with a speed range of 600 – 5400rpm and capable of withstanding peak cylinder pressures of up to 140 bar. The single cylinder engine is unique in that the cylinder heads are interchangeable. The mode of operation is therefore dictated by the head and it can potentially be run as a 2-stroke or 4-stroke and with either gasoline SI or diesel CI.

The cylinder head used for all test work is the standard 3 cylinder head as found on the Mahle 1.2l 3 cylinder downsized engine (Figure 3.1). A cylinder block has been designed to mate the cylinder head to the crankcase. This cylinder block has been designed to provide the cylinder head with the required coolant and oil supplies with as little modification to the cylinder head as possible. The only modification that had to be done to the cylinder head was the drilling of a hole which serves to act as an emergency oil drain should the head overflow with oil.



Figure 3.1 The Mahle 1.2l 3 Cylinder Advanced Downsizing Engine (Hancock, et al [48])

The Mahle 1.2l 3 cylinder downsized engine is an advanced downsizing technology demonstrator engine designed by Mahle (Hancock, et al [48]). It has been designed to replace a 2.4l V6 PFI engine that one would typically find in a class C or D European vehicle with a weight of around 1600kg. It has also been designed to achieve a fuel consumption reduction of around 30% over the V6 over the NEDC cycle, whilst simultaneously complying with Euro 5 and ULEV2 emissions standards. The Mahle 1.2l 3 cylinder downsized engine makes use of central GDI with a piezoelectric fuel injector and injection pressures of up to 200 bar.

The 3 cylinder engine exists in 3 different guises, a single turbo version capable of a peak power and peak torque of 90kW and 210Nm respectively, and a twin turbo version capable of a peak power and peak torque of 144kW and 286Nm respectively. This corresponds to peak BMEP values of 22 bar and 30 bar for the single turbo engine and the twin turbo engine respectively. Both of these engines have a geometric CR of 9.75. A third single turbo variant has also been made, this has a maximum power output of 120kW and a geometric CR of 9.3.

The third variant of this engine (or the second generation engine) has been fitted to a Volkswagen Passat (Figure 3.2). This “mule” test vehicle has achieved an NEDC fuel consumption figure of 5.8l/100km and an NEDC CO₂ output figure of 135 g/km. The engine also achieved a 80-120 km/h fifth gear acceleration time of 8.9 seconds (Fraser, et al [100]).



Figure 3.2 The Mahle Downsized Demonstrator Vehicle

3.2.1.1 Single Cylinder Engine Description

The single cylinder engine (Figure 3.3) has a bore of 83mm and a stroke of 73.9mm, the same as that for the Mahle 3 cylinder engine, and a displacement of 400cc. The single cylinder engine uses the same connecting rod and similar piston as on the 3 cylinder engine, although the piston on the single cylinder engine gives a geometric CR of 9.25. It is possible to alter the geometric CR slightly with the same piston by adding or subtracting shims that are placed between the crank case and the cylinder block. Without changing the piston, this is the only variation in geometric CR that can be obtained.

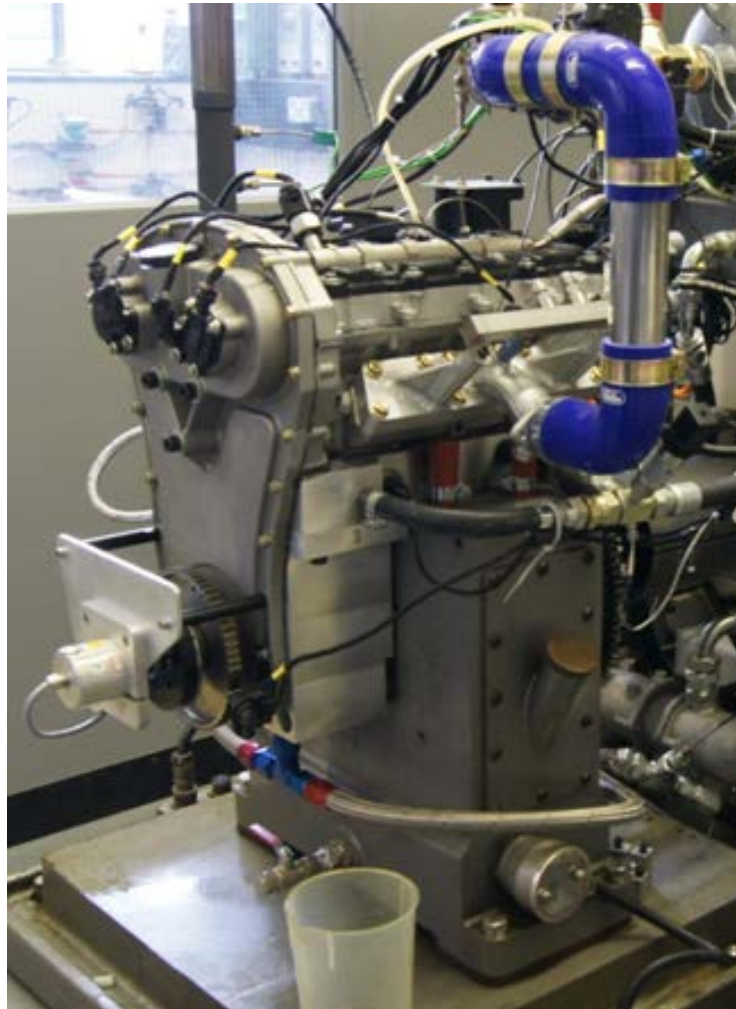


Figure 3.3 The Brunel Single Cylinder Downsized Engine

The engine has a 70lb flywheel. It is this component that imposes the 140 bar average peak cylinder pressure constraint. It is also this component that limits the maximum speed of the engine to 5400rpm.

In total 3 different intake cam profiles (152 CAD short profile, 240 CAD standard profile and 292 CAD long profile) and 1 exhaust cam profile (276 CAD standard profile) were used for all test work (profiles given in appendix A.1). Both the intake and exhaust valves can be phased within ± 20 CAD of a set point.

The single cylinder engine consists of the 3 cylinder head from the standard Mahle 1.2l 3 cylinder downsized engine mated to a single cylinder Ricardo Hydra crankcase by means of a bespoke cylinder block (see section 3.2.1.2).

The middle cylinder of the cylinder head is used as the firing cylinder for this engine, the other 2 cylinders have been blanked off. The valve holes for cylinders 1 and 3 have also been blanked off, as well as the oil gallery for the hydraulic lash adjusters, to ensure that the cavity between the top of the cylinder and the cylinder block does not fill with oil.

The middle cylinder was used because of geometrical constraints imposed by the flywheel. In order to maintain the same geometric CR and stroke of the 3 cylinder engine whilst using the same components as the 3 cylinder engine, the cylinder head had to be mounted just 54mm above the top of the crankcase. The flywheel however projects over the top of the crankcase by 41mm leaving very little clearance between the head and the flywheel, whereas over the front of the engine there is no such constraint. This meant that the cam drive sprockets were projected somewhat forward of the front of the crankcase cam drive system. In order to compensate for this offset a plate had to be designed to house the cam drive system. This plate was mounted on the front of the crankcase and also housed the cam chain tensioner.

3.2.1.2 Cylinder Block Design

The cylinder block had to be designed specifically for this application owing to very tight geometric constraints and the need for a very robust design which can withstand very severe autoignition or “superknock” cylinder pressures of up to 250 bar. The block has a total height of 54mm at its thickest point and incorporates galleries for head coolant, block coolant, oil supplies, oil draining and fixings (Figure 3.4).

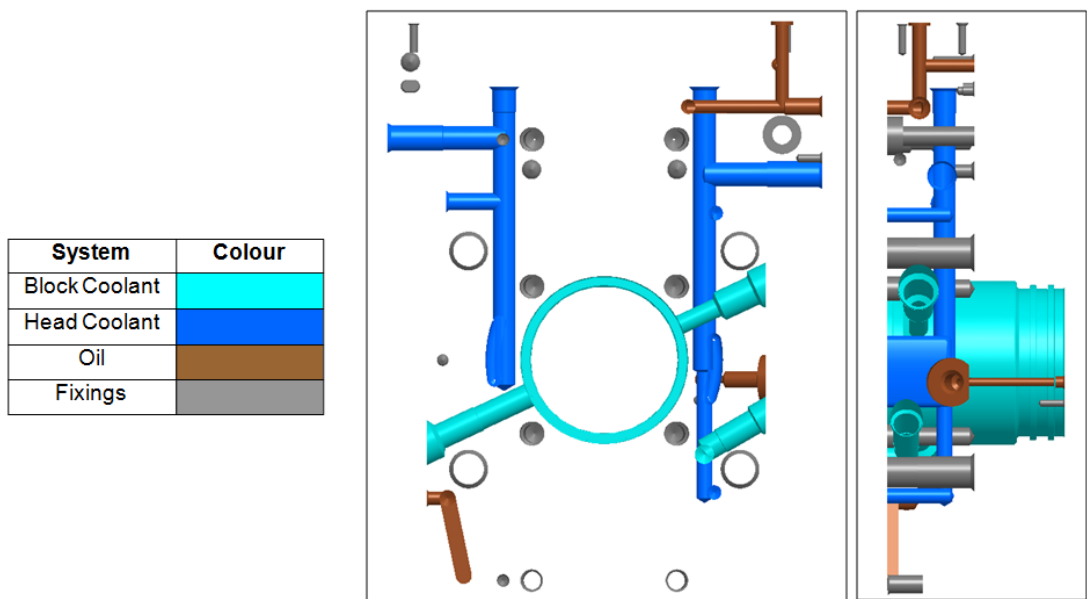


Figure 3.4 Cylinder Block Plumbing

The head is designed for cross flow type coolant flow. This has been maintained for the most part in the cylinder block design however the flow will be more fan like than straight across owing to the fact that there is just 1 orifice on cylinder 2 for head coolant feed and holes for all cylinders on the head coolant return side. This has been done to prevent flow stagnation in the proximity of cylinder 2 while ensuring the majority of the flow goes around cylinder 2.

Figure 3.4 also shows the positions of the cylinder head mounting bolts. There are 8 in total which are located the cylinder side of the 2 main head coolant galleries and running parallel to them. These bolt holes have been designed to provide the

required gasket clamping force of 100kN. A simplified version of this block has been analysed in ANSYS V11.0 [101] in an effort to ascertain where the greatest stresses occur and what material is best suited to its construction (Figure 3.5). Figure 3.5 shows the factor of safety when grey cast iron is used, and also shows that the parts of the structure exposed to the greatest stresses are the fixing holes. In this scenario the entire length of the holes are threaded, however, it was later found that employing a small counter thread of 10mm and a chamfer of 0.5mm reduced the stress concentrations to such an extent that aluminium could be used in the blocks construction instead.

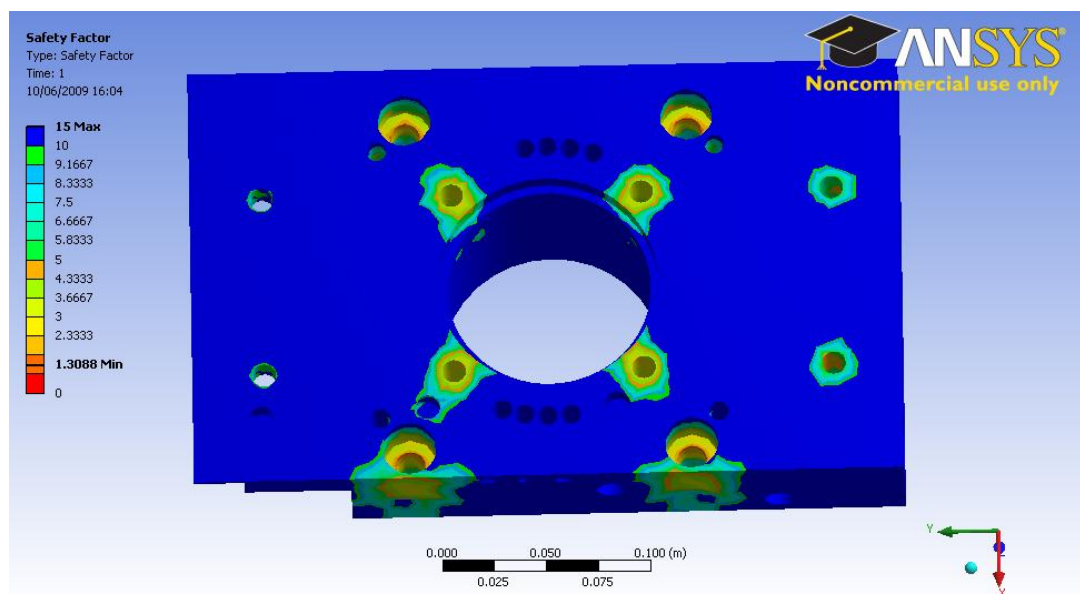


Figure 3.5 Ansys Plot of Factor of Safety

Aluminium is the preferable material to construct the cylinder block out of because of its corrosion inhibiting properties, ease of machining and the fact it has the same coefficient of thermal expansion as the cylinder head (which is also aluminium), which will reduce warping effects and damage to the head gasket.

The block coolant jacket geometry has been designed to accommodate an aluminium liner with Nikasil coating as developed for a previous single cylinder Mahle project and found to be robust.

There is room for minor adjustment of geometric CR by the fitment of shims between the cylinder block and the crankcase. The block also features many dowels

which are used to correctly locate the other components such as cylinder head, crankcase, head gasket and the cam drive plate.

3.2.2. Oil System

The hydra crankcase features a wet sump oil lubrication system, standard Mobil1 0W-40 oil was used for all test work. The crankcase also contains 2 1kW electric oil heaters in the sump to preheat the oil before running. The oil is circulated externally to the engine by means of a single speed 3-phase electric oil pump located at the back of the test cell. This pump imposes no parasitic loss on the engine. The oil is filtered by means of an AC Delco X19 equivalent oil filter mounted on the test bed next to an oil heat exchanger. The maximum heat rejection rate of this heat exchanger is 4kW. The rate of heat rejection is controlled by a Spirax Sarco capillary actuator which is used to control the flow rate of raw cooling water through the heat exchanger.

Oil temperature and pressure are measured at multiple points in the oil system. The pressure is monitored by means of 3 different sensors, 1 is an analogue gauge, another sensor is a Druck 4.20mA feedback pressure sensor which is connected to a low speed data acquisition system, the third sensor is a pressure switch sensor for the dynamometer emergency stop system. Temperature is monitored in 3 different positions. It is measured by 2 Platinum Resistance Thermometers (PRTs) located about 500mm upstream of the crankcase oil gallery, one for the low speed data acquisition system, and the other for the dynamometer emergency stop system. Another PRT is located around 200mm downstream of the oil sump, this is connected to the low speed data acquisition system. The temperature is monitored both before and after the engine so an idea of the rate of heat addition to the oil across the engine can be obtained.

The oil system has a nominal flow rate of 9.1 l/min which is fed to a single oil gallery in the crankcase. This oil gallery distributes oil through 3 different hoses, 1 for lubricating the cams, 1 for the hydraulic lash adjusters and the final one for the cam

drive system (chain tensioner, chain lubricant and cam phasers), there is also a fourth outlet for the oil gallery which is for the piston cooling jet located inside the crankcase. Depending on which cam was employed, there was also a fifth oil feed for the high pressure fuel pump. The oil heaters have no temperature ceiling and are controlled by means of a manually operated instrument panel located on the test bench.

The oil pressure varies greatly depending on the oil temperature, typical pressures are 6.5 bar abs when the oil is at room temperature and 4.25 bar abs when the oil is at 90°C. The oil pressure cannot be regulated. A maximum oil temperature of 90°C was implemented in order to stop the oil pressure dropping below a minimum of 4.25 bar abs.

A schematic diagram of the oil system is shown below (Figure 3.6):

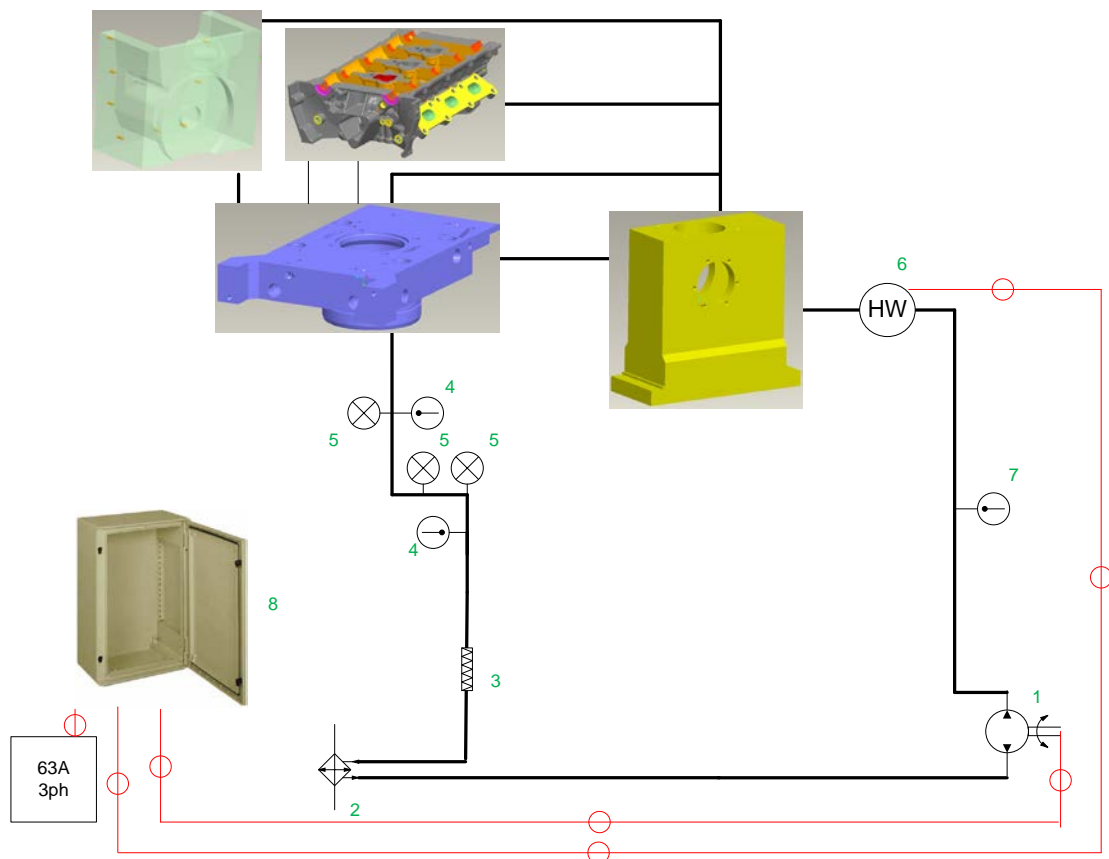


Figure 3.6 Oil System Schematic Diagram

Where the components are numbered as follows:

1. Oil pump 3-phase 9.1l/min

2. Oil heat exchanger (4kW heat rejection)
3. Oil Filter (AC Delco X19 or equivalent)
4. 2 x Inlet PRTs
5. 3 x Pressure sensors (Analogue gauge, pressure switch and Druck PTX 1400 0-10 bar)
6. Oil heaters (2 x 1kW immersion in crankcase)
7. Outlet PRT
8. Power/control cabinet

The cabinet in Figure 3.6 with the red lines leading from it is a 3-phase power supply. Figure 3.6 is slightly inaccurate in that it shows the oil being drained from the cylinder head directly, it is actually drained from the head via the block. It also does not show the oil supply to the high pressure fuel pump.

3.2.3 Coolant System

The coolant system is also external to the engine (3-phase single speed electric pump located at the back of the test cell), and imposes no parasitic losses on the engine. The coolant used for all test work was a mix of 50% de-ionised water and 50% ethylene glycol. The coolant system also features a 3kW immersion heater to preheat the coolant before engine running. The rate of coolant heat rejection is controlled by a capillary actuator which regulates the raw water flow through a coolant heat exchanger. The maximum rate of heat rejection of this heat exchanger is approximately 53kW.

The cooling system for this engine is quite unique in that it has split cylinder head and cylinder block cooling. The test bed has been set up so the flow rate of coolant through the cylinder head and block can be varied independently of each other. There is also a coolant bypass which allows the flow rate of coolant for the entire engine to be varied. To an extent the pressure can also be varied, but not independently of flow.

To ensure that the cylinder head is full of coolant, and that no part of the cooling jacket is not sufficiently submerged in coolant, the coolant tank has been located 121mm (H) higher than the highest point of the coolant jacket (Figure 3.7).

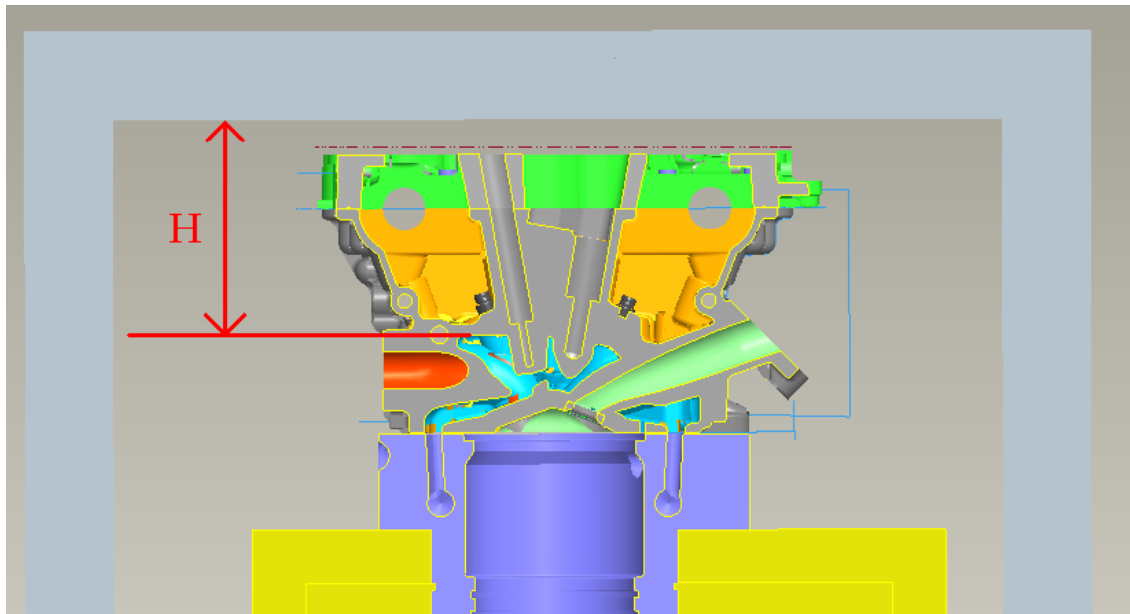


Figure 3.7 Coolant Jacket Height Relative to Coolant Tank Height

The flow rate through each section of the coolant system is controlled by means of 3 ball valves, one for the head coolant, one for the block coolant, and another for the bypass circuit, as shown in Figure 3.8. The 2 coolant flow meters have been located upstream of the ball valves and in straight sections of pipe to ensure the turbine type flow meters give as accurate a reading as possible.

The coolant pressure is monitored by means of a Druck 4.20mA pressure sensor which is located approximately 200mm upstream of the inlet side of the cylinder block at a tee where the flow splits. The feed for both the coolant and the block is common up until this tee. The head and block coolant outlets are isolated from each other from this tee up until the coolant tank where they are recombined. The main purpose of this pressure sensor is to allow a means of monitoring coolant pump health, but also to ensure constant pressure when varying the coolant flow rates. The coolant pressure is typically between 1.2 and 1.5 bar abs depending on the temperature and running condition.

The coolant temperature is monitored in 5 locations by 4 PRTs and 1 thermocouple. One PRT is located approximately 200mm upstream of the inlet of the cylinder block in the same tee as the pressure sensor. This is to monitor the coolant inlet temperature. Another 2 PRTs are located approximately 500mm downstream of the outlet side of the cylinder block and head, this is to monitor the coolant outlet temperatures. The final PRT is located in the coolant tank is used for the dynamometer emergency stop system. A K-type thermocouple is located in the coolant heater reservoir tank to ensure that the coolant heater does not exceed its maximum temperature and that no boiling occurs.

The coolant pump is a 3-phase Beresford pump and has a nominal flow rate of 32 l/min with no ability to change this flow rate. This flow rate was reduced somewhat with the pump in situ on the test bed to a maximum of 11 l/min. The coolant heater has no temperature ceiling although it is fitted with a thermostat that will disable the heating element once the temperature exceeds 80°C. The heaters are controlled by means of a manually operated instrument panel located on the test bench.

The relatively low maximum coolant flow rate imposed a significant constraint on the peak speed and load the engine could be run at. Although the maximum coolant temperature could be regulated with relative ease due to the high heat rejecting capacity of the heat exchanger, the temperature difference across the engine (between the coolant inlet and outlet) is dictated purely by coolant flow rate and no other component. A typical ΔT between the inlet and outlet for a production engine is 2 - 10°C, with poorly designed engines peaking at about 15°C. The engine was run at a maximum ΔT of 14°C for baseline work, but a severe engine failure followed soon after which resulted in a blown head gasket and softening of the cylinder head. After this a ΔT maximum limit of 6°C was imposed.

An additional 12V DC automotive style coolant pump was later employed in an attempt to boost the maximum coolant flow rate. Due to the high resistance nature of the coolant system plumbing, the effectiveness of this pump was compromised and delivered no more than the Beresford pump. For some test work both pumps were

employed and between them managed to deliver a maximum coolant flow rate of 13.5 l/min.

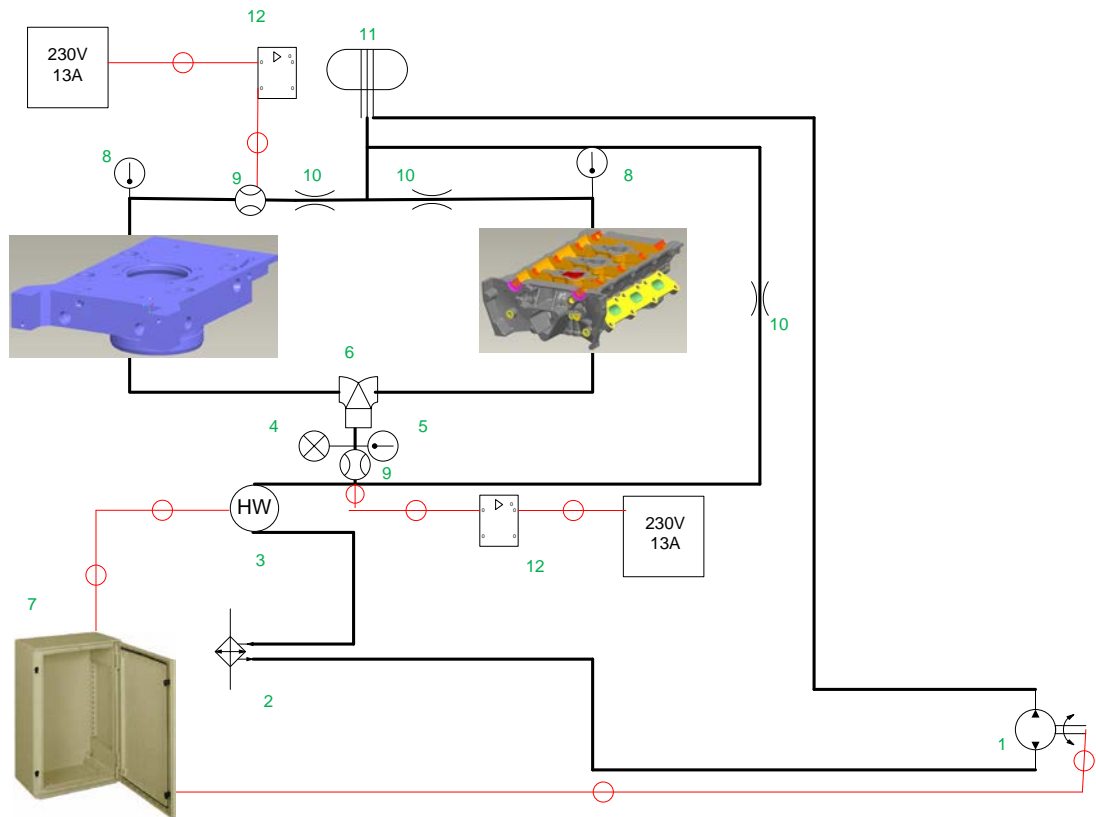


Figure 3.8 Coolant System Schematic Diagram

Where the components are numbered as follows:

1. Coolant pump 3-phase 32l/min
2. Coolant heat exchanger (heat rejecting capacity in the region of 53kW)
3. Coolant heater with thermocouple (3kW Redring immersion heater in a reservoir)
4. Pressure sensor (Druck PTX 1400 0-4 bar)
5. Inlet PRT
6. Tee (0.5")
7. Power/control cabinet
8. 2 x Outlet PRTs
9. 2 x Outlet flow meters (Apollo RN3/15 flow meter and Apollo RN3/20 flow meter)
10. 3 x Ball valves

11. Coolant tank

12. 2 x Flow meter pulse counters (Apollo WFC/5 frequency to current converter)

The cabinet in Figure 3.8 with the red lines leading from it is a 3-phase power supply. Figure 3.8 is slightly inaccurate in that it shows separate coolant flows from the head and the block, in actual fact the flow from the head is output via a completely different gallery within the block.

3.2.4 Fuel System

The fuel used for all test work is standard pump Unleaded Gasoline (ULG) with a Research Octane Number (RON) of 95. The gasoline is circulated around the Brunel University engine laboratory by means of a pump. All of the fuel lines around the laboratory are of stainless steel construction to avoid the contamination effects associated with the use of copper pipes as documented by Pereira, et al [102].

A schematic diagram of the fuel system is shown below (Figure 3.9). The temperature of the fuel was controlled by means of a heat exchanger. Manual control of the fuel temperature was employed throughout all test work. The temperature of the fuel is measured in 2 locations, the first point being a PRT sensor located immediately downstream of the low pressure fuel pumps. The second point where the fuel temperature was measured was in the coriolis flow meter employed to measure the fuel flow rate, although this temperature was not recorded for any test work.

The fuel pressure is monitored in 2 locations, the first point being immediately downstream of the low pressure pumps by means of a 4.20mA Druck pressure sensor. The second pressure sensor is an automotive type pressure sensor located in the common rail. This pressure sensor is connected to the Engine Management System (EMS) only, it was recorded for all test work.

The fuel flow rate was measured with an ABB FCM2000 coriolis flow meter with a DN1.5 size sensor. This flow meter can also output the fuel density and temperature although these values were not recorded for any part of the test work.

A port for the purging of fuel vapours is located in the low pressure circulation part of the fuel system to avoid potential vapour lock issues. This has been installed in case of any problems, but the fuel system is actually void less so this is not anticipated to be an issue and is for redundancy only.

The engine has a PFI system as well as a centrally mounted DI system, although only the DI system was used for this test work.

The fuel is fed from the laboratory fuel supply circuit to the low pressure pumps under the force of gravity. These low pressure pumps are powered by an external 12V supply and impose no parasitic loss on the engine. The fuel pressure is regulated by means of a fuel pressure regulator located approximately 300mm downstream of the pumps. The regulator regulates the pressure to approximately 4.8 bar abs. The fuel that has been purged from the regulator forms a local low pressure fuel circulation system. This low pressure fuel circuit incorporates the heat exchanger and a filter.

The fuel that is not circulated is fed to a high pressure pump via the coriolis flow meter. The high pressure pump is powered by the engine intake camshaft. Its power requirement is unknown but it is expected to be quite large due to the fact it has been designed for much larger multi cylinder engines. This is expected to be one of the largest parasitic losses imposed on the engine. The high pressure pump is a lossless type pump and requires no bypass back to the low pressure system.

The common rail used for all test work is the original common rail used on the 3 cylinder engine with 2 of the ports blanked off. The injector is a piezoelectric type direct injection injector with a maximum design pressure of 200 bar. It is an outward opening type.

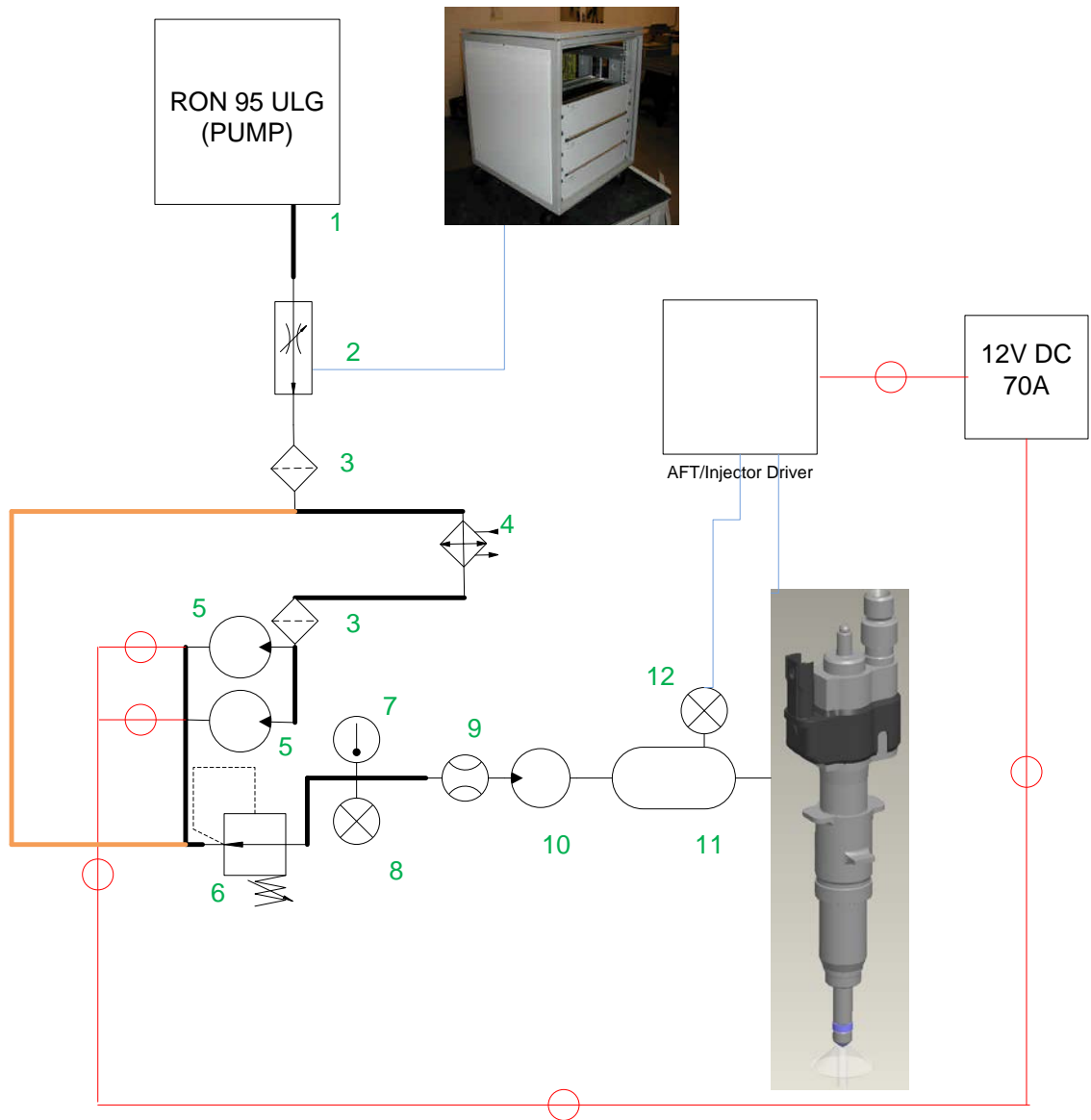


Figure 3.9 Fuel System Schematic Diagram

Where the components are numbered as follows:

1. RON 95 ULG fuel supply (regular pump fuel)
2. Solenoid ball valve
3. 2 x Fuel filters (Delphi)
4. Fuel heat exchanger
5. Low pressure fuel pumps
6. Pressure regulator

7. PRT
8. Low pressure sensor (Druck PTX1400 0-10 bar)
9. Fuel flow meter (ABB FCM2000)
10. High pressure fuel pump
11. Common rail
12. Rail pressure sensor (automotive type)

3.2.5 Intake System

3.2.5.1 Pipes

The intake system is constructed from a mixture of materials including rubber hose (from the compressor to the pressure regulator) which has been rated at pressures of up to 8 bar abs (the automotive style sensors in the system restrict this to 4 bar abs however). This also allows flexibility in terms of the compressor and pressure regulator placement, and has been employed with the intention of reducing the number of pressure reducing elbows in the intake system. The pipe work between the pressure regulator and the plenum is mostly stainless steel construction to support the weight of the charge air heater.

The pipes between the compressor and the plenum are all 1" diameter and have been sized to eliminate the possibility of choking at any point in the system. The pipes downstream of the plenum are all 1.5" and they are a mixture of stainless steel, aluminium and silicon tubing construction. Owing to the vacuous environment downstream of the throttle the use of silicon tubing has been minimised to make "pinching" less likely. The silicon tubing has been designed to be the weak point of the system and is intended to simply blow apart if the pressure in the plenum becomes too high as the result of a pressure regulator fault.

The intake system post throttle has been designed to have as few interruptions in the general airflow as possible in an effort to make the airflow through the intake system more predictable and smooth.

3.2.5.2 System Details

Owing to the fact a single cylinder engine was used for all test work, a turbocharger could not be used. Compressed air was provided by an industrial compressor instead. A schematic diagram of this system (also known as the boost rig) is shown in Figure 3.10. The compressor used was a Compair HV22RS AERD hydrovane type compressor. It consists of a 22kW motor with a hydrovane compressor, an intercooler, a refrigerant drier unit, a 5 micron oil filter and a 250l receiver.

The refrigerant drier was employed for all test work to provide consistent air as humidity has been found to have a minor effect on the properties of the air (Taylor [103]) and will have an impact on the propensity for an engine to start knocking. The refrigerant drier dries the air to <3% humidity, no hygrometer was employed to check the charge air humidity at any point during the test work. Dry air has the highest ratio of specific heats and is therefore detrimental to turbocharged engine efficiency. Therefore the data obtained from all test work will be slightly pessimistic in comparison to data obtained from the 3 cylinder engine running in a typical northern European climate.

This compressor delivers a maximum flow rate of $3.88\text{m}^3/\text{min}$ effective at 1 bar abs ($4.61\text{kg}/\text{min}$) and delivers this at a minimum pressure of 7 bar abs. The pressure is regulated down to more suitable pressures by means of a Parker Hannifin EPDN4 closed loop control pressure regulator located downstream of the compressor in the test cell. This pressure regulator is controlled by the EMS directly. The EMS pressure sensor used to regulate pressure is a standard Bosch automotive pressure/temperature sensor located downstream of the plenum and upstream of the throttle.

The degree of pressure control achievable through this pressure regulator is not very precise due to the fact it was not designed for precise pressure regulation but for regulating large amounts of flow from very high pressures. Pressure control is typically ± 0.15 bar of the requested pressure, therefore where possible the throttle

was used to achieve more refined control of the pressure so that the variability of boost pressure is less than ± 0.08 bar.

A 3kW Secomak 632 charge air heater is located downstream of the pressure regulator to elevate the charge air temperature to a more representative post compressor temperature. A heater is required to heat of the charge air because the compressor intercooler has a very high rate of heat rejection such that the charge air temperature is typically just 8°C above the ambient temperature. The Secomak 632 is not designed as a charge air heater, it therefore had to be modified somewhat by sealing it up with a non-silicone based sealant (because silicone has the possibility of contaminating the air supply). The heater is controlled by means of closed loop control based on the feedback from a K-type thermocouple located in the “plenum” pressure vessel. The precision of control is $\pm 1^{\circ}\text{C}$.

The next component in the system is the plenum which is a 40l stainless steel cylindrical pressure vessel. It has been sized on what experience of previous single cylinder engines has deemed the optimum size for a plenum for an engine of this size. The pipe downstream of the plenum has also been sized depending on what previous experience has deemed most appropriate. Three cylinder engines benefit from the fact that the cylinders are 240 CAD out of phase which is almost exactly the duration of typical intake and exhaust valve events, this means there are very few cylinder to cylinder interaction effects and the flow of air through the engine is fairly constant. This breathing effect is very difficult to duplicate with other engine configurations, particularly on a single cylinder engine. A very large diameter intake manifold was used, as well as a very large plenum volume to try and reduce pressure and rarefaction waves as much as possible.

Located downstream of the plenum is a tee. This tee connects the plenum to the throttle primarily, with the third junction being a ball valve which allows the engine to be run in NA mode. This ball valve can also be left slightly open to enhance boost pressure control at low flow conditions by bleeding some air off thus artificially increasing the flow rate through the compressor and pressure regulator.

The throttle is placed post plenum which is unconventional for most automotive engines, however, given the size of the plenum and the relatively unstable control of the pressure regulator the throttle was located post plenum in an effort to improve control. One and a half inch pipe was also employed post throttle in an effort to create as large a volume as possible. The throttle is a standard automotive electrically actuated throttle (Bosch DV-E5 40mm) with integrated position sensor. The throttle is controlled by the EMS, although the throttle position is dictated by the dynamometer, allowing closed loop control of load if required.

Automotive type pressure and temperature sensors are located both upstream and downstream of the throttle to give the EMS pre and post throttle temperatures and pressures. The post throttle sensor was used to control boost pressure and temperature.

An automotive type Mass Air Flow (MAF) sensor was employed slightly downstream of the post throttle pressure and temperature sensor. This is a 1-way hot wire type sensor and is therefore of limited effectiveness as the air flow in this region of the intake is pulsing rather than steady. The sensor feedback was treated as an indication only. The sensor was located in straight unobstructed section of approximately 4 pipe diameters upstream and downstream of the pipe to ensure the flow was as uniform, and the flow measurement was as accurate, as possible. Location of this sensor in a position of steady flow was not possible because the only section long and straight enough would have been the feed to the pressure regulator which is never below 7 bar abs pressure, which is too great for the sensor.

Approximately 80mm upstream of the intake port is a Kistler 4005BA10FA0 piezoresistive pressure transducer, details of which can be found in the data acquisition section of this chapter (Section 3.3). The final component in the intake system is a PRT temperature sensor which is located directly in the intake port to give the charge temperature going into the engine, or to give an indication of engine breathing.

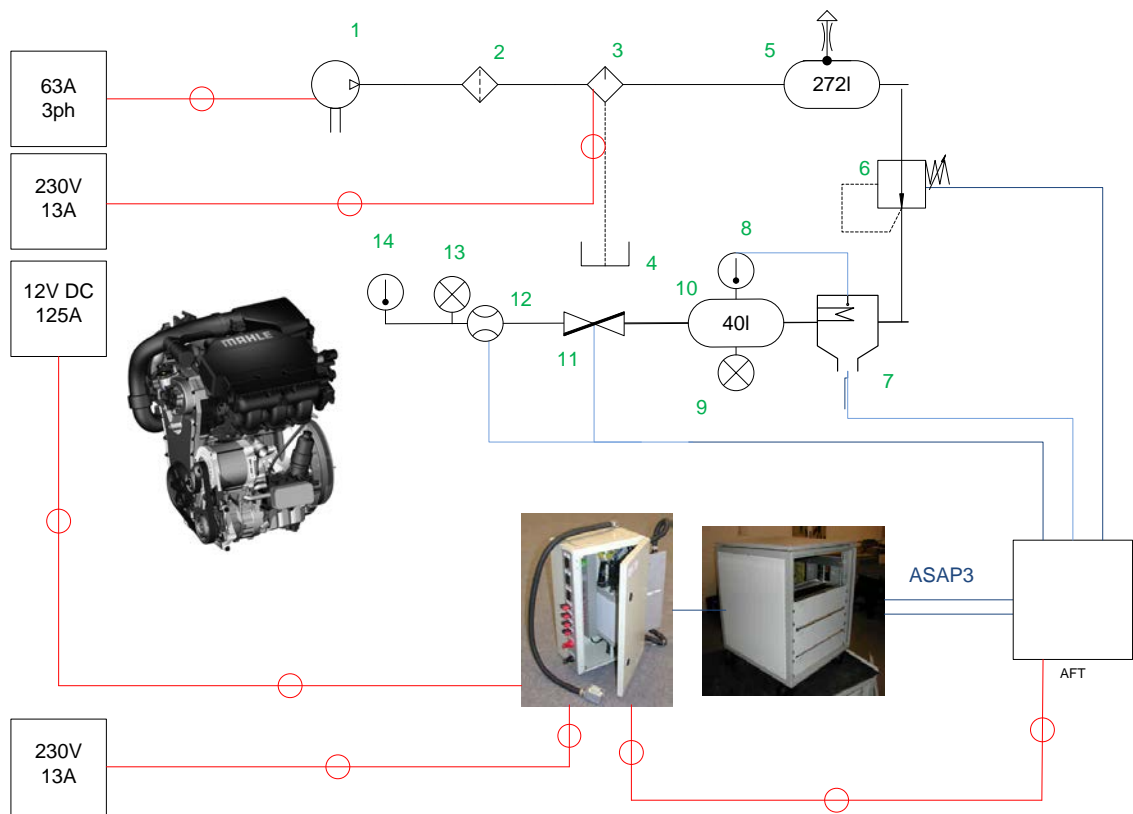


Figure 3.10 Intake System Schematic Diagram

1. Compressor (Compair HV22RS)
2. Filter
3. Air refrigerator dryer (cools to 3⁰C)
4. Drain
5. Receiver 272l
6. Pressure regulator (Parker electronic pressure regulator EPDN4)
7. Intake heater (Secomak 632)
8. K-type thermocouple (RS 397-1539)
9. Analogue pressure gauge
10. Accumulator (40l)
11. Throttle (Bosch DV-E5 40mm)
12. MAF sensor
13. Pressure transducer (Kistler 4005BA10FA0)
14. Temperature sensor (PRT RS 611-8264)

3.2.6 Exhaust System

3.2.6.1 Design

The exhaust system is a mixture of stainless steel and austenitic stainless steel construction and has been designed to withstand exhaust gas temperatures of up to 980⁰C at pressures of up to 4 bar abs average.

Like the intake the exhaust has been designed to have no sudden/step changes in pipe diameter purely in the interest of keeping the exhaust flow as predictable as possible. Also like the intake system, the single cylinder nature of the engine will result in drastically different breathing dynamics compared to the 3 cylinder engine. Although the breathing dynamics can be changed by installing a surge tank, the breathing is still not going to resemble that of the 3 cylinder engine so a surge tank has not been installed.

Where possible the exhaust components have been shrouded in insulation to minimise the possibility of injury. The exhaust system has also been mounted as high as possible in the cell, with as minimal an area possible at operator height.

3.2.6.2 System Details

A schematic diagram of the exhaust system is shown in Figure 3.11. The first component in the exhaust system is a K-type thermocouple that is located in the exhaust port to give the exhaust port temperature. A more precise PRT type temperature sensor would have been used for this application but PRTs cannot withstand temperatures of up to 980⁰C and could therefore not be used.

The cross sectional profile of the exhaust runner changes at this point from the straight oval shaped exhaust port geometry to a 1" circle. The transition between these shapes is achieved by means of a 50mm long variable geometry section. This has

been done to ensure no abnormal flow properties such as any considerable turbulence occur in or close to the exhaust port.

A Kistler 4005BA10FA0 piezoresistive pressure transducer (details of which can be found in section 3.3) with water cooling module is located approximately 100mm downstream of the exhaust port. Approximately 50mm downstream of this is a condensate drain where any condensation that has formed in the exhaust can be drained away. The drain has been sited at the lowest point in the exhaust system. This drain is emptied every day.

Approximately 350mm downstream of this is a low speed Druck PTX1400 pressure sensor (details have been given in section 3.3) to measure the average EBP. The main reason for this is to set the EBP valve correctly. Although the main purpose of this pressure sensor is to control the EBP valve, it is in fact connected to the data acquisition system. Approximately 50mm downstream of this is another K-type thermocouple which has been installed in this location to ensure that the lambda sensor is not being subjected to temperatures out of its design range.

Two hundred millimetres downstream of this is an automotive type Universal Exhaust Gas Oxygen (UEGO) lambda sensor. This is connected directly to the EMS where the lambda is controlled by means of closed loop control as detailed in section 3.2.7. One hundred millimetres downstream of this is a boss for the exhaust gas analysers which have been described in section 3.3.

The next component in the system is an EBP regulating valve. This valve is a butterfly type valve with no plastic components/washers. It seals by means of a gasket and clamps instead of a washer. Owing to design constraints this valve is never in the fully open position, however, the pressure increase caused by this is negligible as the butterfly is so wide open that the restrictive area imposed by the butterfly itself is encompassed entirely in the butterfly shaft area.

This valve is actuated by means of a servo motor connected to the valve by means of a rod. The servo motor is operated remotely through the dynamometer test bed. The pressure control is open loop requiring the user to input a throttle open angle (in %) to give the required EBP.

The exhaust system then exits the cell and exhausts to atmosphere by way of an automotive type muffler and silencer.

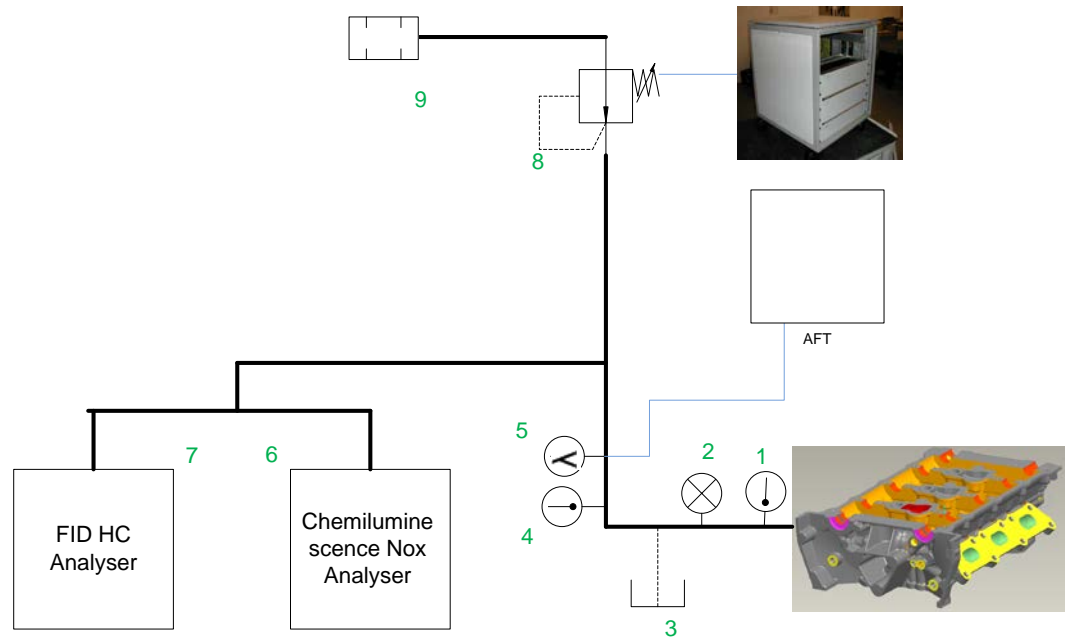


Figure 3.11 Exhaust System Schematic Diagram

1. K-type thermocouple (RS 397-1539)
2. Pressure transducer (Kistler 4005BA10FA0)
3. Condensate Drain
4. K-type thermocouple (RS 397-1539)
5. UEGO AFT Lambda sensor
6. Rotork Analysis Model 443 Chemiluminescence NOx Analyser
7. Rotork Analysis Model 523 FID HC Analyser
8. CPEngineering EBP regulating butterfly valve
9. Silencer (outside building)

3.2.6.3 Conversion of Emissions to Specific Emissions

All emissions were recorded as volume concentrations in parts per million (ppm) initially. These were later converted to indicated specific emissions. This was achieved by firstly converting volume concentrations of the various emissions to mass concentrations, which can then be multiplied by the mass of exhaust gas required to generate 1 kWhr of energy.

Converting volume concentration to mass concentration requires calculation of the ratio of molecular weight of the emission being investigated to the molecular weight of air. Multiplying this by the volume concentration of the emission will give a mass concentration. The molecular weight of NO is 30g/mole. The molecular weight of HCs is the same as that of the span gas used to calibrate the FID analyzer (propane gas) which is 44g/mole. The molecular weight of air is 29 g/mole. The ratio of molecular weights must also be divided by the AFR due to the fact there are many more moles of air per mole of fuel.

This value can be converted from ppm to percentage by firstly dividing by 1,000,000 to obtain a parts per kilogram fraction and then multiplying this by 100 to get a percentage figure. This percentage figure is then multiplied by the amount of fuel required to generate 1 kWhr of power, or the specific fuel consumption. For this work indicated values were used and calculated.

The equation for this conversion (Eq.3.1) is given as,

$$ISem = ISFC * 100 \left(\frac{VC_{em}}{1e^6} \right) \left(\frac{1}{AFR} \right) \left(\frac{M_{em}}{M_{air}} \right) \quad 3.1$$

where $ISem$ is the indicated specific emissions of emission em , VC_{em} is the volumetric concentration of emission em in ppm, and M_{em} and M_{air} is the molecular weight of the emission em and air respectively.

3.2.7 Dynamometer and EMS

The dynamometer used for all test work is a CP Engineering 48kW AC motor with a 4 quadrant AC regenerative inverter drive and an operating envelope as shown in Figure 3.12. The dynamometer is capable of a maximum speed of 6000rpm. The dynamometer is capable of motoring and absorbing 48kW and has a maximum torque rating of 140Nm. The dynamometer is also capable of transient operation although this capability was not used for this test work.

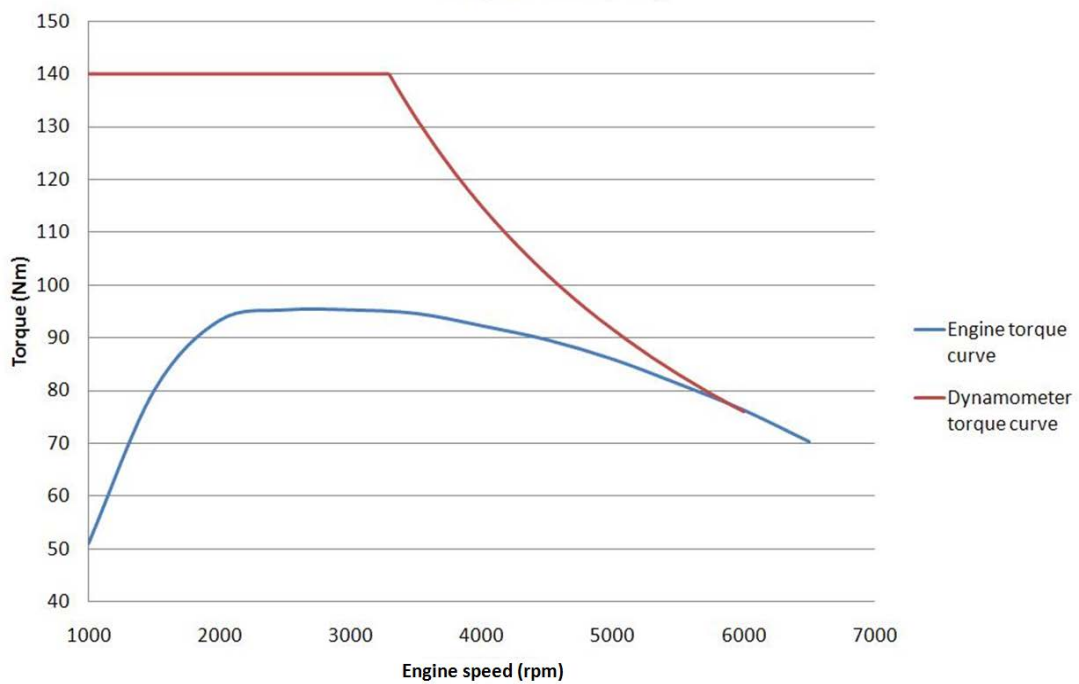


Figure 3.12 Dynamometer Torque Curve and Engine Torque Curve Comparison

Although the CADET V14 light software has limited capability for logging data, it was not used for logging any data for this test work. A dedicated logging system was employed for this purpose instead (see section 3.3). Just one output from the dynamometer was logged and that was the torque reading which was output from the CADET V14 cabinet into the instrumentation system.

A schematic of the dynamometer system is given in Figure 3.13.

Loom 1	Loom 2
Manifold pressure/temp	Connectors:
Fuel rail pressure (DI Only)	Ex cam sensor
Ex cam VCT	Supercharger out pressure
Hot EGR valve	Exhaust pressure
LP fuel pressure (PFI Only)	HP fuel pump (DI Only)
Throttle	Airflow meter
Boost pressure/temp	EGR in temp
Supercharger bypass valve	Supercharger in temp
Coolant temp	Loom 1/loom 2 interface
Exhaust lambda	Power ground
Inlet lambda	Test bed loom interface
Port injector (PFI Only)	Ground
Ignition coil	CAN 1
In cam sensor	CAN 2
In cam VCT	Accelerator pedal
EGR valve	Cylinder pressure
Crank sensor	WO connectors:
Knock sensor	Backpressure valve
Exhaust temp	Injection timing
Cold EGR valve	Ex cam sensor
Throttle position	Error signal
Coil Gnd engine	EGR pump drive
Fuel rail pressure	Ignition
DI INJ (DI Only)	Boost valve drive
Loom 2/loom 1 interface	EGR rate
	Back pressure valve
	Injection enable
	Injection pulse width
	+5V input
	In cam

Figure 3.14 ECU Loom Connection List

The ECU is controlled remotely via a Controller Area Network (CAN) connection which is connected to an ETAS 571.3 interface card which in turn is connected to a computer running ETAS INCA V7.0 [104]. This is the only means of connecting to the ECU with the exception of the ignition and the accelerator pedal inputs which are controlled by the CADET V14 dynamometer control system. The main reason for this is to ensure that some control over the engine is still possible in the event that the computer running the ECU should malfunction. The low pressure fuel pumps are also controlled by the dynamometer and can be used as yet another failsafe in the event of the ECU computer malfunctioning. Besides very primitive control of the engine

through the dynamometer, the only means of controlling the engine is through ETAS INCA V7.0.

Most of the sensor feedbacks can be displayed and logged through ETAS INCA V7.0, shown below is a list of sensor feedbacks that were used for data analysis:

- Manifold pressure
- Throttle position
- Rail pressure
- Injection timing
- Spark timing
- Relative air charge
- Intake cam timing
- Exhaust cam timing
- Exhaust lambda
- Boost pressure

The ECU offers closed loop control of lambda and boost pressure and can be configured to give closed loop control of EBP too, although this feature was not used for this test work. The spark timing is dictated by a map. For this work the ECU was initially configured to use a map of relative air flow and speed to give the spark timing, however, due to the fact that a 1-way flow sensor was used and that the throttle was never truly wide open, the relative air flow value was found to be unreliable so the software was later reconfigured to use a map of MAP and speed instead.

Although the knock sensor was connected it was not used to control spark timing, it was instead connected to an oscilloscope to give an indication to the operator whether or not the engine was knocking. The cylinder pressure was however used almost exclusively to give an indication of whether or not knock was occurring. The main reason for this is because doubts were raised over the effectiveness of the knock sensor given its location at the end of the cylinder head, and the feedback was therefore never fully trusted.

3.3 Data Acquisition and Instrumentation

A list of sensors and their descriptions is given in Appendix A.2.

There are 3 logging systems used for this test work, a device for high speed acquisition, a second one for low speed acquisition and a third for the PRTs. The high speed system is based on a National Instruments (NI) USB-6353, which is capable of logging up to 32 channels (16 differential) and has a maximum sampling speed of 1MS/s when used in a multi-channel configuration. This device logs the following channels:

- Cylinder pressure
- Intake pressure
- Exhaust pressure
- Fuel flow rate
- Shaft encoder clock
- Shaft encoder reference
- Torque

The shaft encoder used with this device is an Encoder Technology EB58-204040. This gives 0.25 CAD resolution which is required for knock analysis, however, the NI USB-6353 uses multiplexing which means all the channels have to be logged at that resolution. At low speeds this is not a problem, but at speeds of up to 5400rpm this card is overwhelmed with data and is not suitable for logging all of the data channels. At 5200rpm this card can handle a maximum of 8 channels. These channels have been configured to run differentially, attempts were made to run them single-ended in an effort to increase the channel count but the noise was found to have too great an impact on the in-cylinder pressure transducer signal.

The low speed system consists of a NI USB 6210. This device is capable of logging up to 16 channels single ended (8 differential). This device logs the following channels:

- Exhaust temperature
- Exhaust manifold temperature
- Total coolant flow
- Block coolant flow
- Oil pressure
- Low pressure fuel pressure
- Coolant pressure
- Average exhaust pressure

The sampling frequency for all test work was 0.5Hz. These channels have also been configured to run differentially.

The PRT acquisition system consists of an eDAM-9015 acquisition card. This card supports up to 7 PRT inputs and connects to the computer by means of a serial connection.

Where possible (and applicable) signal amplifiers have been placed as close as possible to their corresponding sensors in an effort to reduce noise. All sensor cables are also screened and ground to a common ground. This common ground has been used for all instrumentation and is located at the data acquisition card end of the cables. A common ground or “star earth” configuration was used in-order to avoid “ground loops” in the instrumentation. The instrumentation cables have also been placed as far away from power cables as possible, and efforts were made to ensure that power cables never ran parallel to instrumentation cables.

In spite of these efforts the cylinder pressure transducer still exhibited a great deal of noise, so further screening was used on other non-instrumentation cables (the EBP servo cable was found to be a source of considerable noise). The cylinder pressure signal exhibited a maximum of 3mV of noise for this test work. As cylinder pressure is

the most important feedback (noise is indistinguishable from knock and knock cannot be calculated using average values) for this work a disproportionate amount of effort went into ensuring this sensor was noise free in comparison to the other sensors.

Other sensors such as the intake and exhaust pressure transducers exhibited some noise as well, however, these feedbacks can be averaged which cancels out the vast majority of the noise.

3.3.1 Data Acquisition Software

All 3 data acquisition devices pass data to a bespoke software package known as the “Transient Combustion Analyzer” developed at Brunel University by Dr Yan Zhang. The interface of this software package is as shown in Figure 3.15.

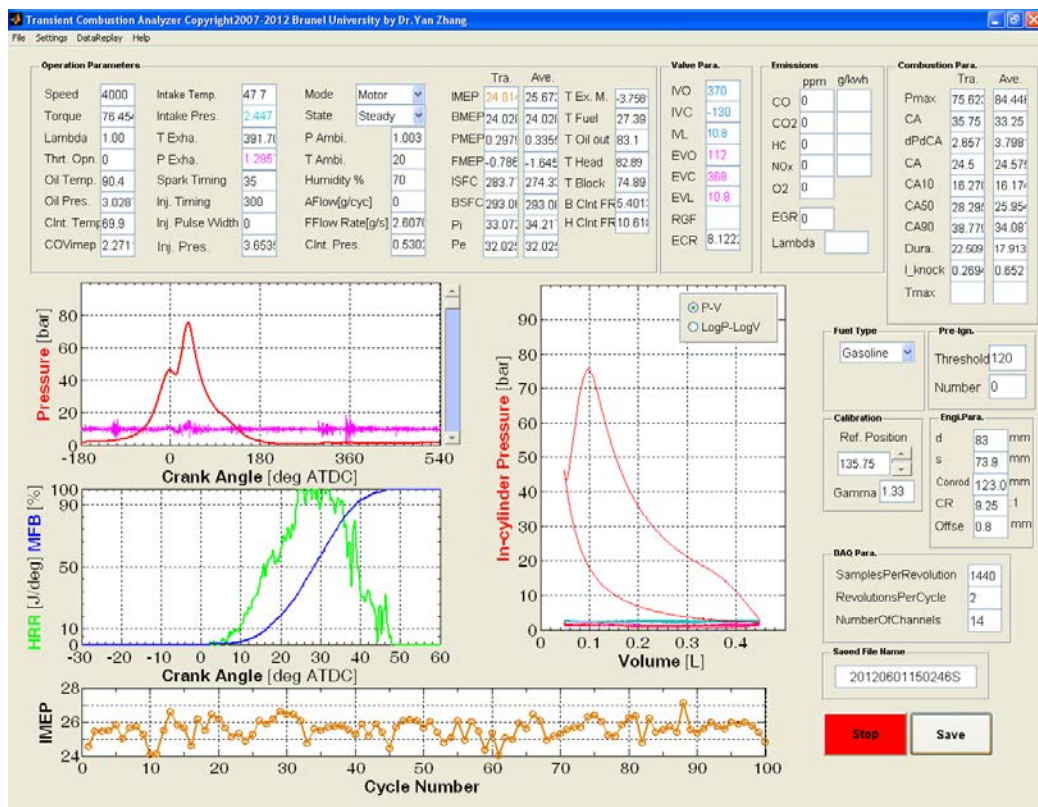


Figure 3.15 Transient Combustion Analyzer Data Acquisition Software Interface

This software gives real time feedback of all low speed channels as well as some of the high speed channels. There are 4 graph windows in the user interface (Figure 3.16) which display the following:

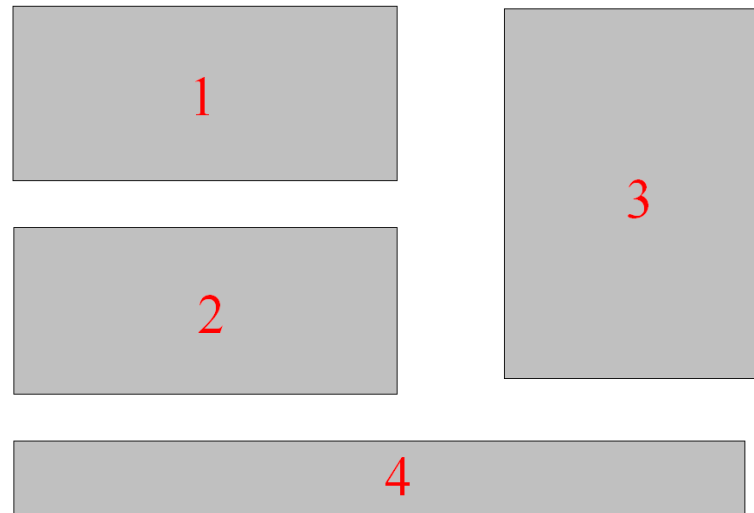


Figure 3.16 Graph Window Layout

Window 1: Cylinder Pressure and knock intensity.

Both of these are updated on a cycle to cycle basis. The cylinder pressure feedback comes directly from the in-cylinder pressure transducer. The Knock Intensity (KI) is a measure of the difference in the actual pressure as reported by the in-cylinder pressure transducer, and the “predicted” pressure. The predicted pressure is calculated by averaging the pressure across the 10 points before and 10 points after the point in question (Eq.3.2). For instance, the predicted pressure (p_n) at a crank angle n is calculated by taking the average of the points from $(n - 2.5)$ up to $(n + 2.5)$ at 0.25 CAD resolution as shown graphically in Figure 3.17. Both cylinder pressure and KI are plotted against the engine crank angle as determined by the shaft encoder clock signal.

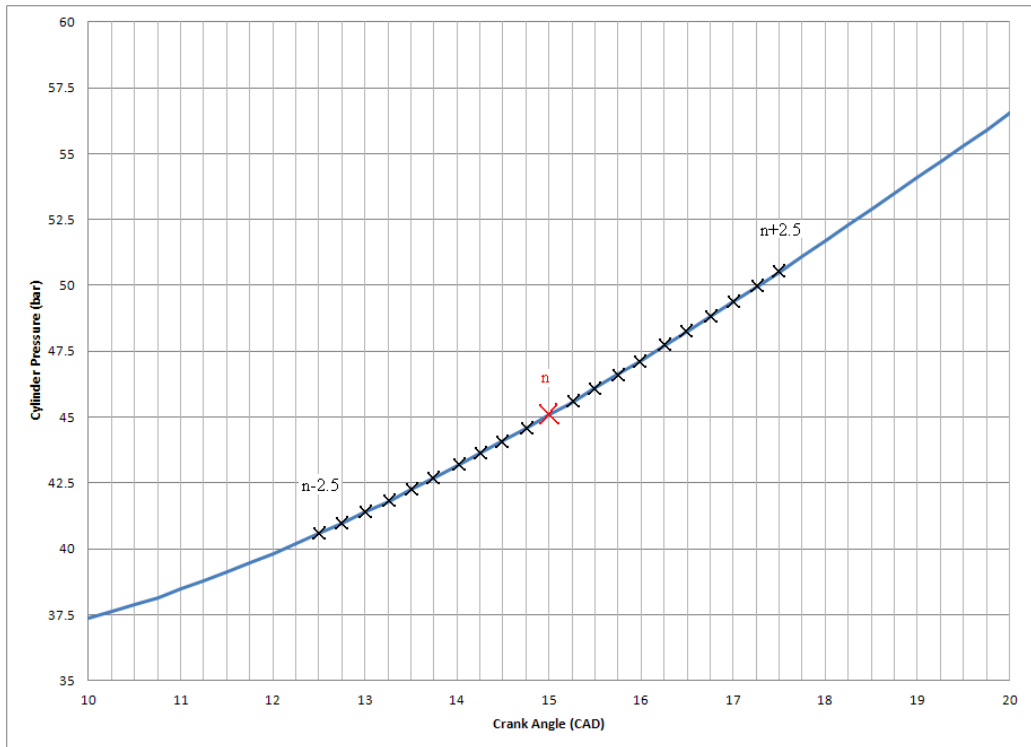


Figure 3.17 Band-pass Filtering Calculation

$$p_n = \frac{\sum_{n-2.5}^{n+2.5} p}{21} \quad 3.2$$

The knock intensity is then calculated using the following formula (Eq.3.3):

$$KI = p_f - p_n \quad 3.3$$

where p_f is the pressure feedback from the in-cylinder pressure transducer. This technique for measuring knock intensity was used because it is computationally much less expensive than using a band-pass filter. This is also an established technique for measuring KI and is used in industry and has been found to be very effective.

This reading has been found to be very sensitive to noise, hence the reason why so much attention was paid to noise reduction for the in-cylinder pressure transducer. The peak rate of cylinder pressure change per CAD ($dp/d\theta$) has not been used to measure KI specifically (although it is logged) because the $dp/d\theta$ in knock free running has been found to be close to a value that would be considered knock. The $dp/d\theta$ method is also a lot more susceptible to noise.

Window 2: Mass Fraction Burn

This is updated on a cycle to cycle basis. The mass fraction burn rate is calculated using the Rassweiler and Withrow method (Rassweiler, et al [105]) which states that there are 2 mechanisms that can bring about a change in cylinder pressure (Δp). They are A) a change in volume (Δp_V), and B) the presence of combustion (Δp_C). This can be expressed as follows (Eq.3.4):

$$\Delta p = \Delta p_V + \Delta p_C \quad 3.4$$

The change in pressure brought about by a change in volume (V) is easily calculated from the relationship based on the polytropic equation (Eq.3.5):

$$\Delta p_V = p_i \left[\left(\frac{V_i}{V_{i+1}} \right)^n - 1 \right] \quad 3.5$$

where i represents a crank angle and $i+1$ represents an incremental difference in crank angle. Combining these 2 equations results in the following (Eq.3.6):

$$\Delta p_C = p_{i+1} - p_i \left(\frac{V_i}{V_{i+1}} \right)^n \quad 3.6$$

The combustion process takes place over a finite period of time and therefore cannot be said to be a constant volume process, and although the above equation will indicate when combustion has finished it is not possible to determine the quantity of fuel burnt at this point. It is therefore necessary to take the sum of the Δp_C up to the point it becomes zero, the crank angle at which this occurs shall be called j , this will then indicate that all the fuel that is going to burn has been burnt by crank angle j . The MFB can then be determined by dividing the sum of the Δp_C up to a crank angle of i by the sum of the Δp_C up to a crank angle of j (Eq.3.7):

$$x = \frac{\sum_1^i \Delta p_C}{\sum_1^j \Delta p_C} \quad 3.7$$

where x is the MFB. It is also necessary to calculate Δp_C relative to a reference position. This reference position can be anywhere but for the purposes of this study the TDC (or the point of minimum volume) was used.

There are a great many assumptions made with this model. The biggest assumption is the value of the polytropic index n which is assumed to be constant at all times during the compression and expansion strokes. This is not accurate as the value can be expected to change slightly. The value of n is determined from the log P-V during the compression process.

Window 3: P-V (or log P-V)

This is updated on a cycle to cycle basis. The cylinder and intake pressures are fed back directly from the in-cylinder and intake pressure transducers respectively. The volume is calculated using the crank angle signal from the shaft encoder using the following formula (Eq.3.8):

$$V = \frac{s\pi \left(\frac{b}{2}\right)^2}{(CR - 1)} + \pi \left(\frac{b}{2}\right)^2 \left(\left(CL + \frac{s}{2} \right) - \frac{s}{2} \cos\theta \right) - \sqrt{(CL)^2 - \left(\frac{s}{2} \sin\theta + x \right)^2} \quad 3.8$$

where V is the volume, s is the stroke, b is the bore, CR is the compression ratio, CL is the connecting rod length, θ is the crank angle in radians, and x is the crank-pin offset.

Window 4: Cylinder IMEP Vs. cycle

This is updated on a cycle to cycle basis. This window displays the Net IMEP (NIMEP) values obtained from the previous 100 cycles and gives an indication of how stable the engine is at that particular running condition akin to a graphical representation of the COV of IMEP.

The NIMEP is calculated from the cylinder pressure data. Owing to the nature of the test work, where one can expect great variations in the size of the pumping loop, the NIMEP value was used as opposed to Gross IMEP (GIMEP) value.

Maintaining a constant NIMEP means any increase in the pumping loop size due to higher or lower EBPs is offset by an increase in the gross work. There is no significant advantage to using NIMEP as opposed to GIMEP, the biggest reason is for convenience in comparing the single cylinder data to the 3 cylinder data. It is also easier to calculate the power “cost” of the turbocharger using NIMEP.

In-order to maintain accuracy of in-cylinder pressure data, a Polytopic Index Pressure Referencing (PIPR) system was used to “peg” the data as described by Brunt, et al [106]. This has been used instead of an Intake Manifold Pressure Referencing (IMPR) system because of noise errors associated with the intake pressure transducer, and the fact that for certain IMOPs and cam durations the intake valves may still be open at BDC with pressure waves present in the intake manifold compromising accuracy. Attempts were made to implement a BDC IMPR system but this technique was found to present an issue with the polytropic exponent which sometimes reached as high as 1.38 which is not accurate for GDI applications, even with dry air. A polytropic exponent of 1.32 was assumed for the PIPR pegging technique between 100 and 65 CAD Before TDC (BTDC). This value was used because it was in closest agreement with the predicted GT-Power value and made comparing the 2 datasets easier.

There are also a great deal of boxes that feedback numerical data in real time, a description of these is given in Appendix A.3.

3.3.2 Calibration of Sensors

Flow meters

The Apollo flow meters are turbine type flow meters and were calibrated April 2011 immediately before being installed to the test rig. These flow meters have been calibrated over their respective ranges of 2-20l/min and 5-50l/min.

The ABB FCM2000 coriolis flow meter was last calibrated in February 2011 across its full flow range.

Pressure sensors

The Druck pressure sensors were tested across their respective ranges using a dead weight tester. The sensors were only tested at their maximum pressures and at atmospheric pressure. No offsetting was required for any of these sensors.

The Kistler in-cylinder pressure transducer was also dead weight tested. Owing to the nature of piezoelectric pressure transducers the sensor cannot be calibrated using a steady state load. In-order to calibrate this sensor the settings on the Kistler 5011B charge amplifier had to be adjusted. The high-pass filter or Time Constant (TC) was set to long and the Low-pass Filter (LF) switched on to allow the Δp to be recorded correctly and to be displayed for such a period so as to ascertain if it was correctly calibrated or not. The transducer was calibrated and the calibration values given by Kistler were found to be correct and no additional corrections were required.

The intake and exhaust pressure transducers were not dead weight tested initially because the pressure transducers and charge amplifiers were brand new and freshly installed immediately before test work commenced.

Temperature sensors

Both the PRTs and the thermocouples were calibrated using water in the vicinity of 90°C. The hot water would be placed in a container and the temperature sensor was then immersed in the water along with an RS 206-3722 temperature probe and the feedbacks from both sensors were compared. This procedure was carried out once before the test work commenced and all instrumentation temperature sensors were found to be in good agreement with the RS 206-3722, with the maximum error being 2°C.

Shaft encoder

The TDC position was determined using a Kistler 2629C capacitance probe TDC sensor which can determine the dynamic TDC accurate to within 0.1 CAD. The thermodynamic loss angle was calculated at 1200rpm to be 0.9 CAD using the horizontal cut principle (by recording the crank angle at the same capacitance either side of the peak capacitance point and interpolating between those 2 points to find TDC). It was assumed to be constant throughout the speed range of the engine. The reason for this assumption is the shaft encoder resolution is relatively coarse, and the software cannot be adjusted to less than 0.25 CAD resolution. The engine was equipped with the TDC sensor and motored over the full engine speed range. Using the horizontal cut principle there was a difference in thermodynamic loss angle, however, this difference was too fine to input into the software, so the same value was used for all speeds.

Exhaust gas analyzers

Both the Rotork Analysis model 443 Chemiluminescence analyzer and the Rotork Analysis model 523 Flame Ionization Detector (FID) analyzer were analyzed whenever used using span gasses. The span gas used for the Chemiluminescence analyzer was 500ppm (nominal) nitric oxide, and the span gas used for the FID analyzer was 500ppm (nominal) propane.

3.3.3 Accuracy of Data and Known Measurement Errors

In order to maintain as high a degree of accuracy as possible 300 cycles were logged at each of the test points. This was done in order to obtain as accurate a value of IMEP and standard deviation as possible as described by Brunt, et al [107].

The long and short cam profile camshafts differed from the standard profile camshaft in geometry, this meant that 2 different types of high pressure fuel pump had to be employed for this test work. The 2 different pumps had very different degrees

of control, with the pump used for the short and long duration cam profiles having a much higher degree of control. A comparison of the 2 pumps is shown in Figure 3.18.

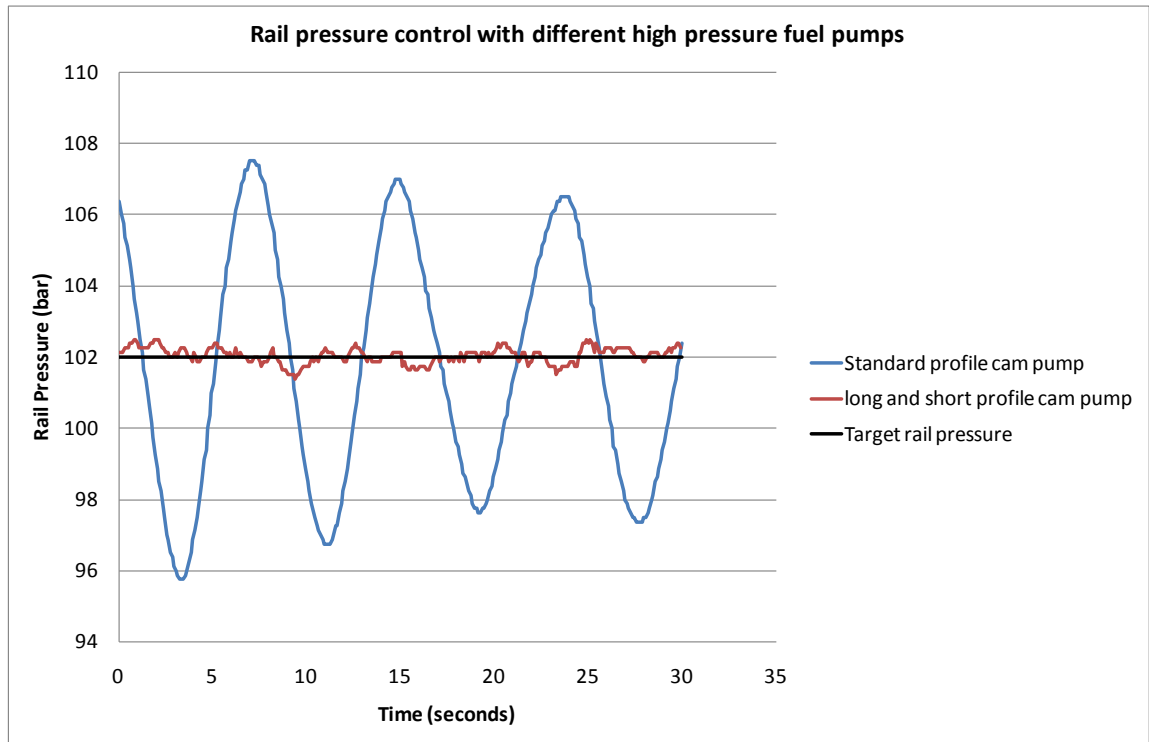


Figure 3.18 Accuracy of Fuel Rail Pressure Control at 3000rpm and 4 bar BMEP

The average pressure with the standard cam high pressure fuel pump can still be seen to average 102 bar which will have negligible impact on the engine HC emissions and burn durations, but it can be found to have a significant impact on the ISFC. The output from the coriolis fuel flow meter can be found to echo this sinusoidal trend, which means that for a constant IMEP the ISFC can also be found to echo this trend.

The degree of control can be found to decline greatly with lower fuel pressures and medium speeds. Figure 3.18 shows the worst case scenario as experienced over the course of 30 seconds at 3000rpm and 4 bar BMEP. To keep the error associated with this control problem to a minimum logs were taken when the fuel pressure equalled the requested pressure. The maximum error associated with this phenomenon was approximately 8 g/kWhr in ISFC at 3000rpm and 4 bar BMEP.

3.4 Daily Test Point

In order to assess the performance and repeatability of the engine and the instrumentation a test point was selected where the engine would run every day in order to see if there was any difference in performance. This test point is as shown in Table 3.1:

Table 3.1 Daily Test Point Test Variables and Control Criteria

Speed	2000rpm
Load	4 bar NIMEP
Spark timing	50%MFB at 8 CAD ATDC
IMOP	100 CAD ATDC
EMOP	120 CAD BTDC
Boost	1.35 bar
Air humidity	dry air
Air temperature	40 deg C
Coolant temperature	80 deg C
Oil temperature	80 deg C
SOI	319CAD BTDC
Rail pressure	134 bar
Throttle position	14.8% open
Emissions	HCs only

Owing to logistical constraints only data from the instrumentation system was saved, the data from the ECU was not saved. Only HCs were recorded because the Chemiluminescence NOx analyzer was not used for all test work.

Chapter 4

Development of a Single Cylinder Engine GT-Power Model

4.1 Introduction

A single cylinder engine GT-Power [4] model has been developed for assessing the benefits of EIVC and LIVC strategies. The main reason for developing a single cylinder engine model is to test the effectiveness of Deep Miller (EIVC and LIVC with very high MAPs) at high engine loads, different geometric CRs and very high EBPs to both complement and compare to the data obtained from the single cylinder experimental engine. An analytical approach has been adopted for the majority of the Deep Miller work due to constraints imposed by the single cylinder experimental engine (such as insufficient ignition energy to ignite the charge with high levels of boost, and the inability to run with fuel enrichment) that would make an equivalent experimental analysis impossible at this moment in time.

A secondary reason is to assist in understanding what is happening in the test results obtained from the single cylinder experimental engine, and to help explain precisely what impact the breathing dynamics of the single cylinder experimental engine is having on the overall results. A second more basic single cylinder engine model was created for this purpose. Although the 3 cylinder engine model had been setup and validated at Mahle Powertrain, it has proven necessary to develop a single

cylinder engine model because the single cylinder engine will have very different breathing dynamics to the 3 cylinder engine, which renders a direct comparison between the 3 cylinder engine model and single cylinder engine experimental results impossible. The single cylinder engine is also a great deal more versatile than the 3 cylinder engine, and the MAP, Charge Air Temperature (CAT) and EBP can be anything the user specifies, rather than being dictated by a turbocharger and intercooler.

The efficacy of the EIVC and LIVC processes is dictated heavily by the MAP/EBP ratio, particularly during the gas exchange period, so introducing independent control of each will allow a more thorough investigation of both processes. One of the main benefits offered by the EIVC and LIVC processes is the possibility of running with a higher geometric CR than would ordinarily be achieved with the standard Otto cycle. This model will therefore be used to analyse and quantify this benefit and to offer a greater deal of understanding of the mechanisms that bring about any performance benefits.

A brief overview of the Mahle Powertrain 3 cylinder engine GT-Power model is also given at the end of this chapter.

4.2 Development of the Single Cylinder Engine Model

There are 2 main variants of the single cylinder engine model that have been developed for this test work. The similarities between both models will be described in section 4.2.1. Of the 2 models, 1 of them is almost entirely automated and features closed loop control of numerous systems, this is described in section 4.3. The second variant contains very little closed loop control and is almost entirely manual and is described in section 4.4.

Both models are geometrically identical with the biggest difference between them being the presence of a knock model in model 1 and numerous other closed loop control systems. Given the similarities of both of these models, with the exception of sections 4.2.1, 4.3 and 4.4 where the differences between both models are described,

both single cylinder models shall henceforth both referred to as the singular “single cylinder engine model”.

The single cylinder engine model has been designed to resemble the single cylinder experimental engine as closely as possible. However, many parts of the intake system have been left out of the model in an effort to reduce the complexity, and because certain aspects of the system introduce anomalies and strange phenomena to the model without contributing to the accuracy.

4.2.1 Single Cylinder Engine Model Details

This section describes the commonalities of the 2 models and discusses their limitations. The flow modelling has been described in section 4.2.1.1 while the combustion modelling has been described in section 4.2.1.2. The limitations of both models have been described in section 4.2.1.3. A summary of the other parameters used in this model is given in section 4.2.1.4.

4.2.1.1 Flow Modelling

The flow of gasses has been modelled one-dimensionally. This approach involves calculating the flow properties by solving the Navier-Stokes equations for the conservation of energy (Eq.4.1), continuity (Eq.4.2) and momentum (Eq.4.3) in one-dimension. This requires the whole system (intake and exhaust) to be divided (or discretized) into sub-volumes. The Navier-Stokes equations are solved over the boundaries of these sub-volumes where scalar values (such as pressure, density and temperature) are averaged across the entire sub-volume, and vector quantities (such as mass flux and velocity) are calculated at the boundaries of the sub-volume. This approach is described as a staggered grid and is shown graphically in Figure 4.1.

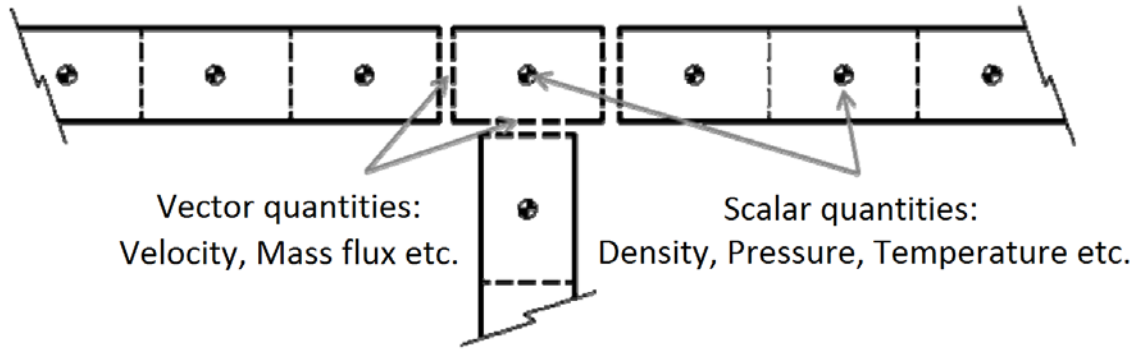


Figure 4.1 Staggered Grid Arrangement

$$\frac{d(me)}{dt} = -p \frac{dV}{dt} + \sum_{boundaries} (\dot{m}H) - hA_s(T_{fluid} - T_{wall}) \quad 4.1$$

$$\frac{dm}{dt} = \sum_{boundaries} \dot{m} \quad 4.2$$

$$\frac{d\dot{m}}{dt} = \frac{dpA + \sum_{boundaries}(\dot{m}u) - 4C_f \frac{\rho u |u|}{2} \frac{dxA}{D} - C_p \left(\frac{1}{2} \rho u |u|\right) A}{dx} \quad 4.3$$

where m is the mass of the volume, e is the total internal energy per unit mass, t is time, p is pressure, V is volume, \dot{m} is the boundary mass flux into the volume, H is total enthalpy, h is heat transfer coefficient, A_s is heat transfer surface area, T_{fluid} is the fluid temperature, T_{wall} is the wall temperature, dp is the pressure differential acting across dx , A is the cross-sectional flow area, C_f is skin friction coefficient, u is the velocity at the boundary, D is equivalent diameter, C_p is pressure loss coefficient, ρ is density and dx is the discretization length.

An explicit solver has been used for all test work in an effort to model the pressure pulsation effects in the intake and exhaust systems (caused by exhaust blowdown pulses) as accurately as possible.

4.2.1.2 Combustion Modelling

A single zone model has been adopted to model the cylinder of the engine for all test work. This assumes that the pressure, temperature and composition of the cylinder gasses are uniform and homogeneous. This model is unable to differentiate between burned and unburned gasses and models combustion as a simple heat addition process. The limitations of this approach have been outlined in section 4.2.1.3. Due to the fact that combustion is not modelled burn rates must be approximated rather than calculated.

The burn rate was approximated using a method developed by Wiebe [108] known as the Wiebe function (Eq.4.4), given by:

$$x_b = 1 - \exp \left\{ -a \left[\frac{\theta - \theta_0}{\Delta\theta_b} \right]^{m+1} \right\} \quad 4.4$$

where a and m are constants (5 and 2 respectively), x_b is the MFB, and θ , θ_0 and $\Delta\theta_b$ denote instantaneous crank angle, crank angle at start of combustion and total combustion duration in CAD respectively.

Although this model gives a very good estimation of the MFB rate profile, it requires the user to input a value for the 10-90% MFB duration first, as this model cannot predict burn duration. The 10-90% MFB duration was taken from 3 cylinder experimental data (obtained by Mahle Powertrain) recorded at a similar speed and load point to the test point being tested in the single cylinder engine model.

The values of a and m used are based on previous experiments by Heywood, et al [109] where the optimum values were determined as 5 and 2 respectively. These values could have been recalculated using the same 3 cylinder data used to obtain the 10-90% MFB duration, however, they were not obtained from this because the MFB duration profile can change dramatically depending on what cam, cam timing, EBP and MAP combination is being tested. Also at the time this model was developed the single cylinder experimental engine was not operational and no directly comparable data was available. At a later stage when the single cylinder experimental engine was

operational, a comparison between the single cylinder experimental engine and the single cylinder engine model was made. With the standard duration cam using values of 5 and 2 for a and m respectively the burn duration profile obtained from the Wiebe function was found to be in good agreement with the burn duration profile from the single cylinder experimental engine.

4.2.1.3 Modelling Limitations

The greatest limitation of the single cylinder engine model is presented by the combustion modelling approach adopted. The single-zone model is the simplest method of modelling combustion, which can be advantageous in that it affords the user the greatest degree of control over the combustion event. However, this requires the user to know key combustion criteria prior to the simulation being carried out.

Multi-zone models go some way to remedying this by modelling a flame front and calculating burn durations, as well as factoring in other phenomena such as crevices and flame quenching, however, most are still incapable of modelling combustion. Some models such as the Blizzard and Keck turbulent entrainment model (Blizard, et al [110]) improve upon this by calculating burn durations, however, this model still requires some assumptions and simplifications to be made.

The Leeds University Spark Ignition Engine (LUSIE) model (Merdjani, et al [111]) is more advanced and accurate still, however, the code still requires work and incorporating this code into this single cylinder engine model is quite difficult and time consuming.

For semi-quantitative analysis of the effect of EIVC and LIVC on the engine's performance, the standard single-zone GT-Power code was deemed adequate, with the understanding that all data obtained from this test work will be indicative only.

4.2.1.4 Other Modelling Parameters

An engine is replicated in GT-Power through the use of *objects* which are linked in sequences to form intricate engine geometry such as the intake and exhaust manifolds for instance. The 2 most commonly used objects in this model are *Pipe* and *PipeRoundBend* which are used to create cylindrical pipes and pipe elbows respectively.

Besides the very important geometrical parameters such as length and diameter of the *object*, GT-Power allows the user to input other parameters for each of these *objects* such as surface roughness and wall temperature. Where applicable these values were determined by following the guidance given in the GT-Power help navigator [112]. For other more important parameters specific to the engine, such as intake and exhaust port geometry, intake and exhaust valve geometry and port flow coefficients, values from the Mahle Powertrain 3 cylinder engine GT-Power model (section 4.5) were used. For components specific to the single cylinder engine such as intake and exhaust manifolds, the geometry of these components was recorded as accurately as possible from the single cylinder experimental engine.

The way in which combustion timing is altered in GT-Power with the Wiebe function is by changing the 50% MFB point instead of the spark timing. Therefore for this chapter and chapter 5 the combustion timing will be referred to as either combustion phasing or the 50% MFB point and not spark timing. Due to the fact the combustion duration and Wiebe function variables were constant for all test work, the spark timing is directly correlated to the 50% MFB point however.

4.3 Single Cylinder Engine Model 1: DoE Based Test Plan

Single cylinder engine model 1 was developed purely to study Deep Miller, and was not employed for any low load work. As mentioned briefly in section 4.1, EIVC and

LIVC processes are dependent upon many variables including MAP, CAT, EBP, CR, Intake Valve Open (IVO) time and intake cam duration. For satisfactory analysis of EIVC and LIVC processes it is necessary to determine the effect of each of the above variables. Testing all of these variables by hand is a very long winded process, which is the reason why a DoE must be employed and why this model requires closed loop control of many different systems.

Model 1 has been developed purely for this application and can run almost entirely independently of any input from the user, which makes it highly dynamic and the perfect tool for executing large DoEs with.

A diagram of model 1 is shown in Figure 4.2.

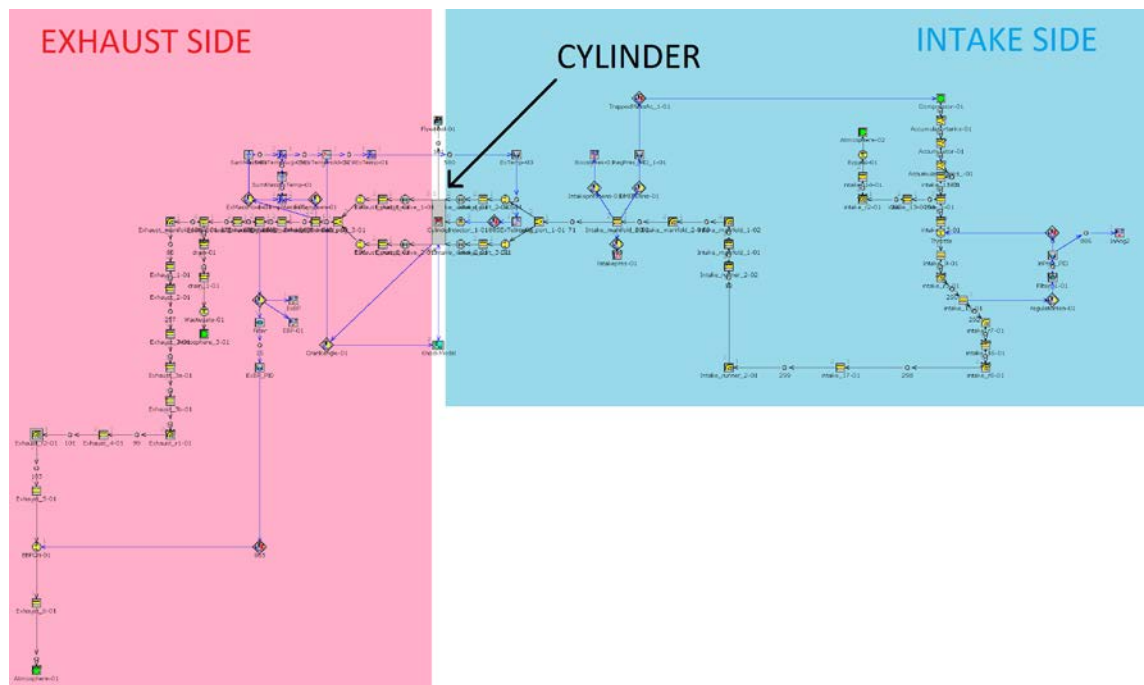


Figure 4.2 Single Cylinder Engine Model 1

This model has closed loop control of the following:

- Intake pressure (by controlling to a requested MAP)
- Intake temperature (by controlling atmospheric temperature)
- Knock intensity (by controlling combustion phasing)
- Exhaust temperature (by controlling lambda)
- Exhaust pressure (by controlling to a requested EBP)

Although the model does feature closed loop control of intake pressure, this can only control to a requested intake pressure. This may not seem necessary as the operator could simply request an intake pressure instead of having to control it, but this was not possible in practice because the pressure at the source of the intake system did not necessarily correspond to the pressure in the intake runner, hence the reason why a throttle with closed loop control was implemented. The same problem also applied to the intake temperature.

Attempts were also made to implement closed loop control of BMEP by regulating intake pressure. This could not be achieved as it was found to interfere with the knock model. The knock model and BMEP control were found to interact negatively and would generate the following scenario. If the combustion phasing was retarded slightly by the knock model the BMEP control would increase the boost pressure to compensate for the resulting loss of BMEP, this in turn would lead to a greater degree of combustion phasing retard which would require yet another rise in boost pressure and the boost pressure was found to progressively increase while the combustion phasing would become more and more retarded.

The exhaust temperature is regulated by changing the degree of enrichment in the cylinder. The temperature was regulated according to the exhaust gas temperature in the exhaust runner. The maximum degree of enrichment was fixed to a lambda of 0.85.

For this model the EBP was regulated by means of a variable diameter orifice rather than a conventional butterfly valve as implemented on the test engine, simply because the variable diameter orifice offered a greater deal of control with the Proportional Integral Derivative (PID) control system. The location of the variable orifice diameter was dictated by the single cylinder experimental engine, hence the reason why it is located so far downstream of the exhaust port. The EBP was regulated according to the average pressure in the exhaust runner over an entire engine cycle.

The knock model is the most complex closed loop system and has been described in section 4.3.1.

4.3.1 Single Cylinder Engine Knock Model

4.3.1.1 Functionality of the Knock Model

The single cylinder engine knock model (henceforth known as just the knock model) has been applied to the engine itself and is calculated, and controlled, in real time. Please note this is a knock model only and not to be confused with an autoignition model. Autoignition encompasses both knocking combustion and pre-ignition, and this model is unable to predict pre-ignition reliably (see section 6.4.4).

This knock model is based on 3 key equations that are fundamental to its operation. The first is the induction time integral described by Livengood, et al [113] known as the Livengood-Wu formula (Eq.4.5). The second is the combustion model developed by Douaud, et al [114] known as the Douaud and Eyzat combustion model (Eq.4.6). The third equation is the knock intensity formula developed by Gamma Technologies [112] (Eq.4.7). The first component is the Livengood-Wu integral which is given by:

$$T = \int_{-100}^{thkn} \frac{1}{\tau} dt \quad 4.5$$

where the integral limits -100 and $thkn$ equal the angle in CAD BTDC where compression is assumed to begin and the angle at which knocking is assumed to have started respectively. Once T is equal to 1 knocking combustion has commenced. The symbol τ represents the Douaud and Eyzat component, given by:

$$\tau = 5.72e6P \left(\frac{ON}{100}\right)^{3.402} p^{-1.7} \exp\left(\frac{3800}{AT_u}\right) \quad 4.6$$

where P is the precursor reaction rate multiplier, ON is the fuel octane number, p is the instantaneous cylinder pressure, A is the activation energy multiplier and T_u is the instantaneous unburned gas temperature. The precursor reaction rate multiplier was

adjusted for each individual engine speed to increase knock model stability and to ensure knock was occurring at the right moment in the cycle.

The start angle of the Livengood-Wu integral is usually the start of compression. The start of compression is however very difficult to determine as it does not necessarily correspond to intake valve closure. The knock model was initially set to start integrating the moment the flow through the intake valves stopped, however, this resulted in added complication to the knock model and introduced another potential issue with knock model functionality. This angle was therefore fixed at 100 CAD BTDC because this was found to have negligible impact on the functionality of the knock prediction point and intensity. The knock model still has the facility to revert back to using the flow through the intake valves however.

As soon as the Livengood-Wu integral equals 1 knocking combustion is present and the magnitude of this knocking combustion is calculated using the following formula:

$$KI = 10000Akm \left(\frac{V_{TDC}}{V_I} \right) e^{\frac{-T_a}{T_u}} \max [0, (1 - (1 - \varphi)^2)] \tau \quad 4.7$$

where A is the knock index multiplier, km is the percentage of cylinder mass unburned at knock initiation, V_{TDC} is the cylinder volume at TDC, V_I is the cylinder volume at knock initiation, T_a is the activation temperature (which has been assumed to be 6000 K) and φ is the equivalence ratio.

In order to solve these equations in real time (as is necessary for the closed loop control of combustion phasing), numerous outputs from the engine must be fed into the knock model. These required outputs are as follows:

- Instantaneous in-cylinder pressure
- Instantaneous in-cylinder unburned zone temperature
- Instantaneous in-cylinder lambda
- Instantaneous in-cylinder unburned gas mass fraction
- Instantaneous intake valve lift
- Instantaneous in-cylinder volume
- Crank angle

The intake valve lift does not appear in any of the knock model equations (Eq.4.5-4.7) but is still required for the satisfactory operation of the knock model. The intake valve lift is fed into the knock model to give the user the option of assuming the start of compression occurs when the intake valve closes instead of having to provide an arbitrary start of compression point.

Of all of the engine outputs the only one required numerous times is the crank angle. This is output from the engine a total of 5 times by 5 different sensors (denoted CAx where x equals 1 – 5) for 5 different purposes as shown in Table 4.1.

Table 4.1 Description of the Various Crank Angle Sensors in the Knock Model

Crank angle sensor	Description
CA1	TDC determination
CA2	BDC determination
CA3	Value of Livengood-Wu integral at the last point before knocking combustion
CA4	Last point before knocking combustion determination
CA5	Knocking combustion point determination

TDC and BDC determination though rather rudimentary still needs to be calculated. As mentioned previously, one of the factors of the DoE is geometric CR, and there is no way to feed back the geometric CR directly in GT-Power, therefore it must be calculated by dividing the volume at BDC by the volume at TDC.

Each of the crank angle sensors is used in the same way and all of them are used as a control input for a *hold object*. A *hold object* requires an input, a control input and a trigger point. The output of the *hold object* is fixed at the value of the input

at the trigger point which is triggered by the control input. This has been demonstrated in Figure 4.3 which shows the TDC determination. For TDC the input is cylinder volume, the control input is the crank angle and the trigger point is 0 CAD.

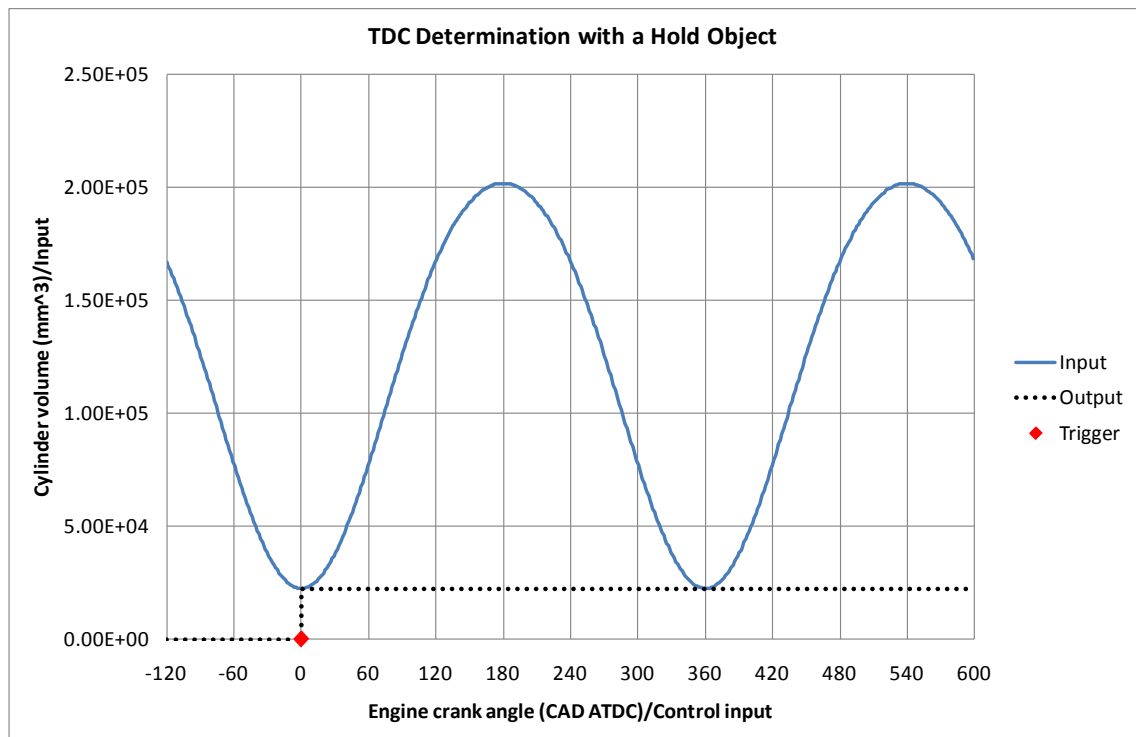


Figure 4.3 TDC Determination with a *Hold Object*

Figure 4.3 depicts the first cycle of a simulation, for every cycle after this one the output of the *hold object* will not until change again until 0 CAD is reached again.

This technique has been employed heavily throughout the knock model, it is used to hold values of pressure, temperature, unburned gas mass fraction and volume at the point where knocking combustion occurs. In these cases the Livengood-Wu component of the knock model was used as the control input and the trigger was set to 1. This ensured the Douaud and Eyzat and knock intensity components were calculated just once per cycle and that they were calculated at the correct time (at the point where knocking combustion occurs).

One of the problems experienced with this system was that the Livengood-Wu component never equalled exactly 1, this is due to the fact that the resolution of the simulation was 1 CAD. Obtaining a Livengood-Wu integral of exactly 1 is not possible due to the fact the resolution of the simulation would have to be infinitely small. This

problem has been illustrated in Figure 4.4 where the accuracy of the point where knocking combustion occurs can be seen.

In this instance the point where knocking combustion occurs would be recorded as 23 CAD After TDC Firing (ATDCF) by the knock model, whereas in actual fact the point where knocking combustion actually occurs is closer to 22.5 CAD ATDCF. This error can be up to almost 1 CAD. This error in itself is acceptable as most ECUs are accurate to 1 CAD, however, this error led to convergence issues within the knock model. An interpolation system was therefore incorporated to interpolate between the points both before and after the knocking combustion line to obtain a very precise crank angle where knocking combustion occurred.

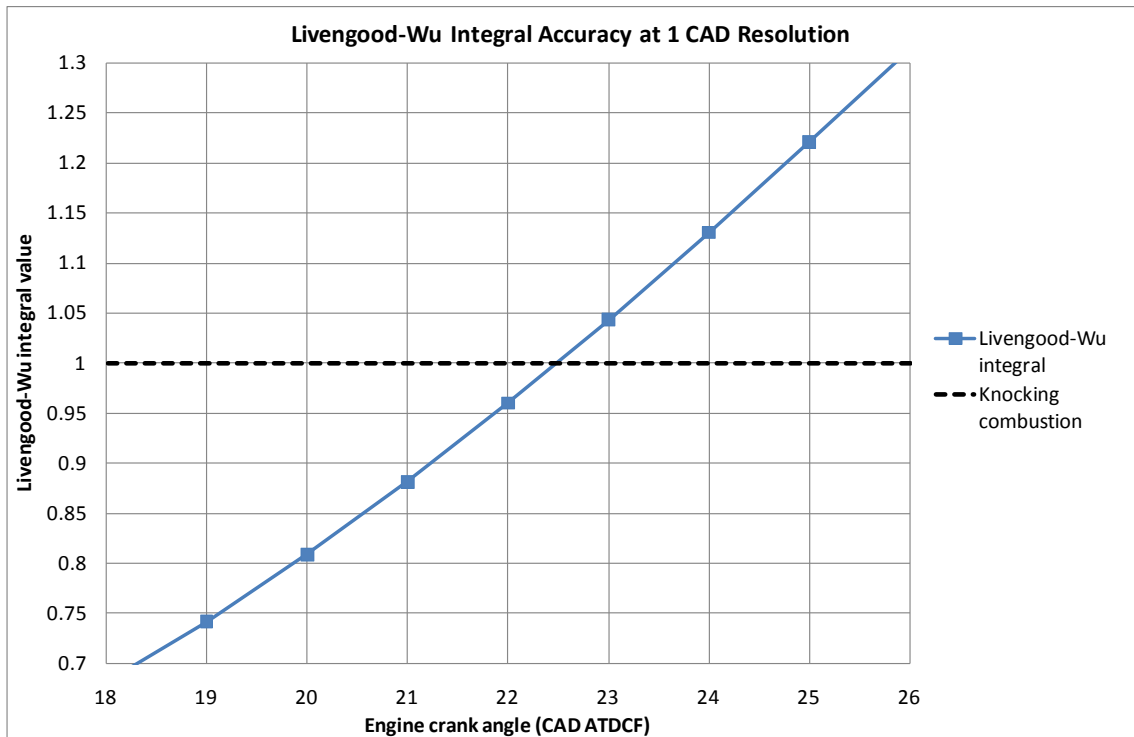


Figure 4.4 Livengood-Wu Integral Accuracy at 1 CAD Resolution

This interpolation system was applied to each of the required inputs for the knock intensity (Eq.4.7) component of the knock model, including τ . The incorporation of this interpolation technique increased the accuracy of the knock model by up to 271%. This example also highlights the difference between crank angle sensors CA3 and CA4 and crank angle sensor CA5. CA3 and CA4 are used to solve the knock model

equations at the last point before knocking combustion commences, and CA5 is used to solve the knock model equations after knocking combustion has begun.

Once the interpolation has taken place a knock intensity number is obtained from Eq.4.7. This number is divided by a target knock intensity as input by the user. It is this number that the PID controller is trying to target, all the time this number is not equal to 1 the combustion phasing will be changed.

4.3.1.2 Irresolvable Issues with the Knock Model

One of the biggest problems encountered with the knock model was the fact that the 50% MFB point was so variable from case to case (which is to be expected when running a large DoE). The closed loop control system for the combustion phasing on its own is incapable of dramatically changing the 50% MFB point in a short space of time due to the fact there are so many other closed loop systems at work on the model. This therefore requires the 50% MFB point to be moved incrementally along with each of the other closed loop systems, else all the closed loop control systems would become unstable.

The speed of convergence was found to dramatically improve when tables were incorporated to offset the default 50% MFB point according to engine operating conditions at that particular test point. These tables increase or decrease the degree of combustion phasing retard automatically before simulation has even commenced, thus allowing the 50% MFB point to converge within a shorter space of time (250 cycles).

There are a total of 4 tables correcting the 50% MFB point. These tables change the 50% MFB point phasing based on:

- MAP (Table 4.2)
- EBP (Table 4.3)
- Geometric CR (Table 4.4)
- IMOP (Table 4.5)

The values in these tables are constant for all speed and load cases.

Table 4.2 MAP Correction Factors

MAP (bar)	Correction factor
2	13.7
4	24.4

Table 4.3 EBP Correction Factors

EBP (bar)	Correction factor
2	6.2
4	12.4

Table 4.4 Geometric CR Correction Factors

Geometric CR	Correction factor
9	27.51428571
12.5	38.21428571

Table 4.5 IMOP Correction Factors

IMOP (CAD ATDC)	Correction factor
-282	-39.41428571
-240	-28.21428571

A general rule of thumb with these tables is the larger the correction factor the more retarded the initial combustion phasing would be.

The values in the these tables have been approximated based on test work carried out with the 3 cylinder engine model involving changing MAP and EBP (Table 4.6), they were not controlled independently, and geometric CR was not changed at all at any point in the test work. It is for these reasons that just one map incorporating this data on its own was insufficient in giving suitable 50% MFB point approximations that were close enough to the actual values to give convergence.

Table 4.6 MAP and IMOP 3 Cylinder Map of BLD 50% MFB Points at a Speed and Load of 5000rpm and 24 bar BMEP Respectively

		IMOP (CAD ATDC)								
		-220	-230	-240	-250	-260	-270	-280	-290	-300
Cam duration (CAD)	177.31	29.7638	27.67556	25.99715	24.7249	23.75866	23.25416	23.154	23.46551	24.07751
	179.28	29.75526	27.6562	25.96599	24.68133	23.69995	23.17142	23.05351	23.33914	23.88449
	181.25	29.74672	27.63685	25.93484	24.63776	23.64124	23.08868	22.95302	23.21277	23.69147
	183.22	29.73818	27.61749	25.90368	24.59419	23.58253	23.00594	22.85253	23.0864	23.49845
	185.19	29.72964	27.59813	25.87253	24.55062	23.52382	22.9232	22.75204	22.96002	23.30542
	187.16	29.7211	27.57878	25.84137	24.50705	23.46511	22.84045	22.65155	22.83365	23.1124
	189.13	29.71256	27.55942	25.81022	24.46348	23.4064	22.75771	22.55106	22.70728	22.91938
	191.1	29.70402	27.54007	25.77906	24.41991	23.34769	22.67497	22.45057	22.58091	22.72636
	193.07	29.69548	27.52071	25.74791	24.37634	23.28898	22.59223	22.35008	22.45454	22.53334
	195.04	29.68694	27.50136	25.71675	24.33277	23.23027	22.50949	22.24959	22.32817	22.34032
	197.01	29.6784	27.482	25.6856	24.2892	23.17156	22.42674	22.1491	22.2018	22.1473
	199.9901	29.2393	27.14799	25.4565	24.18046	23.2353	22.67515	22.56563	22.81887	22.8773
	202.9702	28.8002	26.81398	25.2274	24.07172	23.29904	22.92356	22.98216	23.43594	23.6073
	205.9504	28.3611	26.47997	24.9983	23.96298	23.36279	23.17196	23.39869	24.05301	24.3373
	208.9305	27.922	26.14596	24.7692	23.85424	23.42653	23.42037	23.81522	24.67008	25.0673
	211.9106	27.4829	25.81195	24.5401	23.7455	23.49028	23.66877	24.23175	25.28715	25.7973
	214.8907	27.0438	25.47794	24.311	23.63676	23.55402	23.91718	24.64828	25.90422	26.5273
	217.8708	26.6047	25.14393	24.0819	23.52802	23.61777	24.16558	25.06481	26.52129	27.2573
	220.851	26.1656	24.80992	23.8528	23.41928	23.68151	24.41399	25.48134	27.13836	27.9873
	223.8311	25.7265	24.47591	23.6237	23.31054	23.74526	24.66239	25.89787	27.75543	28.7173
226.8112	25.2874	24.1419	23.3946	23.2018	23.809	24.9108	26.3144	28.3725	29.4473	
250	24	23	23	24.5	24.5	19.9	20.4	20.9	30	

The data available for populating the intake cam duration and IMOP map was quite extensive but only over a relatively short cam duration window, which is another reason why it could not be used directly.

4.4 Single Cylinder Engine Model 2: Correlation of Thermodynamic Data

Single cylinder engine model 2 very closely resembles single cylinder engine model 1 (Figure 4.2), with the only difference being the actuators have been removed from the closed loop systems in model 2. Single cylinder engine model 2 was modified in some instances to provide some closed loop control (most commonly fuel enrichment control was re-employed because it was a very long process to determine the correct AFR manually).

It was used for both low and high load work and was employed heavily for deducing whether or not charge scavenging was occurring with LIVC. It was also used to extract P-V data from GT-Power as this cannot be done from the DoE directly. This

provided a good opportunity to check the integrity of the data obtained from the DoE too.

4.5 Mahle Powertrain 3 Cylinder Engine Model

A 3 cylinder engine GT-Power model has been developed by Mahle Powertrain (Figure 4.5). It is based on the first generation 1.2l 3 cylinder downsized engine with a single turbocharger and a geometric CR of 9.25. The geometry of the engine and cylinder have been replicated very accurately in the model, and the port flow coefficients of the intake and exhaust valves were measured on a flow bench.

This model has been fully correlated by Rothmaier [115] and was found to be a very good correlation to the engine, particularly at part load. This model has also been found to predict the breathing dynamics of the engine very accurately.

This model has been employed mostly for comparing the breathing dynamics of the single cylinder engine to the 3 cylinder engine where no test data from Mahle Powertrain exists or could be obtained. The results of this can be found in section 6.2. It has also been used to help correlate the knock model (Table 4.6).

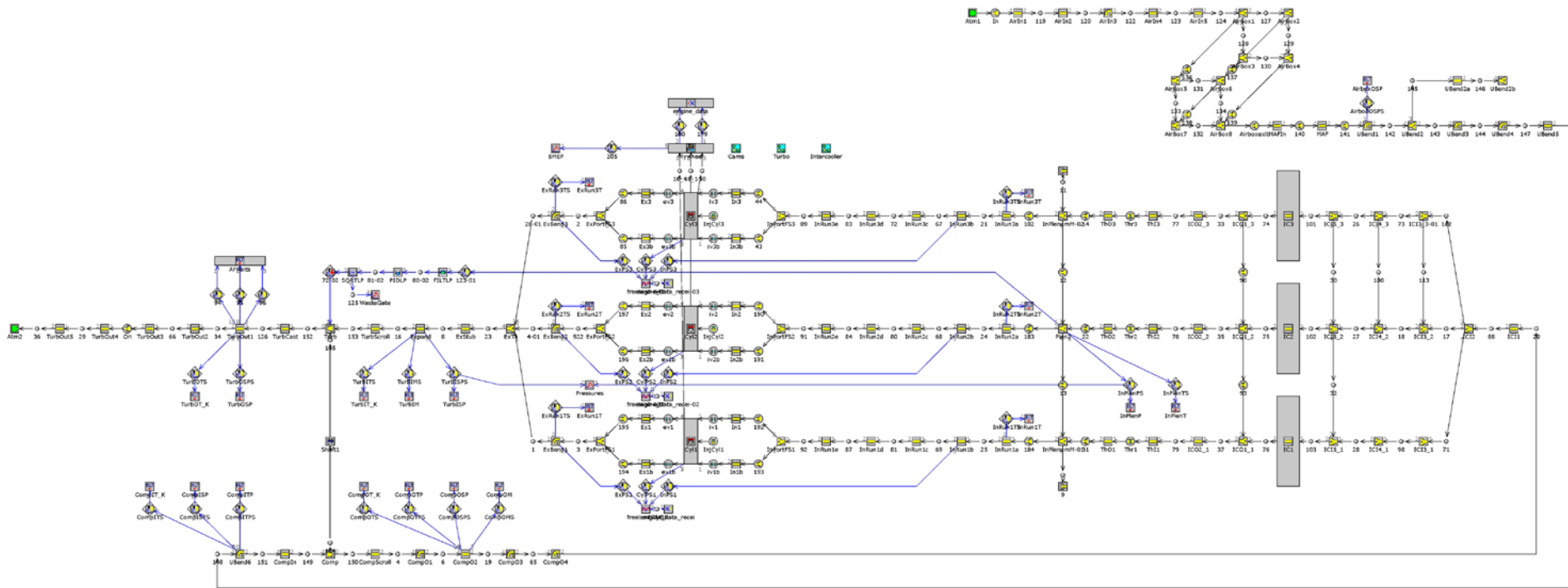


Figure 4.5 Mahle Powertrain 3 Cylinder Engine Model

Chapter 5

Application of the Deep Miller Cycle to Improve Fuel Economy and Increase Maximum Load

5.1 Introduction

This chapter describes the development of a DoE based test plan and presents the results of an analytical study into the Deep Miller cycle process (EIVC and LIVC with very high boost pressures) executed in a single cylinder engine GT-Power model (as described in chapter 4).

The intention of this test work is to ascertain the effects of EBP and geometric CR on the effectiveness of Deep Miller at key speeds and loads that should theoretically yield the most significant fuel economy benefit for a downsized engine.

This chapter has been arranged into 3 major sections, 1 section on describing the DoE based test plan as well as test points, and the other 2 sections showing results. The first section of this chapter explains why, and how, a DoE approach has been adopted. It also explains what type of DoE has been employed and details the screening process used to validate the model. This section also explains the choice of test points and why they have been selected.

The first results section is focussed on the use of EIVC and LIVC to optimize fuel consumption (or ISFC). It has been arranged to show ISFC trends with increasing EBP and geometric CR, followed by an analysis of the cam timings. Following this is an

explanation of the phenomena that impacted very heavily on these results such as cam timing, scavenging and engine breathing. This is followed by a section explaining the positive and negative aspects of increasing geometric CR.

The second section is a study of the maximum loads that can be obtained using Deep Miller. This section studies the impact of EBP on maximum load and explains how the engine is restricted from producing higher loads.

5.2 Development of a DoE Based Test Plan

5.2.1 Introduction

The intention of this test work is to assess the impact of geometric CR and EBP on Deep Miller effects. In order to do this many different cam durations must be tested at many different IMOPs. These can be assessed by Changing One Separate factor at a Time (COST), however, this is a very long winded approach, particularly when several variables will need to be assessed, and it has also been found to give misleading results (in some cases) in comparison to a fractional factorial design (Eriksson, et al [116]). Therefore a fractional factorial DoE approach will be adopted instead.

The DoE approach is used to assess the impact of many different variables in as few experiments as possible. It is widely adopted in many different industries as time is usually a tight constraint and it is usually very important that selected experiments are maximally informative.

5.2.2 Screening

A program of screening tests was constructed to determine the most accurate fractional factorial regime for this particular test work. The screening process in DoE

terms usually refers to a series of tests carried out to determine which variables can be discounted from the DoE because their impact on the overall result is negligible. However, for this work this was not carried out as each of the 5 variables have been well documented to have a significant effect on the ISFC of an engine. For the purposes of this study the screening process refers more to the process of determining a suitable size for the DoE and optimum configuration. Additional screening was also carried out to determine optimum gain values for the various PID control systems.

The majority of the screening process was carried out at the 5000rpm, 24 bar BMEP speed and load point, with only a relatively small amount carried out at other speeds. This point was selected for many reasons, chief among which is because the Miller cycle benefits at high speed and high load are of the greatest interest in this study (for its synergies with downspeeding). A high load point is also necessary to test the knock model and a high speed is also necessary to test the closed loop enrichment control and to gauge its influence on ISFC.

There are 3 main studies that make up the back bone of this screening process, the first of which was a very lengthy process of ensuring the knock model functioned correctly. The impact of this process can be seen in section 4.3.1 where the knock model has been fully described. The other closed loop control systems were also checked for correct functionality during this phase.

The second was to assess which factorial design would be optimum for this application. The initial approach to this was to determine how many levels there should be for each of the variables. Very coarse preliminary Box and Draper DoEs were carried out to determine which of the variables would have the greatest impact on ISFC. CR was found to have a more subtle and predictable impact on ISFC so this had the fewest levels, while cam duration (the focus of this study) required the greatest number of levels. The number of levels selected for each of the factors is as shown in Table 5.1 (bracketed values represent the ranges and resolutions associated with the 1000rpm DoE):

Table 5.1 DoE Ranges, Levels and Resolution (1000rpm)

Factor	Range	Levels	Resolution
Intake cam duration	152 - 312 CAD	16	10 CAD
IMOP	As shown in Table 5.2	As shown in Table 5.2	10 CAD
MAP	2 - 4 bar (1.5 - 3 bar)	5 (4)	0.5 bar
EBP	2 - 4 bar (1.5 - 3 bar)	5 (4)	0.5 bar
CR	9 - 12.5	3	1.75

Table 5.2 Intake Valve IMOP Ranges for Different Duration Cams

Cam duration (CAD)	IMOP range (CAD ATDC)	Levels
152	50 - 120	8
196	60 - 120	7
240	80 - 120	5
276	100 - 140	5
312	110 - 150	5

Speed is another factor that has been investigated but it has not been included in the above list because the knock model must be reconfigured for each speed, also closed loop control of enrichment is not required at lower speeds. Therefore, for the purposes of this study, different speeds shall be considered as different studies rather than a variable.

Owing to the number of factors and the number of levels involved a full factorial COST approach DoE is immediately unfeasible as it will consist of 6000 points per speed and a DoE of this size will require computer resources that are, at this moment in time, unavailable. A fractional factorial model was therefore adopted.

Test work from the experimental engine suggests a quadratic model is best suited to capture the correct response. Quadratic models are also required to locate optimal points. The intention of this study is not to capture the optimal points with a great deal of precision because the knock model and combustion models cannot permit this (due to their inherent weaknesses). The intention of this DoE test plan was therefore not to determine with great accuracy where the optimal points arise but to get an idea of trends across the entire range of all of the variables.

The third stage of this screening process was to determine what type of fractional factorial DoE is best suited to the test range. This has been described in section 5.2.3.

5.2.3 DoE Type

A Latin hypercube (McKay, et al [117]) design was adopted at first but this was later abandoned due to problems experienced with the extreme points of the experimental region, such as the corners of the hypercube where “lips” would form due to the curve fitting algorithm. This is due to the fact that the Latin cube design will never test the same value of a particular variable twice and is therefore very reliant on the curve fitting algorithm. It was found to be very reliant on the knock model functioning correctly over the entire range of the experimental region, which it rarely did. A D-optimum (described by Eriksson, et al [116]) approach was then adopted instead.

Figure 5.1 gives an example of a Latin cube quadratic point distribution and a D-Optimum quadratic point distribution over the same range with the same number of test points with 2 variables. The Latin hypercube points are noticeably more clustered toward the centre of the experimental region and the D-Optimum points are more uniformly distributed and cover the extreme regions of the experimental region.

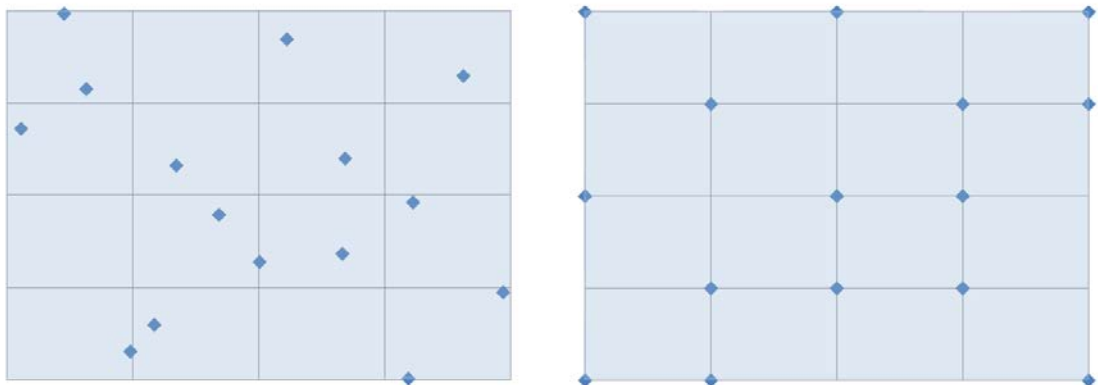


Figure 5.1 Latin Hypercube (left) and D-Optimum (right) Quadratic Point Distribution Comparison

A D-optimum design was found to be more effective at reducing the “lipping” effect at the extreme points of the hypercube (Figure 5.2), and is also better suited to testing asymmetric experimental regions which this is due to the fact the IMOP range changes with cam duration. The experimental region can be found to be highly

asymmetric for this test work, not only because of the IMOP limit but also because certain MAP, EBP, IMOP and cam duration combinations would lead to unfeasibly high volumetric efficiencies and loads. Due to logistical constraints an asymmetric experimental region could not be used and it was instead broken down into regions of different IMOPs, so this advantage of the D-optimum design could not be utilised in practice.

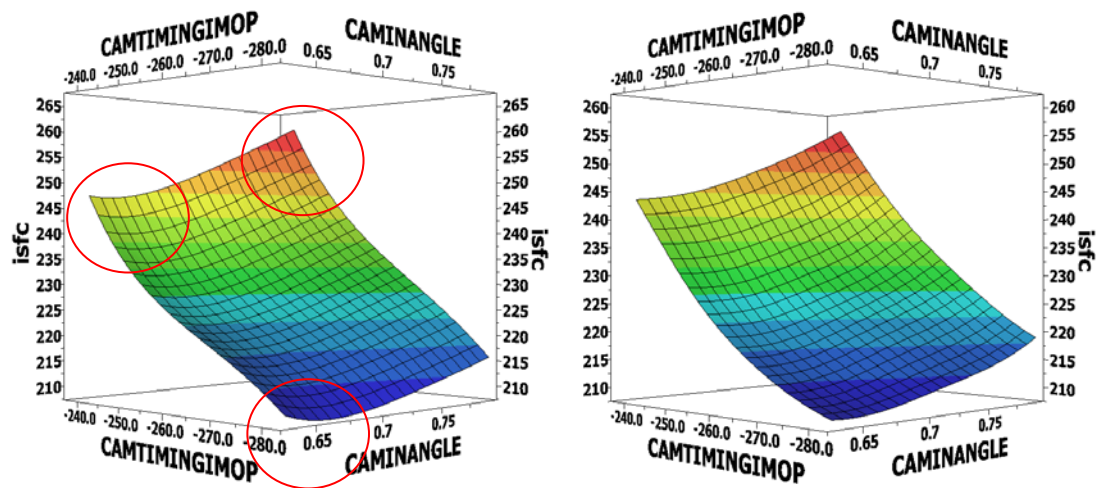


Figure 5.2 Latin Hypercube (left) and D-Optimum (right) Quadratic Curve Fitting Comparison with Lips Circled

A further advantage of the D-optimum design is the ability to extract and add data to the experimental region after it has been carried out. For areas where data integrity was quite low and the knock model was malfunctioning, data could be obtained manually using single cylinder engine model 2 which could be used to manually populate the experimental region.

5.2.4 Limitations of the DoE

Strictly speaking there are many variables besides the 5 tested that can have an impact on ISFC, such as assumed exhaust temperature limit, intake temperature, combustion phasing, fuel quality and age, and, in the case of the single cylinder engine, exhaust and intake geometry and runner lengths. However, some of these variables are not easily controlled such as the exhaust and intake manifold tuning. Fuel age and

fuel quality, which can be shown to have a profound effect on engine autoignition performance, is another variable. Unfortunately it is not possible to replicate different fuels reliably in GT-Power.

The exhaust temperature limit for most turbocharged engines is dictated by the turbocharger. The temperature ceiling for all test work was set to 930⁰C. This is beyond the maximum temperature limit imposed for all experimental test work which was 900⁰C. The reason for setting different temperature limits is because the physical engine was constrained by the lambda sensor to a low maximum exhaust gas temperature, and the majority of the GT-Power work is fundamentally theoretical so a slightly higher exhaust temperature limit was imposed. Modern materials such as austenitic steel and nickel-chromium alloys have raised the allowable exhaust temperature limit, modern technologies such as Water Cooled Exhaust Manifold (WCEM) also increase this limit dramatically (Taylor, et al [118]). The imposed temperature ceiling of 930⁰C is therefore relatively conservative.

The number of experiments used was the maximum number the computational resources would permit in an effort to define the regions where EIVC and LIVC were not feasible, and the optimum points with as high a degree of accuracy as possible. This number is approximately 150 experimental points. For an experimental region of this size and for cam duration to be captured at a resolution of 10 CAD, 150 points is still insufficient so the experimental region was broken down into sub experimental regions each of 150 experimental points. Due to the fact the IMOP ranges changed with cam duration, and the fact the cam duration had to be assessed at such a high resolution, the 4 DoEs were for 4 different cam duration ranges which were as follows:

- 152 – 192 CAD duration
- 192 – 232 CAD duration
- 232 – 272 CAD duration
- 272 – 312 CAD duration

An attempt was made to split this into finer cam duration ranges still but this was later abandoned because it was much more difficult to analyse the data and yielded no improvement in the accuracy of the results.

The cam profiles were calculated by inputting a scale factor for the standard cam, for instance the 152 CAD duration cam profile was determined by scaling the standard cam down a factor of 1.58. The valve lift was kept constant however at 11mm for all cam profiles. Figure 5.3 shows 5 valve profiles of 152, 196, 240, 276 and 312 CAD duration.

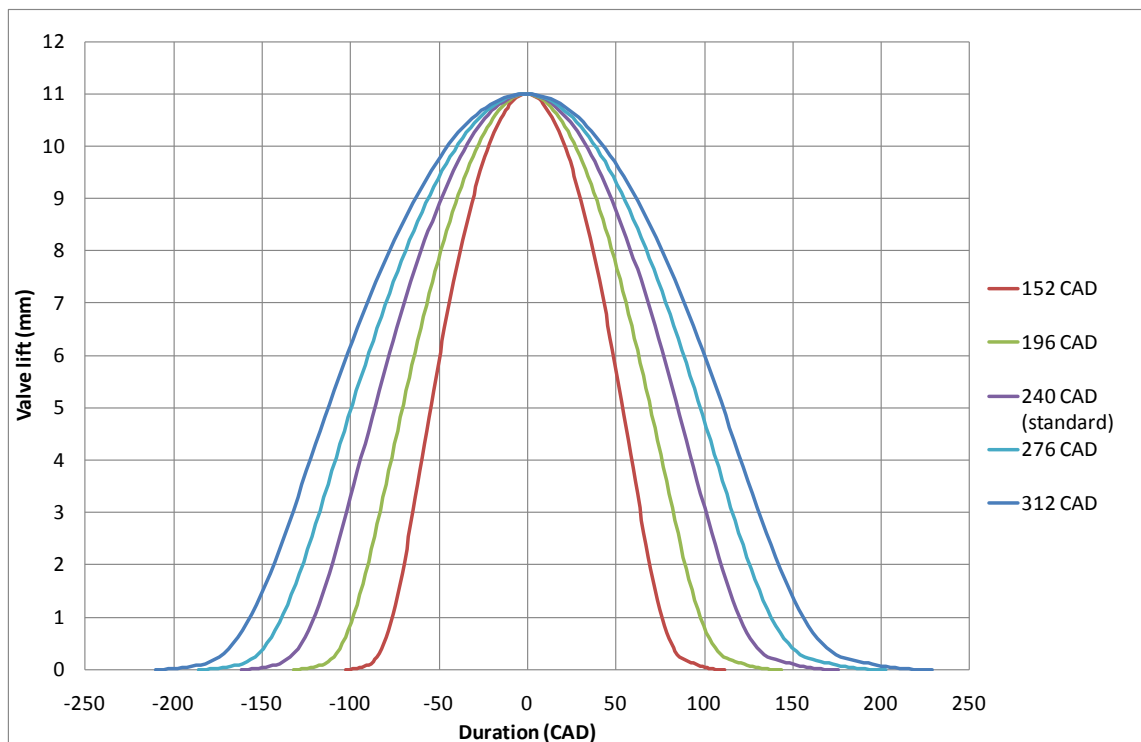


Figure 5.3 Comparison of GT-Power Calculated Intake Cam Profiles for 152, 196, 240, 276 and 312 CAD Durations Cams

A Radial Base Function (RBF) was found to give results most like that acquired from the test work and this was therefore used for curve fitting. The design optimization tool in AutoDOE was used to extract raw data from the DoEs where variables such as EBP, geometric CR, cam duration and IMOP could be fixed and a target power could be requested. The software could interpolate to give the correct MAP for that condition as well as interpolated values of ISFC and numerous other variables, this was found to be the most effective way to analyse the data.

Data was not necessarily obtained at the resolution tested at in the DoE. For instance, cam duration was not obtained at 10 CAD increments but for 5 different cam durations of 152, 196, 240, 276 and 312 CAD. The reason for this is the malfunctioning of the knock model meant trend lines were inaccurate, so the decision was made to test as close as possible to set cam durations so no curve fitting was required due to the fact that the extremities of the DoE are relatively well populated with raw data.

Owing to the great number of closed loop control systems the number of runs per case was set to 250 to allow the numerous closed loop control systems to converge. Any points that had not converged in this number of cycles were removed from the DoE manually and omitted from the analysis. This many runs may alter the result slightly but all cases were run 250 times, so if the results were distorted at all they would all be distorted equally and still give a reliable representation of trends.

5.2.5 Test Point Description

The aim of this test work is to assess the performance benefits that can be realised through the use of EIVC and LIVC at high load across a different range of speeds. The DoE nature of this work means the data can also be used to get a better understanding of which strategy is best for increasing peak load too.

At this moment in time emissions are not key concerns because generally speaking loads as high as those tested are not part of the NEDC cycle and are therefore not of direct interest in this simulated portion of the work. All work is also steady state as there is no turbocharger present so transients are not of great interest or relevance.

The decision was made to adopt a DoE test plan at 3 different speeds and loads where downsized engines are most heavily constrained, and/or where adoption of the Miller cycle could greatly improve performance. The scope of the DoEs is outlined in section 5.2.2 and the speed and load points tested are as follows:

- 1000rpm, 14 bar BMEP (15.14 bar NIMEP)

- 2000rpm, 24 bar BMEP (25.58 bar NIMEP)
- 5000rpm, 24 bar BMEP (26.02 bar NIMEP)

Please note that all BMEP values given are 3 cylinder equivalent loads. The corresponding NIMEP values have been given in brackets. These points can all be seen to be relatively high in load but the phenomena preventing higher loads from being obtained can be seen to be quite different. One thousand and 2000rpm were tested because autoignition is a particular problem at low speed. The final speed of 5000rpm was tested due to the fact that fuel enrichment is required at this speed at high load. A load of 14 bar BMEP at 1000rpm has been selected due to the fact that given the current state of turbocharging/eboosting technology, this is likely to be the limit of what can be achieved using extreme EIVC and LIVC at such a low speed. The 24 bar BMEP load points have been selected so as to enable a direct comparison with the experimental engine. An identical MAP limit of 4 bar abs has also been imposed to make results comparable to the experimental engine. Additional reasons for running at these speeds and loads are explained in the sections 5.2.5.1, 5.2.5.2 and 5.2.5.3 for 1000, 2000 and 5000rpm respectively.

No low load DoEs were carried out because they are out of the scope of this portion of the test work, this is due to the fact that combustion is particularly affected at low loads and the GT-Power model cannot predict COV values, nor can it factor in combustion degradation due to too low EOC temperatures.

For all test work the EMOP was set to the maximum valve overlap position. This was fixed to allow consistency across all test points and to provide the maximum expansion ratio. This may be detrimental with higher EBPs, however, test work carried out on the single cylinder experimental engine suggests that the maximum valve overlap position is optimum for the exhaust valve with the baseline standard cam. EIVC and LIVC work with the 3 cylinder GT-Power model also suggests the maximum valve overlap position is optimum for the exhaust valve.

Although the single cylinder experimental rig has CAT control, the vast majority of engines have very limited CAT control. Accurate determination of the CAT is made

even more difficult when EIVC and LIVC strategies are employed because the charge temperature can be reduced by over pressurising/under pressuring the charge. It is for this reason that the CAT will not be varied during this test work, it will simply be set to a level that can be achieved by the intercooler on the 3-cylinder engine (40⁰C).

The Start Of Injection (SOI) timing has been derived from data obtained from Mahle Powertrain. The SOI timings are different depending on speed and load and are shown in Table 5.3.

Table 5.3 SOI Timings for Each of the Speed and Load Points

Speed (rpm)	BMEP (bar)	SOI (CAD BTDCF)
1000	14	246
2000	24	259
5000	24	349

5.2.5.1 1000rpm, 14 bar BMEP

One thousand revolutions per minute is a very low speed to be running at high load, even for downsizing and downspeeding concepts, however, the requirement for performance is still there at these speeds (Turner, et al [50]) and this is still a very valid speed point for high load.

Although the load is relatively low at this test point, performance can still be seen to be autoignition (specifically knock) limited. In most cases though the combustion phasing has only needed to be retarded a few CAD away from MBT. The 3 cylinder engine is run in the full valve overlap position at this speed and load to allow for as much scavenging as possible in the interest of mitigating knock. Scavenging is very effective at mitigating knock by evacuating the cylinder of as much hot residual gas as possible from the previous cycle. However, allowing fresh air to flow through the cylinder can be detrimental as it has the effect of diluting the exhaust gasses, causing the engine to appear to be running lean at the lambda sensor. As a consequence of this the EMS will inject more fuel to restore the engine to “stoichiometric” when in actual fact it is actually enriching the mixture as seen from the cylinder. This phenomenon has been explained in more detail in section 5.3.4.

In the case of the 3 cylinder engine a map exists that allows the EMS to compensate for this accidental enrichment by running the engine slightly lean (according to the lambda sensor). No such correction has been applied for this DoE.

5.2.5.2 2000rpm, 24 bar BMEP

This is arguably the most important speed to optimise as its one of the most common operating speeds for automotive engines. At 2000rpm knocking combustion still imposes a significant constraint on maximum load but much higher loads can be reached than at 1000rpm due to the higher engine speeds and the faster burn rates associated with greater degrees of in-cylinder turbulence.

For most downsized engines peak (or at least near peak) load can be achieved at 2000rpm. It can also be achieved without the need for enrichment which makes it a very desirable speed to run at.

In the case of the 3-cylinder engine, the MAP exceeds the EBP at this speed and load, the engine is also run at the full valve overlap condition. This means the cylinder will be very well scavenged at this speed, to the point that the EMS is set to run slightly lean to compensate for this scavenging effect. For this DoE analysis the engine was run at $\lambda = 1$ without any compensation for scavenging.

5.2.5.3 5000rpm, 24 bar BMEP

Five thousand revolutions per minute and 24 bar BMEP represents the maximum speed and load point for this test work. At this speed and load the exhaust temperatures are going to be very elevated and fuel enrichment will be required in most cases to regulate this. Although the objective of this work is to optimise ISFC (as with the other 2 speeds and loads), the mechanism by which this is achieved is slightly

different. An improvement in ISFC is yielded here through reduced fuel enrichment rather than through mitigating knock directly.

Knock still imposes a significant constraint at this speed and load but the propensity for the engine to experience pre-ignition is greatly reduced (due to an absence of LSPI). The reason why 5000rpm is being treated as the maximum speed is to ensure consistency with the downspeeding concept. This means that although the engine is seldom run at this speed there is a great need for high peak load at this point because the headline power output of an engine is very important to consumers and vital to the commercial success of an engine.

At this speed and load the 3 cylinder engine would be in the minimum valve overlap position due to the fact the EBP is much greater than the MAP. The 3 cylinder engine also runs with the maximum degree of fuel enrichment at this speed and load, with a lambda of 0.85. As a consequence of this, this speed and load point has the highest BSFC of the entire operating envelope (with the exception of the very low load points) and this speed and load point therefore has the greatest scope for improvement, another reason why a speed of 5000rpm was selected.

5.3 ISFC Optimisation

5.3.1 Introduction

This section contains an analysis of the results from the DoE test plan described in section 5.2. The objective of this section is to focus on the ISFC benefit that can be obtained through the EOC pressure and temperature reducing qualities of the Deep Miller process. The initial portion of this section contains a very detailed analysis of the ISFC trends with varying EBP and geometric CR. This portion highlights particular nuances seen in the data, and highlights several different phenomena that have affected the outcome of this test work. This has been broken down into specific speed

and load sections. Following this is an analysis of the cam timings required for the respective cams.

The second portion of this section is an overview of these phenomena and a more general overview of the impact they have had on the test work as a whole. This includes the impact of scavenging, engine breathing and geometric CR considerations.

5.3.2 ISFC Trends

5.3.2.1 1000rpm, 14 bar BMEP

5.3.2.1.1 EBP Effects

In this analysis the EBP of 1.5 and 2 bar are of much more importance than 2.5 bar because this is the most representative level of EBP that is likely to be required with a typical turbocharger at this speed and load point (based on baseline data obtained by Mahle Powertrain for the 3 cylinder engine). Results with 3 bar EBP have been excluded from this analysis because of data integrity issues. All the data given in this section is for a CR of 9, CR effects are discussed in section 5.3.2.1.2.

Figure 5.4 shows an overlay of the optimum IMOPs for ISFC for each of the different cams and EBPs. The optimum IMOP for ISFC was determined from IMOP cam timing sweeps across the full extent of the cam phasing range, and then selecting the IMOP timing that gave the lowest ISFC.

From a purely theoretical perspective the optimum cam timing and the optimum cam duration will depend heavily on the EBP and the difference in MAP and EBP. For a low EBP extreme EIVC and LIVC are preferable as the more extreme the IVC offset from BDC, the higher the required MAP. The combination of low EBP and high MAP is preferable because this will invert the pumping loop so it contributes work to the cycle, and the low EBP will maximise the energy that can be extracted from the

gross work contribution. However, if the MAP is elevated too high over the EBP too much scavenging will take place during the valve overlap phase which will cause the fuel efficiency to fall away fast (see section 5.3.4).

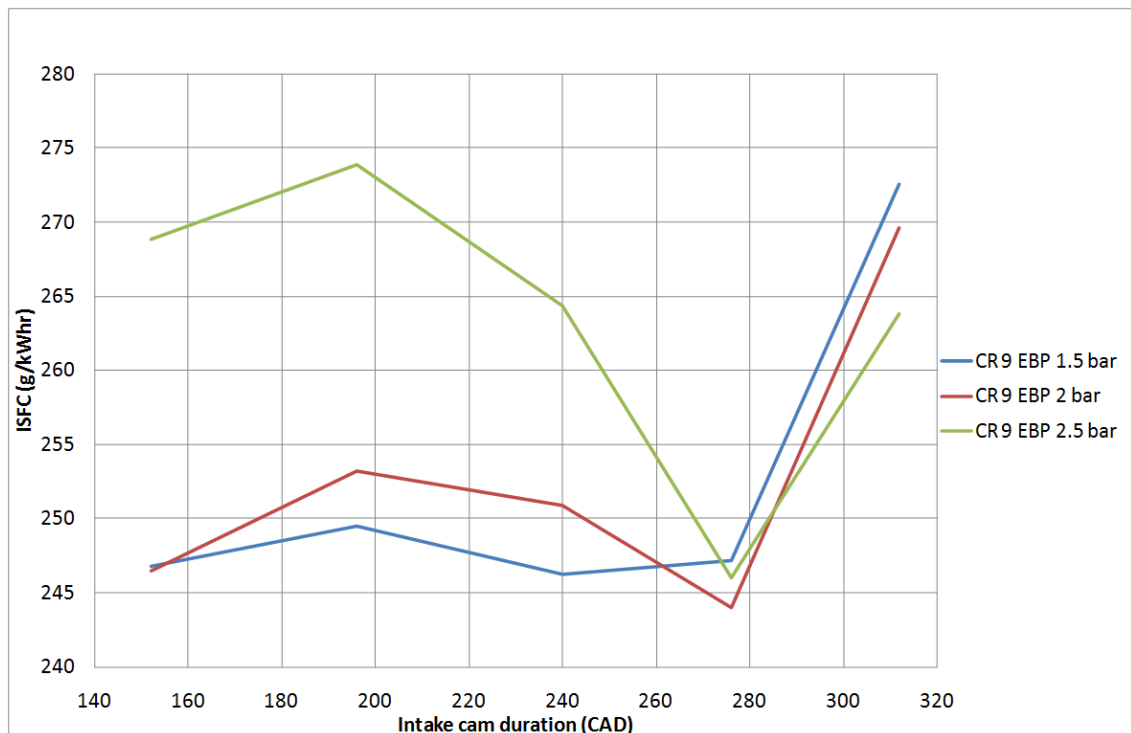


Figure 5.4 Impact of EBP on ISFC at a Geometric CR of 9

The influence of EBP can be seen to be greater for some cams than for others, with the 2 shortest cams showing the greatest sensitivity to EBP. The 276 CAD duration cam shows the least sensitivity to EBP and an apparent point of inflection, as well as the transposition of the 1.5 bar and 2.5 bar EBP lines. The 312 CAD duration cam also exhibits relatively little sensitivity to EBP but all points can be seen to be noticeably higher in ISFC.

The decline in ISFC with the 312 CAD duration cam can be attributed to the fact that the valve is still open so late into the compression stroke. This is advantageous in that it allows the maximum possible over-expansion and EOC temperature reduction benefit, but leaving the valve open during the compression stroke allows charge to escape the cylinder into the intake manifold. It is no longer just air as fuel will be diluted into it at that point due to the fact the SOI is at 246 CAD BTDC Firing (BTDCF), and fuel as well as air will be exhaled from the cylinder into the intake manifold.

Although the fuel is effectively still in the intake manifold and has the potential to be burned with no great impact on the ISFC, a lot of this fuel is lost during the valve overlap period as it is scavenged straight through the cylinder into the exhaust. This happens regardless of IMOP timing, and, to an extent, regardless of EBP to MAP ratio because there is always a small amount of valve overlap with the exhaust valve in its maximum overlap position (which was fixed due to the fact it gives the maximum expansion ratio and optimum ISFCs in this position) and still a certain degree of scavenging. This charge scavenging effect was witnessed using the animation feature in GT-Power, stills from this animation can be found in Appendix A.4.

This effect is similar in appearance to the excess scavenging experienced with the short cam profiles, with both scenarios ultimately culminating in unburned fuel being present in the exhaust. However, with charge scavenging there is the potential to use the unburned fuel in the exhaust as it will be mixed with air (not necessarily stoichiometrically) and can therefore be burned providing more energy to the turbocharger turbine, this may be required for high MAPs. It will also likely cool the cylinder down more than just air during the scavenging process.

It is due to charge scavenging that the EBP of 1.5 bar and 2.5 bar lines have become inverted at the 312 CAD duration cam position. An EBP of 2.5 bar will obviously impede air flow from the intake and inhibit charge scavenging more than an EBP of 1.5 bar. The 2.5 bar EBP in this case is keeping more of the charge in the cylinder at the expense of raised EOC pressure and temperature.

The disadvantage of raised EOC pressure and temperature can be seen to be outweighed by the advantage of reduced charge scavenging at this speed and load condition, which leads to a reduced ISFC for the higher EBP condition.

The charge scavenging effect can be seen to occur with the 276 CAD duration cam as well, however, due to the fact IVC occurs earlier in the compression process and the fact the MAP does not have to be as high as with the 312 CAD duration cam, very little charge completely short circuits the cylinder and goes into the exhaust unburned. It is for this reason that the ISFC values for the 276 CAD duration cam can be seen to be the lowest, because the effective CR is at a very low value while the cycle

is not hindered by charge scavenging or fresh air scavenging issues like the 312 CAD duration cam and the 152 CAD duration cam.

For the 152, 196 and 240 CAD duration cams the 2.5 bar EBP line can be seen to diverge quite sharply from the 1.5 and 2 bar EBP lines. This is due to the fact that the EOC pressures and temperatures are elevated for the high EBP cases (which require the combustion phasing to be retarded away from MBT). The combustion phasing has to be retarded from MBT in every case for the 2.5 bar EBP points for all cam durations (relative to the 1.5 and 2 bar EBP points). This has not manifested itself for the 276 CAD and 312 CAD duration cams in Figure 5.4 because the retarded combustion phasing is compensated by the lack of charge scavenging which has led to points for all 3 EBPs converging together and almost overlaying.

The difference in EOC pressure and temperature between each of the EBP cases is much greater for cams running at a relatively high effective CR, and the combustion phasing has to be retarded to a greater extent at these points as a consequence. Retarding the combustion phasing will result in a lower peak combustion temperature which can be found to be detrimental to ISFC (as dictated by the second law of thermodynamics).

This is the reason why the ISFC profile shapes can be seen to show such a close resemblance to the effective CR profile for each of the cams, as can be seen in Figure 5.5. The 312 CAD duration cam data has been omitted from Figure 5.5 because charge scavenging has elevated ISFC and distorted the trend.

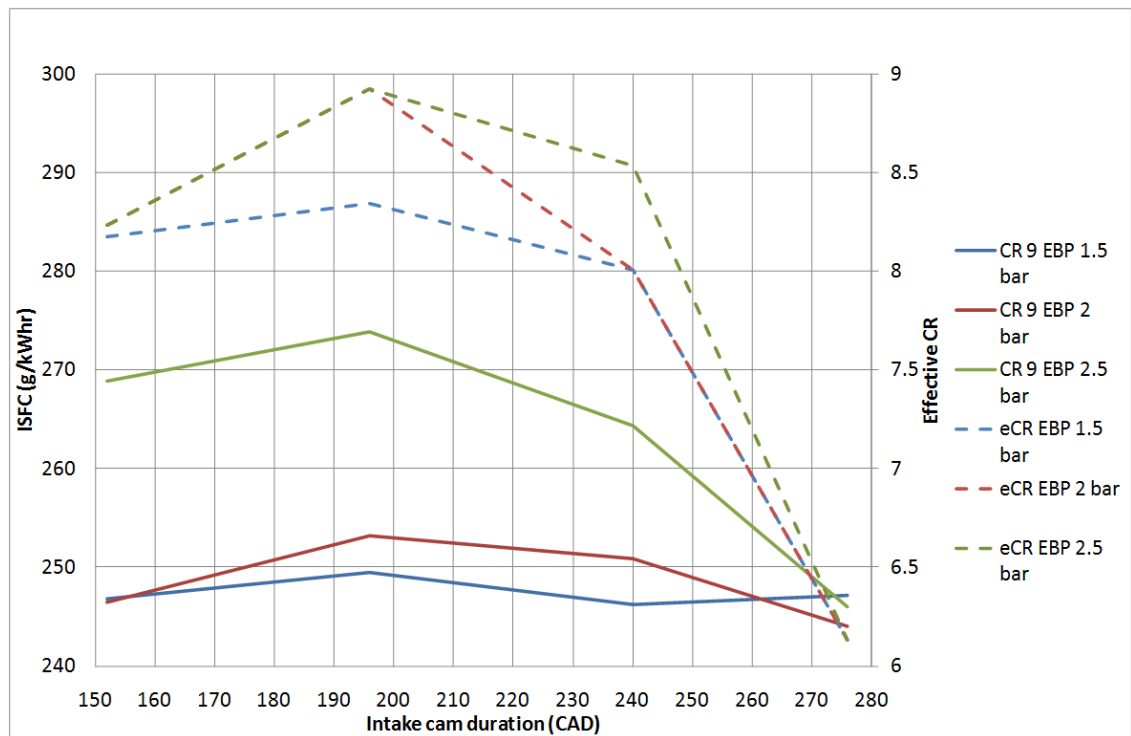


Figure 5.5 Comparison of Effective CR and ISFC for Each EBP at a Geometric CR of 9

5.3.2.1.2 Geometric CR Effects

One of the key advantages of using cam phasing and different duration cams is it affords the ability to operate the engine at different effective CRs in real time. This allows an increase of the geometric CR which in turn yields a theoretical benefit in fuel economy. With this test work the engine will very seldom be run with the effective CR equal to the geometric CR, it is not actually possible to run with the full geometric CR with the 152, 276 and 312 CAD duration cams.

Although theoretically a higher geometric CR should benefit fuel economy, at this speed and load it can actually be found to be detrimental to fuel economy because a high CR (whether effective or geometric) will result in higher EOC pressures and temperatures, this will require the combustion phasing to be retarded which will further exacerbate the high EOC pressure and temperature problem in a vicious circle. This is why typically turbocharged and downsized engines use a relatively low

geometric CR. Lowering the effective CR may circumvent this problem and allow the use of higher geometric CRs.

Owing to data integrity issues no reliable 312 CAD duration cam data at geometric CRs of 10.75 and 12.5 could be obtained and this cam has therefore been omitted from this analysis. The reason for these data integrity issues was the elevated EOC pressure and temperatures encountered with higher geometric CRs. This required the combustion to be extraordinarily retarded to satisfy the knock model. The knock model becomes unstable in these scenarios and ceases to function. Attempts were made to re-acquire the data with the manual single cylinder GT model (model 2) but similar issues were encountered as with model 1 in that no acceptable MAP, IMOP and combustion phasing could be found that gave an acceptable KI value. It should be stressed that the extent to which combustion phasing had to be retarded was beyond the functional limit of the experimental engine, and any data that would have been obtained would have been of no practicable use and purely hypothetical anyway (see section 5.3.6).

The impact of geometric CR increase with constant EBP can be seen in Figures 5.6 to 5.8. These Figures reveal the optimum geometric CR and EBP combinations for each of the different cam profiles. With 2 exceptions (which will be addressed later) the lines peak at roughly the same cam duration for each geometric CR case. The peak ISFC can be also be seen to correspond to the peak effective CR very closely, revealing the correct trend of the higher the effective CR the lower the cycle efficiency.

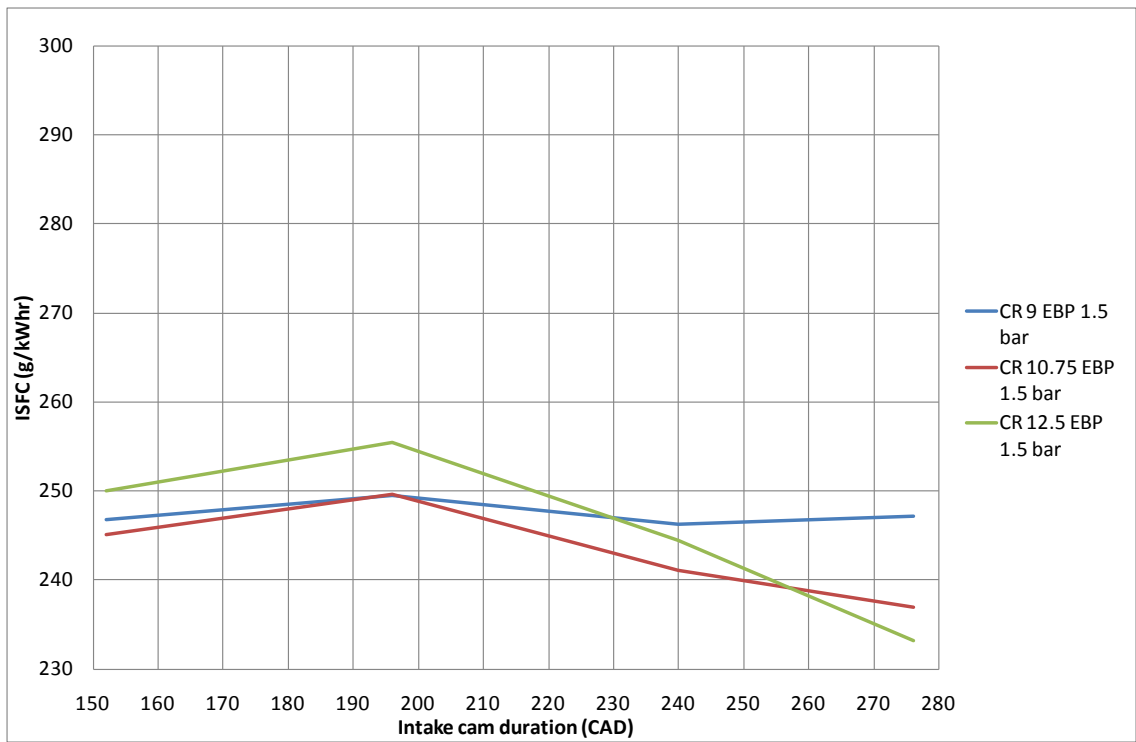


Figure 5.6 Comparison of Different Geometric CRs with an EBP of 1.5 bar

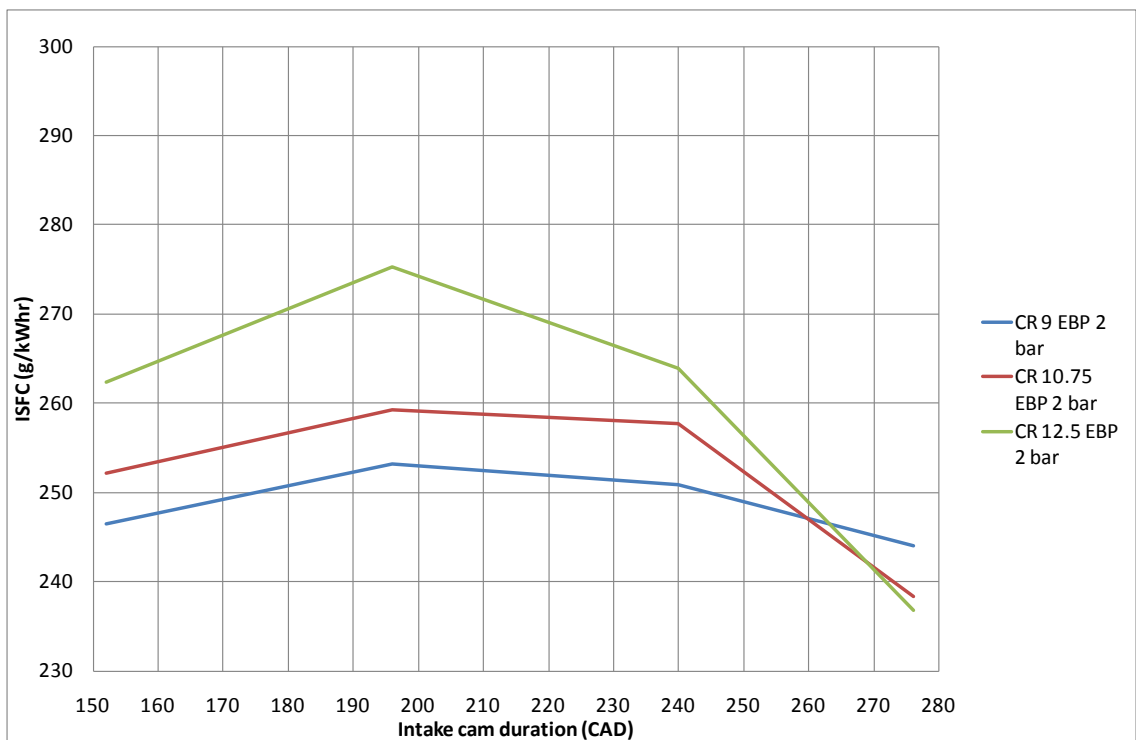


Figure 5.7 Comparison of Different Geometric CRs with an EBP of 2 bar

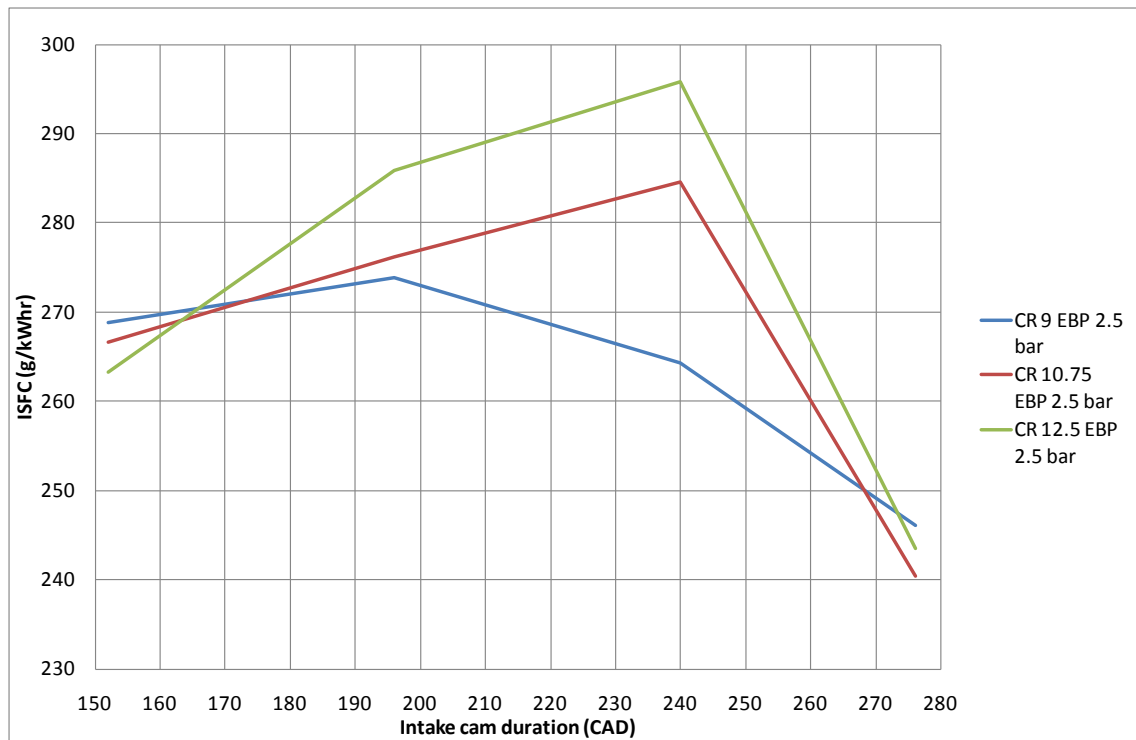


Figure 5.8 Comparison of Different Geometric CRs with an EBP of 2.5 bar

The geometric CR lines can also be observed to diverge the higher the effective CR. For the low effective CR cases, they can be seen to converge or in some cases change positions. The effectiveness of geometric CR increase is almost entirely dependent on EOC pressure and temperature at this running point, which is partly reflected by the fact the red geometric CR of 10.75 line is usually between the geometric CR of 9 and geometric CR of 12.5 lines, and why when going from a cam duration with a high ISFC to a cam duration with a low ISFC the geometric CR of 10.75 can always be seen to intersect the geometric CR of 9 line first.

These results show that a high geometric CR is very rarely optimum for a cam of any duration unless it is either extremely short or extremely long. The reason why extremely short and extremely long cam durations are required for high geometric CR is because they can reduce the effective CR to such a point that the combustion can be phased close enough to the Minimum spark advance for Best Torque (MBT) to give an advantage. There is some sensitivity to EBP with some strong evidence that higher geometric CRs can be employed with lower EBPs.

Observing the geometric CR lines in Figures 5.6 to 5.8 reveals that with low EBPs the benefits of extreme EIVC and LIVC are limited and minimal (the lines exhibit a very shallow gradient). The geometric CR of 10.75 and geometric CR of 12.5 lines suggest that higher geometric CRs are required to obtain considerable benefit from EIVC and LIVC strategies.

The main reason for the minimal performance benefit is the fact that while this is a comparatively high load for 1000rpm, it is overall just a medium load site. The MAP level is relatively modest and for some points is not much above NA. As a result of this EOC pressures and temperatures are moderately low and although EIVC and LIVC can reduce these, the effect is not as pronounced as if they were higher. The variation in ISFC for the 1.5 bar EBP and geometric CR of 9 case is the lowest with a variation of just 3.3 g/kWhr across the entire range of cam durations. This variation changes dramatically with increasing EBP. The variation in ISFC for 2 bar EBP and geometric CR of 9 case is 9.2 g/kWhr and 27.8 g/kWhr with the 2.5 bar EBP geometric CR of 9 case.

The variations for the geometric CR of 10.75 and the geometric CR of 12.5 cases can be seen to be a lot higher than these due to the increased EOC pressure and temperature variations associated with these higher geometric CR cases.

For the most part the peaks in ISFC can be seen to correspond very well with the peak effective CR. There are however 2 notable exceptions to that, both shown in Figure 5.8 which shows the peak ISFC values to occur at the second highest effective CR point for the 10.75 and 12.5 geometric CR cases. This offset appears to be due in part to the pressure/rarefaction wave caused by the blowdown pulse in the exhaust interacting with the intake manifold breathing (see section 5.3.5 for more details).

Although a high geometric CR offers an ISFC benefit, the combustion phasing is in general much more retarded for high geometric CRs. This may be feasible for an engine simulation but for the experimental engine this could lead to combustion instability and a very high COV (as explained in section 5.3.6).

5.3.2.2 2000rpm, 24 bar BMEP

5.3.2.2.1 EBP Effects

An ISFC comparison at a geometric CR of 9 and EBPs of 2, 3 and 4 bar can be seen in Figure 5.9 (unfortunately no data is available for the 312 CAD duration cam at an EBP of 4 bar due to data integrity issues). The profiles of the lines are broadly similar but can be seen to change slightly (particularly between the 196 CAD duration cam and the 240 CAD duration cam).

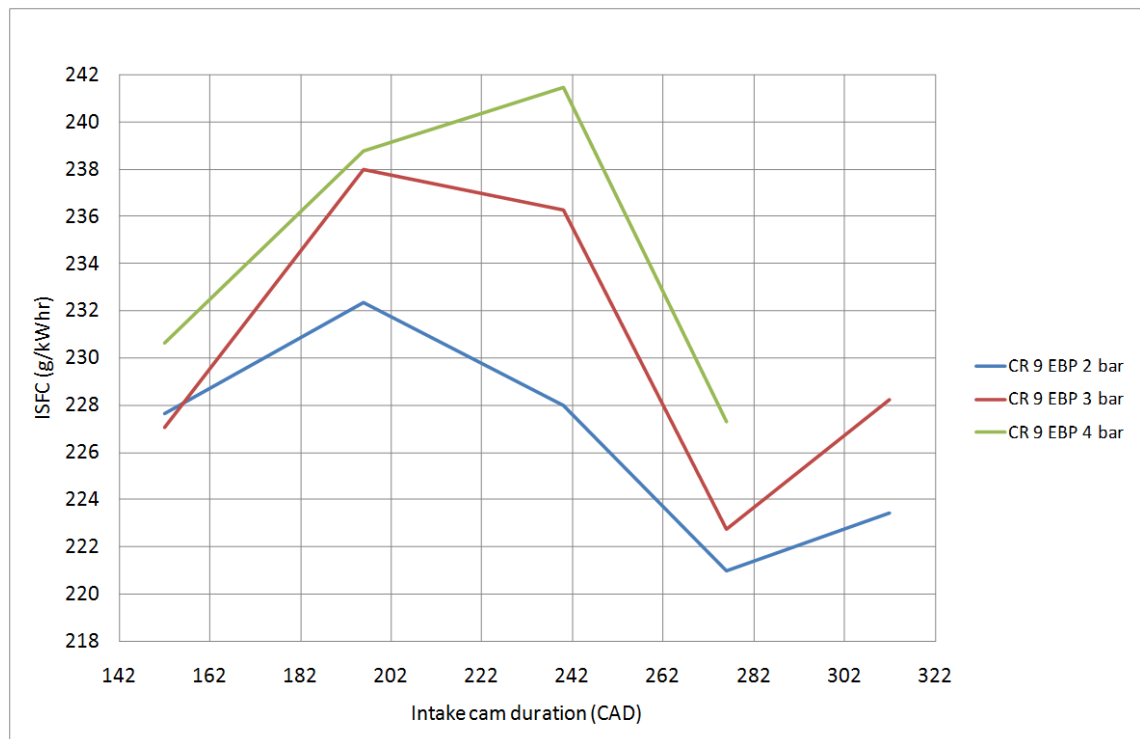


Figure 5.9 Impact of EBP on ISFC at a Geometric CR of 9

The most likely explanation for this is that each cam had a different optimum cam timing and a different optimum effective CR. Figures 5.10, 5.11 and 5.12 show the IVC, IVO and effective CR for the optimum cam position for each cam duration at a geometric CR of 9 and an EBP of 2, 3 and 4 bar respectively.

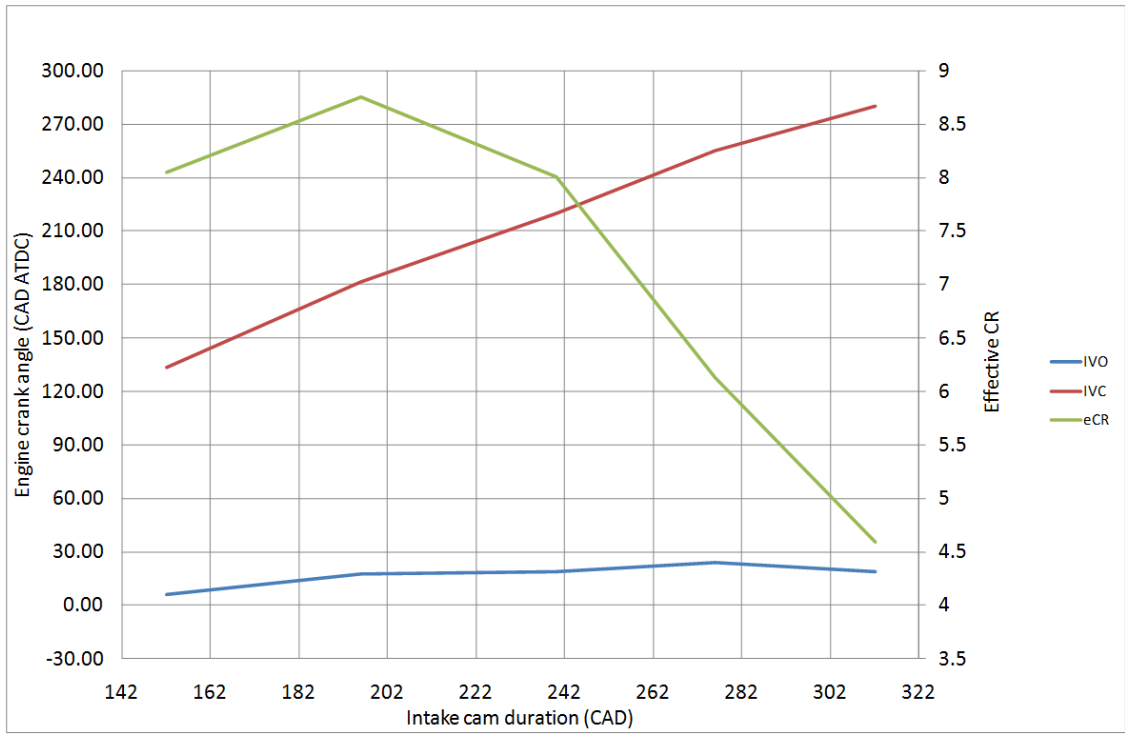


Figure 5.10 Optimum ISFC Cam IMOPs for an EBP of 2 bar at a Geometric CR of 9

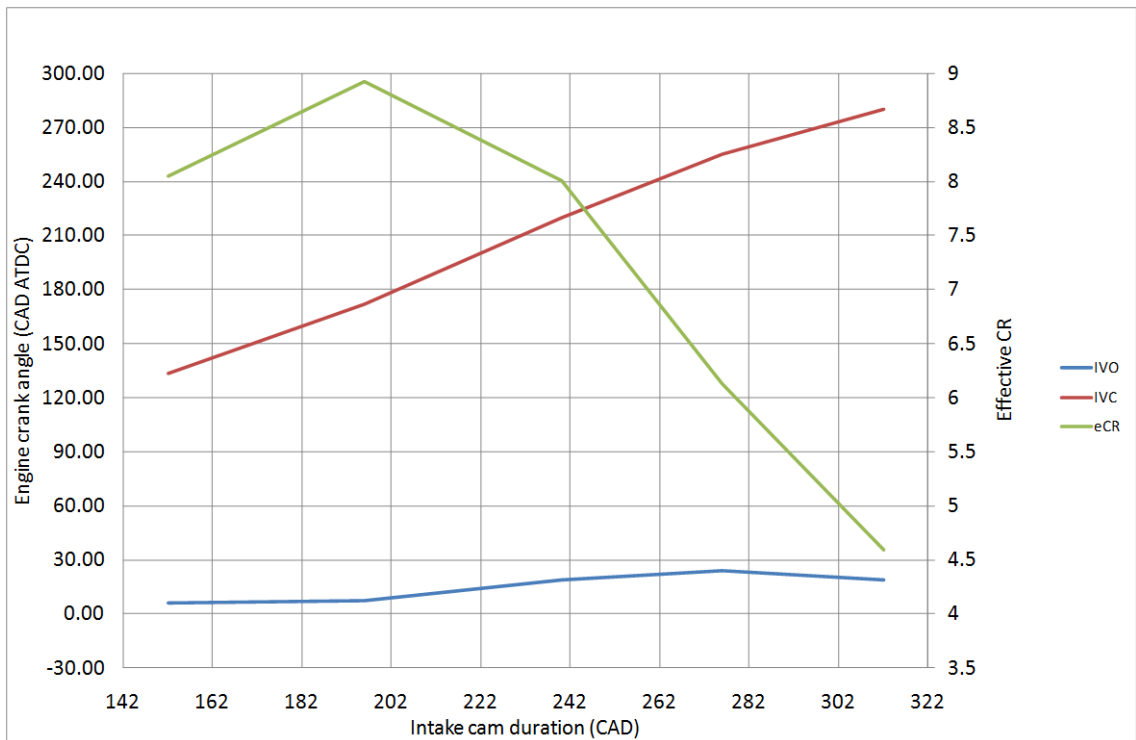


Figure 5.11 Optimum ISFC cam IMOPs for an EBP of 3 bar at a Geometric CR of 9

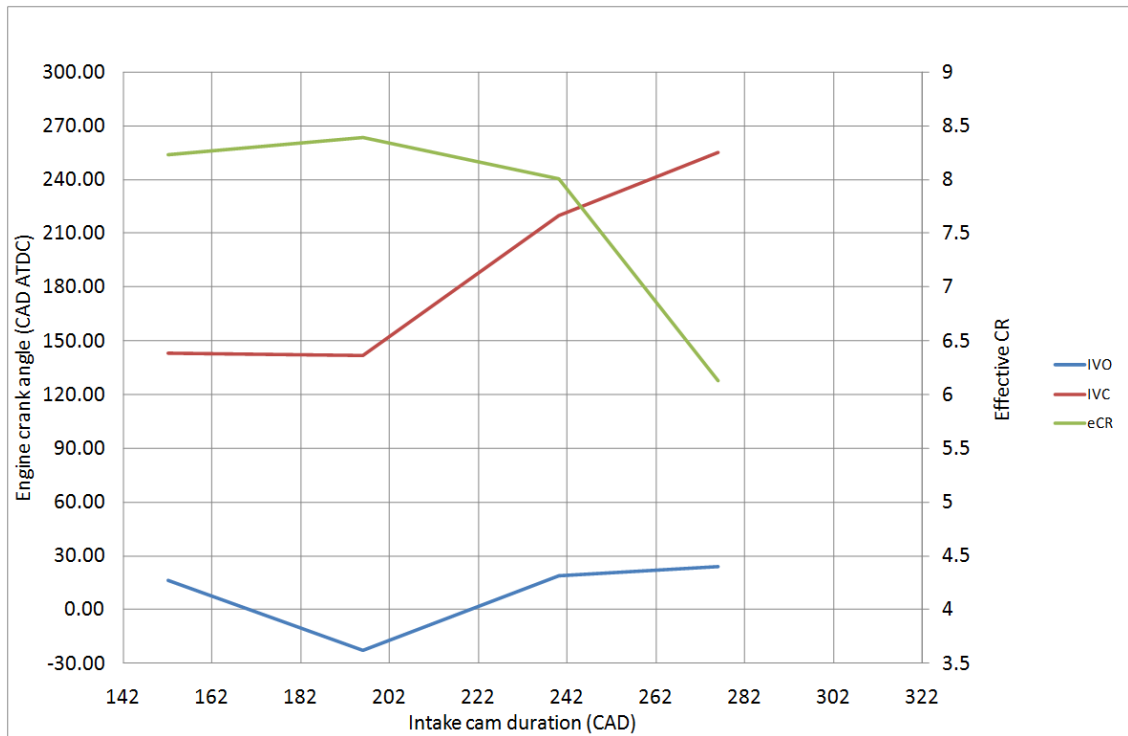


Figure 5.12 Optimum ISFC cam IMOPs for an EBP of 4 bar at a Geometric CR of 9

There is a clear trend for each of these points, they all favour a very small degree of valve overlap (with the exception of the 196 CAD duration cam at 4 bar EBP), the long cam profiles in particular. Figure 5.13 reveals where the optimum IVO opening is relative to the IVO limit for this test work. In all cases the IVC can be seen to be close to the limit but for durations of 240 CAD and above, the optimum IVC can be seen to be on the very limit of testing.

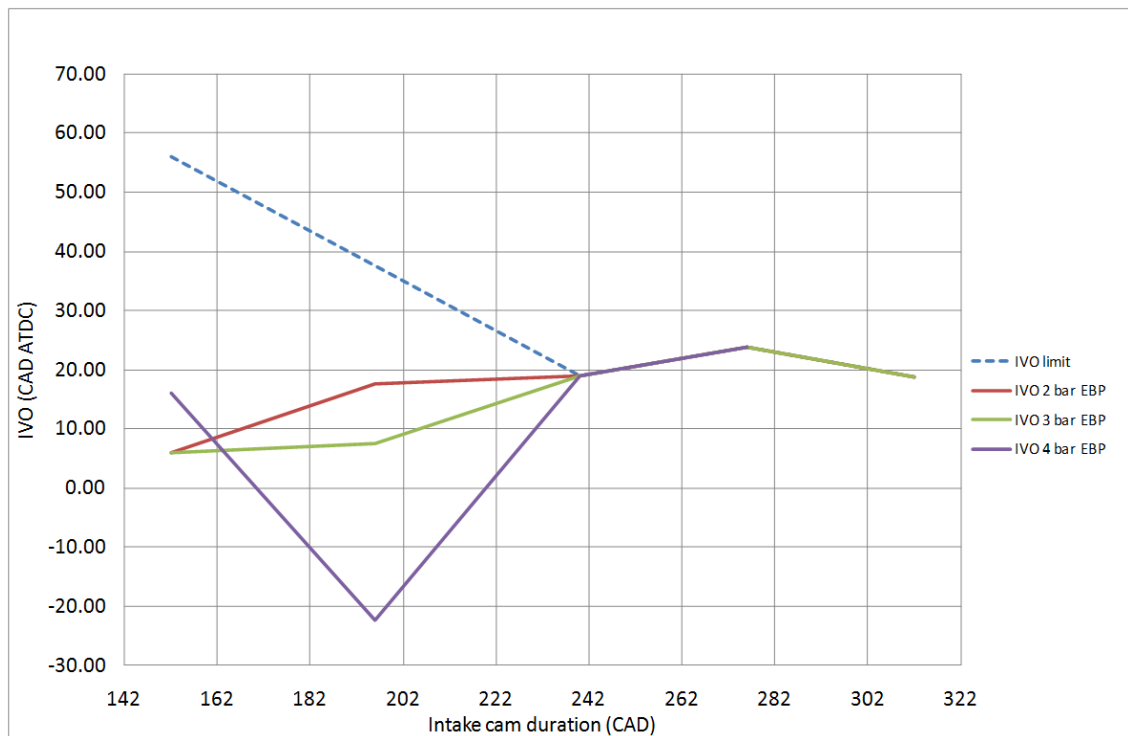


Figure 5.13 Optimum IVO Cam Timing Points for EBPs of 2 and 3 bar Compared to the IVO Limit for a Geometric CR of 9

The IVO time can be delayed until much later with the short cams owing to the fact that even with an IVO of nearly 60 CAD After TDC (ATDC) the IVC point still occurs at just 3 CAD After BDC (ABDC). With the longer cams however, even with a relatively conservative IVO of 20 CAD ATDC, IVC occurs at 100 CAD ABDC which requires a very high MAP. Going beyond 20 CAD ATDC IVO with the longest 312 CAD duration cam by just 10 CAD will require an MAP of 4.84 bar which logistically is not feasible with current technology and falls out of the scope of this project. The 276 CAD duration cam has similar issues although the IVO time can be delayed slightly beyond the 312 CAD duration cam but only by 6 CAD. The 240 CAD duration cam IVO time could be delayed until later but was not for this test work as the intention was to use the standard cam for baseline comparison purposes only. Further work has revealed that the ISFC can be improved by 2 g/kWhr if the 240 CAD duration cam IVO time is delayed by a further 10 CAD, if it is delayed any more than this ISFC begins to increase. The reason for this increase in ISFC beyond a certain IVO delay time can be attributed to the increase of residuals in the cylinder.

All of this test work was carried out with the exhaust valve in the maximum valve overlap position and the Exhaust Valve Closing (EVC) point fixed at 16 CAD ATDC. Therefore between TDC and the EVC point the piston will begin to draw hot exhaust gasses back into the cylinder. If there is no valve overlap period at all these gasses will remain in the cylinder for the next cycle. Cool residual gasses have the effect of reducing the propensity to knock, however, in this scenario they are hot and if they are present in the cylinder in sufficient quantities they will considerably elevate the charge temperature above the manifold temperature of 40⁰C. This in turn will lead to elevated EOC pressure and temperature and potentially an increased propensity to knock.

This phenomenon is particularly present for the 196 CAD duration cam where a reduction in effective CR can be seen to result in an increase in EOC pressures and temperatures (Figures 5.14 and 5.15 respectively). This can be attributed to the breathing dynamics of the engine which have been explained in section 5.3.5.

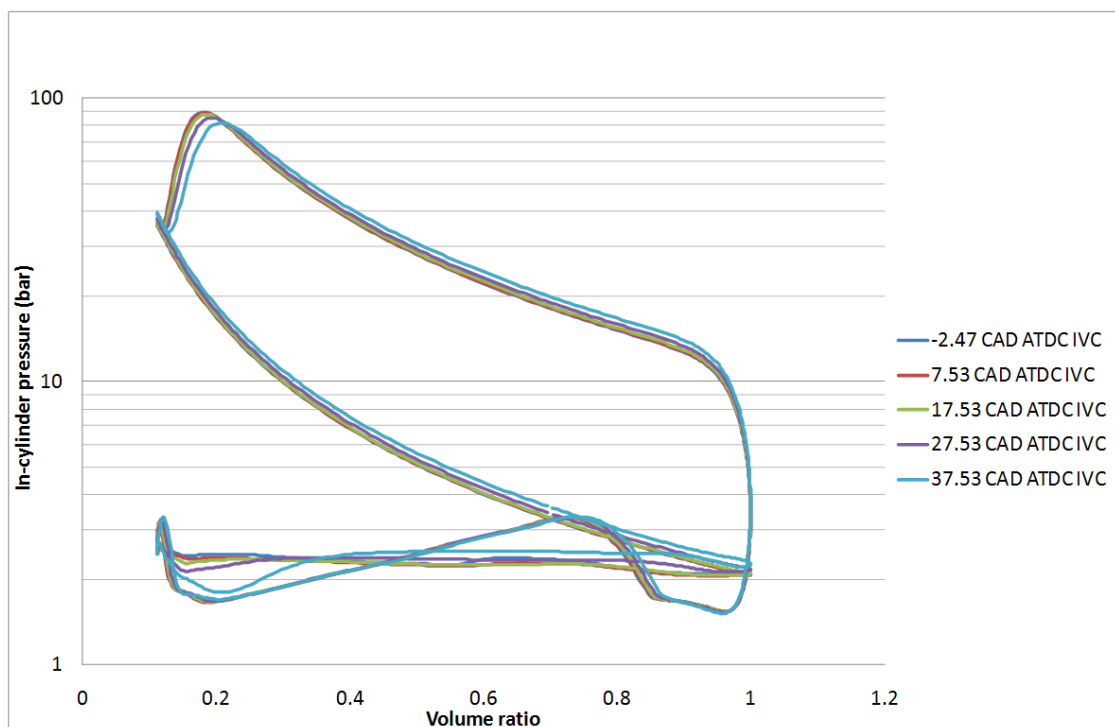


Figure 5.14 Log P-V IVC Sweep for 196 CAD Duration Intake Cam at a Geometric CR of 9 and an EBP of 2 bar

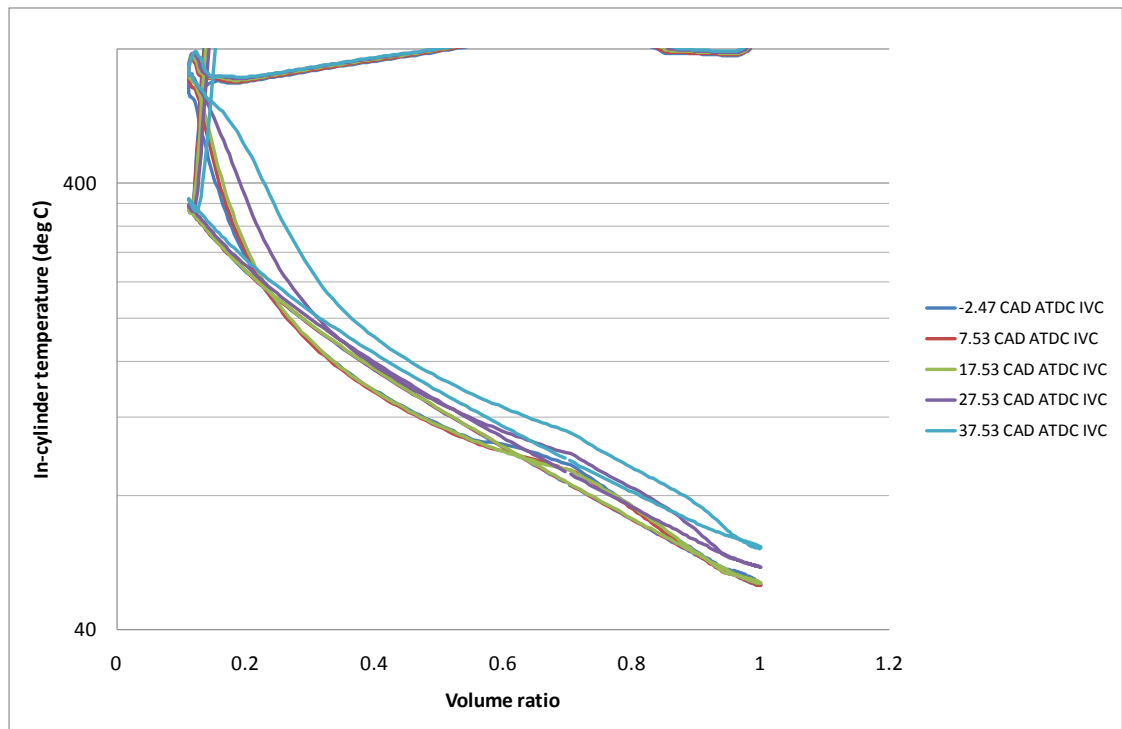


Figure 5.15 Log Temperature Vs. Volume Ratio IVC Sweep for 196 CAD Duration Intake Cam at a Geometric CR of 9 and an EBP of 2 bar

The 4 bar EBP points are of limited relevance for this speed and load condition because for most of the optimum IMOP timings the MAP was not so high as to warrant an EBP of 4 bar, unless a very poorly specified turbocharger was employed. The EBP points of 2 and 3 bar were of greater relevance, however, the 152 CAD and 312 CAD duration cams required very high MAPs, typically in excess of 3 bar, and the 4 bar EBP points may be relevant to them.

The integrity of the data at 4 bar EBP is noticeably worse than at 2 and 3 bar, particularly for points with a very late IVC. The EOC pressures and temperatures and quantity of residuals in the cylinder were sufficiently high to cause the knock model to malfunction and predict what is effectively (although not actually because the knock model cannot predict pre-ignition) very severe pre-ignition. Even with IVCs that allowed a high degree of valve overlap the cylinder would not scavenge because the EBP was almost always elevated above the MAP. This also resulted in malfunctioning of the knock model in some instances.

A comparison of the optimum IMOP timings for each of the cams at EBPs of 2, 3 and 4 bar can be found in Figure 5.13. The optimum IMOP timings can be seen to be much more variable at 4 bar EBP than for the 2 and 3 bar EBP cases due to the fact that scavenging no longer occurs during valve overlap periods. The biggest difference between the 2 and 3 bar EBP cases and the 4 bar EBP case is with the 196 CAD duration cam. The optimum IMOP has shifted from a very little valve overlap IMOP timing to the maximum valve overlap IMOP timing.

The reason for this shift is the engine breathing dynamics and the presence of pressure/rarefaction waves in the exhaust system (see section 5.3.5).

The EBP can be seen to have a different impact on the engine depending on cam duration. Figure 5.9 shows the sensitivity with the 152 CAD duration cam to be very low at 4 g/kWhr variation between the 3 different EBPs, whereas the variation with the 240 CAD duration cam is very high at 13 g/kWhr. An insensitivity to EBP is obviously desirable because increasing EBP is always detrimental to engine efficiency due to the inability to scavenge and inability to keep the cylinder cool.

The burn duration can be expected to increase in duration with rising EBPs because of the greater quantities of residuals in the cylinder at cycle start, this makes the ISFC values given in Figure 5.9 slightly optimistic for the 3 and 4 bar EBP cases in comparison to the 2 bar EBP case.

5.3.2.2.2 Geometric CR Effects

Figures 5.16, 5.17 and 5.18 show overlays of the optimum ISFC points for each of the different cam durations for 3 different geometric CRs of 9, 10.75 and 12.5 respectively. Due to data integrity issues Figure 5.18 had to be truncated.

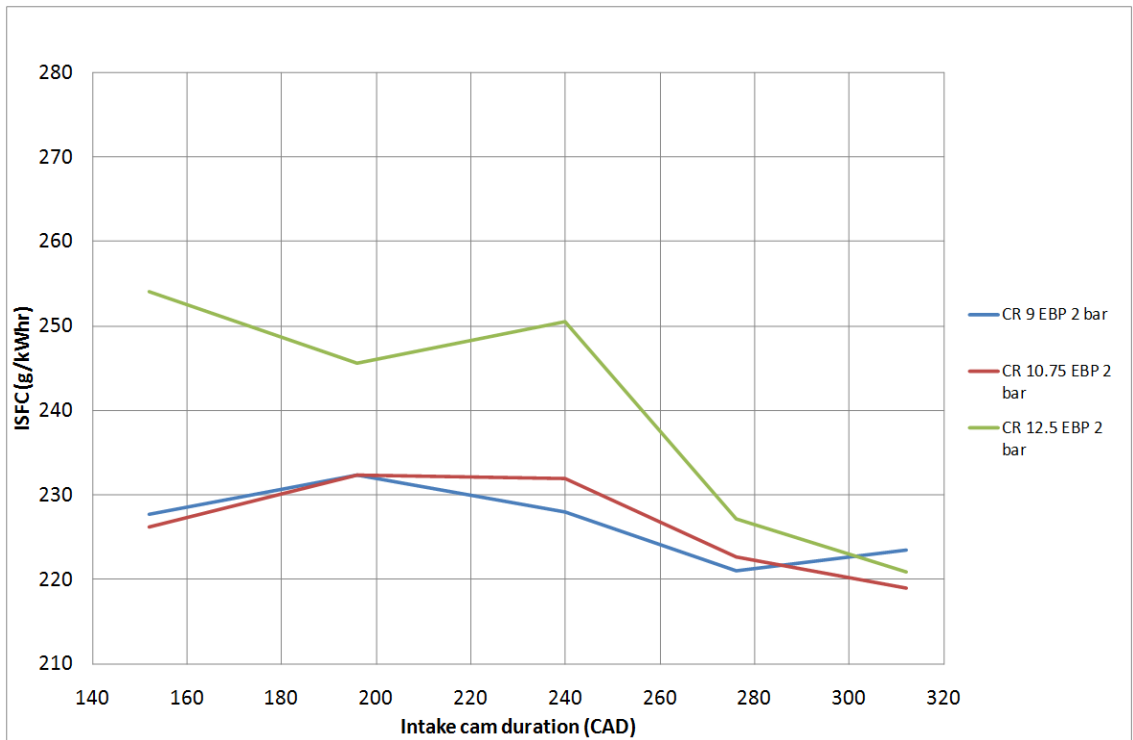


Figure 5.16 Comparison of Different Geometric CRs with an EBP of 2 bar

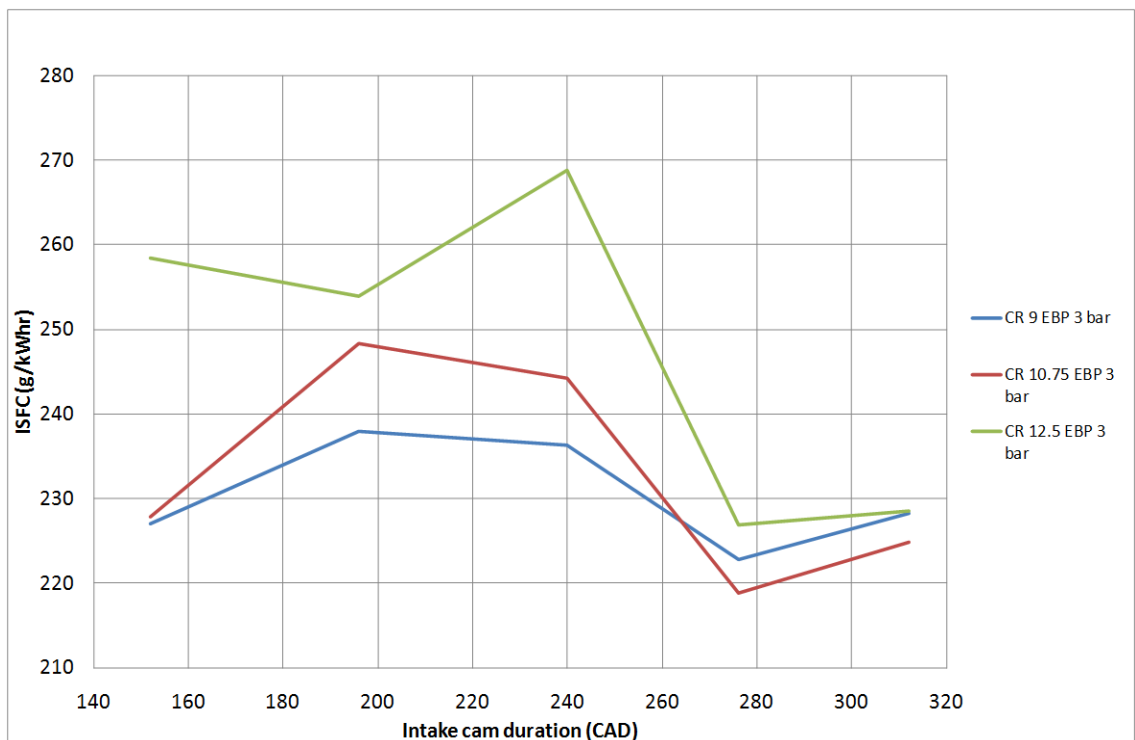


Figure 5.17 Comparison of Different Geometric CRs with an EBP of 3 bar

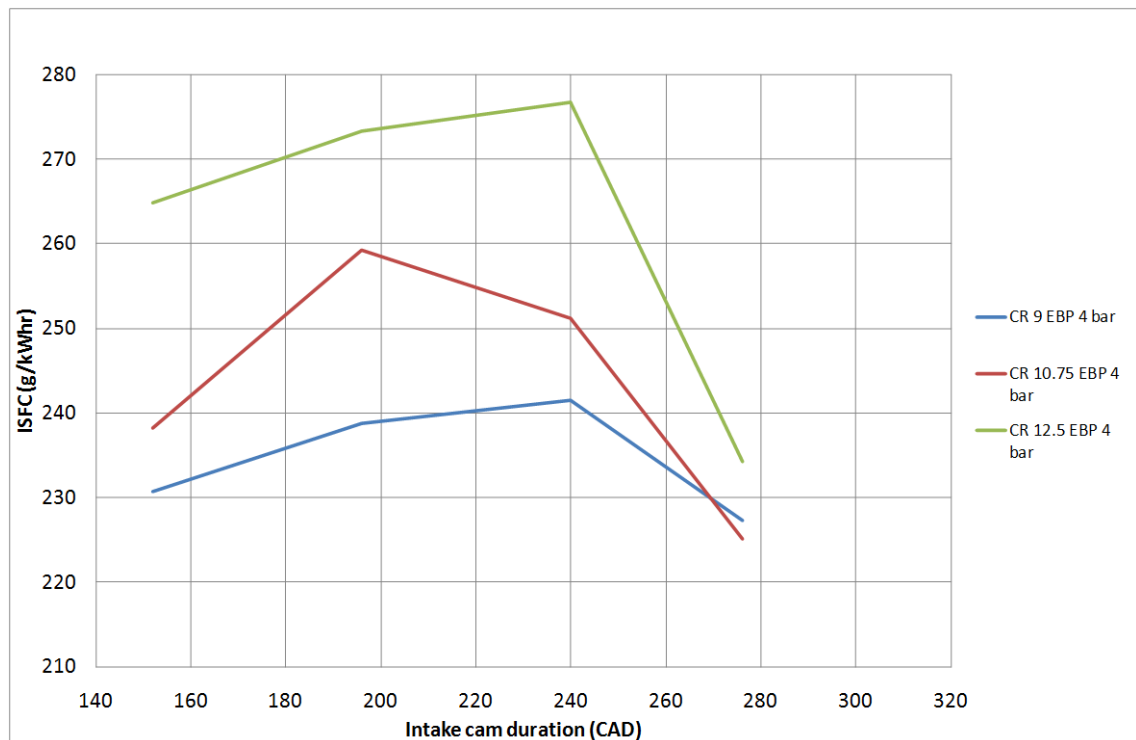


Figure 5.18 Comparison of Different Geometric CRs with an EBP of 4 bar

The data reveals that the long cams show the greatest potential for running at high geometric CRs. At this load point, where the engine is particularly susceptible to knock, a higher geometric CR is actually beneficial to engine running. The very short cam with a high geometric CR can be beneficial to ISFC too, but the results show a very high sensitivity to EBP at this condition. The 196 CAD and 240 CAD duration cams generally have a detrimental effect on ISFC with increasing geometric CR.

Generally speaking the cam profiles that offer the lowest effective CRs show the greatest synergy with geometric CR increase. This is to be expected because increasing geometric CR has the effect of undoing any effective CR reduction that has already been applied. If the cam duration is such that not much effective CR reduction can be applied, a geometric CR increase of 1.75 will increase the effective CR beyond the previous geometric CR. With very long or very short cam durations this does not occur, and even with an increase in geometric CR of 3.5, the effective CR can still be seen to be far below the initial geometric CR.

The engine breathing at geometric CRs of 10.75 and 12.5 is very similar to the engine breathing behaviour at a geometric CR of 9. The optimum load points occur at

very similar cam timings as the geometric CR of 9 line, however, there is a slight offset in some cases. For low EBPs the optimum cam timing can be observed to be offset slightly toward the minimum valve overlap point. The reason for this is a high geometric CR results in a reduced clearance volume. The rate of scavenging can be seen to be near enough constant for different geometric CRs therefore a low clearance volume will be scavenged more rapidly than a larger clearance volume and more fresh air will be scavenged into the exhaust. This results in more accidental fuel enrichment which is detrimental to ISFC. For large degrees of valve overlap this makes ISFC markedly worse for high geometric CRs compared to low geometric CRs.

In Figure 5.16 the geometric CR of 10.75 line can be seen to overlay the geometric CR of 9 line very closely. With rising EBP the 2 lines can be seen to diverge slightly, particularly for the 196 CAD and 240 CAD duration cams. This can be attributed in part to the extended pumping loop afforded by the increase in geometric CR.

5.3.2.3 5000rpm, 24 bar BMEP

5.3.2.3.1 EBP Effects

Figure 5.19 shows an EBP sweep at a geometric CR of 9. The profile of the lines can be seen to be drastically different to the lower speed and load profiles (Figures 5.4 and 5.9). This is attributed almost wholly to the requirement for enrichment to reduce exhaust gas temperatures.

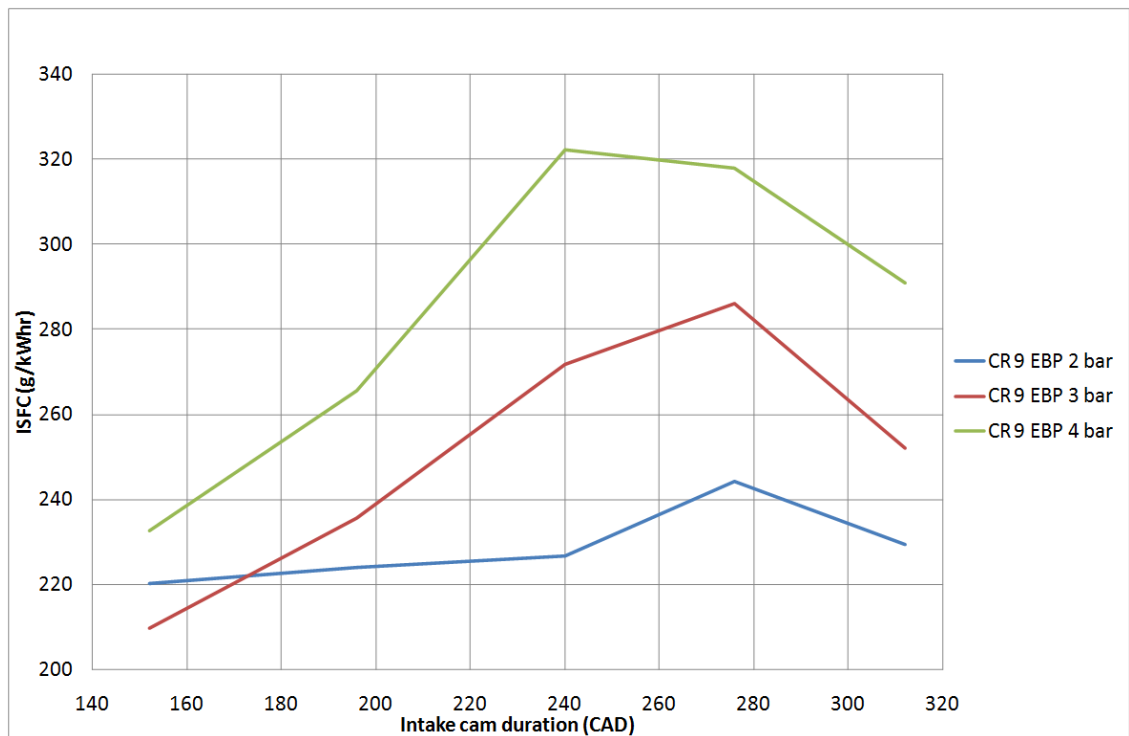


Figure 5.19 Comparison of 2, 3 and 4 bar EBPs at a Geometric CR of 9

Almost the exact opposite trend can be seen compared to the lower speeds and loads where enrichment was not necessary. The short cams are required for optimum ISFC for all EBP cases at this speed and load. At the lower speed points excessive scavenging was identified as the cause for high ISFCs. This could have potentially been offset by mapping the required lambda at the speed and load condition but was not, and therefore represented one of the worse cam durations for these speeds.

Running at this high a speed gives the engine less time to induct and exhaust gasses, and as a consequence of this the MAP was typically a lot higher at this speed than at the equivalent point at 2000rpm. Several points were excluded from this analysis in spite of the fact they were the optimum for that particular cam duration, geometric CR and EBP combination. The reason for this is that the engine would fail to achieve the required load of 24 bar BMEP even with the MAP set to the maximum of 4 bar. The points most afflicted by this problem were the points with a very low effective CR, where typically a lot of boost would be required. This has had a notable impact on some trend lines obtained and these points will be identified throughout the course of this section.

The breathing dynamics of the engine are very similar to the 1000rpm and 2000rpm cases in that the MAP to EBP ratio and valve overlap timings still dictate how much scavenging or backflow takes place. At 5000rpm there is far less time to scavenge the cylinder or for backflow to propagate into the intake manifold, so although scavenging still takes place there is not as much as there would be at 1000 and 2000rpm. For the 152 CAD duration cam scavenging can still be seen to take place, this results in accidental over enrichment of cylinder charge, however, at this speed fuel enrichment would be required to regulate the exhaust temperature for some EBPs anyway.

The degree of accidental over enrichment at a common running point of geometric CR of 9, IMOP of 50 CAD ATDC and an EBP of 2 bar is 23.32% at 2000rpm as opposed to just 6.81% at 5000rpm. With an over enrichment percentage this low the 152 CAD duration cam begins to provide an ISFC similar in magnitude to that predicted by the use of lambda mapping at lower speeds (see section 5.3.4), and represents a much more viable cam duration choice at this speed.

Another major advantage offered by the 152 CAD duration cam is that scavenging air through the cylinder will have the effect of diluting the exhaust gasses, thus reducing the exhaust gas temperature. This phenomena as well as the fact the effective CR ratio is very low at this IMOP with this cam results in an exhaust gas temperature of 787.8°C , well below the maximum limit of 930°C . Accidental over enrichment is partly responsible for such a low exhaust gas temperature. Removing the accidental over enrichment results in an exhaust gas temperature of 827.67°C which is still well below the maximum temperature limit thus rendering any quantity of enrichment unnecessary, however, a lower exhaust gas temperature does have a small impact on the EOC pressure and temperature for the subsequent cycle. Over enrichment also has the effect of lowering the polytropic exponent which serves to reduce EOC pressure and temperature through charge cooling. This will influence the combustion phasing and permits it to be moved closer to MBT for the accidental over enrichment case. It is for this reason that a 6.81% reduction in fuel flow rate yields a benefit in ISFC of 6.62% and not 6.81%, and the combustion must be retarded 0.266 CAD further away from MBT for the compensated case.

The 152 CAD duration cam exhibits the least sensitivity to EBP at this speed and load condition. All of the EBP conditions can be seen to benefit from the reduced scavenging, and for the 3 and 4 bar EBP cases the optimum cam timing is the maximum valve overlap condition. The optimum cam timing for 4 bar EBP is also the maximum valve overlap condition, however, this point was excluded from this analysis because even with an MAP of 4 bar the engine could not reach a BMEP of 24 bar, therefore the IMOP with the second largest degree of valve overlap, and the second lowest ISFC, was selected instead.

As with the other cases the general profile of the lines in Figure 5.19 can be seen to mimic the effective CR quite closely. The degree of divergence in each of the lines can also be seen to grow as effective CR is increased too, reflecting the increasing EOC pressures and temperatures associated with higher EBPs and higher effective CRs. The peak ISFC does not occur at peak effective CR though, it is instead offset slightly toward the longer duration cams, occurring at 240 CAD duration cam for the 4 bar EBP case and 276 CAD duration cam for the 2 and 3 bar EBP cases.

Analysis of the 276 CAD duration cam data has revealed that the optimum IMOP timing for an EBP of 2 bar is the maximum valve overlap position, whereas it is the minimum valve overlap position for 3 and 4 bar EBP cases. The reason for this is the pressure difference between MAP and EBP. For the 2 bar EBP case the MAP is greater than the EBP hence scavenging occurs during the valve overlap phase, for the 3 and 4 bar cases EBP exceeds MAP leading to back flow through to the intake.

Maximum valve overlap is optimum for the 276 CAD duration cam with 2 bar EBP case, however, the difference in ISFC across the entire IMOP sweep can be seen to be very small in comparison to most of the other IMOP sweeps for other speed/load/EBP/geometric CR combinations, showing a variation of just 7.84 g/kWhr in ISFC across the entire sweep. This shows that the balance between scavenging and effective CR reduction is very fine at this condition. The maximum valve overlap point corresponds to the highest effective CR point for the 276 CAD duration cam whereas the minimum valve overlap corresponds to the lowest effective CR point. Enrichment is required at every point in the IMOP sweep to regulate exhaust gas temperature. Less

enrichment is required at the maximum valve overlap point due to the fresh air scavenging that is taking place whereas more is required at the minimum valve overlap point due to the presence of hot exhaust gasses in the cylinder during compression. Very small amounts of charge can be seen to propagate into the intake manifold at the minimum valve overlap point, but there is no evidence of charge scavenging.

Figure 5.20 shows the lambda, effective CR and ISFC for the geometric CR of 9, EBP 2 bar IMOP sweep. The lambda line can be seen to resemble a V shape, the first peak at an IMOP of 100 CAD ATDC (maximum valve overlap) is a result of fresh air scavenging diluting the exhaust gasses and resulting in a reduction of exhaust gas temperature. The first peak is the highest, however, the value given is exhaust lambda which, as discussed before, is slightly lean of the cylinder lambda due to accidental over enrichment. The second peak occurring at an IMOP of 140 CAD ATDC is as a result of the very low effective CR reducing the EOC pressure and temperature.

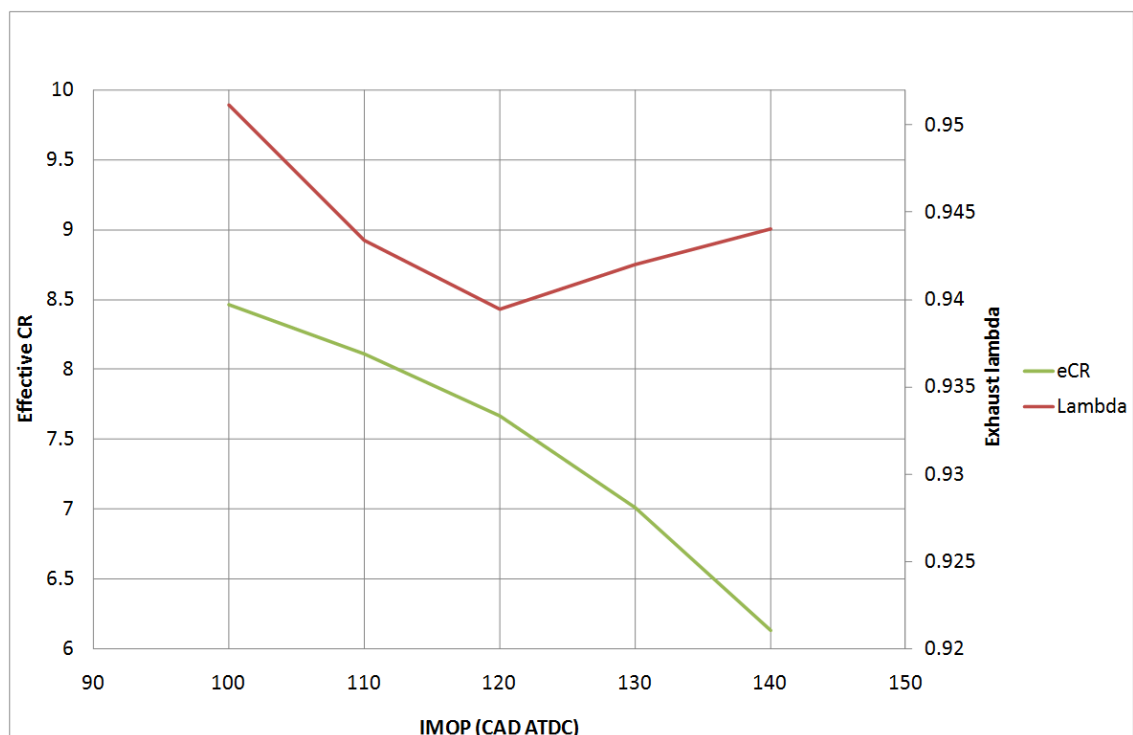


Figure 5.20 Effective CR and Lambda Plots at a Geometric CR of 9, EBP of 2 bar and a Cam Duration of 276 CAD

For this cam duration this is the key determinant in what the optimum cam timing is, and it is for this reason that the optimum cam timing shifts directly from a

maximum valve overlap position to a minimum valve overlap position with increasing EBP (when fresh air scavenging is no longer possible).

Unlike the 1000rpm and 2000rpm points, at 5000rpm and 24 bar BMEP on a turbocharged engine the EBP is almost inevitably above the MAP and 3 bar. Therefore running in the maximum valve overlap position is not going to be a possibility and effective CR reduction is the only means of yielding an ISFC improvement. Something else that must be taken into consideration is that the air and fuel that has been scavenged could react when in the exhaust system thus raising exhaust gas temperature considerably. GT-Power is not able to model secondary combustion outside the cylinder and this effect has therefore not been factored in.

At higher EBPs the lambda line can still be seen to resemble a V shape as shown in Figure 5.20. The peak in lambda at the maximum valve overlap position is attributed to accidental over enrichment giving the impression the engine is running leaner than it actually is. The minimum valve overlap point (IMOP of 140 CAD ATDC) can be observed to go from the optimum IMOP timing to the worst IMOP timing with increasing EBP. The transition between optimum and worst is moderately slow occurring over the course of a change of EBP of 1.3 bar, however, the transition from worst to best for the minimum valve overlap point (IMOP of 100 CAD ATDC) is very fast, occurring over the course of a change of EBP of just 0.2 bar.

This same trend can also be observed for the 312 CAD duration cam profile. In spite of the fact the IVC point does not occur until well into the compression stroke for all IMOP cases, very little charge scavenging can be seen to take place in comparison to the equivalent 2000rpm point. Although due to the fact over enrichment is used charge scavenging cannot be easily observed in the GT-Power data owing to the fact the vapour fuel fraction in the exhaust is not zero or almost zero even during normal running. As with the 276 CAD duration cam, the ISFC figures suggest that there is not a considerable amount of charge scavenging otherwise it would not be the optimum IMOP timing for ISFC.

Although the highest effective CR occurs at a cam duration of 240 CAD, the ISFC peaks there for just the 4 bar EBP case. The reason why it does not peak there for the 2

and 3 bar EBP cases is because of the IMOP timing. For both the 240 and 276 CAD duration cams at 2 bar EBP the optimum IMOP timing for ISFC is the maximum valve overlap point. The extent of the maximum valve overlap differs for each cam however. The IVO angle for the 240 CAD duration case is 21 CAD BTDC gas exchange, for the 276 CAD duration cam it is 16.15 CAD BTDC gas exchange. This allows a considerable amount more scavenging to take place for the 240 CAD duration cam in spite of the fact the MAP is lower. This has the effect of reducing the exhaust gas temperature. For the 240 CAD duration cam this lowers the temperature enough to not warrant the use of enrichment. The reduced exhaust gas temperature has a lower speed of sound meaning the pressure/rarefaction wave caused by the EBP valve is slightly later in the cycle, the significance of this is covered in section 5.3.5.

5.3.2.3.2 Geometric CR Effects

Figures 5.21, 5.22 and 5.23 show optimum ISFC points for each of the different geometric CRs at EBPs of 2, 3 and 4 bar respectively.

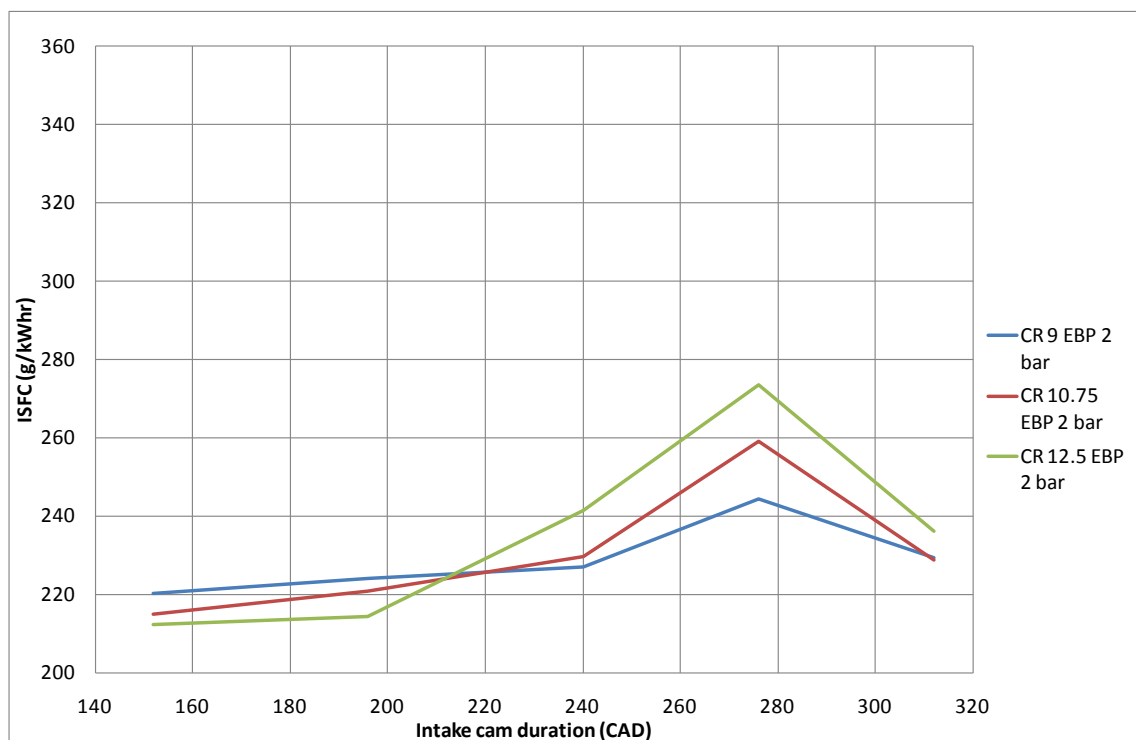


Figure 5.21 Comparison of Different Geometric CRs with an EBP of 2 bar

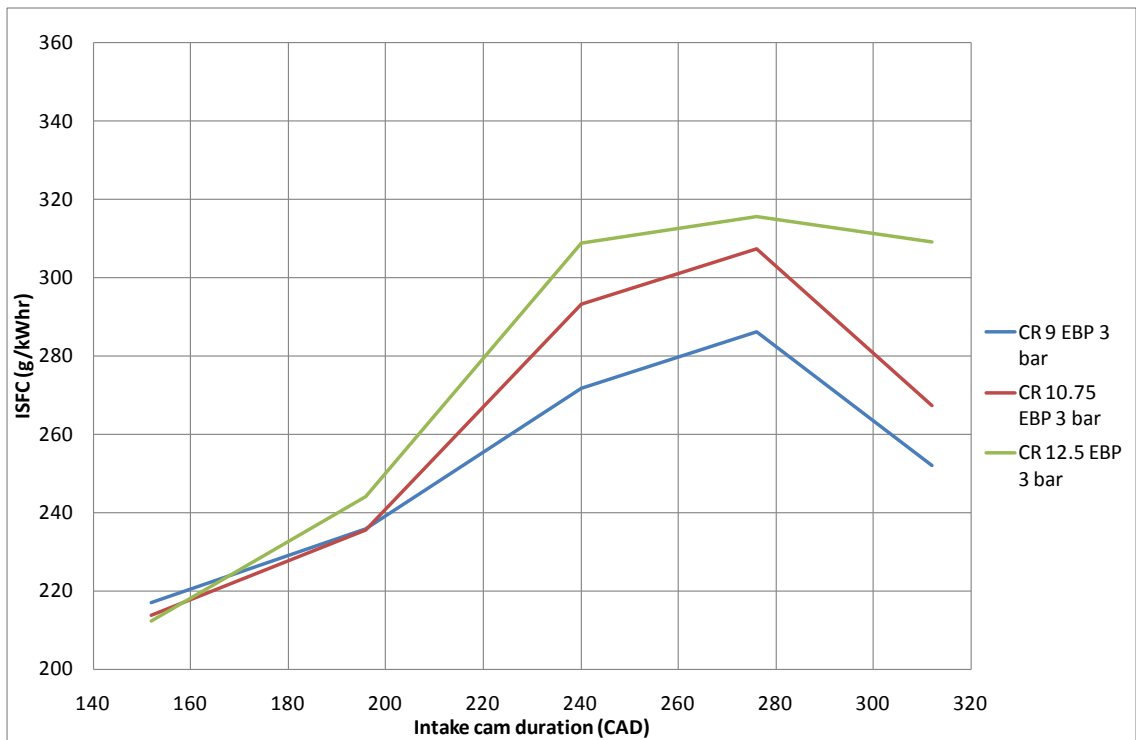


Figure 5.22 Comparison of Different Geometric CRs with an EBP of 3 bar

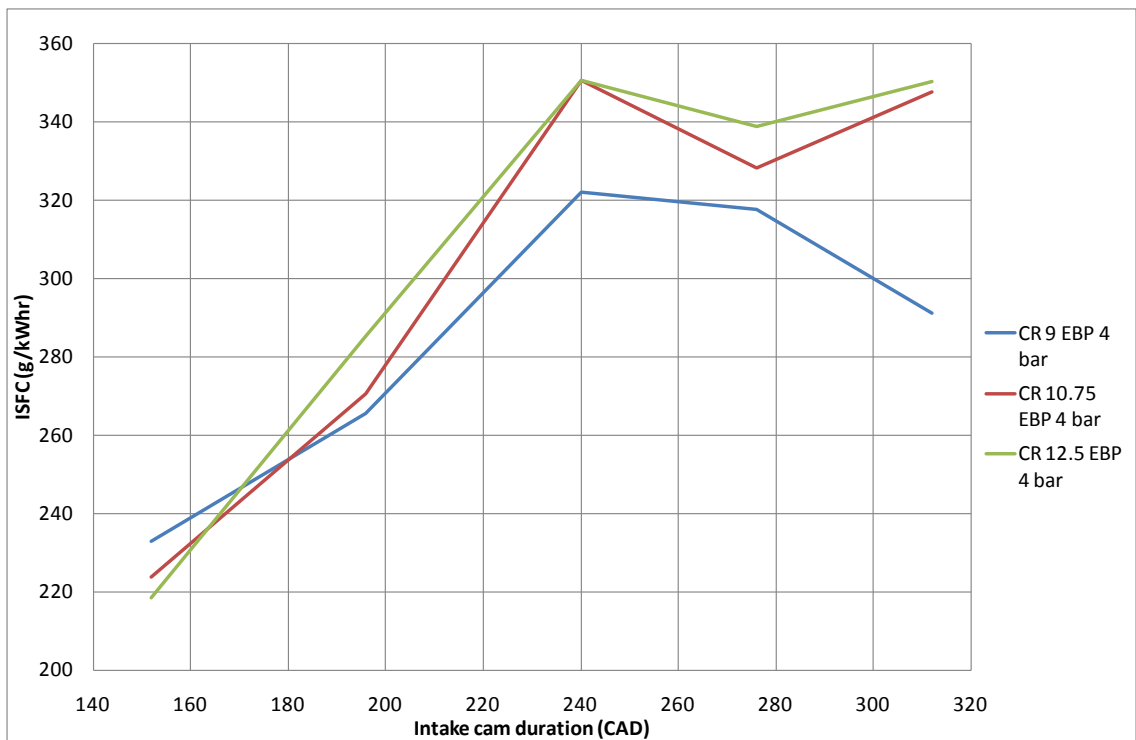


Figure 5.23 Comparison of Different Geometric CRs with an EBP of 4 bar

In Figures 5.21 to 5.23 all the geometric CR lines can be seen to show the same trend and all peak at the same positions. Of the 3 EBPs only the 4 bar EBP case can be seen to follow the effective CR trend where the peak ISFC occurs at the peak effective

CR. The reason for the offset for the 2 and 3 bar EBP cases can be attributed to scavenging. The optimum cam IMOP can also be seen to change between the maximum valve overlap point for the lower EBP cases to the minimum valve overlap point for the 4 bar EBP case. As the difference in MAP and EBP is reduced the engine breathing will be altered accordingly as described in section 5.3.2.3.1.

Figures 5.21 to 5.23 also reveal significantly less sensitivity to EBP for the 152 CAD duration cam than for any of the other cam durations for all geometric CRs. This can be attributed in part to the reduced EOC pressures and temperatures which greatly increases the tolerance to EBP, and also to the fact higher EBPs inhibit scavenging and accidental over enrichment. The benefit offered by higher geometric CRs can be seen to become less and less with increasing EBP due to the fact the EOC pressure and temperature is elevated by higher EBPs.

With the exception of the 2 bar EBP case the 312 CAD duration cam can be seen to break the trend of decreasing ISFC with decreasing effective CR. The reason for this is the choice of IMOP points is simply very restricted for this long cam because of the imposed 4 bar MAP limit. Therefore the chosen IMOP in this case does not necessarily mean it is the optimum, just that it is the only point that achieved the load with an MAP of 4 bar. There was just 1 IMOP timing that resulted in adequate load being achieved for the geometric CR of 12.5 and 4 bar EBP point, and that was the maximum valve overlap position because of the high effective CR it affords. Although this point has been displayed in Figure 5.23 as being valid, the exhaust gas temperature (even with the full degree of enrichment) is well above the temperature ceiling at 1013.6⁰C which actually renders it an invalid point too. The same applies to the 4 bar EBP and geometric CR of 10.75 case too, which is MAP restricted for the 312 CAD duration cam. The point shown in Figure 5.23 for this is also the maximum valve overlap point and it is also not strictly valid because the exhaust gas temperature exceeds the temperature limit. In both of the above cases the minimum valve overlap point would be optimum if a higher MAP limit was instated (because of the reduced effective CR).

The geometric CR of 9 point is also dictated by the MAP restriction, however, the IMOP point that gave acceptable load at this condition was the one that gave the second lowest degree of valve overlap, which is much closer to the optimum cam timing. The reason why adequate load could be achieved with the lower geometric CR is because the EOC pressure and temperature is much lower which allows the combustion phasing to be advanced slightly more than the geometric CR of 10.75 and 12.5 cases, the cycle efficiency is improved by this and the MAP therefore does not have to be as high. The exhaust gas temperature will also be reduced by the increased degree of combustion phasing advance.

The MAP limit has also manifested itself in Figure 5.22 (3 bar EBP) for the 312 CAD duration cam and has resulted in a point being selected that is not the optimum, hence the reason why it does not follow the reduced ISFC with reduced effective CR trend as closely as the 2 and 3 bar EBP lines.

Although not as visible as for the 312 CAD duration cam, the 152 CAD duration cam is also restricted in places by the MAP limit. As with the 312 CAD duration cam the MAP limit is only a problem at the higher EBPs where scavenging is impeded. The IMOP must be shifted to a lower valve overlap point when maximum valve overlap is optimum for this cam. Shifting the IMOP to a lower valve overlap point increases the effective CR which increases ISFC. The effect is far less marked though due to the fact less valve overlap results in less scavenging and less accidental over enrichment, this helps to offset the increase in EOC pressure and temperature.

5.3.3 Cam Timing Trends

Section 5.3.2 highlighted the impact of scavenging and various other phenomena on the ISFC performance of the single cylinder engine model. The purpose of this section is to highlight the impact of these phenomena on the optimum cam timing position for ISFC, and how far away this is from the theoretical optimum position for the cam in terms of effective CR reduction.

Figure 5.24 gives a general indication of the theoretical percentage gain in efficiency that can be obtained through using the theoretically optimum cam timing compared to what was found to be the optimum cam timing in the test work. This is shown for each cam. The frequency of the use of a theoretically non-optimal cam timing is shown in Figure 5.25.

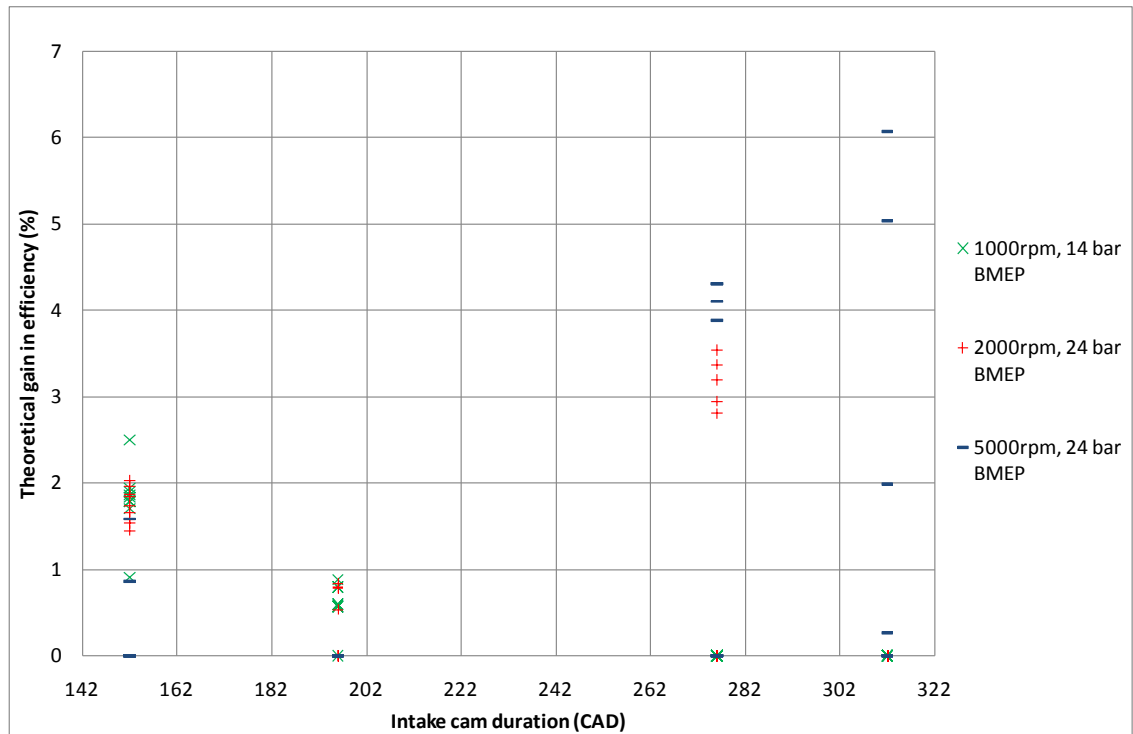


Figure 5.24 The Theoretical Gain in Thermodynamic Efficiency Through the Adoption of Optimum Cam Positioning

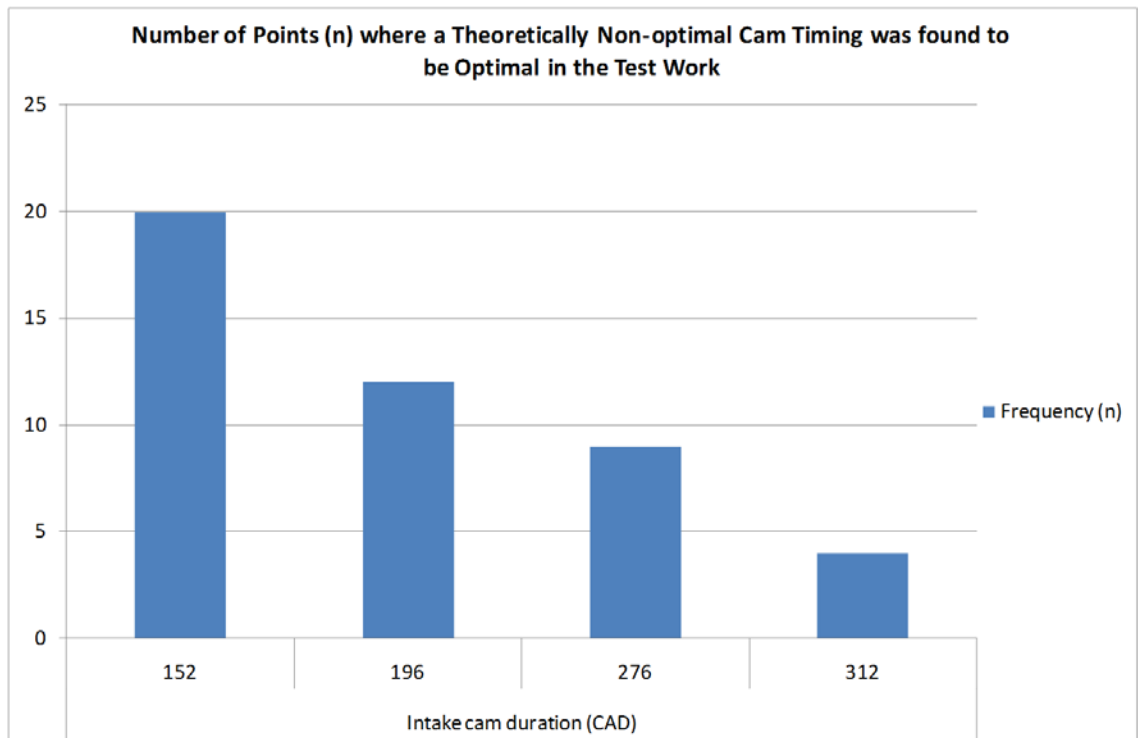


Figure 5.25 Number of Points where a Theoretically Non-optimal Cam Timing was found to be Optimal in the Test Work

Although the number of theoretically non-optimal cam timings with the 152 CAD duration cam is far greater than for any other cam, the theoretical loss of efficiency is not as considerable as it is for the 296 and 312 CAD durations cams. This is due to the fact that a higher degree of effective CR reduction can be adopted with the 276 and 312 CAD duration cams. Due to a hard point limitation with the 152 CAD duration cam, the effective CR can never be as low as with the longer cams. The impact of this on theoretical efficiency benefit is shown in Figure 5.26. Please note, the profiles of the lines are not perfectly parabolic due to the fact slightly more cam phasing was used with the 276 CAD duration cam.

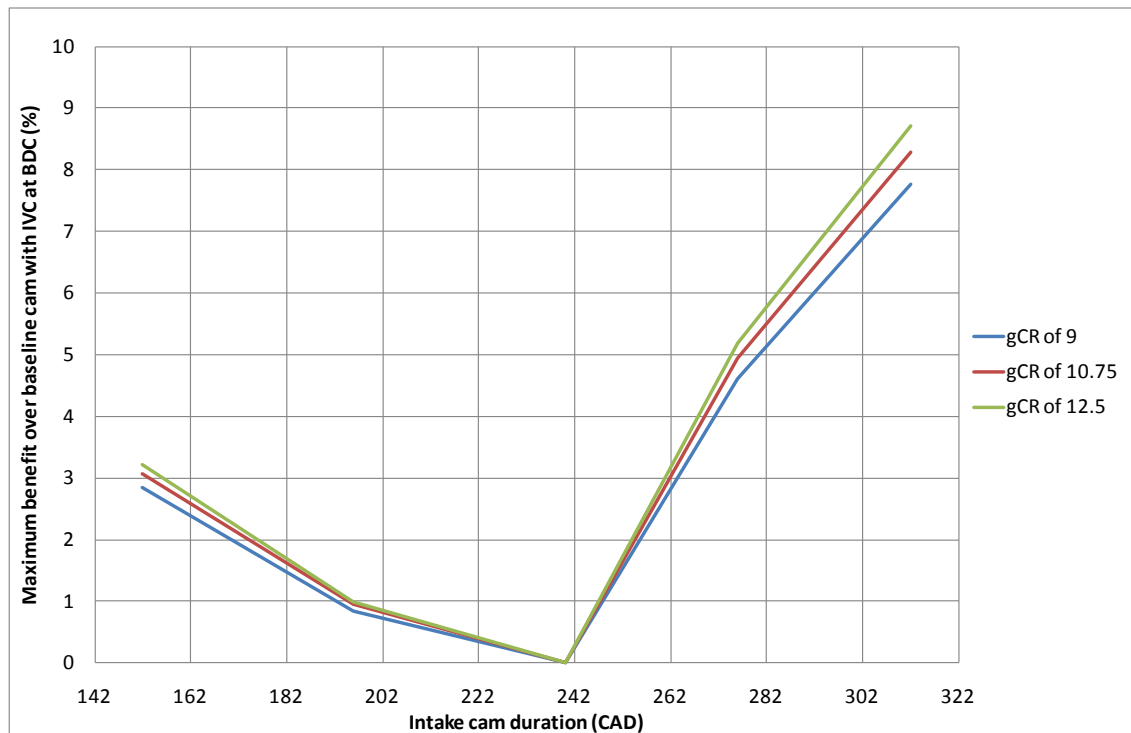


Figure 5.26 Maximum Benefit over Baseline Case (IVC at BDC) with each Cam at each Geometric CR

This means that it is not as critical to run at the optimum cam timing with the 152 CAD duration cam as it is with the 312 CAD duration cam.

Figure 5.24 reveals a clear trend with regard to engine speed. Of the 1000rpm 14 bar BMEP points, the ones that are not optimally timed all occur at short cam durations where scavenging was found to have a detrimental impact on ISFC. The 5000rpm 24 bar points generally did not experience the same issue with scavenging (due to the fact that the optimal timing is the minimum valve overlap position) so the cam could be placed in the optimal position, unlike at low speed. It was however heavily affected for the longer cam durations. The reason for this is the cam timing had to be reduced because the volumetric efficiency was so low with the cam in the optimum position that even with an MAP of 4 bar a load of 24 bar BMEP was unattainable.

The impact of geometric CR increase has very little effect on the cam timing with the exception of 5000rpm, this is due to the fact that the MAP limit was reached earlier with higher geometric CRs. This is likely due to the fact that a higher geometric

CR results in a lower overall cylinder volume for a constant swept cylinder capacity, hence a higher charge density is required to compensate for this.

EBP also shows no strong trends. Although elevated EBPs were found to inhibit scavenging this effect was not significant enough to shift the IMOP a whole 10 CAD (which was the resolution tested at for this work). It may be possible to observe cam timing effects at finer IMOP resolutions.

5.3.4 Scavenging Effects

Two different forms of scavenging were observed to take place during this study, one form is the scavenging of fresh air (called simply “scavenging” for this study) and the other is the scavenging of charge (called “charge scavenging”). The effects of these 2 forms of scavenging are particularly marked for the 152 CAD duration cam and the 312 CAD duration cam. Although both EIVC and LIVC are both very susceptible to the effects of scavenging, the effects are usually less noticeable with LIVC due to the fact the optimum cam timing is the minimum valve overlap point. Figure 5.27 demonstrates this.

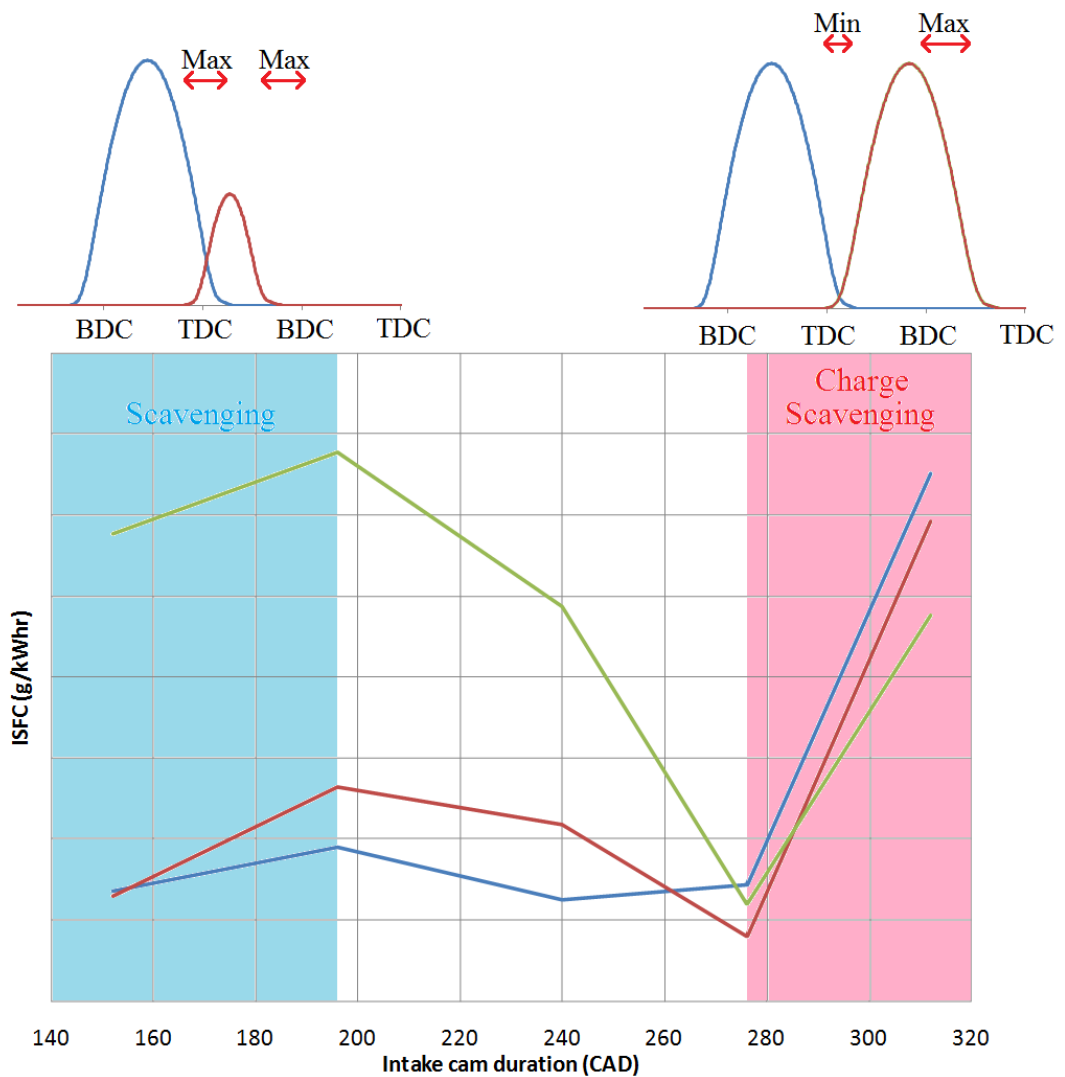


Figure 5.27 Demonstration of Optimum Cam Timings for EIVC and LIVC

5.3.4.1 Scavenging

Although scavenging is generally beneficial to cycle efficiency, it can have the effect of diluting the exhaust gases with fresh air and causing the exhaust gas to appear lean. As a consequence of this the EMS will inject more fuel than is necessary to restore the engine to “stoichiometric” when in actual fact in-cylinder lambda is too rich (accidental over enrichment).

Scavenging (the blue region of Figure 5.27) was found to be particularly dependent on speed, load, EBP and geometric CR. Scavenging is particularly marked at

low speed and high load where the MAP is usually greater than the EBP, and the valve overlap period is usually quite long in terms of a period of time (no different when measured in CAD). This affect has been mapped on the engine operating envelope and is denoted by the blue region in Figure 5.28, which was obtained from the 3 cylinder engine at Mahle Powertrain.

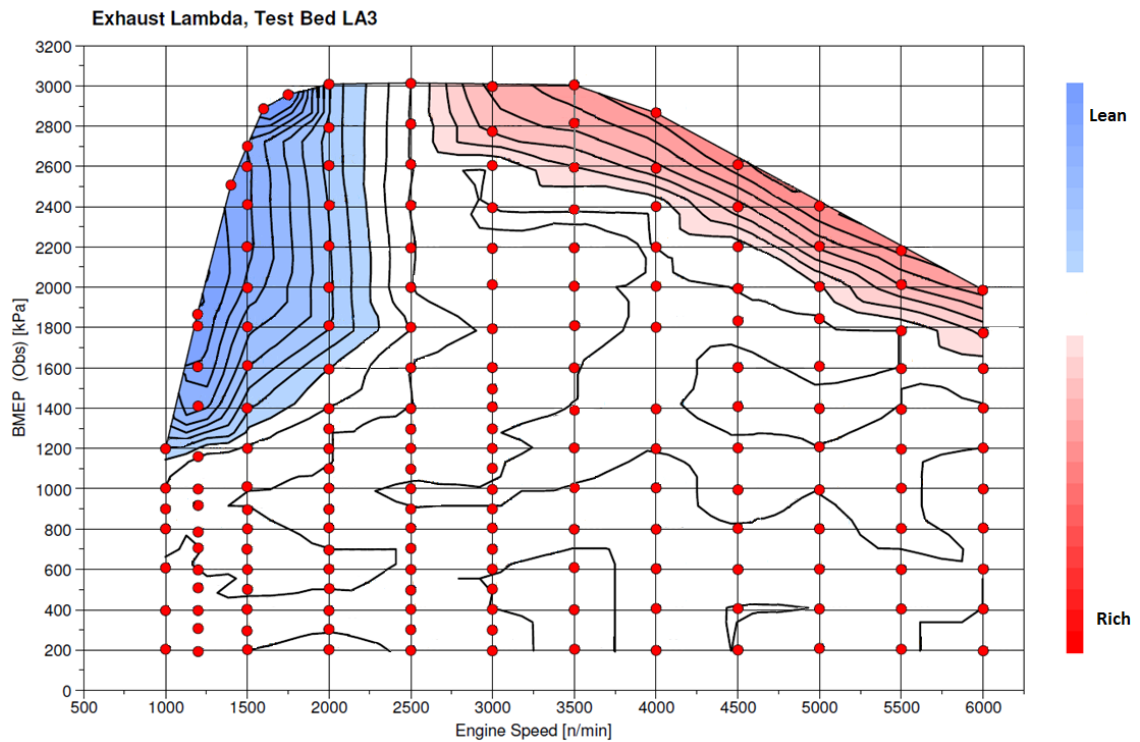


Figure 5.28 3 Cylinder Engine Speed and Load Map Showing where Exhaust Lambda Enrichment and Leaning is Used

This map could not be used at any point in this test work though, not even for the 240 CAD duration standard cam. This is because the engine breathing is very different for the single cylinder engine, as well as the MAP and EBP combinations which, for the 3 cylinder engine, are dictated by the turbocharger and fixed. The huge degree of variation available for the single cylinder engine, as well as the different cam durations, made creating maps like that in Figure 5.28 a huge task. This could theoretically be carried out in GT-Power by incorporating closed loop control of exhaust lambda based on in-cylinder lambda but the complexity of the model would be increased significantly and places even more onus on the in-cylinder combustion modelling for accurate results.

Instead the decision was made to run the engine at lambda 1 for all test work and to compensate for the accidental over enrichment at a later date. The method employed for compensating for accidental over enrichment was to extract the in-cylinder lambda from the DoE data and multiply it by the ISFC. This is a very simplistic approach and fails to take into account the added charge cooling effect of the fuel. This makes the ISFC after this calculation slightly optimistic.

The accidental over enrichment has had the effect of skewing the results slightly, and is the reason why the optimum IMOP position for ISFC recorded for the standard 240 CAD duration cam for speeds of 1000rpm and 2000rpm is not the maximum valve overlap position as is the case with the 3 cylinder engine. The decision to not use lambda correction for accidental over enrichment has the biggest impact at low EBP points with high MAPs and with large degrees of valve overlap. The impact on the quoted ISFCs for the worst case speed and load point of 1000rpm, 14 bar BMEP in percentage terms can be seen in Figure 5.29. The tables show the maximum percentage difference between the compensated and uncompensated values for each cam, EBP and CR combination. The percentage values refer to how much larger the ISFC is for the uncompensated value in comparison to the compensated value.

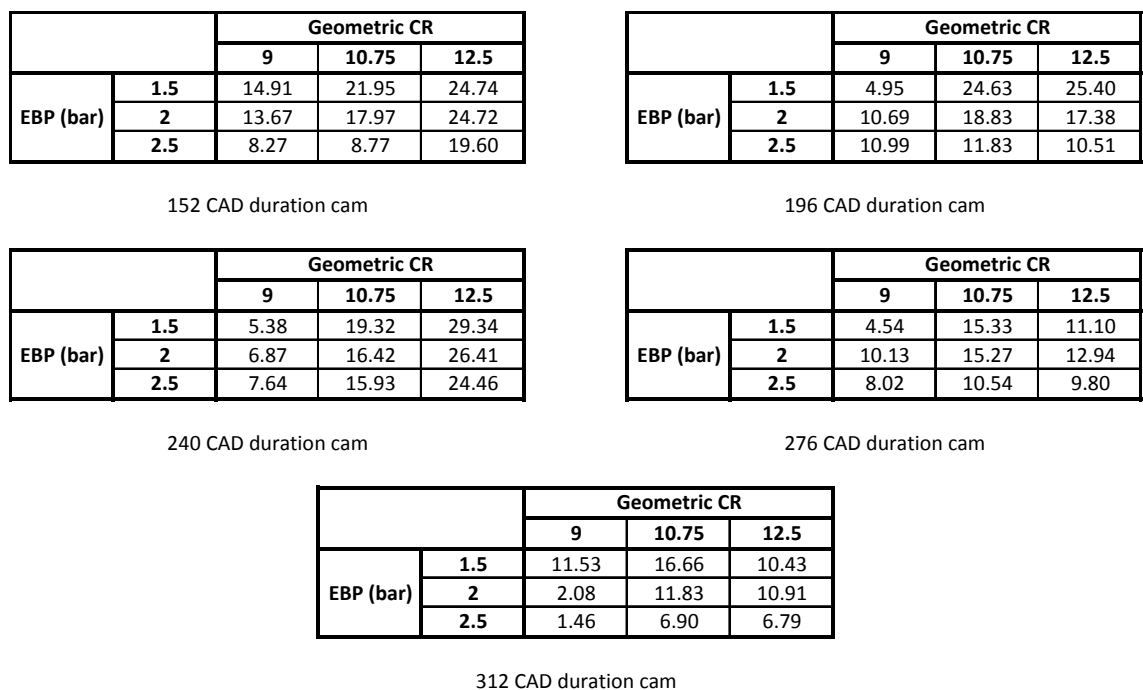


Figure 5.29 Scavenging Compensation (%) for each of the Different Cams at each EBP and CR for 1000rpm and 14 bar BMEP

The cams that are most affected by accidental over enrichment are the shorter cams. The main reason is the longer duration cams gain efficiency through the reduction of effective CR, which is generally not achieved with high degrees of valve overlap. The values are generally larger for the higher CR points because the smaller clearance volume for higher CRs is quicker to scavenge than for lower CRs, therefore more fresh air short circuits to the exhaust than with lower CRs. The shorter cam also requires the highest MAP at the maximum valve overlap point of all of the cams being tested, which will increase scavenging.

Accidental over enrichment is still present at 2000rpm (Figure 5.30) and is similar in magnitude to the 1000rpm case, in spite of the fact the cylinder has the half the amount of time to scavenge at this speed. The reason for this is the load is much higher at the 2000rpm point and the MAP is much greater as a consequence of this.

		Geometric CR		
		9	10.75	12.5
EBP (bar)	2	18.20	29.64	30.69
	3	13.47	18.93	23.00
	4	11.05	14.28	24.56

152 CAD duration cam

		Geometric CR		
		9	10.75	12.5
EBP (bar)	2	12.54	11.87	12.47
	3	7.17	7.78	7.35
	4	2.46	2.43	2.94

196 CAD duration cam

		Geometric CR		
		9	10.75	12.5
EBP (bar)	2	6.12	6.05	8.51
	3	2.89	2.27	7.30
	4	1.22	1.89	5.48

240 CAD duration cam

		Geometric CR		
		9	10.75	12.5
EBP (bar)	2	21.55	19.38	24.68
	3	9.05	10.01	18.26
	4	2.21	4.47	9.20

276 CAD duration cam

		Geometric CR		
		9	10.75	12.5
EBP (bar)	2	34.91	29.55	32.66
	3	11.21	10.57	17.85
	4	3.31	4.90	8.73

312 CAD duration cam

Figure 5.30 Scavenging Compensation (%) for each of the Different Cams at each EBP and CR for 2000rpm and 24 bar BMEP

The extent of the scavenging at 5000rpm cannot be easily quantified from this data due to the fact fuel enrichment was used, which has distorted the in-cylinder lambda values. The data that could be extracted is shown in Figure 5.31. The only data shown is that obtained at a requested lambda of 1, or in other words where the

exhaust temperature is below the temperature limit without the need for fuel enrichment. An overlay of the in-cylinder lambdas (Figure 5.32) demonstrates the impact of speed on scavenging at a point where the ISFC is not influenced by the use of fuel enrichment to give an idea of the different effect of scavenging at different speeds and loads.

		Geometric CR		
		9	10.75	12.5
EBP (bar)	2	1.59	5.72	8.31
	3	1.30	1.55	3.88
	4	0.72	3.12	2.18

152 CAD duration cam

		Geometric CR		
		9	10.75	12.5
EBP (bar)	2	2.77	2.88	4.25
	3	2.81	4.04	N/A
	4	N/A	N/A	N/A

196 CAD duration cam

		Geometric CR		
		9	10.75	12.5
EBP (bar)	2	3.07	5.37	5.00
	3	N/A	N/A	N/A
	4	N/A	N/A	N/A

240 CAD duration cam

		Geometric CR		
		9	10.75	12.5
EBP (bar)	2	N/A	N/A	N/A
	3	N/A	N/A	N/A
	4	N/A	N/A	N/A

276 CAD duration cam

		Geometric CR		
		9	10.75	12.5
EBP (bar)	2	2.77	5.56	4.62
	3	N/A	N/A	N/A
	4	N/A	N/A	N/A

312 CAD duration cam

Figure 5.31 Scavenging Compensation (%) for each of the Different Cams at each EBP and CR for 5000rpm and 24 bar BMEP

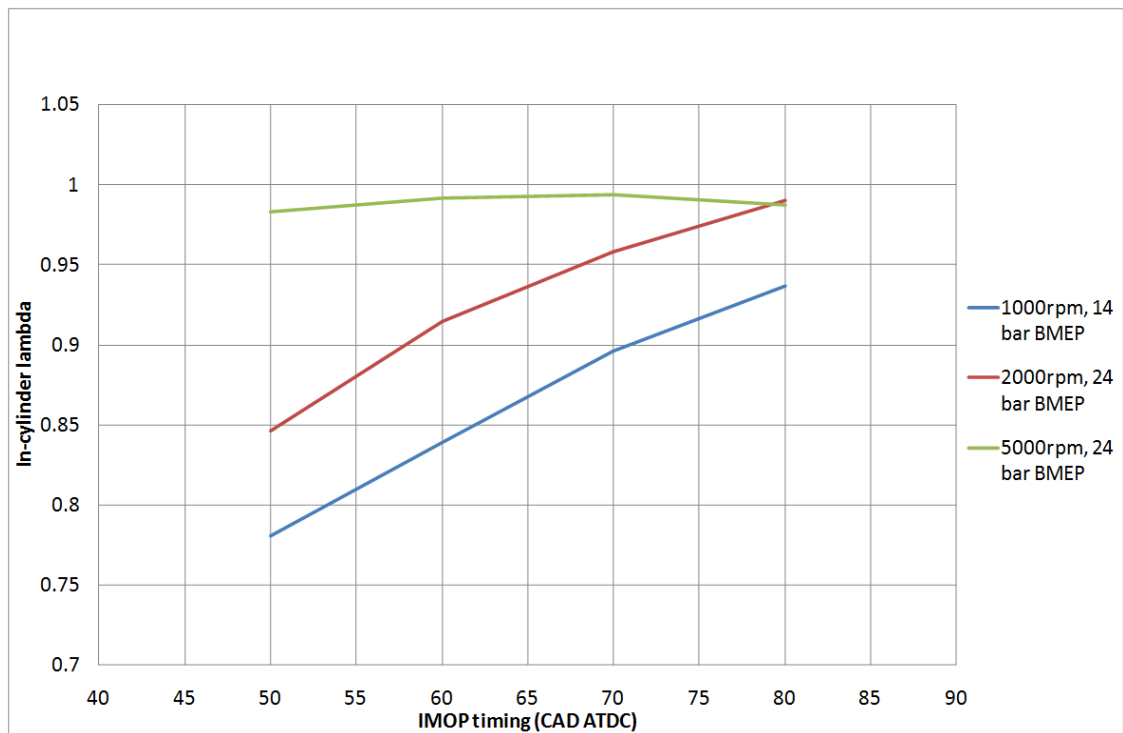


Figure 5.32 Comparison of In-cylinder Lambdas for the 152 CAD Duration Cam at 2 bar EBP and a Geometric CR of 9 for All Speeds

Even at a reduced load of 14 bar BMEP the extent of the scavenging is still relatively high for the 1000rpm case. In spite of the far greater MAP to EBP ratio, the scavenging at 5000rpm is barely noticeable, showing a peak difference of just 8.31%. It is for this reason that the maximum valve overlap condition was the optimum for the 152 CAD duration cam for 5000rpm and not for 1000 and 2000rpm. The optimum running point for the 152 CAD duration cam theoretically is the maximum valve overlap point because of the reduced effective CR.

The with and without compensation ISFC curves for each of the different speed and load points can be seen in Figures 5.33, 5.34 and 5.35 for speeds of 1000rpm, 2000rpm and 5000rpm respectively. All of these figures are for an EBP of 2 bar (1.5 bar EBP for the 1000rpm case) and a geometric CR of 9.

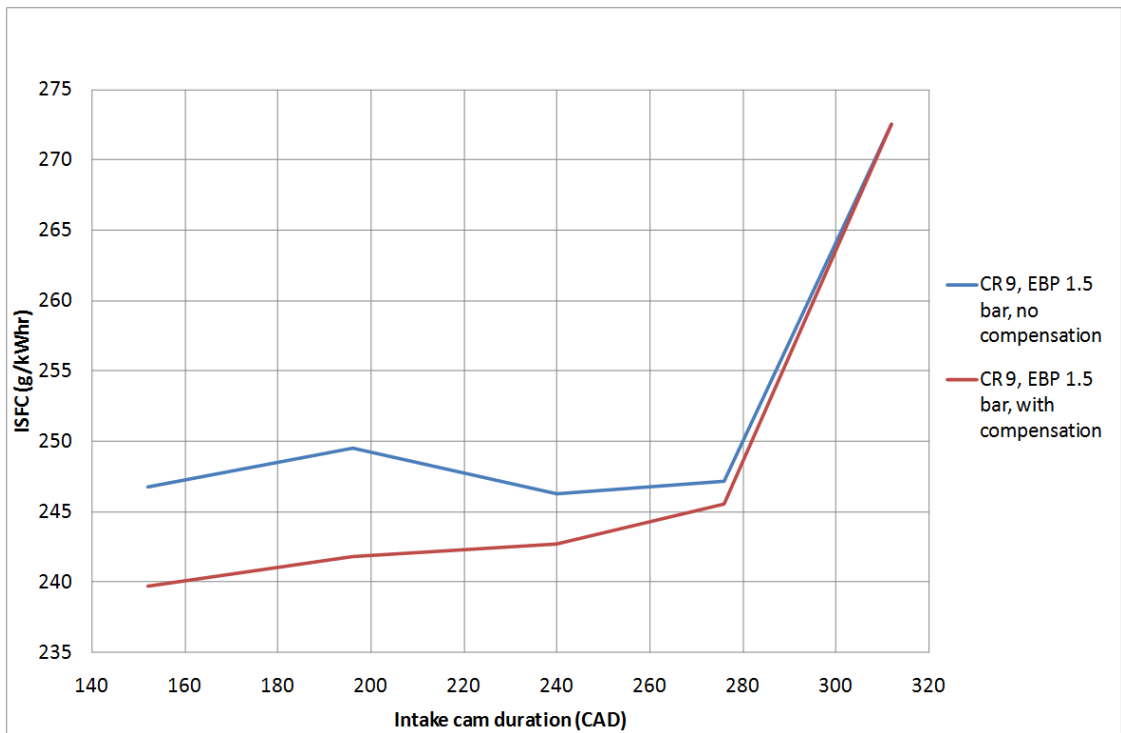


Figure 5.33 1000rpm, 14 bar BMEP, EBP of 1.5 bar, Geometric CR of 9. With and without Scavenge Compensation

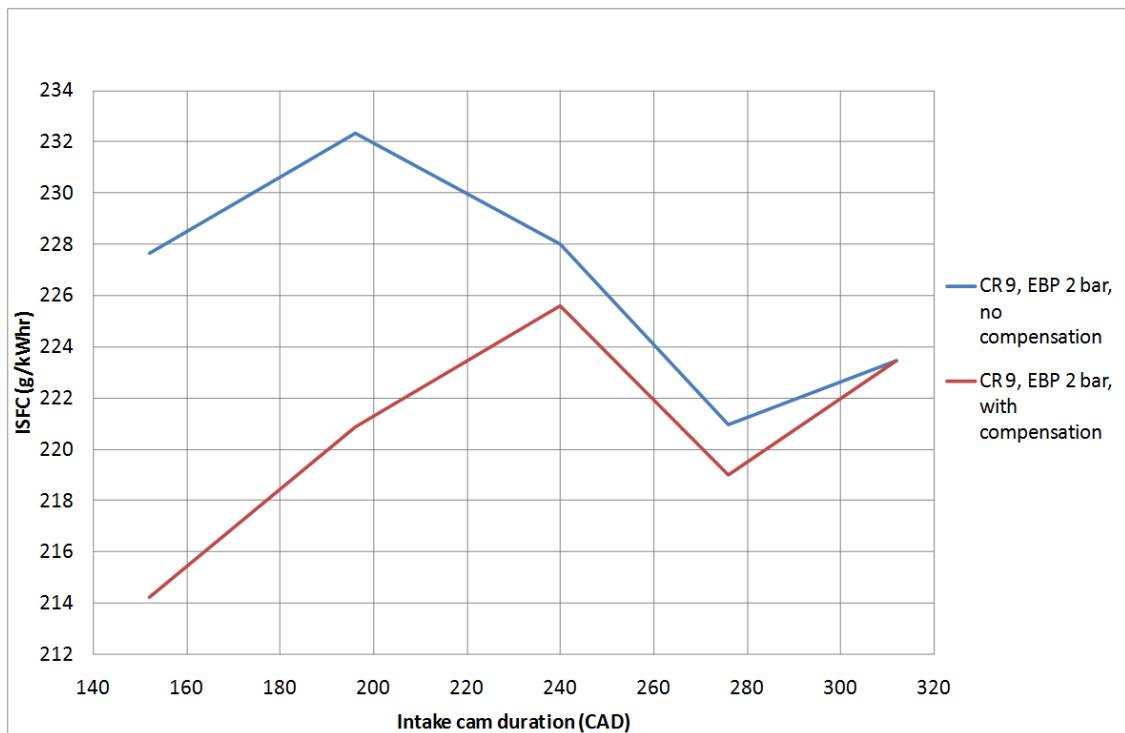


Figure 5.34 2000rpm, 24 bar BMEP, EBP of 2 bar, Geometric CR of 9. With and without Scavenge Compensation

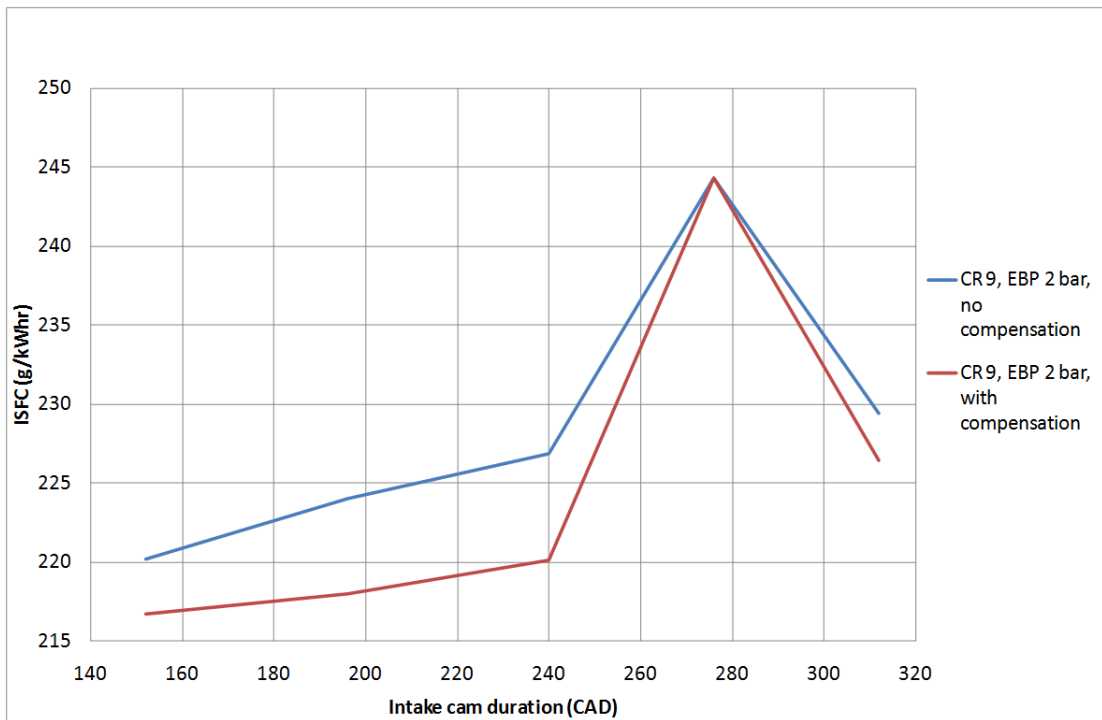


Figure 5.35 5000rpm, 24 bar BMEP, EBP of 2 bar, Geometric CR of 9. With and without Scavenge Compensation

The actual benefit to the cycle is much less than Figures 5.29 to 5.31 would imply. The reason for this is Figures 5.29 to 5.31 show the difference between exhaust lambda and in-cylinder lambda at the IMOP where the maximum difference was found, not the difference between the IMOP with the highest degree of scavenging and the optimum from the plot without compensation as can be seen in Figures 5.33 to 5.35. Table 5.4 demonstrates this for the 152 CAD duration cam IMOP sweep.

Table 5.4 1000rpm, 14 bar BMEP, Geometric CR of 9, EBP of 1.5 bar. With and without Scavenge Compensation Effects on ISFC for an IMOP Sweep with the 152 CAD Duration Cam

IMOP	ISFC (w/o compensation)	ISFC (with compensation)	% Difference between points
50	281.704307	239.6956692	14.91231648
60	265.072522	240.8037164	9.155534273
70	252.091628	241.8045279	4.080698824
80	247.161895	243.1013907	1.642852074
90	246.775231	244.9863621	0.724898081
100	249.81143	248.0040081	0.723514481
110	256.110358	254.1515305	0.764837273
120	264.871743	263.4493316	0.537018947

Figures 5.29 to 5.31 refer to the “% Difference between points” column whereas Figures 5.33 to 5.35 refer to the difference between the optimum points

(highlighted in green). This reveals that scavenging, and compensating for scavenging, though producing a significant difference at the maximum valve overlap point ultimately has a relatively minor effect on the ISFC in this case.

This effect is more pronounced at other running points, particularly at high CRs and EBPs where running with a very low effective CR is crucial to efficiency. This has the tendency of pushing the optimum IMOP back toward the maximum valve overlap point, even though scavenging is taking place. This is more a problem for the medium length cams of 196 and 240 CAD duration where the effective CR is very high regardless of IMOP. The peak difference in optimum ISFC with and without compensation occurs at a geometric CR of 12.5, an EBP of 2.5 bar and a cam duration of 196 CAD. The optimum IMOP in both cases is the maximum valve overlap position, which equates to a difference in ISFC of 10.22% higher for the without compensation case in comparison to with compensation.

The 2000rpm case exhibits the greatest sensitivity to scavenging (maximum of 6.3%), with the 1000rpm and 5000rpm cases showing much reduced levels of sensitivity (maximum of 3.1% and 1.8% respectively). The reason for the greater sensitivity at 2000rpm is the fact the speed is relatively low and the load is relatively high.

5.3.4.2 Charge Scavenging

Charge scavenging (the red region of Figure 5.27) occurs only with LIVC. It has been found to be similar in magnitude to scavenging in some low speed cases, but the exact amount depends heavily on the ratio of MAP to EBP. It is only a problem with LIVC due to the fact that LIVC purges a great deal of charge into the intake manifold during the compression process. If the MAP is quite high and the EBP quite low scavenging of this purged charge can take place and result in unburned charge being short circuited straight through the cylinder and into the exhaust.

Calculation of the impact of this on ISFC is not possible with GT-Power V6.1. If the scavenged charge is stoichiometric it will appear invisible to both the in-cylinder lambda and exhaust lambda feedbacks. It is possible to estimate it using the animation feature of GT-Power, this is achieved through observation of the vapour fuel fraction in the exhaust. This technique does not work with 5000rpm though, due to the fact fuel enrichment is used as a matter of course.

The volume of the exhaust port on the cylinder head and the exhaust manifold was estimated using the geometry of the GT-Power model and an estimation of the volume of unburned charge was obtained by observing how far downstream the vapour fuel fraction propagated through the exhaust system after EVC. It was assumed that this vapour fuel fraction cloud was a stoichiometric mix of air and fuel, and from this assumption an estimate of the amount of scavenging can be obtained.

Figure 5.36 shows the effect of EBP on charge scavenging at the 1000rpm and 14 bar BMEP point. The charge scavenging is reduced by 60.3% by running with an EBP of 2.5 bar compared to 1.5 bar.

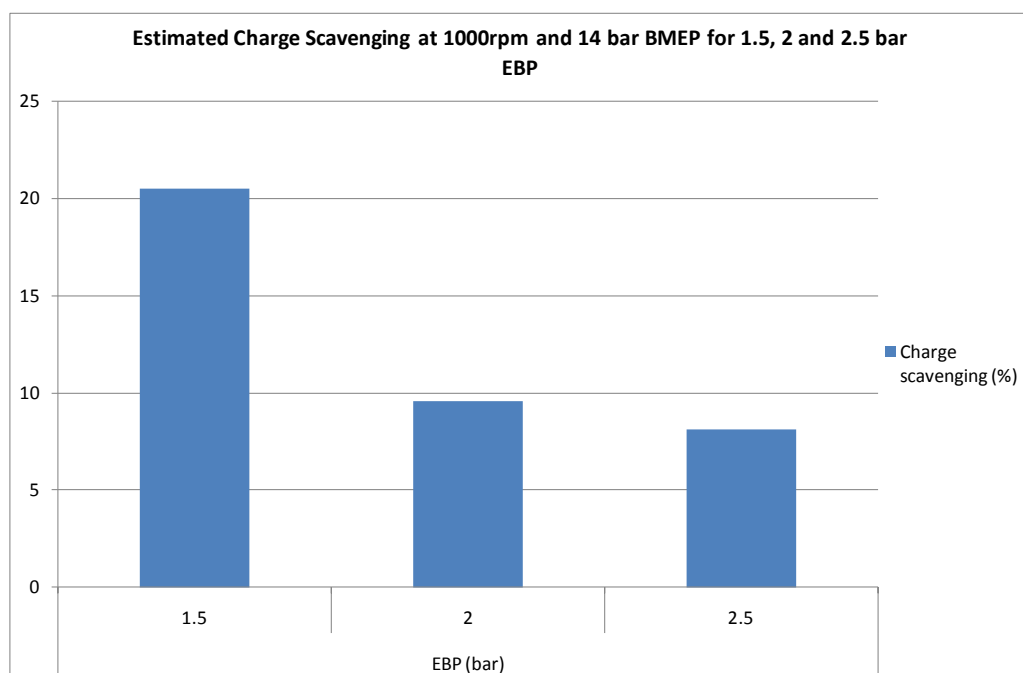


Figure 5.36 Estimated Charge Scavenging at 1000rpm and 14 bar BMEP for 1.5, 2 and 2.5 bar EBP

Figure 5.37 shows the effects of charge scavenging at the higher speed and load point of 2000rpm and 24 bar BMEP. The degree of charge scavenging has dropped

considerably in comparison to the 1000rpm case in spite of the fact the MAP is much higher. Geometric CR has been found to increase the degree of charge scavenging at this speed and load, likely due to the fact that the MAP is slightly higher for higher geometric CRs and because the clearance volume is slightly reduced. In this instance the degree of charge scavenging has increased by 30% through an increase in geometric CR of 39%.

No data could be obtained at higher EBPs due to the fact that not enough charge scavenging was occurring to become visible in the animation window. A similar problem was encountered at 5000rpm, even with low EBPs where fuel enrichment was not applied.

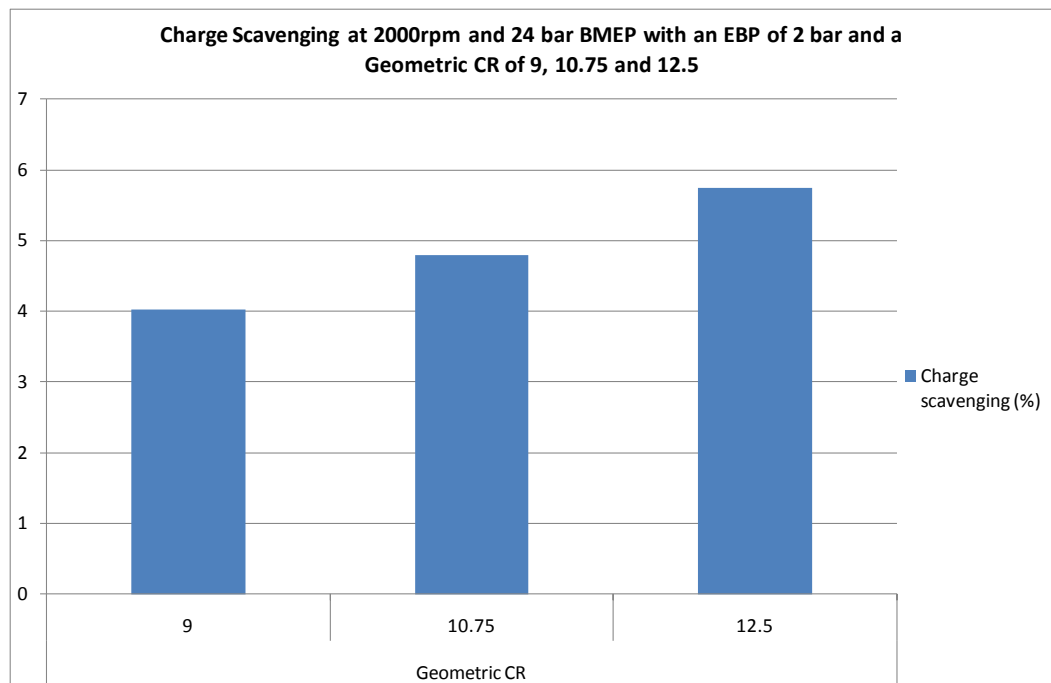


Figure 5.37 Charge Scavenging at 2000rpm and 24 bar BMEP with an EBP of 2 bar and a Geometric CR of 9, 10.75 and 12.5

5.3.5 Engine Breathing

The single cylinder exhaust system geometry exhibits some very pronounced tuning effects, particularly when EBP is applied. This is noticeable with both this single cylinder model and the single cylinder experimental engine. A very large pressure wave

is present in the system at all speeds and can be found to originate from the exhaust back pressure regulating valve itself (see section 6.2.3.4). This pressure wave is a reflection of the exhaust blowdown pulse and similar in magnitude to it. The effect of this pressure wave is different depending on the speed and load condition. In the case of 2000rpm and 24 bar BMEP the initial pressure wave reflection occurs during the exhaust stroke when only the exhaust valve is open so is of limited significance. The second reflection however peaks at almost exactly TDC during the gas exchange process and has a huge impact on the residuals in the cylinder for the subsequent cycle.

Overlays of the EBP on a crank angle degree basis and log P-V diagram effects have been shown in Figures 5.38 and 5.39 respectively. These figures show the optimum IMOP points at a geometric CR of 9 and an EBP of 2 bar.

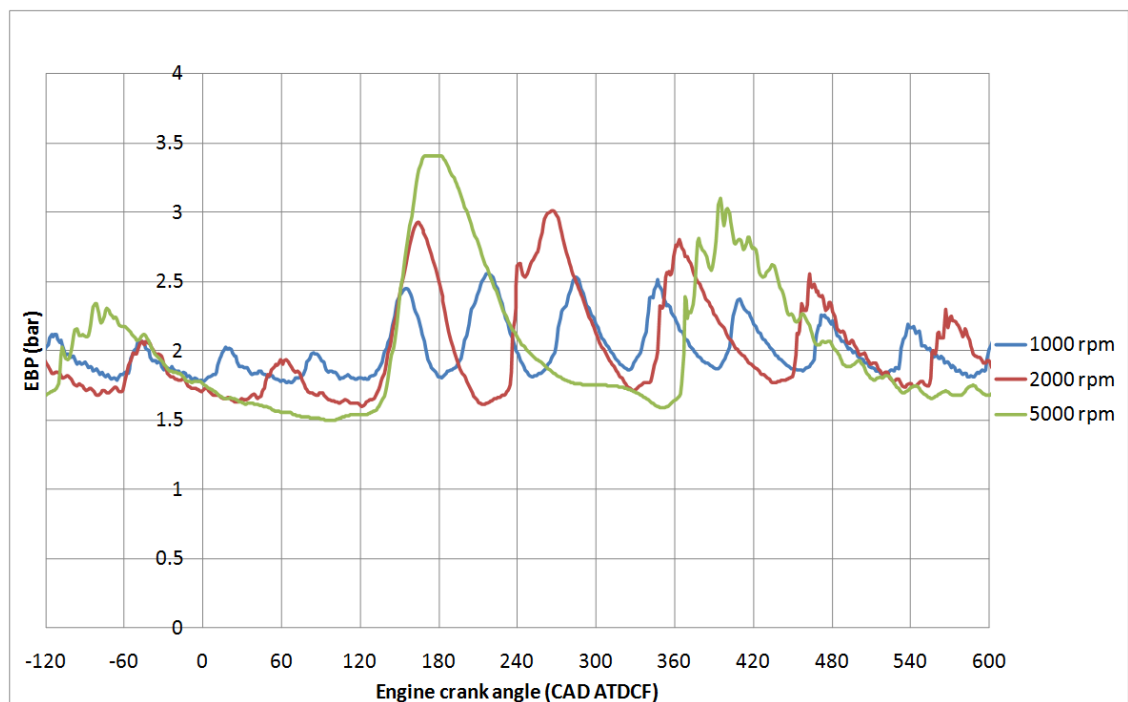


Figure 5.38 EBP Resolved on a CAD Basis for an EBP of 2 bar, a Cam Duration of 152 CAD for Speeds of 1000, 2000 and 5000rpm

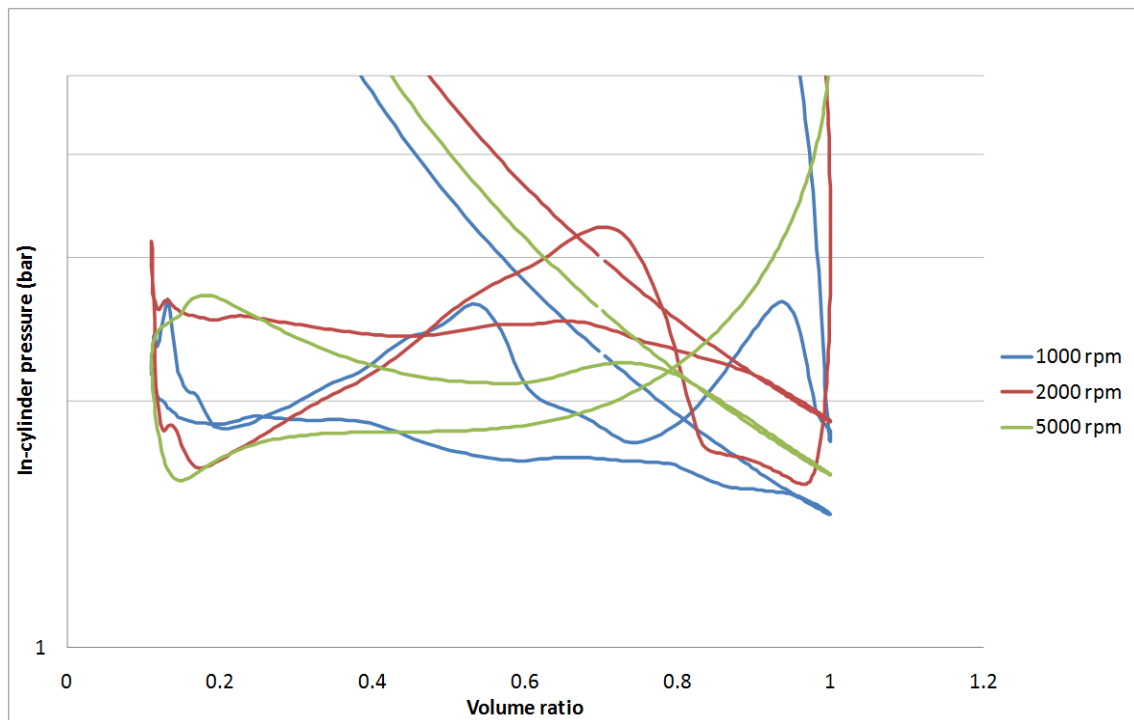


Figure 5.39 Log P-V Overlay at an EBP of 2 bar, a Cam Duration of 152 CAD, and for Speeds of 1000, 2000 and 5000rpm

Even at this relatively low EBP condition the peak magnitude of the pressure waves in Figure 5.38 can be seen to have a profound effect on the P-V diagram (Figure 5.39). As can be expected the pressure waves occur at a higher frequency at the lower speed condition because the speed of sound in the exhaust is comparable for all 3 speeds whilst the engine speed is dramatically different.

For a supposedly constant EBP the pressure peaks can be seen to be dramatically different in magnitude indicating that the 2000rpm case is more heavily affected than the 1000rpm case. The period of greatest importance for predictable exhaust flow is the valve overlap period. Any pressure waves that are present during the valve overlap period can be seen to propagate through to the intake manifold and drastically alter the engines breathing performance.

The influence of EBP and pressure waves present in the system has been analysed at the 1000rpm condition where it can be seen to result in unpredictable performance with the 240 CAD duration cam. The intake manifold mass flow rates for the 3 240 CAD duration cam cases in Figure 5.8 are shown in Figure 5.40.

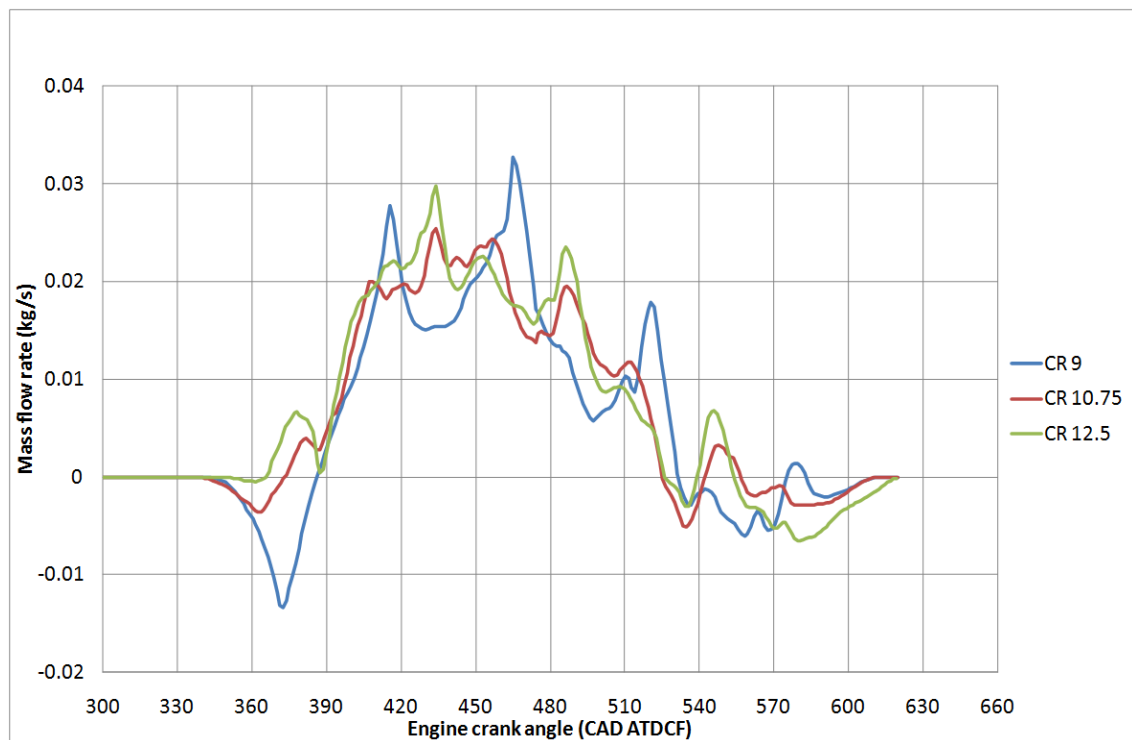


Figure 5.40 Intake Mass Flow Rate Overlay for 240 CAD Cam Duration at an EBP of 2.5 bar, and a Speed and Load of 1000rpm and 14 bar BMEP

The pressure waves are very evident in Figure 5.40 and manifest themselves as very large mass flow spikes. Notice the phasing of the pressure waves is different for the geometric CR of 9 case and the geometric CR of 10.75 and geometric CR of 12.5 cases. The phasing for the geometric CR of 10.75 and geometric CR of 12.5 cases is identical, and both profiles exhibit very large negative mass flow rates immediately before IVC. This will result in charge being drawn into the intake manifold. Notice too the large mass flow spike shortly after IVO, particularly for the geometric CR of 12.5 case. This is caused by a rarefaction wave in the exhaust system drawing air straight through the cylinder. This is scavenging occurring which is having a detrimental effect on the ISFC for these 2 cases.

At higher EBPs the peak pressure spikes can be seen to increase in magnitude considerably which can heavily influence the MAP required to maintain a certain load. This occurs at all engine speeds but is most noticeable at the 2000rpm, 24 bar BMEP point with a 196 CAD duration cam, a geometric CR of 9 and an EBP of 4 bar.

For the 60 CAD ATDC IMOP point the pressure wave in the exhaust can be seen to travel through the cylinder and into the intake manifold. Because the intake manifold is considerably shorter than the exhaust manifold this pressure wave travels at a much higher frequency through the intake and causes a considerable peak in intake valve flow rate whilst the intake valve is still open. This is visible at approximately 440 CAD ATDCF (Figure 5.41). This air ramming effect means the MAP can be reduced significantly, in spite of the fact the effective CR is comparatively low (Figure 5.42).

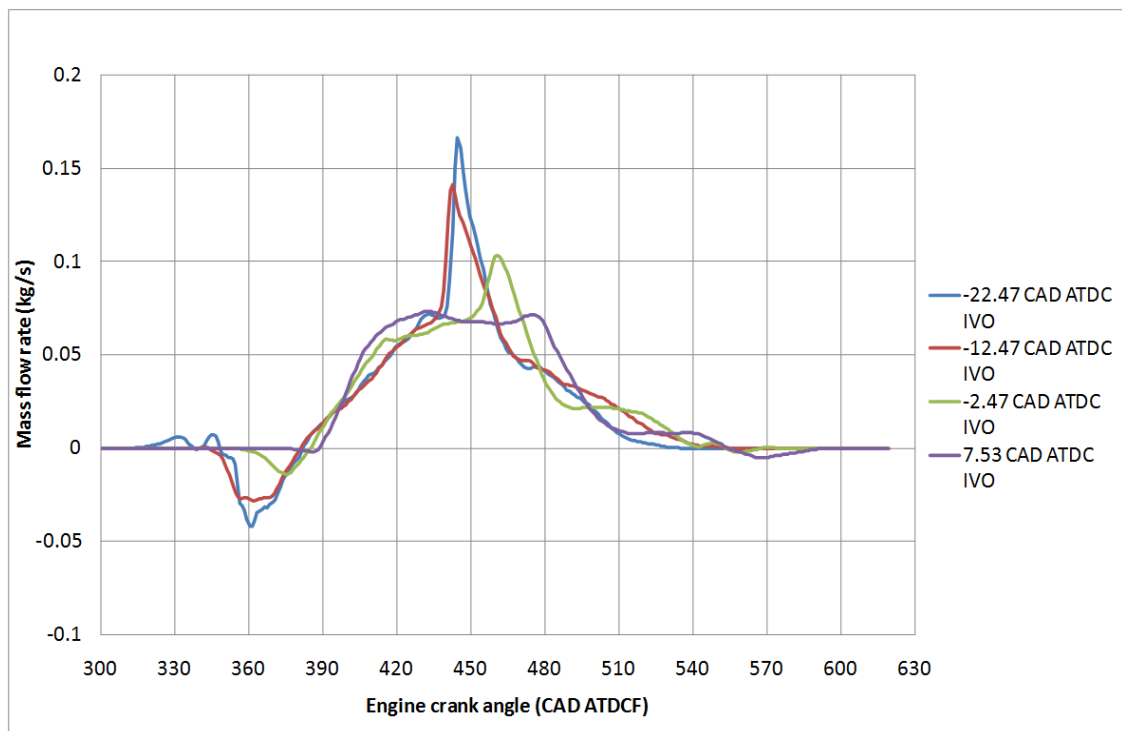


Figure 5.41 2000rpm, 24 bar BMEP, 196 CAD Duration Cam, EBP 4 bar, Geometric CR of 9. Intake Valve Mass Flow Rate Profiles from an IMOP Sweep

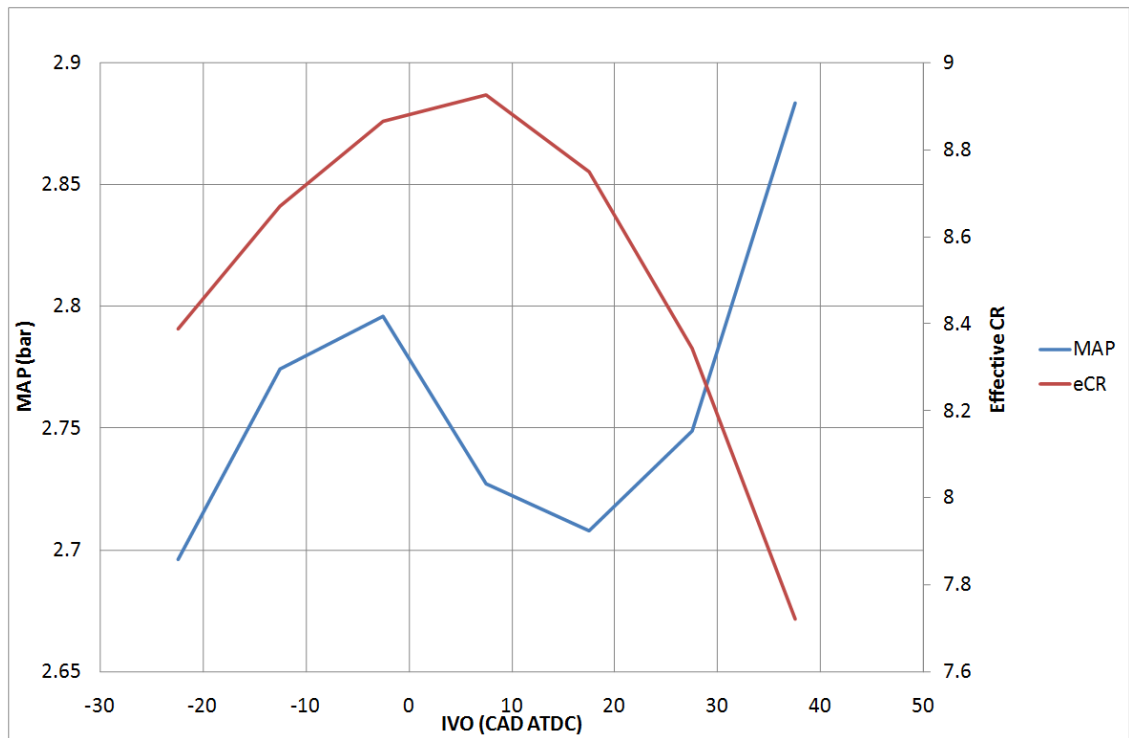


Figure 5.42 2000rpm, 24 bar BMEP, 196 CAD Duration Cam, EBP 4 bar, Geometric CR of 9. MAP Requirements for an IMOP Sweep

The result of this pressure wave propagation through to the intake results in a great deal of exhaust gas entering the intake manifold and mixing with the fresh intake air, as can be seen by the briefly negative mass flow rate through the intake valve in Figure 5.41. This has the effect of raising the intake port temperature approximately 19⁰C in comparison to the minimum valve overlap case, but ultimately the EOC temperature and pressure is much lower for the maximum valve overlap case.

This phenomenon is present at lower EBPs too, its impact is much less noticeable at these conditions though. It is also noticeable with the shorter 152 CAD duration cam too, although it is most pronounced with the 196 CAD duration cam due to the fact the pressure wave in the intake occurs almost precisely at the MOP point of the cam. It occurs slightly too late with the 152 CAD duration cam which greatly reduces the peak amplitude (0.13 kg/s peak mass flow rate for the 152 CAD duration cam Vs. 0.17 kg/s peak mass flow rate for the 196 CAD duration cam) of the pressure spike in the intake manifold, and slightly too early for the 240 CAD duration cam, again, making its impact on the cycle almost negligible. The MAP is also much higher for the 152 CAD duration cam which impedes reverse flow through the intake valve

(0.03 kg/s peak mass flow rate for the 152 CAD duration cam Vs. 0.04 kg/s peak mass flow rate for the 196 CAD duration profile).

The impact of the variability in the speed of sound on the exhaust pressure wave at the 5000rpm, 24 bar BMEP, 2 bar EBP and geometric CR of 9 point is shown in Figure 5.43. Figure 5.43 shows the 5 lines corresponding to each of the different duration cams. In brackets is the exhaust gas temperature in °C. The exhaust gas temperature is the main factor influencing the speed of sound, however, residuals and enrichment will have the effect of changing the exhaust gas density somewhat, but not considerably.

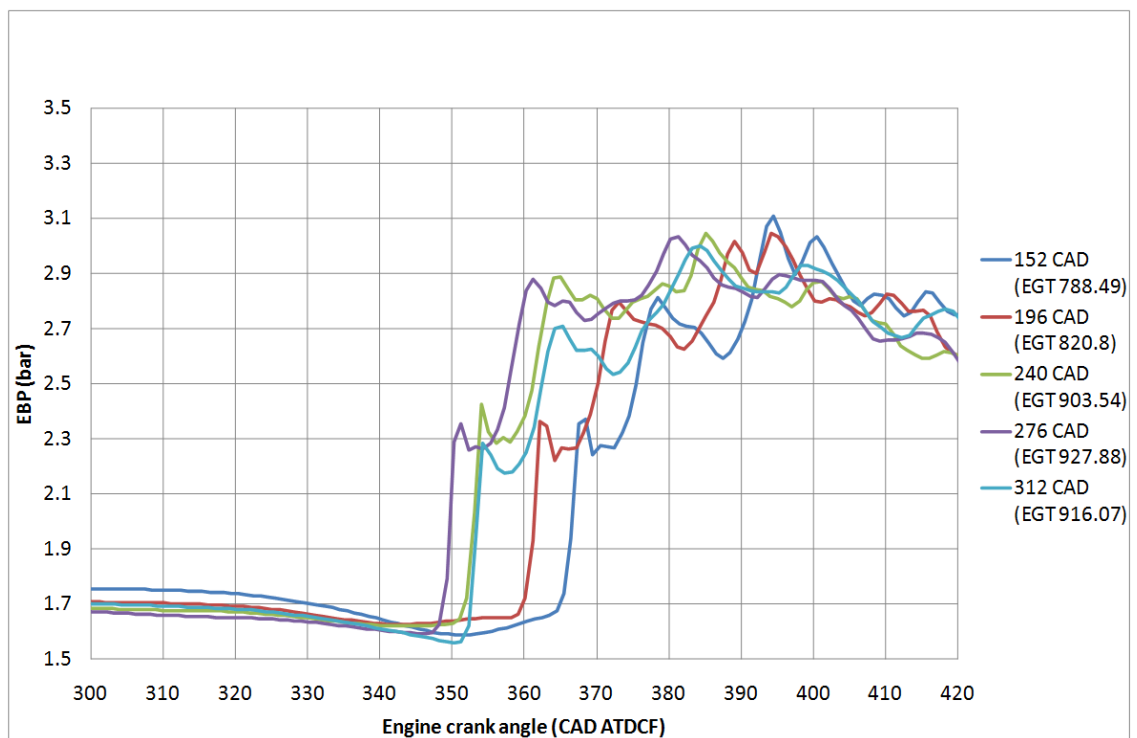


Figure 5.43 Influence of Exhaust Gas Temperature (EGT) on Exhaust Pressure/Rarefaction Wave at 5000rpm, 24 bar, 2 bar EBP and a Geometric CR of 9

For lower exhaust gas temperatures the pressure wave can be seen arrive at shortly after TDC gas exchange (this pressure data was obtained at the exhaust pressure transducer site, the pressure wave will not reach the cylinder until approximately 5 CAD later than shown in Figure 5.43). The fact that the pressure wave arrives later for the 240 CAD duration cam coupled with the fact IVC occurs at an

earlier point is the reason why the scavenging is much improved at 240 CAD duration site compared to the 276 CAD duration site.

Similar engine behaviour can be seen at an EBP of 3 bar also. At this point the 276 CAD duration cam optimum point has shifted from the maximum valve overlap position to a minimum valve overlap position. The 240 CAD duration cam exhibits significant scavenging akin to the 2 bar EBP case, the 276 CAD duration point exhibits little to no perceivable scavenging due to the IMOP being shifted to the minimum valve overlap position. At this IMOP the efficiency of the cycle is dictated by the effective CR which is not sufficiently low enough to be more efficient than the 240 CAD duration cam point.

At an EBP of 4 bar though the scavenging can be seen to be greatly reduced for the 240 CAD duration cam (although the maximum valve overlap position is still optimum for this cam) which requires more fuel enrichment to regulate the temperature as opposed to fresh air. With both the 240 CAD duration cam and 276 CAD duration cam now requiring enrichment, the benefit afforded by the reduction in effective CR by the 276 CAD duration cam has reduced the ISFC at this point to less than that at the 240 CAD duration cam point.

Determining the precise effect of the pressure waves in the exhaust system is impossible without modifying the exhaust geometry and re-doing all test work. It has a different and unpredictable effect on engine breathing at almost every single test point. The most noticeable effect of this exhaust tuning is an offset in the worst ISFC point with decreasing EBP or geometric CR changes. The point of optimum ISFC can be seen to be relatively insensitive to EBP however, this is likely to be because of the fact that in most cases the 276 CAD duration cam was optimum, and in all cases this was with a very small degree of valve overlap so any exhaust tuning effects will likely stay in the exhaust and not manifest themselves in the intake in a manner as can be seen in Figure 5.41.

Charge scavenging may be influenced to a small degree by exhaust manifold tuning but the impact will be minimal due to the fact charge scavenging happens with the long duration cams only which also run with a small degree of valve overlap.

The exhaust manifold tuning for a speed of 5000rpm is quite closely matched to that of the 3 cylinder engine (Figure 5.44), with the pressure peaks occurring close to 240 CAD apart and the pressure peaks being similar in magnitude, so for this speed the single cylinder engine would be quite comparable to the 3 cylinder engine if it were not for the fact the blowdown pulse changes depending on the engine running conditions and the local speed of sound at 5000rpm (Figure 5.43).

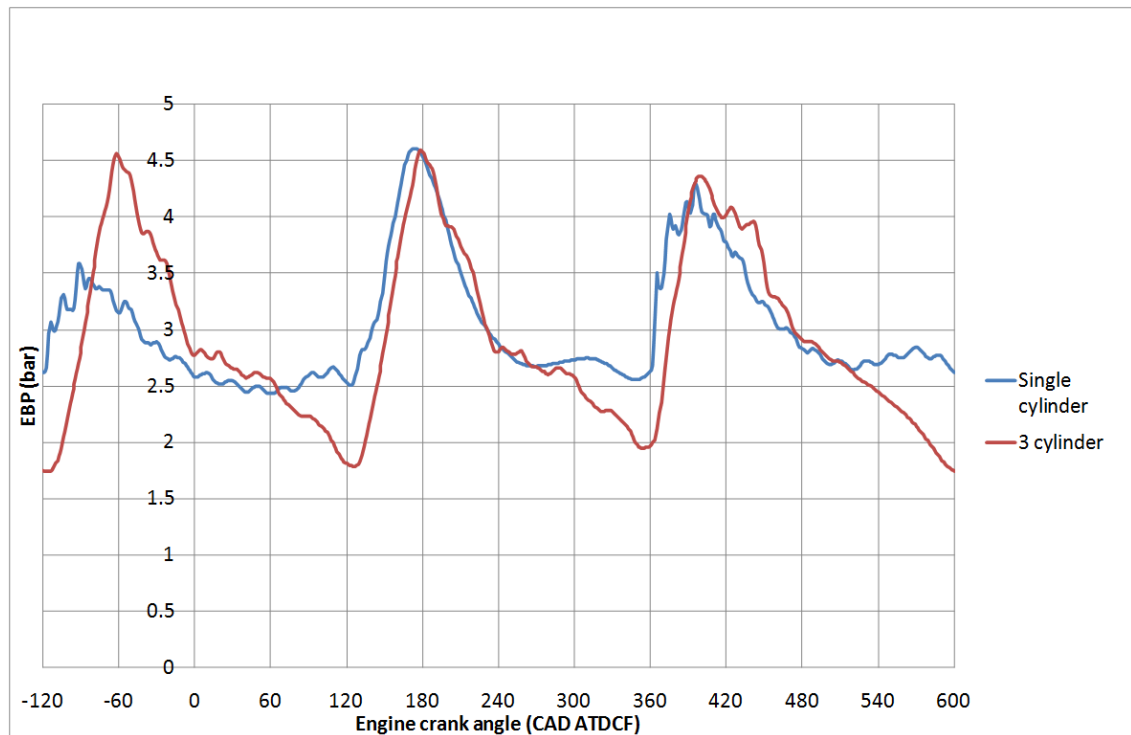


Figure 5.44 Comparison of Single Cylinder and 3 Cylinder EBP Profiles Resolved on CAD Basis at 5000rpm and 24 bar BMEP

5.3.6 General Compression Ratio Effects

Increasing geometric CR has the theoretical effect of increasing the cycle efficiency as can be determined from the Otto cycle efficiency formula (Eq.5.1).

$$\eta_{Otto} = 1 - \frac{1}{r_v^{n-1}} \quad 5.1$$

where η_{Otto} is the Otto cycle efficiency, r_v is the geometric CR and n is the polytropic exponent.

It can also be seen to extend the pumping loop. Whether or not this is beneficial or detrimental to the overall cycle efficiency is dictated by the MAP to EBP ratio

Figure 5.45 reveals the extent of this increase in pumping loop at the 2000rpm, 24 bar BMEP point with a cam duration of 312 CAD.

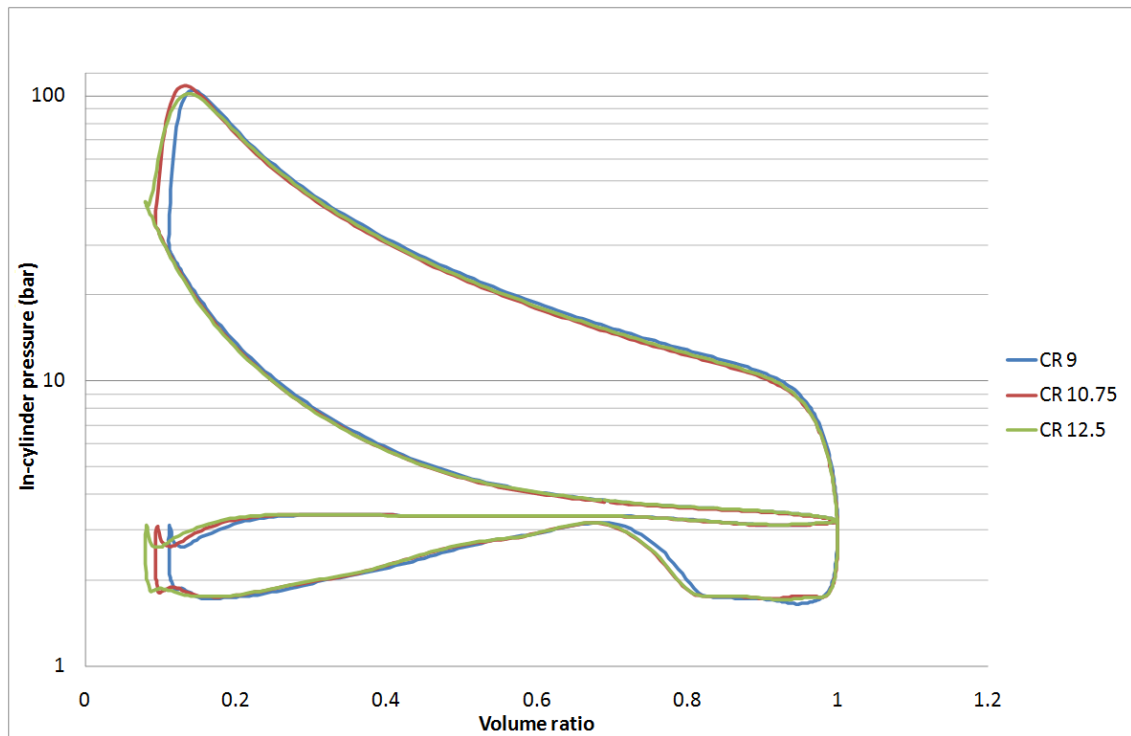


Figure 5.45 Log P-V Diagram at 2000rpm, 24 bar BMEP, 312 CAD Duration Cam, EBP of 2 bar. Comparison of Different Geometric CRs

At 2 bar EBP the pumping loop contribution is positive and can yield an ISFC improvement of 0.5 g/kWhr or 2.3 J/cycle. Extra work can be extracted from the gross work too which is much more significant and results in an extra energy yield of 119 J/cycle. It should be noted though that for the geometric CR of 12.5 case the EOC pressure is considerably higher. For the case demonstrated in Figure 5.45 the temperature and pressure history is such that the combustion phasing can be advanced and this extra portion of gross work can be extracted. Extracting this extra portion of power from the cycle is difficult when running at BLD and in most cases it was not possible with a geometric CR of 12.5. Under certain circumstances an advantage in ISFC could be yielded with a geometric CR of 10.75.

Evidence of this can be seen in the Figures 5.16 to 5.18 which show all but 1 of the geometric CR of 12.5 points to be far less efficient than the geometric CR of 9 and geometric CR of 10.75 points. In every one of the cases where the geometric CR of 12.5 point is higher than the geometric CR of 9 point the EOC pressure can be seen to be at least 8 bar higher. The 50% MFB points have also had to be retarded dramatically for BLD running with the geometric CR of 12.5 points as can be seen.

For all speeds the 50% MFB point had to be retarded with higher geometric CRs. Figures 5.46 to 5.48 show the 50% MFB for each of the cam durations, geometric CRs and EBPs.

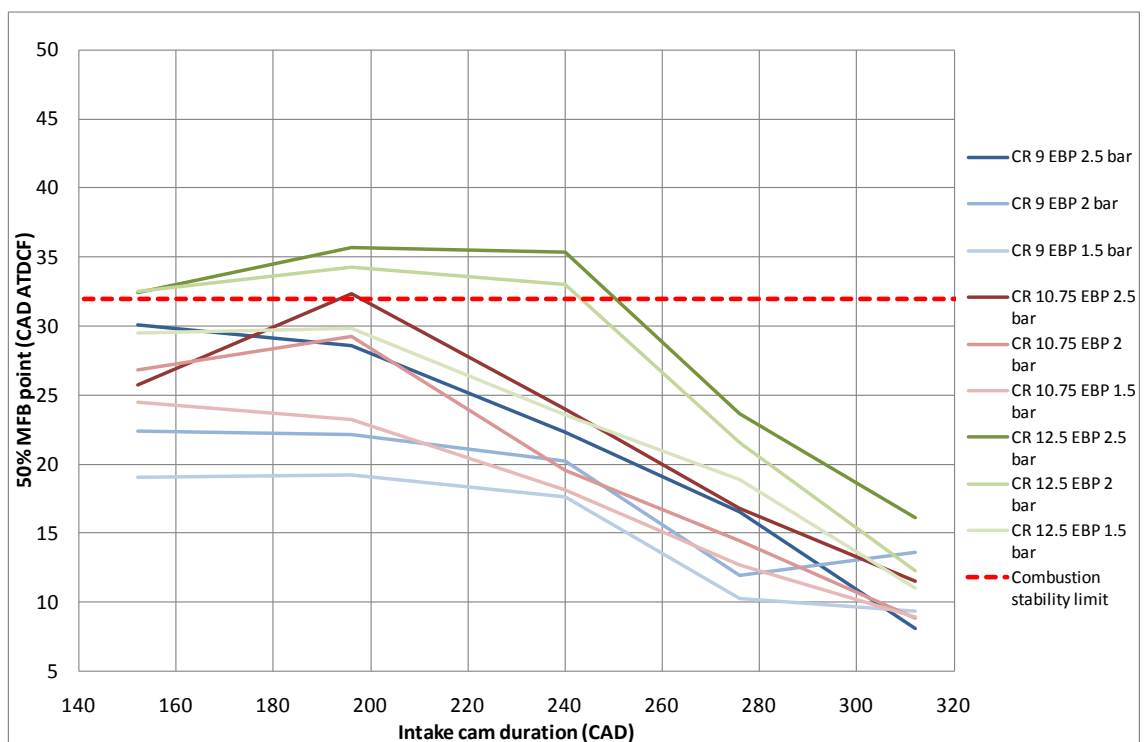


Figure 5.46 1000rpm, 14 bar BMEP 50% MFB Points for EBPs of 1.5, 2 and 2.5 bar at Geometric CRs of 9, 10.75 and 12.5

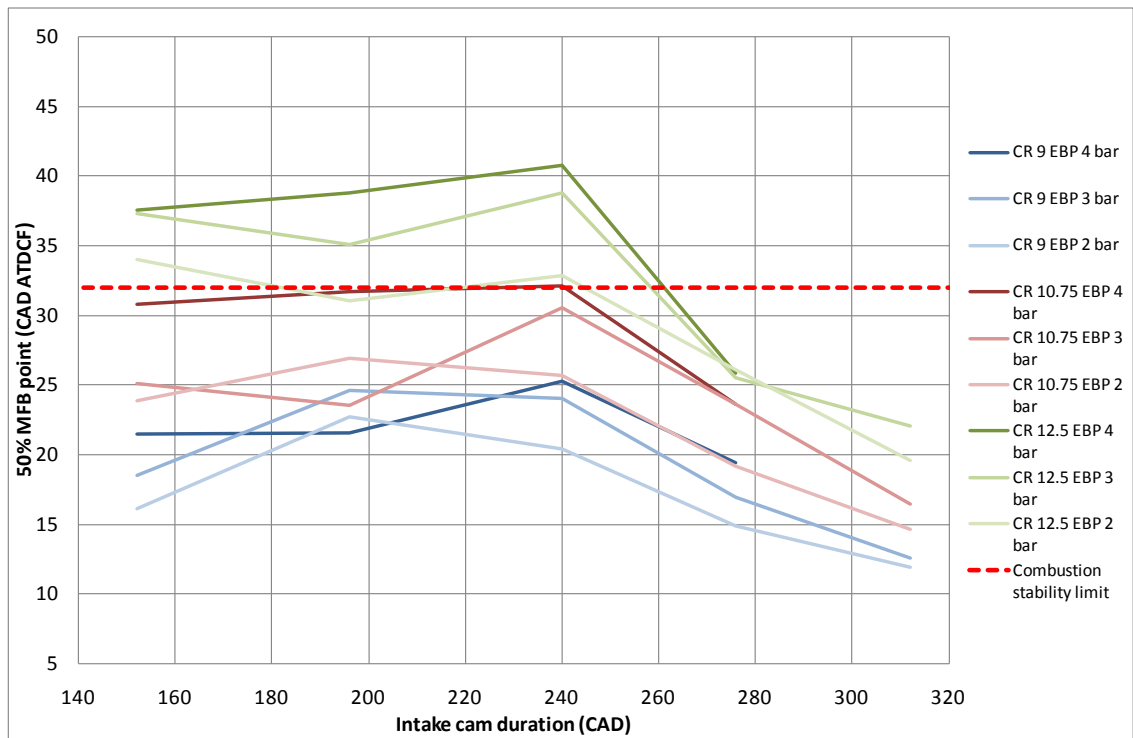


Figure 5.47 2000rpm, 24 bar BMEP 50% MFB Points for EBPs of 2, 3 and 4 bar at Geometric CRs of 9, 10.75 and 12.5

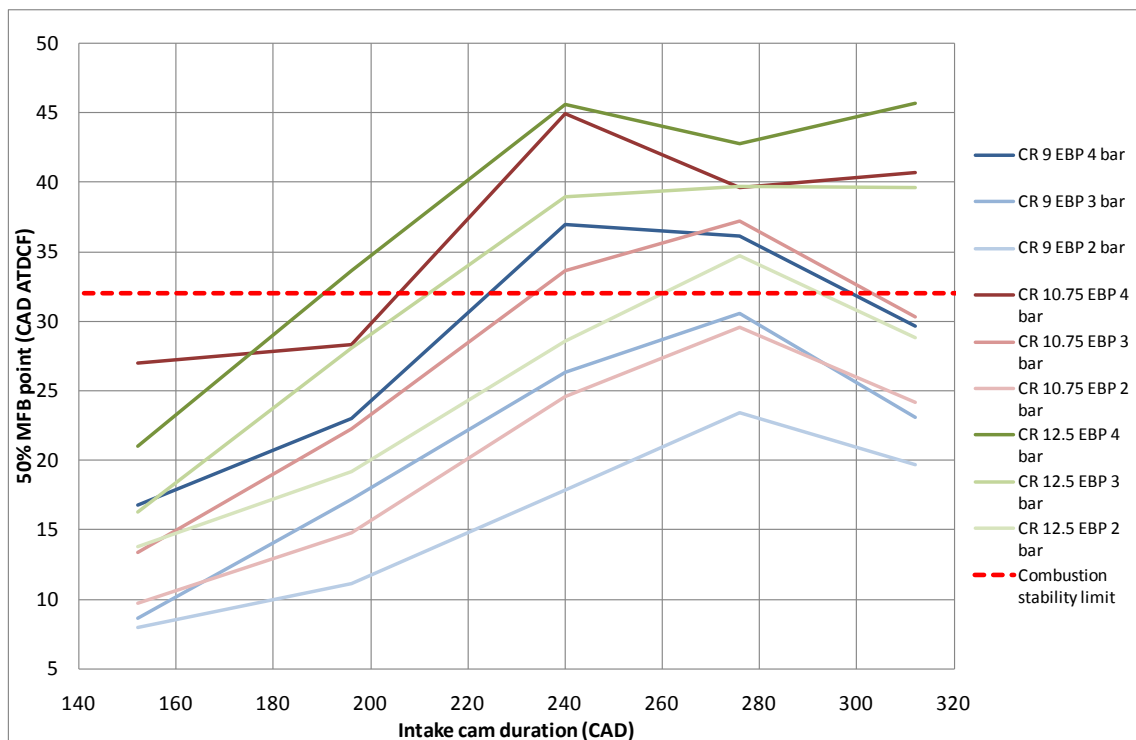


Figure 5.48 5000rpm, 24 bar BMEP 50% MFB Points for EBPs of 2, 3 and 4 bar at Geometric CRs of 9, 10.75 and 12.5

Figures 5.46 to 5.48 clearly show very strong correlations with their respective ISFC plots in Figures 5.6, 5.9 and 5.19. Both geometric CR and EBP can be observed to

have a significant effect on the combustion phasing at all speeds. Some cam durations arguably exhibit less sensitivity to EBP than others. Generally the longer cams are less sensitive to EBP than the shorter ones, although this is not visible for the 5000rpm case (Figure 5.48), this can be attributed to the fact that the cam IMOP timing was not optimised due to the MAP limit restricting it. The shorter cam durations can be expected to be more sensitive to EBP due to the scavenging inhibiting properties of higher EBPs and the fact that the valve overlap period is generally a lot longer with the shorter cams.

Figure 5.46 to 5.48 highlight the extent to which combustion must be retarded to run at the BLD condition. It should be noted that it may not be possible to retard the 50% MFB point to this extent for the high geometric CR and high EBP points. There are 2 reasons for this, the ignition energy to ignite the charge may be insufficient with an EOC pressure above approximately 50 bar. This constraint can be rectified with a higher energy ignition system. The second reason (which is far bigger constraint) is the fact that the experimental engine has been found to misfire and experience abnormal combustion with 50% MFB points later than 32 CAD ATDC at all speeds. This limit is shown in Figures 5.46 to 5.48 as a bright red dashed line.

The trends shown in Figures 5.46 to 5.48 reveal that high geometric CRs can only be employed effectively when the effective CR is low enough, or in other words, only for the extremely short or long cam durations. Even when effective CRs are low it still may not be possible to run at high geometric CRs depending on the cam timing.

The extent of the benefit afforded by operating at a geometric CR of 12.5 and 10.75 is generally greatest for low EBPs. As can be expected, the greatest advantage of running at a higher geometric CR can be shown at the lower speed and load case of 1000rpm and 14 bar BMEP. At this point the geometric CR of 10.75 benefits the ISFC for each of the cam duration points in comparison to a geometric CR of 9. The load is however still slightly too high to be of considerable benefit for a geometric CR of 12.5 for all but the very long 312 CAD duration cam. Although the engine can still run with the 50% MFB phased to 32 CAD ATDCF it is not advisable due to the fact LSPI has a much higher propensity to occur at these speeds.

5.4 Maximum Load Comparisons

For the purposes of this section the focus shall be shifted away from optimisation of ISFC and shall be shifted to which cam profile is best suited for maximum load generation. The qualities to look out for when determining the maximum load point are similar to those for minimum ISFC. A low EOC pressure and temperature for as high a mass of air in the cylinder will provide the highest load, a relatively high degree of combustion phasing advance will also be required to keep the exhaust gas temperature as low as possible.

Mechanical constraints may also be a limiting factor in the pursuit for maximum load, for this work the maximum acceptable cylinder pressure will be 140 bar. A maximum degree of combustion phasing retard will also be imposed to ensure the maximum load outputs are realistic in the real world. The limit is a maximum 50% MFB anchor point phasing of 32 CAD ATDCF.

Figures 5.49 and 5.50 show the theoretical maximum load outputs for each of the different cams at an EBP of 2 and 3 bar respectively (the dashed lines between the points represent trend lines for each of the 5 cams).

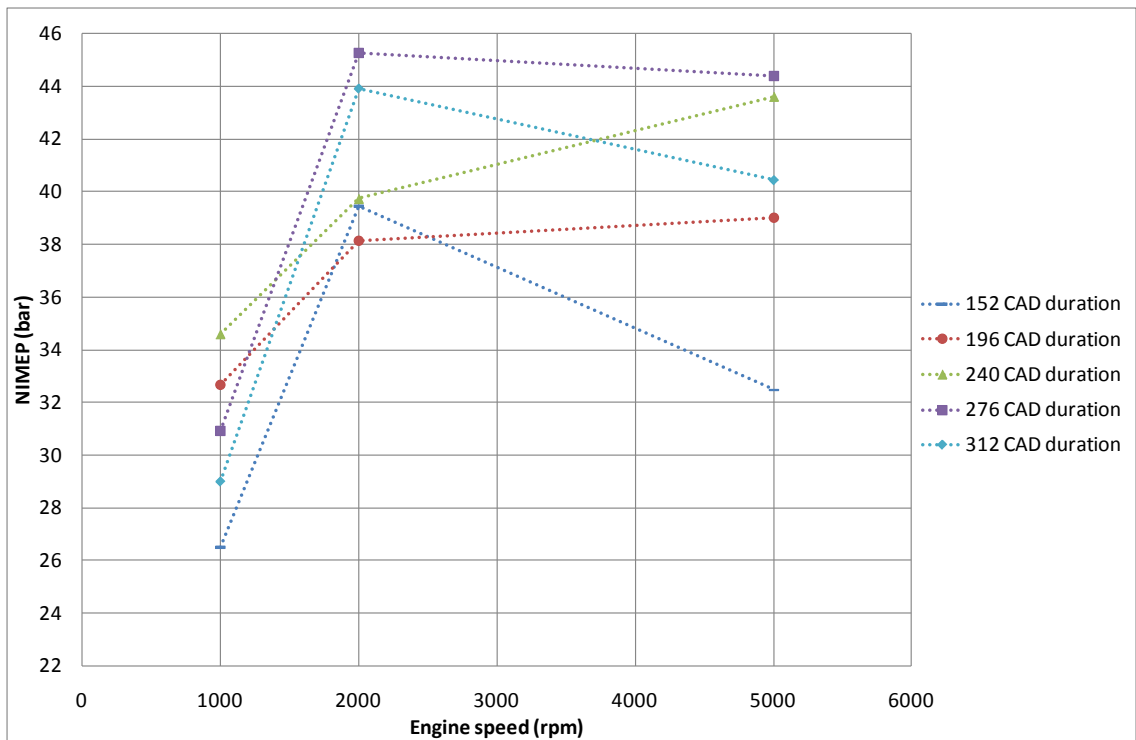


Figure 5.49 Peak Load (NIMEP) at 1000, 2000 and 5000rpm for each Cam Profile for an EBP of 2 bar

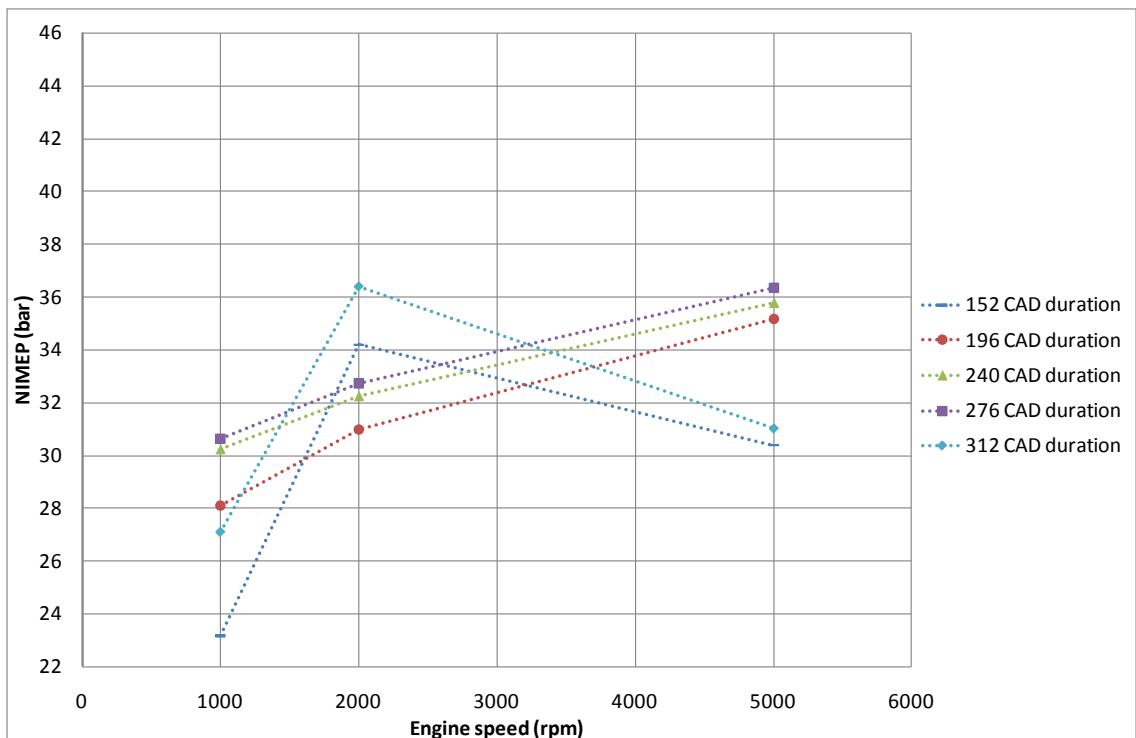


Figure 5.50 Peak Load (NIMEP) at 1000, 2000 and 5000rpm for each Cam Profile for an EBP of 3 bar at 2000 and 5000 rpm, and an EBP of 2.5 bar at 1000rpm

The 2 bar EBP case NIMEP figures can be seen to be very high in comparison to the 3 bar/2.5 bar figures which are more like what can be seen on the 3 cylinder engine. The reason for this is the lack of EBP leading to very low EOC pressure and

temperature. In almost all cases the MAP limit of 4 bar (3 bar for 1000rpm) can be seen to be the limiting factor on peak power with the exception of the 2000rpm point with the 276 CAD duration cam which had to be reduced slightly because of the 140 bar cylinder pressure limit. The only 2 points in Figure 5.49 that were not MAP limited were the 2000rpm 196 CAD duration cam and 240 CAD duration cam points which were limited by the elevated EOC pressures and temperatures at these points.

The MAP limit manifests itself most clearly at the 5000rpm cases in both Figures 5.49 and 5.50 where the short 152 CAD duration cam and long 312 CAD duration cam can be seen to be down in peak load in spite of the fact the EOC pressures and temperatures are lowest at these points. This is due to the very low volumetric efficiency afforded by these cams.

The 3 bar/2.5 bar EBP point (Figure 5.50) showed a similar MAP limit constraint at 1000 and 5000rpm but the 2000rpm points are very much knock limited with the full MAP being required for just the 152 CAD duration cam point. These points can be seen to follow the logical trend of the lower effective CR resulting in the highest load being achieved for the most part, with the notable exception of the 196 and 240 CAD duration cam points that appear to be inverted. One of the possible explanations for this is the tuning phenomena that affects the 196 CAD duration cam (see section 5.3.5) which resulted in the anomaly seen in Figure 5.12.

The 276 CAD duration cam is optimum for maximum load for 4 of the 6 speed and EBP combinations because of good low effective CR and high mass trapping qualities. Although the 152 CAD duration cam offers similar effective CRs to the 312 CAD duration cam (slightly greater even) it can be seen to be below the 312 CAD duration cam at every point. The reason for this is that although the effective CR is comparable the trapped charge mass is less than with the 312 CAD duration cam. This due to the fact that IVC is classed as the 1mm valve lift point and not the actual valve closing point. It is also dependent on the direction of piston motion when the valve closes. With EIVC the piston is moving downwards, therefore flow is restricted into the cylinder, whereas the piston motion is upwards with LIVC and flow is being restricted

out of the cylinder. This means that the mass of air trapped in the cylinder will always be greater with LIVC than EIVC for equivalent effective CRs.

5.5 Summary

The effectiveness of EIVC and LIVC changes dramatically depending on the speed, load, EBP and geometric CR combination. In most cases LIVC offers the greatest benefit but only at low speeds. This was not always achieved with the maximum degree of LIVC (312 CAD duration cam), in some cases moderate LIVC was more efficient (276 CAD duration cam), particularly at low speeds and low EBPs where charge scavenging was observed to take place.

EIVC was also observed to offer a benefit but only at high speeds where the degree of scavenging was reduced to the extent that accidental over enrichment no longer had a significant impact on the ISFC. EIVC can be seen to offer greater benefits at lower speeds if the EMS is somehow able to compensate for the scavenging. If compensation is used EIVC is generally more effective at reducing ISFC than LIVC.

The efficiency benefits offered by EIVC and LIVC are heavily dependent on EBP. Increasing EBP generally yielded a greater performance benefit for both EIVC and LIVC, however, there were some notable exceptions to this trend, particularly for EIVC at very high EBPs (4 bar).

Geometric CR increase was found to benefit extreme cases of EIVC and LIVC for almost every speed, load and geometric CR case, and lesser degrees of EIVC and LIVC for low EBP cases. It was found to be detrimental to ISFC for the standard duration cam and detrimental to lesser degrees of EIVC and LIVC in some cases.

The results from this test work were heavily influenced by the exhaust manifold tuning. The influence of the exhaust manifold was found to be particularly great for higher EBP cases where the blowdown pulse (and the corresponding pressure/rarefaction wave) were greater in magnitude than for lower EBP cases. For

high degrees of valve overlap the exhaust tuning could be found to influence the intake system and distort the required MAPs slightly. This was found to be detrimental to cam profiles that favoured a high degree of valve overlap, in most cases.

Both EIVC and LIVC show the potential to increase the maximum load (relative to the standard cam profile) but the requirement for high MAPs is much greater. At a speed of 2000rpm the MAP requirement is typically the maximum limit of 4 bar for the extreme EIVC and LIVC cases, this results in higher loads being reached for these cases, but at a speed of 5000rpm, where the MAP requirement for the standard cam profile is also 4 bar, the load can be seen to be reduced relative to the standard cam profile. A similar effect can be observed at 1000rpm too where the maximum MAP was limited to 3 bar.

Chapter 6

Single Cylinder Engine Performance Evaluation

6.1 Introduction

The objective of the first part of this chapter is to assess how the single cylinder experimental engine performs in comparison to the 3 cylinder engine and the single cylinder engine model, in an attempt to better ascertain what impact engine breathing will have on the successful implementation of EIVC and LIVC strategies.

Autoignition has also been studied extensively. The single cylinder experimental engine has shown a greater propensity for severe autoignition events (severe meaning cylinder pressures in excess of 30% higher than the average peak cylinder pressure) in comparison to the 3 cylinder engine, particularly at low engine speeds. The source of this severe autoignition behaviour has been investigated, including whether or not it is caused by LSPI or simply by knocking combustion. The impact of coolant flow rate effects and fuel age effects on autoignition tendency has also been investigated.

6.2 Comparison of the Single Cylinder Experimental Engine to the 3 Cylinder Engine

6.2.1 Introduction

The purpose of this investigation is to see how the single cylinder experimental engine compares to the 3 cylinder engine. Ultimately the intention of this study is to apply what has been learned here to the 3 cylinder engine, and the objective of this test work is to ascertain whether or not the data and the trends seen on the single cylinder experimental engine are going to be a good representation of the behaviour of the 3 cylinder engine.

The engines will be compared at equivalent speed and load sites across the engine operating range. All of the other criteria such as injection timing, rail pressure, coolant and oil temperatures and CAT as used on the 3 cylinder engine will be duplicated on the single cylinder engine as closely as possible.

6.2.2 Description of Test Points

Cam timing sweeps were carried out in various regions of the operating map to both obtain some baseline data (which can be compared to the GT-Power model of both the single cylinder and 3 cylinder engines) and also to compare the different profile cams to one another. The test points are shown in Figure 6.1 and are given in Table 6.1. This baseline data was obtained with the standard 240 CAD duration 3 cylinder engine intake cam.

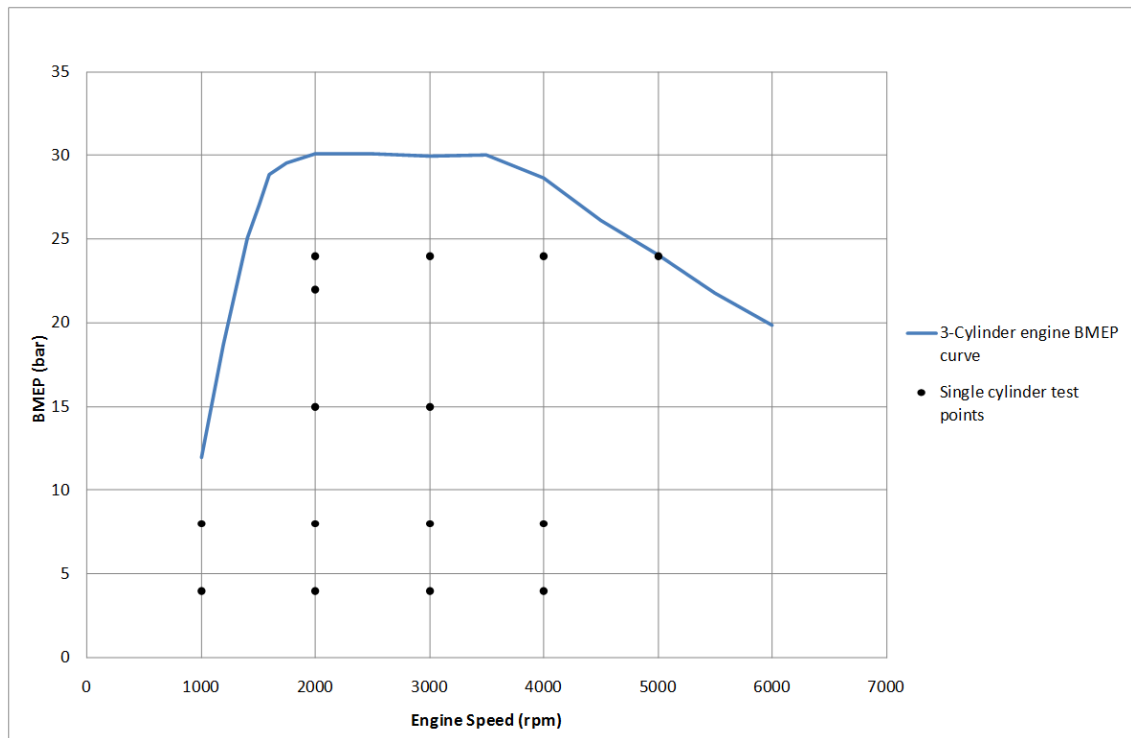


Figure 6.1 Baseline Data Test Points

Table 6.1 Baseline Data Test Points

Speed (rpm)	BMEP (bar)	NIMEP (bar)	EBP valve position (% closed)	SOI (CAD BTDC)	Rail pressure (bar)
1000	4	4.56	0	320	85.93
1000	8	8.83	0	276	132.63
2000	4	4.64	0	320	91.93
2000	8	8.90	0	319	131.06
3000	4	4.80	0	320	101.83
3000	8	8.98	0	319	134.45
4000	4	4.98	0	291	110.81
4000	8	9.05	0	297	140.56
2000	15	16.04	0	290	168.54
2000	15	16.04	45	290	168.54
3000	15	16.44	0	303	167.8
3000	15	16.44	45	303	167.8
2000	22	23.48	0	262	169.36
2000	22	23.48	40	262	169.36
2000	24	25.58	0	259	169.26
2000	24	25.58	* 2 bar EBP	259	169.26
3000	24	25.49	0	300	169.2
3000	24	25.49	35	300	169.2
4000	24	25.84	0	326	169.3
5000	24	26.02	0	349	170.01

* - EBP in bar, not valve position

The maximum load tested is relatively conservative in comparison to the 3 cylinder engine BMEP curve. The 3 cylinder comparison was obtained from baseline data carried out by Mahle Powertrain on the second generation Mahle 1.2l 3 cylinder downsized engine with Bosch-Mahle TurboSystems turbocharger and a CR of 9.3. A

maximum BMEP of 24 bar was imposed because of mechanical constraints. The single cylinder test points in Figure 6.1 correspond to 3 cylinder engine effective BMEP values, for example, 24 bar BMEP at 5000rpm for the 3 cylinder engine requires a NIMEP of 26.02 bar, the single cylinder engine was therefore run at an NIMEP of 26.02 bar at this point. The single cylinder brake values will not be used in this chapter because they are artificially low due to the fuel pump and 3 cylinder camshaft (as opposed to a single cylinder specific camshaft) parasitic losses rendering them unrepresentative.

A list of the test variables and control criteria are given in Table 6.2.

Table 6.2 Test Variables and Control Criteria

Variable	Control criteria
Air	<3% humidity, temperature maintained at +/- 3 degC of 40 degC intake port temp
Coolant	Temperature maintained at +/- 3 degC of 80 degC
Oil	Temperature maintained at +/- 3 degC of 90 degC
Fuel	Fresh ULG RON 95, supply temperature regulated to +/- 5 degC of 25 degC
Speed	See Table 6.1
Loads	See Table 6.1
Intake cam	Standard 240 CAD profile
Exhaust cam	Standard 278 CAD profile
IMOP	80 - 120 CAD ATDC (swept in 10 CAD increments)
EMOP	100 - 140 CAD BTDC (swept in 10 CAD increments)
Spark timing	BLD or MBT depending on load
Exhaust	For EBPs see Table 6.1. Temperature control not required
Data acquisition	300 cycles logged

6.2.3 Results

6.2.3.1 ISFC

A direct comparison of ISFC (Figure 6.2) shows that the single cylinder engine is higher in ISFC at every point in comparison to the 3 cylinder engine, with the exception of 5000rpm and 24 bar BMEP, where the ISFC on the single cylinder can be seen to be below that of the 3 cylinder. The reason for this is likely to be the employment of fuel enrichment.

Enrichment could not be applied reliably at this point on the single cylinder engine, which imposed an EBP constraint at high speed and load. The reason for this is the lambda sensor was found to malfunction at very high temperatures. Attempts were made to re-site the lambda sensor and to cool the sensor down but the problem persisted. Different types of lambda sensor were used but exhibited similar issues. Attempts were made to run the engine with open loop control of lambda but due to boost pressure fluctuations from the boost rig, stable lambda values were unobtainable. This fault is the reason why the 4000 and 5000rpm 24 bar BMEP points “with EBP” and the “no EBP” points align perfectly, because no EBP could be employed.

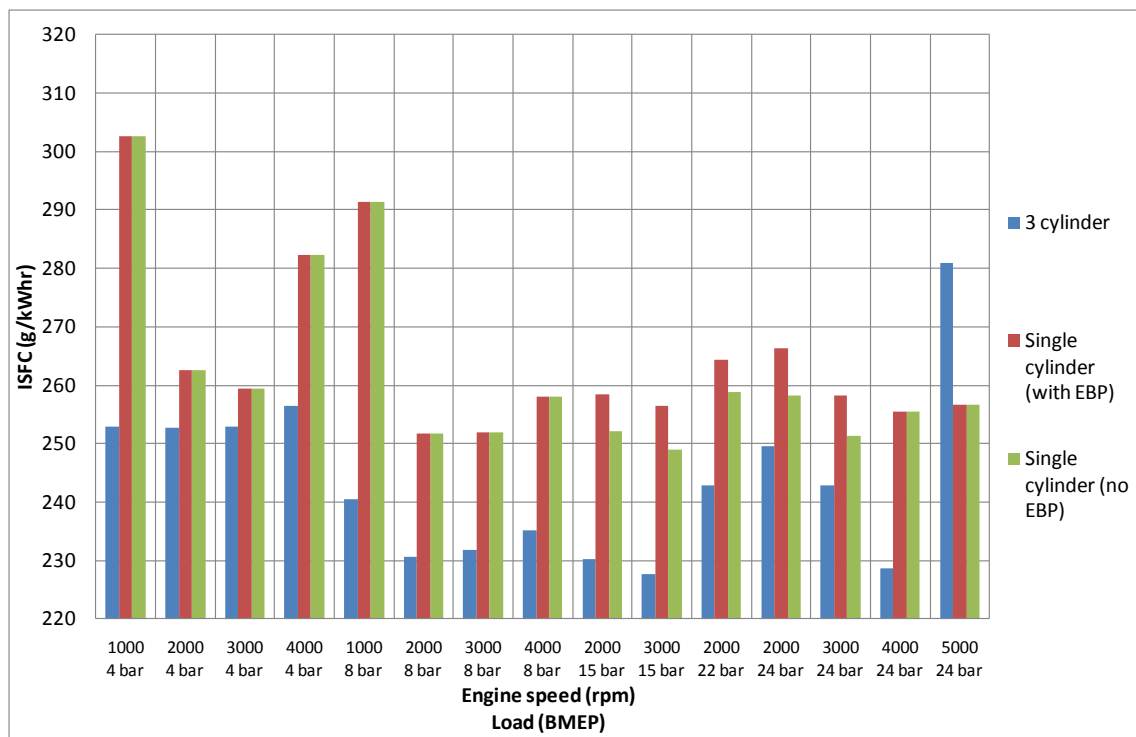


Figure 6.2 ISFC Comparison of 3 Cylinder and Single Cylinder Engines

There are many possible reasons why the ISFC may be higher on the single cylinder engine including; inaccurate in-cylinder pressure reading, inaccurate fuel flow rate reading, incorrect TDC position, incorrect lambda sensor feedback, elevated heat losses in the cylinder, large cycle to cycle COV, MFB rate, intake and exhaust manifold tuning, combustion phasing, residuals in the cylinder and air humidity. It is unlikely that the increase in ISFC for the single cylinder engine can be attributed to just one of these things. The in-cylinder pressure transducer and fuel flow meter are both

calibrated and accurate. A capacitive TDC sensor is used to determine dynamic TDC (see section 3.3.2). This TDC probe is applied at one speed only (1200rpm) when this is not ideal as the thermodynamic loss angle can change dramatically with engine speed, however, the biggest difference in ISFC occurs at low engine speed and reduces as engine speed rises which demonstrates the incorrect trend to make incorrect TDC measurement the cause of the discrepancy seen in Figure 6.2.

The difference in ISFC between the 2 engines can be seen to be, for the most part, insensitive to either engine speed or load. This trend rules out elevated heat losses because although the surface area of the single cylinder engine is relatively large in comparison to the 3 cylinder engine (possibly even greater than the actual 3 cylinder engine) provided the engine is kept at the same temperature the heat flux through it (although far greater than the 3 cylinder engine when calculated on a per-cylinder basis) should be constant regardless of engine speed and load.

6.2.3.2 Engine Breathing

A more viable explanation for the difference in ISFC between the 2 engines could be engine breathing and in-cylinder flow structure. The impact of the difference in engine breathing dynamics is very clear at low speed, particularly at low load. The largest discrepancy between the single cylinder engine and 3 cylinder engine is at the 1000rpm, 4 bar BMEP condition. The reason for this can be partly attributed to the difference in MFB durations between the 2 different engines, which shows the single cylinder engine is characterised with a much longer combustion duration as defined by the 10-90% MFB duration than the 3 cylinder engine (3 cylinder data obtained from Mahle Powertrain). The 10-90% MFB duration and spark timing for the single cylinder is 20.9 CAD and 28.6 CAD BTDC respectively, compared to 17.2 CAD and 19.4 CAD BTDC respectively for the 3 cylinder engine.

Given the different intake and exhaust manifold configurations and flow properties the engine breathing between the 2 engines can be expected to be significantly different. The difference in the spark timing and combustion duration

would suggest that the single cylinder engine either has a greater residual mass fraction at cycle start than the 3 cylinder engine and/or that there is less turbulence in the cylinder meaning the flame front propagates through the end gas at a lower speed.

Figure 6.3 shows a spark timing comparison between the single cylinder and 3 cylinder engines. It shows that at low speed the spark timing had to be advanced to achieve the same 50% MFB timing of approximately 8 CAD ATDC (MBT point). This could be indicative of reduced charge motion or increased residual gas concentration with the single cylinder engine. At higher loads this trend can be seen to reverse at 2000rpm and 8 bar BMEP. Figure 6.4 shows a 50% MFB point comparison of the 3 cylinder and single cylinder engine with and without EBP. The fact that there is no considerable difference in the MBT timings at low loads means the MFB duration is longer at 1000rpm and low loads, and faster at medium loads. This is confirmed by a comparison of 10-90% MFB durations too (Figure 6.5). All of these signs point strongly to different breathing behaviour.

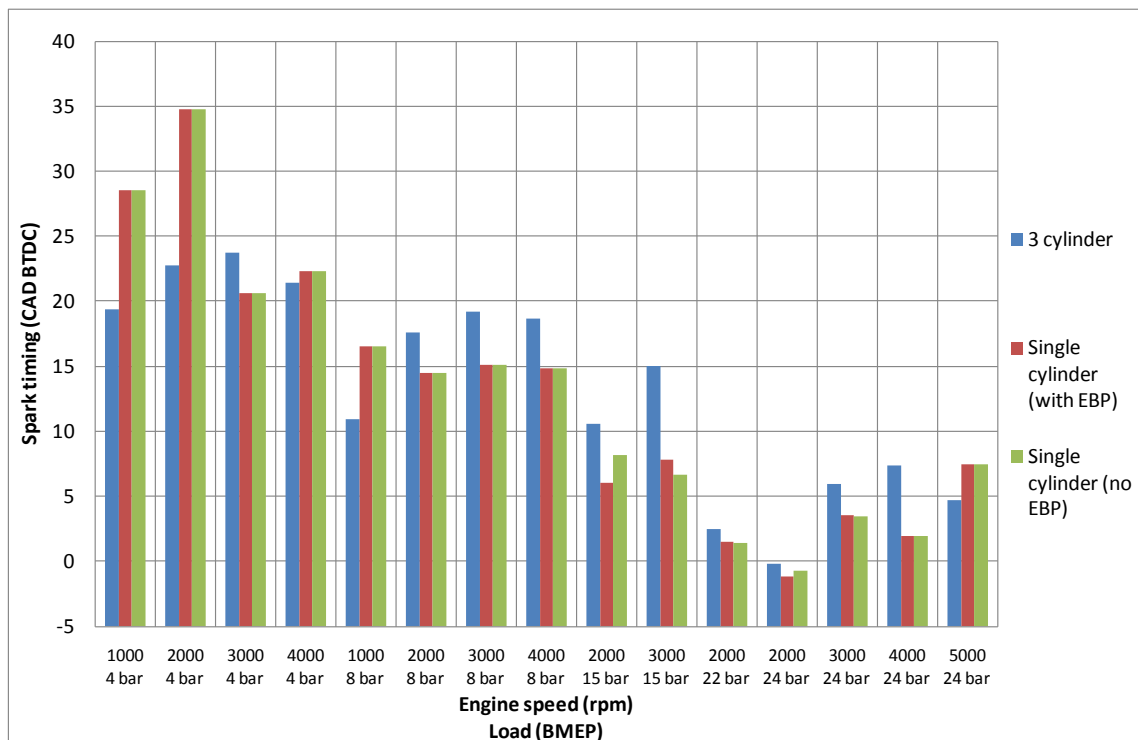


Figure 6.3 Single Cylinder and 3 Cylinder Spark Timing Comparison

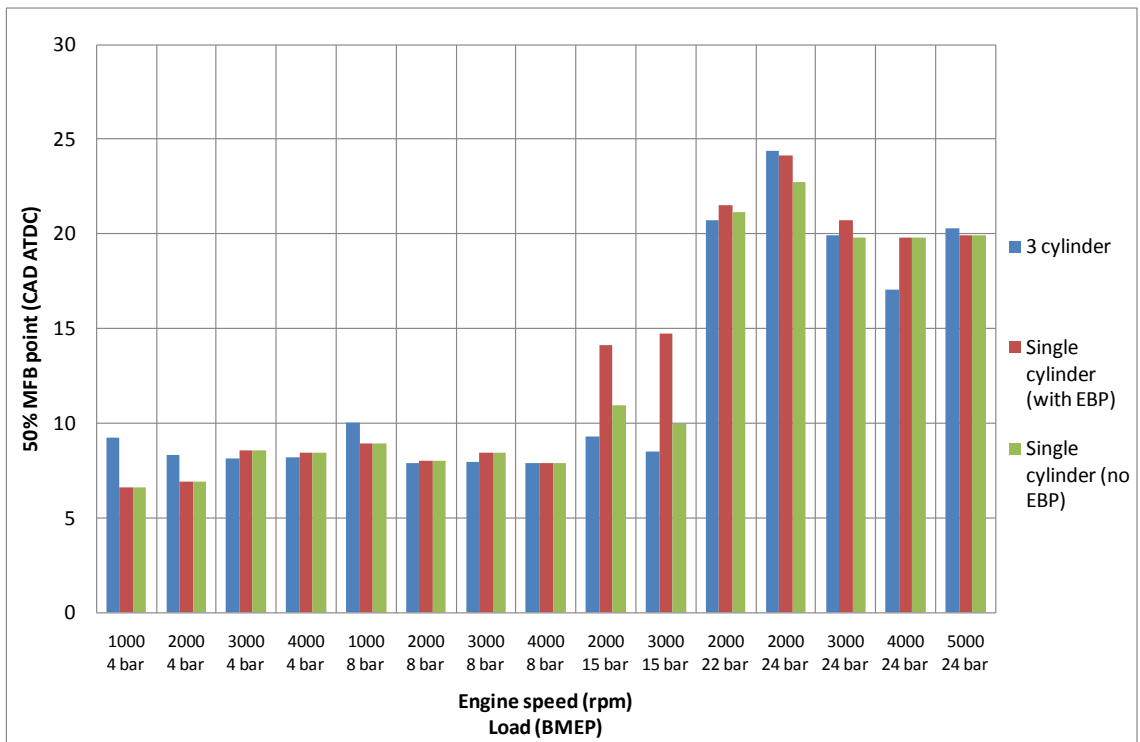


Figure 6.4 Single Cylinder and 3 Cylinder 50% MFB Point Comparison

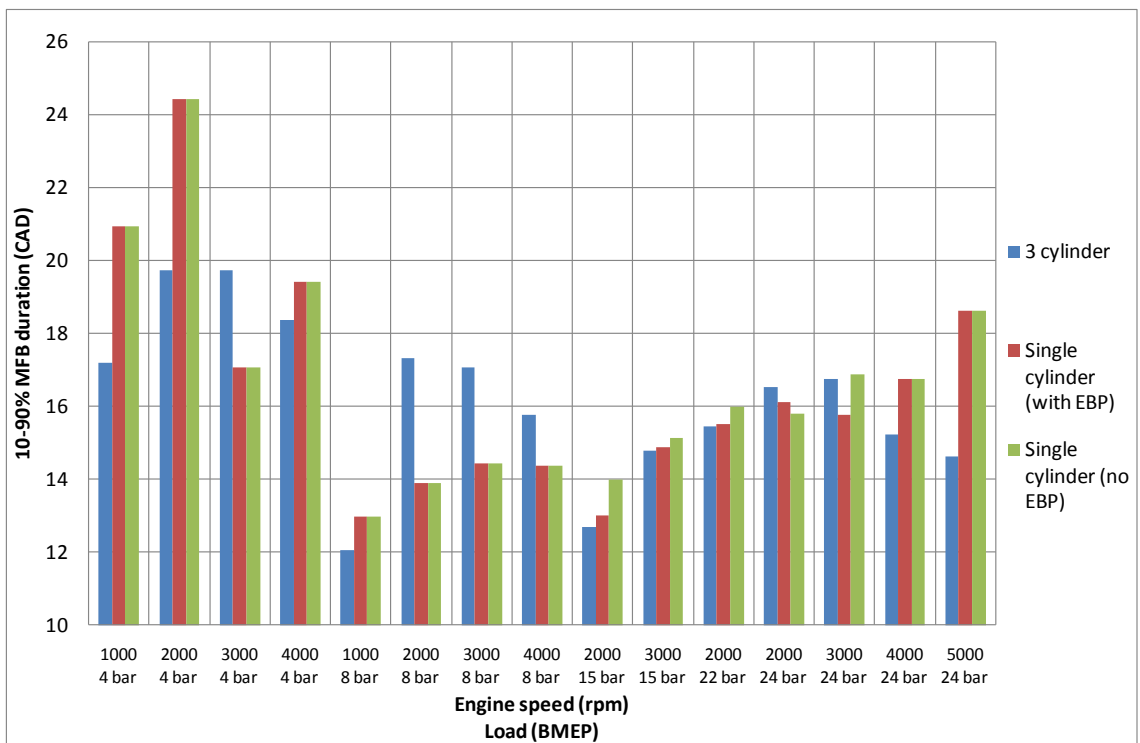


Figure 6.5 Single Cylinder and 3 Cylinder 10-90% MFB Duration Comparison

The difference in the breathing performance is perhaps best illustrated by the difference in boost pressure requirement for the equivalent speed and load points for both engines (Figure 6.6) and by the EBP (Figure 6.7).

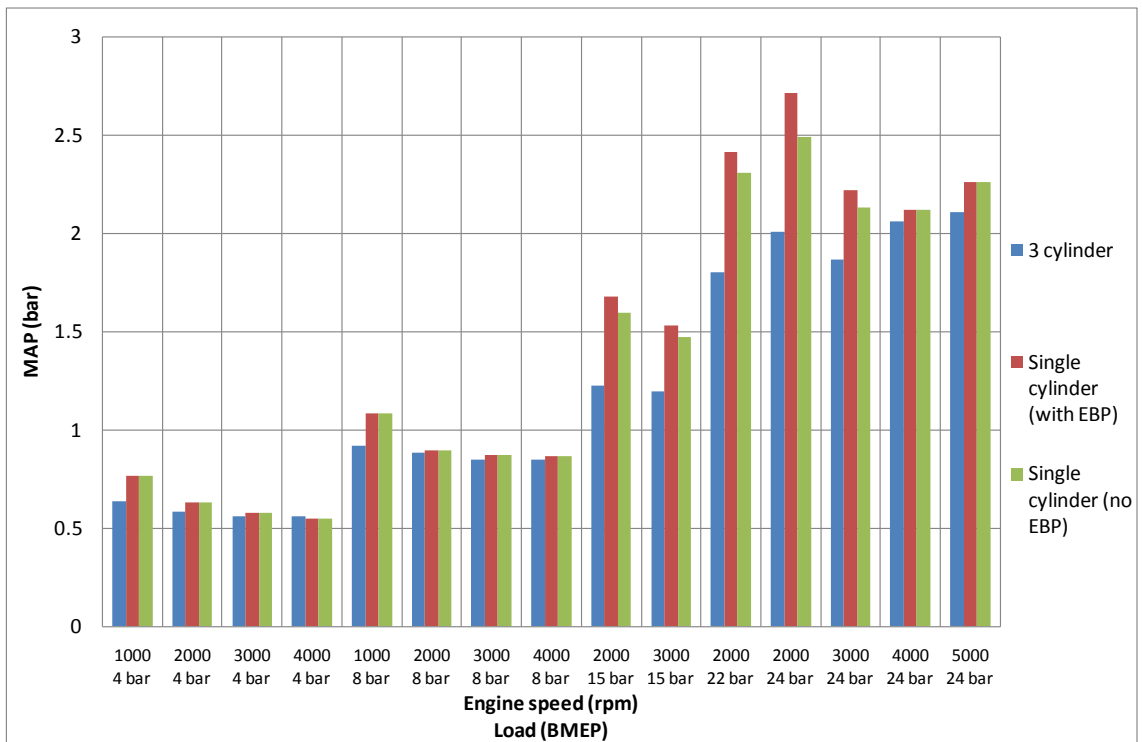


Figure 6.6 Single Cylinder and 3 Cylinder MAP Requirement Comparison

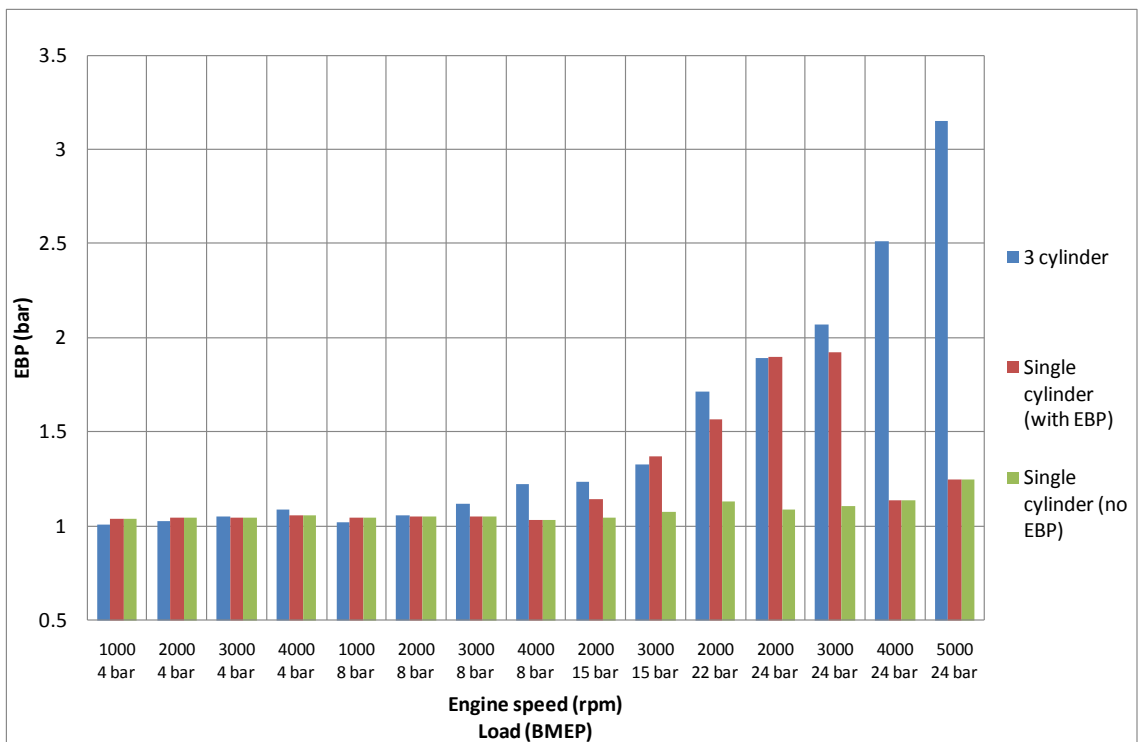


Figure 6.7 Single Cylinder and 3 Cylinder EBP Comparison

In spite of the fact the single cylinder engine is run with a similar EBP to that of the 3 cylinder, it requires a much higher MAP in comparison to the 3 cylinder engine.

One possible explanation for this massive increase in boost requirement is the rate at which air flows through the intake manifold. In the case of the 3 cylinder engine the phase difference between the cylinders and the cam durations result in a near continuous flow through the intake system, whereas for the single cylinder engine the air in the intake manifold is continuously stopping and starting through the entire intake system.

The position of the plenum relative to the intake port will influence engine breathing and is supposed to help the engine maintain a constant MAP. The influence of the plenum position can be seen in Figure 6.8. Pressure waves can be seen for each of the 3 solid lines, but the waves can be seen to be vastly different for the single and 3 cylinder engines. These waves are caused by the blowdown pulse that occurs when a valve is initially opened and are inevitable regardless of engine configuration, but the magnitude of the waves across the entire cycle can be seen to be lower for the 3 cylinder engine simulation than for the single cylinder simulation. It must also be noted that for the single cylinder engine the throttle has been located downstream of the plenum whereas on the 3 cylinder engine the throttle is located upstream of the plenum.

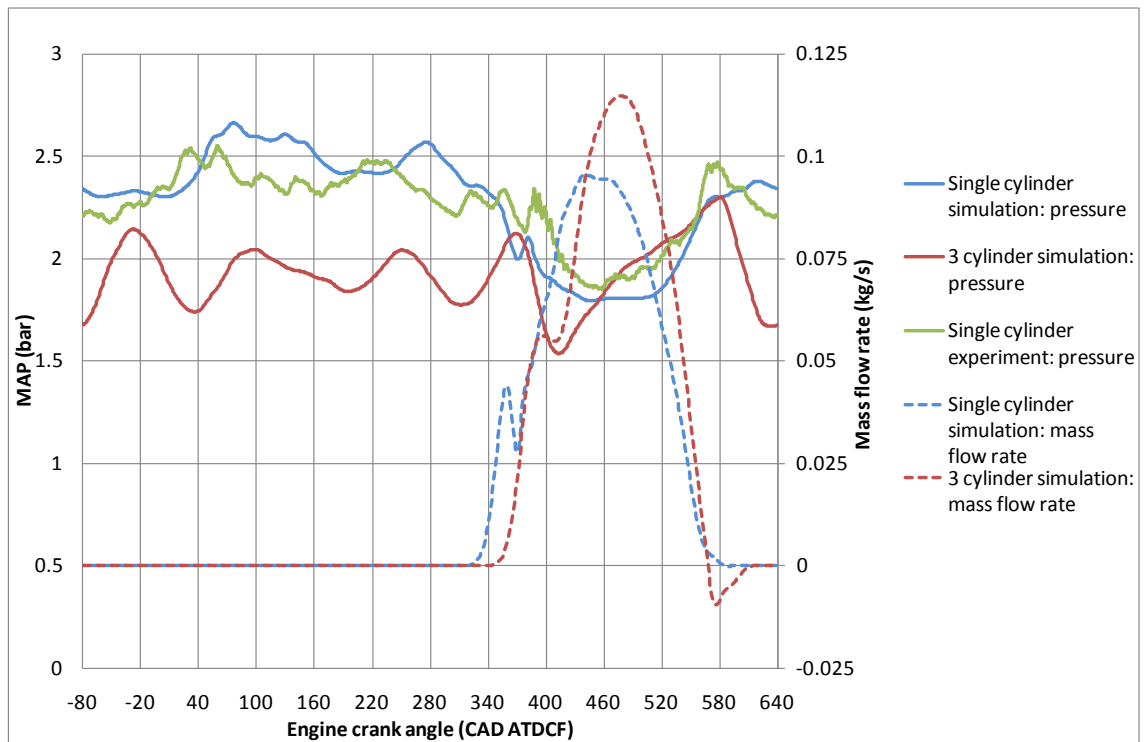


Figure 6.8 Comparison of Intake Manifold Pressures and Intake Valve Mass Flow Rate at 5000rpm and 24 bar BMEP

The blowdown pulse itself is roughly equal in magnitude between both single cylinder scenarios and the 3 cylinder simulation, however, the instantaneous MAP for the 3 cylinder engine can be found to recover much more quickly in comparison to the single cylinder engine, this results in a greatly increased flow rate through the valve in spite of the greatly elevated EBP. The MAP for the 3 cylinder engine can also be found to be much more consistent throughout the cycle, and the average MAP is a good indication of what the cylinder actually sees when the intake valve is opened. In the case of the single cylinder engine the MAP whilst the intake valve is open can be seen to be more approximately 0.4 bar down on the average MAP across the entire cycle.

This can be found to have an impact on ISFC in the form of a slightly larger pumping loop (Figure 6.9) by forming a slight downward lip as highlighted by the circle. In total though the 3 cylinder engine can be found to have a much larger pumping loop in this instance, owing to the fact the EBP has been massively elevated by the turbocharger. The positive contribution of the pumping loop for the single cylinder engine is very small in comparison, and is confined to a very small area by a volume

ratio of approximately 0.8 to 1. The rest of the pumping loop is actually negative which means positive work is applied to the piston during the gas exchange process.

This positive work contribution during the pumping loop is provided solely by the boost rig in this instance.

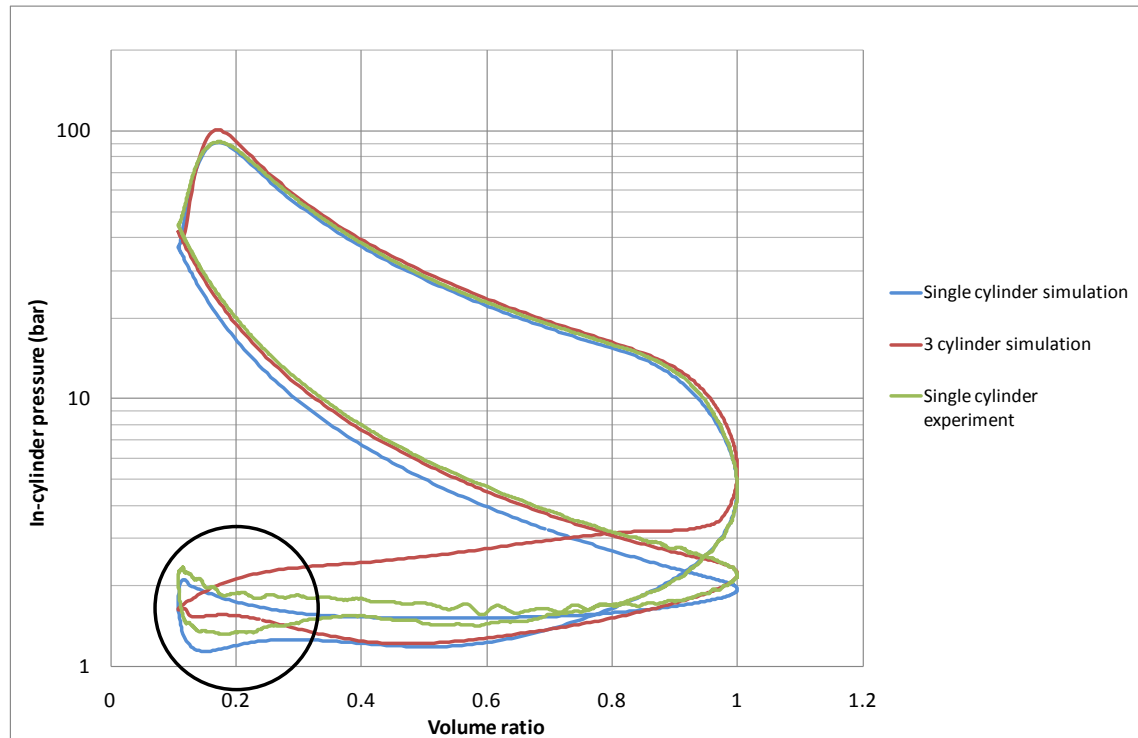


Figure 6.9 5000rpm 24bar BMEP logP-V Comparison

The positive pumping loop work contribution can be found to impact the rest of the cycle too. As mentioned previously, the BMEP figures quoted in this chapter are 3 cylinder effective BMEPs, in order to obtain these effective BMEPs a NIMEP figure was targeted. NIMEP encompasses all 4 strokes of the thermodynamic cycle, therefore if a constant NIMEP is to be maintained, a different sized pumping loop work contribution must be compensated for by a different sized compression and expansion (gross) work contribution.

At this test point the extra work required to drive the turbocharger is 1.428 bar Mean Effective Pressure (MEP) which equates to 2.38kW per cylinder. The actual cost however is more than this as boosting the GIMEP 1.428 bar requires the combustion phasing to be retarded to a greater extent (which is visible in Figure 6.9) and a higher

peak cylinder pressure. The elevated EBP has also resulted in a higher EOC pressure which will require the combustion phasing to be retarded to a greater extent still.

The impact of this phenomenon on ISFC is pronounced, and is best demonstrated by Figure 6.2. A comparison of the single cylinder engine with and without EBP lines shows this effect and reveals a reduction in ISFC of up to 3.2% when turbocharger representative levels of EBP are employed.

The single cylinder engine can be seen to benefit from this lack of considerable EBP, not only through a reduction in the pumping loop losses but also through the lower end of induction pressure and temperature. However, this beneficial effect of lower pressure and temperature has been lost during the compression process. The exact reason for this is likely to be down to different residual gas concentrations at the beginning of compression, or perhaps a difference in the way the fuel evaporation is modelled in GT-Power and how the fuel evaporates in the physical engine.

GT-Power simulations of the single cylinder and 3 cylinder engines reveal that at the 5000rpm, 24 bar BMEP point the single cylinder will have 1.57% residual burned gas at cycle start, and the 3 cylinder engine will have 2.76% residual burned gas at cycle start. Exhaust gasses can be found to have a higher heat capacity than fresh air and fuel mixture because exhaust gas contains more large molecules than fresh air does. Sonntag, et al [119] documents that large molecules (such as typical exhaust gas molecules) have greater capacity for storing heat and can store energy in more ways such as vibrational and rotational energy in comparison to smaller molecules (such as air molecules).

This means that residuals have the effect of reducing the polytropic exponent during the compression phase leading to lower EOC pressures and temperatures. This theory does not explain what is apparent in Figure 6.9 however. Although the increased residuals will have the effect of reducing the polytropic exponent slightly, the influence of the raised EBP in the case of the 3 cylinder engine will result in an EOC pressure and temperature far higher than that of the single cylinder engine. This can be seen by the EOC pressure offset between the single cylinder simulation and the 3 cylinder simulation in Figure 6.9.

6.2.3.3 Knocking Tendency

In terms of knocking performance the single cylinder engine appears to be in very good agreement with the 3 cylinder engine for the most part. Figure 6.4 shows the differences in 50% MFB points between both engines.

The most noticeable difference between the engines is the 2000 and 3000rpm 15 bar BMEP points. Without EBP the single cylinder engine is in very good agreement with the 3 cylinder engine, however, even with a modest amount of EBP, combustion has to be retarded significantly.

The reason for this is the tuning state of the exhaust manifold of the single cylinder engine. The rarefaction/pressure wave caused by the blowdown pulse is sufficiently large enough to greatly impede the flow of burned gasses out of the cylinder, thus leading to a greater residual gas concentration at the start of cycle. This has the effect of elevating the EOC pressure and temperature in comparison to the 3 cylinder engine, and also serves to reduce the MFB duration. A comparison of the cylinder pressures and EBPs at 2000rpm and 15 bar BMEP is given in Figures 6.10 and 6.11 respectively.

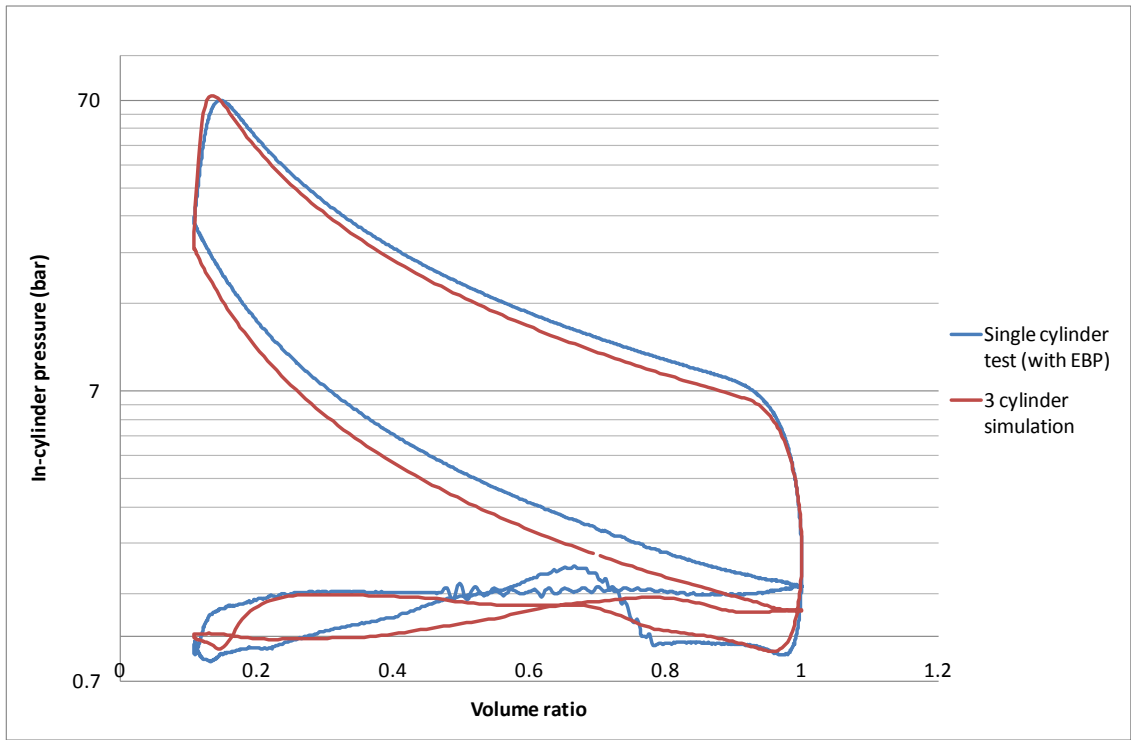


Figure 6.10 2000rpm, 15 bar BMEP Single Cylinder and 3 Cylinder Simulation In-cylinder Pressure Comparison

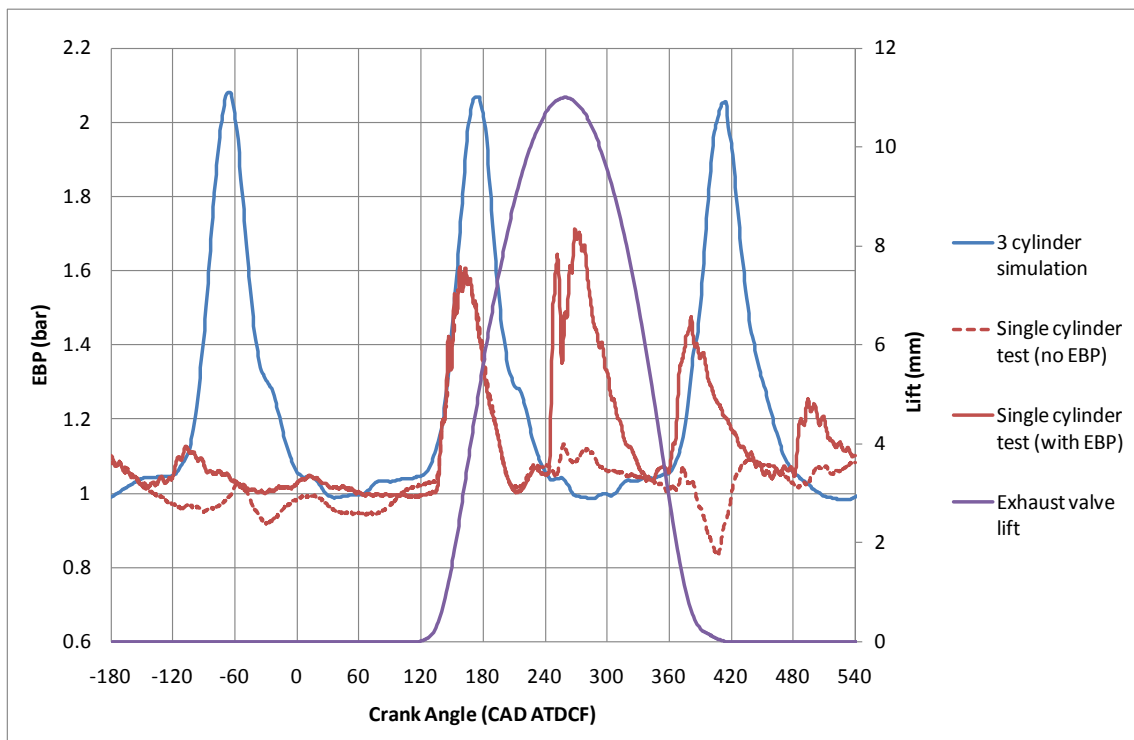


Figure 6.11 2000rpm, 15 bar BMEP Single Cylinder and 3 Cylinder Simulation EBP Comparison

A similar phenomenon can be seen at the 3000rpm, 15 bar BMEP condition also. Figure 6.12 shows the impact of the EBP on in-cylinder pressure and Figure 6.13 shows the actual EBP data.

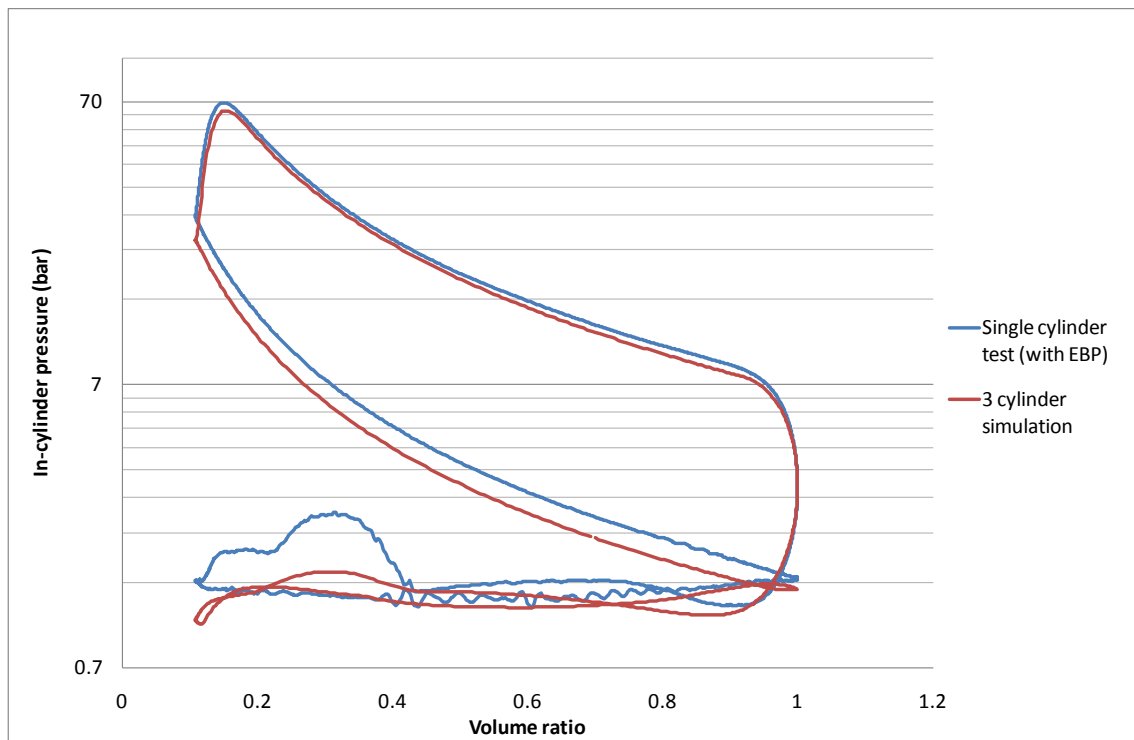


Figure 6.12 3000rpm, 15 bar BMEP Single Cylinder and 3 Cylinder Simulation In-cylinder Pressure Comparison

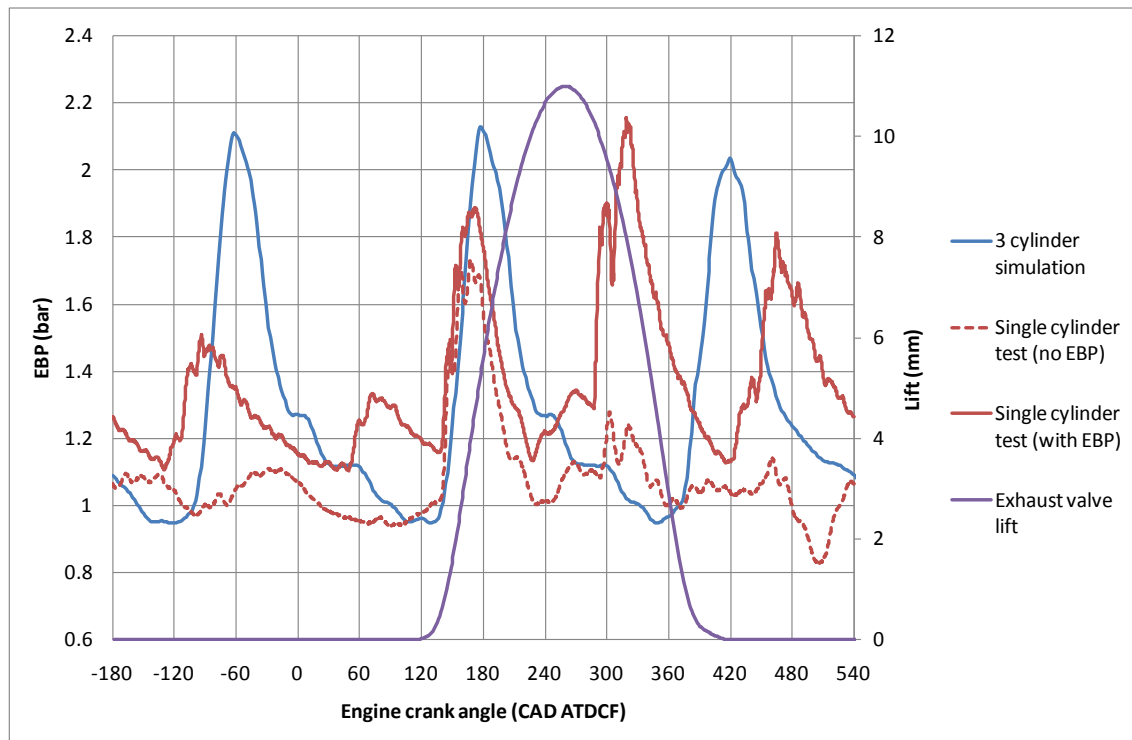


Figure 6.13 3000rpm, 15 bar BMEP Single Cylinder and 3 Cylinder Simulation EBP Comparison

6.2.3.4 Correct EBP Determination

Accurately simulating a turbocharger on a single cylinder engine is very difficult and virtually impossible with just a butterfly valve. Setting the butterfly valve to an angle that gives the same average pressure as a turbocharger can result in the sort of phenomena that is apparent in Figures 6.10 to 6.13 where the flow is choking through the partially closed orifice leading to very severe pressure waves.

The method used for setting the appropriate EBP was to adjust the valve so the average EBP for the single cylinder engine across the entire cycle was equal, or close to the EBP for the 3 cylinder engine across the entire cycle. Figures 6.11 and 6.13 reveal that for these speed and load conditions this was not the correct approach, and that the average EBP while the exhaust valve is open is very different to the average EBP across the entire cycle.

Table 6.3 reveals that the average EBP across while the exhaust valve was open is higher for the single cylinder engine than it is for the 3 cylinder engine with supposedly the same EBP.

Table 6.3 Table of Average EBP during the Exhaust Valve Open Phase

Case	Average EBP (bar)
2000rpm, 15 bar single cylinder (no EBP)	1.136
2000rpm, 15 bar single cylinder (with EBP)	1.275
2000rpm, 15 bar 3 cylinder simulation	1.268
3000rpm, 15 bar single cylinder (no EBP)	1.192
3000rpm, 15 bar single cylinder (with EBP)	1.526
3000rpm, 15 bar 3 cylinder simulation	1.330

For both speeds the average EBP is raised by the pressure/rarefaction wave and for both speeds, from a profile point of view, and from a residuals point of view, the single cylinder without EBP data is a more reliable representation of the 3 cylinder engine than the single cylinder with EBP data.

This pressure/rarefaction wave is common to all 2000 and 3000rpm test points where the EBP valve has been applied, as can be seen from Figure 6.14 for the 2000rpm cases. Frequency analysis confirms that the CAD interval between peaks corresponds to a distance of about 4m when approximating the speed of sound in the exhaust based on exhaust port temperature. This is almost exactly twice the distance between the exhaust pressure transducer and the EBP valve.

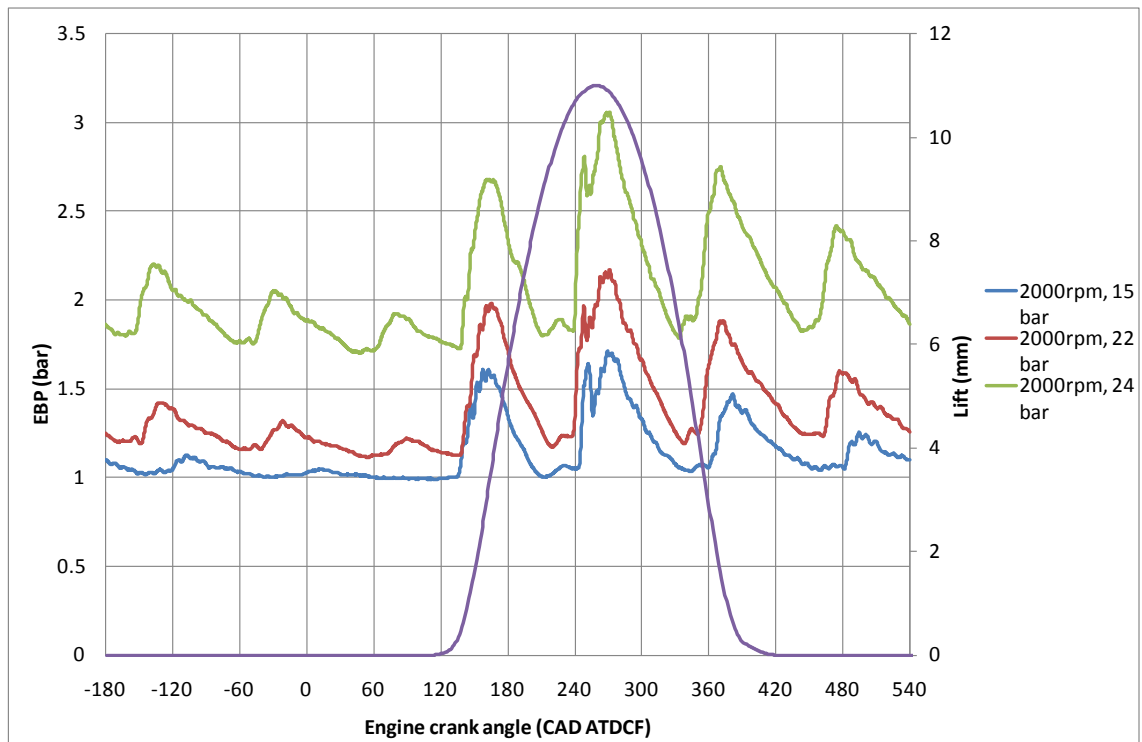


Figure 6.14 2000rpm EBP Comparison at Various Loads with the EBP Valve Applied

The presence of this pressure wave during the exhaust stroke will undoubtedly have an impact on engine performance and on the residuals present in the cylinder for the subsequent cycle. However due to its position in the cycle its influence will be minimised, the third pressure wave (in the region of 340 to 440 CAD ATDCF) will have a far greater impact on residuals as this coincides exactly with the valve overlap point. Figure 6.15 shows where the exhaust pressure waves fall in comparison with the valve overlap position.

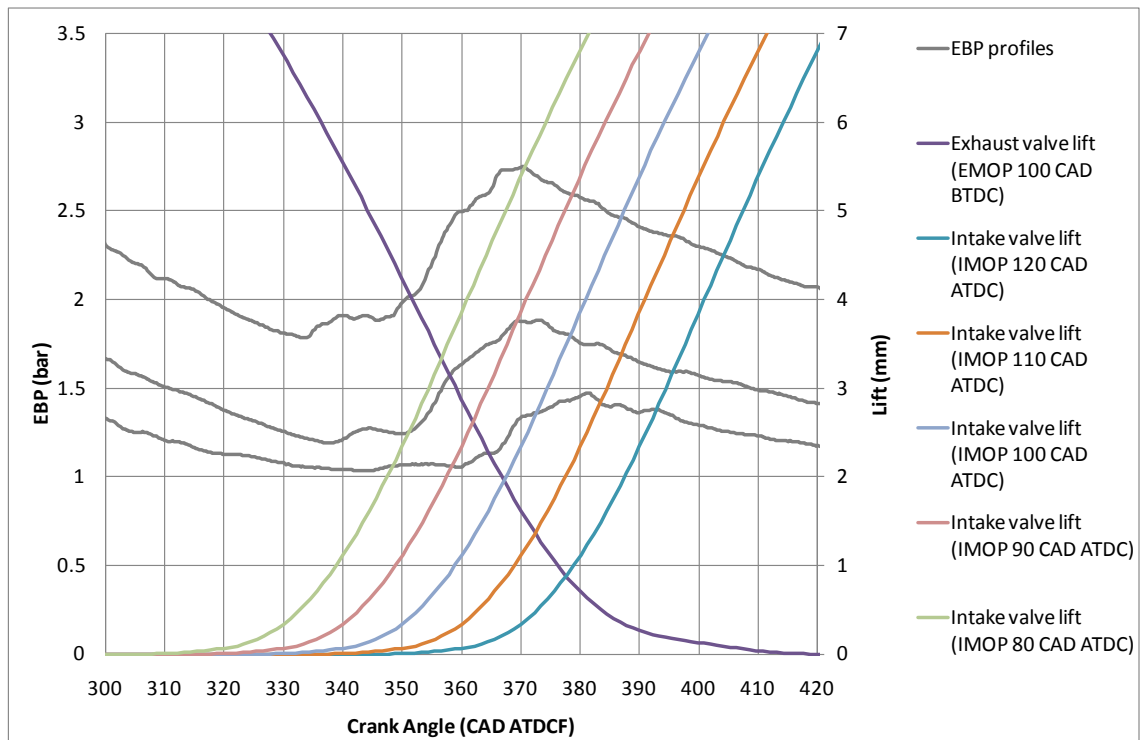


Figure 6.15 2000rpm, Various Loads Single Cylinder EBP Overlay Vs. Valve Overlap Period

This will greatly limit the scavenging ability of the engine and will distort the result regardless of what cam timing combination is being tested.

6.3 Impact of Coolant Flow Rate on Autoignition Tendency

6.3.1 Introduction

Owing to the intricate geometry that the COSCAST process allows (Smith, et al [120]), and the fact the coolant jacket has been designed for high specific power outputs, the coolant jacket geometry on the Mahle 1.2l 3 cylinder downsized head is capable of dissipating heat very effectively from all parts of the cylinder head and greatly reduces the likelihood of any hot spots occurring.

The coolant jacket geometry was dictated by the results of a Computational Fluid Dynamics (CFD) study, and has been designed to create flow of a 3D nature. Fins

within the coolant jacket are used to guide coolant flow to further ensure optimum cooling is taking place.

A standard 12V DC coolant pump was initially installed to the Mahle 1.2l 3 cylinder downsized engine, which is capable of pumping coolant at a rate of up to 100 l/min. With a coolant jacket this sophisticated and effective, the very valid question of whether or not the coolant pump needs to be this large and whether or not the head can function correctly, particularly at low speed, with a lower coolant flow rate is raised.

In order to establish whether or not this was the case a test plan was devised which involved regulating the coolant flow rate to the head, the block, and to the entire engine independently of one another to determine which component would have the biggest effect (if any at all) on autoignition tendency.

The work was split into 2 phases. In the first phase of test work the coolant flow rate has been regulated to give a certain coolant temperature difference between the engine coolant inlet side and the engine coolant outlet side which will henceforth be called the ΔT . Because this engine has a split cooling system and a certain hardware setup it is possible to regulate the coolant flow for the cylinder head and the coolant flow for the cylinder block independently of one another. It is also possible to measure the coolant flows for the head and the block separately by means of 2 turbine type flow meters.

6.3.2 The Effect of Coolant Temperature Gradient

The objective of this first phase of test work was to try and regulate the flow to produce a predetermined ΔT across the head and the block. Owing to the dangers involved in going in to the test cell whilst the engine is running and adjusting the coolant flow rates, the engine was run with full coolant flow rate initially and run at the 2000rpm, 20 bar NIMEP running condition and left to stabilize for 10 minutes. A

log was then taken of the coolant flow rates and ΔT s across the head and block, as well as spark timing and manifold pressure data.

The ΔT s and corresponding flow rates are shown below:

Component	Coolant flow rate (l/min)	Delta T (deg C)
Head	5.23	6.4
Block	5.37	6.7

Using this data flow rates for ΔT s of 9, 12 and 15⁰C were calculated using the following relationship (Eq.6.1):

$$Q = mC_p\Delta T \quad 6.1$$

where the Q is heat rejection, m denotes mass (coolant mass flow rate in this instance) and C_p is specific heat capacity at constant pressure. For this test work the value of Q is constant (because the speed and load are constant) and C_p is constant. With this in mind Eq.6.1 can be rearranged to give a relationship of the variation of ΔT with coolant mass flow rate m (Eq.6.2).

$$\frac{m_2}{m_1} = \frac{\Delta T_1}{\Delta T_2} \quad 6.2$$

Using this formula it is then possible to derive a table of flow rates for the desired ΔT s as shown in Table 6.4. Please note that at the head and block ΔT of 15⁰C point (the lowest total coolant flow rate point) the flow rate is so low that it is out of the calibrated range of one of the flow meters. This point was still tested but may have been compromised by this.

Table 6.4 Test Plan Showing Desired ΔT s and the Corresponding Flow Rate Required to Achieve that ΔT

		Block Coolant Delta T (deg C)			
		6.7	9	12	15
Head Coolant Delta T (deg C)	6.4	5.369581	3.997355	2.998016	2.398413
		5.230148	5.230148	5.230148	5.230148
	9	5.369581	3.997355	2.998016	2.398413
		3.719216	3.719216	3.719216	3.719216
	12	5.369581	3.997355	2.998016	2.398413
		2.789412	2.789412	2.789412	2.789412
	15	5.369581	3.997355	2.998016	2.398413
		2.23153	2.23153	2.23153	2.23153

	Block Coolant Flow Rate (l/min)
	Head Coolant Flow Rate (l/min)

The engine was then run at each of these points for 3 minutes with 100 cycles being logged every minute unless a severe autoignition was witnessed, in which case that was logged as well. The total number of autoignition events was recorded by means of a counter which is triggered every time the peak cylinder pressure of a cycle goes above a certain threshold. The threshold for this work was set to 100 bar.

Other test variables and their control criteria are shown in Table 6.5.

Table 6.5 Test Variables and Control Criteria

Variable	Control criteria
Air	<3% humidity, temperature maintained at +/- 3 degC of 45 ⁰ C intake port temp
Coolant	Temperature maintained at +/- 3 degC of 80 ⁰ C
Oil	Temperature maintained at +/- 3 degC of 90 ⁰ C
Fuel	Aged ULG 95, no temperature control
Speed	2000rpm
Loads	20 bar NIMEP
Intake cam	Standard 240 CAD profile
Exhaust cam	Standard 278 CAD profile
IMOP	100 CAD ATDC
EMOP	120 CAD BTDC
Spark Timing	BLD
Exhaust	Pressure not regulated, temperature control not required
Data acquisition	Averaged over 100 cycles

6.3.2.1 Results

In total 9 severe autoignition events were experienced during this test work. Figure 6.16 shows the distribution of these events across the range of coolant flow rates tested, the z-axis represents the number of severe autoignition cycles at each coolant flow rate combination over the period of 3 minutes. This data showed a vague trend but no statistically significant results were obtained.

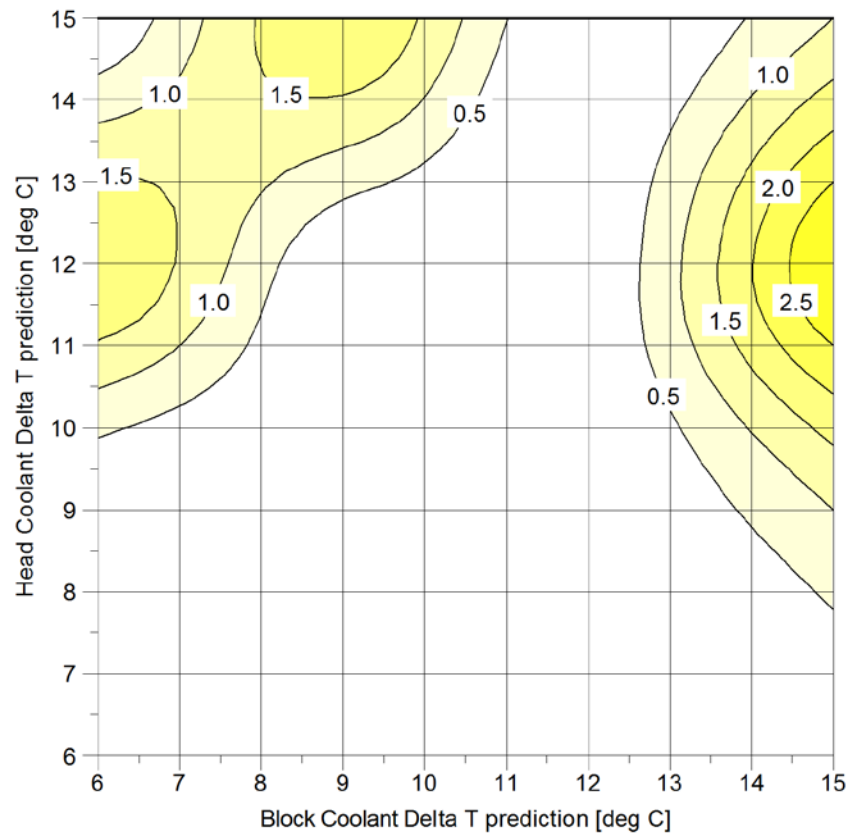


Figure 6.16 Severe Autoignition Frequency

The autoignition events were slightly different in character depending on the ΔT condition. The autoignition frequency showed a vague trend with coolant flow rate (Figure 6.17) and showed that block coolant temperature is perhaps of greater importance than head coolant temperature in the prevention of autoignition (Figure 6.18).

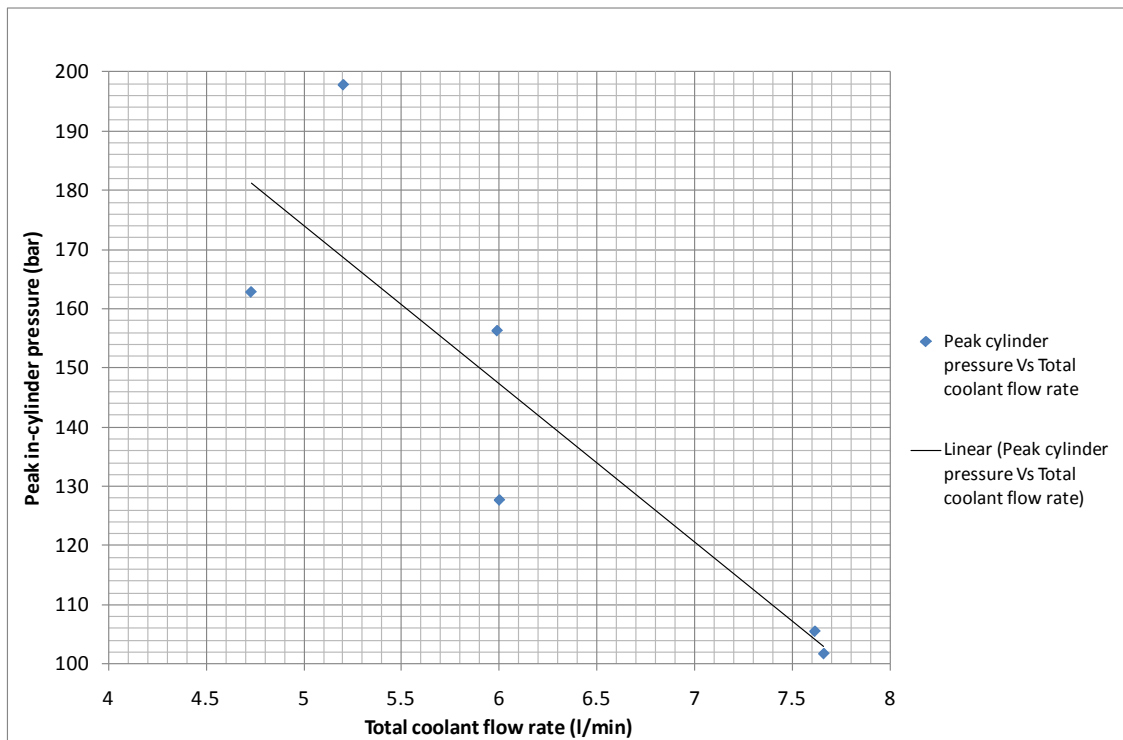


Figure 6.17 Peak Autoignition Cylinder Pressure Vs. Total Engine Coolant Flow Rate

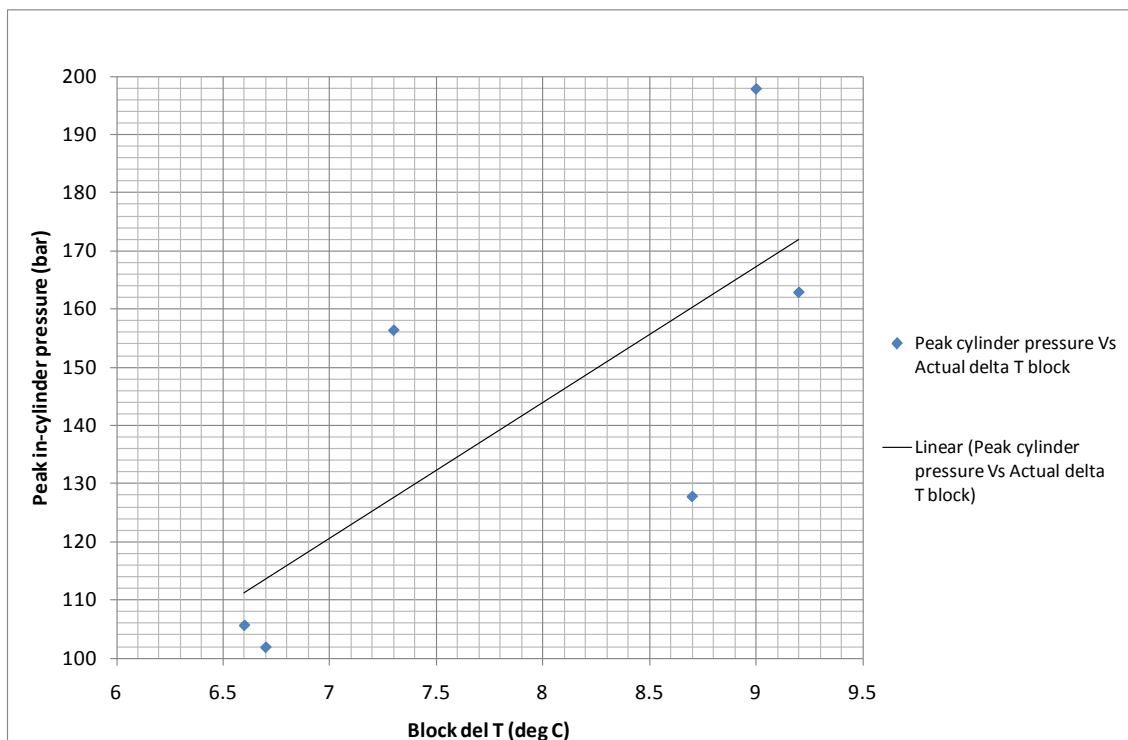


Figure 6.18 Peak Autoignition Cylinder Pressure Vs. Block Coolant Flow Rate

Trend lines have been added to Figures 6.17 and 6.18, although the trend line in Figure 6.18 is not as close a fit as that in Figure 6.17. Figure 6.17 shows that the

lower the coolant flow rate the more severe the autoignition event is likely to be. However, the manner in which autoignition events occur also changes with coolant flow rate. The 128 bar, 102 bar, 105 bar and 167 bar autoignition events were all isolated events, whereas the 156 bar and 198 bar events were not isolated but occurred as a cluster of 2 or 3 autoignition events.

The presence of more severe autoignitions at lower coolant flow rates suggest that perhaps hot spots are forming in the cylinder. There is also an unusual variation in coolant flow rate with lower head coolant flow rates, implying that perhaps the method of cooling is changing from forced convection to nucleate boiling.

The trend line in Figure 6.18 is made even more questionable by the fact the coolant flow for the head also passes through the block both on its way to and from the head. The coolant gallery for the head extends along a significant length of the block (Figure 3.4) and at low head coolant flow rates will give sufficient time for the head coolant to reject a great deal of heat to the block. This will also result in some uncertainty of the true ΔT s obtained from the head and block respectively with the most likely result being that the actual head ΔT is going to be much greater than the measured head ΔT , and the actual block ΔT being less than the measured block ΔT .

The ΔT s for the head and block are shown in Figures 6.19 and 6.20 respectively.

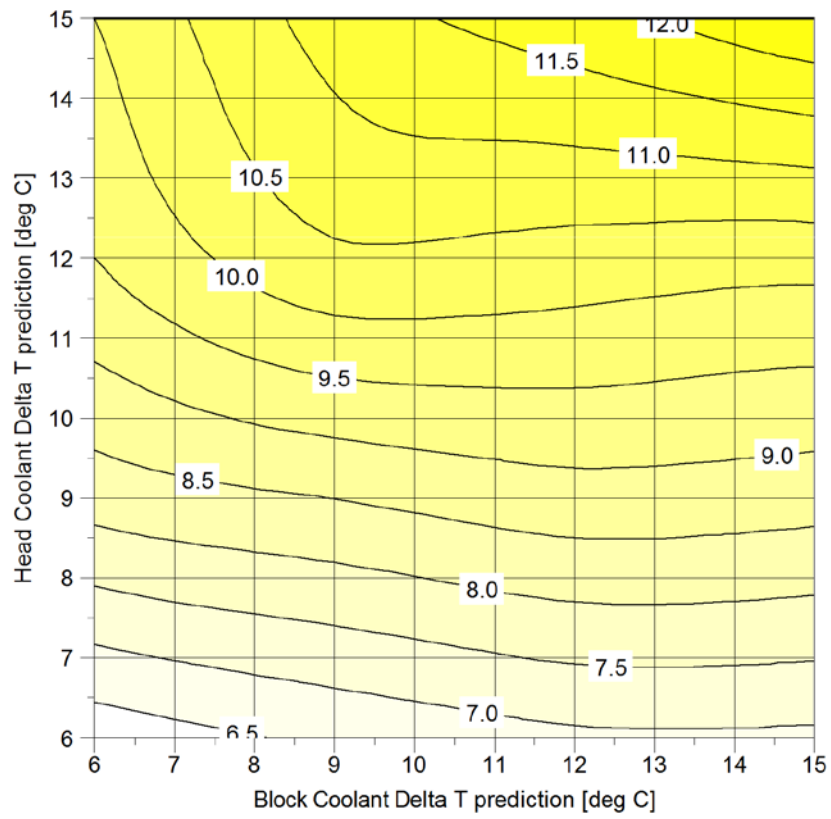


Figure 6.19 Head Coolant Delta T (deg C)

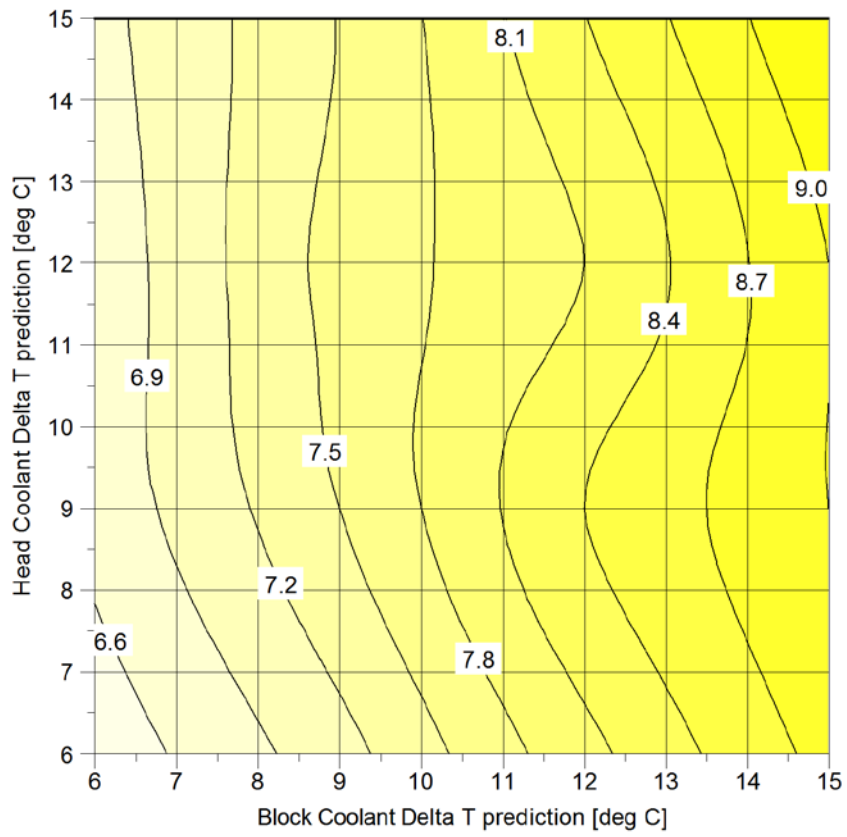


Figure 6.20 Block Coolant Delta T (deg C)

As can be seen from both Figures 6.19 and 6.20, the actual ΔT is far less than the predicted ΔT . There are many potential reasons for this, the most likely of which is that as the coolant flow rate is reduced more heat is lost through the plumbing because the coolant is taking longer to reach the temperature measuring PRTs. This will therefore mean the coolant is cooled down to a greater extent at low flow rates. Another reason is that the way in which the coolant is flowing may result in a greater heat flux for the coolant, for example if nucleate boiling is occurring the rate of heat rejection will increase dramatically compared to film boiling and forced convection, as has been documented by Robertson, et al [121].

Figure 6.20 is a map of block coolant temperature for each of the test points. It can be seen that the block temperature is largely insensitive to head temperature, however, Figure 6.19, a map of head temperatures at each of the test points, can be found to show a large dependence on the block temperature, particularly at large head coolant ΔT predictions (very low head coolant flow rates). This dependence is so large in fact that at a predicted head ΔT of 15⁰C, when the block predicted ΔT is swept from 6⁰C to 15⁰C the actual block ΔT is the same in magnitude as the actual head ΔT .

This could be attributed partly to a discrepancy in head coolant flow rate (Figure 6.21) at high predicted head ΔT s. The isolines in Figure 6.21 should be horizontal, the fact that they are not means that something is changing the flow rate. This discrepancy can be attributed to user error to an extent, but all flows were set at a 2000rpm, 4 bar NIMEP condition to within a maximum error of ± 0.1 l/min. The extent of this user error is perhaps most visible in Figure 6.22 which shows a map of block coolant flow rate, and can be seen to be relatively insignificant.

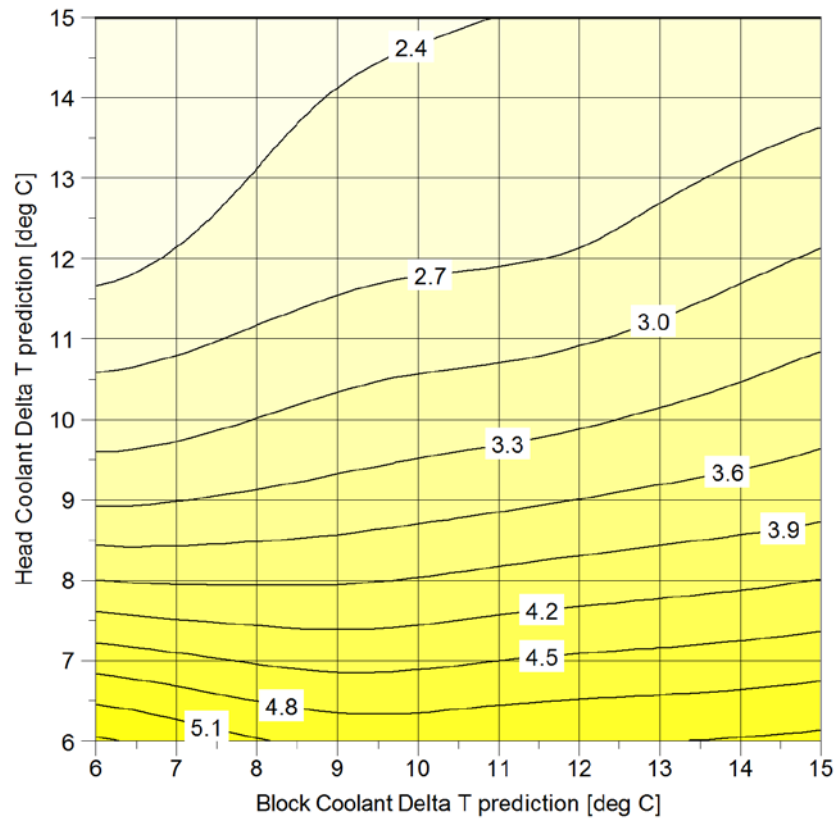


Figure 6.21 Head Coolant Flow Rate (l/min)

One possible reason for this discrepancy in head coolant flow rate is that as the flow rate is reduced, the flow behaviour through the head coolant jacket is changing. The coolant jacket features complex 3 dimensional flow geometry (Figure 6.23) which has not been designed for flows as low as these. However, if the flow was drastically different it would manifest itself at the 2000rpm 4 bar NIMEP condition too, implying that the discrepancy in flow would more likely be caused by increased load and heat rejection.

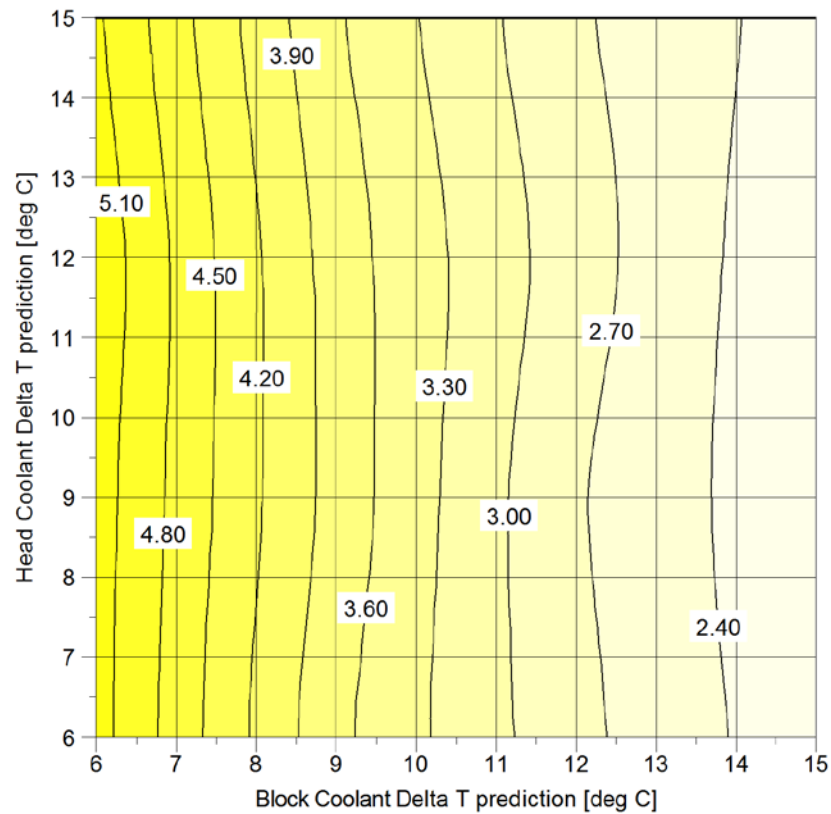


Figure 6.22 Block Coolant Flow Rate (l/min)

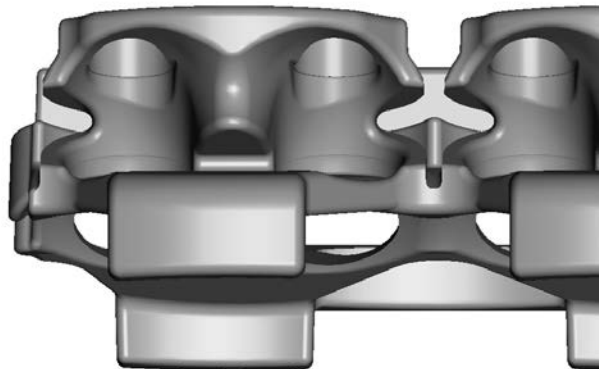


Figure 6.23 Cylinder Head Coolant Jacket Geometry (Hancock, et al [48])

Although the maximum temperature was always controlled to 80°C for this test work it is highly likely that the local temperatures in the head (and block) will go far in excess of this, (particularly if the intended coolant jacket 3D flow has been destroyed by insufficient flow rate) resulting in stagnating pools of coolant in the coolant jacket where nucleate boiling or even film boiling is occurring. This will likely change the coolant pressure in the head and reduce/increase the coolant flow rate correspondingly. To an extent this is supported by Figure 6.19 which shows greatest heat rejection in the top portion of the map where the isolines can be found to be

more vertical than in the bottom portion of the map. This implies that more of the block's heat is being absorbed through the head, a side effect of the coolant in the head having a higher heat flux. As mentioned previously coolant in a nucleate boiling condition has a higher heat flux than coolant in a forced convection condition.

There was no perceivable increase in KI (Figure 6.24) across the entire range of the coolant flow rates tested. For each test point the BLD point was located and for each test point it was almost exactly the same (Figure 6.25) with slight differences between test points but no obvious trends.

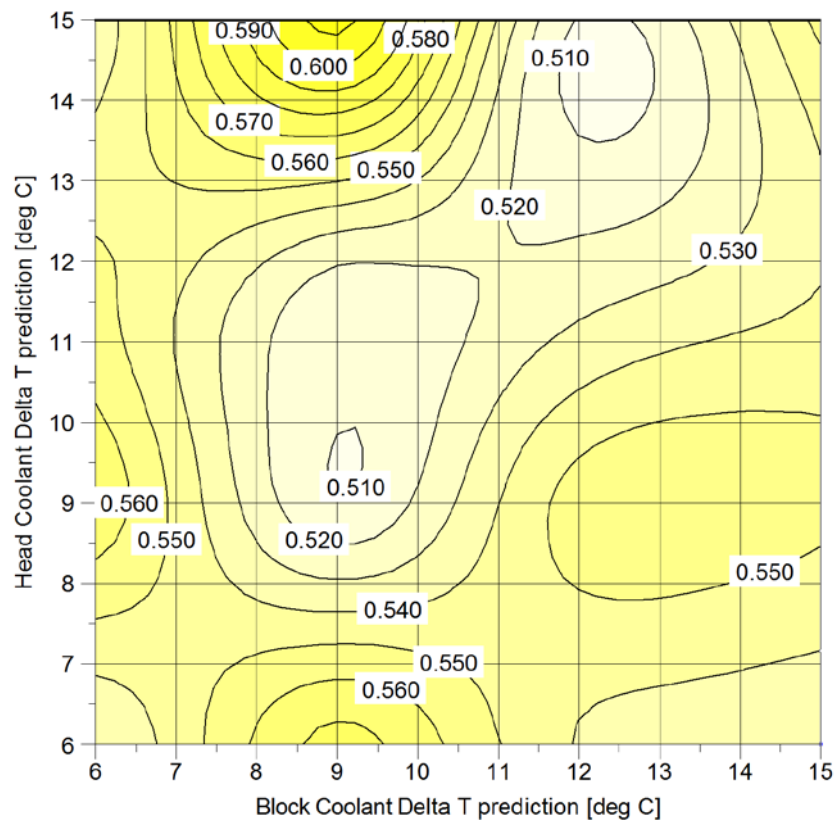


Figure 6.24 Average Band-pass Filtered KI (bar)

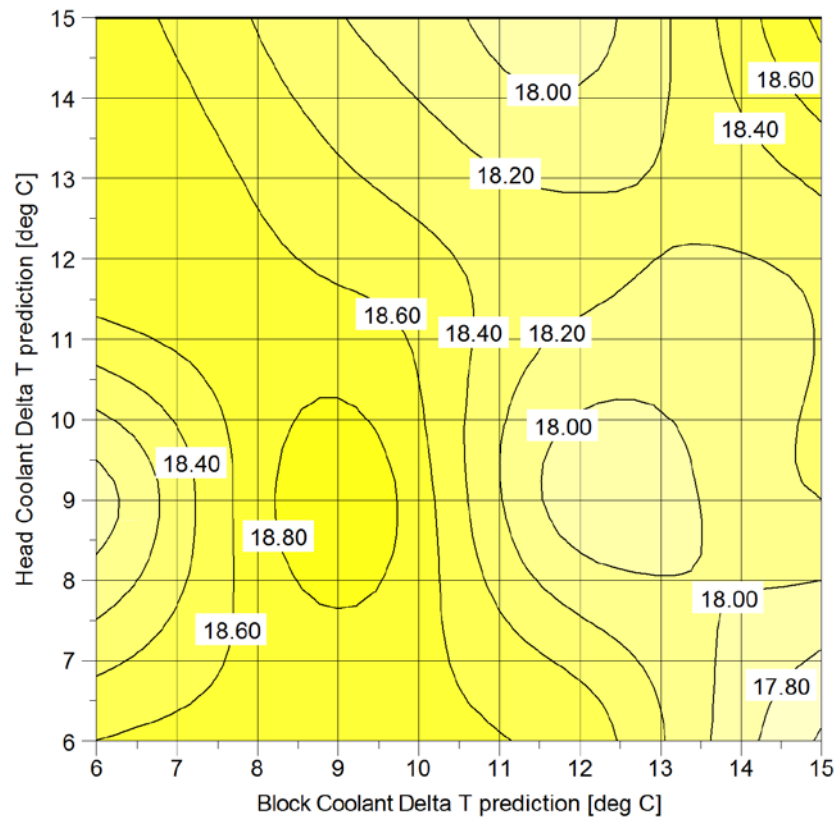


Figure 6.25 BLD 50% MFB (CAD ATDCF)

6.3.3 Effect of Coolant Flow Rate at Higher Load Operations

The second phase of this test work involved running at a higher load for a longer duration to get some statistically significant autoignition data following the inconclusive results obtained from the first phase.

The load was increased from 20 bar NIMEP to 24 bar NIMEP and the duration the engine was held there for increased from 3 minutes to 15 minutes, or limited by the time it took 6 autoignitions to occur, whichever came first. Other than that this test is identical to the test plan in the first phase and the criteria outlined in Table 6.5.

Owing to the elevated load the coolant flow rates required for specific ΔT s had to be recalculated. The same technique for determining the correct flow rates as in the first phase of the test work was adopted for the second phase, which was firstly running the engine at the test condition with maximum coolant flow rate and then

using Eq.6.2 to calculate a table of corresponding theoretical coolant flow rates to give a required ΔT .

The ΔT s and corresponding maximum flow rates are shown below:

Component	Coolant flow rate (l/min)	Delta T (deg C)
Head	4.90	6.9
Block	5.40	3.4

From this a map of test points was produced as shown in Table 6.6.

Table 6.6 Test Plan Showing Desired ΔT s and the Corresponding Flow Rate Required to Achieve that ΔT

		Block Coolant Delta T (deg C)				
		3.4	6	9	12	15
Head Coolant Delta T (deg C)	6.9	5.396921	3.05825546	2.038837	1.529128	1.223302
		4.904733	4.9047326	4.904733	4.904733	4.904733
	9	5.369581	3.05825546	2.038837	1.529128	1.223302
		3.760295	3.760294993	3.760295	3.760295	3.760295
	12	5.369581	3.05825546	2.038837	1.529128	1.223302
		2.820221	2.820221245	2.820221	2.820221	2.820221
	15	5.369581	3.05825546	2.038837	1.529128	1.223302
		2.256177	2.256176996	2.256177	2.256177	2.256177

	Block Coolant Flow Rate (l/min)
	Head Coolant Flow Rate (l/min)

Some of these values have been highlighted in red. These represent points that are below the calibrated range of the flow meters and were therefore not tested. One hundred cycles were logged every 5 minutes for this test work, unless the autoignition was so frequent that the engine could not be run at that test point for the full 15 minutes, in which case they were logged at more regular intervals. As with the first phase of this work a threshold and counter were used to log the number of autoignitions, and every time an autoignition event that exceeded this threshold occurred it was logged. The peak cylinder pressure threshold for this was 120 bar.

6.3.3.1 Results

The results showed no real trend for autoignition but it did show a great deal of difference in frequency, as can be seen from Figure 6.26. The reason for this is

unknown but could be attributed to the fact that in some instances 2 autoignitions would happen within a few cycles of each other (with 1 occurring as a consequence of the other), and this elevates the frequency somewhat. The decision was made to count all of these autoignitions separately. This decision was made because ultimately each severe autoignition event is damaging to the engine, regardless of whether or not they occur relative to each other or if one occurs as a consequence of another. The distribution of these “run-on” autoignition events is also random and would therefore have no influence on the trend.

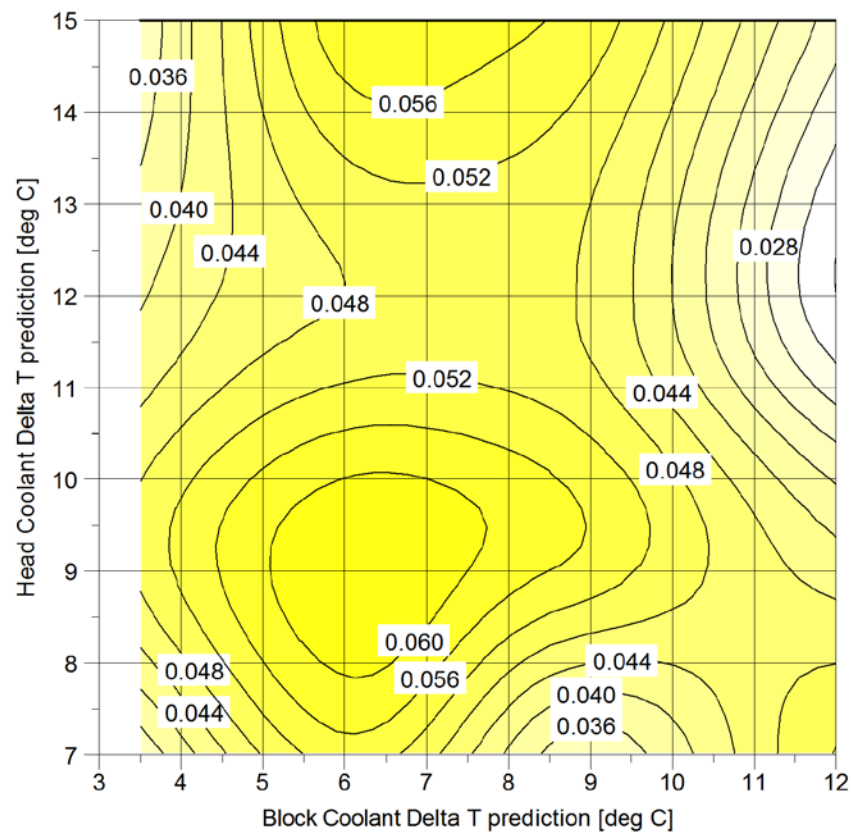


Figure 6.26 Autoignition Frequency in Percentage of Autoignition Cycles at Different Coolant Flow Points

This phase of the test work also revealed no correlation between coolant flow rate and the BLD point, no correlation between coolant flow rate and autoignition frequency. It has also shown that there is no correlation between peak autoignition cylinder pressure and coolant flow rate, contrary to what Figure 6.17 might have suggested.

From this test work it would appear as though this cylinder head can be run at a significantly lower flow rate than the 3 cylinder coolant pump currently delivers, however, the cylinder liner was found to have cracked soon after completing this test work. Although there is no conclusive evidence this failure was caused by this test work, least of all by the reduction in coolant flow rate, it should be taken into consideration for all future test work.

6.4 Impact of Cam Timing on Autoignition Tendency

6.4.1 Introduction

The single cylinder engine has been found to be much more prone to severe autoignition than the 3 cylinder engine. This issue of severe autoignition has imposed a heavy constraint on the maximum permissible load the single cylinder engine can operate at, and has forced the implementation of a 26 bar NIMEP load limit when the 3 cylinder engine can achieve almost 32 bar NIMEP.

The fact that this issue is only present at low engine speeds suggests that LSPI could be the cause of this issue. One of the intentions of this study is to determine whether or not these severe autoignitions are the result of LSPI.

6.4.2 Test Plan

The main objective of this test work was to try and find the optimum cam timing from an autoignition perspective, and whether or not there was a difference in the type of autoignition event depending on the cam timing. This work has also been carried out in a GT-Power simulation in an effort to better understand the mechanisms behind this increased tendency to autoignite (section 6.4.4).

In order to find an optimum cam timing a cam timing sweep was carried out which involved sweeping both inlet and exhaust cams through their full operable ranges (IMOP 80–120 CAD ATDC, EMOP 100–135 CAD BTDC) in 5 CAD increments. This was done to ascertain what impact valve overlap had on autoignition tendency and whether or not the autoignition was being caused by residuals in the cylinder or some other sort of deposit from a previous cycle.

The other test variables and their control criteria can be found in Table 6.7.

Table 6.7 Test Variables and Control Criteria

Variable	Control criteria
Air	<3% humidity, temperature maintained at +/- 3 degC of 45 ⁰ C intake port temp
Coolant	Temperature maintained at +/- 3 degC of 80 ⁰ C
Oil	Temperature maintained at +/- 3 degC of 90 ⁰ C
Fuel	Aged ULG RON 95, no temperature control
Speed	2500 rpm
Loads	20 bar NIMEP
Intake cam	Standard 240 CAD profile
Exhaust cam	Standard 278 CAD profile
IMOP	80 - 120 CAD ATDC (swept in 5 CAD increments)
EMOP	100 - 135 CAD BTDC (swept in 5 CAD increments)
Spark Timing	BLD
Exhaust	Pressure not regulated, temperature control not required
Data acquisition	Averaged over 100 cycles

6.4.3 Results

The test work revealed potential hotspots for autoignition in terms of cam timing combinations. Very severe autoignition or “superknock” (peak cylinder pressure above 200 bar, knock intensity above 100 bar) cycles were encountered twice during this phase of the test work. Plots of autoignition locations, peak magnitudes and frequency are shown in Figures 6.27 and 6.28 respectively.

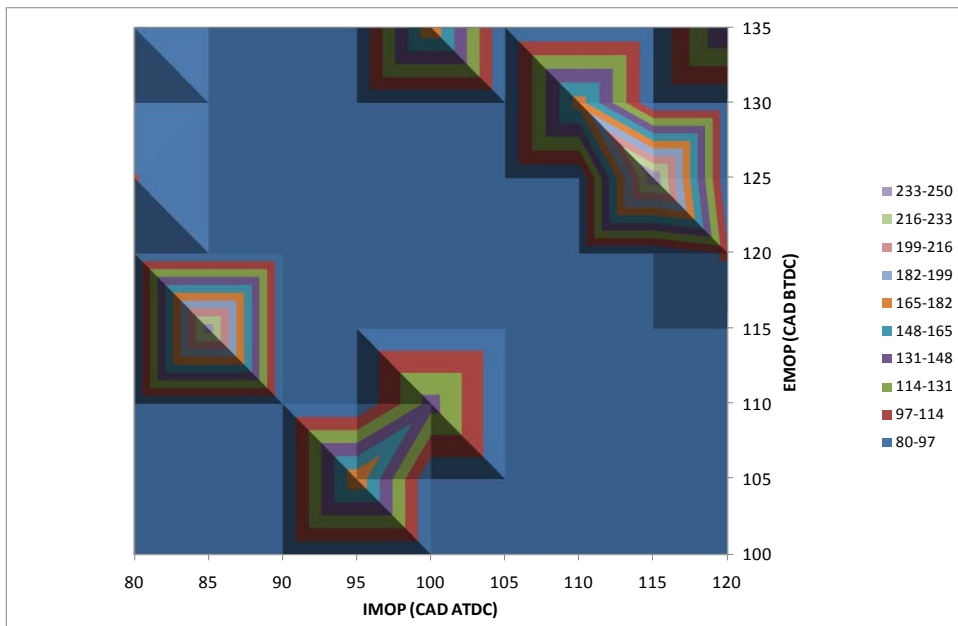


Figure 6.27 Peak Autoignition Cylinder Pressure

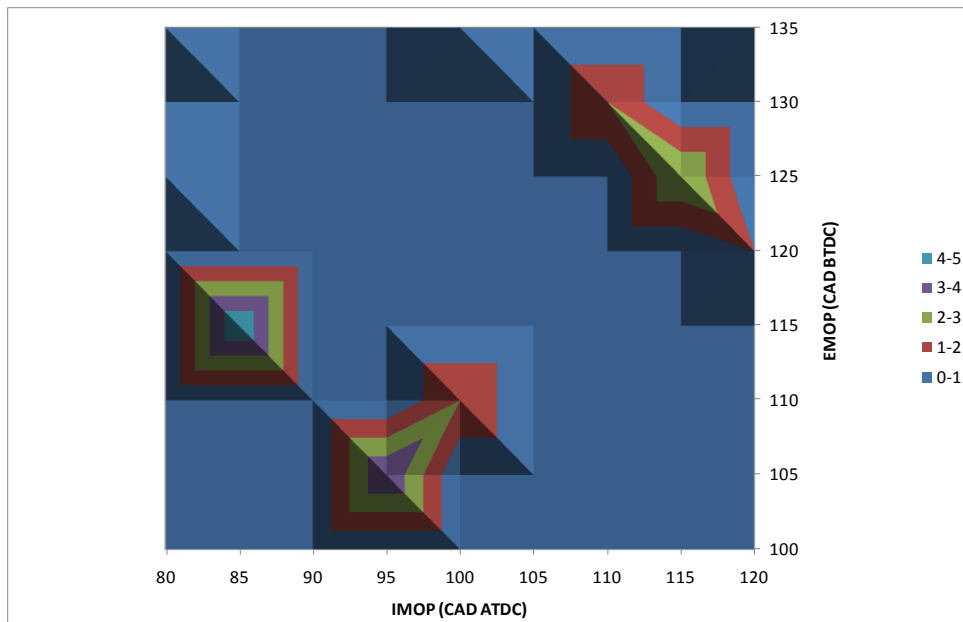


Figure 6.28 Frequency of Autoignition Events at Specific Cam Timings

Figures 6.27 and 6.28 reveal 2 potential autoignition hotspots, for the purposes of this test work these hotspots will be broken down into “ridges” named as shown in Figure 6.29.

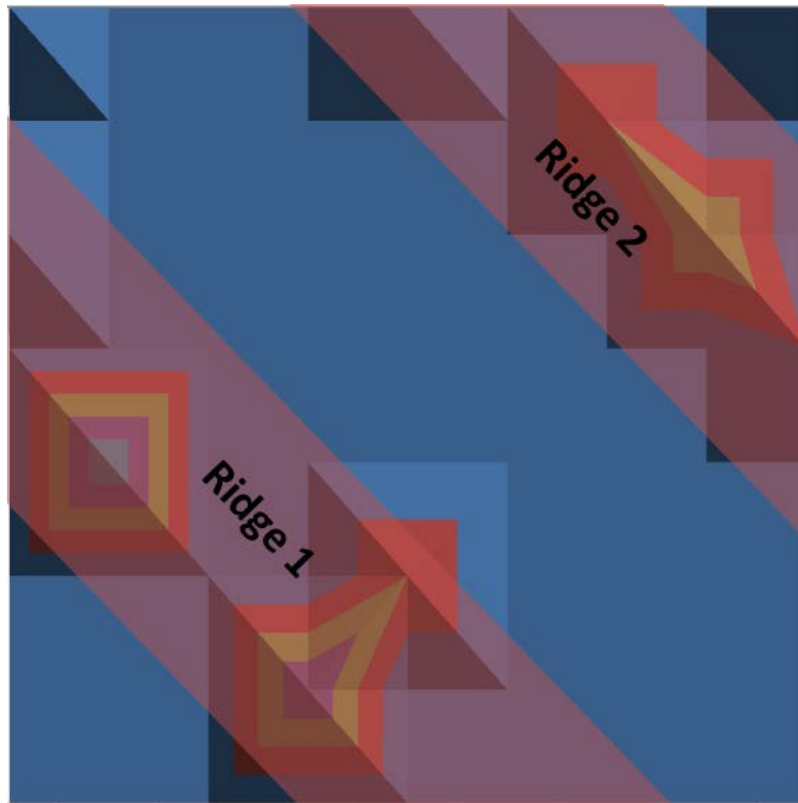


Figure 6.29 Ridge 1 and Ridge 2 Definitions

These ridges encompass 87% of the autoignition events witnessed during this test work, what is more they are also lines of constant valve overlap indicating that valve overlap is of great importance when it comes to autoignition, and where this overlap occurs with respect to piston TDC is of less importance.

A well known source of autoignition is residuals, therefore it may be logical to assume that valve timings that offer less valve overlap will be more prone to autoignition. This can be seen to an extent in Figure 6.29 as ridge 2 highlights an area of very little valve overlap, and an autoignition event that falls just outside the boundary of ridge 2 with an even lesser degree of valve overlap also shows a relatively light autoignition event. Ridge 1 however highlights an area of large valve overlap where the pressure differential between intake and exhaust will strongly encourage scavenging. A GT-Power simulation was carried out to determine the impact on engine breathing and knocking performance. The results of this study are presented in section 6.4.4.

As can be seen from Figure 6.27 superknock events can be found to occur under both ridge 1 and ridge 2. Although they are both very severe autoignition superknock events they can be found to be different when analysing the in-cylinder pressure traces (Figure 6.30).

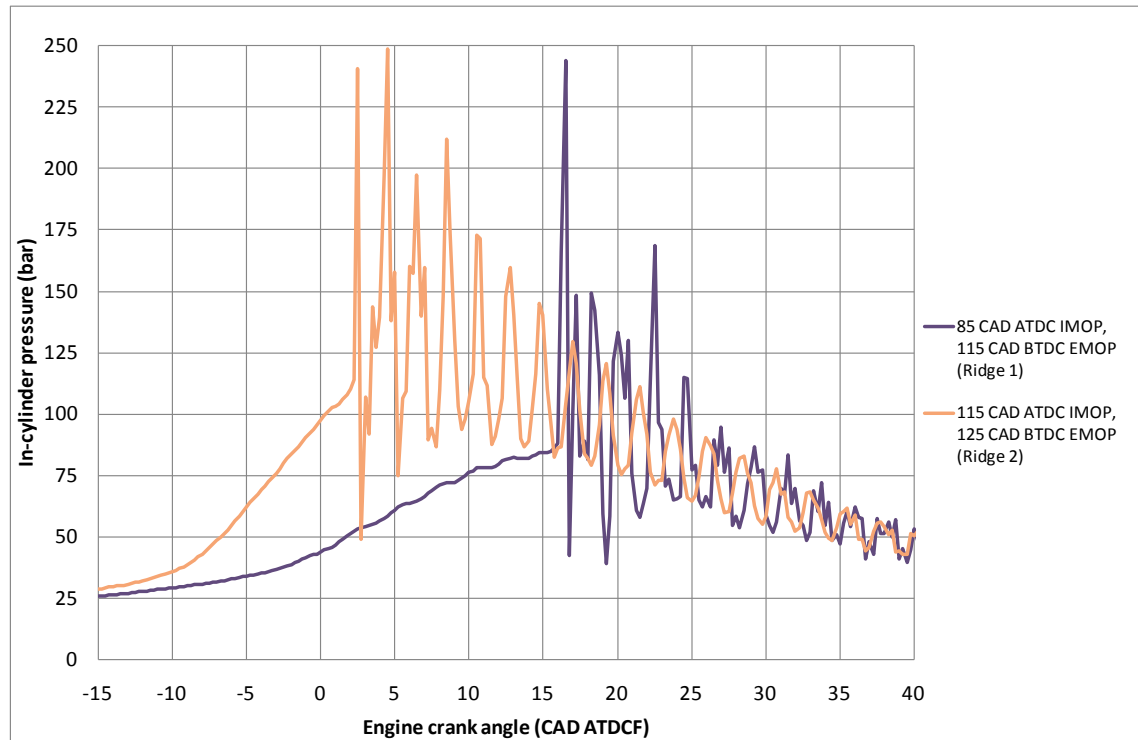


Figure 6.30 Comparison of 2 Superknock Events, 1 Occurring Under Ridge 1, the Other Under Ridge 2

One of the superknock events occurs at a much earlier crank angle than the other. In the case of Figure 6.30 this offset in superknock angle can be attributed to the pressure history of the cylinder prior to autoignition (Figure 6.31). In both of these cases the superknock cycles were caused by LSPI, as can be seen clearly from Figure 6.31. The ridge 2 case is very clearly caused by LSPI, while the ridge 1 case is still LSPI it does not occur until later into the cycle.

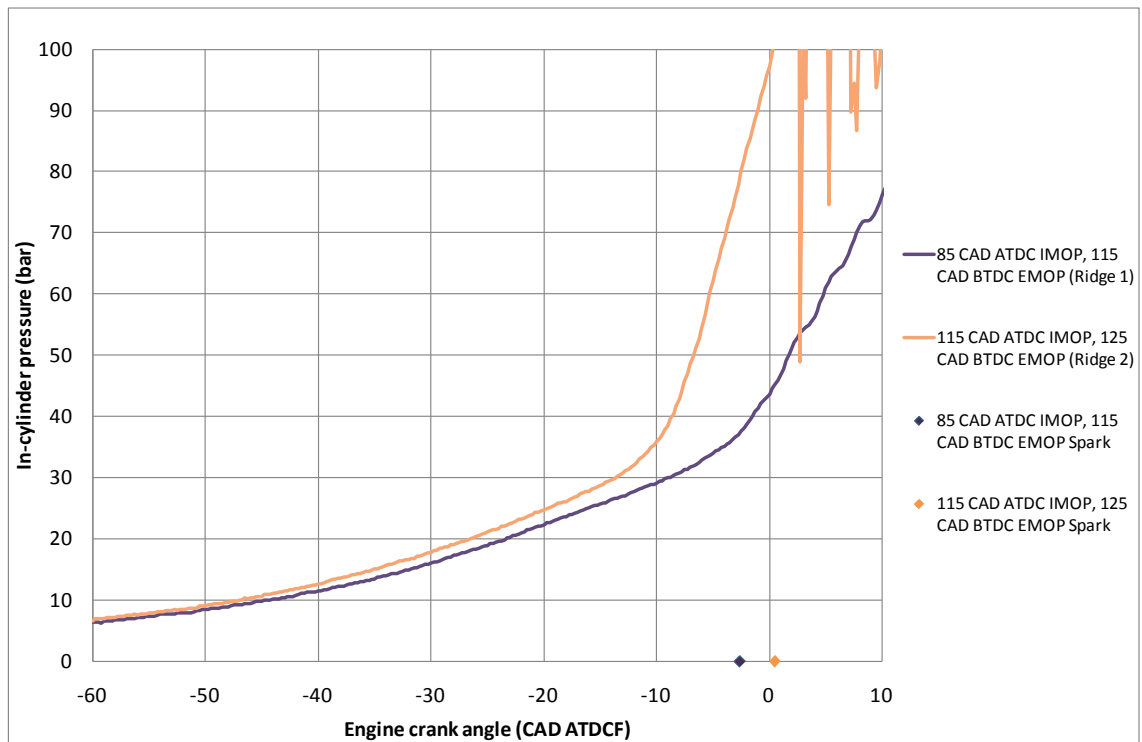


Figure 6.31 Comparison of Pressure Histories for 2 Superknock Events, 1 Occurring Under Ridge 1, the Other Under Ridge 2

There are a few potential explanations for the greater EOC pressure for the cases encompassed by ridge 2. These include the fact that no EBP was applied at any point during this test work, but the MAP was still relatively high. This means that during the valve overlap phase only scavenging will take place, and with high degrees of valve overlap (such as under ridge 1) the scavenging will be much greater than with smaller degrees of valve overlap (such as under ridge 2). This scavenging will be beneficial to the engine but will also result in slight accidental over enrichment, and the engine running slightly rich under ridge 1, whereas the AFR will be much closer to stoichiometric under ridge 2.

Fuel enrichment is well known to result in a reduction in polytropic exponent, so for this test work the PIPR pegging technique was abandoned in favour of pegging using the MAP instead (as described in section 3.3.1) to try and ascertain the extent of this scavenging effect. The polytropic exponent can be seen to be lower for the high valve overlap cases (Figure 6.32) implying that accidental over enrichment is occurring as a result of the scavenging. The polytropic exponent values obtained from this are somewhat higher than expected, it is suspected that the reason for this is the lack of

an intake pressure transducer when this work was carried out, the automotive style MAP sensor had to be used instead. Although this is not ideal or particularly accurate each of the cases were pegged using the same method and the same sensor, so the trend shown should be accurate.

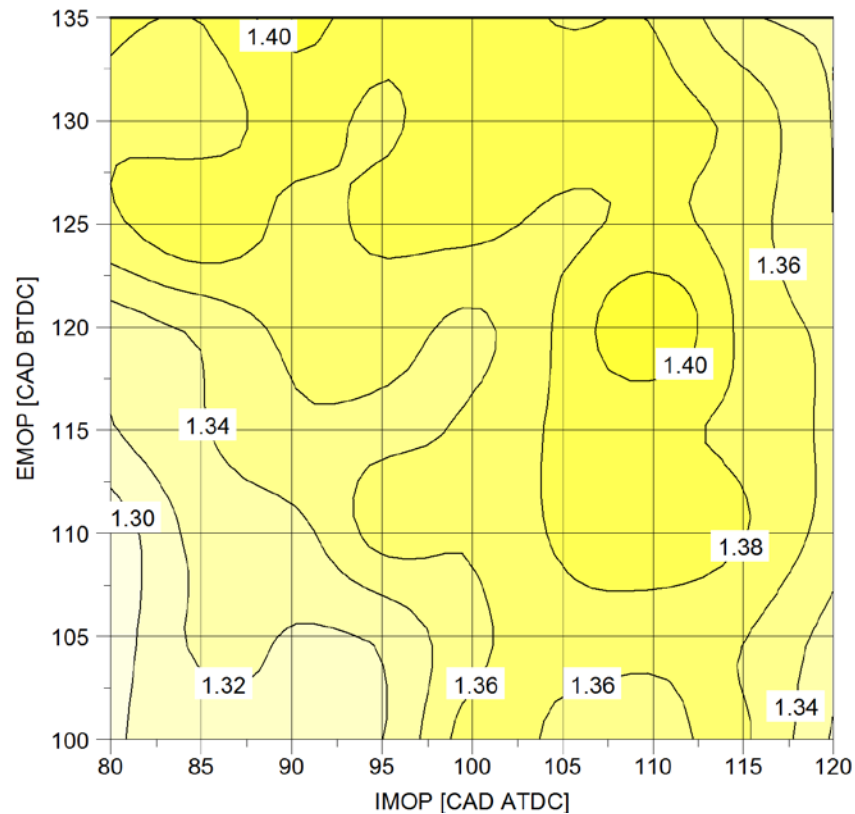


Figure 6.32 Polytypic Exponents

Lower EOC pressures will reduce the knocking propensity and the spark can be advanced several CAD as a result of this. Figure 6.33 shows that the 50% MFB angle for the points under ridge 1 is much more advanced than for the points under ridge 2. The lower EOC pressure is the most probable explanation for this but the spark timing will also be influenced by the EMOP timing. Late EMOP timings will reduce the degree of valve overlap but they will also reduce the effective expansion ratio, this will have the effect of reducing the size of the gross work contribution. This reduction of expansion ratio will need to be compensated for by an increase in boost pressure thus effectively shifting the engine to a higher load point (Figure 6.34). This will consequently require the spark timing to be retarded.

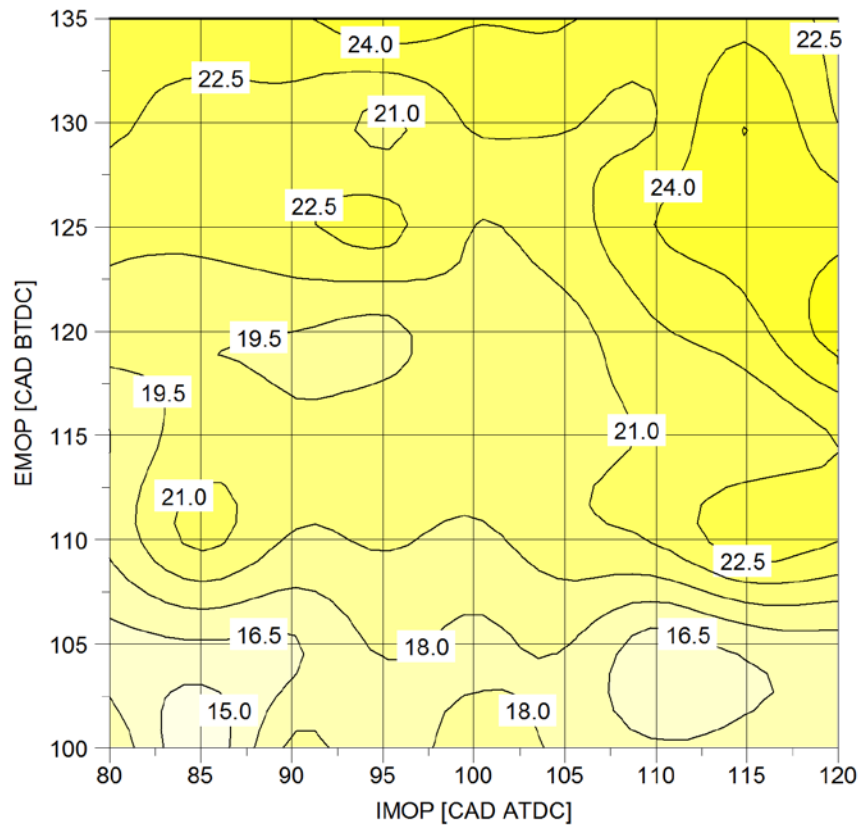


Figure 6.33 50% MFB Angle (CAD ATDCF)

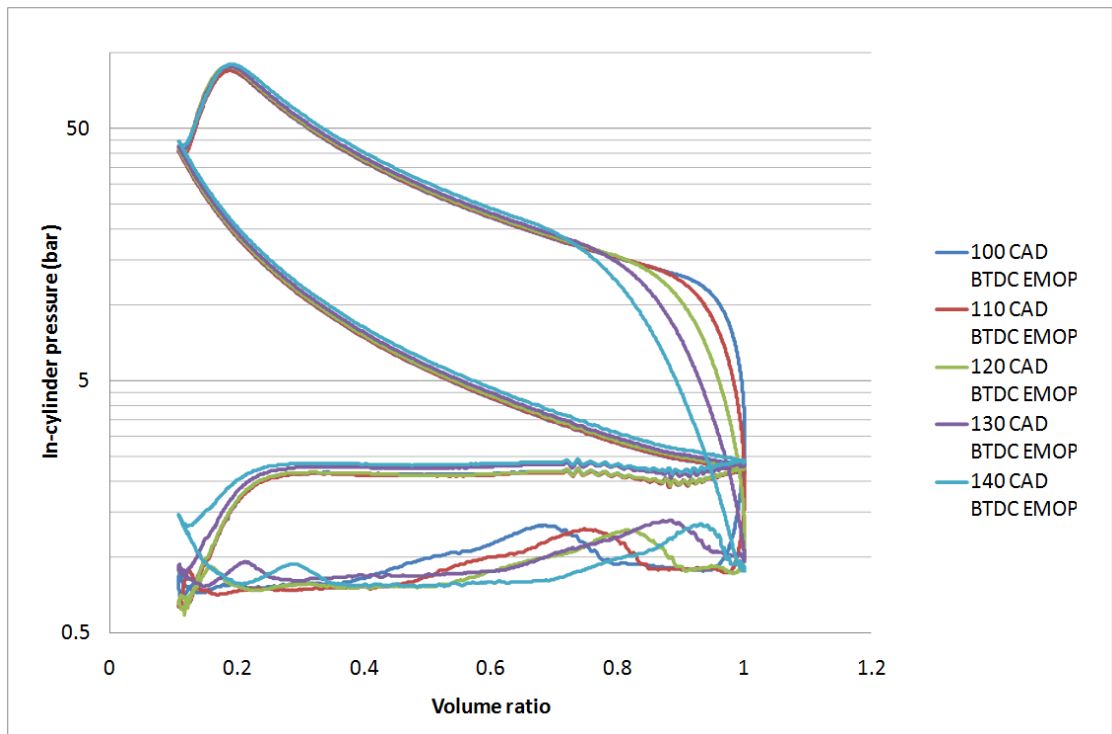


Figure 6.34 EMOP Sweep at Constant Load and IMOP Demonstrating the Impact of EMOP Timing on GIMEP

Strangely the standard autoignition events under ridge 1 and ridge 2 echo this trend (Figures 6.35 and 6.36) when perhaps the opposite trend would be expected and might suggest that the autoignitions under ridge 1 and ridge 2 could be caused by different mechanisms. Five of the autoignition events that occurred under ridge 1 were very clearly caused by LSPI when spark timings are compared to in-cylinder pressure, however, for the rest of the autoigniting cycles it was not possible to determine with certainty the cause of autoignition.

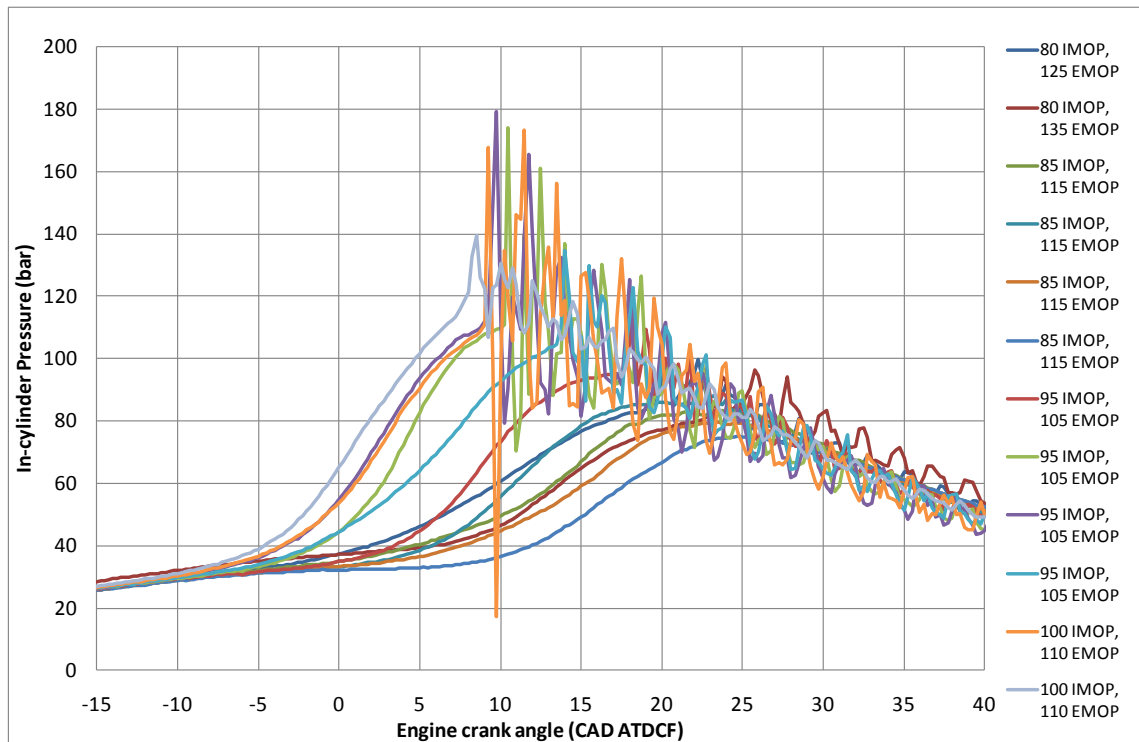


Figure 6.35 Autoignitions Under Ridge 1 (Units of IMOP and EMOP are CAD ATDC and CAD BTDC Respectively)

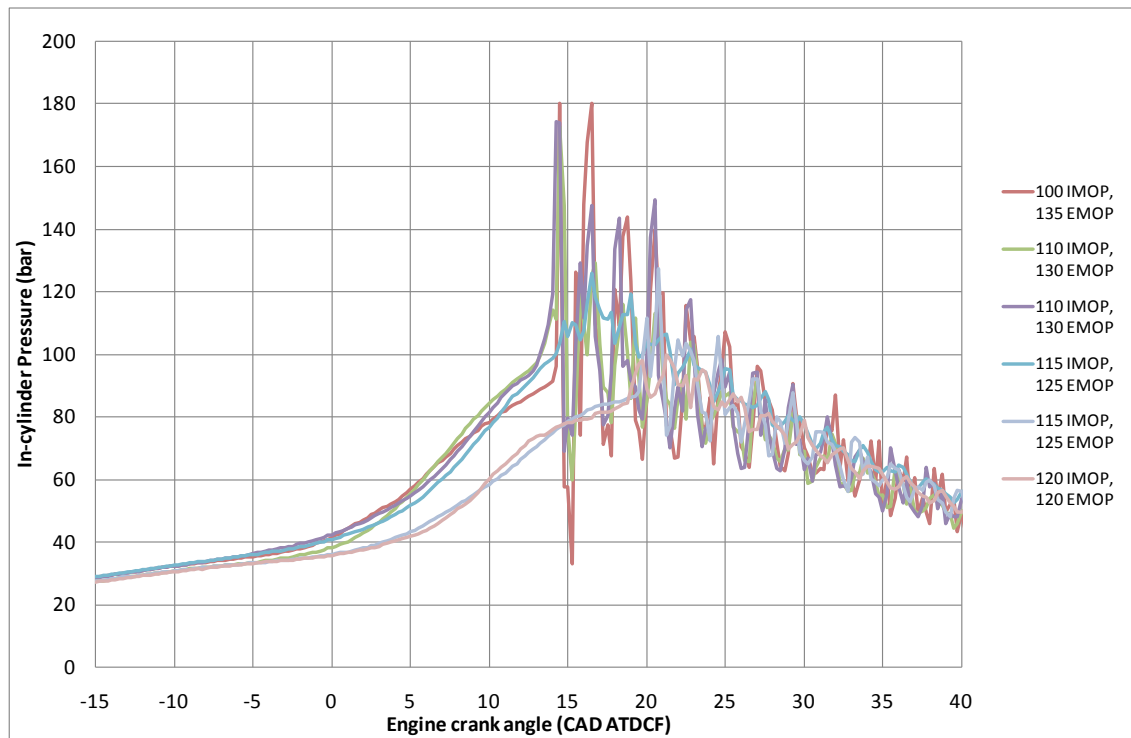


Figure 6.36 Autoignitions Under Ridge 2 (Units of IMOP and EMOP are CAD ATDC and CAD BTDC Respectively)

Zahdeh, et al [122] discovered that Fuel-Oil interactive effects were a cause of LSPI, however, fuel enrichment had also been found to eliminate LSPI in the same study. The exact degree of in-cylinder fuel enrichment was unknown in the study by Zahdeh, et al, as it is unknown here, which may explain why it is still autoigniting under ridge 1 but the autoignitions have stopped at the very corner point (IMOP 80 CAD ATDC, EMOP 100 CAD BTDC). Figure 6.32 would imply that the charge is significantly richer at the bottom left hand corner than under ridge 1, in spite of their close proximity. The difference in fuel enrichment from the bottom left hand corner and ridge 1 is also very apparent from a plot of exhaust gas temperatures (Figure 6.37). Unfortunately no physical effective AFR data is available from this test work due to the use of a 1-way air flow meter which gives unreliable readings (see section 3.2.5.2 for details). The effective AFR has been analysed in the GT-Power work as shown in section 6.4.4.

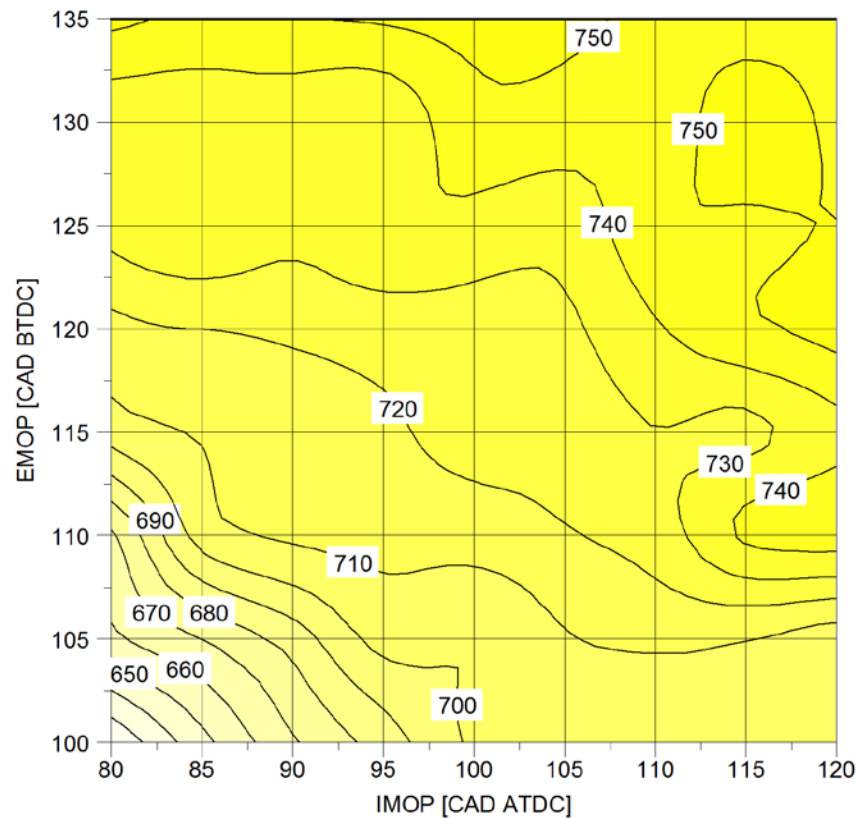


Figure 6.37 Exhaust Port Temperatures ($^{\circ}\text{C}$)

6.4.4 GT-Power Analysis

6.4.4.1 Introduction

In order to better gauge what is happening in the engine a GT-Power analysis was carried out using a modified version of single cylinder model 2 (see section 4.4) which was modified to give closed loop control of NIMEP.

The test plan adopted for the GT-Power work was the same as for the experimental test work. The IMOP and EMOP were changed in 5 CAD increments between their respective limits (80–120 CAD ATDC IMOP and 100–135 CAD BTDC EMOP). A full factorial DoE was used after disappointing results were obtained with a Latin hypercube type DoE. Once the test had been carried out the response fitting algorithm employed was a complex RBF emulator. This was found to give a response most like that obtained in the physical test work, superior to all the polynomial models

(the polynomial models were found to give “lips” at the extremities of the maps, whereas RBF had a lesser propensity to do this).

To compensate for the lack of closed loop combustion phasing control the 50% MFB points obtained from the physical test work were used. These were mapped against IMOP and EMOP angles. To further increase the accuracy of the results the 10-90% MFB duration was also mapped with respect to IMOP and EMOP. At first the average 10-90% MFB duration was used for all test points, however, it was later found that the 10-90% MFB duration had a large impact on the quality of results, so it was later mapped.

6.4.4.2 Results

The general pattern of the GT-Power data is fairly similar to the experimental test results, however, it predicts the minimum ISFC region very accurately and clearly has similar trends to the experimental data, as can be seen in Figure 6.38. As this ISFC map corresponds so closely to the test rig data it has been assumed that the data from the model will give a strong indication of the performance and trends of the experimental engine, but absolute values will not be trusted.

The data obtained from this test work is therefore of use as the main purpose of it is to ascertain what is happening in the cylinder in terms of residual gasses and scavenging. It is also hoped that this model will be able to give some indication as to what is causing the autoignition events.

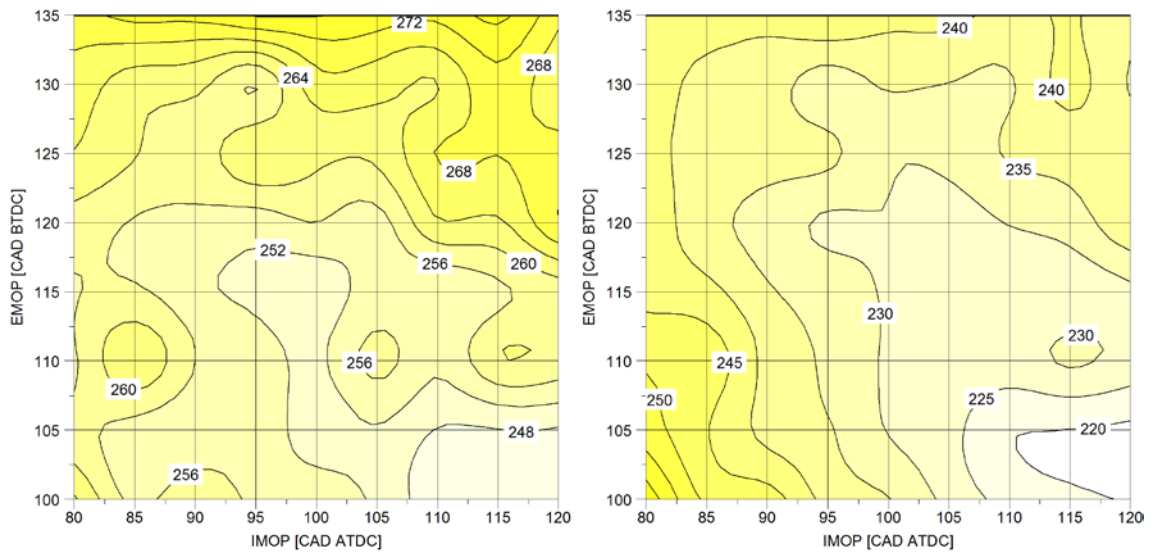


Figure 6.38 Experimental (left) and Simulated (right) ISFC Comparison

Figure 6.39 is a plot of equivalent cylinder AFR which also factors in the air used to scavenge the cylinder, and it confirms to an extent what was seen in the physical test work. It clearly shows that the effective AFR under ridge 1 is a lot richer than under ridge 2, although ridge 2 is still slightly rich of stoichiometric. Figure 6.40 is a plot of residual gas concentration at cycle start. It confirms that the residual gas concentration at cycle start is less for cycles that fall under ridge 1 as opposed to those that fall under ridge 2.

Although this simulation is not reliable in terms of absolute values, it provides a strong indication that the effective AFR is rich under ridge 1, and that there is a strong correlation between ridge 1 and ridge 2 in terms of AFR. However, it provides no obvious reason why the maximum valve overlap point should not also fall under ridge 1. The only reasonable explanation is that the charge cooling effect of the extra fuel will reduce the EOC pressure and temperature considerably, which in turn will reduce the tendency for autoignition to occur. The minimum difference in the 50% MFB point between the maximum valve overlap point and ridge 1 (as can be seen in Figure 6.33) is 1 CAD. The corresponding EOC pressure and temperature benefit afforded by this enrichment/scavenging is shown in Figures 6.41 and 6.42 respectively.

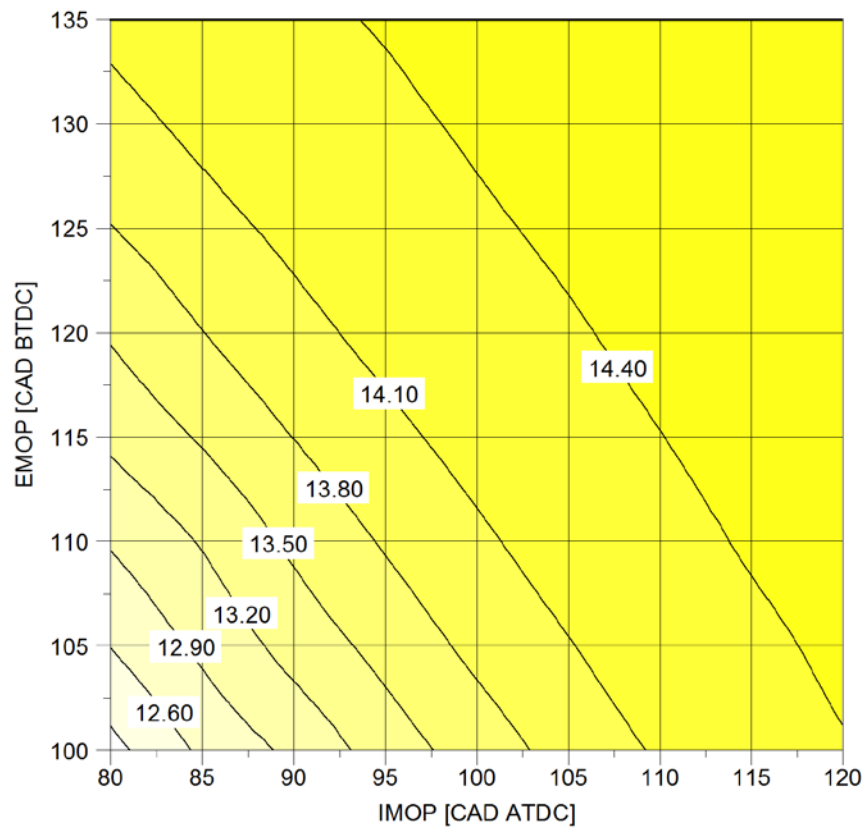


Figure 6.39 Equivalent AFR at Cycle Start

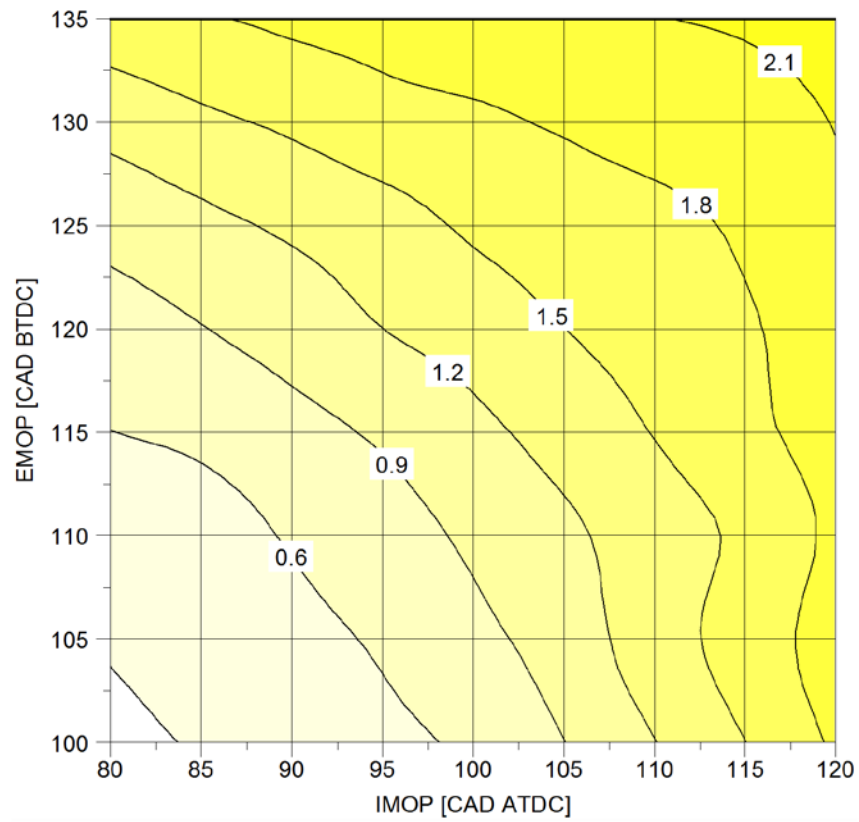


Figure 6.40 Residual Gas Concentration at Cycle Start

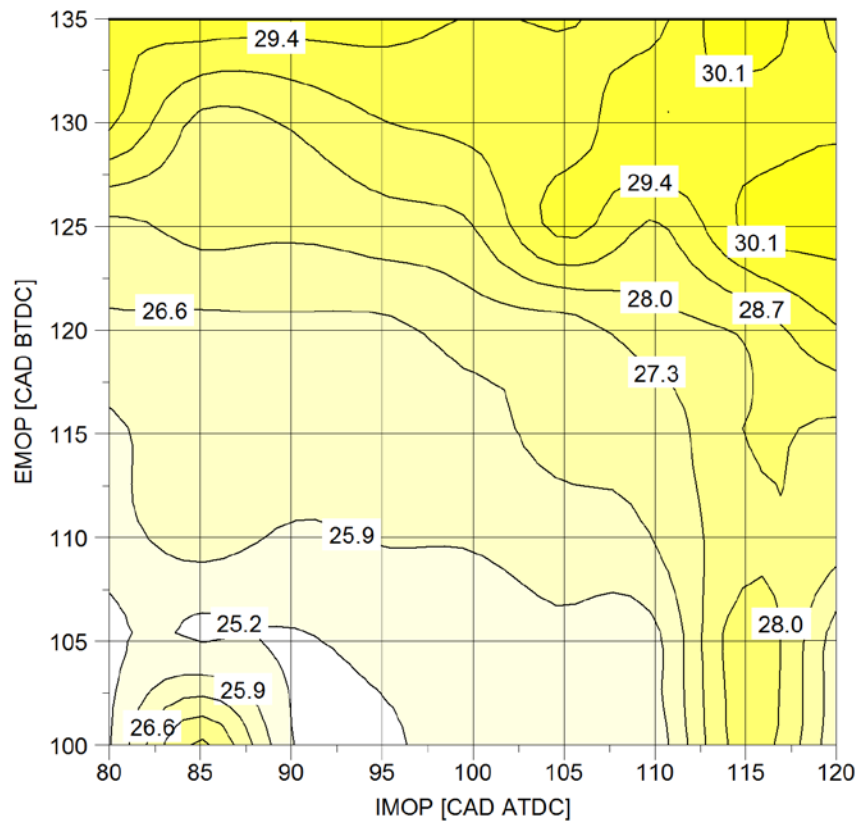


Figure 6.41 EOC Pressure (bar)

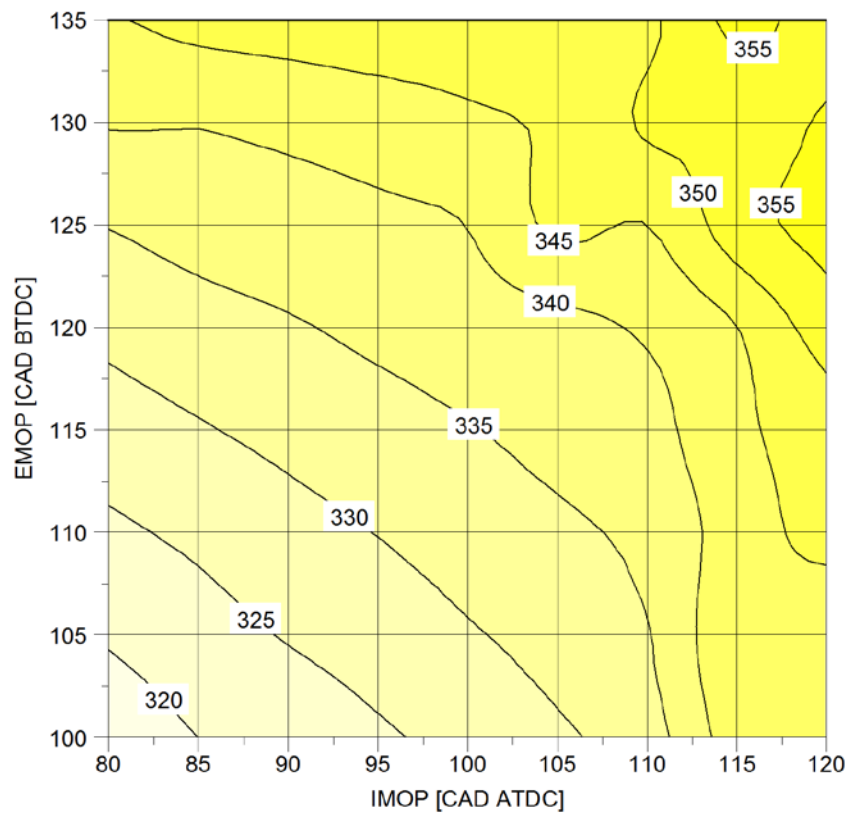


Figure 6.42 EOC Temperature (°C)

An attempt was made to predict pre-ignition with the single cylinder knock model. The reason why this was attempted is because the predicted KI is quite high in the vicinity of ridge 1. There is also a point under ridge 2 where the intensity can be seen to be very high. In order to test the models ability to predict pre-ignition all spark values in the map were retarded 5 CAD, the plot of knock intensity was then analysed to see if any of the points (particularly under ridge 2) had become incredibly high. Previous experience with the single cylinder engine model has revealed that if the EOC pressures and temperatures are too high the engine will “knock” before any of the cylinder charge has actually been burned, this leads to an incredibly high knock intensity (as knock intensity is calculated on the percentage of fuel unburned at the time of knock). Results from this experiment revealed that the knock models ability to predict pre-ignition is not effective at this running condition.

6.5 Effects of Fuel Age

6.5.1 Introduction

One of the biggest disadvantages for downsized engines and their worldwide success is the requirement for very high RON fuels. In Europe gasoline with a RON of 95 and 98 and even higher still are widely available, however, the downsized engine must also cater to the likes of large emerging markets such as China and India where the RON values are generally lower and high RON fuels, though available, are generally less commonplace.

With China now having the largest automotive market in the world it is of great importance that all future downsized engines can run on Chinese grade fuels so as not to compromise the downsized engine’s global success.

In an effort to try and assess the sensitivity of downsized engines to different fuel types, the single cylinder engine was run with 2 samples of pump ULG RON 95. One of these samples was a year old, the other was fresh.

Over time the lighter components can be found to evaporate which generally has the effect of decreasing RON. Unfortunately the facility to analyse both the aged and fresh fuel chemically was unavailable at the time this test work was carried out.

6.5.2 Test Plan

This test work consisted of running the engine at steady load for 15 minutes with the 2 different fuels, one being aged (12 months) ULG RON 95 and the other being fresh (<1 month old) ULG RON 95, and observing the autoignition frequency. The test criteria was as shown in Table 6.8.

Table 6.8 Test Variables and Control Criteria

Variable	Control criteria
Air	<3% humidity, temperature maintained at +/- 3 degC of 45 degC intake port temp
Coolant	Temperature maintained at +/- 3 degC of 80 degC
Oil	Temperature maintained at +/- 3 degC of 90 degC
Fuel	Aged and fresh ULG RON 95, no temperature control
Speed	2000rpm
Loads	24 bar NIMEP
Intake cam	Standard 240 CAD profile
Exhaust cam	Standard 278 CAD profile
IMOP	100 CAD ATDC
EMOP	120 CAD BTDC
Spark timing	BLD
Exhaust	Pressure not regulated, temperature control not required
Data acquisition	500 cycles logged
Test duration	15 minutes

6.5.3 Results

The fresh fuel resulted in a considerable decline in autoignition frequency. Over the course of 15 minutes 6 autoignition cycles were observed with the aged fuel and 3 were observed with the fresh fuel. A comparison of the autoignition cycles obtained with the aged and fresh fuels is shown in Figures 6.43 and 6.44 respectively. Six cycles were obtained with the fresh fuel because the test was run twice.

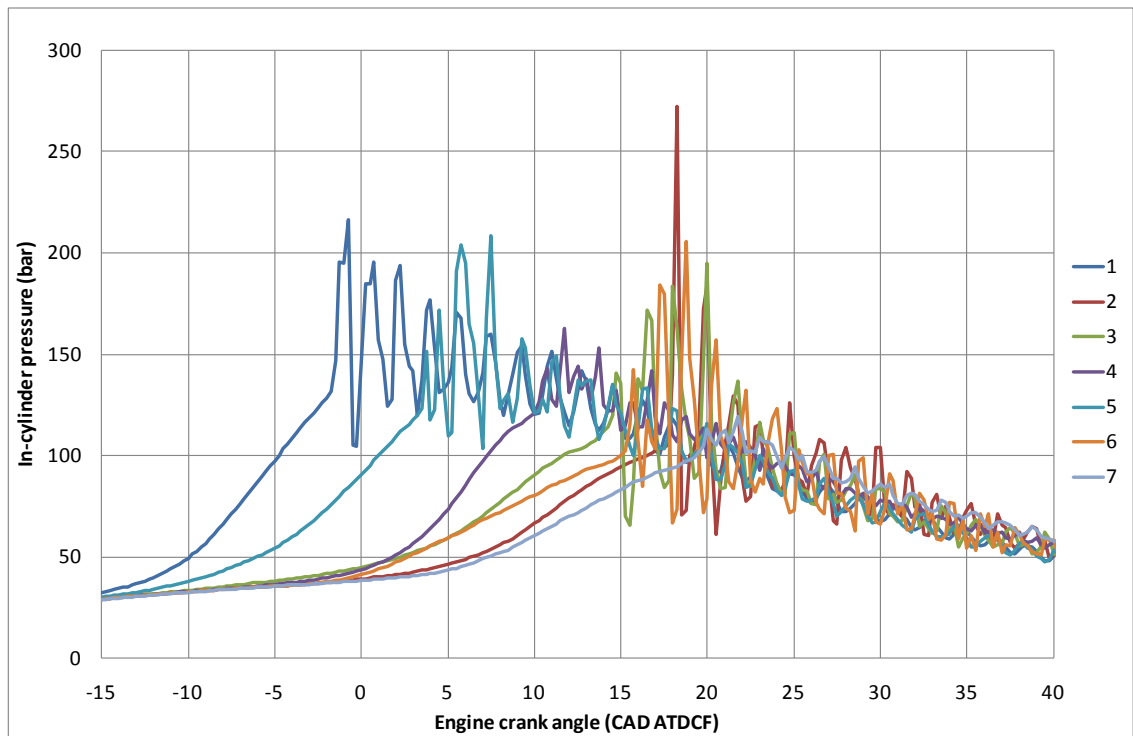


Figure 6.43 Autoignitions with Aged ULG95

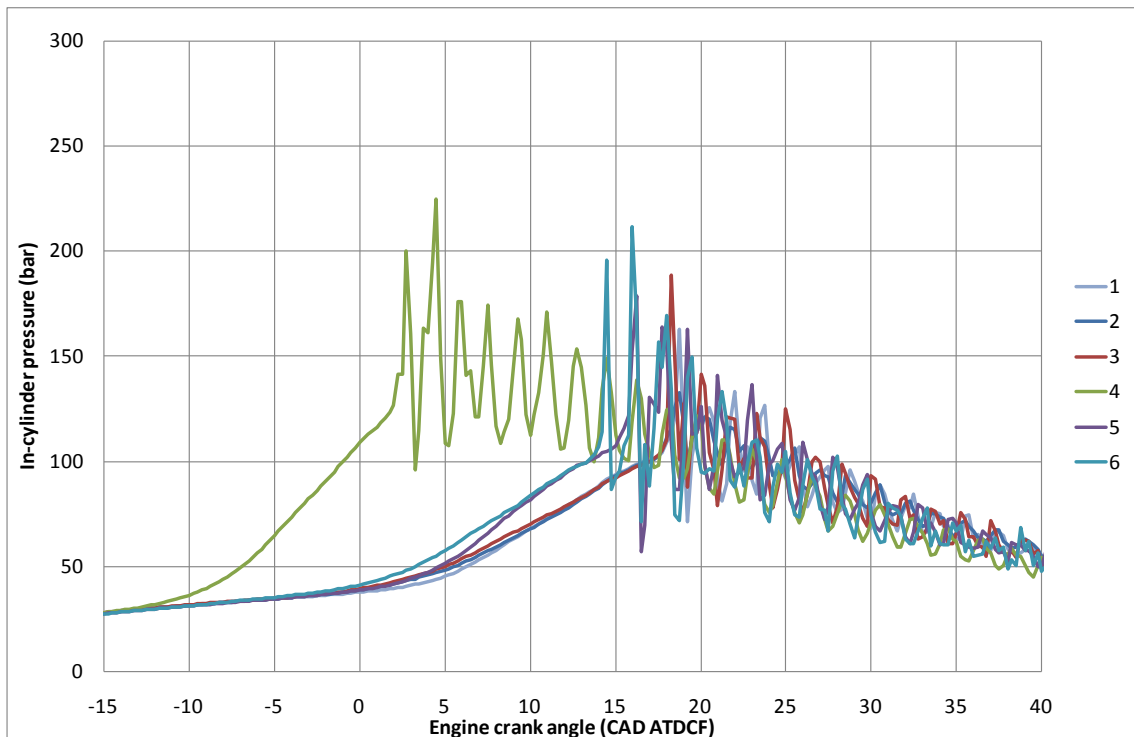


Figure 6.44 Autoignitions with Fresh ULG95

The maximum pressure and intensity can be seen to be fairly similar for both fuels (with the exception of 1 autoignition cycle with the aged fuel). However, the peak cylinder pressure is reached earlier with the aged fuel from the autoignition events

observed. This suggests that the aged fuel had a greater propensity for LSPI in comparison to the fresh fuel. The very high peak cylinder pressures appear to be caused by a different mechanism with the fresh fuel which was very severe knock, although from the data obtained it is not possible to say with certainty whether LSPI or knock was the cause of the autoignition events. One potential reason for the later peak cylinder pressures with the fresh fuel is that over time fuel can react with oxygen to create long chain olefins and diolefins. Sasaki, et al [123] documents that owing to their size, long chain olefins and diolefins are more likely to autoignite as they have an overall larger and correspondingly weaker structure.

Other than the considerable reduction in autoignition frequency there were no considerable differences between the different fuels. The 50% MFB point could be advanced 0.4 CAD with the fresh fuel but there was no difference with the 10-90% MFB duration. The aged fuel exhibited a 0.81% improvement in ISFC, in spite of the fact the BLD point was retarded in comparison to the fresh fuel. The exhaust temperature was also 14⁰C lower for the aged fuel, which is where the improvement in ISFC might have come from.

The COV of IMEP was slightly higher for the aged fuel but not significantly. Unfortunately no emissions data was obtained from this test work.

Chapter 7

Experimental Studies of Miller Cycle on Engine Performance and Fuel Consumption

7.1 Introduction

The purpose of this chapter is to explore the benefits that can be yielded through the adoption of the Miller cycle on the single cylinder experimental engine.

This chapter has been arranged into 2 major sections. The first section is a study of the benefits that can be yielded through the de-throttling effect of the Miller cycle at low loads. The second section of this chapter is an exploration of the autoignition mitigating effects of Deep Miller at low speed and high load.

The components that bring about a benefit over the standard Otto configuration of the engine have also been explored, as well as other phenomena that have been found to influence engine performance. These phenomena include engine breathing, cam timings and combustion phasing observations. The feasibility of supercharging/turbocharging with Deep Miller has also been investigated.

7.2 Achieving EIVC and LIVC

In order to carry out this work the experimental engine (described in section 3.2.1) had to be fitted with different geometry intake cams. In total 3 different duration intake cams were tested. The cam durations were defined as the number of CAD between the End Of Ramps (EORs). The first was a short low-lift cam with an EOR to EOR duration of 152 CAD and a maximum lift of 5mm. The second was the standard Mahle intake cam with an EOR to EOR duration of 240 CAD and a maximum lift of 11mm. The third was a standard-lift long cam with an EOR to EOR duration of 292 CAD and a maximum lift of 11mm. Figure 7.1 shows an overlay of these 3 cams in their maximum overlap positions.

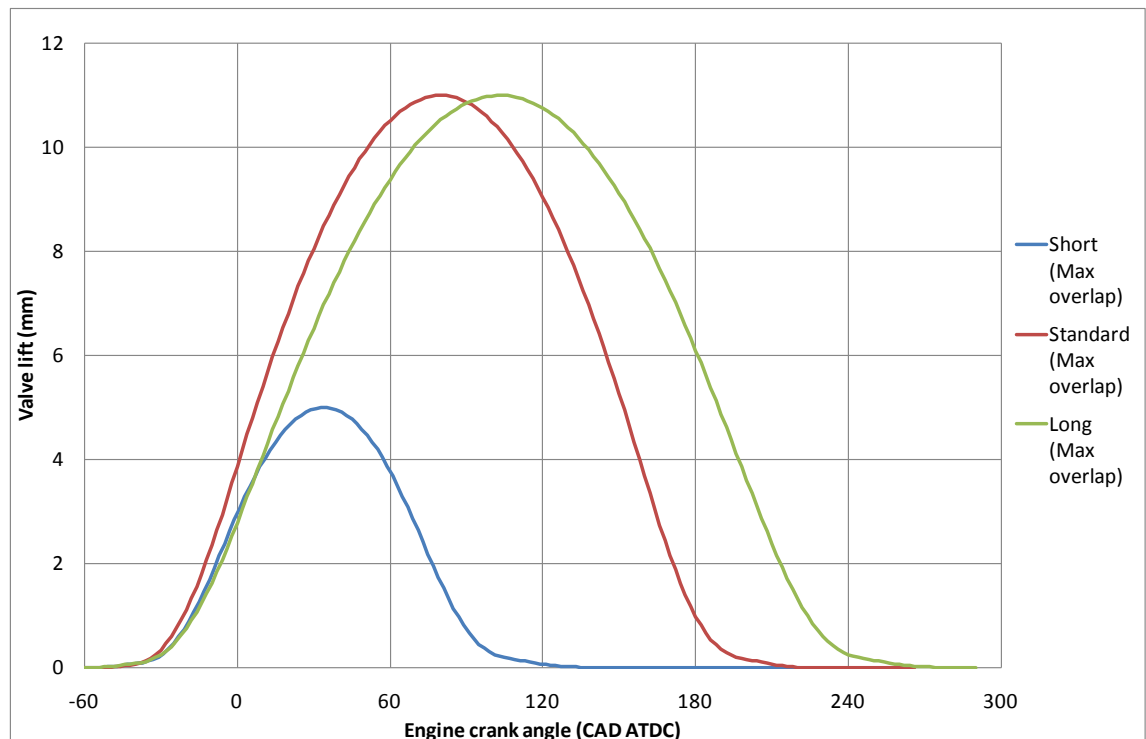


Figure 7.1 Cam Profile Comparison (as Shown in Their Maximum Valve Overlap Positions)

These were all tested with the standard Mahle exhaust cam with an EOR to EOR duration of 278 CAD and a maximum lift of 11mm. The geometry of all of the cams is given in Appendix A.1.

The cams can also be phased by up to 40 CAD to reduce the valve overlap. Figure 7.2 shows the minimum and maximum limits of the cam phasing.

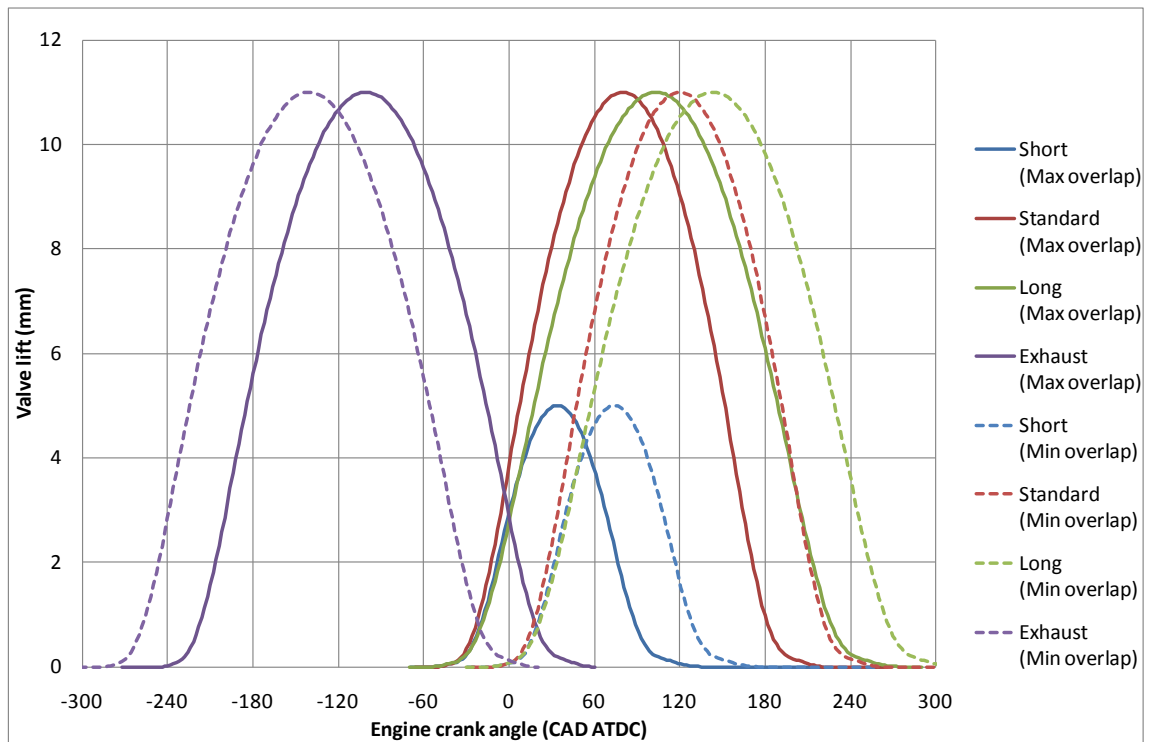


Figure 7.2 Cam Phasing Ranges

Using the cam phasers the effective CR can be reduced to as low as 5.57 and 6.16 (as calculated from the 1mm lift point) with the 152 CAD duration cam and 292 CAD duration cam respectively. All cams were swept across their respective ranges in 10 CAD increments for all test work.

7.3 Description of Test Points

The Miller cycle performance benefits were assessed in the following 2 regions (Figure 7.3)

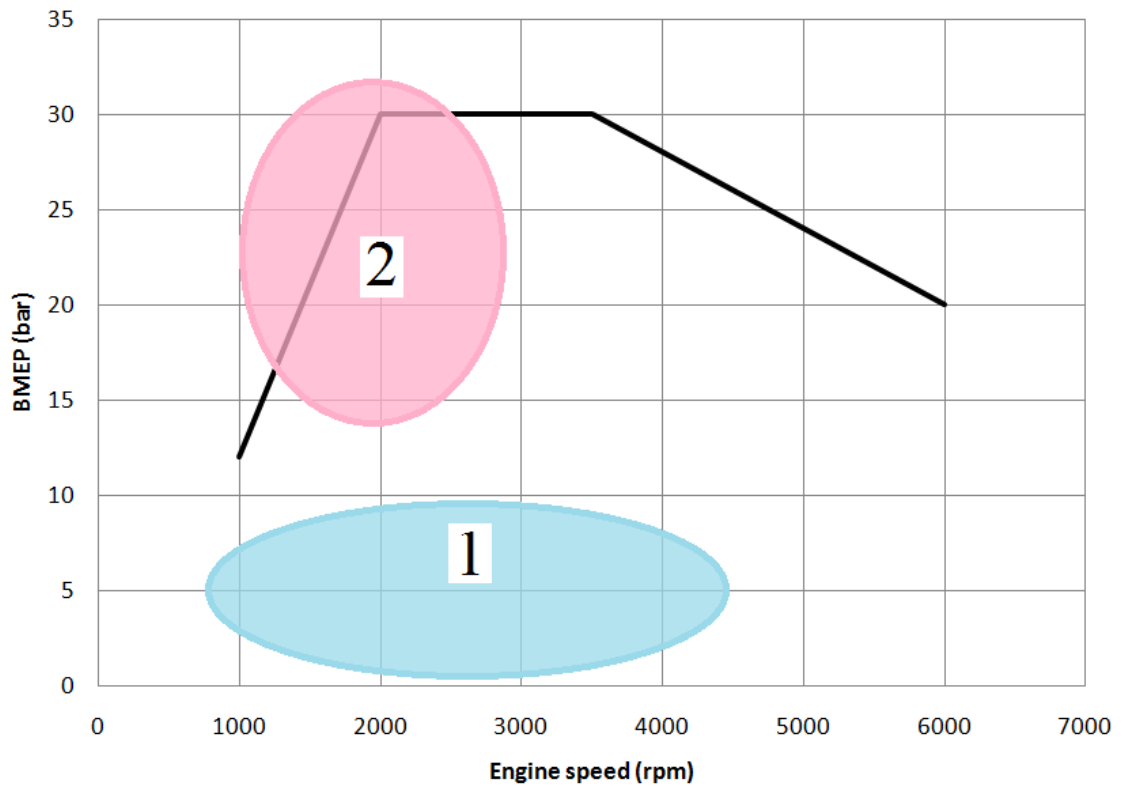


Figure 7.3 Regions of Miller Cycle Studied

These regions can be broken down as follows:

Region 1: De-throttling effect at part-load conditions

De-throttling is the technique of using the intake valves to throttle the air flow to the engine instead of a conventional throttle. The advantage of this is the pumping losses can be reduced by elevating the manifold pressure and then implementing either EIVC (stopping the air from going into the cylinder during the induction stroke) or (LIVC exhaling charge from the cylinder during the compression stroke) to regulate the mass of air in the cylinder.

The test points in Table 7.1 were selected to study the de-throttling effect on part-load fuel economy. The minimum load is constrained by engine misfire below certain loads.

Table 7.1 Test Points for De-throttling Studies (BMEPs are the 3 Cylinder Equivalent Values)

Speed (rpm)	BMEP (bar)	NIMEP (bar)	EBP valve position (% closed)
1000	4	4.56	0
1000	8	8.83	0
2000	4	4.64	0
2000	8	8.90	0
3000	4	4.80	0
3000	8	8.98	0
4000	4	4.98	0

Region 2: Effective CR reduction for autoignition mitigation at full-load and low speed operations

In this region EIVC and LIVC will be employed to reduce the effective CR, this will allow the combustion to be phased closer to MBT without autoignition occurring. In this region even at maximum load no fuel enrichment will be required, but owing to the low speed of the engine there will be a greater propensity for autoignition to take place. It is in this region that the effectiveness of EIVC is questioned as it has been found to reduce in-cylinder charge motion considerably at lower loads. Table 7.2 gives the test points for region 2.

Table 7.2 Test Points for Region 2 (BMEPs are the 3 Cylinder Equivalent Values)

Speed (rpm)	BMEP (bar)	NIMEP (bar)	EBP valve position (% closed)
2000	15	16.04	0
2000	15	16.04	45
2000	24	25.58	0
2000	24	25.58	* 2 bar EBP

* - EBP in bar, not valve position

Due to rig constraints this test plan had to be truncated considerably from the original intended test plan that included some high speed and high load sites. The engine was found to be incapable of running at higher speeds and loads due to the insufficient coolant flow rate of the coolant pump.

A list of the test variables and control criteria are given in Table 7.3.

Table 7.3 Test Variables and Control Criteria

Variable	Control criteria
Air	<3% humidity, temperature maintained at +/- 3 degC of 40 degC intake port temp
Coolant	Temperature maintained at +/- 3 degC of 80 degC
Oil	Temperature maintained at +/- 3 degC of 90 degC
Fuel	Fresh ULG RON 95, supply temperature regulated to +/- 5 degC of 25 degC
Speed	See Tables 7.1 and 7.2
Loads	See Tables 7.1 and 7.2
Intake cam	Short 152 CAD profile, standard 240 CAD profile and long 292 CAD profile
Exhaust cam	Standard 278 CAD profile
IMOP	See Table 7.4 (swept in 10 CAD increments)
EMOP	100 - 140 CAD BTDC (swept in 10 CAD increments)
Spark timing	BLD or MBT depending on load
Exhaust	For EBPs see Tables 7.1 and 7.2. Temperature control not required
Data acquisition	300 cycles logged

The IMOP timing is dependent on the cam being tested. Table 7.4 gives the ranges of IMOPs for the 3 different cams and their respective IVO and IVC points. Also shown are the exhaust EMOP ranges and corresponding EVO and EVC points.

Table 7.4 MOPs and Corresponding Valve Opening/Closing Points for Each of the Cams

Cam	Maximum overlap phasing			Minimum overlap phasing		
	MOP	IVO/EVO (1mm lift)	IVC/EVC (1mm lift)	MOP	IVO/EVO (1mm lift)	IVC/EVC (1mm lift)
152 CAD Intake	35 CAD ATDC	-18 CAD ATDC	87 CAD ATDC	75 CAD ATDC	22 CAD ATDC	127 CAD ATDC
240 CAD Intake	80 CAD ATDC	-21 CAD ATDC	180 CAD ATDC	120 CAD ATDC	19 CAD ATDC	220 CAD ATDC
292 CAD Intake	104 CAD ATDC	-17 CAD ATDC	224 CAD ATDC	144 CAD ATDC	23 CAD ATDC	264 CAD ATDC
278 CAD Exhaust	100 CAD BTDC	215 CAD BTDC	16 CAD ATDC	140 CAD BTDC	255 CAD BTDC	-24 CAD ATDC

7.4 Low Load Operations with EIVC and LIVC (Region 1)

7.4.1 Introduction

Low load points can typically be found to be less efficient than medium to high load points. This is due to the problem of pumping losses at low load being of a similar magnitude to the gross power output. Downsizing an engine has the effect of reducing these pumping losses relative to the gross power by running at what is effectively a higher load point (load point shifting). There is still scope for improving this further still by throttling with the valve instead of a throttle. The scope of this benefit has not been investigated before with an aggressively downsized engine with a very high degree of load point shifting.

The objective of this portion of the work is to assess the extent of the benefit of throttling with the valve at low load, and what impact this has on the size of the pumping loop.

The single cylinder engine is relatively limited in how low a load it can run at satisfactorily, and the minimum load it can sustain for all IMOP and EMOP combinations was 4 bar BMEP. The test work involved carrying out IMOP and EMOP sweeps at speeds of 1000, 2000 and 3000rpm at loads of 4 and 8 bar BMEP, and 4000rpm and 4 bar BMEP, as shown in Table 7.1.

7.4.2 Results

Comparisons of the optimum cam timing combinations at each speed and load site for each cam are shown in Figure 7.4. As stated previously, BMEPs are the 3 cylinder equivalent values.

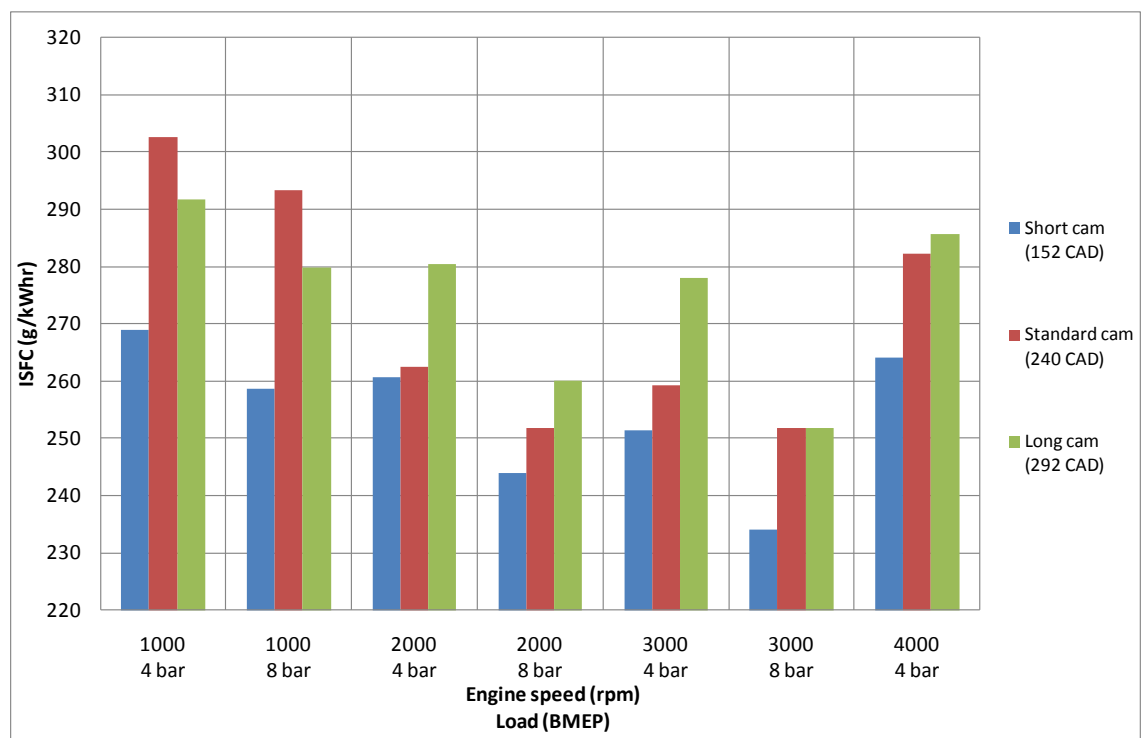


Figure 7.4 ISFC Comparison of Short, Standard and Long Cams at Low Loads

The short cam (152 CAD duration) exhibits the lowest ISFC values for every speed and load combination, and the long cam (292 CAD duration) showed the highest values typically. There is a slight break from this trend at 1000rpm where the standard cam (240 CAD duration) exhibits the highest ISFCs.

One possible explanation for this is the fact that the effective CR and the volumetric efficiency are highest for the standard cam. This therefore results in the standard cam requiring the lowest MAP of the 3 different cams, and in a GT-Power simulation carried out reveals that this results in the largest back flow of exhaust gas to the intake of the 3 cams during the valve overlap period. As a consequence of this the residual gas concentration at cycle start for the standard cam can be seen to be the largest of the 3 cams.

This is not detrimental in itself but very high residual gas concentration can have the effect of reducing the flame front speed (at this speed and load) which will make cycles less repeatable. As a consequence of this lambda control is also made more difficult, particularly for the single cylinder engine where the lambda sensor is located 800mm downstream of the exhaust port.

The residual gas concentration at cycle start according to the GT-Power model is more elevated for the standard cam than for the other 2 cams. However, the short and long cams still exhibit elevated levels of residuals in the cylinder and still suffer from very high COVs, this is therefore not (on its own) a suitable explanation for the discrepancy seen with the standard cam at these 1000rpm points.

It should be noted that of the standard cam tests the 1000rpm points were the last to be done before a blown head gasket was observed. The head gasket failure allowed combustion gasses to leak past the gasket and pressurise the coolant circuit. This manifested itself on the instrumentation as a low coolant flow rate. The coolant flow rate for these points was approximately 4% lower than for other test points, however, gas leakage would manifest itself on a P-V diagram by way of a reduced polytropic exponent during the expansion stroke. No appreciable difference can be seen between the short, long and standard cams in polytropic exponent during the expansion stroke (Figure 7.5), and the head gasket issue was rectified for the short and

long cams. This is also not a satisfactory explanation on its own for the break in ISFC trend at 1000rpm.

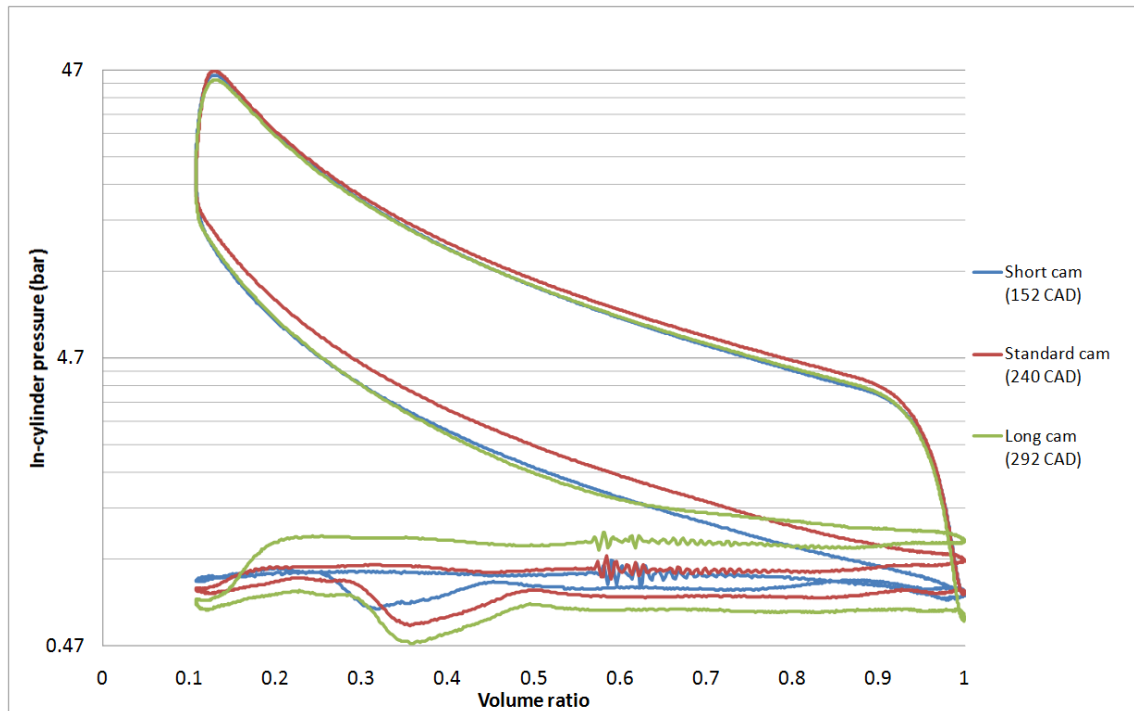


Figure 7.5 1000rpm, 8 bar BMEP Short, Standard and Long Cam Overlay

There are several reasons why the short cam exhibits lower ISFCs at every single point. The short cam gave the minimum pumping loop size of the 3 cams for every single point, as can be seen in Figure 7.6 (short cam PMEP values are closest to zero).

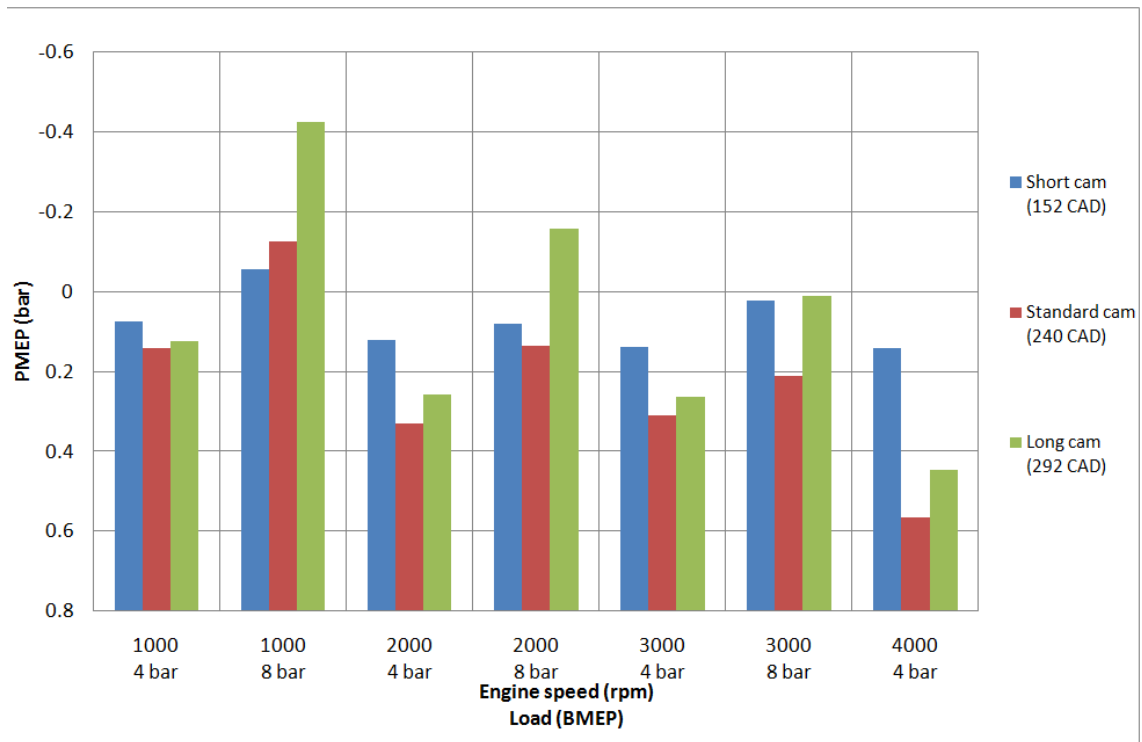


Figure 7.6 PMEP Comparison of Short, Standard and Long Cams at Low Loads

The minimisation of the pumping loop is achieved by the effective elimination of part of the pumping loop as can be seen in Figure 7.7. The in-cylinder pressure for the short cam can be seen to start reducing (through polytropic expansion) at a volume ratio of approximately 0.6. From this point on therefore the cylinder effectively becomes a closed system and the mass of air trapped in the cylinder is fixed. The rest of the intake stroke is therefore polytropic expansion and is “cancelled out” of the pumping loop by the polytropic compression that occurs during the compression stroke (although not quite due to charge heating).

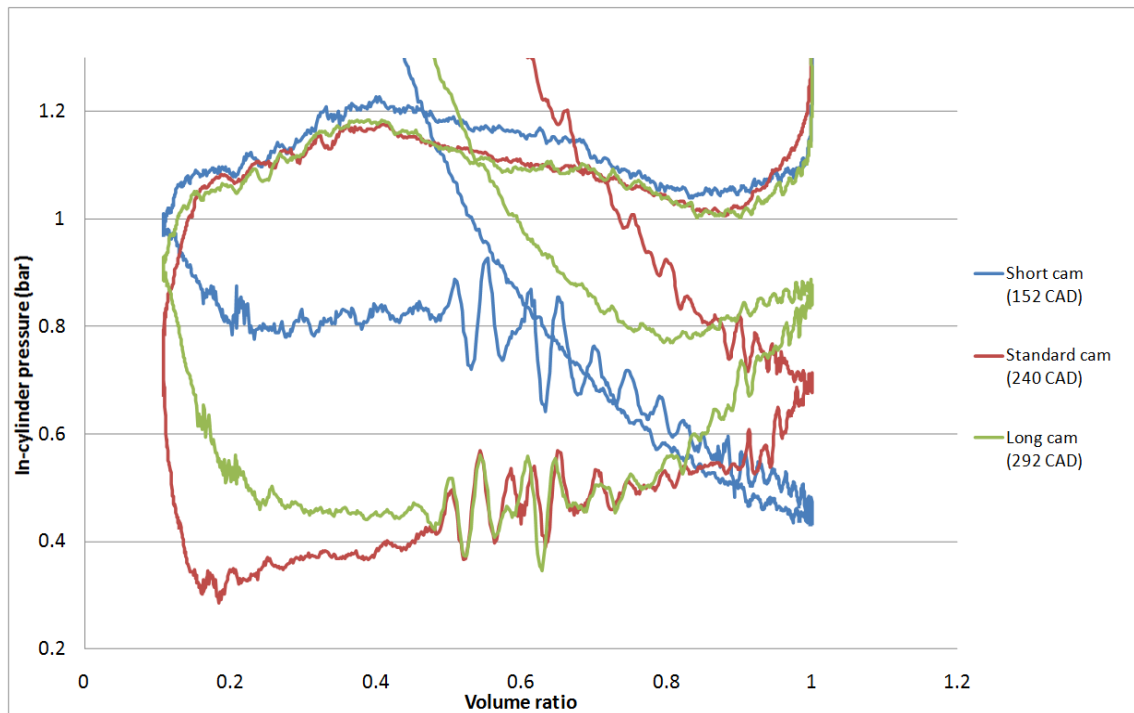


Figure 7.7 4000rpm, 4 bar BMEP Short, Standard and Long Cam Overlay

In Figure 7.6 the pumping loop size was determined from BDC to TDC to BDC rather than calculating the size of just the pumping loop itself, between the intersections of the lines (as can be seen in Figure 7.7).

Although both EIVC and LIVC reduce the pumping loop size, EIVC reduces it to a greater extent than LIVC, even for the same effective CR. It must be stressed that reducing the pumping loop size does not necessarily mean reducing pumping losses. Reducing effective CR requires a higher MAP to ensure the correct mass of air is trapped in the cylinder to make the required load, it is this principle that (at low loads) reduces the vertical size of the pumping loop. EIVC offers a further decrease in pumping loop size by reducing the horizontal size of the pumping loop and in the case of Figure 7.7 leaving the horizontal portion of the pumping loop between a volume ratio of 0.6 and 1 almost entirely unpopulated. It is for this reason that the short cam line in Figure 7.6 is significantly flatter than the other 2 cams. While LIVC reduces the horizontal size of the pumping loop somewhat, the portion between a volume ratio of 0.6 and 1 is still partially populated.

Restricting the geometric size of the pumping loop is not always optimum for higher load cases where the MAP is above the EBP. In these cases the pumping loop

contribution becomes negative and is beneficial to the cycle. It would therefore be logical to assume that the larger the pumping loop the better in these cases. Although a larger negative pumping loop is theoretically beneficial to the cycle (because the gross power contribution can be made smaller as a consequence of this), in the cases where the negative pumping loop is very large for the long cam in comparison to the short and standard cams (1000rpm, 8 bar BMEP and 2000rpm, 8 bar BMEP for example), this does not translate to a lower ISFC. Potential reasons for this are given in section 7.4.2.1.

Although the pumping loop is comparatively large at these speed and load points its impact on ISFC is quite conservative. The peaks and troughs in Figure 7.6 correspond quite well to the profiles of the lines in Figure 7.4, however the difference in ISFC brought about by the change in pumping loop size is much smaller than the theoretical gain obtained from the change in pumping loop size (see section 7.4.2.3). The most likely explanation for this is that at these low load points the efficiency gained through the decrease in power loop size (to maintain constant NIMEP) is offset by a low EOC temperature and pressure and a corresponding degradation of combustion efficiency.

The long cam demonstrating the highest ISFCs is an unexpected result. Some literature suggests that LIVC is not as effective at reducing ISFC as EIVC at low load, but cases of LIVC performing this much worse than the standard cam are unheard of. This is suspected to be a result of differences in charge motion exhibited by the different cams (see section 7.4.2.1) leading to incomplete combustion for the long cam. According to GT-Power studies no charge scavenging will take place at any of the speed and loads tested for this portion of the test work. Charge will however still be exhaled to the intake manifold during the compression process, this will likely contain some fuel. Figure 7.8 is a plot of intake port temperatures for each of the cams and speed and load points, and demonstrates the presence of residual gasses and charge in the intake manifold for the long cam by elevated temperatures.

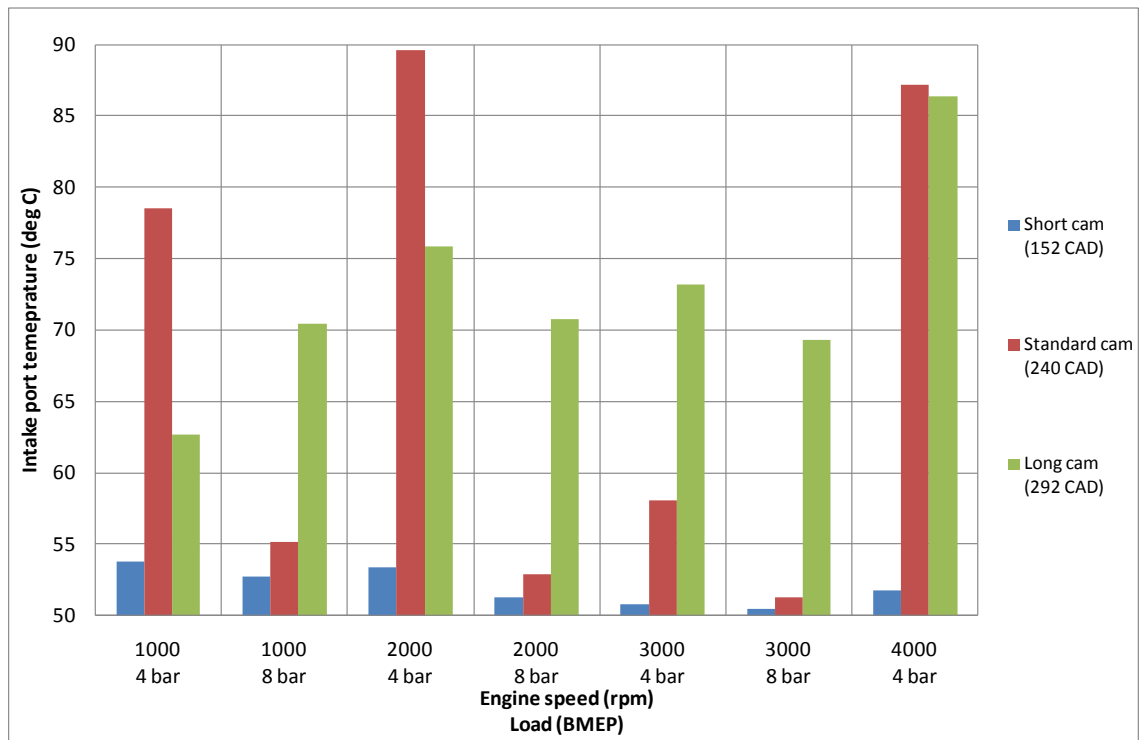


Figure 7.8 Intake Temperature Comparison of Short, Standard and Long Cams at Low Loads

7.4.2.1 Discrepancy at 1000rpm

The 1000rpm 4 bar BMEP test point (with all 3 cams) has been repeated in a GT-Power simulation to give a direct comparison to the single cylinder experimental engine. The GT-Power simulation was found to be very accurate at predicting engine breathing dynamics but very inaccurate at predicting the ISFC trends observed.

One potential reason for this was the difference in effective CRs. In order to better gauge what the theoretical thermal efficiency should be for each of the cams an approximation was made based on the data retrieved from the GT-Power model. Relative to the standard cam the long cam (with the second highest degree of effective CR reduction) is 1.90% more efficient, and the short cam is 6.06% more efficient. This trend is consistent for both of the 1000rpm cases with the experimental test data, however, the actual improvement in efficiency was far greater than the theory stipulates. The long cam returned an ISFC benefit of 3.73% relative to the standard cam, and the short cam returned an ISFC benefit of 12.55% relative to the standard

cam. The GT-Power model presented the greatest efficiency disparity by predicting a 0.08% decline in efficiency for the long cam relative to the standard cam, and a 3.14% decline in efficiency for the short cam relative to the standard cam.

Another notable inaccuracy is the required MAP for the long cam. GT-Power predicts an MAP of 0.9 bar whereas the physical engine required an MAP of 1.096 bar. This discrepancy is considerable, as well as the discrepancy between the ISFCs for the long cam (247 g/kWhr in GT-Power Vs. 292 g/kWhr for the experimental engine).

The suspected reason for all of these discrepancies is the in-cylinder charge motion during the compression stroke, and the difference in the quantity of residuals present. The impact of neither charge motion nor residuals can be simulated in GT-Power, changing the properties of the Wiebe combustion model is as close as it is possible to get.

The charge motion can be expected to differ for each of the different cams. The short cam for instance combines a very low lift with a very short duration whereas the long cam exhibits a high degree of lift for a longer duration. The impact of this on the mass flow rate through the intake valves is considerable (Figure 7.9).

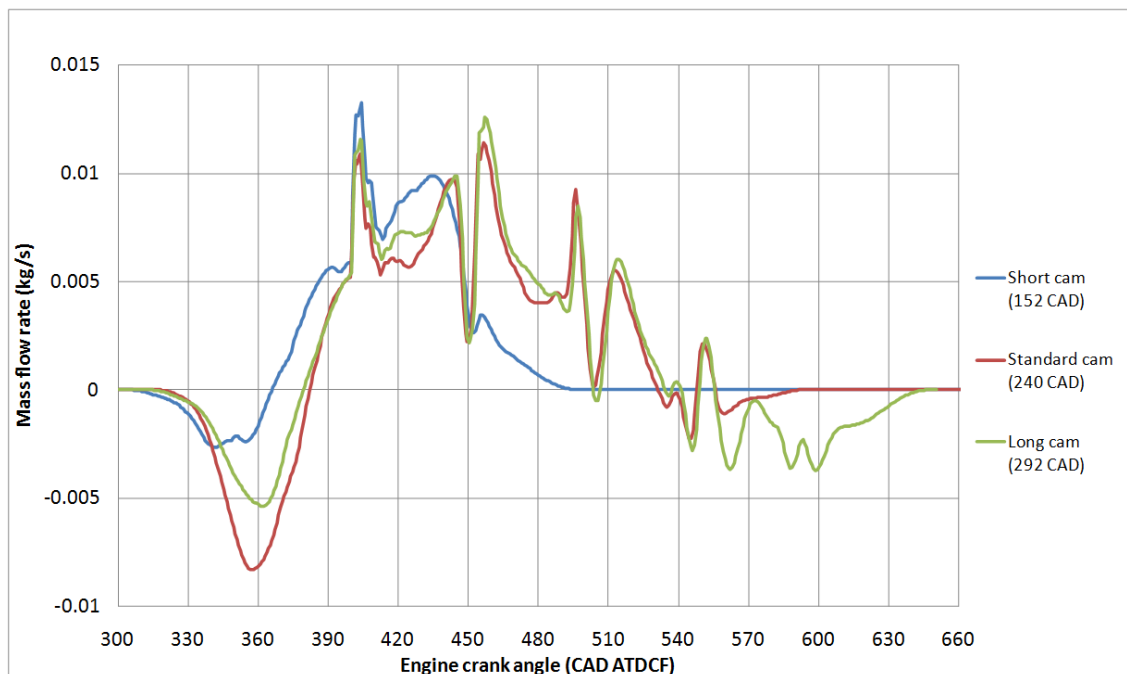


Figure 7.9 Comparison of the Intake Valve Mass Flow Rates for the 3 Different Duration Cams at 1000rpm and 4 bar BMEP

The short cam can be found to exhibit peak mass flow rates greater than both the standard and the long cams, even with a reduced valve lift. This will result in the flow velocity through the valves being far greater for the short cam than for the other 2 cams. High flow velocity can be found to result in very high levels of TKE but relatively low levels of bulk flow such as tumble (Matsumoto, et al [66]). The higher TKE will result in a more homogeneous charge but the lack of bulk flow will reduce overall charge motion and increase the burn duration. The standard and long cams however have high levels of lift which will promote bulk flow but drastically reduce the TKE. As a result of this the overall charge motion will be relatively high but the charge itself will be relatively in-homogeneous. Figure 7.10 supports this theory and shows the difference in the MFB duration for the 3 different cams.

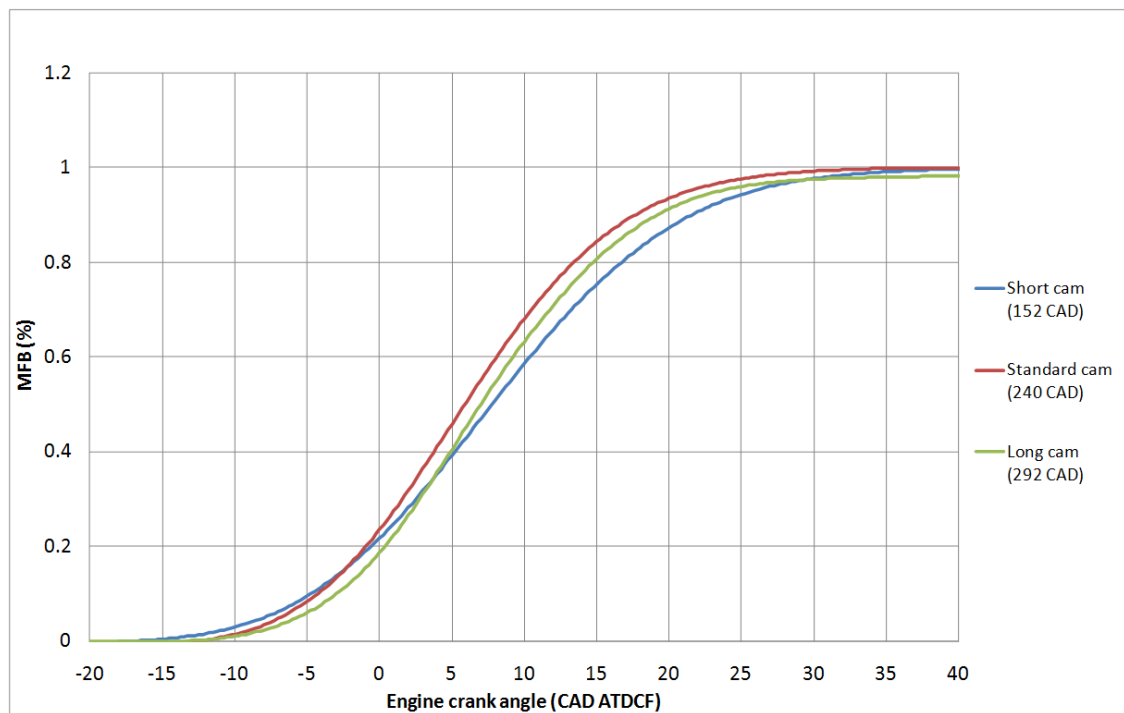


Figure 7.10 MFB Profiles for the 3 Different Cams at 1000rpm and 4 bar BMEP

Both the standard and long cams exhibit very similar profiles which would imply the in-cylinder flow is very similar for both cams. Both the standard and long cams have very similar 10-90% MFB durations too, with durations of 25.2 CAD, 20.9 CAD and 20.4 CAD for the short, standard and long cams respectively. The only point where the profiles can be seen to differ is at the very high MFB points (~0.95 MFB) very late into the expansion stroke where the total fuel mass burned for the long cam

fails to reach the full 100%. In reality 100% MFB cannot be achieved but the short and standard profile get much closer to full 100% MFB than the long cam. The most likely reason for this is that the majority of the charge expelled to the intake during the compression stroke with the long cam is air and that it contains relatively little fuel, this would lead to enrichment in the cylinder and an excess of fuel.

In order for this to occur the HC emissions must be elevated, which they are not markedly for the long cam, however, the high quantity of residuals present at cycle start will contain the majority of the unburned HCs from the previous cycle, which will be burned during the current cycle. This will cause the HC emissions to appear lower than they effectively are.

The COV of IMEP can also be observed to be higher for the standard and long cams (Figure 7.11). Higher COV values can be indicative of increased residuals in the cylinder, they can also be indicative of higher degrees of tumble motion in some circumstances (Zhao, et al [96]). Another potential reason is the reduced EOC temperature associated with the use of EIVC and LIVC. This is a valid explanation for increased COV and decreased combustion stability, but if low EOC temperature was the main reason for it it would have manifested itself to a greater extent with the short cam than it has.

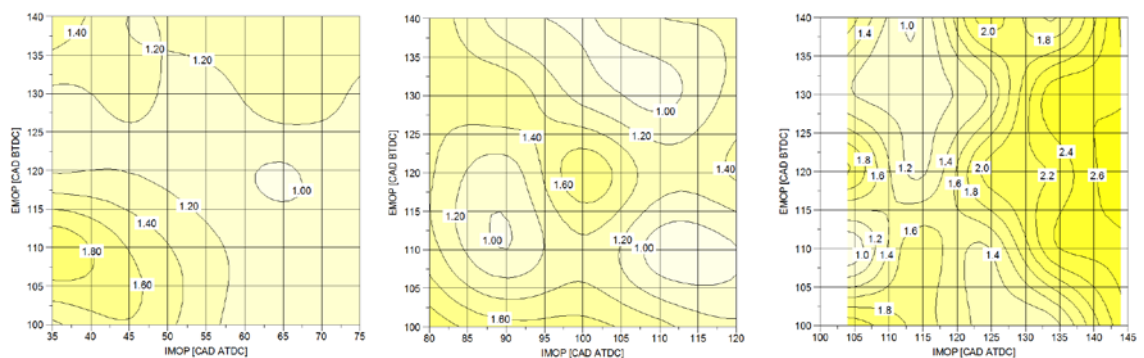


Figure 7.11 Comparison of COV for 1000rpm and 4 bar BMEP for Short (left), Standard (middle) and Long (right) Cams

Most of the above factors are present for all engines running with EIVC and LIVC, however, this is the first time on average that LIVC has returned a considerably lower thermal efficiency than the standard cam to the author's best knowledge. This would suggest that it is one of the above issues or a separate issue that is present on

this single cylinder engine. The fact that this engine is a single cylinder as opposed to a multi-cylinder engine (as used for the majority of the other studies) could change the behaviour slightly, as well as the intake and exhaust tuning dynamics that had such a great impact on the results shown in chapter 5.

The disparity mentioned earlier about the MAP requirement for the single cylinder model being so different to that required for the single cylinder engine indicates that the engine breathing is having an effect, even at low speeds. It has also been found that the minimum load achievable with the single cylinder engine is 4 bar BMEP because below this misfiring occurs.

The reason for this was investigated, and a back to back GT-Power study of the single cylinder and 3 cylinder engines revealed that residuals are massively elevated as a result of the engine breathing differences. For the same degree of valve overlap at the 1000rpm, 4 bar BMEP load point the residuals were found to be 49.5% higher for the single cylinder engine. At 2000rpm and 4 bar this can be seen to drop to 34.1% higher for the single cylinder engine. As the standard cam exhibits the greatest quantity of residuals this is the most likely reason why the single cylinder engine performed so poorly with the standard cam at 1000rpm in comparison to the other 2 cams.

7.4.2.2 Emissions

Data has been obtained for both HCs and NO_x emissions at all test points. The main objective of recording this emissions data is to assess the differences in combustion and using it as an additional tool to determine what is happening in the engine rather than having a mind to reduce them. For this test work the injection timing and pressure was fixed to the standard 3 cylinder values at the equivalent running conditions. Analysis of more emissions would have been required if this had been altered but, as it was not, HCs and NO_x were deemed adequate. Data obtained from the 3 cylinder also suggests that other emissions such as CO, O₂, CO₂ and smoke number were all fairly constant over this speed and load region. Smoke emissions may

have proven useful, and attempts were made to monitor smoke number, however, the smoke emissions were so low that an AVL 415 smoke meter was unable to reliably collect data from the engine. Smoke emission monitoring was therefore abandoned.

HC emissions and NO_x emissions are shown in Figures 7.12 and 7.13 respectively.

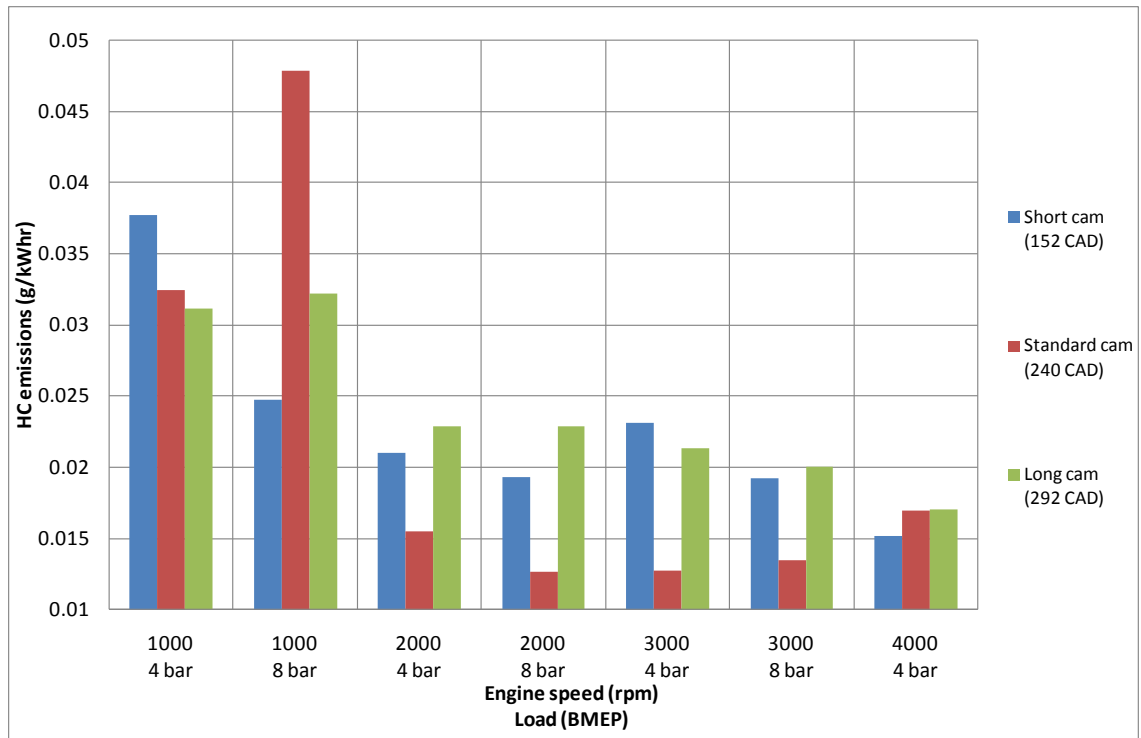


Figure 7.12 HC Emissions Comparison of Short, Standard and Long Cams at Low Loads

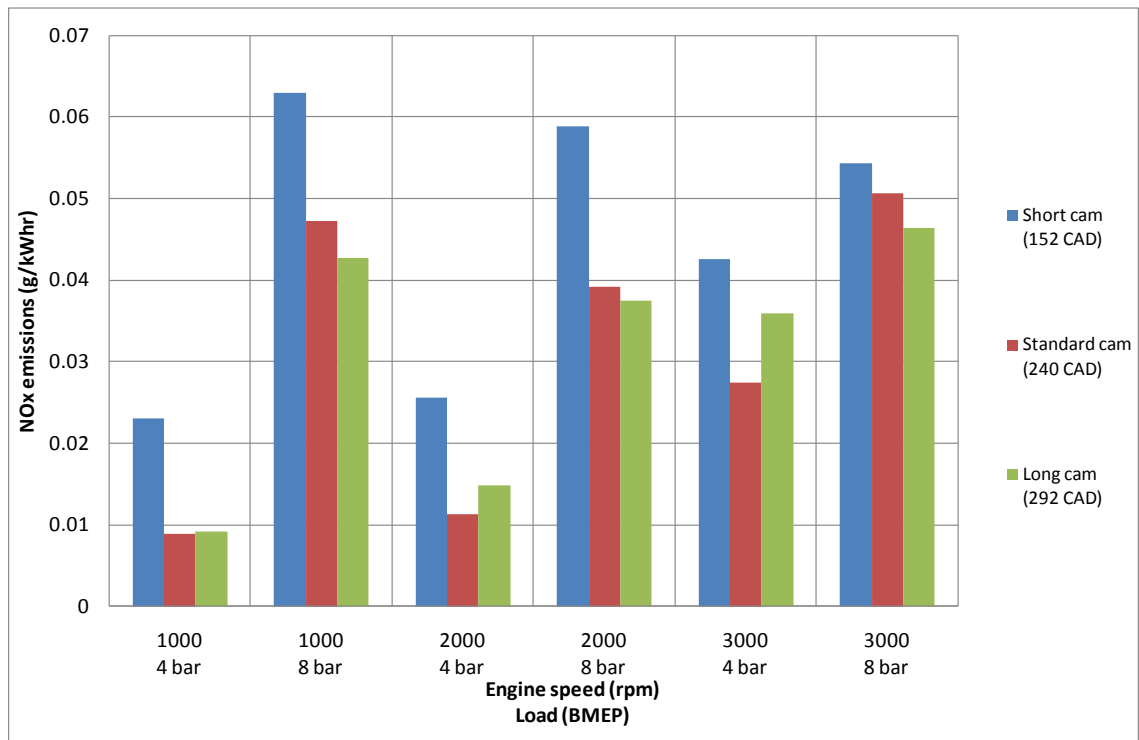


Figure 7.13 NOx Emissions Comparison of Short, Standard and Long Cams at Low Loads

Figure 7.12 shows a considerable increase in HC emissions for the 1000rpm points for all cams, which is caused by a decline in combustion stability at this speed. With the exception of 1000rpm the HC emissions stabilize for all other speeds with the standard cam in all cases returning the fewest HC emissions. This is most likely due to the fact that the standard cam exhibited the highest quantity of residual gasses at cycle start of the 3 cams, thus providing the greatest opportunity to burn off any HC emissions from the previous cycle. The shortest cam would be expected to have the highest HC emissions because it has consistently the lowest quantity of residual gasses at cycle start, a reduced EOC temperature in comparison to the standard cam, and it has the least opportunity to burn off any HC emissions from previous cycles.

Studies with the 3 cylinder engine show that HC emissions should generally decline with higher loads (Figure 7.14). This trend cannot be seen in Figure 7.12, in fact the long cam actually demonstrates the opposite trend to this. This is likely to be due to the engine breathing and the fact that at higher loads there is considerably less residual gas concentration at cycle start due to the higher MAP inhibiting back flow.

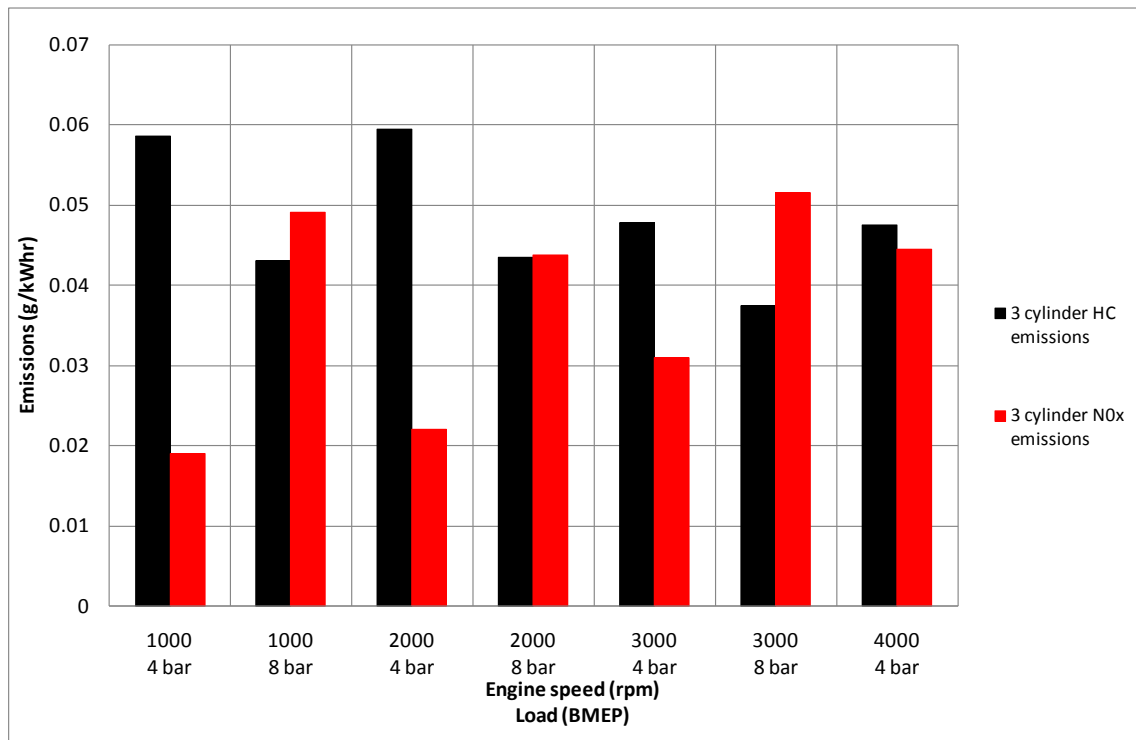


Figure 7.14 HC and NOx Emissions as Obtained from Test Work Carried out by Mahle Powertrain

The HC emissions can also be observed to be low in comparison to the 3 cylinder engine. The exact reason for this is unknown but is most likely to be due to higher rates of internal EGR for the single cylinder engine. The absolute numbers output from the FID analyser were not trusted for this reason, the values relative to each other and trends observed are likely to be accurate however.

The NOx emissions provide a better indication of the residual gas concentration at cycle start with the short cam being consistently higher than the other 2 cams. This is an unexpected result as the literature suggests NOx emissions should be reduced with lower EOC temperatures, however, the residual gas concentration at cycle start with the standard cam and long cam will inhibit NOx formation considerably, and this is the most likely explanation for this unexpected result.

The overall trends are also more like what was observed with the 3 cylinder engine in that higher load increases NOx emissions drastically. The reason for this is a reduction in residual gas concentration at cycle start in combination with higher EOC temperatures leading to higher combustion temperatures.

With such an elevated MAP requirement (Figure 7.15) for the long cam the NO_x emissions could be expected to be slightly higher than they are (due to a higher EOC temperature) but it is important to remember that in the case of the long cam the MAP can be quite misleading because the values given in Figure 7.15 correspond to the average pressure across the 4-stroke cycle, not the pressure whilst the valve is open which is of greatest importance, the same applies to the short cam MAP requirement too. The flow of charge from the cylinder to the intake will also distort the MAP slightly. The theoretical MAP requirement for the long cam is approximately 15% greater than what is required for the standard cam, so the NO_x emissions should be 15% higher but the peak combustion temperature is lower for the long cam due to the lower effective CR, so the fact that both the standard cam and long cam overlay each other closely is coincidental and not to be unexpected.

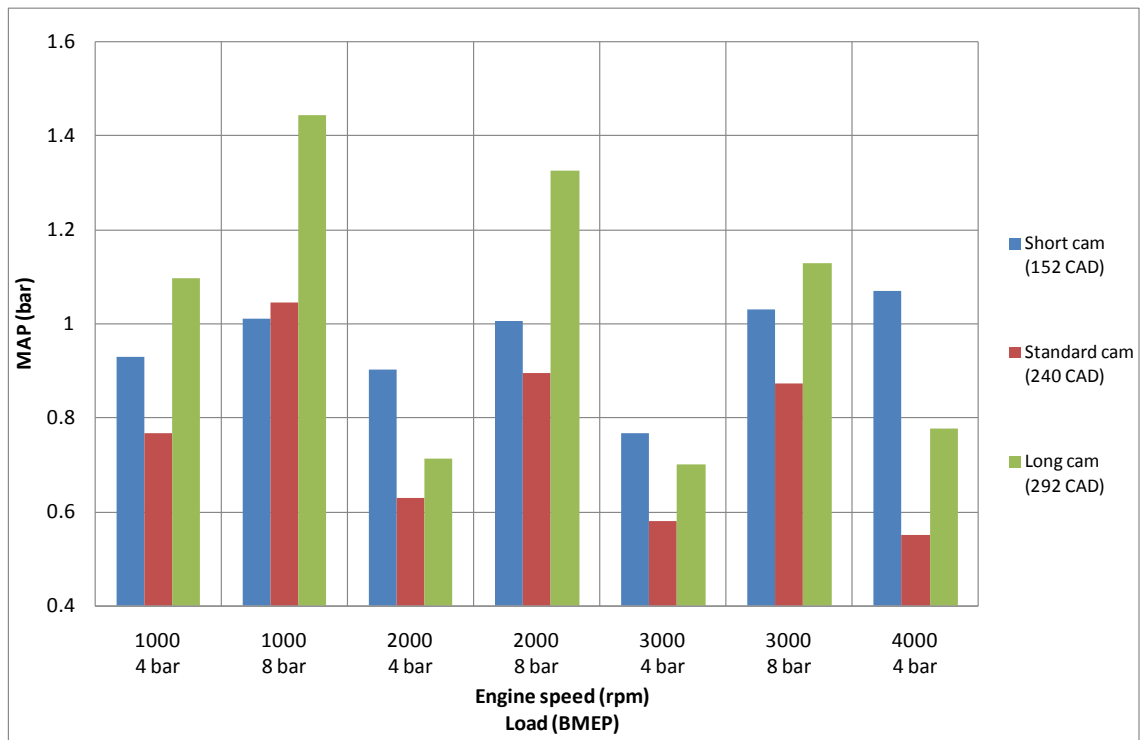


Figure 7.15 MAP Comparison of Short, Standard and Long Cams at Low Loads

7.4.2.3 Analysis of the Individual Components of EIVC and LIVC

This section contains a breakdown of the individual components that cause an increase or decrease in the overall efficiency for both EIVC and LIVC in comparison to the standard cam. The 3000rpm and 4 bar BMEP point was analyzed in this section because it is arguably the most typical point recorded without any nuances.

The theoretical efficiency was calculated on a theoretical cycle basis rather than through the use of a formula. The reason for this is the formulas quoted for the Atkinson cycle process such as those given in Stone [30] and Heywood [21] calculate the thermodynamic efficiency for a 2-stroke cycle and not a 4-stroke cycle.

A major limitation of the equations given in Stone and Heywood is that the system is closed throughout the entire cycle, otherwise by definition it cannot be considered a cycle. This means that the isobaric processes must result in a change of temperature (according to the perfect gas law), this change of temperature is directly proportional to the volume ratio swept. When the cycle is considered open for the duration of the isobaric processes (as is the case with a 4-stroke engine) no temperature change takes place.

What this means is the thermal efficiency of a realistic Atkinson cycle can be calculated using the same formula used to calculate Otto cycle efficiency (Eq.7.1) given by,

$$\eta_{Otto} = 1 - \frac{T_4 - T_1}{T_3 - T_2} \quad 7.1$$

where T_1 , T_2 , T_3 , and T_4 are temperatures at the respective positions shown in Figure 7.16.

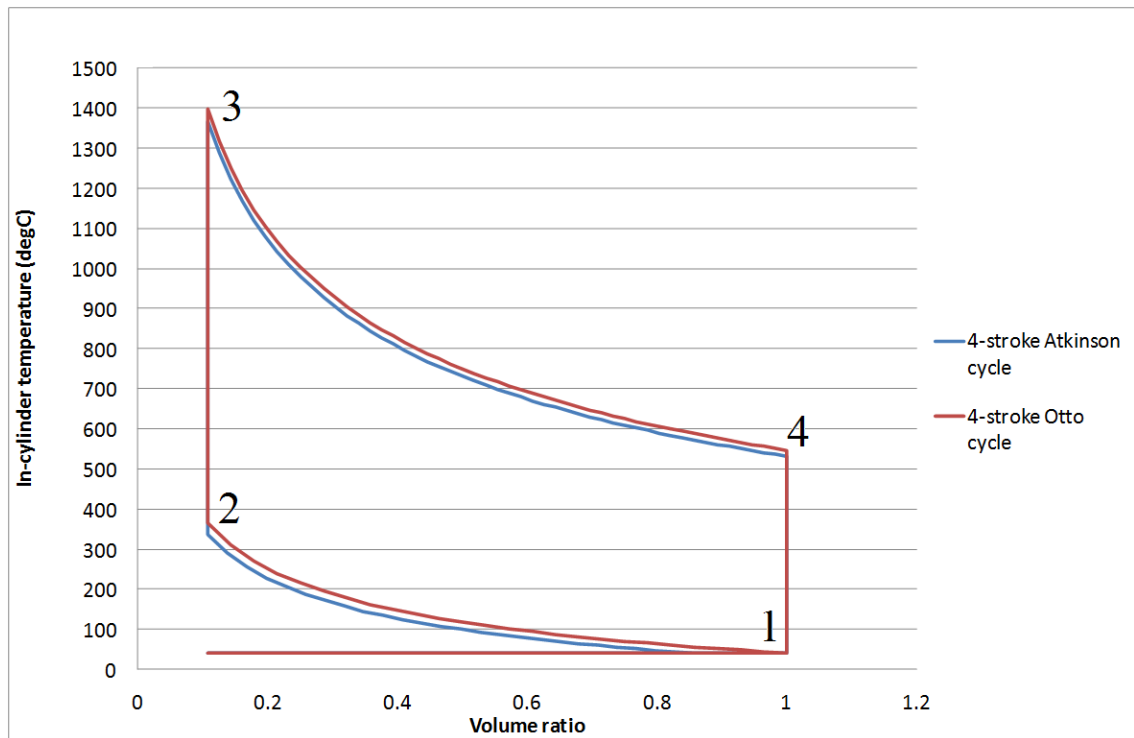


Figure 7.16 Theoretical Temperatures at Various Points in the 4-Stroke Atkinson and Otto Cycles

For a constant heat input (as is the case in Figure 7.16) the Atkinson cycle can be seen to yield a benefit by virtue of the fact T_4 is reduced.

Stone and Heywood both neglected the pumping loop contributions in their derivations, this limits the efficiency calculation to the gross work of the cycle only. At low loads the pumping contributions will be considerable and they cannot be neglected.

The only way to incorporate the pumping losses is to calculate the entire cycle manually. The magnitude of the pumping losses will also affect the size of the gross contribution of the cycle (if the net work is kept constant).

A comparison of the 2-stroke and 4-stroke Miller/Atkinson cycles is shown in Figure 7.17. Both cycles depict the same theoretical gross power output with realistic MAP.

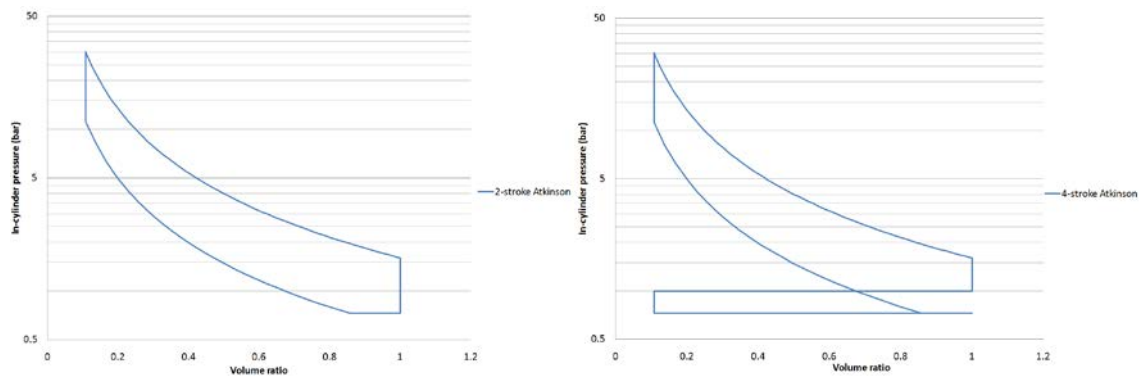


Figure 7.17 Comparison of 2-Stroke (left) and 4-Stroke (right) Theoretical Atkinson Cycles

The biggest difference between the 2-stroke and 4-stroke processes is the isobaric processes. The isobaric processes refer to the processes that take place at constant pressure. In the 2-stroke cycle there is just 1 very small isobaric process that occurs before the polytropic compression process. In the 4-stroke cycle there are 3 isobaric processes at 2 different in-cylinder pressures, this creates a work contribution that is not present in the 2-stroke case.

In the following section the net work of the cycle was kept constant which required the gross work to change depending on the size of the pumping loop. A reduction of the gross work was instigated by changing the theoretical mass of air trapped in the cylinder at cycle start according to Eq.6.1. This was done by changing the MAP. The ΔT was associated with the heat addition process of combustion was kept constant for all theoretical work, so the only change in heat input was through a change of mass alone.

The theoretical benefits offered by the use of EIVC are shown in Figure 7.18, these can be compared to the actual benefits observed from the test work (Figure 7.19).

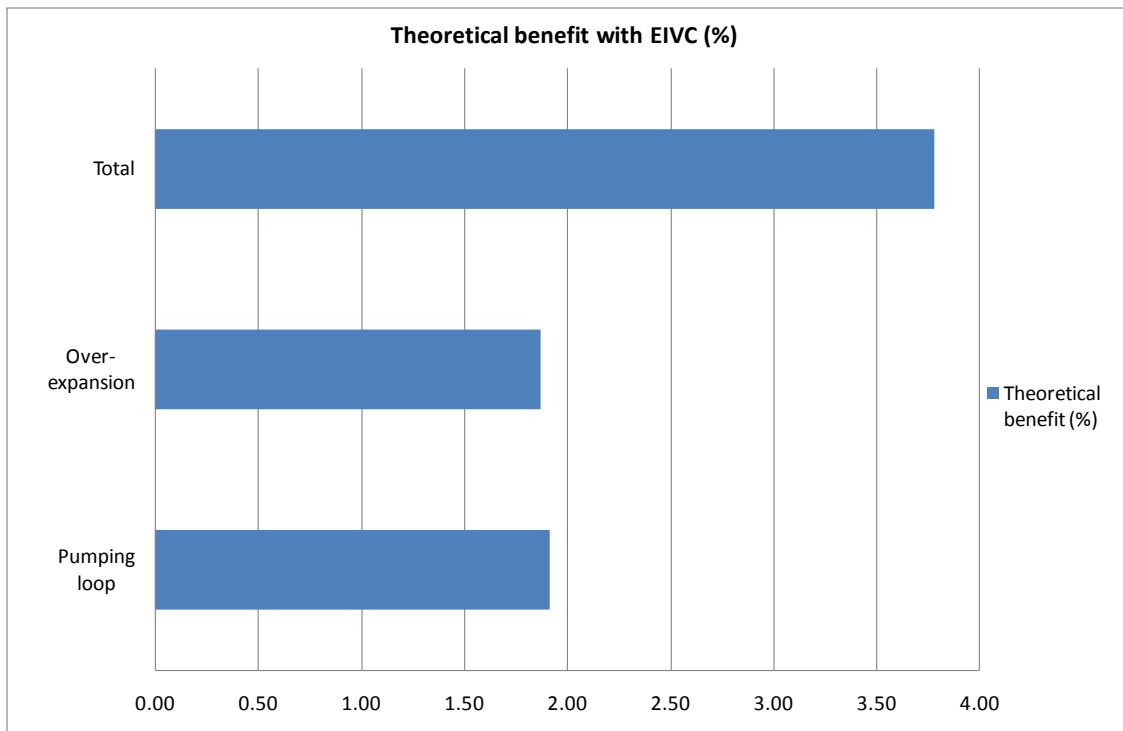


Figure 7.18 Theoretical Benefit with EIVC at 3000rpm and 4 bar BMEP

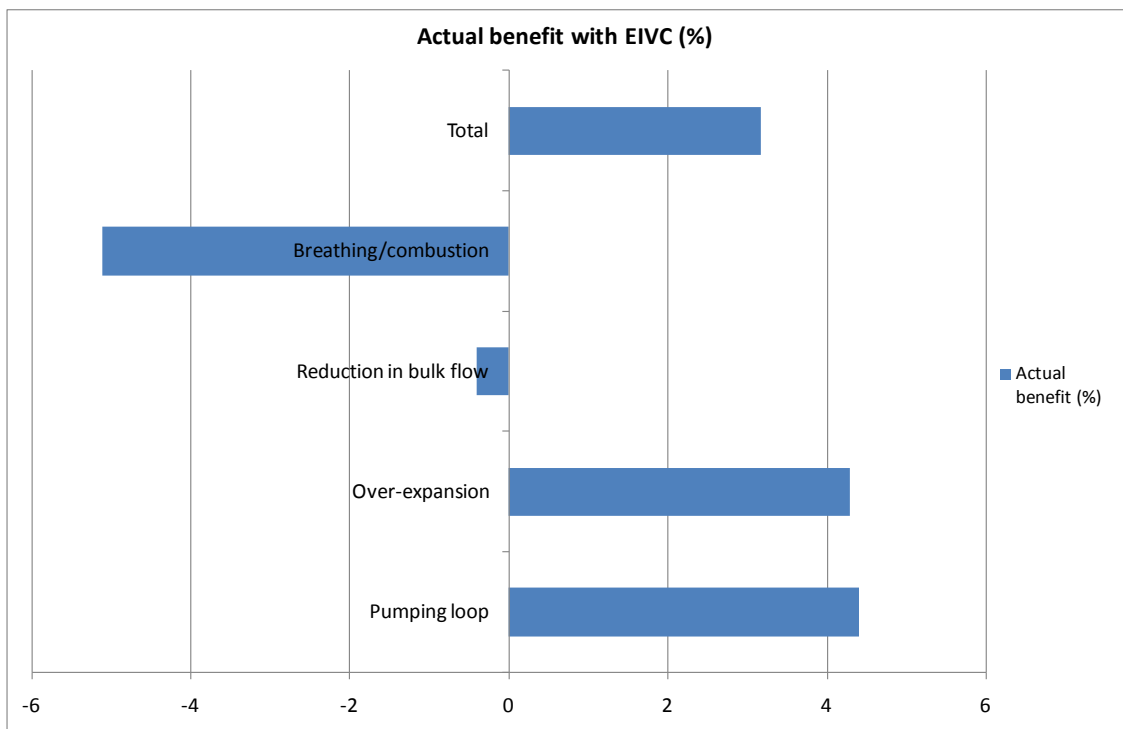


Figure 7.19 Actual Benefit with EIVC at 3000rpm and 4 bar BMEP

The mechanisms that have influenced the theoretical efficiency have been listed in Figure 7.18 where “Pumping loop” corresponds to the benefit associated with

a reduction in pumping loop size. “Over-expansion” refers to the benefit associated with running with over-expansion as opposed to the standard Otto cycle. The over-expansion value is influenced by the pumping loop size because constant NIMEP was maintained. In order to factor the influence of the pumping loop out of the gross work component, the influence of over-expansion was calculated at a constant GIMEP point, or by subtracting the “Pumping loop” component from the “Total” component. The “Total” value is calculated based on the thermal efficiency as calculated from the theoretical open system 4-stroke Atkinson cycle, or the 4-stroke Otto cycle efficiency.

For the actual data (Figure 7.19) “Pumping loop” refers to the difference in PMEP between the standard and the short cam as derived from the experimental data. “Over-expansion” was calculated by subtracting the experimental pumping loop value from the theoretical thermal efficiency as calculated from the theoretical open system 4-stroke Atkinson cycle (4-stroke Otto cycle) analysis. The “Reduction in bulk flow” refers to the influence of the increased burn duration associated with EIVC. It has been called the reduction of bulk flow because that is the theorized cause for the slow burn (see section 7.4.2.1). It has been calculated using GT-Power. The “Breathing/combustion” component is the efficiency benefit associated with combustion deterioration caused by either low EOC pressure and temperature, residuals, low in-cylinder charge motion, or a high COV. This has been calculated by adding the other components and subtracting this from the “Total” which has been calculated as the difference in ISFC for the standard and short cam derived from the experimental data.

The influence of pumping loop size and over-expansion can be seen to be roughly equal in size. The over-expansion component is of the same magnitude as the pumping loop contribution due to the fact that the effective CR is so low. The over-expansion component can be expected to reduce in size with higher effective CRs approaching the geometric CR.

The pumping loop component is entirely dependent on load and will not necessarily decrease with increasing effective CR, as can be seen in Figure 7.6. In this

example the pumping loop component is very large for the standard cam due to the fact the engine is being run at very low load.

The reduction in bulk flow can be seen to be quite inconsiderable in comparison to the loss associated with the engine breathing/combustion deterioration according to Figure 7.19. However, it was not possible to determine precisely how much of the combustion deterioration was caused by the reduction of bulk flow, likewise, it was not possible to determine accurately what effect an increase in TKE had on the overall efficiency either.

The theoretical gain in efficiency can be seen to match the actual gain in efficiency quite closely. This is likely to be more coincidence than proof that the 4-stroke Atkinson cycle analysis is an accurate measure of the efficiency of EIVC and LIVC, as the components of pumping and over-expansion can be expected to be far different in reality due to engine breathing behaviour.

Figures 7.20 and 7.21 show the theoretical and actual advantages of LIVC (compared to the standard cam).

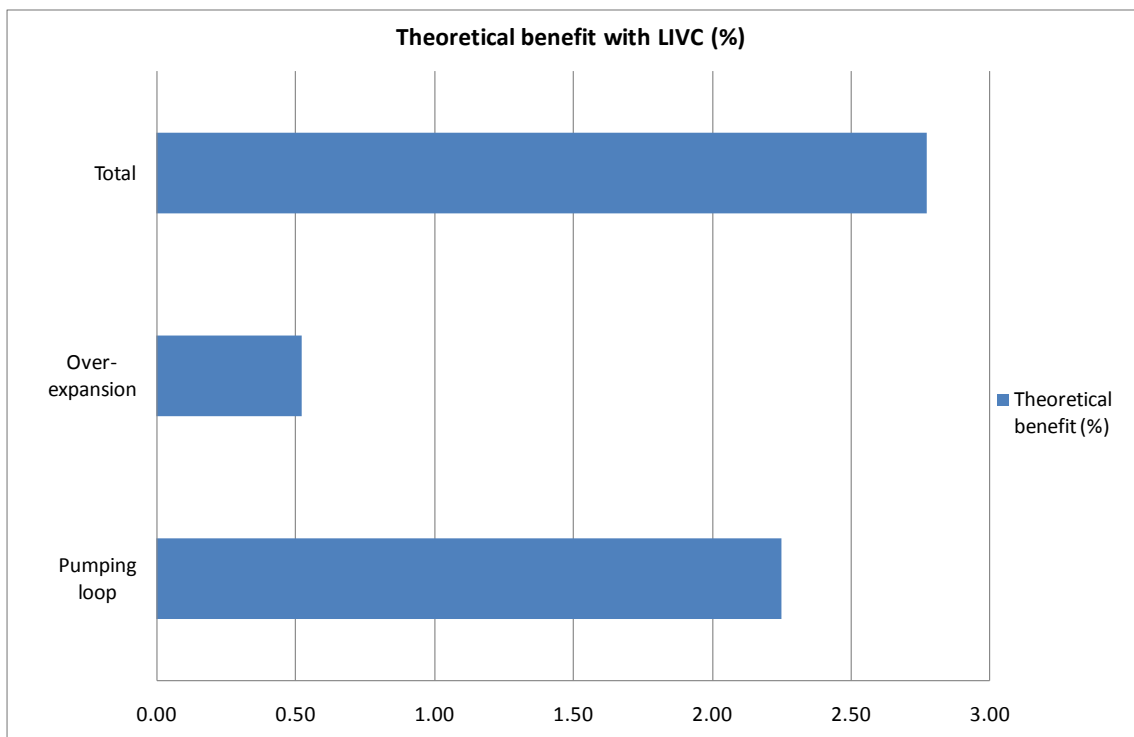


Figure 7.20 Theoretical Benefit with LIVC at 3000rpm and 4 bar BMEP

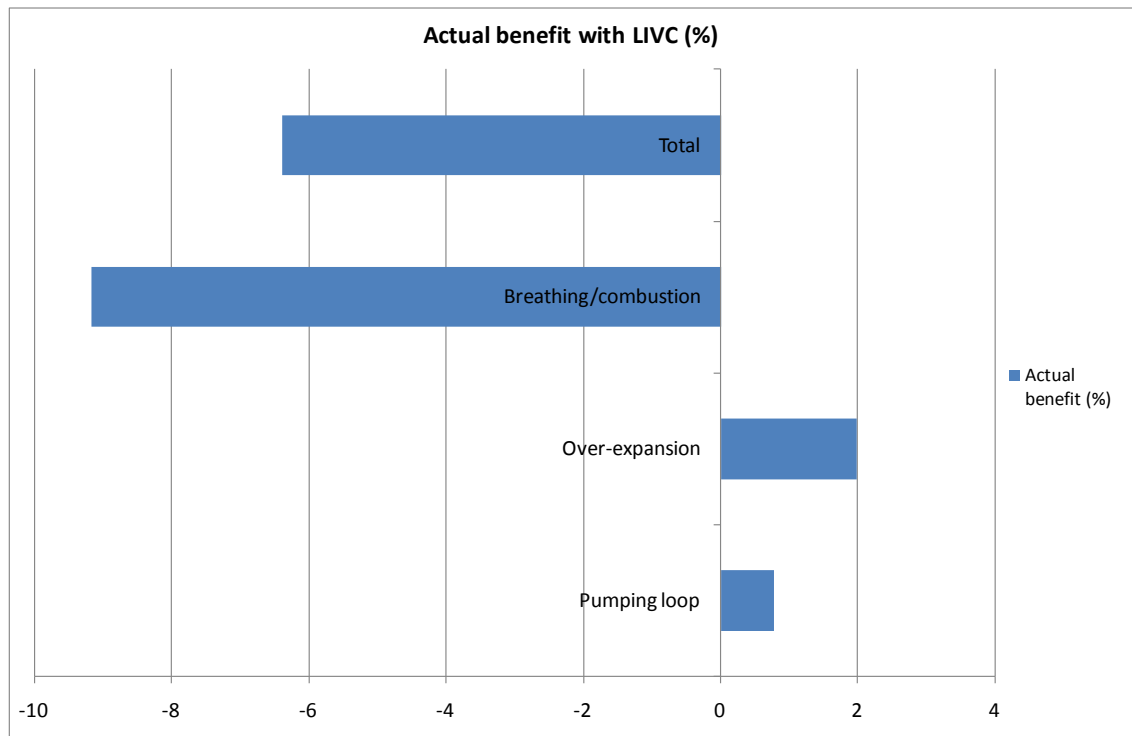


Figure 7.21 Actual Benefit with LIVC at 3000rpm and 4 bar BMEP

The pumping loop contributions can be seen to be markedly different for LIVC. The predicted contribution is a lot higher than the actual contribution. This is due to the fact that the long cam at this point requires an MAP similar to the standard cam, thus resulting in similar pumping loop sizes, whereas the MAP requirement in theory should be 0.1 bar lower for the standard cam.

The combustion deterioration that affects LIVC can also be seen more clearly here and is accountable for an ISFC increase of 9%. This could likely be improved to a level similar to the level obtained with EIVC if the maximum valve lift with the long cam were reduced to encourage more turbulent mixing, although the lack of bulk flow could impact on this benefit somewhat.

For both EIVC and LIVC cases the losses of efficiency associated with combustion deterioration could potentially be reduced by adopting a higher geometric CR. A higher geometric CR will increase the degree of in-cylinder turbulence toward TDC and will also elevate the EOC temperature and pressure which will further aid combustion stability. If combustion deterioration issues could be eliminated completely this would yield an ISFC improvement of 5% with EIVC and 9% with LIVC.

7.4.2.4 Optimum Cam Timing Observations

The optimum cam timings make it very clear that the full potential of the short and long cams could not be yielded at speeds and loads as low as these with this particular engine. The optimum cam timing for the short cam was the maximum valve overlap point (the point for minimum effective CR) for 3 of the 7 test points. The optimum cam timing for the long cam was the minimum valve overlap point (the point for minimum effective CR) for 3 of the 7 test points as well.

Analysis of the results shows that on almost every occasion the cam timing that gave the highest EOC pressure was the optimum for the 4 bar BMEP cases. Eight bar BMEP proved to be sufficient to run with the full extent of effective CR reduction with the long cam, however, the optimum cam timing for the short cam at 8 bar BMEP was typically in the middle of the cam phase range, offering neither optimum effective CR nor a great deal of scavenging. Generally speaking the favoured cam timing was that which offered the highest EOC pressure again.

The cam sweeps carried out show quite clearly the impact of effective CR (IMOP sweeping) and residuals (EMOP sweeping) on the combustion stability and impact on burn rate, however, the impact on ISFC could not be isolated due to the fact that effective CR and effective expansion ratio change when IMOP and EMOP (respectively) are adjusted. Figure 7.22 is an example of a 10-90% MFB IMOP-EMOP sweep map extracted from the test data. The sensitivity to EMOP differed across the speed and load range with the 8 bar BMEP points typically showing a reduced sensitivity to EMOP and residuals. The most likely explanation for this is the elevated MAP is resulting in scavenging of the cylinder rather than allowing back flow.

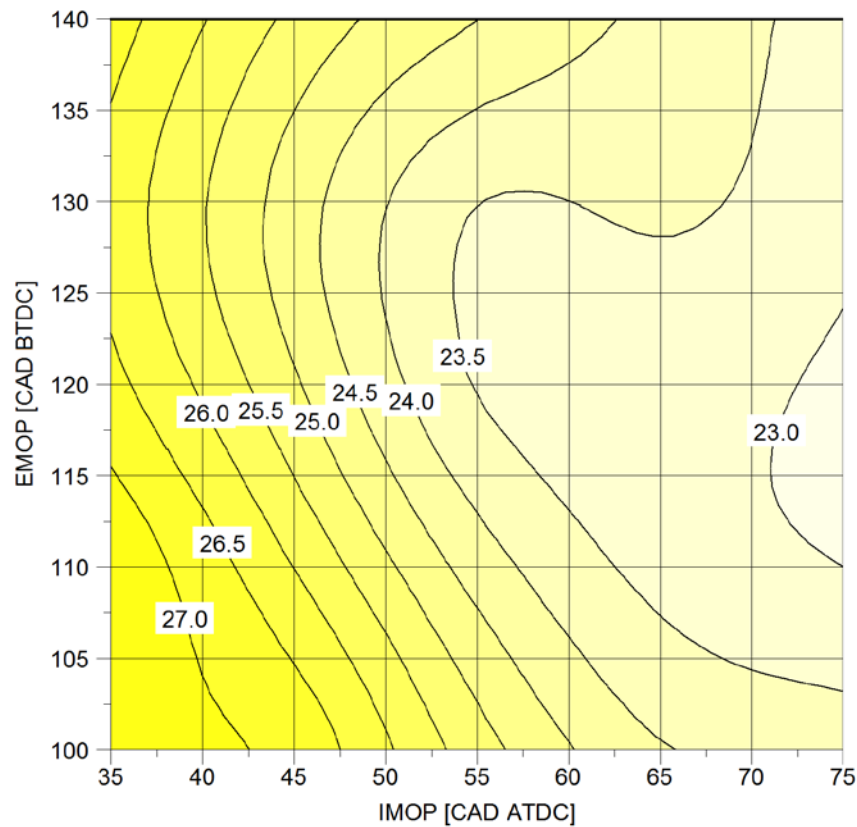


Figure 7.22 Map of 10-90% MFB Rates for an IMOP-EMOP Sweep with the Short Cam at 3000rpm and 4 bar BMEP

The sensitivity of 10-90% MFB duration to IMOP (or effective CR) can be seen to be similar in magnitude for all speed and load points. The COV however is not particularly sensitive to the degree of IMOP or EMOP but is typically greater with extremes of IMOP, so either with maximum valve overlap or minimum valve overlap for both the short and long cams. The COV typically increases with later IMOPs (tending toward minimum valve overlap) because the effective CR is increasing. Although the quantity of residuals will reduce with later IMOPs, the MAP will also reduce allowing more back flow of exhaust gasses to the intake, so the quantity of residuals cannot be expected to decline that predictably with increasing later IMOPs.

7.4.2.5 Combustion Phasing Observations

The MBT timing exhibited very little sensitivity to cam duration and fell between 6 and 9 CAD ATDC for all test work (Figure 7.23).

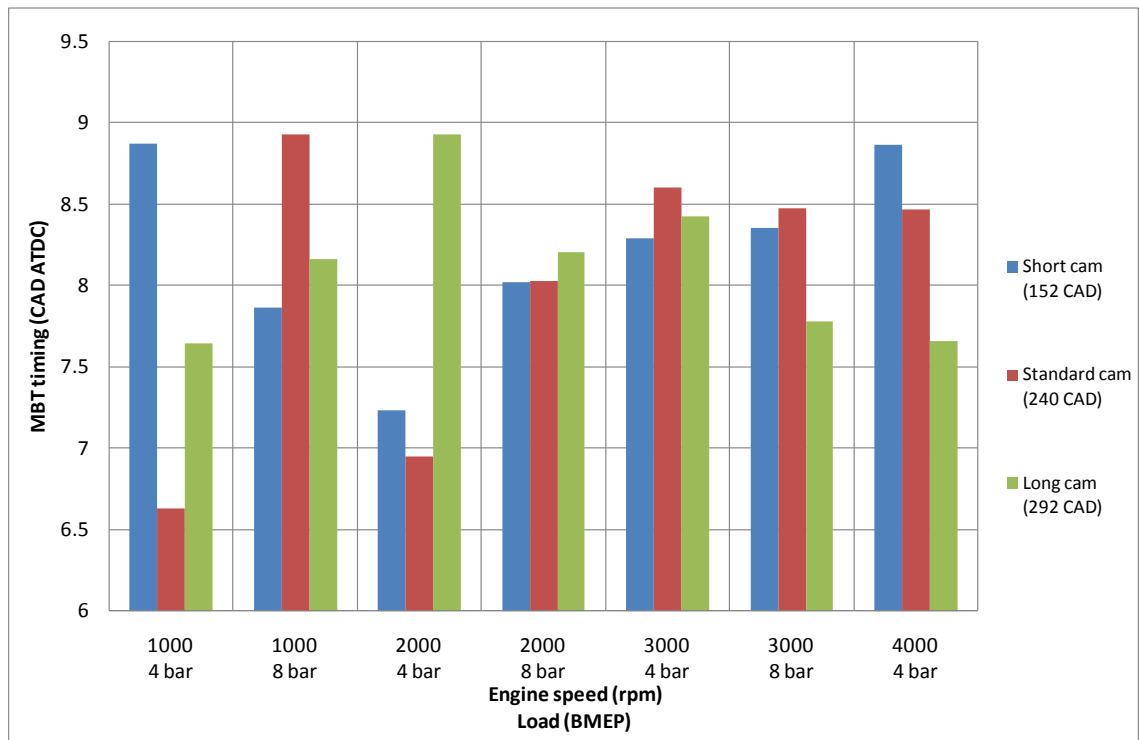


Figure 7.23 MBT Comparison of Short, Standard and Long Cams at Low Loads

Figure 7.24 reveals the spark timings to be dramatically different with the short cam requiring a great deal more spark advance than the other 2 cams, which can be seen to be broadly the same. The short cam can be seen to exhibit a slight upward trend with increasing speed, which would imply that increasing engine speed does not address the problem of reduced charge motion to the same extent as it does with the longer cam.

The spark timing can be seen to be highly dependent on load with the short and standard cams, with the higher load points requiring the spark to be retarded significantly as can be expected. The long cam however exhibits a much smoother profile and shows a far reduced sensitivity to load in comparison to the other 2 cams. Figure 7.8 illustrates that intake port temperatures are very elevated at certain speeds and loads in the case of the standard cam. This indicates a large amount of back flow through the intake valves. The standard cam line can be seen to have a very erratic profile. This is explained by the optimum IMOP timing for each of the different speed and load points. For every speed and load point the optimum EMOP was the maximum valve overlap position, therefore the quantity of residuals in the cylinder is influenced purely by the IMOP timing. The optimum IMOP timing for the 4 bar BMEP cases (with

the exception of 3000rpm) was either the maximum valve overlap position or the second highest degree of valve overlap position (Figure 7.25). This allowed a great deal of back flow from the cylinder into the intake manifold during the valve overlap period which elevated the intake port temperatures significantly. The 8 bar BMEP cases generally favoured significantly lower degrees of valve overlap, and the MAP was higher for these points. Both of these result in greatly reduced backflow of residual/exhaust gasses to the intake thus resulting in a considerably reduced intake port temperature.

Figures 7.12 and 7.13 also suggest that the residual gas concentration with the standard cam at the 1000 and 2000rpm 4 bar BMEP points is particularly high, this will likely result in the very pronounced variations in spark timing seen with the standard cam. The standard cam would be expected to exhibit the highest MFB durations due to the fact the EOC temperatures are inherently higher than with the short and long cams.

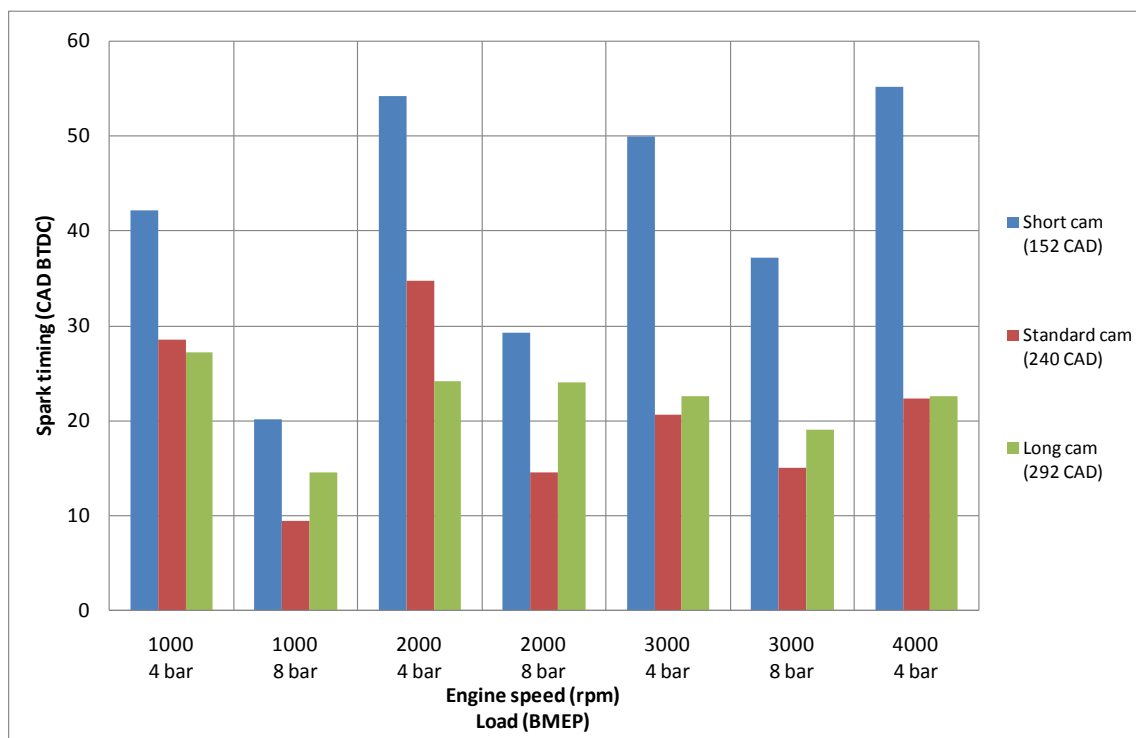


Figure 7.24 Spark Timing Comparison of Short, Standard and Long Cams at Low Loads

The reason for the very erratic profile of the short cam line can likely be attributed to the cam timing (Figure 7.25). The cam timings for the short cam at the

low load points tends to be toward the maximum valve overlap position, which for the short cam is the position that inherently produces the lower EOC temperatures due to the low effective CR. At higher loads the short cam favours the reduced valve overlap positions, this will result in a higher EOC temperature.

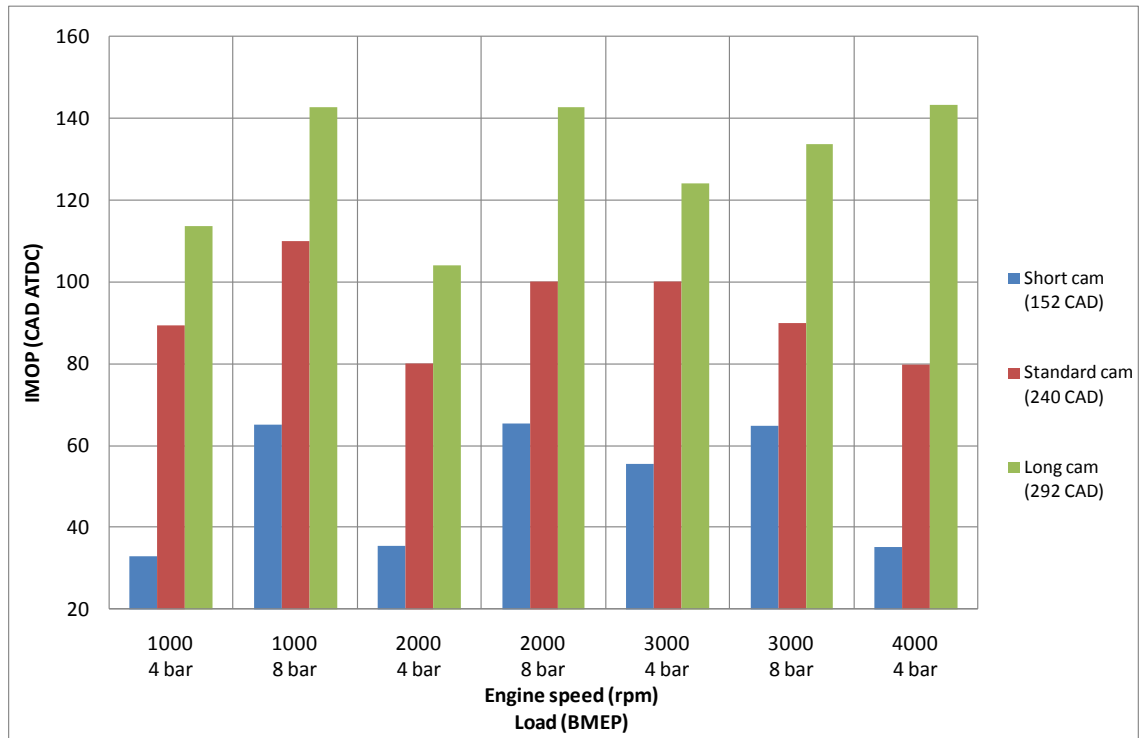


Figure 7.25 Optimum IMOP Timing Comparison of Short, Standard and Long Cams at Low Loads

7.4.3 Summary

EIVC proved to be the optimum strategy for reducing ISFC at low load. The reason for this is a reduction in effective CR and a consequent increase in MAP. The increase in MAP ensured back flow of exhaust gasses into the intake manifold and the consequent residual gas concentration at cycle start was kept to a minimum. The increase in MAP also resulted in a reduction of the pumping loop size.

LIVC was found to be hindered by combustion degradation issues. The cause of this is unknown but is suspected to be due to the fact charge is exhaled into the intake manifold where it may react and spoil before it is readmitted to the cylinder for the

next cycle. Both GT-Power and HC emissions analysis confirm that no significant quantities of charge scavenging are taking place.

It is suspected that both EIVC and LIVC strategies at these low load conditions would benefit from an increase of geometric CR to help raise the EOC pressure and temperature and to ensure higher levels of turbulence are generated in the cylinder to allow thorough mixing.

7.5 High Load Operations with EIVC and LIVC (Deep Miller)

7.5.1 Introduction

High load EIVC and LIVC are arguably of greatest importance to the downsizing concept. The mechanism by which an improvement in fuel economy and performance is theorized to take place is as described in section 7.3. The reduction of EOC pressure and temperature is of great importance because it will advance the BLD limit (in comparison to the standard cam).

Unfortunately the test plan for this work had to be truncated to just the 2000rpm, 15 bar BMEP and 24 bar BMEP points because of a severe failure of the engine believed to have been brought about by running at high speeds and loads.

The focus of this work was on reducing ISFC rather than increasing maximum load for the reasons given above. The 24 bar BMEP points were carried out at 2 different EBPs, one scenario was with no EBP and the other with an EBP of 2 bar. The 15 bar BMEP points were also carried out at 2 different EBPs, one scenario was with no EBP the other was setting the EBP valve to 45% closed. This was determined as the correct EBP valve position to give turbocharger representative levels of EBP at this speed and load.

No emissions were logged for this test work except HC. The reason for not logging NO_x is that this no longer falls in the remit of the NEDC cycle.

The test points are shown in Table 7.2, and the test variables and control criteria are defined in Table 7.3.

7.5.2 Results

A comparison of all 3 cams with no EBP and 2 bar EBP is shown in Figure 7.26.

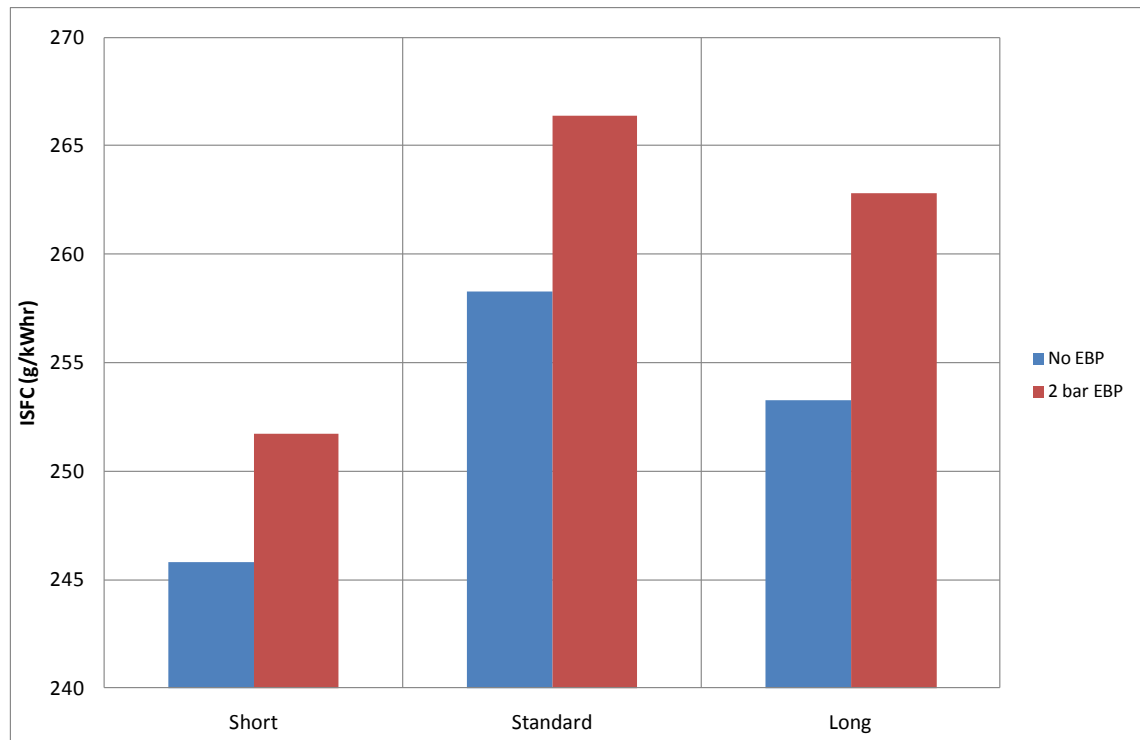


Figure 7.26 2000rpm, 24 bar BMEP ISFC Comparison for Short, Standard and Long Cams at 2 EBPs

The increase in load has been found to greatly increase the combustion stability for both the short and long cam, but particularly for the long cam which, for this work, was phased to its maximum extent (minimum valve overlap). The short cam could not be phased to provide the minimum effective CR however, due to the fact that at maximum valve overlap (the optimum timing for low effective CR for the short cam) scavenging was resulting in accidental enrichment of the charge as evidenced by the profile of HC emissions Vs. IMOP angle (Figure 7.27).

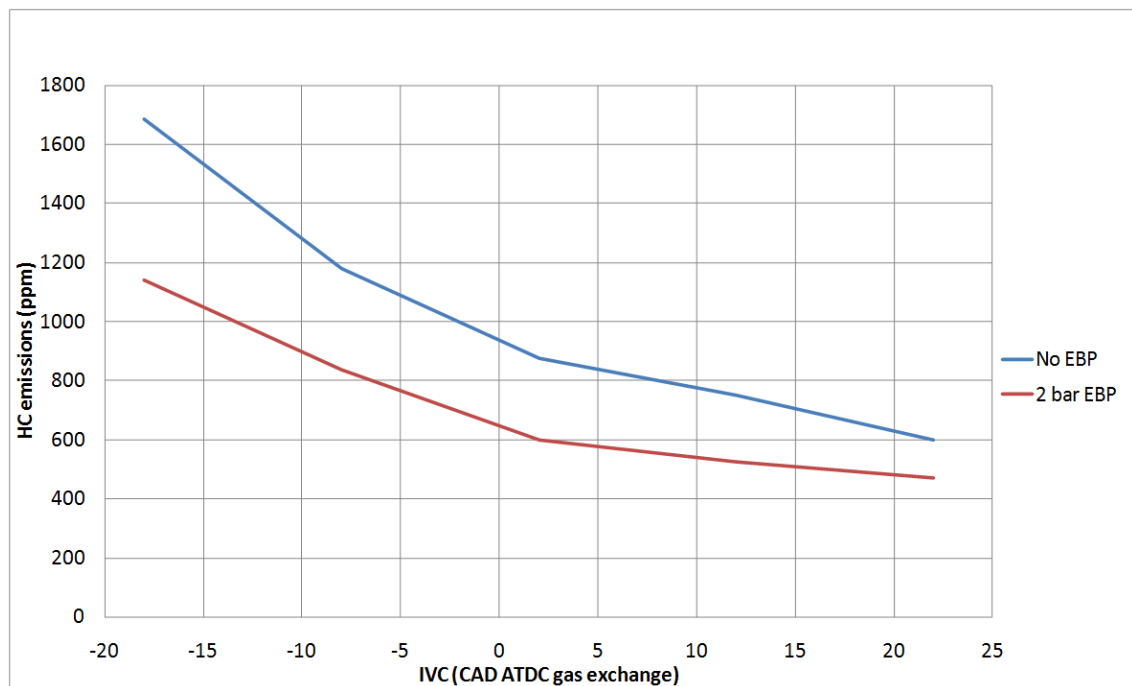


Figure 7.27 HC Emissions for Different IVC Timings and 2 Different EBPs with the Short Cam at 2000rpm and 24 bar BMEP with an EMOP of 100 CAD BTDC (Maximum Valve Overlap Position)

The accidental over enrichment is reduced in magnitude for the 2 bar EBP case but can still be seen to occur owing to the low effective CR requiring an MAP well in excess of the EBP. EBP effects have been analysed in greater depth in section 7.5.2.1.

In spite of the fact the short cam could not be phased to provide the maximum degree of effective CR reduction it still offers the greatest improvement in ISFC in comparison to the long cam. One of the reasons for this is that the EOC pressure was lower for the short cam. This can likely be attributed (to an extent) to the fact that the degree of effective CR reduction obtainable with the short cam is slightly greater than that with the long cam.

The degree of effective CR reduction obtainable with the short cam is even greater still due to fact the effective CR is calculated from the 1mm lift position. In reality the flow through the intake valve will begin to reduce at valve lifts of more than 1 mm which in the case of EIVC means cylinder depressurisation will occur before the 1mm lift point is reached, and for LIVC cylinder pressurisation will occur before the 1mm lift point. The difference between EIVC and LIVC is that the flow into the cylinder will begin to reduce earlier for EIVC and the flow out of the cylinder will reduce earlier for LIVC. This means that the effective mass of air trapped in the cylinder with EIVC will

be less than the effective CR will imply, while the mass of air trapped in the cylinder with LIVC will be more than the effective CR will imply.

Another one of the reasons why the ISFC improvement is not as marked for the long cam as it is for the short cam is the fact that charge scavenging is taking place. This has been confirmed by a GT-Power simulation and is accountable for a 1.91% drop in ISFC (this is less than the values quoted in section 5.3.4.2 due to the fact that a stoichiometric charge was assumed to be scavenged in that instance). The presence of charge scavenging has also manifested itself in the HC emissions results obtained from the experimental engine (With HC emissions of 0.0225, 0.0243 and 0.039 g/kWhr for the short, standard and long cams respectively). There is no appreciable rise in exhaust gas temperature which indicates that the charge that has been scavenged has not been burning in the exhaust gasses, however, this is the temperature as measured at the exhaust port so this is not necessarily a good indicator. There is a small increase in EBP for the no EBP case (please note: no EBP means the EBP valve was set to 0% closed, not necessarily a complete absence of EBP and/or pressure/rarefaction waves) for the 24 bar BMEP point, and also a small increase for both 15 bar BMEP with and without EBP points. This could indicate that some combustion is occurring in the exhaust manifold, but not enough data has been obtained to determine with any degree of certainty whether there is any combustion at any point in the exhaust system.

Although the combustion stability is considerably improved (relative to the low load performance) the COV for the short cam is markedly worse than for the other 2 cams, but only at the 24 bar BMEP points (Figure 7.28).

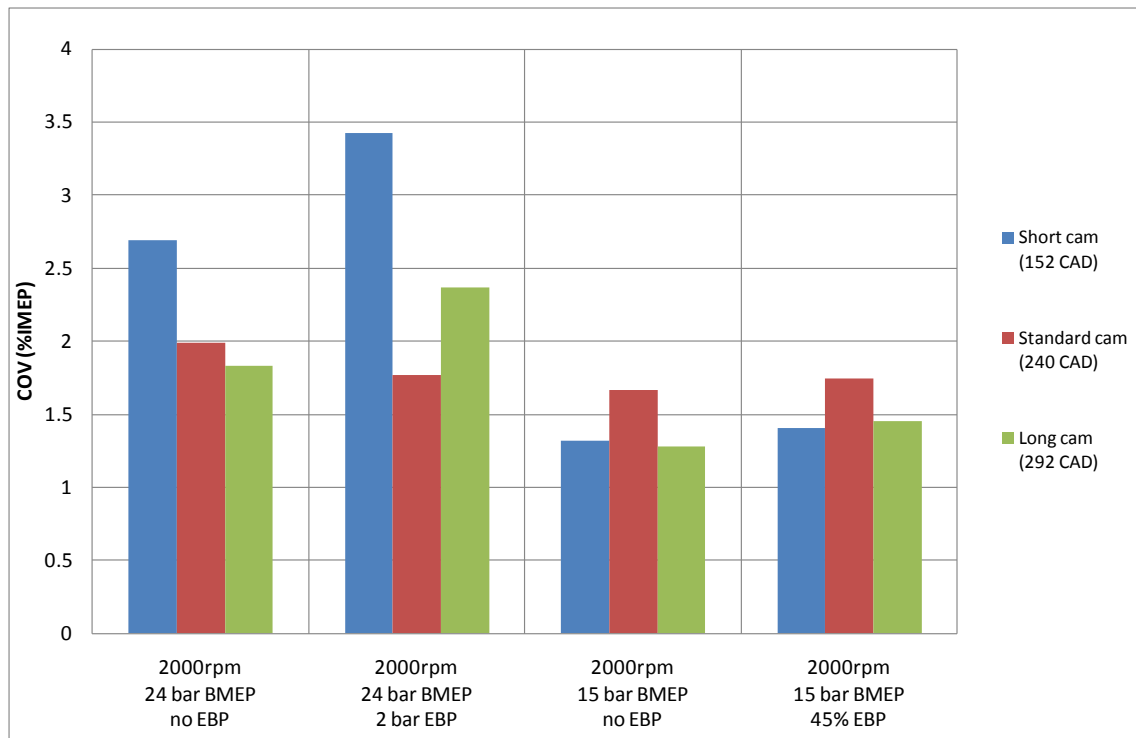


Figure 7.28 COV for Short, Standard and Long Cams at 2000rpm, High Load with and without EBP

The lack of combustion stability is also visible (and understandable) when observing the 10-90% MFB duration results (Figure 7.29). At every point the 10-90% MFB duration is markedly longer for the short and long cams in comparison to the standard cam. The burn rate is particularly long for the short cam which, as with the low load points, is probably due to a lack of bulk flow in the cylinder as well as lower EOC pressure and temperature. The 10-90% MFB durations are still long for the long cam but considerably better than for the short cam. The reason for this is the in-cylinder charge motion is likely to be comparable to the standard cam and consist of a great deal of bulk fluid motion, but the effective CR reduction will result in lower EOC pressures and temperatures which will reduce flame front speed.

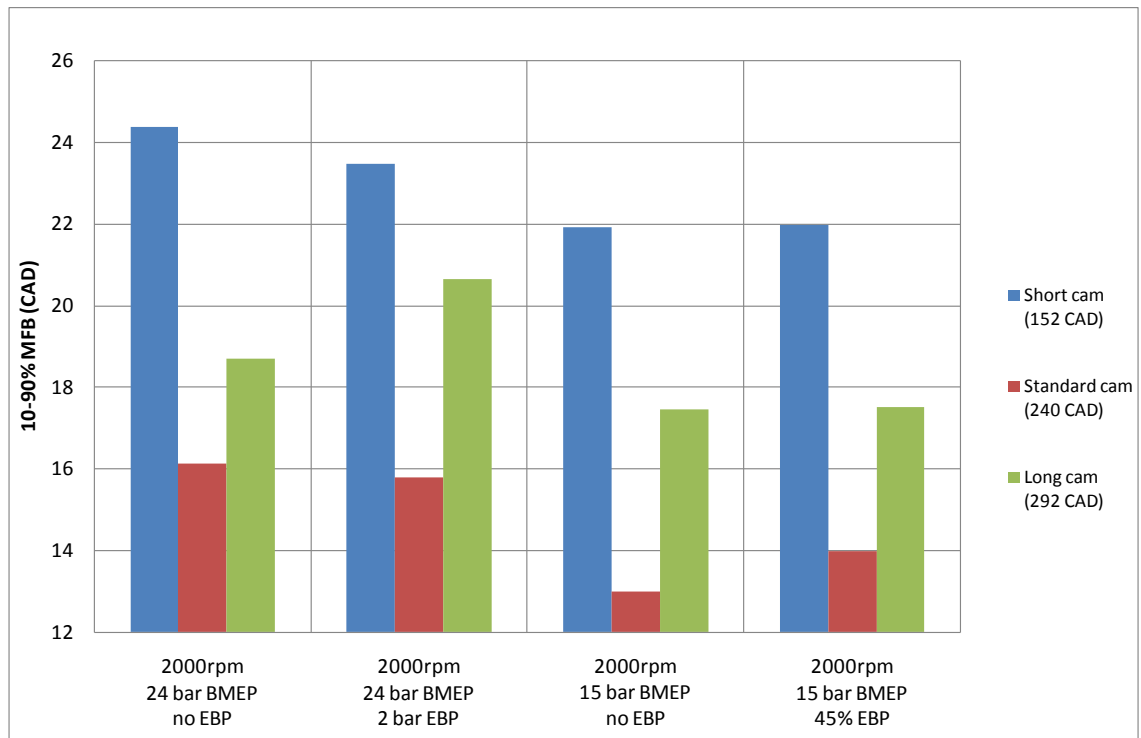


Figure 7.29 10-90% MFB Duration for Short, Standard and Long Cams at 2000rpm, High Load with and without EBP

The increase in 10-90% MFB duration is highly unlikely to be caused by residuals because a GT-Power simulation has revealed there to be no considerable residual gas concentration at cycle start with all 3 cams. The very long 10-90% MFB duration has not had a great impact on the BLD point at the 24 bar BMEP point, with no strong trends to suggest the short cam requires a greater deal of combustion phasing retard as a consequence of a longer burn duration (Figure 7.30). However, the impact of a longer burn duration on the 50% MFB point is more noticeable at 15 bar BMEP.

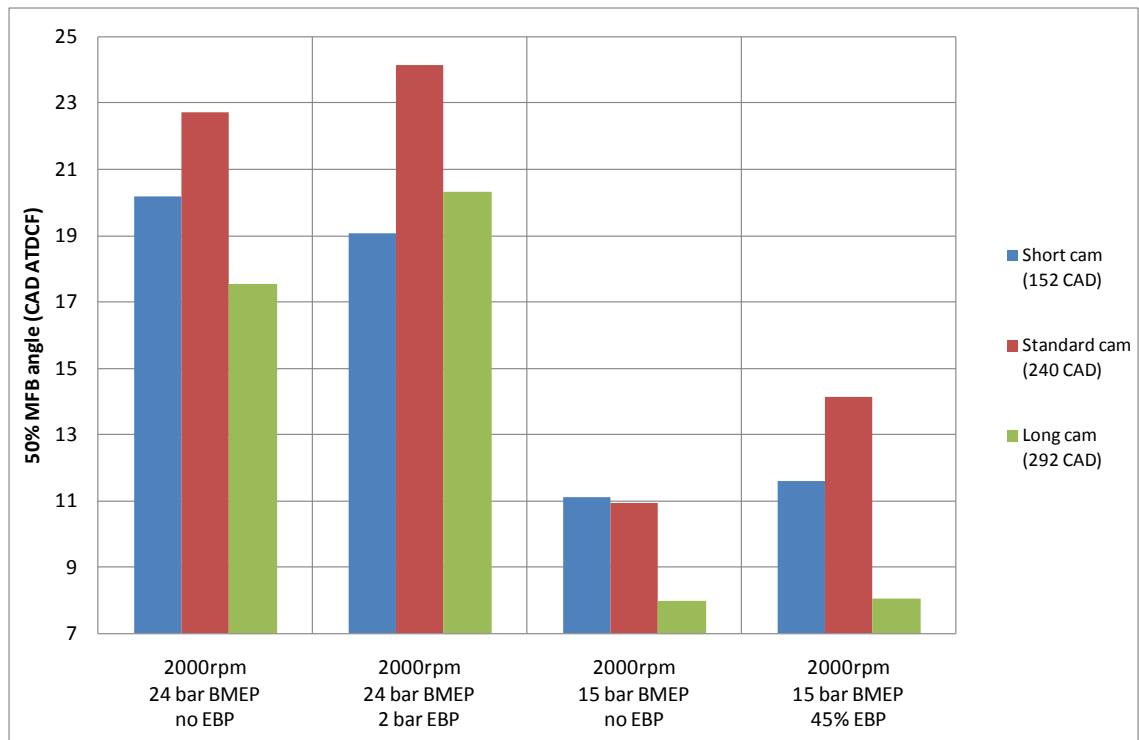


Figure 7.30 50% MFB Angle for Short, Standard and Long Cams at 2000rpm, High Load with and without EBP

The short cam also demonstrates the lowest EOC pressure at the 15 bar BMEP site too. This can be found to manifest itself by the degree of spark advance that can be achieved with the short cam (Figure 7.31). Owing to a lack of charge motion associated with low lift, this is not corresponding to a 50% MFB benefit. A similar trend can be seen with the long cam too where the spark can be considerably advanced due to reduced EOC temperature but this is not yielding a benefit in the 50% MFB due to reduced charge motion.

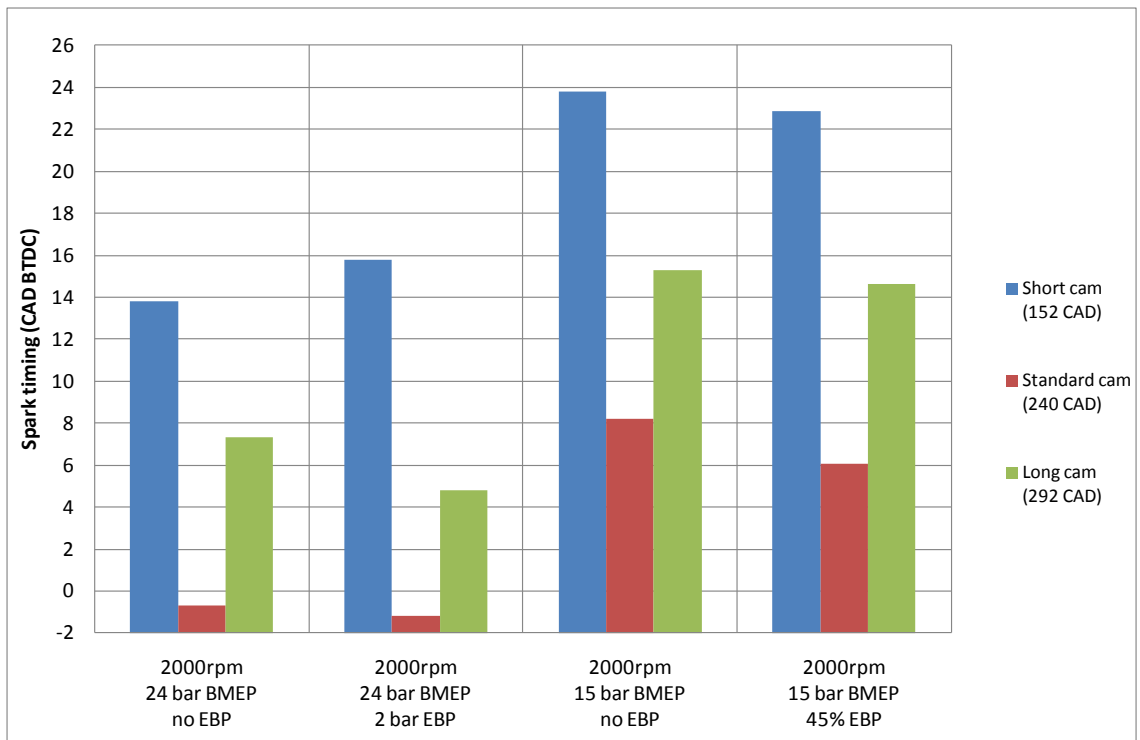


Figure 7.31 Spark Timing for Short, Standard and Long Cams at 2000rpm, High Load with and without EBP

The 15 bar BMEP ISFC trends can be seen to match the 24 bar BMEP trends quite closely (Figure 7.32).

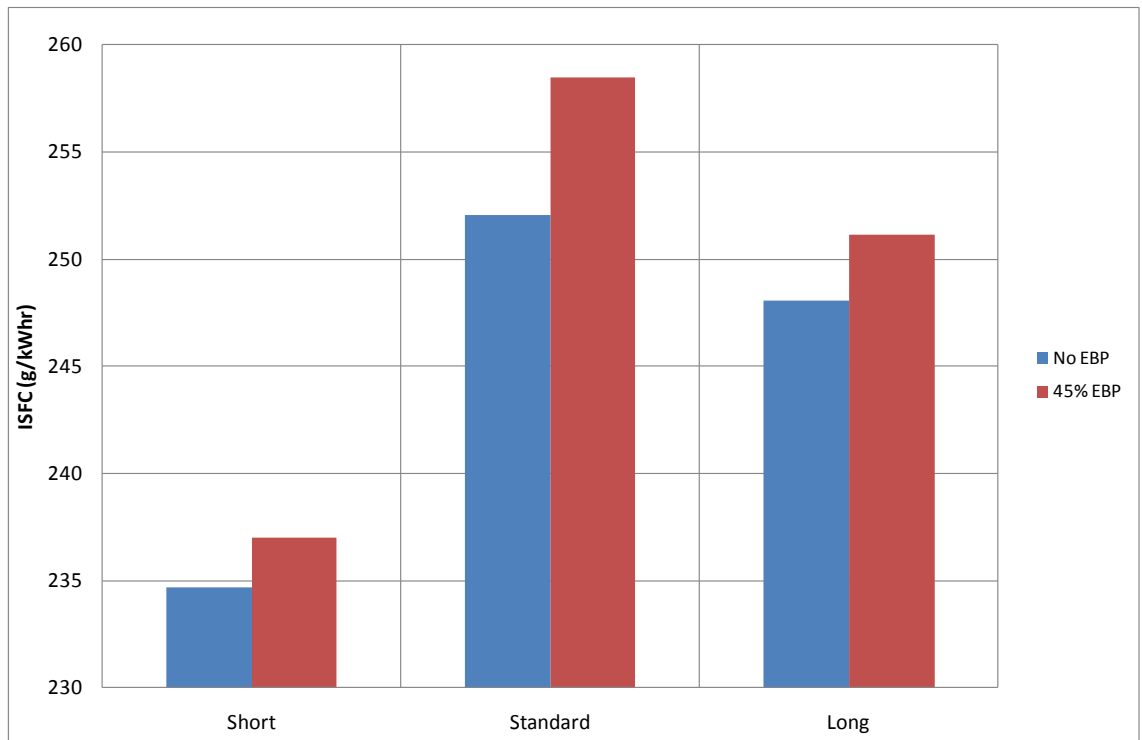


Figure 7.32 2000rpm, 15 bar BMEP ISFC Comparison for Short, Standard and Long Cams at 2 EBPs

Although the absolute ISFC benefit afforded by the long cam is similar in magnitude at 15 bar BMEP and 24 bar BMEP, relative to the short cam it appears less effective at this load. Although 15 bar BMEP is quite a way down in load compared to 24 bar BMEP, it is still high enough for the test results to indicate the theoretical optimum cam timing is the actual optimum cam timing, which shows that the benefits offered by over-expansion are not outweighed by the problems associated with combustion instability.

The EBP can be seen to have very little effect here, the reason for this is 45% EBP valve closure corresponds to an EBP of approximately 1.2 bar abs which is considerably less than the 2 bar EBP applied to the 24 bar BMEP point.

A GT-Power analysis has confirmed that a small amount of charge scavenging still takes place at this load, however, the experimental test data shows no strong indication of this with only a minor increase in the HC emissions for the long cam in comparison to the short and standard cams.

7.5.2.1 EBP Effects

The presence of EBP has only a slight effect on the ISFC (Figure 7.26) but it can be seen to have a significant effect on the COV which drastically increases with EBP. This is most likely caused by an increase of MFB duration associated with increased residuals (Figure 7.29). The long cam is the only cam to exhibit this trend of longer combustion duration with increasing EBP, with the other 2 cams exhibiting faster combustion. Figure 7.27 shows that higher EBPs can afford the use of lower effective CRs with the short cam by inhibiting scavenging, however the optimum cam timings for ISFC for the short cam still do not match the theoretical optimum cam timings.

One such point where the increase in EBP has permitted the use of a lower effective CR is the 2000rpm, 24 bar BMEP point with the short cam. In spite of the increased in-cylinder pressure and temperature associated with higher EBPs the combustion phasing could be advanced to closer to MBT with an EBP of 2 bar than it

could with no EBP (Figure 7.30). This has yielded no benefit to ISFC however because of the reduced combustion stability associated with higher residual gas concentration.

Employing the EBP valve has also produced an effect similar to that shown in chapter 5 in that pressure waves in the exhaust can be seen to influence the in-cylinder pressure profile (on a CAD basis) as seen in Figure 7.33.

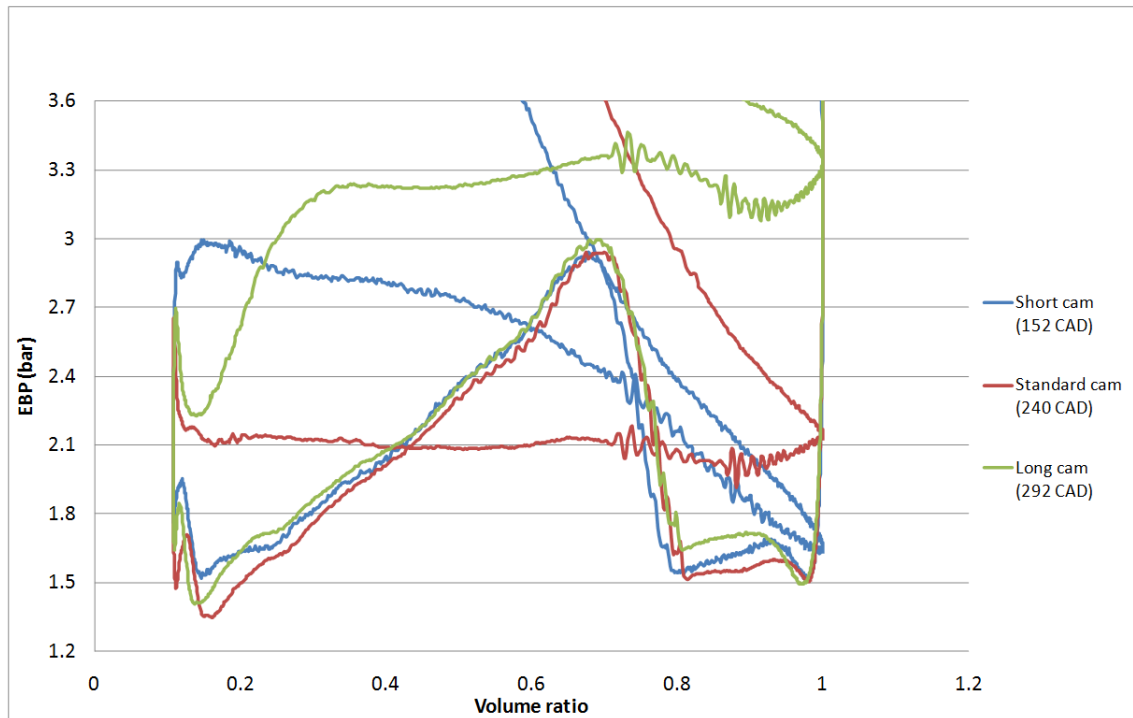


Figure 7.33 EBP Profile Comparison between Short, Standard and Long Cams with 2 bar Average EBP at 2000rpm and 24 bar BMEP

This has the effect of either reducing or increasing the pumping loop size depending on the MAP. This will have the most significant effect on the short cam because that is the only 1 of the 3 cams that is running with the maximum degree of valve overlap. The impact of this on the thermodynamic cycle is very hard to determine but an attempt has been made in the following section (section 7.5.2.2).

7.5.2.2 Analysis of the Individual Components of EIVC and LIVC

This section contains a breakdown of the individual components that cause an increase or decrease in the overall efficiency for both EIVC and LIVC in comparison to

the standard cam. The 24 bar BMEP point has been selected for analysis both with and without EBP.

The theoretical analysis is as shown in Figures 7.34 and 7.35 with no EBP and 2 bar EBP respectively.

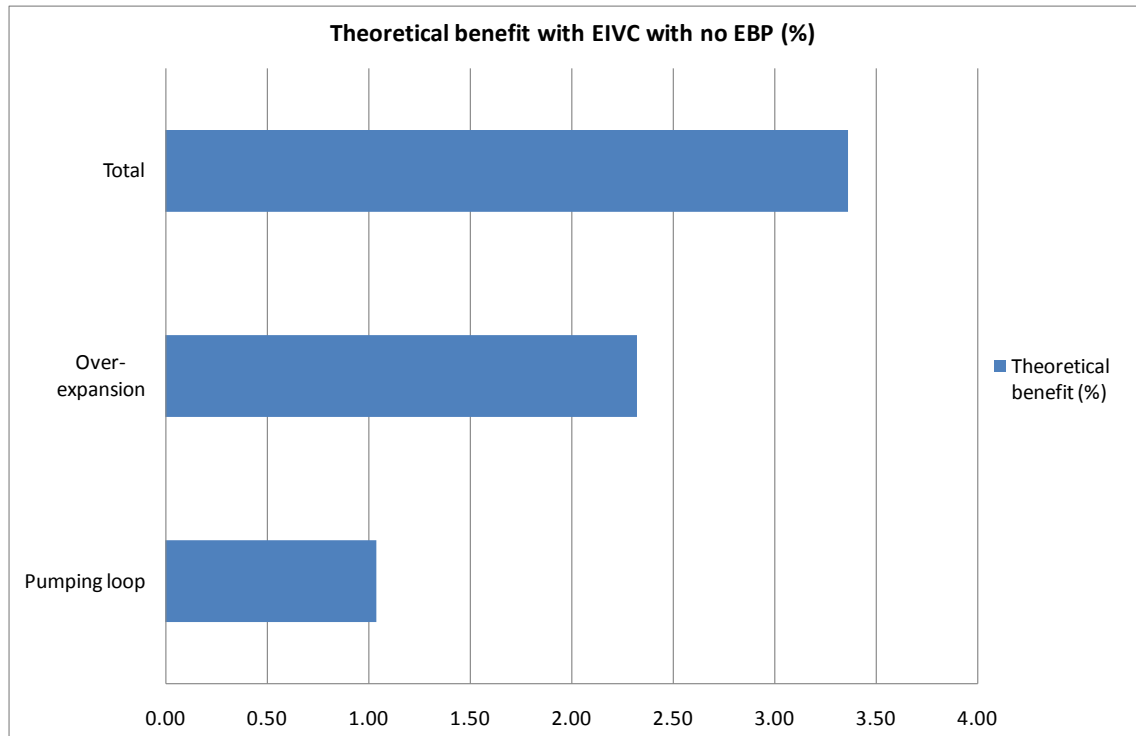


Figure 7.34 Theoretical Benefit with EIVC at 2000rpm and 24 bar BMEP with no EBP

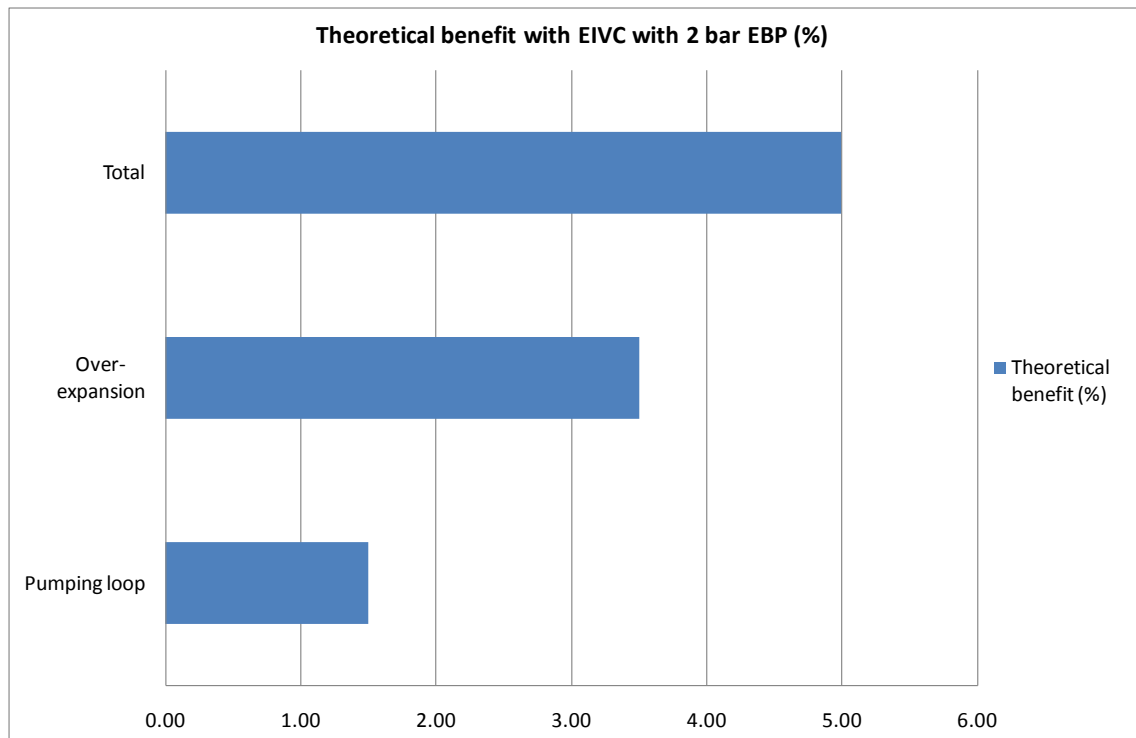


Figure 7.35 Theoretical Benefit with EIVC at 2000rpm and 24 bar BMEP with an EBP of 2 bar

The gain in efficiency predicted with the 2 bar EBP case over the no EBP case can be attributed to the fact the short cam can be phased 10 CAD closer to maximum valve overlap position with an EBP of 2 bar, as discussed in section 7.5.2.1. In the case of the experimental engine an efficiency benefit (relative to the standard cam) can be yielded by increasing the EBP. Figures 7.36 and 7.37 show the actual components and their impact on the cycle efficiency for the no EBP and 2 bar EBP cases respectively.

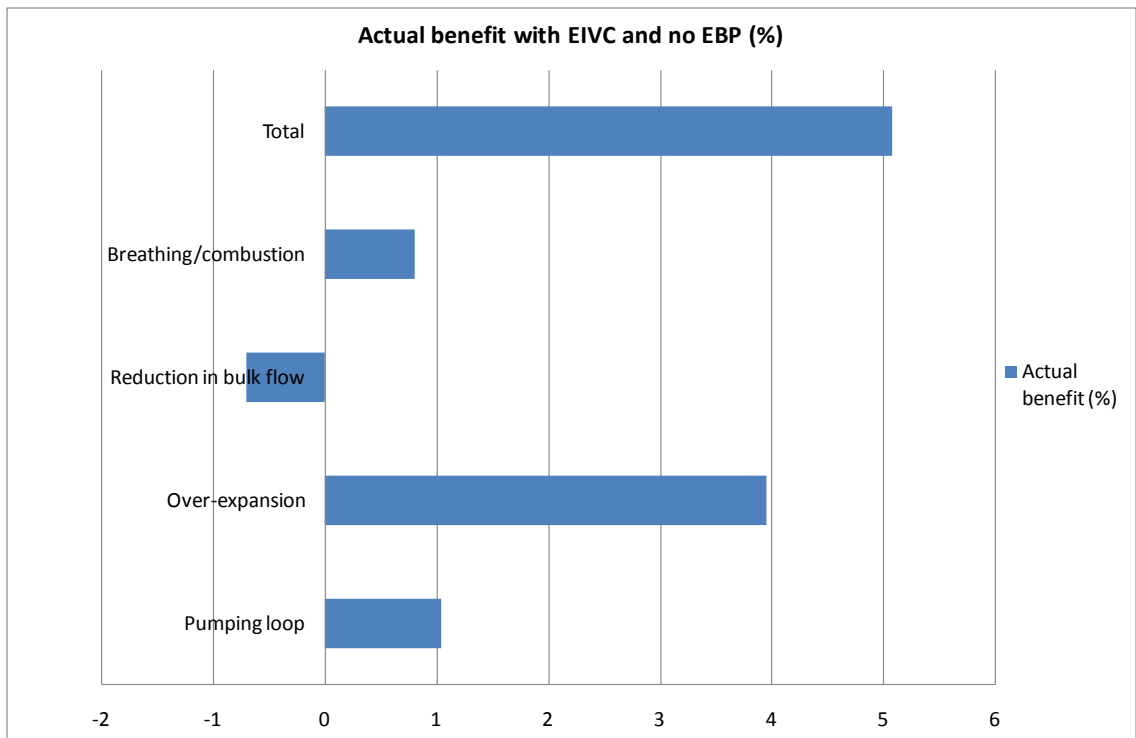


Figure 7.36 Actual Benefit with EIVC at 2000rpm and 24 bar BMEP with no EBP

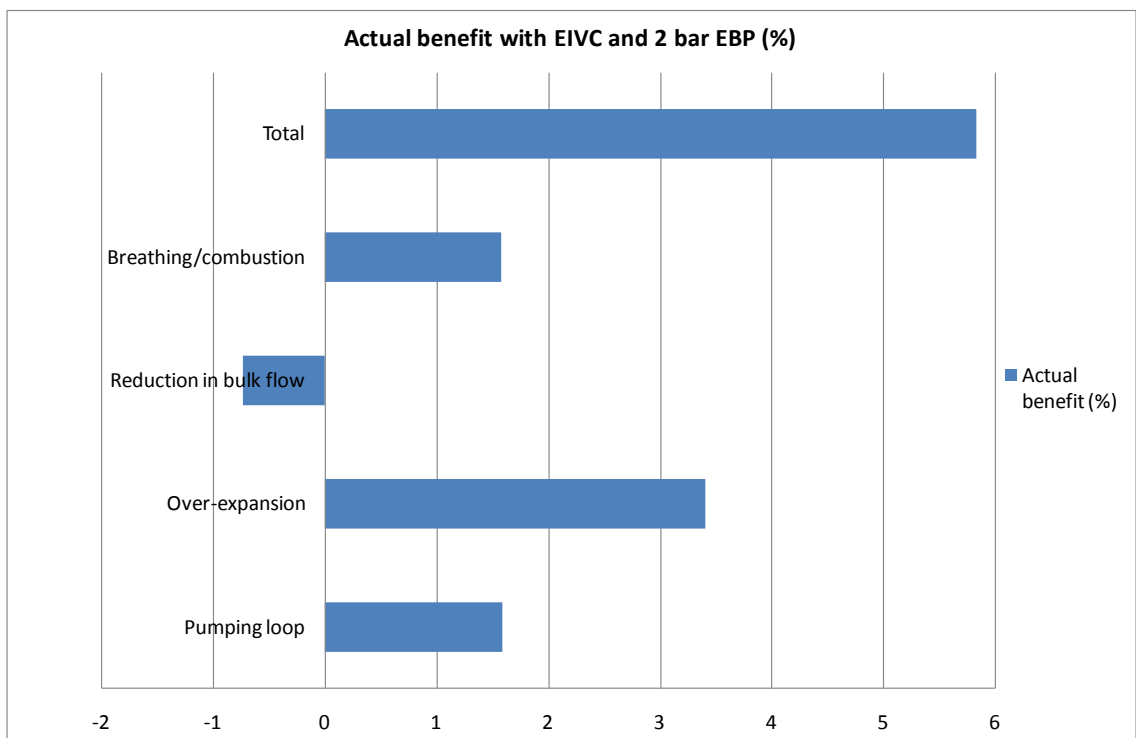


Figure 7.37 Actual Benefit with EIVC at 2000rpm and 24 bar BMEP and 2 bar EBP

The pumping loop and breathing/combustion components offer the majority of the improvement in performance when an EBP of 2 bar has been employed. The

breathing/combustion component refers to the influence of EOC pressure and temperature leading to a greater deal of spark advance, this was found to be of more importance than the reduction of bulk flow/increased MFB duration.

The over-expansion component can be seen to decrease in size slightly with increasing EBP. This is an indication that the exhaust temperature was elevated to a greater extent than expected by the increase in EBP.

Due to the tuning effects discussed in section 7.5.2.1 the theoretical benefit afforded by the reduced pumping loop size component with no EBP is not realised in practise. The pumping loop contribution can actually be seen to decrease with decreasing EBP.

The theoretical benefit offered by LIVC with an EBP of 2 bar is shown in Figure 7.38. The no EBP case has not been shown due to the fact the effective CR does not change, this therefore results in a negligible difference between both scenarios.

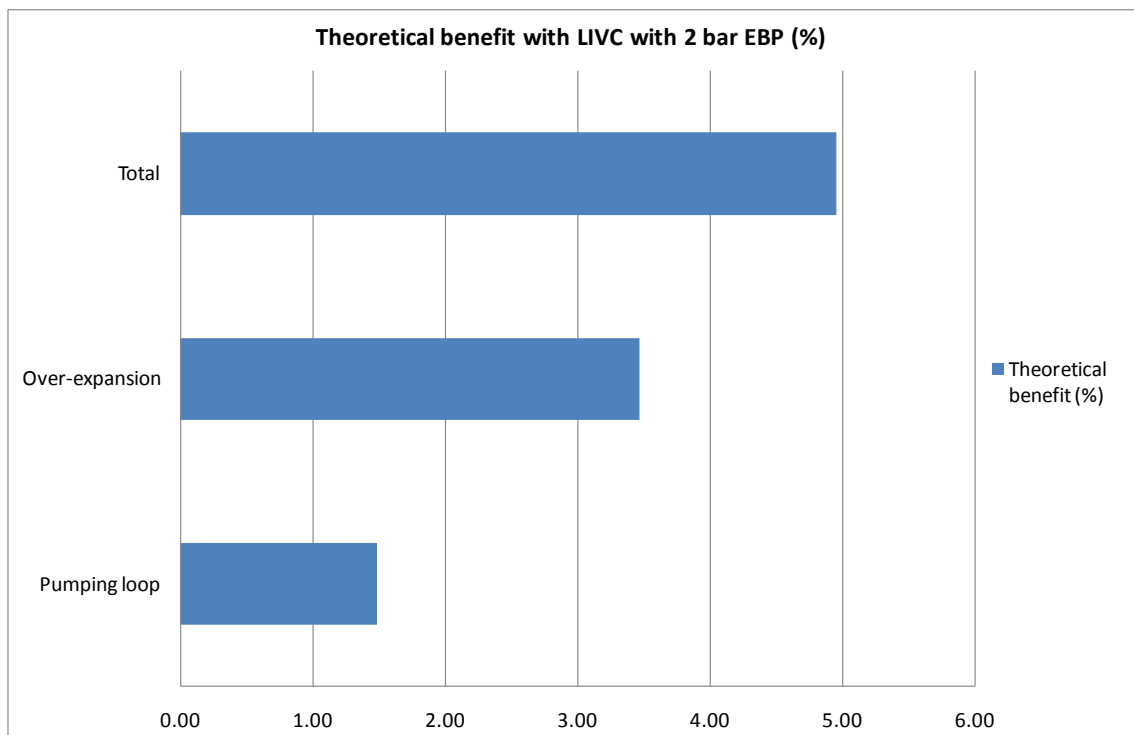


Figure 7.38 Theoretical Benefit with LIVC at 2000rpm and 24 bar BMEP with an EBP of 2 bar

This is not much different to the LIVC case due to the fact the effective CRs are almost the same for both cases. The actual benefits for the no EBP and the 2 bar EBP cases are shown in Figures 7.39 and 7.40.

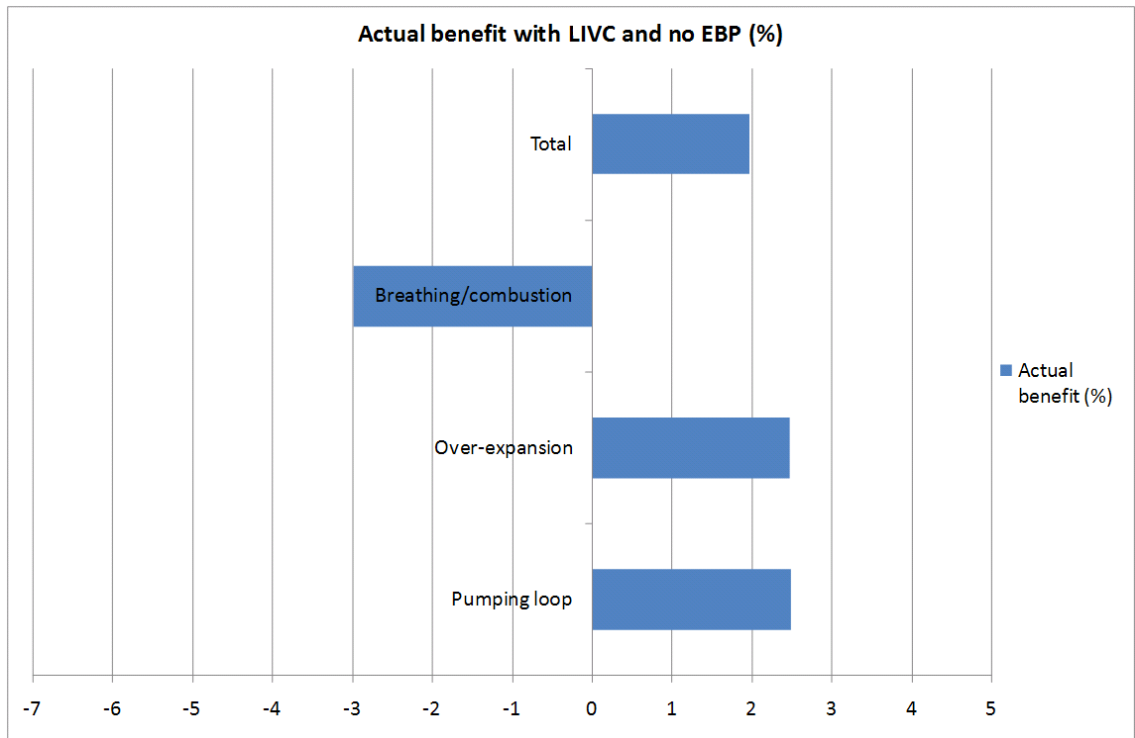


Figure 7.39 Actual Benefit with LIVC at 2000rpm and 24 bar BMEP with no EBP

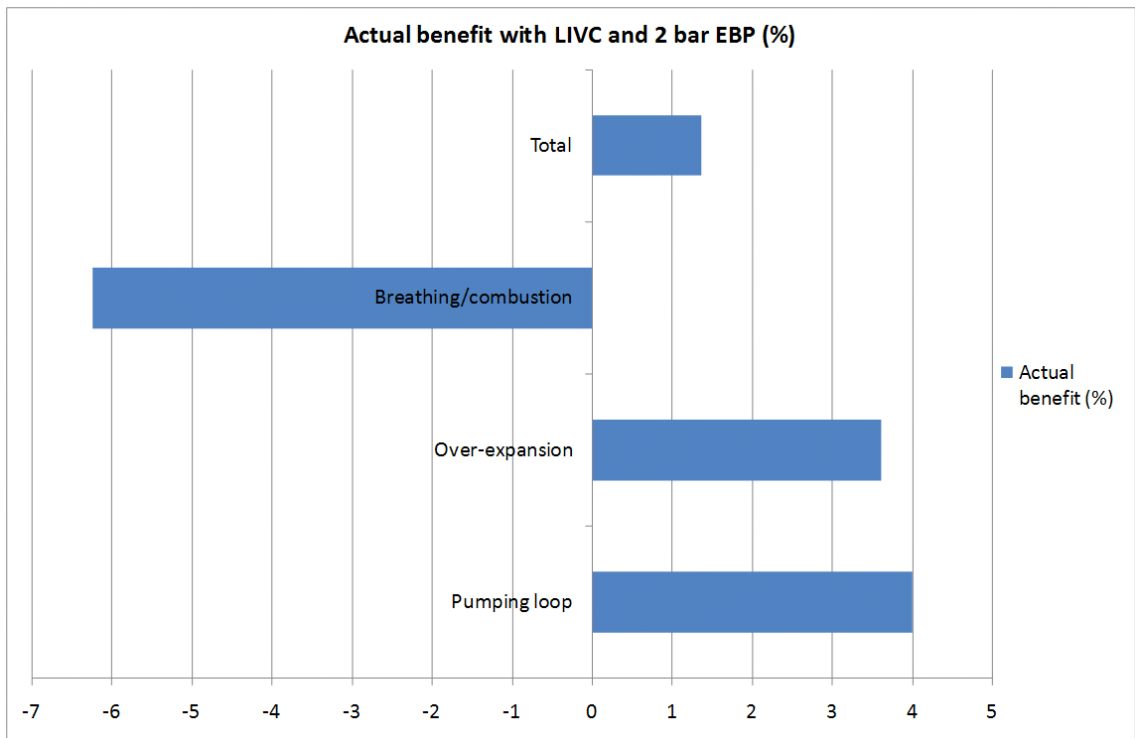


Figure 7.40 Actual Benefit with LIVC at 2000rpm and 24 bar BMEP with an EBP of 2 bar

The most noticeable difference between the 2 EBP cases is the size of the pumping loop which increases drastically with EBP. The breathing/combustion contribution can also be seen to increase dramatically with EBP. The

breathing/combustion issues worsen with increasing EBP which is somewhat contradictory. The reason why the breathing/combustion contribution is so large is because of the charge scavenging that takes place. At an EBP of 2 bar the ratio of MAP to EBP is lower so it would be logical to assume less charge scavenging will be taking place. The HC emissions obtained from this test work suggest that the degree of charge scavenging at 2 bar EBP is reduced compared to the no EBP case, GT-Power also suggests that less charge scavenging is taking place at 2 bar EBP.

The only other possible explanation is that an exhaust rarefaction wave during the brief valve overlap period is resulting in charge scavenging, and that the elevated exhaust gas temperature is causing the air/fuel mixture to combust before a sample reaches the exhaust gas analyser. As was the case previously though, not enough evidence exists to prove that this is happening.

7.5.2.3 Turbocharging/Supercharging Feasibility for Deep Miller

From the data obtained from both the GT-Power work and the experimental test work, the penalty to ISFC for running with turbocharger representative levels of EBP is not sufficient to justify supercharging, as this will almost certainly be less efficient.

There is however just argument for supercharging at some of the points tested because of the need to run at high MAPs even at relatively conservative loads. For instance Figure 7.15 reveals the MAPs required to run at the part load points. For some speeds the required MAP for 4 bar BMEP is exceeding 1 bar for both the short and long cams. Even at loads as low as this, at 4000rpm most turbochargers will be capable of providing very light boost as required, but at 1000rpm the mass flow rate of air through the turbine will be insufficient for even light boost.

There are turbochargers that can provide significant boost at 2000rpm and 24 bar BMEP however, it is unlikely that they will be able to achieve the required MAP of 3.5 bar abs, as is required for the long cam with 2 bar EBP.

The long cam generally had a greater need for high MAPs at low speeds and loads. The short cam on the other hand required elevated MAPs in comparison to the standard cam, but these generally did not exceed atmospheric pressure. For low speeds therefore LIVC will likely require some sort of supercharging/e-boosting system whereas EIVC is better suited to turbocharged applications.

LIVC also required higher MAPs than EIVC at higher loads too, as can be seen in Figure 7.41 for an engine speed of 2000rpm.

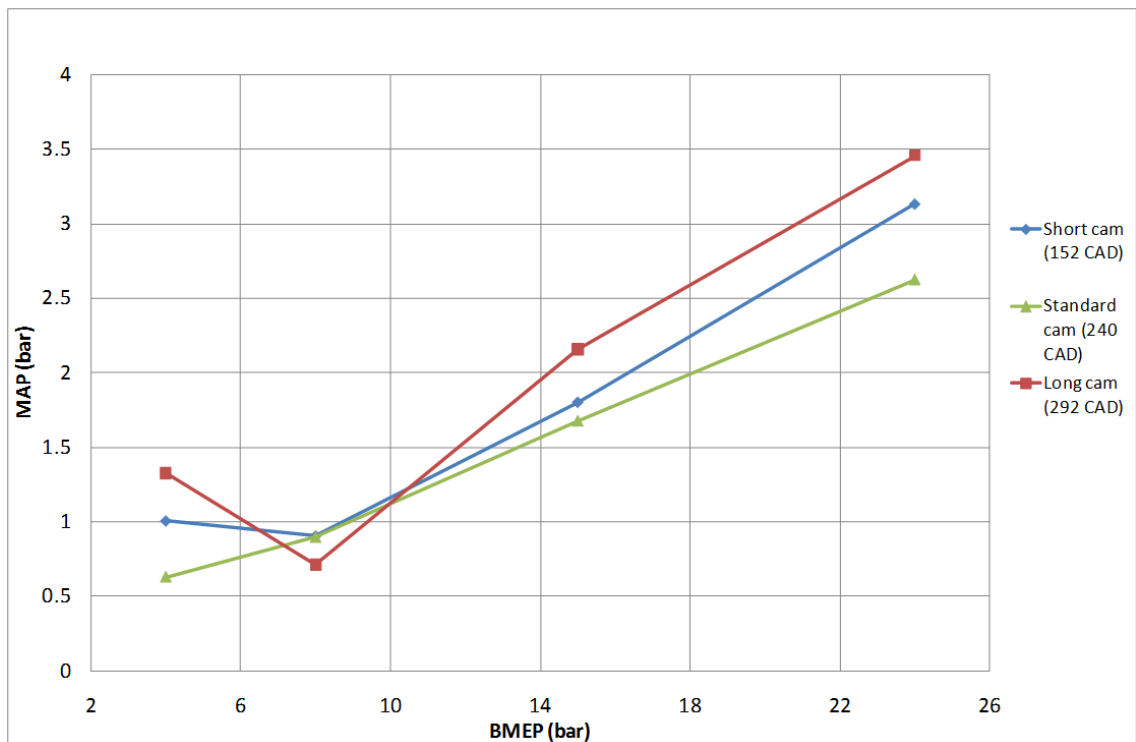


Figure 7.41 MAP Requirement Vs. BMEP for Short, Standard and Long Cams at an Engine Speed of 2000rpm

The reason for the higher MAP requirement is as mentioned previously, the definition of the intake valve close point is at 1mm lift, in reality the charge will not stop escaping to the manifold at 1mm lift thus reducing the effective CR to a level below that of the short cam.

7.5.3 Summary

EIVC was found to be the more effective strategy for reducing ISFC at every load and EBP condition tested. This benefit amounted to between 4.9 and 9% depending on the load point and EBP. LIVC also delivered a slight benefit at these elevated loads but it was a lot more conservative than that offered by EIVC and amounted to 1.1 to 2.9% depending on the load point and EBP.

The main reason for the modest increase in efficiency from LIVC is charge scavenging which was found to occur with very high MAP to EBP ratios. The impact of this on the cycle efficiency is very difficult to determine but ranged from 0.2% to 1.9% according to GT-Power simulations.

It is also suspected that the valve lift for the long cam might have benefitted from being reduced to promote more turbulence in the cylinder which would aid mixing. There was evidence of insufficient mixing apparent from the MFB duration data, the MFB duration was consistently longer than with the standard cam, this could be due to the bulk flow in the cylinder being destroyed as charge is expelled back into the intake during compression. There was also evidence of less mass being burned in total with LIVC, even though the 10-90% MFB duration was quite reasonable. It is suspected that this is due to in-cylinder accidental over enrichment caused by non-homogeneous charge being expelled to the intake during the compression stroke.

EIVC exhibited the longest MFB durations which are suspected to be the result of reduced bulk flow in the cylinder. The low lift valve is suspected to compensate for this somewhat by increasing the flow velocity through the valve, which will be converted into high amounts of TKE which will ensure good mixing.

Both EIVC and LIVC resulted in an increase in the COV of IMEP. At lower loads LIVC generally exhibited greater COV of IMEP values than EIVC and the standard cam. EIVC exhibited greater COV of IMEP values at higher loads than LIVC, LIVC was found to be similar to the standard cam.

The EBP valve is suspected to influence the results, particularly at the 2 bar EBP points where the blowdown pulse could be seen to bounce between the EBP valve and the engine. The exact impact of this on engine performance is very difficult to gauge but comparing the data with the EBP valve with the data with no EBP indicates that the effect is not massively significant.

Although both the long and short cams were selected to give similar ranges of effective CR reduction through equal degrees of LIVC and EIVC respectively. The maximum degree of LIVC will always be slightly greater than the maximum degree of EIVC because the effective CR was calculated at the 1mm lift point. In reality air/charge will continue to flow beyond these points. The error this has resulted in could not be calculated due to the presence of pressure waves and ram air effects distorting how much air is actually trapped in the cylinder at the point of valve closure.

Chapter 8

Summary and Conclusions

8.1 Introduction

This thesis contains a thorough and in-depth exploration of both low and high load Miller cycle processes on a modern aggressively downsized engine. A Ricardo Hydra based single cylinder experimental engine with a 3 cylinder head from a Mahle downsized DI gasoline engine was designed and commissioned. Its performance was analysed both thermodynamically and analytically across the speed and load range of the engine. The Miller cycle process was applied successfully and at loads that were hitherto untested and/or unpublished in the public domain.

Both a thermodynamic and an analytical comparison were made between the single cylinder experimental engine, the single cylinder model and the Mahle 3 cylinder engine (using a 3 cylinder model developed by Mahle Powertrain and baseline data acquired by Mahle Powertrain to assist). The differences in key performance criteria such as efficiency, engine breathing, autoignition propensity and effective exhaust back pressures were identified and analysed.

An analytical analysis of “Deep Miller” was carried out in a one-dimensional GT-Power model, and the impact of EIVC and LIVC strategies at speeds of 1000, 2000 and 5000rpm and loads of 14, 24 and 24 bar BMEP respectively were assessed. A thorough analysis of the trends in the results was also carried out. Analysis of the maximum load

that could be obtained was also carried out to obtain an estimate of the performance benefit that could be expected when running with the Miller cycle at high load.

In engine experiments both EIVC (152 CAD duration cam) and LIVC (292 CAD duration cam) operating regimes were tested with a VVT system applied to both intake and exhaust cams, and the cams swept across their entire ranges of operation. Extensive test work with the standard cam was carried out to provide a suitable comparison. An exhaust back pressure valve was applied to both the experimental and analytical engine to simulate a turbocharger, and an intake heater applied to ensure the incoming air temperature was at turbocharger representative levels.

Further test work was carried out into autoignition and “superknock” tendency in an effort to better understand the causes of autoignition and why it is so prevalent on the single cylinder engine in comparison to the 3 cylinder engine.

8.2 Analytical Study of Deep Miller

The impact of Deep Miller was assessed using a DoE based test plan which allowed the assessment of other variables such as intake cam timing, exhaust back pressure and geometric compression ratio too. Three DoEs were carried out at different speeds to assess the increase in boosting requirement at low speed, the autoignition imposed limitations at low to medium speeds and the fuel enrichment requirement at high speed.

Both EIVC and LIVC were observed to offer a benefit over the baseline case but the extent of the EIVC and LIVC that could be employed were both constrained by various factors. A great deal of scavenging was observed to take place with EIVC due to the fact the intake manifold pressure had to be elevated considerably over the baseline case. This was found to be an issue in particular for EIVC because the effective compression ratio is lowest (the optimum position) when the short cam is in the maximum valve overlap position. Scavenging, though good for exhaust gas

temperature reduction and purging the cylinder of residuals, resulted in accidental over enrichment of the charge in the cylinder which elevated ISFC considerably.

It was discovered that if the engine management system is capable of compensating for this scavenging and maintaining a stoichiometric charge in the cylinder, EIVC resulted in a 5.3% improvement in thermal efficiency compared to a maximum of 3% for LIVC at realistic exhaust back pressures. With no compensation applied the optimum strategy for fuel economy varied depending on speed, load, and very much so on exhaust back pressure. In almost all of the 1000rpm and 2000rpm cases moderate LIVC was found to be the optimum strategy and yielded a maximum benefit of up to 7% at very elevated exhaust back pressures. EIVC was hindered by excessive scavenging leading to accidental enrichment.

At 5000rpm the maximum extent of EIVC was favoured due to the fact that fuel enrichment was required to regulate the exhaust gas temperature, which makes the fact it was occurring by accident academic. The maximum benefit achieved over the standard baseline cam was 3.2%.

It was also found that the engine was highly sensitive to geometric compression ratio, particularly for cams that exhibited very low effective compression ratio reduction. For some exhaust back pressures an increase in geometric compression ratio was beneficial to thermal efficiency, but only for extreme EIVC and LIVC cases. This gain in efficiency peaked at 5.8% and was typically greater at lower exhaust back pressures.

The potential to increase maximum engine load using Deep Miller was explored. LIVC was found to offer the greatest increase in load. The greatest increase at higher exhaust back pressures was obtained with the longest (most extreme LIVC) cam but the moderate LIVC cam was found to be optimal for the lower EBP cases. The most extreme EIVC and LIVC cams were greatly limited by the peak intake manifold pressure however. This was not such a constraint at lower speeds but at 5000rpm the maximum load obtained with extreme LIVC was lower than that obtained with the moderate LIVC cam by virtue of the fact that the volumetric efficiency of the extreme LIVC cam was the bottleneck. The maximum load increase at turbocharger

representative levels of exhaust back pressure was 1.3% at 1000rpm, 12.3% at 2000rpm and 1.7% at 5000rpm.

8.3 Experimental Engine Study of Miller Cycle

The effect of both EIVC and LIVC was assessed at numerous points over the speed and load map, and hydrocarbon and NO_x emissions were both recorded in order to gain an understanding of the impact of Miller cycle on emissions performance.

At low load EIVC was found to give thermal efficiency benefits for every single low speed point of up to 7.2% over the baseline cam. LIVC however exhibited lower thermal efficiency than the standard baseline cam at all low load points with the exception of the 1000rpm points. The reduction of thermal efficiency was found to be up to 7.1% with LIVC.

It was found that the unexpected result with LIVC could be attributed to the breathing behaviour of the single cylinder experimental engine. An analytical analysis of the same test points revealed that the long cam (LIVC) had a considerably higher residual gas concentration than the equivalent EIVC point. It is also suspected that exhaling charge into the intake manifold had a detrimental effect on thermal efficiency.

The PMEP component was found to be greatly reduced for both EIVC and LIVC strategies. The PMEP component for EIVC was found to be minimised in size considerably, however, the pumping component for LIVC was generally less than that of the standard cam baseline, but its contribution to the overall cycle was much higher than with EIVC. At low speeds the PMEP component for LIVC was found to be negative and actually contributed work to the cycle from loads as low as 8 bar BMEP. This work contribution was as high as 4.7% to the entire (net) cycle at low speed.

The effect of Miller cycle at low speed and high load operations was also assessed and it was found that both EIVC and LIVC resulted in a thermal efficiency increase over the standard cam baseline. EIVC was found to give a greater efficiency

benefit of 6% at 24 bar BMEP and 8.8% at 15 bar BMEP, while LIVC gave an efficiency benefit of 1.3% at 24 bar BMEP and 2.8% at 15 bar BMEP, both were at turbocharger representative levels of exhaust back pressure.

The limited benefit offered by LIVC was attributed to increased rates of charge scavenging which were confirmed both by hydrocarbon emissions and in an analytical study. It was discovered that the intake port temperature was massively elevated (up to 90°C) beyond anything reported in the literature.

Both EIVC and LIVC strategies exhibited greater COV of IMEP values in comparison to the standard cam baseline point, even at loads as high as 24 bar BMEP. The COV of IMEP showed a dramatic increase when exhaust back pressure was applied. It was discovered that the exhaust back pressure valve created considerable pressure waves within the exhaust system that resulted in a pressure wave reaching the cylinder at the valve overlap point, it is suspected that this may have had an adverse affect on the COV of IMEP values obtained.

The mass fraction burn rate for EIVC and LIVC were longer than with the standard baseline cam. EIVC exhibited the longest mass fraction burn duration, which indicates that reduced charge motion is still an issue, even at very high loads, but that its effect on thermal efficiency was minimal.

A summary of the different components that led to an increase in thermal efficiency was also carried out. Two studies were carried out, one assessing the theoretical benefits that should be yielded and the other showing the actual benefits that were yielded based on thermodynamic and analytical data. The loss of thermodynamic efficiency due to combustion was found to be considerable for both EIVC and LIVC (up to 5.1% and 9.2% respectively) while the loss of thermodynamic efficiency due to a lack of bulk flow with EIVC was relatively small in comparison (0.5%).

8.4 Recommendations for Future Work

This study has investigated the use of the Miller cycle at both low and high loads, the first study of its kind. It has revealed that the Miller cycle, particularly EIVC shows great high load potential. LIVC showed some potential but was hindered by the engine breathing dynamics of the single cylinder experimental engine, and it would be unfair to rule it out as a result of this study. It would be a worthwhile investment of time to optimise the intake and exhaust tuning for LIVC for future work and perhaps trying both strategies on the 3 cylinder engine.

Deep Miller appears to be a very viable future technology for increased fuel efficiency from the analytical work and experimental work carried out in this study. Whilst it is perhaps not a good idea to increase the boost pressure ceiling beyond 4 bar abs for near term future work at this moment in time, it would be useful to assess the experimental benefits of Deep Miller at more speeds such as at 1500rpm and 5000rpm.

It would also be beneficial to test different piston geometries in future work such as different geometric compression ratios and piston bowls designed to give more turbulence and tumble motion, mainly for the benefit of EIVC. Valve deactivation almost certainly is not feasible with EIVC with Deep Miller, but may be feasible with LIVC. This is another avenue that could potentially be explored in future work. With the current state of tune of the single cylinder engine, full load EGR is likely not viable, the residual gas concentration for LIVC has been seen to have a very detrimental impact on thermal efficiency and EGR will likely exacerbate this problem.

References

- [1] Smil, V., "The Two Prime Movers of Globalization: History and Impact of Diesel Engines and Gas Turbines", *Journal of Global History* 2, pp 373-394, 2007.
- [2] Zhao, H., "Advanced Direct Injection Combustion Engine Technologies and Development Volume 1: Gasoline and Gas Engines", Woodhead Publishing Limited, 2009.
- [3] Clean Air Act 1956, 4 & 5 Eliz.2 Ch. 52, Parliament of the United Kingdom, 1956.
- [4] GT-SUITE V6.1.0, Gamma Technologies Inc, Westmont, Illinois, 2004.
- [5] Fuglestedt, J., Bernsten, T., Myhre, G., Rypdal, K., Skeie, R.B., "Climate Forcing from the Transport Sectors", *Proceedings of the National Academy of Sciences*, Vol. 105, No. 2, pp 454-458, 2008.
- [6] "EU Transport in Figures: Statistical Pocketbook 2011", European Commission, 2011.
- [7] "World Oil Outlook 2011", Organization of the Petroleum Exporting Countries (OPEC), 2011.
- [8] Regulation (EC) No 443/2009 of the European Parliament and of the Council of 23 April 2009 Setting Emission Performance Standards for New Passenger Cars as Part of the Community's Integrated Approach to Reduce CO₂ Emissions from Light-Duty Vehicles (Text with EEA Relevance), 2009.
- [9] Proposal 2012/0190 (COD) for a Regulation of the European Parliament and of the Council Amending Regulation (EC) No 443/2009 to Define the Modalities for Reaching the 2020 Target to Reduce CO₂ Emissions from New Passenger Cars, 2012.
- [10] "Worldwide Emissions Standards: Passenger Cars and Light Duty Trucks", Delphi, 2012.
- [11] Regulation (EC) No 715/2007 of the European Parliament and of the Council of 20 June 2007 on Type Approval of Motor Vehicles with Respect to Emissions from Light Passenger and Commercial Vehicles (Euro 5 and Euro 6) and on Access to Vehicle Repair and Maintenance Information (Text with EEA Relevance), 2007.
- [12] US EPA Clean Air Act Title II Part A – Motor Vehicle Emission and Fuel Standards, 1990.

- [13] US EPA Control of Air Pollution from Motor Vehicles: Tier III Motor Vehicle Emission and Fuel Standards, 2011.
- [14] California Exhaust Emissions Standards and Test Procedures for 2001 Through 2014 Model Criteria Pollutant Exhaust Emissions Standards and Test Procedures and 2009 Through 2016 Model Greenhouse Gas Exhaust Emission Standards and Test Procedures for Passenger Cars, Light-duty Trucks and Medium-duty Vehicles, California Environmental Protection Agency Air Resources Board (CARB), 1999.
- [15] Lyons, J. M., Carlson, T. R., Austin, T. C., "Evaluation of California Greenhouse Gas Standards and Federal Energy Independence and Security Act – Part 1: Impacts on New Vehicle Fuel Economy", SAE Paper 2008-01-1852, 2008.
- [16] Air Pollution Control Law Chapter III, Ministry of the Environment, Government of Japan, 1996.
- [17] Resolution No 415 of 24 September 2009, Conama 415/2009, Federal Government of Brazil, 2009.
- [18] "Gasoline and Diesel Fuel Update", U.S. Energy Information Administration, 2012.
- [19] Bolton, P., "Petrol and Diesel Prices", House of Commons Library, 2012.
- [20] Sher, E., "Handbook of Air Pollution from Internal Combustion Engines: Pollutant Formation and Control", Academic Press, 1998.
- [21] Heywood, J. B., "Internal Combustion Engine Fundamentals", McGraw Hill, 1988.
- [22] Cole, R. L., Poola, R. B., Sekar, R., "Exhaust Emissions of a Vehicle with a Gasoline Direct-injection Engine", SAE Paper 982605, 1998.
- [23] Harrington, J. A. and Shishu, R. C., "A Single Cylinder Study of the Effects of Fuel Type, Fuel Stoichiometry, and Hydrogen to Carbon Ratio and CO, NO and HC Exhaust Emissions", SAE Paper 730476, 1973.
- [24] Shimotani, K., Oikawa, K., Horada, O., Kagawa, Y., "Characteristics of Gasoline In-cylinder Direct Injection Engine", Proceedings of the Internal Combustion Engine Symposium – Japan, 1995.
- [25] Bowman, C. T., "Kinetics of Pollutant Formation and Destruction in Combustion", Progress in Energy and Combustion Science, Vol. 1, pp 33-45, 1975.
- [26] Johnson, G. L., Caretto, L. S., Starkman, E. S., "The Kinetics of CO Oxidation in Reciprocating Engines", The Combustion Institute Spring Meeting, 1970.
- [27] Zhao, F., Lai, M. C., Harrington, D. L., "The Spray Characteristics of Automotive Port Fuel Injection – A Critical Review", SAE Paper 950506, 1995.

- [28] Daniel, W. A., "Flame Quenching at the Walls of an Internal Combustion Engine", Proceedings of the Sixth International Symposium on Combustion, 1957.
- [29] Wentworth, J. T., "The Piston Crevice Volume Effect on Exhaust Hydrocarbon Emission", Combustion Science and Technology, Vol. 4, pp 97-100, 1971.
- [30] Stone, R., "Introduction to Internal Combustion Engines", Third Edition, Palgrave Macmillan, 1999.
- [31] Miller, J.A. and Bowman, C. T., "Mechanism and Modelling of Nitrogen Chemistry in Combustion", Progress in Energy and Combustion Science, Vol. 15, pp 287-338, 1989.
- [32] Zeldovich, Y. B., "The Oxidation of Nitrogen in Combustion and Explosions", Acta Physiochim URRS, Vol. 21, pp 577-628, 1947.
- [33] Lavoie, G. A., Heywood, J. B., Keck, J. C., "Experimental and Theoretical Study of Nitric Oxide Formation in Internal Combustion Engines", Combustion Science and Technology, Vol. 1, pp 313-326, 1970.
- [34] Komiyama, K. and Heywood, J. B., "Predicting NO_x Emissions and Effects of Exhaust Gas Recirculation in Spark-ignition Engines", SAE Paper 730475, 1973.
- [35] Kummer, J. T., "Catalysts for Automobile Emission Control", Progress in Energy and Combustion Science, Vol. 6, pp 177-199, 1981.
- [36] Helms, H., Pehnt, M., Lambrecht, U., Liebich, A., "Electric Vehicle and Plug-in Hybrid Energy Efficiency and Life Cycle Emissions", Eighteenth International Symposium Transport and Air Pollution, Session 3: Electro and Hybrid Vehicles, 2010.
- [37] Thomas, C. E., "Fuel Cell and Battery Electric Vehicles Compared", International Journal of Hydrogen Energy, Vol. 34, pp 6005-6020, 2009.
- [38] Plotkin, S., Santini, D., Vyas, A., Anderson, J., Wang, M., He, J., Bharathan, D., "Hybrid Electric Vehicle Technology Assessment: Methodology, Analytical Issues, and Interim Results", Centre for Transportation Research, Argonne National Laboratory, ANL/ESD/02-2, 2001.
- [39] Bassett, M. D., Hall, J., Darkes, D., Fraser, N. A. J., Warth, M., "Design and Development of a Dedicated Range Extender Engine", Internal Combustion Engines: Improving Performance, Fuel Economy and Emissions, Institute of Mechanical Engineers, 2011.
- [40] Lee, C. Y., Zhao, H., Ma, T., "Analysis of a Cost Effective Air Hybrid Concept", SAE Paper 2009-01-1111, 2009.

- [41] Schwarz, C., Schünemann, E., Durst, B., Fischer, J., Witt, A., “Potentials of the Spray-guided BMW DI Combustion System”, SAE Paper 2006-01-1265, 2006.
- [42] Missy, S., Schwarz, C., Schünemann, E., “Brennverfahrensentwicklung am Beispiel der Neuen BMW Sechs – Und Vierzylinder Ottomotoren mit High Precision Injection und Schichtbrennverfahren”, Direkteinspritzung im Ottomotor IV, 2007.
- [43] Lake, T., Stoke, J., Murphy, R., Osborne, R., Schamel, A., “Turbocharging Concepts for Downsized DI Gasoline Engines”, SAE Paper 2004-01-0036, 2004.
- [44] Zhao, H., Li, J., Ma, T., Ladommatos, N., “Performance and Analysis of a 4 Stroke Multi-cylinder Gasoline Engine with CAI Combustion”, SAE Paper 2002-01-0420, 2002.
- [45] Osborne, R. J., Li, G., Sapsford, S. M., Stoke, J., Lake, T. H., Heikal, M. R., “Evaluation of HCCI for Future Gasoline Powertrains”, SAE Paper 2003-01-0750, 2003.
- [46] Cairns, A., Blaxill, H., Irlam, G., “Exhaust Gas Recirculation for Improved Part and Full Load Fuel Economy in a Turbocharged Gasoline Engine”, SAE Paper 2006-01-0047, 2006.
- [47] Friedfeldt, R., Zenner, T., Ernst, R., Fraser, A., “Three-cylinder Gasoline Engine with Direct Injection”, ATZ Autotechnology, Vol. 12, No. 2, 2012.
- [48] Hancock, D., Fraser, N., Jeremy, M., Sykes, R., Blaxill, H., “A New 3 Cylinder 1.2l Advanced Downsizing Technology Demonstrator Engine”, SAE Paper 2008-01-0611, 2008.
- [49] <http://www.mce-5.com/english/index.html> accessed on 24/11/2012 (see appendix A.5).
- [50] Turner, J., Pearson, R., Luard, N., “Investigation of Appropriate Technologies for a Highly-downsized DISI Engine”, Engine Downsizing Conference, Institute of Mechanical Engineers, 2011.
- [51] Lumsden, G., OudeNijeweme, D., Fraser, N., Blaxill, H., “Development of a Turbocharged Direct Injection Downsizing Demonstrator Engine”, SAE Paper 2009-01-1503, 2009.
- [52] <http://en.wikipedia.org/wiki/Twincharger/> accessed 23/11/2012 (see appendix A.5).
- [53] Copeland, C., Martinex-Botas, R., Turner, J., Pearson, R., Luard, N., Carey, C., Richardson, S., Di Martino, P., Chobola, P., “Boost System Selection for a Heavily Downsized Spark Ignition Prototype Engine”, Tenth IMechE International Conference on Turbochargers and Turbocharging, 2012.

- [54] Fraser, N. and Bassett, M., "Extreme Engine Downsizing with a Single Turbocharger – 100kW/l and 30 bar BMEP", Engine Downsizing Conference, Institute of Mechanical Engineers, 2011.
- [55] Fraser, N., Blaxill, H., Lumsden, G., Bassett, M., "Challenges for Increased Efficiency Through Gasoline Engine Downsizing", SAE Paper 2009-01-1053, 2009.
- [56] Amann, M., Alger, T., Mehta, D., "The Effect of EGR on Low-speed Pre-ignition in Boosted SI Engines", SAE Paper 2011-01-0339, 2011.
- [57] Anderson, M. K., Assanis, D. N., Filipi, Z. S., "First and Second Law Analyses of a Naturally-aspirated, Miller Cycle, SI Engine with Late Intake Valve Closure", SAE Paper 980889, 1998.
- [58] Miller, R., "Supercharging and Internal Cooling Cycle for High Output", Oil and Gas Power Division Proceedings of the National Conference, ASME 46-OGP-4, pp 1-5, 1946.
- [59] <http://world.honda.com/powerproducts-technology/exlink/> accessed 23/11/2012 (see appendix A.5).
- [60] Kapus, P. E., Denger, D., Holland, T., "Intelligent Simplification – Ways Towards Improved Fuel Economy", SAE Paper 2002-01-0236, 2002.
- [61] Stansfield, P. A., Wigley, G., Garner, C. P., Patel, R., Ladommatos, N., Pitcher, G., Turner, J. W. G., Nuglisch, H., Helie, J., "Unthrottled Engine Operation using Variable Valve Actuation: The Impact on the Flow Field, Mixing and Combustion", SAE Paper 2007-01-1414, 2007.
- [62] Stansfield, P. A., Wigley, G., Garner, C. P., Patel, R., Ladommatos, N., Pitcher, G., Turner, J. W. G., Nuglisch, H., "Comparison Between Unthrottled, Single and Two-valve Induction Strategies Utilising Direct Gasoline Injection: Emissions, Heat-release and Fuel Consumption Analysis", SAE Paper 2008-01-1626, 2008.
- [63] Battistoni, M. and Mariani, F., "Fluid Dynamic Study of Unthrottled Part Load SI Engine Operations with Asymmetric Valve Lifts", SAE Paper 2009-24-0017, 2009.
- [64] Taylor, J., Fraser, N., Dingelstadt, R., Hoffmann, H., "Benefits of Late Inlet Valve Timing Strategies Afforded Through the Use of Intake Cam in Cam Applied to a Gasoline Turbocharged Downsized Engine", SAE Paper 2011-01-0360, 2011.
- [65] Moore, W., Foster, M., Lai, M. C., Xie, X. B., Zheng, Y., Matsumoto, A., "Charge Motion Benefits of Valve Deactivation to Reduce Fuel Consumption and Emissions in a GDI, VVA Engine", SAE Paper 2011-01-1221, 2011.

- [66] Matsumoto, A., Zheng, Y., Xie, X., Lai, M. C., Moore, W., "Interactions of Multi-hole DI Sprays with Charge Motion and Their Implications to Flexible Valve-trained Engine Performance", SAE Paper 2011-01-1883, 2011.
- [67] Cleary, D. and Silvas, G., "Unthrottled Engine Operation with Variable Intake Valve Lift, Duration, and Timing", SAE Paper 2007-01-1282, 2007.
- [68] Sellnau, M., Kunz, T., Sinnamon, J., Burkhard, J., "2-step Variable Valve Actuation: System Optimization and Integration on an SI Engine", SAE Paper 2006-01-0040, 2006.
- [69] Turner, J. W. G., Pitcher, G., Burke, P., Garner, C. P., Wigley, G., Stansfield, P., Nuglisch, H., Ladommatos, N., Patel, E., Williams, P., "The HOTFIRE Homogeneous GDI and Fully Variable Valve Train Project – An Initial Report", SAE Paper 2006-01-1260, 2006.
- [70] Hara, S., Nakajima, Y., Nagumo, S. I., "Effects of Intake-valve Closing Timing on Spark-ignition Engine Combustion", SAE Paper 850074, 1985.
- [71] Akihisa, D. and Sawada, D., "Research on Improving Thermal Efficiency Through Variable Super-high Expansion Ratio Cycle", SAE Paper 2010-01-0174, 2010.
- [72] Sellnau, M. and Rask, E., "Two-step Variable Valve Actuation for Fuel Economy, Emissions, and Performance", SAE Paper 2003-01-0029, 2003.
- [73] Lee, K., Bae, C., Kang, K., "The Effects of Tumble and Swirl Flows on Flame Propagation in a Four-valve S.I. Engine", Applied Thermal Engineering, Vol. 27, pp 2122-2130, Elsevier, 2007.
- [74] Hitomi, M., Sasaki, J., Hatamura, K., Yano, Y., "Mechanism of Improving Fuel Efficiency by Miller Cycle and Its Future Prospect", SAE Paper 950974, 1995.
- [75] Ishizuki, Y., Shimizu, Y., Hikino, H., Kawashima, Y., "A New Type of Miller Supercharging System for High Speed Engines Part 2 – Realization of High BMEP Diesel Engines", SAE Paper 851523, 1985.
- [76] Kamo, R., Mavinahally, N. S., Bryzik, W., Reid, M., "Emission Characteristics of a Turbocharged Multi-cylinder Miller Cycle Diesel Engine", United States of America Department of Energy, 1995.
- [77] Kado, T., Osaka, Y., Noguchi, T., Horimoto, K., Ogawa, M., Narita, H., "The Development of 1 MW Class Gas Engine and its Application to Cogeneration Systems", Technical Review, Vol. 45, No. 1, 2008.
- [78] <http://www.getransportation.com/rail/rail-products/locomotives/powerhaul-series-locomotive.html> accessed 23/11/2012 (see appendix A.5).

- [79] Sakai, H., Noguchi, H., Kawauchi, M., and Kanesaka, H., "A New Type of Miller Supercharging System for High-speed Engines - Part 1 Fundamental Considerations and Application to Gasoline Engines", SAE Paper 851522, 1985.
- [80] Goto, T., Hatamura, K., Takizawa, S., Hayama, N., Abe, H., Kaneska, H., "Development of V6 Miller Cycle Gasoline Engine", SAE Paper 940198, 1994.
- [81] <http://www.edmunds.com/mazda/millenia/2002/features-specs.html> accessed 28/11/2012 (see appendix A.5).
- [82] Takabe, S., Hatamura, K., Kanesaka, H., Kurata, H., Iguchi, Y., Matsubara, H., "Development of the High Performance Lysholm Compressor for Automotive Use", SAE Paper 940843, 1994.
- [83] Ichimaru, K., Sakai, H., Kanesaka, H., Winterborne, D. E., "A Rotary Valve Controlled High Expansion Ratio Gasoline Engine", SAE Paper 940815, 1994.
- [84] Ueda, N., Sakai, H., Iso, N., Sasaki, J., "A Naturally Aspirated Miller Cycle Gasoline Engine – Its Capability of Emission, Power and Fuel Economy", SAE Paper 960589, 1996.
- [85] The Law Concerning Special Measures for Total Emission Reduction of Nitrogen Oxides from Automobiles in Specified Areas: Law No. 70 of 1992, Ministry of the Environment: Government of Japan, 1992.
- [86] Blakey, S. C., Saunders, R. J., Ma, T. H., Chopra, A., "A Design and Experimental Study of an Otto Atkinson Cycle Engine Using Late Intake Valve Closing", SAE Paper 910451, 1991.
- [87] Rabia, S. M. and Korah, N. S., "Knocking Phenomena in a Gasoline Engine with Late-intake Valve Closing", SAE Paper 920381, 1992.
- [88] Urata, Y., Umlyama, H., Shimizu, K., Fujiyoshi, Y., Sono, H., Fukuo, K., "A Study of Vehicle Equipped with Non-throttling S.I. Engine with Early Intake Valve Closing Mechanism", SAE Paper 930820, 1993.
- [89] Boggs, D. L., Hilbert, H. S., Schechter, M. M., "The Otto-atkinson Cycle Engine - Fuel Economy and Emissions Results and Hardware Design", SAE Paper 950089, 1995.
- [90] Theobald, M. A., Lequesne, B., Henry, R., "Control of Engine Loads via Electromagnetic Valve Actuators", SAE Paper 940816, 1994.
- [91] Tuttle, H., "Controlling Engine Load by Means of Late Intake Valve Closing", SAE Paper 800794, 1980.

- [92] Tuttle, H., "Controlling Engine Load by Means of Early Intake Valve Closing", SAE Paper 820408, 1982.
- [93] Ke, Y. and Pulcher, H., "Controlling the Load and the Boost Pressure of a Turbocharged SI Engine by Means of Early Intake-valve Closing", SAE Paper 960588, 1996.
- [94] Söderberg, F. and Johansson, B., "Fluid Flow, Combustion and Efficiency with Early or Late Inlet Valve Closing", SAE Paper 972937, 1997.
- [95] Koga, H. and Watanabe, S., "Research on Extended Expansion General-purpose Engine – Heat Release and Friction", SAE Paper 2007-32-0003, 2007.
- [96] Zhao, F., Lai, M. C., Harrington, D. L., "Automotive Spark-ignited Direct-injection Gasoline Engines", Progress in Energy and Combustion Science, Vol. 25, pp 437-562, Pergamon, 1999.
- [97] Wang, Y., Lin, L., Roskilly, A. P., Zeng, S., Huang, J., He, Y., Huang, X., Huang, H., Wei, H., Li, S., Yang, J., "An Analytic Study of Applying Miller Cycle to Reduce NOx Emission from Petrol Engine", Applied Thermal Engineering, Vol. 27, pp 1779-1789, Elsevier, 2007.
- [98] Gould, L. A., Richeson, W. E., Erickson, F. L., "Performance Evaluation of a Camless Engine Using Valve Actuators with Programmable Timing", SAE Paper 910450, 1991.
- [99] Sakata, Y., Yamana, K., Nishida, K., Shimuzu, T., Shiga, S., Araki, M., Nakamura, H., Obokata, T., "A Study on Optimization of an Over-expansion Cycle Gasoline Engine with Late-closing of Intake Valves", SAE Paper 2007-24-0089, 2007.
- [100] Fraser, N., Korte, V., Rückauf, J., Harms, K., Miersch, J., Brandt, M., Münz, S., Rauscher, M., "Das MAHLE-Bosch Downsizing Demonstrator Fahrzeug", Aachener colloquium Fahrzeug- und Motorentchnik 2010, 2010.
- [101] ANSYS, Release 11.0, ANSYS Inc, Canonsburg, PA, 2007.
- [102] Pereira, R. C. C. and Pasa, V. M. D., "Effect of Alcohol and Copper Content on the Stability of Automotive Gasoline", Energy Fuels, Vol. 19, No. 2, pp 426-432, 2005.
- [103] Taylor, C. F., "The Internal Combustion Engine in Theory and Practice, Volume 1", MIT press, 1960.
- [104] ETAS INCA V7.0, ETAS GmbH, Stuttgart, Germany, 2011.
- [105] Rassweiler, G. M. and Withrow, L., "Motion Pictures of Engine Flames Correlated with Pressure Cards", SAE Transactions, Vol. 83, pp 185-204, 1938.

- [106] Brunt, M. and Pond, C., "Evaluation of Techniques for Absolute Cylinder Pressure Correction", SAE Paper 970036, 1997.
- [107] Brunt, M. and Emtage, A., "Evaluation of IMEP Routines and Analysis Errors", SAE Paper 960609, 1996.
- [108] Wiebe, L., "Halbermpirische Formel für die Verbrennungsgeschwindigkeit", Verlag der Akademie der Wissenschaften der UdSSR, 1967.
- [109] Heywood, J. B., Higgins, J. M., Watts, P. A., Tabaczynski, R. J., "Development and Use of a Cycle Simulation to Predict SI Engine Efficiency and NOx Emissions", SAE Paper 790291, 1979.
- [110] Blizard, N. C. and Keck, C. J., "Experimental and Theoretical Investigation of Turbulent Burning Model for Internal Combustion Engines", SAE Paper 740191, 1974.
- [111] Merdjani, S. and Sheppard, C. G. W., "Gasoline Engine Cycle Simulation using the Leeds Turbulent Burning Velocity Correlations", SAE Paper 932640, 1993.
- [112] GT-Suite Help Navigator, Gamma Technologies Inc, Westmont, Illinois, 2004.
- [113] Livengood, J. C. and Wu, P. C., "Correlation of Auto-ignition Phenomena in Internal Combustion Engines and Rapid Compression Machines", The Fifth International Symposium on Combustion, 1955.
- [114] Douaud, A. M. and Eyzat, P., "Four-octane Number Method for Predicting the Anti-knock Behaviour of Fuels in Engines", SAE Paper 780080, 1978.
- [115] Rothmaier, A., "NGM 1.2 GT-Power Baseline Correlation", Mahle Powertrain Internal Report, 2010.
- [116] Eriksson, L., Johansson, E., Kettaneh-Wold, N., Wilkström, C., Wold, S., "Design of Experiments: Principles and Applications", Umetrics, 2000.
- [117] McKay, M. D., Beckman, R. J., Conover, W. J., "A Comparison of Three Methods for Selecting Values of Input Variables in the Analysis of Output From a Computer Code", Technometrics, Vol. 42, pp 55-61, 2000.
- [118] Taylor, J., Fraser, N., Wieske, P., "Water Cooled Exhaust Manifold and Full Load EGR Technology Applied to a Downsized Direct Injection Spark Ignition Engine". SAE Paper 2010-01-0356, 2010.
- [119] Sonntag, R. E. and Borgnakke, C., "Fundamentals of Thermodynamics", Eighth edition, Wiley, 2013.
- [120] Smith, R. A. and Wilkins, P. S. A. W., "Low Pressure Sand Casting: Current Experience with a New Process", AFS Transactions, pp 785-792, 1986.

[121] Robertson, A., Hartland, J., Gil-Martinez, A., "Heat Flux Estimation and the Control of Nucleate Boiling in a Laboratory Test Rig", SAE Paper 2005-01-2007, 2005.

[122] Zahdeh, A., Rothenberger, P., Nguyen, W., Anbarasu, M., Schmuck-Soldan, S., Schaefer, J., Goebel, T., "Fundamental Approach to Investigate Pre-ignition in Boosted SI Engines", SAE Paper 2011-01-0340, 2011.

[123] Sasaki, N., Nakata, K., Kawatake, K., Sagawa, S., Watanabe, M., Sone, T., "The Effect of Fuel Compounds on Pre-ignition Under High Temperature and High Pressure Condition", SAE Paper 2011-01-1984, 2011.

Appendix

A.1 Cam Profiles

Cam Angle	Intake Cam Profile Lift (mm)			Exhaust Cam Profile Lift (mm)
	152 CAD	240 CAD	292 CAD	276 CAD
-90	0	0	0	0
-89.5	0	0	0	0
-89	0	0	0	0
-88.5	0	0	0	0
-88	0	0	0	0
-87.5	0	0	0	0
-87	0	0	0	0
-86.5	0	0	0	0
-86	0	0	0	0
-85.5	0	0	0	0
-85	0	0	0	0
-84.5	0	0	0	0
-84	0	0	0	0
-83.5	0	0	0	0
-83	0	0	7.28E-07	0
-82.5	0	0	5.1E-06	0
-82	0	0	2.26E-05	0
-81.5	0	0	7.28E-05	0
-81	0	0	0.000195	0
-80.5	0	0	0.000454	0
-80	0	0	0.00095	0
-79.5	0	0	0.001808	0
-79	0	0	0.003166	0

-78.5	0	0	0.005128	0
-78	0	0	0.007755	0
-77.5	0	0	0.011043	0
-77	0	0	0.014955	0
-76.5	0	0	0.019426	0
-76	0	0	0.024384	0
-75.5	0	0	0.029749	0
-75	0	0	0.035443	0
-74.5	0	0	0.041391	0
-74	0	0	0.047542	0
-73.5	0	0	0.053873	0.00021603
-73	0	0	0.060426	4.32E-04
-72.5	0	0	0.067302	0.00129617
-72	0	0	0.074692	0.00216028
-71.5	0	0	0.082848	0.00518011
-71	0	0	0.092094	0.00819994
-70.5	0	0	0.102777	0.013412325
-70	0	0	0.115281	0.01862471
-69.5	0	0	0.12996	0.02581042
-69	0	0	0.147183	0.03299613
-68.5	0	0	0.167246	0.04163922
-68	0	0	0.190452	0.05028231
-67.5	0	0	0.217007	0.06046157
-67	0	0	0.247122	0.07064083
-66.5	0	0.000236	0.280906	0.08435545
-66	0	0.000471	0.318484	0.09807007
-65.5	0	0.001413	0.359884	0.11804255
-65	0	0.002356	0.405167	0.13801503
-64.5	0	0.005568	0.454308	0.16620477
-64	0	0.008781	0.507328	0.19439451
-63.5	0	0.014157	0.564174	0.231860675
-63	0	0.019532	0.624843	0.26932684
-62.5	0	0.026117	0.689265	0.3165987

-62	0	0.032702	0.757428	0.36387056
-61.5	0	0.039838	0.829249	0.42114724
-61	0	0.046974	0.904704	0.47842392
-60.5	0	0.055465	0.983702	0.54568351
-60	0	0.063955	1.066207	0.6129431
-59.5	0	0.075863	1.152118	0.6899893
-59	0	0.08777	1.241385	0.7670355
-58.5	0	0.105504	1.333898	0.85352975
-58	0	0.123237	1.429591	0.940024
-57.5	0	0.148944	1.528341	1.03550565
-57	0	0.17465	1.630068	1.1309873
-56.5	0	0.209846	1.734634	1.23489
-56	0	0.245043	1.841939	1.3387927
-55.5	0	0.290575	1.951832	1.45045805
-55	0	0.336108	2.064192	1.5621234
-54.5	0	0.392334	2.178848	1.68081145
-54	0	0.44856	2.295655	1.7994995
-53.5	0	0.515502	2.414421	1.9243951
-53	0	0.582444	2.534973	2.0492907
-52.5	0	0.659919	2.657098	2.1795061
-52	0	0.737394	2.780604	2.3097215
-51.5	0	0.825091	2.905278	2.4442979
-51	0	0.912789	3.03093	2.5788743
-50.5	0	1.010309	3.157371	2.7167828
-50	0	1.107829	3.284438	2.8546913
-49.5	0	1.214711	3.411976	2.99485325
-49	0	1.321592	3.539856	3.1350152
-48.5	0	1.437346	3.667959	3.276355
-48	7.28E-07	1.5531	3.796181	3.4176948
-47.5	5.1E-06	1.677199	3.924429	3.5592215
-47	2.26E-05	1.801298	4.052619	3.7007482
-46.5	7.28E-05	1.933107	4.180675	3.8416804
-46	0.000195	2.064917	4.308526	3.9826126

-45.5	0.000454	2.203632	4.436109	4.1224098
-45	0.00095	2.342347	4.563358	4.262207
-44.5	0.001808	2.486946	4.690221	4.400499
-44	0.003166	2.631545	4.816638	4.538791
-43.5	0.005129	2.780842	4.942562	4.6753072
-43	0.007756	2.930139	5.067938	4.8118234
-42.5	0.011044	3.082874	5.192724	4.94635705
-42	0.014957	3.235609	5.316869	5.0808907
-41.5	0.019428	3.390545	5.440334	5.21327685
-41	0.024387	3.54548	5.563071	5.345663
-40.5	0.029752	3.701464	5.685045	5.475767
-40	0.035447	3.857448	5.806209	5.605871
-39.5	0.041398	4.013478	5.926531	5.73358
-39	0.047559	4.169507	6.045966	5.861289
-38.5	0.053919	4.324772	6.164485	5.9865048
-38	0.06054	4.480037	6.282044	6.1117206
-37.5	0.067561	4.633911	6.398616	6.2343563
-37	0.075227	4.787785	6.514158	6.356992
-36.5	0.083857	4.93979	6.628646	6.4769705
-36	0.093864	5.091795	6.742039	6.596949
-35.5	0.105684	5.241558	6.854315	6.7142007
-35	0.119803	5.39132	6.965437	6.8314524
-34.5	0.136665	5.538542	7.075384	6.9459142
-34	0.156733	5.685763	7.18412	7.060376
-33.5	0.180381	5.8302	7.291629	7.17198935
-33	0.207987	5.974636	7.397877	7.2836027
-32.5	0.239806	6.116081	7.502851	7.39231485
-32	0.2761	6.257526	7.606518	7.501027
-31.5	0.317	6.395807	7.708867	7.6067888
-31	0.362651	6.534088	7.809868	7.7125506
-30.5	0.413074	6.66905	7.909513	7.8153162
-30	0.468323	6.804013	8.007772	7.9180818
-29.5	0.528334	6.935522	8.10464	8.0178084

-29	0.593093	7.067031	8.200088	8.117535
-28.5	0.66248	7.194965	8.294114	8.2141825
-28	0.736429	7.322899	8.38669	8.31083
-27.5	0.81478	7.447147	8.477815	8.40436
-27	0.897426	7.571394	8.567462	8.49789
-26.5	0.984174	7.691855	8.655631	8.5882685
-26	1.074882	7.812316	8.742297	8.678647
-25.5	1.169328	7.928897	8.827462	8.7658385
-25	1.267335	8.045478	8.911101	8.85303
-24.5	1.368651	8.158093	8.993216	8.9370035
-24	1.473052	8.270708	9.073784	9.020977
-23.5	1.580239	8.379279	9.152808	9.10170125
-23	1.689918	8.487849	9.230265	9.1824255
-22.5	1.801713	8.592301	9.30616	9.25987125
-22	1.915238	8.696754	9.380471	9.337317
-21.5	2.030051	8.797018	9.453201	9.4114565
-21	2.145719	8.897282	9.52433	9.485596
-20.5	2.261805	8.993294	9.593862	9.5564015
-20	2.377905	9.089305	9.661778	9.627207
-19.5	2.493649	9.181004	9.728082	9.694653
-19	2.608699	9.272702	9.792754	9.762099
-18.5	2.722758	9.360031	9.855801	9.82616125
-18	2.835545	9.447359	9.917203	9.8902235
-17.5	2.946824	9.530263	9.976966	9.95087875
-17	3.056356	9.613167	10.03507	10.011534
-16.5	3.163954	9.691595	10.09153	10.068761
-16	3.269416	9.770023	10.14631	10.125988
-15.5	3.372594	9.843927	10.19943	10.1797665
-15	3.47332	9.917831	10.25088	10.233545
-14.5	3.571479	9.987166	10.30065	10.28385625
-14	3.66693	10.0565	10.34872	10.3341675
-13.5	3.759588	10.12122	10.39512	10.38099275
-13	3.849334	10.18594	10.43982	10.427818

-12.5	3.936107	10.24601	10.48282	10.471142
-12	4.019804	10.30608	10.52412	10.514466
-11.5	4.100381	10.36146	10.56371	10.554274
-11	4.177749	10.41684	10.60159	10.594082
-10.5	4.251877	10.46749	10.63777	10.630359
-10	4.322687	10.51814	10.67222	10.666636
-9.5	4.390158	10.56404	10.70495	10.699372
-9	4.454219	10.60993	10.73595	10.732108
-8.5	4.514859	10.65104	10.76524	10.7612905
-8	4.572012	10.69215	10.79279	10.790473
-7.5	4.625675	10.72844	10.81861	10.8160935
-7	4.675787	10.76473	10.84269	10.841714
-6.5	4.722347	10.79619	10.86504	10.8637655
-6	4.765299	10.82765	10.88564	10.885817
-5.5	4.804646	10.85425	10.90451	10.904292
-5	4.840334	10.88085	10.92162	10.922767
-4.5	4.872369	10.90257	10.937	10.9376615
-4	4.900701	10.92429	10.95063	10.952556
-3.5	4.92534	10.94112	10.96251	10.963866
-3	4.946238	10.95795	10.97264	10.975176
-2.5	4.96341	10.96988	10.98102	10.9828995
-2	4.976813	10.9818	10.98765	10.990623
-1.5	4.986467	10.98881	10.99253	10.9947605
-1	4.992333	10.99582	10.99565	10.998898
-0.5	4.994435	10.99791	10.99702	10.999449
0	4.99274	11	10.99664	11
0.5	4.987277	10.99716	10.9945	10.9969685
1	4.978017	10.99433	10.99061	10.993937
1.5	4.964997	10.98656	10.98497	10.987326
2	4.948192	10.97879	10.97757	10.980715
2.5	4.927645	10.9661	10.96843	10.9705315
3	4.903336	10.9534	10.95753	10.960348
3.5	4.875313	10.93578	10.94488	10.9465985

4	4.843562	10.91817	10.93048	10.932849
4.5	4.808135	10.89563	10.91433	10.9155415
5	4.769022	10.87309	10.89643	10.898234
5.5	4.726279	10.84564	10.8768	10.8773805
6	4.679904	10.81819	10.85541	10.856527
6.5	4.629954	10.78585	10.83229	10.8321385
7	4.576432	10.7535	10.80742	10.80775
7.5	4.519404	10.71627	10.78081	10.7798395
8	4.458879	10.67904	10.75247	10.751929
8.5	4.394928	10.63693	10.7224	10.72051225
9	4.32757	10.59483	10.6906	10.6890955
9.5	4.256886	10.54788	10.65707	10.65418775
10	4.182905	10.50094	10.62181	10.61928
10.5	4.105717	10.44916	10.58484	10.580898
11	4.025365	10.39738	10.54614	10.542516
11.5	3.941951	10.3408	10.50573	10.5006785
12	3.855537	10.28423	10.46361	10.458841
12.5	3.766239	10.22287	10.41978	10.4135695
13	3.674139	10.16152	10.37425	10.368298
13.5	3.579375	10.09543	10.32702	10.31961175
14	3.482054	10.02934	10.2781	10.2709255
14.5	3.382338	9.958539	10.22749	10.21884975
15	3.280362	9.887739	10.17519	10.166774
15.5	3.176315	9.812269	10.12121	10.1113305
16	3.070364	9.736799	10.06556	10.055887
16.5	2.962725	9.656701	10.00824	9.997102
17	2.8536	9.576603	9.949247	9.938317
17.5	2.743234	9.491921	9.888605	9.876216
18	2.631865	9.407238	9.826306	9.814115
18.5	2.51977	9.318021	9.762367	9.7487245
19	2.407228	9.228803	9.696782	9.683334
19.5	2.294547	9.135103	9.629571	9.614683
20	2.182051	9.041402	9.560728	9.546032

20.5	2.070079	8.943275	9.490273	9.474149
21	1.958991	8.845148	9.418201	9.402266
21.5	1.84914	8.742655	9.344534	9.3271815
22	1.740899	8.640162	9.269265	9.252097
22.5	1.634603	8.533368	9.192417	9.173843
23	1.5306	8.426574	9.113985	9.095589
23.5	1.429179	8.315548	9.033993	9.0141985
24	1.33065	8.204522	8.952436	8.932808
24.5	1.235256	8.08934	8.869338	8.8483165
25	1.143272	7.974157	8.784696	8.763825
25.5	1.0549	7.854897	8.698535	8.676268
26	0.970387	7.735638	8.610853	8.588711
26.5	0.889897	7.612388	8.521675	8.498127
27	0.81364	7.489138	8.431001	8.407543
27.5	0.741731	7.36199	8.338857	8.3139715
28	0.674334	7.234842	8.245246	8.2204
28.5	0.611508	7.103897	8.150193	8.123884
29	0.553362	6.972952	8.053702	8.027368
29.5	0.499895	6.838317	7.955803	7.92794965
30	0.451149	6.703682	7.856499	7.8285313
30.5	0.40705	6.565477	7.755822	7.72625965
31	0.367557	6.427271	7.653779	7.623988
31.5	0.332503	6.285625	7.550402	7.5189113
32	0.301735	6.143978	7.445702	7.4138346
32.5	0.274972	5.999035	7.339711	7.3060055
33	0.251929	5.854093	7.232445	7.1981764
33.5	0.232207	5.706016	7.123937	7.0876512
34	0.215406	5.55794	7.014207	6.977126
34.5	0.201044	5.406918	6.903291	6.8639645
35	0.188664	5.255896	6.79121	6.750803
35.5	0.177783	5.102155	6.678004	6.63506985
36	0.167984	4.948414	6.563698	6.5193367
36.5	0.158889	4.792236	6.448335	6.4011011

37	0.15022	4.636057	6.331942	6.2828655
37.5	0.141774	4.477812	6.214564	6.16220355
38	0.133434	4.319567	6.096232	6.0415416
38.5	0.125144	4.159788	5.976992	5.9185368
39	0.116889	4.00001	5.85688	5.795532
39.5	0.108679	3.83952	5.735944	5.670278
40	0.100539	3.67903	5.61422	5.545024
40.5	0.092501	3.519037	5.491761	5.417627
41	0.084603	3.359044	5.368607	5.29023
41.5	0.076886	3.201033	5.244812	5.1608127
42	0.069394	3.043021	5.120422	5.0313954
42.5	0.062165	2.888521	4.995493	4.9001037
43	0.055243	2.734021	4.870076	4.768812
43.5	0.04866	2.584468	4.744232	4.635821
44	0.042455	2.434914	4.618018	4.50283
44.5	0.036651	2.291627	4.491499	4.368358
45	0.031278	2.148339	4.364738	4.233886
45.5	0.02635	2.01254	4.237808	4.09821475
46	0.021884	1.87674	4.110782	3.9625435
46.5	0.017883	1.749547	3.983739	3.8260541
47	0.014349	1.622355	3.856764	3.6895647
47.5	0.011273	1.504749	3.729945	3.55278765
48	0.008643	1.387143	3.603382	3.4160106
48.5	0.006438	1.27989	3.477176	3.27963065
49	0.004634	1.172637	3.351442	3.1432507
49.5	0.0032	1.076205	3.226293	3.00803805
50	0.002105	0.979773	3.101863	2.8728254
50.5	0.001306	0.894347	2.97828	2.7396078
51	0.000761	0.808921	2.855694	2.6063902
51.5	0.000414	0.734523	2.734244	2.47605895
52	0.000212	0.660125	2.614099	2.3457277
52.5	0.000102	0.596683	2.495407	2.2192391
53	4.53E-05	0.533241	2.378347	2.0927505

53.5	1.79E-05	0.480564	2.263072	1.9711282
54	5.89E-06	0.427888	2.149768	1.8495059
54.5	1.4E-06	0.385597	2.038583	1.73381305
55	2E-07	0.343307	1.929699	1.6181202
55.5	0	0.310758	1.823257	1.50939285
56	0	0.27821	1.719427	1.4006655
56.5	0	0.254335	1.618334	1.2998511
57	0	0.23046	1.520133	1.1990367
57.5	0	0.213599	1.424926	1.10694265
58	0	0.196737	1.332853	1.0148486
58.5	0	0.184664	1.243994	0.932099465
59	0	0.17259	1.158471	0.84935033
59.5	0	0.162851	1.076345	0.776365465
60	0	0.153112	0.997724	0.7033806
60.5	0	0.143965	0.922652	0.64036415
61	0	0.134817	0.851223	0.5773477
61.5	0	0.125685	0.783467	0.52427295
62	0	0.116553	0.719466	0.4711982
62.5	0	0.107416	0.659234	0.427776025
63	0	0.098279	0.602838	0.38435385
63.5	0	0.089141	0.550273	0.349973265
64	0	0.080004	0.501586	0.31559268
64.5	0	0.070922	0.456742	0.28923157
65	0	0.061839	0.41575	0.26287046
65.5	0	0.053082	0.378534	0.243068905
66	0	0.044324	0.345044	0.22326735
66.5	0	0.036485	0.315138	0.20827593
67	0	0.028646	0.288687	0.19328451
67.5	0	0.022349	0.265462	0.18130754
68	0	0.016052	0.245236	0.16933057
68.5	0	0.011613	0.227688	0.158891145
69	0	0.007174	0.212498	0.14845172
69.5	0	0.004595	0.199281	0.138611075

70	0	0.002016	0.187668	0.12877043
70.5	0	0.001296	0.177271	0.119067715
71	0	0.000576	0.167752	0.109365
71.5	0	0.000288	0.158806	0.09968151
72	0	0	0.150206	0.08999802
72.5	0	0	0.141787	0.08041351
73	0	0	0.133456	0.070829
73.5	0	0	0.125167	0.061529965
74	0	0	0.116911	0.05223093
74.5	0	0	0.1087	0.0436178
75	0	0	0.100558	0.03500467
75.5	0	0	0.092518	0.02770376
76	0	0	0.084619	0.02040285
76.5	0	0	0.0769	0.01494349
77	0	0	0.069406	0.00948413
77.5	0	0	0.062176	0.00612099
78	0	0	0.055252	0.00275785
78.5	0	0	0.048668	0.001772905
79	0	0	0.042461	7.88E-04
79.5	0	0	0.036657	0.00039398
80	0	0	0.031282	0
80.5	0	0	0.026354	0
81	0	0	0.021887	0
81.5	0	0	0.017884	0
82	0	0	0.01435	0
82.5	0	0	0.011273	0
83	0	0	0.008644	0
83.5	0	0	0.006438	0
84	0	0	0.004635	0
84.5	0	0	0.003201	0
85	0	0	0.002105	0
85.5	0	0	0.001306	0
86	0	0	0.000761	0

86.5	0	0	0.000415	0
87	0	0	0.000212	0
87.5	0	0	0.000102	0
88	0	0	4.54E-05	0
88.5	0	0	1.79E-05	0
89	0	0	5.91E-06	0
89.5	0	0	1.4E-06	0
90	0	0	2E-07	0
90.5	0	0	0	0
91	0	0	0	0
91.5	0	0	0	0
92	0	0	0	0
92.5	0	0	0	0
93	0	0	0	0
93.5	0	0	0	0
94	0	0	0	0
94.5	0	0	0	0
95	0	0	0	0
95.5	0	0	0	0
96	0	0	0	0
96.5	0	0	0	0
97	0	0	0	0
97.5	0	0	0	0
98	0	0	0	0
98.5	0	0	0	0
99	0	0	0	0
99.5	0	0	0	0
100	0	0	0	0

A.2 Sensor List

Thermocouples:

- Exhaust temp
- Exhaust manifold temp
- Plenum air temp

PRT's:

- Head and block coolant temp in
- Head coolant temp out
- Block coolant temp out
- Oil temp in
- Oil temp out
- Low pressure fuel temp
- Intake port temp

Voltage output:

- **Flow meters**

- Total coolant (Apollo RN3/15)
- Block coolant (Apollo RN3/10)
- Fuel (ABB FCM2000)

- **Pressure sensors**

- Oil (Druck PTX 1400 0-6 bar)
- Barometric (Mercury barometer)
- Low pressure fuel (Druck PTX 1400 0-10 bar)
- Coolant (Druck PTX 1400 0-4 bar)
- Average exhaust (Druck PTX 1400 0-10 bar)
- Intake (Kistler 4005BA10FA0)
- Exhaust (Kistler 4005BA10FA0)
- In-cylinder (Kistler 6041A0)

- Exhaust gas analysers

- NOx (Rotork Analysis Model 443)
- HC (Rotork Analysis Model 523)

Apollo RN3



Range	2 - 20 l/min and 5 - 50 l/min
Pressure range	1 - 36 bar abs
Temperature range	-30 - 110 degC
Linearity	± 0.5%
Repeatability	± 0.1%
Size	0.5" BSP and 0.75" BSP
Construction	316 Stainless Steel
Warm up	N/A
Output	0 - 10V

ABB FCM2000



Range	0 - 65 kg/hr
Pressure range	1 - 41 bar abs
Temperature range	-50 - 125 degC
Linearity	± 0.15%
Repeatability	± 0.1%
Size	DN1.5
Construction	316 Stainless Steel
Warm up	30 mins
Output	0 - 10V

Druck PTX1400



Range	1 - 5, 1 - 7 and 1 - 11 bar abs
Pressure range	1 - 5, 1 - 7 and 1 - 11 bar abs
Temperature range	-20 - 80 degC
Linearity	N/A
Repeatability	± 0.15%
Size	0.25" BSP
Construction	316 Stainless Steel
Warm up	N/A
Output	4 - 20mA

Kistler 4005BA10FA0



Range	0 - 10 bar abs
Pressure range	0 - 10 bar abs
Temperature range	-20 - 125 degC (1100deg C w/cooling adapter)
Linearity	± 0.2%
Repeatability	± 0.2%
Size	M5 (M10 w/cooling adapter)
Construction	316 Stainless Steel
Warm up	30 mins
Output	0 - 10V

Kistler 6041A0



Range	0 - 250 bar abs
Pressure range	0 - 250 bar abs
Temperature range	-50 - 350 degC
Linearity	± 0.5%
Repeatability	± 0.5%
Size	M8
Construction	316 Stainless Steel
Warm up	30 mins
Output	0 - 10V

Rotork Analysis 443 FID analyser



Range	0 - 10000 ppm
Pressure range	N/A, 1.5l/min sample flow
Temperature range	10 - 30 degC
Linearity	± 1%
Repeatability	± 1%
Size	3 x 19" rack mount
Construction	316 Stainless Steel
Warm up	40 mins
Output	Analogue display

Rotork Analysis 523 Chemiluminescence analyser



Range	0 - 10000 ppm
Pressure range	N/A, 3l/min sample flow
Temperature range	10 - 30 degC
Linearity	± 1%
Repeatability	± 1%
Size	19" rack mount
Construction	316 Stainless Steel
Warm up	40 mins
Output	Analogue display

A.3 Feedback Descriptions

Label	Description
Speed	Engine speed. Input manually
Torque	Engine brake torque. As feedback from the dynamometer force transducer. High speed

	feedback
Lambda	Feedback from independent lambda sensor. Not used for this test work. This data is saved using INCA instead
Thrt. Opn.	Throttle angle. Not used for this test work. This data is saved using INCA instead
Oil Temp.	Oil in temperature. Low speed feedback
Oil Pres.	Oil pressure. Low speed feedback
Clnt. Temp.	Coolant in temperature. Low speed feedback
COVimep	<p>The coefficient of variation in NIMEP. Calculated using the following formula:</p> $\frac{\sqrt{\sum_1^n (NIMEP - \overline{NIMEP})^2} / (n - 1)}{\overline{NIMEP}}$ <p>n = number of samples (calculated over 100 cycles)</p>
Intake Temp.	Intake port temperature. Low speed feedback
Intake Pres.	Intake pressure as determined by taking the average pressure from the high speed intake pressure transducer from the entire cycle
T Exha.	Exhaust port temperature. Low speed feedback
P Exha.	Exhaust pressure as determined by taking the average pressure from the high speed exhaust pressure transducer from the entire cycle
Spark Timing	The spark timing. Not used for this test work. This data is saved using INCA instead

Inj. Timing	Injection timing. Not used for this test work. This data is saved using INCA instead
Inj. Pulse Width	Injection duration. Not used for this test work. This data is saved using INCA instead
Inj. Pres.	Fuel pressure going into the high pressure pump. The main reason for this is to ensure that the high pressure fuel pump has sufficient pressure. Low speed feedback
Mode	Allows the user to select how the engine is being driven, whether it is being motored or fired
State	Allows the user to select how many cycles are recorded. "Steady" records 100 cycles. "Transient" records cycles until the user requests it to stop
P Ambi	Ambient pressure. Input manually
T Ambi	Ambient Temperature. Input manually
Humidity %	Air Humidity. Input manually. Set to 0
AFlow[g/cyc]	Air Flow through the engine. Not used for this test work
FFlowRate[g/s]	Fuel flow rate through the engine. High speed feedback
Clnt. Pres.	Coolant pressure. Low speed feedback
IMEP	NIMEP. Both the "Tra." And "Ave." boxes are updated on a cycle to cycle basis. "Tra." Gives the NIMEP from the previous cycle. "Ave." gives the average NIMEP from the last 100 cycles

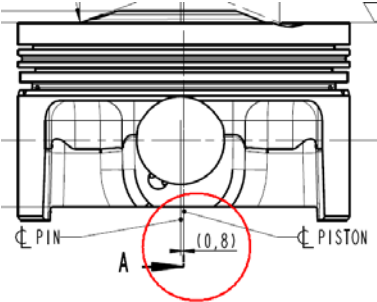
BMEP	Brake Mean Effective Pressure (BMEP). Both the "Tra." And "Ave." boxes are updated on a cycle to cycle basis. "Tra." Gives the BMEP from the previous cycle. "Ave." gives the average BMEP from the last 100 cycles
PMEP	Pumping Mean Effective Pressure (PMEP). Both the "Tra." And "Ave." boxes are updated on a cycle to cycle basis. "Tra." Gives the PMEP from the previous cycle. "Ave." gives the average PMEP from the last 100 cycles. PMEP is calculated using the following formula and the Gross IMEP (GIMEP): $PMEP = NIMEP - GIMEP$
FMEP	Friction Mean Effective Pressure (FMEP). Both the "Tra." And "Ave." boxes are updated on a cycle to cycle basis. "Tra." Gives the FMEP from the previous cycle. "Ave." gives the average FMEP from the last 100 cycles. FMEP is calculated using the following formula: $FMEP = GIMEP - BMEP$
ISFC	Indicated Specific Fuel Consumption (ISFC). Updated on a cycle to cycle basis. Calculated using the following formula: $ISFC = \frac{4.32e^8 F}{NIMEP * V * N}$ <i>F</i> = Fuel flow, <i>V</i> = Swept volume, <i>N</i> = Engine speed
BSFC	Brake Specific Fuel Consumption (BSFC). Updated on a cycle to cycle basis. Calculated

	<p>using the following formula:</p> $BSFC = \frac{4.32e^8 F}{BMEP * V * N}$ <p>F= Fuel flow, V= Swept volume, N= Engine speed</p>
Pi	<p>Indicated power. Updated on a cycle to cycle basis. Calculated using the following formula:</p> $P_i = \frac{NIMEP * V * N}{120}$ <p>V= Swept Volume, N= Engine speed</p>
Pe	<p>Brake power. Updated on a cycle to cycle basis. Calculated using the following formula:</p> $P_e = \frac{BMEP * V * N}{120}$ <p>V= Swept Volume, N= Engine speed</p>
T Ex. M.	Exhaust manifold temperature. Low speed feedback
T Fuel	Low pressure fuel temperature. Low speed feedback
T Oil out	Oil out temperature. Low speed feedback
T Head	Coolant temperature out of the cylinder head. Low speed feedback
T Block	Coolant temperature out of the cylinder block. Low speed feedback
B Clnt FR	Coolant flow rate through the cylinder block. Low speed feedback
H Clnt FR	Coolant flow rate through the cylinder head.

	Low speed feedback
IVO	Intake Valve Opening (IVO) timing. Input manually. Not used for this test work. This data is saved using INCA instead
IVC	Intake Valve Closing (IVC) timing. Input manually. Not used for this test work. This data is saved using INCA instead
IVL	Maximum intake valve lift. Input manually. Not used for this test work
EVO	Exhaust Valve Opening (EVO) timing. Input manually. Not used for this test work. This data is saved using INCA instead
EVC	Exhaust Valve Closing (EVC) timing. Input manually. Not used for this test work. This data is saved using INCA instead
EVL	Maximum exhaust valve lift. Input manually. Not used for this test work
RGF	Residual gas fraction. Input manually. Not used for this test work
ECR	Effective CR. Not used for this test work
CO	Carbon monoxide emissions. Not used for this test work
CO2	Carbon dioxide emissions. Not used for this test work
HC	Hydrocarbon emissions. Not used for this test work. This data was logged by hand instead
NOx	Nitrogen oxides emissions. Not used for this test work. This data was logged by hand

	instead
O2	Oxygen emissions. Not used for this test work
EGR	Exhaust Gas Recirculation (EGR) quantity. Not used for this test work
Lambda	Secondary lambda reading obtained from an exhaust gas analyzer. Not used for this test work
Pmax	Peak cylinder pressure. Both the "Tra." And "Ave." boxes are updated on a cycle to cycle basis. "Tra." Gives the peak cylinder pressure from the previous cycle. "Ave." gives the average peak cylinder pressure from the last 100 cycles
CA	Crank angle of peak cylinder pressure. Both the "Tra." And "Ave." boxes are updated on a cycle to cycle basis. "Tra." Gives the CA of peak cylinder pressure from the previous cycle. "Ave." gives the average CA of peak cylinder pressure from the last 100 cycles
dPdCA	Peak Dp/Dθ. Both the "Tra." And "Ave." boxes are updated on a cycle to cycle basis. "Tra." Gives the peak Dp/Dθ from the previous cycle. "Ave." gives the average peak Dp/Dθ from the last 100 cycles
CA	Crank angle of peak Dp/Dθ. Both the "Tra." And "Ave." boxes are updated on a cycle to cycle basis. "Tra." Gives the CA of peak Dp/Dθ from the previous cycle. "Ave." gives the average CA of peak Dp/Dθ from the last 100 cycles

CA10	The crank angle at 10% MFB. Both the "Tra." And "Ave." boxes are updated on a cycle to cycle basis. "Tra." Gives the 10% MFB angle from the previous cycle. "Ave." gives the average 10% MFB angle from the last 100 cycles
CA50	The crank angle at 50% MFB. Both the "Tra." And "Ave." boxes are updated on a cycle to cycle basis. "Tra." Gives the 50% MFB angle from the previous cycle. "Ave." gives the average 50% MFB angle from the last 100 cycles
CA90	The crank angle at 90% MFB. Both the "Tra." And "Ave." boxes are updated on a cycle to cycle basis. "Tra." Gives the 90% MFB angle from the previous cycle. "Ave." gives the average 90% MFB angle from the last 100 cycles
Dura.	The 10–90% MFB duration. Both the "Tra." And "Ave." boxes are updated on a cycle to cycle basis. "Tra." Gives the 10–90% MFB duration from the previous cycle. "Ave." gives the average 10–90% MFB duration from the last 100 cycles
I_Knock	The peak KI value. Both the "Tra." And "Ave." boxes are updated on a cycle to cycle basis. "Tra." Gives the peak KI value from the previous cycle. "Ave." gives the average peak KI value from the last 100 cycles
Tmax	Not used for this test work
Fuel Type	Either Gasoline or Diesel. This was set to

	Gasoline for all test work
Threshold	Allows the user to specify a maximum cylinder pressure above which it is assumed a pre-ignition event has taken place. This was set to 20% above the maximum cylinder pressure obtained during normal running at that particular test condition
Number	The number of cycles the cylinder pressure has exceeded the threshold pre-ignition value
Ref. Position	Allows the user to input a shaft encoder signal offset to allow the setting of Top Dead Centre (TDC) position using software as opposed to hardware
Gamma	Allows the user to specify a gamma value (ratio of specific heats) for the air. This was set to 1.32 for all test work
d	The cylinder bore measurement
s	The stroke length
Conrod	The connecting rod length
CR	The engine geometric CR
Offse	<p>The crank pin offset as shown below:</p>  <p>A common practice for circumventing NVH</p>

	issues, the crank pin offset had to be factored in because it will impact on the accuracy of NIMEP measurements
SamplesPerRevolution	The resolution of the shaft encoder. For all test work a 0.25 CAD shaft encoder was used, this was therefore set to 1440
RevolutionsPerCycle	The number of engine crank revolutions per cycle. This was set to 2 for all test work
NumberOfChannels	The number of channels going into the data acquisition system
Saved File Name	The name of the folder containing the last recorded set of data

A.4 GT-Power Animation Showing Charge Scavenging

The following Figures show freeze frames from various points on an animated 4 stroke cycle obtained from a GT-Power simulation. The test point is 1000rpm, 14 bar BMEP, 2.5 bar EBP, CR of 9 with a cam duration of 312 CAD and an IMOP of 150 CAD ATDC. At this running condition fuel vapours can be demonstrated to flow back into the intake manifold and then scavenge straight through the cylinder during the gas exchange process resulting in unburned charge being short circuited into the exhaust manifold.

Unburned charge is shown on the Figures A.1 to A.7 as a scarlet coloured red with areas without unburned charge being shown as green. Fuel vapours can be demonstrated to flow as far upstream as the end of the variable section in the intake manifold. Figure A.1 shows the cycle starting at BDC at the end of the intake stroke.

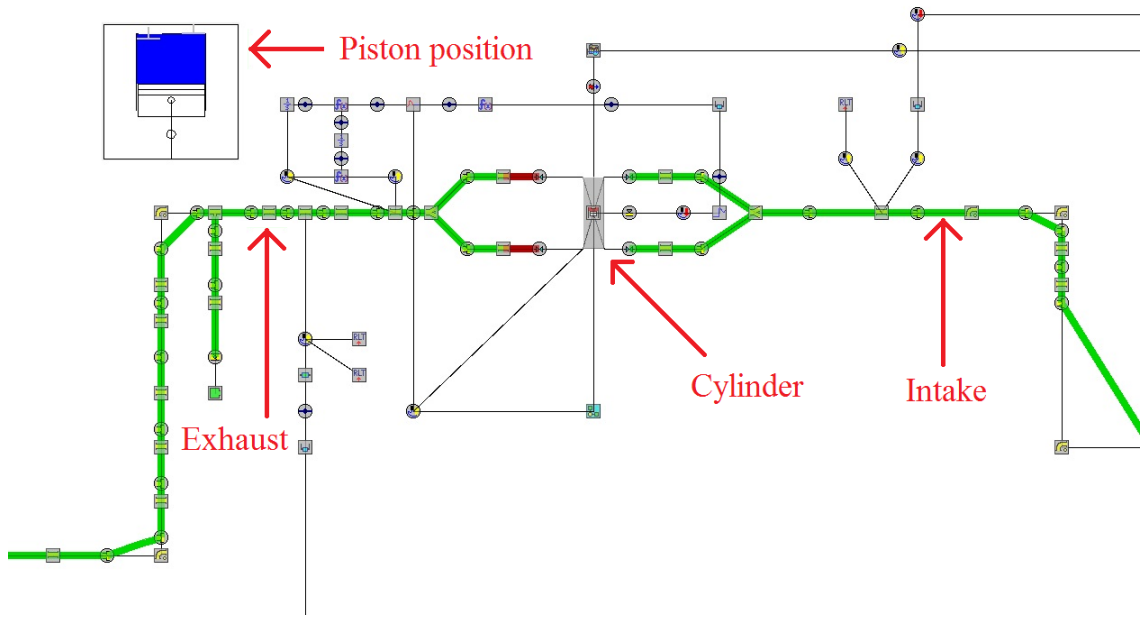


Figure A.1 Piston at End of Intake BDC

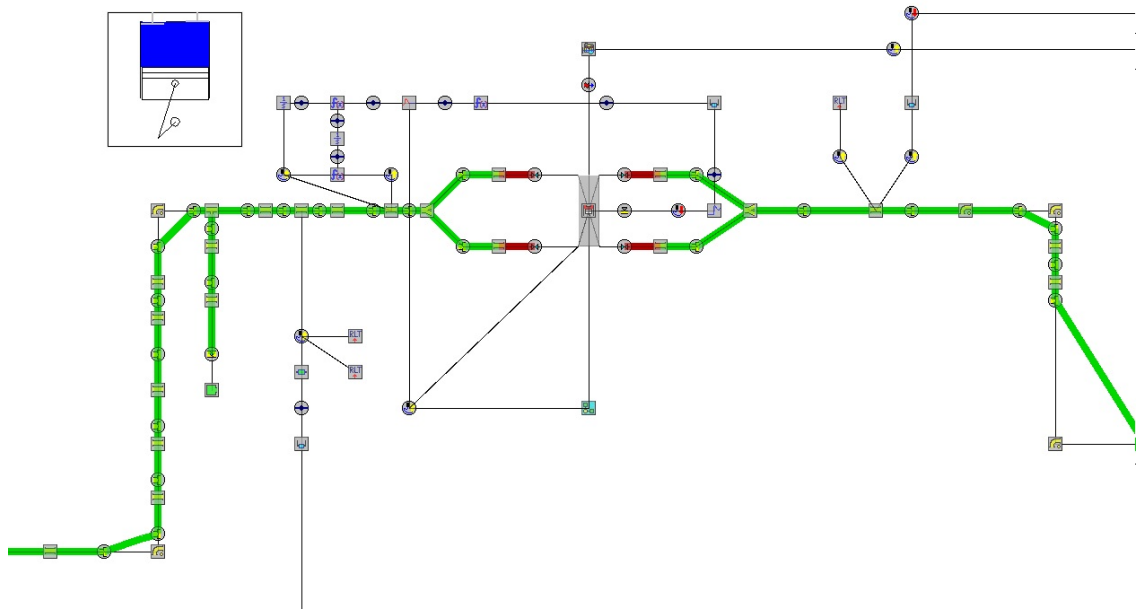


Figure A.2 Charge Beginning to Flow Back Up the Intake Manifold

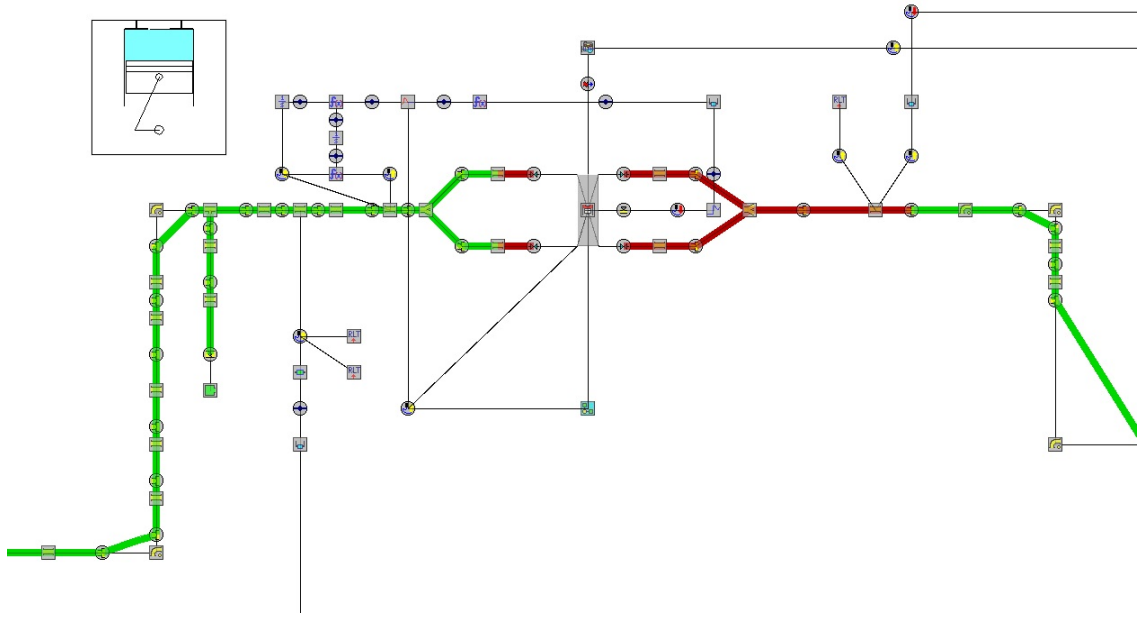


Figure A.3 Charge Still Continuing to Flow Even at 90 CAD BTDCF

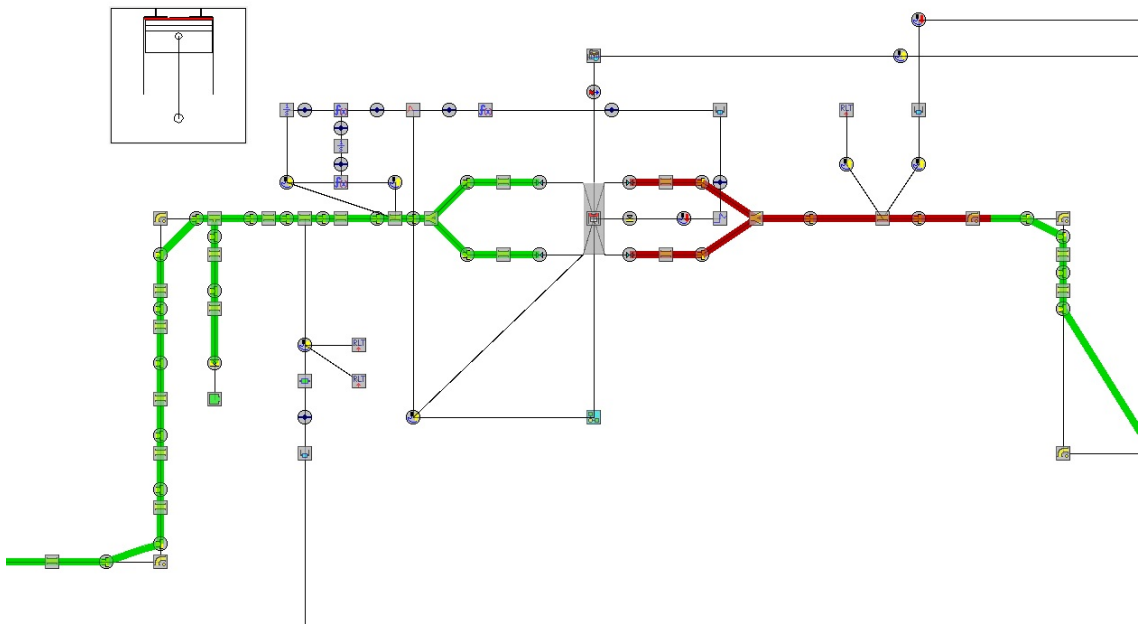


Figure A.4 Piston at TDCF. Charge Still Trapped in Intake Manifold

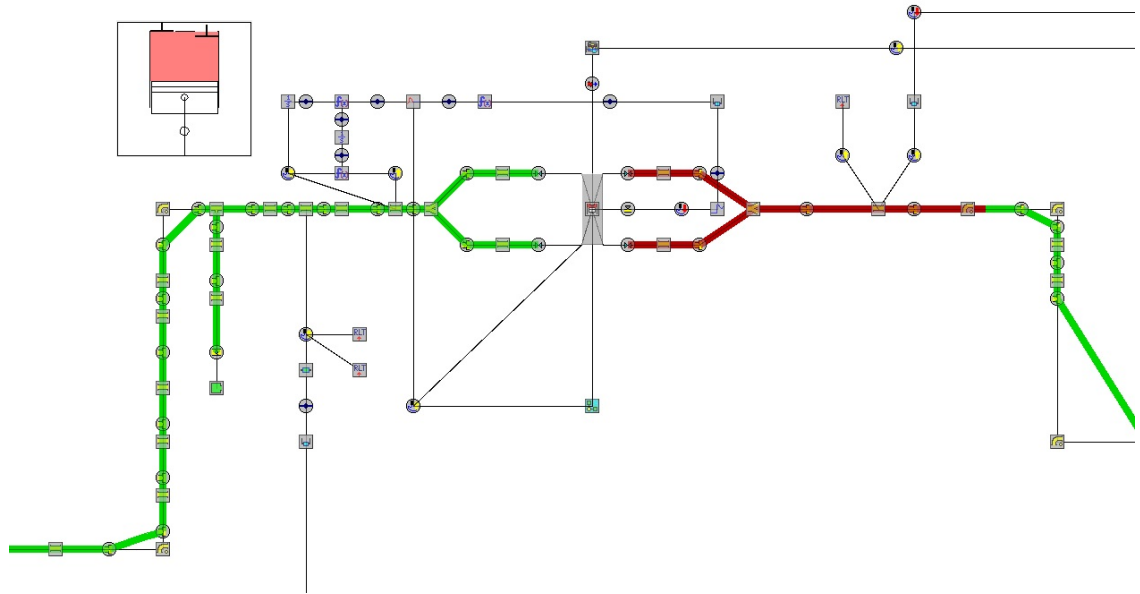


Figure A.5 Piston at End of Power BDC. Exhausting has Commenced, No Unburned Vapours Present in Exhaust Gasses

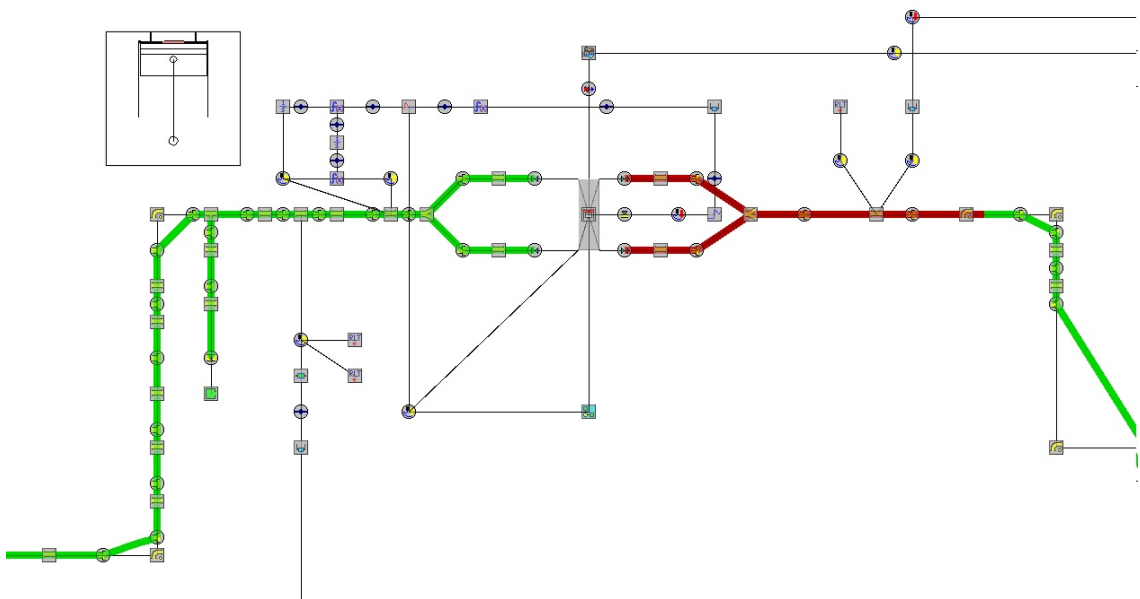


Figure A.6 Piston at Gas Exchange TDC. No Scavenging has yet Begun Despite Both Valves Being Open

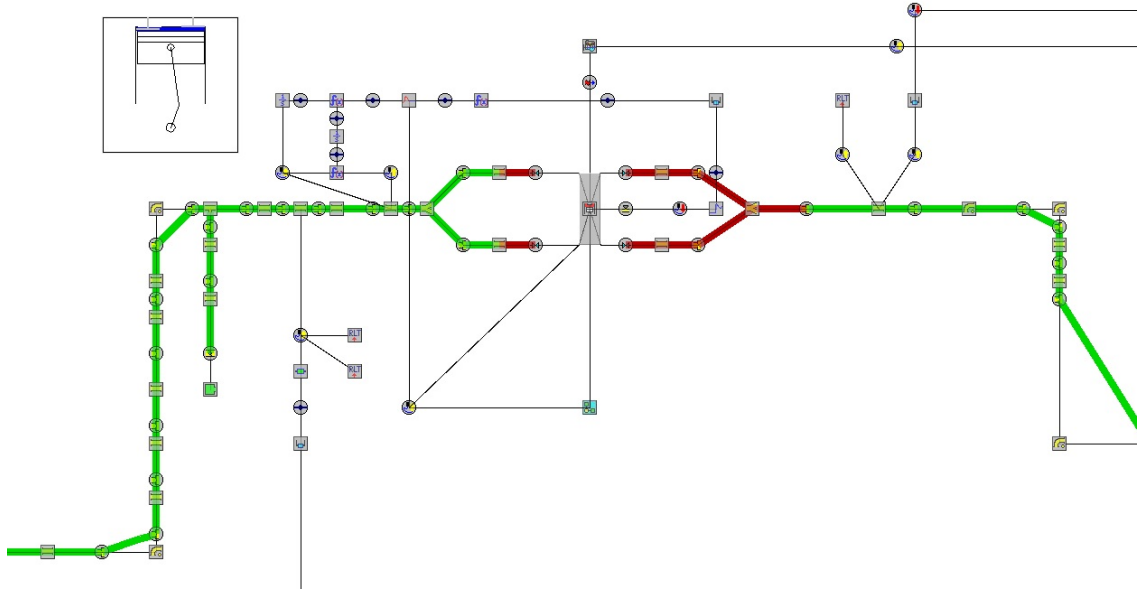


Figure A.7 Charge Scavenging Beginning at Approximately 15 CAD ATDC

A.5 References

Reference 49:



MCE-5 VCRi: Pushing back the fuel consumption reduction limits



- Home page
- What is VCR?
- VCR: pushing back engine efficiency limits
- MCE-5 VCRi technology
- Technological assets
- Strategic assets
- Key results
- False preconceptions

- News
- MCE-5 DEVELOPMENT
The company
- Inventor of
MCE-5 VCRi technology
- MCE-5 VCRi R&D
programs
- Partners
- Careers
- Contacts



MCE-5 VCRi prototype
1.5 L 2-stage turbo MPFI
420 Nm at 1500 rpm
180 kW (220 hp)
from 4000 to 5000 rpm

Video presentation 

**MCE-5 VCRi, environment, energy, economy:
mechanical and technological excellence serving essential strategic objectives**

MCE-5 VCRi is not only a machine to optimize the efficiency, performance and pollutant emission levels of car engines. Through the association of technologies, it's also a fabulous tool to optimize the cost price of the engine, its transmission and after-treatment.

MCE-5 DEVELOPMENT S.A. - 21 avenue Georges Pompidou - F-69486 LYON Cedex 03 | [Shareholders](#) | [Investors](#)

Twincharger

From Wikipedia, the free encyclopedia

Twincharger refers to a compound forced induction system used on some piston-type internal combustion engines. It is a combination of an exhaust-driven turbocharger and an engine-driven supercharger, each mitigating the weaknesses of the other. A belt-driven supercharger offers exceptional response and low-rpm performance as it has no lag time between the application of throttle and pressurization of the manifold. Combined with a large turbo which would offer unacceptable lag and poor response in the low-rpm range, the proper combination of the two can offer a zero-lag powerband with high torque at lower engine speeds and increased power at the higher end. Twincharging is therefore desirable for small-displacement motors (such as VW's 1.4TSD), especially those with a large operating rpm, since they can take advantage of an artificially broad torque band over a large speed range.

Twincharging does not refer to a twin-turbo arrangement, but rather when two different kinds of compressors are used.

Contents

- 1 Technical description
 - 1.1 Series
 - 1.2 Parallel
- 2 Disadvantages
- 3 Commercial availability
- 4 Alternative systems
 - 4.1 Anti-lag system
 - 4.2 Variable geometry turbocharger
 - 4.3 Nitrous oxide
- 5 Water injection
- 6 References
- 7 External links

Technical description

A twincharging system combines a supercharger and turbocharger in a complementary arrangement, with the intent of one component's advantage compensating for the other component's disadvantage. There are two common types of twincharger systems: series and parallel.

Series

The series arrangement, the more common arrangement of twinchargers, is set up such that one compressor's (turbo or supercharger) output feeds the inlet of another. A sequentially-organized Roots type supercharger is connected to a medium- to large-sized turbocharger. The supercharger provides near-instant manifold pressure (eliminating turbo lag, which would otherwise result when the turbocharger is not up to its operating speed). Once the turbocharger has reached operating speed, the supercharger can either continue compounding the pressurized air to the turbocharger inlet

<http://en.wikipedia.org/wiki/Twincharger>

(yielding elevated intake pressures), or it can be bypassed and/or mechanically decoupled from the drivetrain via an electromagnetic clutch and bypass valve (increasing efficiency of the induction system).

Other series configurations exist where no bypass system is employed and both compressors are in continuous duty. As a result, compounded boost is always produced as the pressure ratios of the two compressors are multiplied, not added. In other words, if a supercharger which produced 10 psi (0.7 bar) (pressure ratio = 1.7) alone blew into a turbocharger which also produced 10psi alone, the resultant manifold pressure would be 27 psi (1.9 bar) (PR=2.8) rather than 20 psi (1.4 bar) (PR=2.3). This form of series twincharging allows for the production of boost pressures that would otherwise be unachievable with other compressor arrangements and would be inefficient.

However, the efficiencies of the turbo and supercharger are also multiplied, and since the efficiency of the supercharger is often much lower than that of large turbochargers, this can lead to extremely high manifold temperatures unless very powerful charge cooling is employed. For example, if a turbocharger with an efficiency of 70% blew into a Roots blower with an efficiency of 60%, the overall compression efficiency would be only 42% -- at 2.8 pressure ratio as shown above and 20 °C (68 °F) ambient temperature, this would mean air exiting the turbocharger would be 263 °C (505 °F), which is enough to melt most rubber couplers and nearly enough to melt expensive silicone couplers. A large turbocharger producing 27 psi (1.9 bar) by itself, with an adiabatic efficiency around 70%, would only produce 166 °C (331 °F). Additionally, the energy cost to drive a supercharger is higher than that of a turbocharger; if it is bypassed, the load of performing compression is removed, leaving only slight parasitic losses from spinning the working parts of the supercharger. The supercharger further be disconnected electrically (using an electromagnetic clutch such as those used on the VW 1.4TSI or Toyota's 4A-GZE) which eliminates this small parasitic loss.

With series twincharging, the turbocharger can be of a less expensive and more durable journal bearing variety, and the sacrifice in boost response is more than made up for by the instant-on nature of displacement superchargers. While the weight and cost of the supercharger assembly are always a factor, the inefficiency and power consumption of the supercharger are almost totally eliminated as the turbocharger reaches operating rpm and the supercharger is effectively disconnected by the bypass valve.

Parallel

Parallel arrangements typically always require the use of a bypass or diverter valve to allow one or both compressors to feed the engine. If no valve were employed and both compressors were merely routed directly to the intake manifold, the supercharger would blow backwards through the turbocharger compressor rather than pressurize the intake manifold, as that would be the path of least resistance. Thus a diverter valve must be employed to vent turbocharger air until it has reached the pressure in the intake manifold. Complex or expensive electronic controls are usually necessary to ensure smooth power delivery.

Disadvantages

The main disadvantage of twincharging is the complexity and expense of components. Usually, to provide acceptable response, smoothness of power delivery, and adequate power gain over a single-compressor system, expensive electronic and/or mechanical controls must be used. In a spark-ignition engine, a low compression ratio must also be used if the supercharger produces high boost levels, negating some of the efficiency benefit of low displacement.

<http://en.wikipedia.org/wiki/Twincharger>

Commercial availability

The concept of twincharging was first used by Lancia in 1985 on the Lancia Delta S4 Group B rally car and its street legal counterpart, the Delta S4 Stradale. The idea was also successfully adapted to production road cars by Nissan, in their March Super Turbo.^[1] Additionally, multiple companies have produced aftermarket twincharger kits for cars like the Subaru Impreza WRX, Mini Cooper S, Ford Mustang, Nissan Skyline GT-R, Toyota MR2, as well as the GM 3800 Engine, as in the Pontiac Bonneville SSEI, Pontiac Grand Prix GTP, and the Chevrolet Cobalt SS among others.

The Volkswagen 1.4 TSI is a 1400 cc engine – utilised by numerous automobiles of the VW Group – that sees use of both a turbocharger and a supercharger, and is available with eight power ratings:

103 kilowatts (140 PS; 138 bhp) @ 5,600 rpm; 220 newton metres (162 lbf·ft) @ 1,500-4,000 rpm — VW Golf V, VW Jetta V, VW Touran
 110 kilowatts (150 PS; 148 bhp) @ 5,800 rpm; 220 newton metres (162 lbf·ft) @ 1,250-4,500 rpm — SEAT Ibiza IV
 110 kilowatts (150 PS; 148 bhp) @ 5,800 rpm; 240 newton metres (177 lbf·ft) @ 1,500-4,000 rpm — (CNG version) VW Passat VI, VW Passat VII, VW Touran
 110 kilowatts (150 PS; 148 bhp) @ 5,800 rpm; 240 newton metres (177 lbf·ft) @ 1,750-4,000 rpm — VW Sharan II, VW Tiguan, SEAT Alhambra
 118 kilowatts (160 PS; 158 bhp) @ 5,800 rpm; 240 newton metres (177 lbf·ft) @ 1,500-4,500 rpm — VW Eos, VW Golf VI, VW Jetta VI
 125 kilowatts (170 PS; 168 bhp) @ 6,000 rpm; 240 newton metres (177 lbf·ft) @ 1,500-4,500 rpm — VW Golf V, VW Jetta V, VW Touran
 132 kilowatts (179 PS; 177 bhp) @ 6,200 rpm; 250 newton metres (184 lbf·ft) @ 2,000-4,500 rpm — VW Polo V, SEAT Ibiza Cupra, Škoda Fabia II
 136 kilowatts (185 PS; 182 bhp) @ 6,200 rpm; 250 newton metres (184 lbf·ft) @ 2,000-4,500 rpm — Audi A1

Alternative systems

Anti-lag system

Twincharging's largest benefit over anti-lag systems in race cars is its reliability. Anti-lag systems work in one of two ways: by running very rich AFR and pumping air into the exhaust to ignite the extra fuel in the exhaust manifold; or by severely retarding ignition timing to cause the combustion event to continue well after the exhaust valve has opened. Both methods involve combustion in the exhaust manifold to keep the turbine spinning, and the heat from this will shorten the life of the turbine greatly.

Variable geometry turbocharger

Main article: Variable geometry turbocharger

A variable-geometry turbocharger provides an improved response at widely-varied engine speeds. With variable-incidence under electronic control, it is possible to have the turbine reach a good operating speed quickly or at lower engine speed without severely diminishing its utility at higher engine speed.

<http://en.wikipedia.org/wiki/Twincharger>

Nitrous oxide

Nitrous oxide (N₂O), is mixed with incoming air, providing more oxidizer to burn more fuel for supplemental power when a turbocharger is not spinning quickly. This also produces more exhaust gases so that the turbocharger quickly spools up, providing more oxygen for combustion, and the N₂O flow is reduced accordingly. The expense of both the system itself and the consumable N₂O can be significant.

Water injection

Main article: Water injection (engines)

For more engine power, and to augment the benefits of forced induction (by means of turbocharging or supercharging), an aftermarket water injection system can be added to the induction system of both gasoline and diesel internal combustion engines.

References

- [^] *grandJDM* >> *March Superturbo: Mighty Mite!* (<http://grandjdm.com/2007/12/09/march-superturbo-mighty-mite/>) (2007-12-09)

External links


- http://www.greencarcongress.com/2005/08/inside_vws_new_.html

Retrieved from "<http://en.wikipedia.org/w/index.php?title=Twincharger&oldid=540967725>"

Categories: Superchargers | Turbochargers

-
- This page was last modified on 27 February 2012 at 15:45.
 - Text is available under the Creative Commons Attribution-ShareAlike License; additional terms may apply. See Terms of Use for details.
Wikipedia® is a registered trademark of the Wikimedia Foundation, Inc., a non-profit organization.

Honda Worldwide | Technology Picture Book | EXlink
Page 1 of 3


Honda World Links
Honda Worldwide

Honda Worldwide Home
Products & Technology
Technology
Technology Picture Book(Power Products)
EXlink

Performing more work with less fuel—EXlink (Extended Expansion Linkage Engine)


Taking energy efficiency to a new level—the revolutionary EXlink
(Extended Expansion Linkage Engine)

Performing more work with less fuel... Energy efficiency has been of prime importance in engine design, driving the development of seemingly countless new models over the years.

With the goal of taking energy efficiency to a new level, Honda developed its own linkage engine design based on Atkinson's extended-expansion cycle engine, invented some 130 years ago. The first small engine of its type to be commercially produced, the revolutionary EXlink has an expansion stroke longer than its compression stroke to realize an expansion ratio higher than its compression ratio.

In contrast to a conventional Otto cycle engine, in which the piston strokes are typically of the same length, the EXlink has expansion and exhaust strokes that are longer than its intake and compression strokes. The result is an expansion ratio that is more than 1.4 times higher than the compression ratio, allowing EXlink to offer lower pumping losses and substantially higher thermal efficiency than a conventional engine.

*EXlink, "short for Extended Expansion Linkage Engine, is a trademark of Honda Motor Co., Ltd.

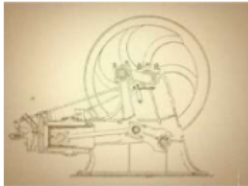


A hint from the Atkinson cycle engine—invented some 130 years ago.

Serving as the inspiration for the Honda EXlink engine, the Atkinson cycle is a technology first implemented by James Atkinson some 130 years ago.

In the 19th century, Atkinson's engine was celebrated for its excellent fuel efficiency, but due to its complicated structure, however, this engine was difficult to construct on a compact scale, and it disappeared thereafter from the main stream of engine development.

Right:Atkinson engine



Source: Kiyoshi Tomizuka, History of the Internal Combustion Engine, San-eishobo Publishing Co., Ltd., 1969

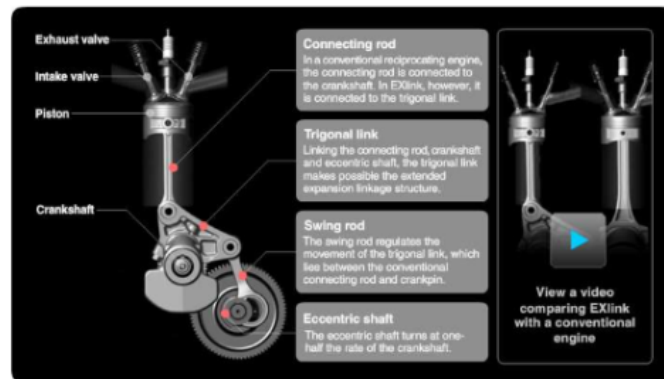
EXlink structure

EXlink features a trigonal link that lies between the connecting rod and crankshaft found in conventional engines. The trigonal link is connected via a swingrod to an eccentric shaft, completing the extended expansion linkage design. The eccentric shaft turns at one-half the speed of the crankshaft, making possible pairs of piston strokes that alternate between short and long.

To realize a high expansion ratio, EXlink uses the short strokes for intake and compression and the long strokes for expansion and exhaust, expanding 110 cm³ of intake to 163 cm³. The key benefit of the Atkinson cycle is taking in a smaller

<http://world.honda.com/powerproducts-technology/exlink/>

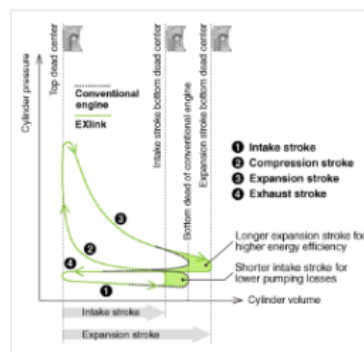
amount of air and fuel and performing more work with it for greatly enhanced fuel efficiency, and in EXlink it is implemented in a simple, compact design.



How EXlink enhances thermal efficiency

In an internal combustion engine, the expansion ratio determines the level of thermal efficiency. Since, in a conventional Otto cycle engine, the expansion ratio is the same as the compression ratio, enhancing fuel efficiency by increasing the expansion ratio also ends up increasing the compression ratio. The higher compression ratio results in undesirable engine knocking.*

In EXlink, however, the compression ratio is 12.2:1, which is low enough to avoid the knocking that can occur in a gasoline engine, while the expansion ratio is a high 17.6:1 to enhance thermal efficiency.



*Engine knocking is the metallic sound and vibration that occur due to abnormal combustion in the cylinder of an engine. Knocking can even lead to engine breakdown. Common causes of engine knocking are premature combustion and an overly high compression ratio.

**Pumping losses are the energy lost from moving air into and out of an engine's cylinder during intake and exhaust.

Engine friction-reducing technologies


Because of EXlink's linkage structure, increased engine friction might seem to be an issue. EXlink, however, features technologies that help reduce engine friction and prevent fuel efficiency losses.

In a conventional engine, when the combusting air-fuel mixture puts the piston under pressure during the expansion stroke, side forces act on the cylinder wall, generating a large amount of friction. Since the amount of side force is in large degree determined by the connecting rod angle, EXlink has been designed so that the connecting rod is nearly parallel to the cylinder walls during the expansion stroke. As a result, the friction loss due to piston side forces is less than half that of a conventional engine. Even with its extra linkage expansion parts, EXlink has the same amount of engine friction as a conventional engine, thereby reaping the full fuel efficiency benefit of the Atkinson cycle.

<http://world.honda.com/powerproducts-technology/exlink/>



Honda Worldwide site
[Home](#) | [Site Map](#) | [Site Index](#) | [About this Site](#)
Copyright, 2013 Honda Motor Co., Ltd. and its subsidiaries and affiliates. All Rights Reserved.



[About Us](#)
[Customer Center](#)
[Resources](#)
[Contact Us](#)
[Security](#)

Rail


Marine

Mining

Drilling

Stationary Power

Energy Storage



Rail Blog

Products

Services


Resources

Software

PowerHaul Series Locomotive

The PowerHaul Series -- GE's most technologically advanced locomotive

Today's global rail industry is challenged with the need for a more powerful locomotive that can operate on existing railways and comply with stringent emissions standards while saving fuel. As it has for more than a century, GE Transportation responded with a technology-leading solution -- the PowerHaul Series Locomotive. The PowerHaul is more powerful, cleaner and fuel-efficient compared to competitive locomotives. The PowerHaul Series also is compliant with EU Stage IIIa emissions standards and features a flexible platform that readily adapts to local requirements.




Features:

- * V-16, twin-turbo 3,700-GHP engine
- * Advances AC traction systems
- * Superior dynamic braking
- * Flexible global platform in locations such as Africa, Asia, Continental Europe, South America, the United Kingdom, and other regions around the globe
- * Cab is ergonomically designed and provides maximum efficiency
- * Dual air conditioning
- * Easy-to-read gauges
- * Unobstructed front windscreen for clear track view

Benefits & Value:

- * 9% reduction in fuel consumption compared to current operating fleet averages
- * Engineered for greater hauling power
- * 9% reduction in CO2
- * 25% increase in train consists



Product Finder

SELECT

SUBSCRIBE TO RSS FEED

Tags

[locomotive](#)
[battery](#)
[marine](#)
[wind hybrid](#)
[motor boat](#)
[stationary](#)
[signaling](#)
[drilling](#)
[mining](#)
[tier tier 3 emissions](#)
[US](#)
[Environmental Protection Agency](#)
[overhaul](#)
[Stockholm AB](#)
[Storstockholms Lokaltrafik](#)
[Tvärbanan](#)
[light rail](#)
[towboat](#)
[L250 Engine](#)
[diesel](#)
[marine](#)
[engine](#)
[Parker Towing](#)
[Company Inc.](#)
[haul truck](#)
[GDY106 AC electric drive](#)
[electric drive systems](#)
[wheel motors](#)
[water jacket](#)
[motor](#)
[oil rig](#)
[ac motor](#)
[dc motor](#)
[enclosed motor](#)
[Brooklyn Genset V250](#)
[enclosed gensets](#)
[Skanska USA backup power](#)
[Durathon energy storage](#)
[uninterruptible power supply](#)
[UPS](#)
[Schenectady New York](#)
[drilling motor](#)
[EPA offshore](#)
[drilling](#)
[Tvärbanan](#)
[light rail system](#)

Connect With Us

[Facebook](#)
[Twitter](#)
[Flickr](#)
[YouTube](#)

Ask the Car People.™


[Learn More](#) | [Sign In](#) | [Mobile](#) | [Help](#) | [Newsletter](#) | [Dealers](#)

[New Cars](#) | [Used Cars](#) | [Inventory](#) | [Car Reviews](#) | [Tips & Advice](#) | [About Us](#) | [Contact Us](#)

Home > [Used Cars](#) > [Mazda](#) > [Millenia](#) > [2002 Millenia](#) > Features & Specs

Used Car History Report


Take the unknown out of buying pre-owned.



[LEARN MORE >](#)

Your chance to win a \$1500 gift card!


Predict which cars consumers prefer. Play the vehicle rating game.



[PLAY NOW >](#)

Let us find your next new car


Search vehicle inventory in our local dealership listings.



[LEARN MORE >](#)

2002 Mazda Millenia - Features & Specs

Overview | Inventory | Appraise | Photos | MPG | More...



S Sedan
(2.3L V6 Supercharger 4-speed Automatic)

Select a different Millenia model

[Change Vehicle](#)

[View photos](#)

Highlights

FUEL ECONOMY (CTY/HWY)	17/25 mpg	ENGINE TYPE	Gas
CAR TYPE	Sedan	TOTAL SEATING	5
TRANSMISSION	4-speed Automatic	CYLINDERS	V6
BASIC WARRANTY	3 Yr./50000 Mi.	CONSUMER RATING	

Colors

Exterior Colors


Brilliant Black	Brilliant Black/Gentry	Emerald Mica	Millennium Red Mica
Platinum Silver Metallic	Sand Mica	Snow Flake White Pearl Mica	Snow Flake White Pearl Mica/Sand Mica

Interior Colors

Beige	Gray
-------	------

Specifications

ADVERTISEMENT



ADVERTISEMENT


Nearby Inventory [UPDATE](#)

There is no inventory for this vehicle


New Car Resources

- [10 Steps to Buying a New Car](#)
- [Incentives and Rebates](#)
- [New Car Buying Guides](#)
- [New Car Inventory](#)
- [Car Finder](#)
- [Guide for First-Time New-Car Buyers](#)

ADVERTISEMENT



ADVERTISEMENT



Get discount deals for your brand new wheels.

<http://www.edmunds.com/mazda/millenia/2002/features-specs.html?style=100003481...>

GROUND CLEARANCE
 DR: 4.9 in. (125.1 mm)

WIDTH 5ft 9.7in

Body style illustration may not reflect the actual shape of this vehicle.

Exterior Measurements

WIDTH	5 ft. 9.7 in. (69.7 in.)	HEIGHT	4 ft. 6.9 in. (54.9 in.)
LENGTH	15 ft. 11.6 in. (191.6 in.)	GROUND CLEARANCE	0 ft. 4.9 in. (4.9 in.)
FRONT TRACK	4 ft. 11.8 in. (59.8 in.)	REAR TRACK	4 ft. 11.8 in. (59.8 in.)
WHEEL BASE	9 ft. 0.3 in. (108.3 in.)		

Interior Measurements

FRONT HEAD ROOM	37.9 in.	FRONT LEG ROOM	43.3 in.
FRONT SHOULDER ROOM	55.1 in.	REAR HEAD ROOM	36.5 in.
REAR LEG ROOM	34.1 in.	REAR SHOULDER ROOM	54.2 in.

Fuel

ENGINE TYPE	Gas FUEL TYPE	Premium unleaded (required)
FUEL TANK CAPACITY	18 gal. RANGE IN MILES (CTY/HWY)	306/450 ml.
EPA MILEAGE EST. (CTY/HWY)	17/25 mpg	

Weights and Capacities

EPA INTERIOR VOLUME	51.4 cu.ft.	CURB WEIGHT	3488 lbs.
CARGO CAPACITY, ALL SEATS IN PLACE	13.3 cu.ft.	MAXIMUM CARGO CAPACITY	13.3 cu.ft.

DriveTrain

DRIVE TYPE	Front wheel drive	TRANSMISSION	4-speed automatic
------------	-------------------	--------------	-------------------

Engine & Performance

BASE ENGINE SIZE	2.3 L	CAM TYPE	Double overhead cam (DOHC)
CYLINDERS	V6	VALVES	24
TORQUE	210 ft.-lbs. @ 3500	HORSEPOWER	210 hp @ 5300 rpm
TURNING CIRCLE	37.4 ft.		

Suspension

- Multi-link front suspension
- Multi-link rear suspension
- Four-wheel independent suspension

Warranty

BASIC	3 yr./ 50000 ml.	DRIVETRAIN	3 yr./ 50000 ml.
ROADSIDE	3 yr./ 50000 ml.		

Features

Interior Features

Front Seats

- 8-way power passenger seat
- 8-way power driver seat
- Driver seat with manual adjustable lumbar support
- Height adjustable driver seat
- Height adjustable passenger seat
- Leather
- Bucket front seats

Rear Seats

- Folding with storage and pass-thru center armrest
- Rear ventilation ducts

Power Features

- Remote power door locks
- Power mirrors

- 1 one-touch power windows

Instrumentation

- Clock
- External temperature display
- Tachometer
- Low fuel level warning

Convenience

- Cruise control
- Front and rear cupholders
- Remote trunk release
- Speed-proportional power steering
- Tilt-adjustable steering wheel
- Front console with storage
- Front door pockets
- Front seatback storage
- 12V front power outlet(s)
- Audio and cruise controls on steering wheel

Comfort

- Interior air filtration
- Trunk light
- Front and rear reading lights
- Leather steering wheel
- Dual illuminating vanity mirrors
- Climate control
- Simulated wood trim on center console
- Leather trim on shift knob
- Front and rear floor mats

Memorized settings

- Memorized settings includes steering wheel

In Car Entertainment

- Diversity antenna
- Bose premium brand speakers
- 200 watts stereo output
- Bose premium brand stereo system
- 9 total speakers
- AM/FM In-dash single CD player stereo

Exterior Features

Roof and Glass

- Variable Intermittent wipers
- Power glass sunroof
- Rear defogger

Tires and Wheels

- Alloy wheels
- Steel spare wheel
- All season tires
- 17 x 7.0 in. wheels
- P215/50R V tires
- Temporary spare tire

Safety Features

- 4-wheel ABS
- Child seat anchors
- Ventilated front disc / solid rear disc brakes
- Engine immobilizer
- Auto delay off headlamps
- 2 rear headrests
- Traction control
- Front height adjustable headrests
- Dual front side-mounted airbags
- Anti-theft alarm system
- Rear door child safety locks
- Front fog/driving lights
- 2 front headrests
- Rear center lap belt
- Electronic brakeforce distribution
- Rear height adjustable headrests

More on 2002 Mazda Millenia

- [2002 Mazda Millenia Consumer Discussions](#)
- [2002 Mazda Millenia Consumer Reviews](#)
- [2002 Mazda Millenia Features and Specs](#)
- [2002 Mazda Millenia Review](#)
- [2002 Mazda Millenia Reliability](#)
- [2002 Mazda Millenia Safety](#)

Explore Edmunds

Search Site

Ask the Car People.™


[Learn More](#) | [Sign In](#) | [Mobile](#) | [Help](#) | [Newsletter](#) | [Dealers](#)

[New Cars](#) | [Used Cars](#) | [Inventory](#) | [Car Reviews](#) | [Tips & Advice](#) | [What's Hot](#) | [Search Site](#)

[Home](#) > [Used Cars](#) > [Mazda](#) > [Millenia](#) > [2002 Millenia](#) > Features & Specs

Used Car History Report


Take the unknown out of buying pre-owned.



[LEARN MORE](#)

Edmunds will predict your next car.


Your preferences. Our recommendations. Try it today!



[MATCH YOUR CAR NOW](#)

Compare the cost of buying new vs used


In the current economic climate, buying new may save you money.



[COMPARE COSTS NOW](#)

2002 Mazda Millenia - Features & Specs

Overview | Inventory | Appraise | Photos | MPG | More...



Premium Sedan
(2.5L V6 4-speed Automatic)

Select a different Millenia model

[Change Vehicle](#)

[View photos](#)

Highlights

FUEL ECONOMY (CTY/HWY)	17/24 mpg	ENGINE TYPE	Gas
CAR TYPE	Sedan	TOTAL SEATING	5
TRANSMISSION	4-speed Automatic	CYLINDERS	V6
BASIC WARRANTY	3 Yr./ 50000 Mi.	CONSUMER RATING	

Colors

Exterior Colors

Brilliant Black

Interior Colors

Black/Ivory


Specifications

LENGTH 15ft 11.8in	WIDTH 5ft 9.7in
HEIGHT 4ft 8.9in	
GROUND CLEARANCE 6ft 4.9in	

Body style illustration may not reflect the actual shape of this vehicle.

Exterior Measurements

Before you visit the dealer
Compare the latest car incentives and rebates available to you



[CLICK HERE](#)

Nearby Inventory [UPDATE](#)

There is no inventory for this vehicle

New Car Resources

- [10 Steps to Buying a New Car](#)
- [Incentives and Rebates](#)
- [New Car Buying Guides](#)
- [New Car Inventory](#)
- [Car Finder](#)
- [Guide for First-Time New-Car Buyers](#)

What Can I Afford?
Find out with Edmunds Affordability Calculator

Tell us your desired monthly payment, and we'll give you a price range for your next car.

[GET STARTED](#)



State Farm™

State Farm offers discounts up to 40% on auto insurance.

Get A Quote ▶

*Not available in all states.

<http://www.edmunds.com/mazda/millenia/2002/features-specs.html?style=100075073>

WIDTH	5 ft. 9.7 in. (69.7 in.)	HEIGHT	4 ft. 6.9 in. (54.9 in.)
LENGTH	15 ft. 11.6 in. (191.6 in.)	GROUND CLEARANCE	0 ft. 4.9 in. (4.9 in.)
FRONT TRACK	4 ft. 11.8 in. (59.8 in.)	REAR TRACK	4 ft. 11.8 in. (59.8 in.)
WHEEL BASE	9 ft. 0.3 in. (108.3 in.)		

Interior Measurements

FRONT HEAD ROOM	37.9 in.	FRONT LEG ROOM	43.3 in.
FRONT SHOULDER ROOM	55.1 in.	REAR HEAD ROOM	36.5 in.
REAR LEG ROOM	34.1 in.	REAR SHOULDER ROOM	54.2 in.

Fuel

ENGINE TYPE	Gas	FUEL TYPE	Regular unleaded
FUEL TANK CAPACITY	18 gal.	RANGE IN MILES (CTY/HWY)	306/432 mi.
EPA MILEAGE EST. (CTY/HWY)	17/24 mpg		

Weights and Capacities

EPA INTERIOR VOLUME	51.4 cu.ft.	CURB WEIGHT	3358 lbs.
CARGO CAPACITY, ALL SEATS IN PLACE	13.3 cu.ft.	MAXIMUM CARGO CAPACITY	13.3 cu.ft.

DriveTrain

DRIVE TYPE	Front wheel drive	TRANSMISSION	4-speed automatic
------------	-------------------	--------------	-------------------

Engine & Performance

BASE ENGINE SIZE	2.5 L	CAM TYPE	Double overhead cam (DOHC)
CYLINDERS	V6		VALVES 24
TORQUE	160 ft.-lbs. @ 4800	HORSEPOWER	170 hp @ 5800 rpm
TURNING CIRCLE	37.4 ft.		

Suspension

- Multi-link front suspension
- Multi-link rear suspension
- Four-wheel independent suspension

Warranty

BASIC	3 yr./ 50000 ml.	DRIVETRAIN	3 yr./ 50000 ml.
ROADSIDE	3 yr./ 50000 ml.		

Features

Interior Features

Front Seats

- 8-way power passenger seat
- 8-way power driver seat
- Driver seat with manual adjustable lumbar support
- Height adjustable driver seat
- Height adjustable passenger seat
- Leather
- Bucket front seats

Rear Seats

- Folding with storage and pass-thru center armrest
- Rear ventilation ducts

Power Features

- Remote power door locks
- Power mirrors
- 1 one-touch power windows

Instrumentation

- Clock
- Tachometer
- External temperature display
- Low fuel level warning

Convenience

- Cruise control
- Front and rear cupholders
- Remote trunk release
- Speed-proportional power steering
- Tilt-adjustable steering wheel
- Front console with storage
- Front door pockets
- Front seatback storage
- 12V front power outlet(s)
- Audio and cruise controls on steering wheel

Comfort

- Interior air filtration
- Trunk light
- Front and rear reading lights
- Leather steering wheel
- Dual illuminating vanity mirrors
- Climate control
- Leather trim on center console
- Leather trim on shift knob
- Front and rear floor mats

Memorized settings

- Memorized settings includes steering wheel

In Car Entertainment

- Diversity antenna
- 100 watts stereo output
- 6 total speakers
- AM/FM in-dash single CD player stereo

Exterior Features

Roof and Glass

- Variable Intermittent wipers
- Power glass sunroof
- Rear defogger

Tires and Wheels

- Alloy wheels
- Steel spare wheel
- All season tires
- 17 x 7.0 in. wheels
- P215/50R V tires
- Temporary spare tire

Safety Features

- 4-wheel ABS
- Child seat anchors
- Ventilated front disc / solid rear disc brakes
- Engine immobilizer
- Auto delay off headlamps
- 2 rear headrests
- Electronic brakeforce distribution
- Rear height adjustable headrests
- Dual front side-mounted airbags
- Anti-theft alarm system
- Rear door child safety locks
- Front fog/driving lights
- 2 front headrests
- Rear center lap belt
- Front height adjustable headrests

More on 2002 Mazda Millenia

- [2002 Mazda Millenia Consumer Discussions](#)
- [2002 Mazda Millenia Consumer Reviews](#)
- [2002 Mazda Millenia Features and Specs](#)
- [2002 Mazda Millenia Review](#)
- [2002 Mazda Millenia Reliability](#)
- [2002 Mazda Millenia Safety](#)

Explore Edmunds

Search Site

- | | | | | | |
|--|-----------------------------------|---|---|---|------------------------------|
| New Cars | Used Cars | Car Reviews | Tips & Advice | Maintenance | What's Hot |
| Calculators | Search Inventory | Car Reviews and Road Tests | Buying a Car | Maintenance Costs & Recalls | Car News |
| Car Finder | Appraise Your Car | Track Tests & Walkarounds | Leasing a Car | True Cost to Own® | Car Pictures |
| Compare Cars | Certified Cars | Long-Term Road Tests | Selling a Car | Find a Repair Shop | Car Videos |
| Find a Dealer | Selling Tips | Comparison Road Tests | Family and Car Safety | How-To Articles | Car Forums |
| Get Monthly Payment | True Cost to Own® | Auto Shows | Fuel Economy & Green Cars | Maintenance Articles | |
| Incentives & Rebates | | Feature Stories | Car Technology | Dealer Service Reviews | |